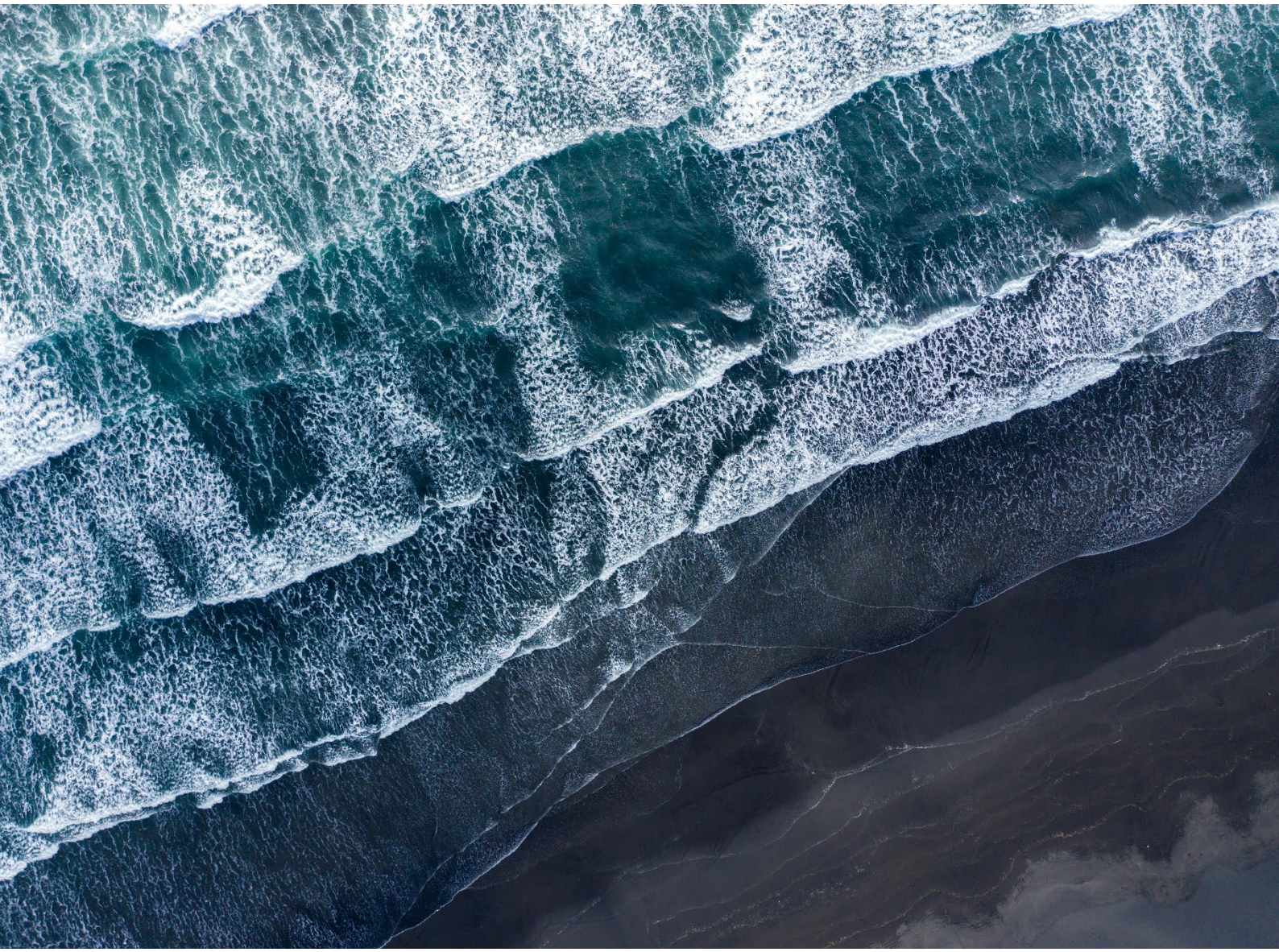
Newfoundland & Labrador Atlas of Storm Surge and Wave Climates

Technical Documentation

June 26, 2024

Prepared for Water Resources Management Division (WRMD)



The expert in WATER ENVIRONMENTS

1964-2024
60 years of solving
water challenges

Newfoundland & Labrador Atlas of Storm Surge and Wave Climates

Technical Documentation

Prepared for: Water Resources Management Division (WRMD)
Represented by: Paula Dawe

Approved by



X
Approved

This document was prepared for the party indicated herein and the purposes outlined in this document. The material and information in the document reflect the opinion and best judgment of DHI Water & Environment, Inc. based on the information available at the time of preparation. Any use of this document or reliance on its content by third parties is the responsibility of the third party. DHI Water & Environment, Inc. accepts no responsibility for any damages suffered as a result of third-party use of this document or for uses other than the intended purposes stated herein.

Contact person:	Paula Dawe
Project Manager:	Méven Robin Huiban
Quality Supervisor:	Danker Kolijn
Author:	Gabriel Vieira de Carvalho; Aline Kaji; Méven Robin Huiban
Project No.:	42803838
Approved by:	Danker Kolijn
Approval date:	June 26, 2024
Revision:	Final 1.1
Classification:	**Restricted:** This document may be shared within DHI whereas sharing it outside the DHI Group entities is subject to the client's prior approval.
File name:	NL_Atlas_StormSurge_Waves_Documentation_Finalv1.1_Logo

DHI Water & Environment, Inc. • PO Box 32120 Preston • Cambridge, ON • N3H 5M2 • Canada
Telephone: +1 519 650 4545 • mhu@dhigroup.com • www.dhigroup.com • Company Reg. No.: 85760 3765

Contents

Nomenclature **1**

Glossary **2**

Plain Language Summary **3**

1 Introduction **4**

2 NL Atlas of Storm Surge and Wave Climate Contents **6**

3 Underlying Datasets **11**

3.1 Model Forcing 11
3.1.1 Wind and Pressure Hindcast (ECMWF ERA5) 11
3.1.2 Astronomical Tide (DTU10) 11
3.1.3 Sea Ice Coverage Hindcast (CIS + NSIDC) 11
3.1.4 DHI Global Wave Model (GWM) 12
3.2 Storm Surge Model - DHI $HD_{NL\text{-}ERA5}$ 13
3.2.1 Model Setup 13
3.2.2 Storm Surge Model Validation 15
3.3 Wave Model 21
3.3.1 MIKE Metocean Simulator 21
3.3.2 Model Setup 23
3.3.3 Wave Model Validation 25
3.4 Climate Projections 42

4 Extreme Value Analysis **44**

4.1 Methodology 44
4.2 Results 46
4.3 Sources of Uncertainty 48

5 Considerations on Climate Projections **50**

6 Discussion **52**

6.1 Typical Use Cases 52
6.2 Limitations 53
6.3 Recommendations 54

7 Closing **56**

8 References **57**

Appendices

Appendix A Quality Indices

Appendix B EVA Methodology

Appendix C EVA Results

Figures

Figure 2.1 Output locations for the metocean parameters timeseries output locations along the coasts of Newfoundland and Labrador 9
Figure 2.2 Overview of raster maps tiles for storm surge statistics covering the entire province ... 9
Figure 2.3 Output locations for the Extreme Value Analyses (EVA)..... 10
Figure 3.1 Example of a Sea Ice Concentration map (CIS + NSIDC) 12
Figure 3.2 Illustration of the GWM model domain and computational mesh 13
Figure 3.3 DHI $HD_{NL\text{-}ERA5}$ – Regional Atlantic Storm Surge Model domain 14
Figure 3.4 DHI $HD_{NL\text{-}ERA5}$ Water Level Validation Stations 15
Figure 3.5 Comparison between measured (CHS-Residual) and modelled (DHI-Residual) water level residual at Bonavista 17
Figure 3.6 Comparison between measured (CHS-Residual) and modelled (DHI-Residual) water level residual at Port aux Basques..... 17
Figure 3.7 Comparison between measured (CHS-Residual) and modelled (DHI-Residual) water level residual at St. John's 18
Figure 3.8 Comparison between measured (CHS-Residual) and modelled (DHI-Residual) water level residual at Holyrood Bay..... 18
Figure 3.9 Comparison between measured (CHS-Residual) and modelled (DHI-Residual) water level residual at Long Cove..... 19
Figure 3.10 Comparison between measured (CHS-Residual) and modelled (DHI-Residual) water level residual at Corner Brook..... 19
Figure 3.11 Comparison between measured (CHS-Residual) and modelled (DHI-Residual) water level residual at Lark Harbour 20
Figure 3.12 Surge water levels time series for hurricanes Igor (2010) and Fiona (2022) 21
Figure 3.13 Schematic representation of the MIKE MS modelling process 22
Figure 3.14 Example of the selected events after completion of the PCA and the MDA steps 23
Figure 3.15 Subdomains of the wave model (left) Examples of the model bathymetry for subdomains NFL_4 and LBR_4 (right) 24
Figure 3.16 Location of wave buoys for the validation of the wave model 26
Figure 3.17 Wave Model Validation – Port aux Basques..... 29
Figure 3.18 Wave Model Validation – Placentia Bay Mouth..... 30
Figure 3.19 Wave Model Validation – Placentia Bay Head 31
Figure 3.20 Wave Model Validation – Fortune Bay..... 32
Figure 3.21 Wave Model Validation – Bonavista 33
Figure 3.22 Wave Model Validation – St. Johns 34
Figure 3.23 Wave Model Validation – Burgeo (MEDS C44235)..... 35
Figure 3.24 Wave Model Validation – Burgeo (MEDS C44235) – Hurricane Earl (Sep 2010)..... 36
Figure 3.25 Locations used for comparison with other hindcast products..... 37
Figure 3.26 Time series of significant wave height based for the overlapping period (1980-2018) between MIKE MS, MSC50 and ERA5 for various locations around Newfoundland and Labrador 38
Figure 3.27 Scatter plots comparing MIKE MS results with MSC50 hindcast (left) and ERA5 (right) for various locations around Newfoundland and Labrador..... 39
Figure 3.28 Scatter plots comparing MIKE MS results with MSC50 hindcast (left) and ERA5 (right) for various locations around Newfoundland and Labrador..... 40
Figure 3.29 Comparison of significant wave height at Burgeo wave buoy (MEDS C44235) during Hurricane Earl in 2010 41
Figure 3.30 Comparison of significant wave height at Port aux Basques during Hurricane Bertha in 1990..... 42

Figure 3.31 Comparison of significant wave height at Port aux Basques during the January 2000 storm 42
Figure 4.1 Example of Extreme Value Analysis of H_{m0} 45
Figure 4.2 Summary of the Sensitivity Analysis of the EVA Parameters 46
Figure 5.1 Projected changes in the 99th percentile of storm surges by end-of-century compared to the baseline (1984-2014 to 2070–2100) for SSP5-8.5 51
Figure 5.2 Projected changes in the 99th percentile of significant wave height by end-of-century compared to the baseline (1984-2014 to 2071–2100) for SSP5-8.5 51

Tables

Table 2.1 Summary of the Atlas deliverables for the Hindcast period (1980-2022) 7
Table 2.2 Summary of the Atlas deliverables for the Climate Change projections (2015-2100) ... 8
Table 3.1 Storm Surge model forcings and boundary conditions for the hindcast and climate change projections simulations 14
Table 3.2 DHI $HD_{NL\text{-}ERA5}$ Model Settings 15
Table 3.3 DHI $HD_{NL\text{-}ERA5}$ Water Level Validation Stations 16
Table 3.4 DHI $HD_{NL\text{-}ERA5}$ Summary of Quality Indices 16
Table 3.5 Wave model forcings and boundary conditions for the hindcast and climate change projections simulations 24
Table 3.6 DHI MIKE MS Wave Model Setup 25
Table 3.7 Wave buoys stations used to compare the wave model results 27
Table 3.8 Comparison Metrics Summary 27
Table 3.9 Locations used for comparison with other hindcast products 37
Table 4.1 Summary of Extreme Value Analyses Results for 20-year and 100-year Return Periods 46

Nomenclature

Abbreviation	Definition / Description
AR6	IPCC Sixth Assessment Report
C3S	Copernicus Climate Change Service
CC	Correlation Coefficient
CHS	Canadian Hydrographic Service
CIS	Canadian Ice Services
CMIP6	Coupled Model Intercomparison Project (Phase 6)
CSIRO	Commonwealth Scientific and Industrial Research Organisation
ECMWF	European Centre for Medium-Range Weather Forecasts
ERA5	Fifth generation ECMWF atmospheric reanalysis of the global climate
EVA	Extreme Value Analysis
FDRP	Federal Damage Reduction Program
FHIMP	Flood Hazard Identification and Mapping Program
GCM	Global Climate Models
GEBCO	General Bathymetric Chart of the Oceans
IPCC	Intergovernmental Panel on Climate Change
MDA	Maximum Dissimilarity Algorithm
MSL	Mean Sea Level
MWD	Mean Wave Direction [°N from] of Total Wave Spectrum
NDMP	National Disaster Mitigation Program
NL	Newfoundland & Labrador
NONNA	Canadian Hydrographic Service Non-Navigational Bathymetric Data
NSIDC	National Snow and Ice Data Center
PCA	Principal Component Analysis
RBF	Radial Basis Function
RCM	Regional Climate Models
RMSE	Root Mean Squared Error
SLR	Sea Level Rise
SSP5-8.5	Shared Socioeconomic Pathway 5-8.5
T_r	Return period [years]
WRMD	Water Resources Management Division

Glossary

Term	Definition / Description
Hindcast	A hindcast is the process of using historical data and models to recreate past environmental conditions for a specific location and period. In the Atlas context, the Hindcast is the simulation of past conditions of storm surge and wave conditions along the coasts of the province.
Climate Change Projection	In the context of the project, Climate Change Projection refers to the prediction of storm surge and wave conditions along Newfoundland and Labrador coasts based on selected Global Climate Models and scenarios. It represents possible future scenarios considering different projected socioeconomic global changes as outlined in the IPCC Sixth Assessment Report [1].
Offshore	Offshore typically refers to the area of the ocean further from the coastline, often characterized by deeper waters, in contrast to nearshore (see below)
Nearshore	Nearshore refers to the zone closer to the coast where waves interact with the seabed and shoreline, in contrast to offshore (see above).
Water Level Residuals	Water Level Residuals (WL_{Res}) refers to the difference between the total water level and the predicted astronomical tide. Water Level Residuals typically comprises of contributions from several phenomena such as storm surge but also large-scale oceanographic processes, long-term oscillations, local anomalies, freshwater discharge, etc.
Mean Sea Level (MSL)	Mean Sea Level is the average sea level height at a specific location and can serve as a reference point for measuring elevations.
Total Wave Spectrum / Wave Parameters	The Total Wave Spectrum refers to the comprehensive distribution of wave energy across different frequencies and wavelengths at a precise location and over a defined period. Wave parameters can be derived from the total spectrum, such as: • Significant Wave Height ($H_{m0,}$ in m): average height of the highest one-third of waves in a given wave spectrum. • Peak Wave Period ($T_{p,}$ in s): time interval between the passage of successive wave crests with the highest energy in a wave spectrum. • Mean Wave Direction (MWD, in °.N): average direction from which waves are propagating in a specific area over a period of time
Sea / Swell waves	In the total wave spectrum, Sea waves generated by local winds coexist with Swell waves originating from distant storms, exhibiting a range of wavelengths and characteristics. Sea waves are influenced by factors such as wind speed, duration, and fetch, and tend to have shorter wavelengths. Swell waves, originate from distant weather systems and travel long distances with more uniform characteristics. They usually have longer wavelengths and a more regular, periodic pattern.
Bi-Model Sea States	Refers to a situation where there are two dominant types of waves present simultaneously in a body of water. A bi-modal wave spectrum would typically exhibit two distinct peaks or modes, each representing a dominant wave frequency or direction within the spectrum.

Plain Language Summary

The Newfoundland & Labrador Atlas of Storm Surge and Wave Climates is a comprehensive resource providing insight into the present and future patterns and characteristics of storm surges and waves along the province's coastlines. It includes detailed maps, charts, tables, and time series data, consolidating a vast array of information to support the assessment of coastal flooding hazards.

The Atlas is a valuable tool for researchers, decision-makers, coastal engineers and planners involved in coastal management, as it aids in understanding the potential risks and impacts of extreme weather events, assessing the high-level design of coastal infrastructures and allowing for informed decision-making and effective planning for flood risk mitigation. It also serves as a dataset to support community-level coastal floodplain mapping initiatives across the province, by providing boundary conditions for the development of local models by consultants, researchers, and government agencies.

At the core of the Atlas lies a set of advanced numerical models developed specifically for this initiative which cover the entire province's coastline with spatial resolutions as fine as 1.5 km. These models have been validated against measurements at various points around the province, where measurements are available, demonstrating their capacity to represent the storm surges and waves in the area.

Within this technical documentation, a comprehensive description of the data is provided, exploring the methodology employed and the models used to generate the datasets. The application of statistical techniques, such as extreme value analysis, is also explained, emphasizing its significance in evaluating the frequency of occurrence and magnitude of extreme events.

Acknowledging the inherent uncertainties associated with climate projections, we emphasize the need for a nuanced interpretation of results and underscore the importance of effective communication when disseminating information derived from the Atlas. The Atlas aims to provide users with an overview of potential future scenarios to support planning and decision making, while ensuring that uncertainties are communicated and understood. At present the Atlas contains results from two Global Climate Models (GCM) and should be considered as a first step towards developing a more comprehensive and robust climate projection product, with a larger ensemble of models.

Additionally, the document addresses the limitations of the data and methods, providing users with a clear understanding of the constraints associated with the information presented in the Atlas and offering practical recommendations and best practices for users to interpret and integrate the information to assess coastal flooding hazards across the province. Regional planning, high-level vulnerability assessments, public information and awareness, downscaling to detailed community level assessments incorporating climate change impacts are examples of use cases for the Atlas. Ensuring that the Atlas is employed for its intended purposes and making thoughtful modifications and adaptations can enhance its effectiveness in specific contexts.

1 Introduction

This report introduces the Newfoundland & Labrador Atlas of Storm Surge and Wave Climates, developed for the Government of Newfoundland & Labrador Water Resources Management Division (WRMD). The Atlas is intended to inform coastal floodplain mapping efforts throughout the province, and to provide a consistent basis for the modelling and interpretation of coastal processes and hazards related to flooding. This technical note describes the data that is provided within the Atlas, including a description of the methodology and the models used to generate the datasets, the limitations of the data, and guidance on how this information can be used to inform coastal floodplain mapping.

As part of the Federal Damage Reduction Program (FDRP), the Government of Newfoundland and Labrador completed flood risk mapping projects for several communities where coastal, fluvial, and pluvial flooding had historically occurred. These flood risk mapping projects were completed between 1981, when the Government of Newfoundland and Labrador joined the FDRP, and 1996, including the completion of flood risk mapping studies for Gould's, Petty Harbour, and Ferryland in 1996, for the communities of Carbonear, Victoria, Salmon Cove, Whitbourne, Heart's Delight - Islington, Winterton and Hant's Harbour in 1996, and for Brigus in 1997.

After the completion of the FDRP, the Government of Newfoundland and Labrador announced a new Climate Change Adaptation initiative to update existing flood risk mapping studies and undertake new flood risk mapping studies with specific considerations for the anticipated impacts of climate change. Additionally, the Government of Canada introduced the National Disaster Mitigation Program (NDMP), which committed ongoing funding to reduce the impacts of natural disasters, including via the completion of flood risk mapping studies until March 31, 2022.

Following the completion of the NDMP, the Government of Canada initiated the Flood Hazard Identification and Mapping Program (FHIMP), which provided extensive funding to provincial and territorial governments in support of the development or updating of flood risk maps, considering fluvial, pluvial and coastal hazards. As part of this effort, a series of coastal hydrodynamic and wave models were developed using DHI's MIKE 21 FM modelling suite to estimate extreme nearshore surge levels and wave conditions based on a hindcast and a forecast of future trends to the local surge and wave climate along the entire coast of Newfoundland and Labrador.

The outcome of this project is the **Newfoundland & Labrador Atlas of Storm Surge and Wave Climates** (from herein referred to as the "Atlas"), a comprehensive dataset which can be leveraged to address present- and future- flood risk planning and management activities. In addition to this document, the Atlas encompasses a series of digital products, including maps, tables, and time series, which can be made available upon request to WRMD.

REPORT STRUCTURE

- Chapter 2 presents the content of the Newfoundland & Labrador Atlas of Storm Surge and Wave Climates, including a description of the various digital files.
- Chapter 3 describes the methodology and models used to derive the storm surge and wave climate datasets.
- Chapter 4 describes the Extreme Value Analysis (EVA) performed on the significant wave height and storm surge.
- Chapter 5 explores the uncertainties associated to climate projections and considerations when interpreting results and communicating the information from this Atlas.
- Chapter 6 discusses limitations of the results and provides recommendations on best practices in using the Atlas.

2 NL Atlas of Storm Surge and Wave Climate Contents

This chapter describes the digital content of the Newfoundland & Labrador Atlas of Storm Surge and Wave Climates.

The Atlas encompasses a diverse range of data, such as time series, extreme value tables, GeoJSON[1] and raster maps[2], which can be made available digitally upon request from the WRMD. The different deliverables and data types are described below and outlined in Table 2.1 and Table 2.2. The data package is split into **hindcast** (historical period covering 1980-2022) and the **climate change projections** (covering 2015-2100). More details of the distinction between these two data packages, as well as the underlying datasets and methodologies used to derive these results are described in subsequent chapters of this report. References to each relevant section are included for each item described below.

HINDCAST

- Timeseries (Chapter 3):
  - Hourly timeseries of Water Level Residual (Storm Surge), Ice Concentration, Significant Wave Height, Peak Period and Mean Wave Direction.
  - The timeseries are provided for 5,830 output points along the coast of Newfoundland and Labrador, with increasing resolution towards the coast - from 10 km offshore to 3 km (Newfoundland) and 5 km (Labrador) near the coast. The output points are depicted in Figure 2.1 and are provided as a shapefile for referencing the output point names and associated bathymetry.
- Extreme Value Analysis (EVA) (Chapter 4):
  - Extreme values for various return periods (1-, 2-, 5-, 10-, 25-, 50- and 100-years) for Water Level Residual (Storm Surge) and Significant Wave Height.
  - Extreme wave Peak Periods associated with each Significant Wave Height extreme values for the various return periods.
  - The EVA outputs are provided for 78 points along the Newfoundland and Labrador coast (Figure 2.3) which were defined in consultation with WRMD to be representative for communities and areas of importance.
  - For each analysis points, the EVA is provided as tables in a text file (.csv). Additionally, a GeoJSON is provided with all EVA results for each analysis points to facilitate the visualization in GIS software.
- Statistical Maps:
  - Maps of Water Level Residual (Storm Surge) and Significant Wave Height 50th and 99th percentile and Average Annual Maximum values.
  - For Water Level Residual (Storm Surge), the statistical maps are provided as raster maps, subdivided into 8 tiles (Figure 2.2).
  - For Significant Wave Height, the statistics are provided as text files (.csv) and GeoJSON for each wave model output point (Figure 2.1) and subdivided into 12 areas corresponding to each wave model subdomain.

[1] GeoJSON is an open standard format designed for representing simple geographical features, along with non-spatial attributes. It can be opened by any GIS software for visualization and explored as a text file.
[2] Raster maps are provided in GeoTIFF format (*.tif*), which is used as an interchange format for georeferenced raster imagery. It can be opened by any GIS software for visualization.

CLIMATE CHANGE PROJECTIONS

- Timeseries (Chapter 3.3):
  - 3-Hourly timeseries of Water Level Residual (Storm Surge), Ice Concentration, Significant Wave Height, Peak Period and Mean Wave Direction. The Climate Change projections timeseries are provided for the same output points as for the Hindcast.
- Projected changes statistical maps:
  - Mid-Century (2041-2070) and Late-Century (2071-2100) maps of projected changes in Water Level Residual (Storm Surge) and Significant Wave Height statistics (50th and 99th percentile and Average Annual Maximum).
  - The projected changes are relative to the historical baseline (1985-2015), considering the SSP5-8.5 scenario for two Global Climate Models (EC-EARTH3 and ACCESS-CM2)[3].
  - The projected changes statistical maps are provided in absolute values (meters for both Water Level Residual and Significant Wave Height).

Table 2.1 Summary of the Atlas deliverables for the Hindcast period (1980-2022)

Run	Item	Description	Location/Data Format
Hindcast (1980-2022)	Timeseries	Hourly time series of storm surge and waves hindcast for the period 1980 to 2022 Variables: - Hm0_Total: Significant Wave Height of Total Wave Spectrum (m) - Tp_Total: Peak Period of Total Wave Spectrum (s) - MWD_Total: Mean Direction of Total Wave Spectrum (degN from) - WL_Res: Residual Water Level - Storm Surge (m) - Ice_Conc: Ice Concentration	5830 high density output points along the NL coast and offshore Results provided as .csv files.
	Extreme Value Analysis	Extreme Significant Wave Height of Total Wave Spectrum (Hm0) - Omnidirectional for 1, 2, 5, 10, 25, 50, 100-year return periods - Directional (30° bins) for 1, 2, 5, 10, 25, 50, 100-year return periods Associated Extreme Peak Period of Total Wave Spectrum (Tp) - 5th percentile of wave peak period associated with extreme Hm0 - 50th percentile of wave peak period associated with extreme Hm0 - 95th percentile of wave peak period associated with extreme Hm0 Extreme Residual Water Level - Storm Surge (WL_Res) - For 1, 2, 5, 10, 25, 50, 100-year return periods	78 analysis points near key NL coastal communities. Results provided as .txt and GeoJSON files.
	Statistical Maps	Maps of Significant Wave Height of Total Wave Spectrum (m) statistics for the Hindcast run (1980-2022) Variables (full name / short name): - Hm0_Total 50th Percentile / Hm0_50p - Hm0_Total 99th Percentile / Hm0_99p - Hm0_Total Average Annual Maximum / Hm0_AAM	5830 high density output points along the NL coast and offshore. Statistical results are divided into 12 areas corresponding to the wave model subdomains. Results provided as .csv and GeoJSON files.
		Maps of Residual Water Level - Storm Surge (m) statistics for the Hindcast run (1980-2022) Variables: - WL_Res 50th Percentile - WL_Res 99th Percentile - WL_Res Average Annual Maximum	Raster maps along the NL coast and offshore. Statistical maps are divided into 8 raster tiles. Results provided as .tif files.

[3] A description of the climate projections used in this study is provided in Section 3.3

Table 2.2 Summary of the Atlas deliverables for the Climate Change projections (2015-2100)

Run	Item	Description	Location/ Data Format
Climate Change - Historical Baseline (1984-2014) and Future Projections (2015-2100)	Timeseries	3-hourly time series of storm surge and wave bulk parameters for a historical baseline (period of 1984-2014) and for the SSP5-8.5 climate change scenario (period of 2015-2100) forced by two Global Climate Models (EC-EARTH3 and ACCESS-CM2). Variables: - Hm0_Total: Significant Wave Height of Total Wave spectrum (m) - Tp_Total: Peak Period of Total Wave Spectrum (s) - MWD_Total: Mean Direction of Total Wave Spectrum (degN from) - WL_Res: Residual Water Level - Storm Surge (m) - Ice_Conc: Ice Concentration	5830 high density output points along the NL coast and offshore. Results provided as .csv files.
	Statistical Maps	Maps of projected changes in Significant Wave Height of Total Wave Spectrum (m) statistics relative to the historical baseline for mid- and late-century, considering the SSP5-8.5 climate change scenario and two Global Climate Models (EC-EARTH and ACCESS-CM2). Variables (Full Name / Short Name): - Hm0_Total Mid-Century 50th Percentile Difference (SSP5-8.5 ACCESS-CM2): - dHm0_MC_50p_AC2 - Hm0_Total Mid-Century 99th Percentile Difference (SSP5-8.5 ACCESS-CM2): - dHm0_MC_99p_AC2 - Hm0_Total Mid-Century Avg Annual Max Difference (SSP5-8.5 ACCESS-CM2): - dHm0_MC_AAM_AC2 - Hm0_Total Late-Century 50th Percentile Difference (SSP5-8.5 ACCESS-CM2): - dHm0_LC_50p_AC2 - Hm0_Total Late-Century 99th Percentile Difference (SSP5-8.5 ACCESS-CM2): - dHm0_LC_99p_AC2 - Hm0_Total Late-Century Avg Annual Max Difference (SSP5-8.5 ACCESS-CM2): - dHm0_LC_AAM_AC2 - Hm0_Total Mid-Century 50th Percentile Difference (SSP5-8.5 EC-EARTH3): - dHm0_MC_50p_EC3 - Hm0_Total Mid-Century 99th Percentile Difference (SSP5-8.5 EC-EARTH3): - dHm0_MC_99p_EC3 - Hm0_Total Mid-Century Avg Annual Max Difference (SSP5-8.5 EC-EARTH3): - dHm0_MC_AAM_EC3 - Hm0_Total Late-Century 50th Percentile Difference (SSP5-8.5 EC-EARTH3): - dHm0_LC_50p_EC3 - Hm0_Total Late-Century 99th Percentile Difference (SSP5-8.5 EC-EARTH3): - dHm0_LC_99p_EC3 - Hm0_Total Late-Century Avg Annual Max Difference (SSP5-8.5 EC-EARTH3): - dHm0_LC_AAM_EC3	5830 high density output points along the NL coast and offshore. Statistical results are divided into 12 areas corresponding to the wave model subdomains. Results provided as .csv and GeoJSON files.
		Maps of projected changes in Storm Surge Residual Water Level (m) statistics relative to the historical baseline for mid- and late-century, considering the SSP5-8.5 climate change scenario and two Global Climate Models (EC-EARTH and ACCESS-CM2). Variables: - WL_Res Mid-Century 50th Percentile Difference (SSP5-8.5 ACCESS-CM2) - WL_Res Mid-Century 99th Percentile Difference (SSP5-8.5 ACCESS-CM2) - WL_Res Mid-Century Avg Annual Max Difference (SSP5-8.5 ACCESS-CM2) - WL_Res Late-Century 50th Percentile Difference (SSP5-8.5 ACCESS-CM2) - WL_Res Late-Century 99th Percentile Difference (SSP5-8.5 ACCESS-CM2) - WL_Res Late-Century Avg Annual Max Difference (SSP5-8.5 ACCESS-CM2) - WL_Res Mid-Century 50th Percentile Difference (SSP5-8.5 EC-EARTH3) - WL_Res Mid-Century 99th Percentile Difference (SSP5-8.5 EC-EARTH3) - WL_Res Mid-Century Avg Annual Max Difference (SSP5-8.5 EC-EARTH3) - WL_Res Late-Century 50th Percentile Difference (SSP5-8.5 EC-EARTH3) - WL_Res Late-Century 99th Percentile Difference (SSP5-8.5 EC-EARTH3) - WL_Res Late-Century Avg Annual Max Difference (SSP5-8.5 EC-EARTH3)	Raster maps along the NL coast and offshore. Statistical climate change maps are divided into 8 raster tiles. Results provided as .tif files.

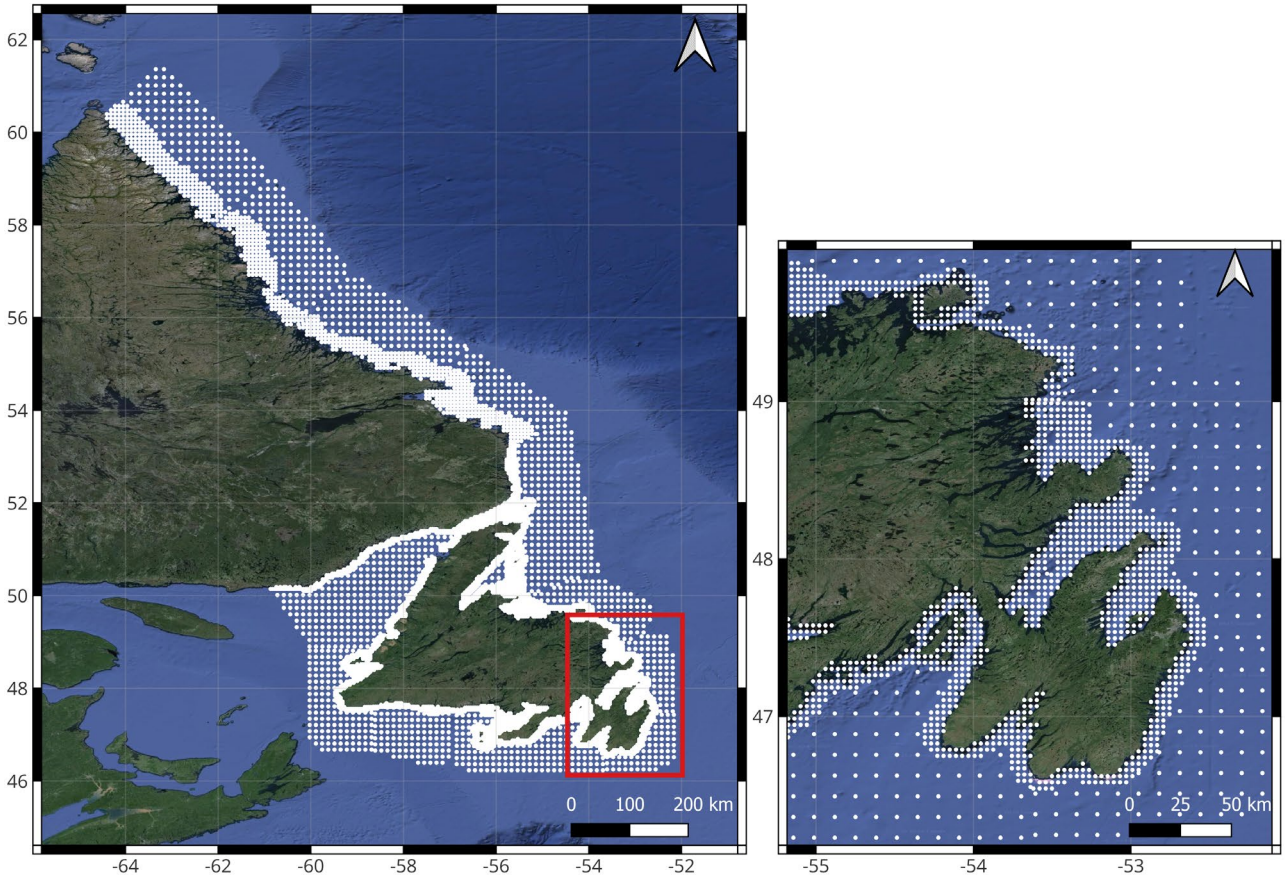


Figure 2.1 Output locations for the metocean parameters timeseries output locations along the coasts of Newfoundland and Labrador

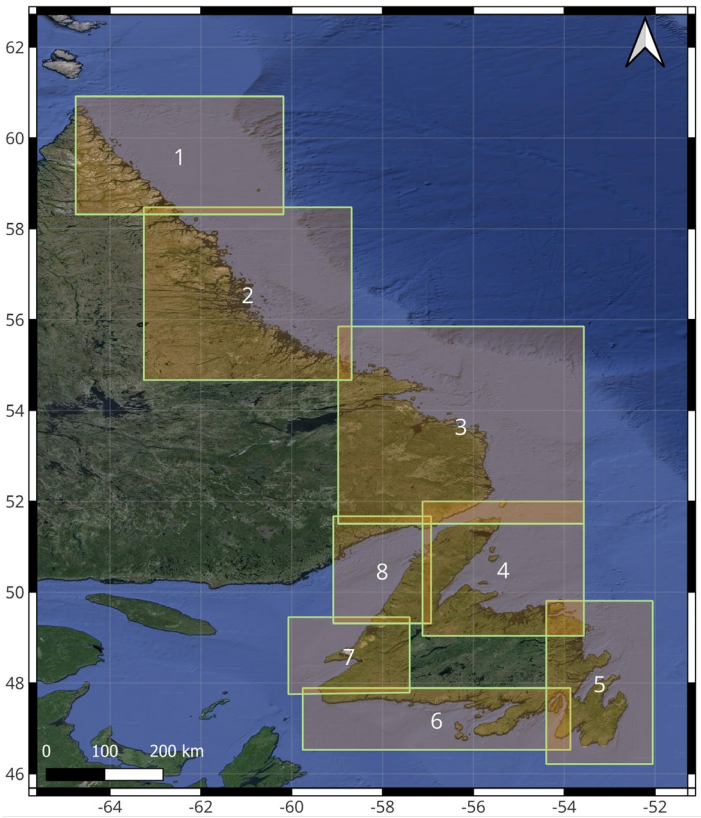


Figure 2.2 Overview of raster maps tiles for storm surge statistics covering the entire province

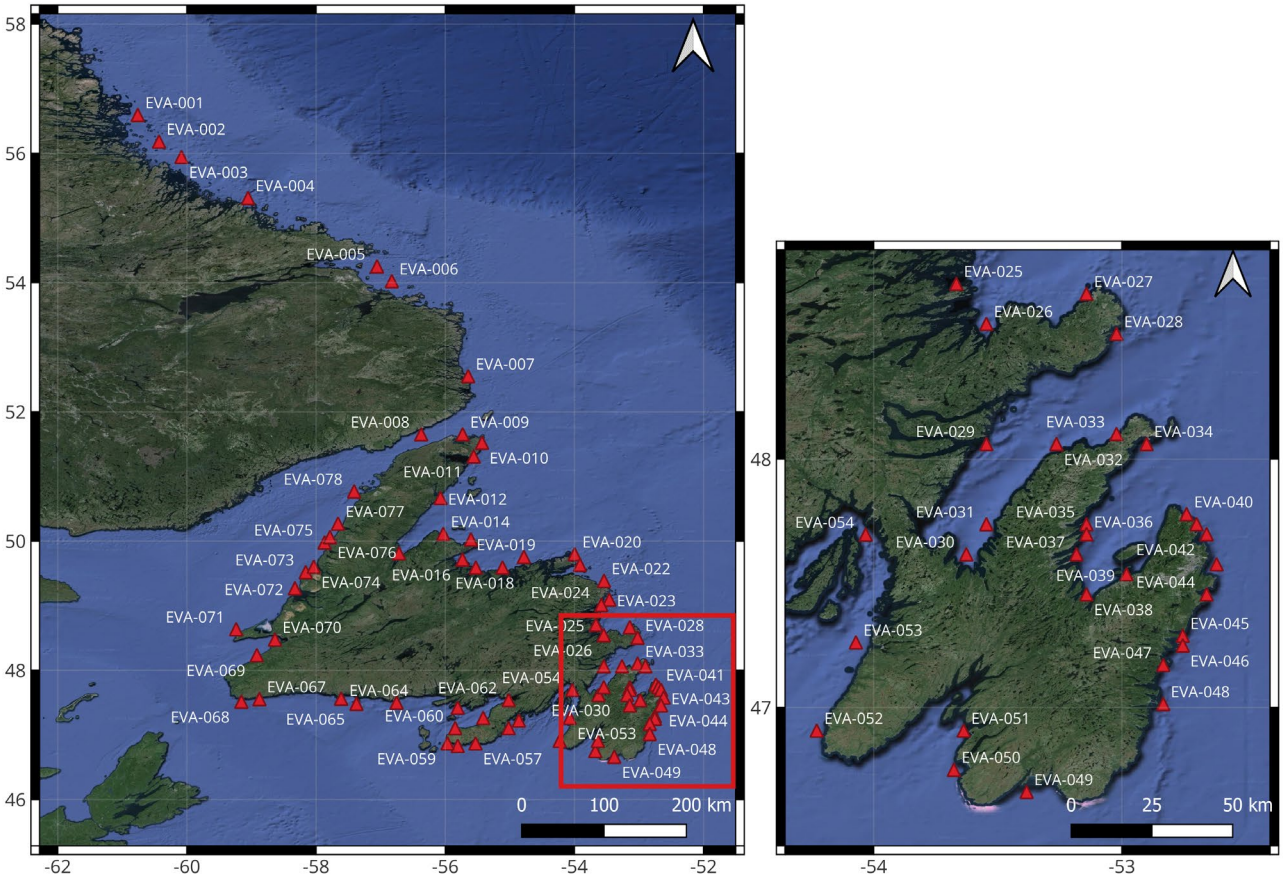


Figure 2.3 Output locations for the Extreme Value Analyses (EVA)

3 Underlying Datasets

This chapter describes the methodology and models used to derive the storm surge and wave climate datasets presented in the Atlas.

3.1 Model Forcing

A combination of publicly available and internal DHI data sources were used as forcing and boundary conditions to the storm surge and wave models.

3.1.1 Wind and Pressure Hindcast (ECMWF ERA5)

ERA5 is the fifth generation European Centre for Medium-Range Weather Forecasts (ECMWF) atmospheric reanalysis of the global climate covering the period from January 1940 to present [2]. ERA5 is produced by the Copernicus Climate Change Service (C3S) at ECMWF and provides hourly estimates of many atmospheric, land and oceanic climate variables. The data cover the Earth on a (approximately) 30 km grid and resolve the atmosphere using 137 levels from the surface up to a height of 80 km. Note that for the future projections, wind and pressure from the Global Climate Models (GCM) were used as input (see Section 3.4).

3.1.2 Astronomical Tide (DTU10)

DTU10 is a global tide model, developed by DTU Space [3], is provided on a grid with a resolution of 0.125 x 0.125 degrees, covering the major 10 tidal constituents. This model incorporates 17 years of data from multi-mission satellite altimetry, including TOPEX/Poseidon (phases A and B), Jason-1 (phases A and B), and Jason-2, for the analysis of sea level residuals. The constituents accounted for in the model include the semidiurnal constituents M2, S2, K2, N2, diurnal constituents S1, K1, O1, P1, Q1, and the shallow water constituent M4.

3.1.3 Sea Ice Coverage Hindcast (CIS + NSIDC)

The historical sea ice cover is derived from weekly ice charts provided by the Canadian Ice Services (CIS) [4], supplemented with satellite-derived ice concentration data from the National Snow and Ice Data Center (NSIDC). The CIS ice charts for the "East Coast" and "Hudson Bay" regions were merged to create a continuous ice concentration surface for the coastal areas. This process required synchronizing the dates of each published weekly chart, often published for different periods, and ensuring uniformity in ice cover throughout the interface regions. To complete the offshore regions not covered by the ice charts, satellite-derived ice concentration data from NSIDC was incorporated. The outcome was weekly maps depicting ice concentration, which served as input for the models (as illustrated in Figure 3.1). Ice Concentration is expressed in tenths describing the area of the water surface covered by ice as a fraction of the whole area.

Note that for the future projections, maps of ice concentration from the Global Climate Models (GCM) were used directly as input (see Section 3.4).

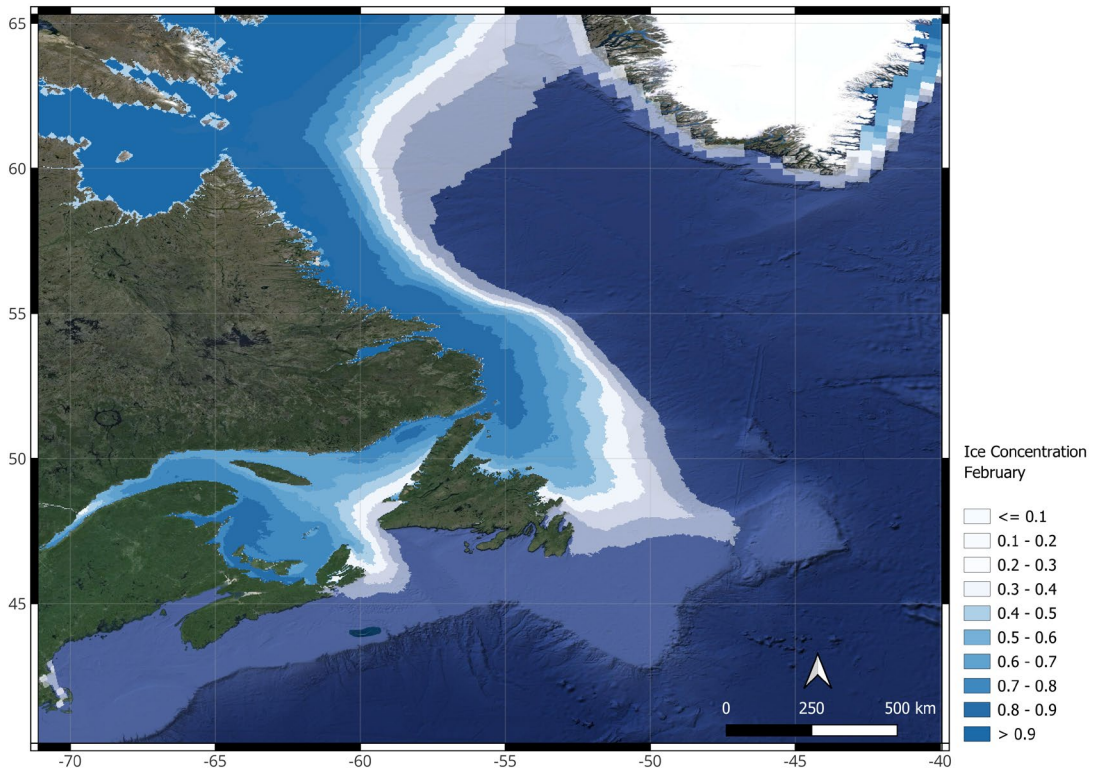


Figure 3.1 Example of a sea ice concentration map (CIS + NSIDC)

3.1.4 DHI Global Wave Model (GWM)

The DHI global wave model dataset (GWM) is based on DHI's 3rd generation MIKE[4] 21 Spectral Wave Model and on the high accuracy global ERA5 wind dataset from ECMWF. The ERA5 wind dataset is a good basis for global (and regional) wave modelling, and Wind Speeds > 12 m/s have been corrected for a better representation of wave modelling. The model has been validated against wave and satellite altimetry observations[5].

The GWM uses a computational mesh with a varying element size resulting in a resolution of ~50 km in offshore areas up to ~15 km near the coastline (see illustration in Figure 3.2). GWM model hindcast was run, including the following:

- Cap on wind friction.
- Stability corrected wind fields.
- Temporal and spatially varying ratio of air/sea density (based on ERA5).

The GWM was used to provide boundary conditions to the Wave Model presented in Section 3.3.

[4] https://www.mikepoweredbydhi.com/

[5] https://www.metocean-on-demand.com/metadata/waterdata-dataset-Global_SW_ERA5

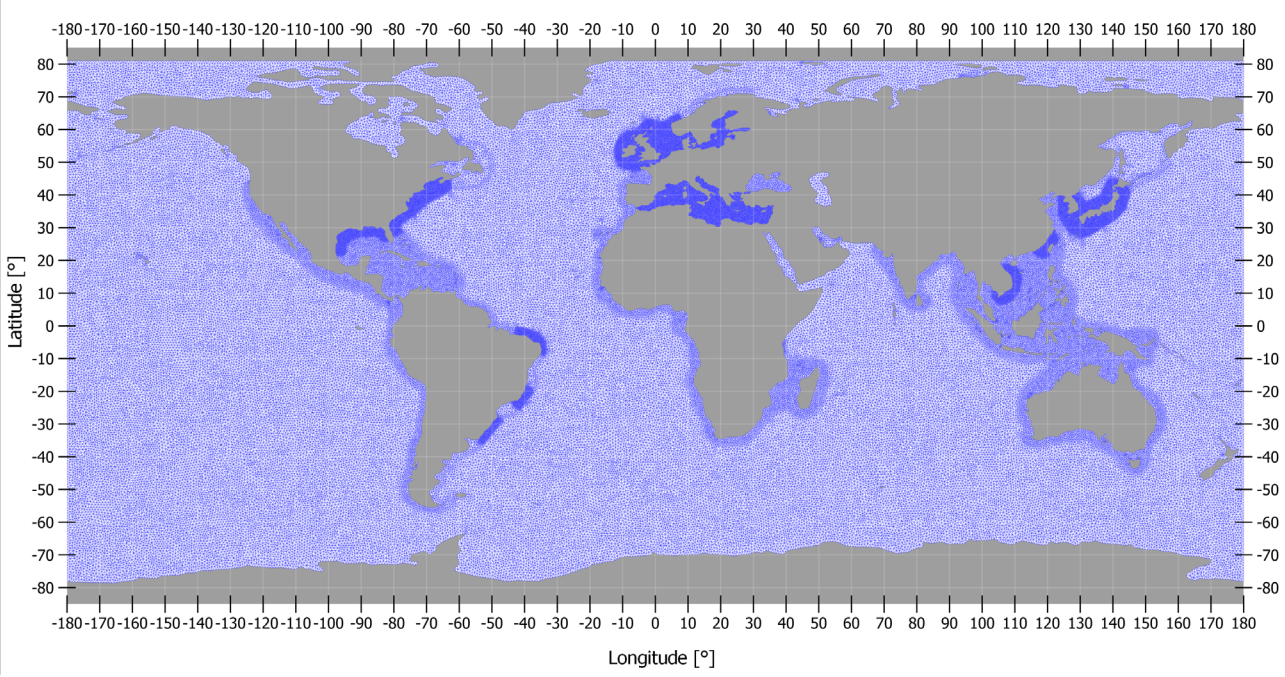


Figure 3.2 Illustration of the GWM model domain and computational mesh

3.2 Storm Surge Model - DHI $HD_{NL\text{-}ERA5}$

A regional storm surge model was developed using DHI MIKE 21 FM HD for the North-Atlantic and the Labrador Sea, with higher resolution around the Province of Newfoundland and Labrador (DHI $HD_{NL\text{-}ERA5}$). The model water level is static and set to Mean Sea Level (MSL), thereby only producing the storm surge residual of the total coastal water levels due to atmospheric pressure and wind-induced setup. Processes such as wave effects (including wave set-up), non-linear tide-surge interactions and other local processes that may contribute to the total water level are not accounted for as part of the regional modelling.

While non-linear tide-surge interactions may manifest in certain areas of the east coast of Canada (notably the Northumberland Strait), they are sporadic and highly localized [5]. In Newfoundland and Labrador, the Strait of Belle-Isle has the potential for (limited) tide-surge interaction; however, its contribution to the total surge levels is very limited [5].

Wave setup can be an important contributor to the total surge levels during more extreme events, such as hurricanes. However, given the complexity of wave setup and its dependence on local bathymetric features, the simulation of these processes in a regional context is not practical and recommendations for downscaling from the Atlas and inclusion of local processes are provided in Section 6.3.

3.2.1 Model Setup

The unstructured mesh model employs triangular elements with a horizontal resolution that varies from 5 km to 1.5 km near the shoreline around Newfoundland and from 8 km to 3 km around Labrador. The bathymetry was obtained from the Canadian Hydrographic Service Non-Navigational (NONNA) Bathymetric Data [6] and complemented with the General Bathymetric Chart of the Oceans (GEBCO) dataset [7] and digital navigation charts from MIKE C-MAP [8]. The DHI $HD_{NL\text{-}ERA5}$ model domain is presented in Figure 3.3. Model settings are described in Table 3.1 and Table 3.2.

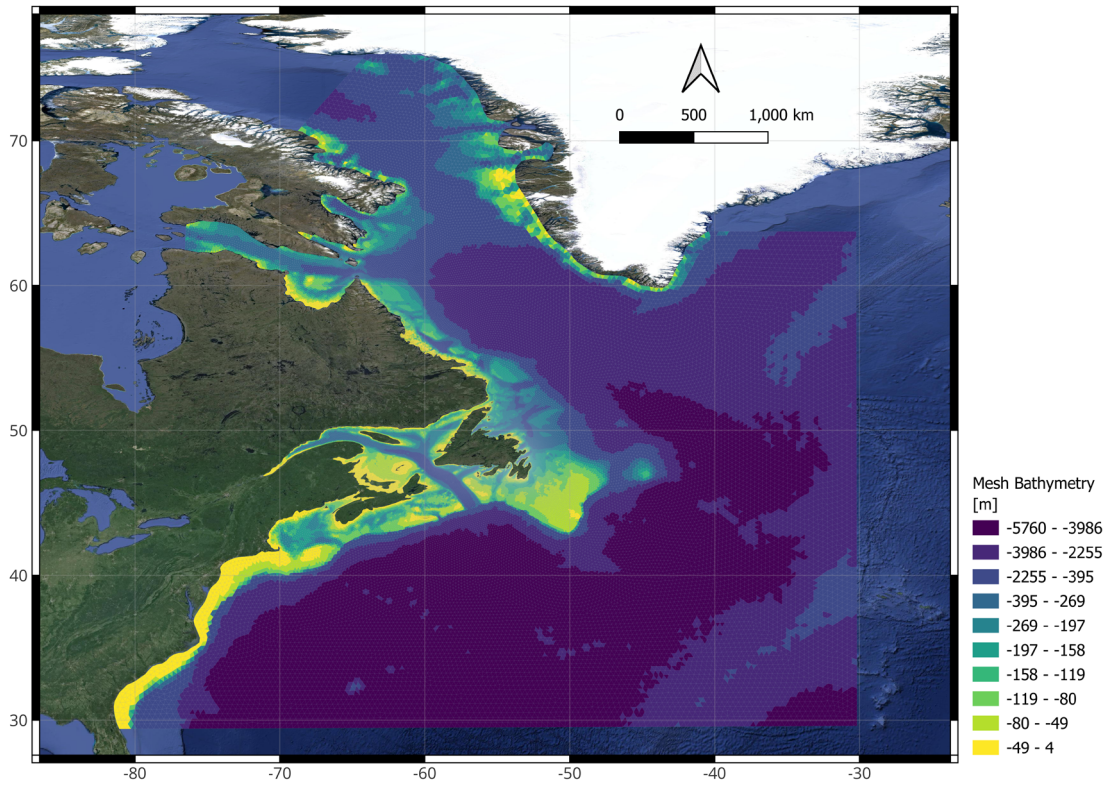


Figure 3.3 DHI $HD_{NL\text{-}ERA5}$ – regional storm surge model domain

For the assessment of historical conditions, the models were forced with wind and pressure fields from the European Centre for Medium-Range Weather Forecasts (ECMWF) ERA5 model hindcast (see Section 3.1.1). For the future climate assessment, the models were forced with two global climate models (GCM) from the Coupled Model Intercomparison Project (Phase 6) (CMIP6): EC-Earth3 and ACCESS-CM2 for the SSP5.8.5 scenario. A description of the climate projection models is provided in Section 3.4.

The historical sea ice cover is derived from weekly ice charts provided by the Canadian Ice Services (CIS) [4], supplemented with satellite-derived ice concentration data from the National Snow and Ice Data Center (NSIDC). For the future projections, maps of ice concentration from the GCMs were used directly as input. The impact of the sea ice cover is integrated in the surge model as spatially and temporally varying specified sea ice concentration. The sea ice concentration impacts the air-sea interaction: in areas where the ice concentration is larger than a specified critical concentration (0.9), the wind stress is excluded from the model calculation. A summary of the boundary conditions used in the hydrodynamic model is provided in Table 3.1.

Table 3.1 Storm surge model forcings and boundary conditions for the hindcast and climate change projections simulations

	Hindcast	Climate Change Projections (SSP5-8.5)
	ECMWF ERA5	ACCESS-CM2 EC-Earth3
	None	AR6 NASA SLR
	Composite (CIS Ice Charts + NSIDC)	ACCESS-CM2 EC-Earth3

Table 3.2 DHI $HD_{NL-ERA5}$ model settings

Setting	$HD_{NL-ERA5}$
Mesh Resolution	40 km offshore ~ 1.5 km nearshore - Regional
Simulation Period	1980-01-01 – 2022-12-31 (43 years)
Output Time Step	1 hr
Density	Barotropic
Eddy Viscosity	Smagorinsky formulation with a constant value of 0.28
Bed Resistance	Manning number of 36 $m^{1/3}/s$
Wind & Pressure Forcing	ERA5 atmospheric data
Bathymetry	NONNA dataset, digital navigation charts and GEBCO

3.2.2 Storm Surge Model Validation

Measured total water level data is available at several tide gauge stations along the Newfoundland coast and were used to assess the storm surge model (DHI $HD_{NL-ERA5}$). Figure 3.4 and Table 3.3 present the available water level stations – name, geographic location, and period with available data. The measured total water level signal at the stations was analysed to isolate the water level residual by extracting the astronomical tide using harmonic analysis. The extracted water level residual was then compared to the results from the regional DHI $HD_{NL-ERA5)}$ model. It is important to note that the obtained measured water level residuals can contain the influence of processes other than only storm surge (i.e., seasonal and interannual baroclinic effects, wave setup, river discharges).

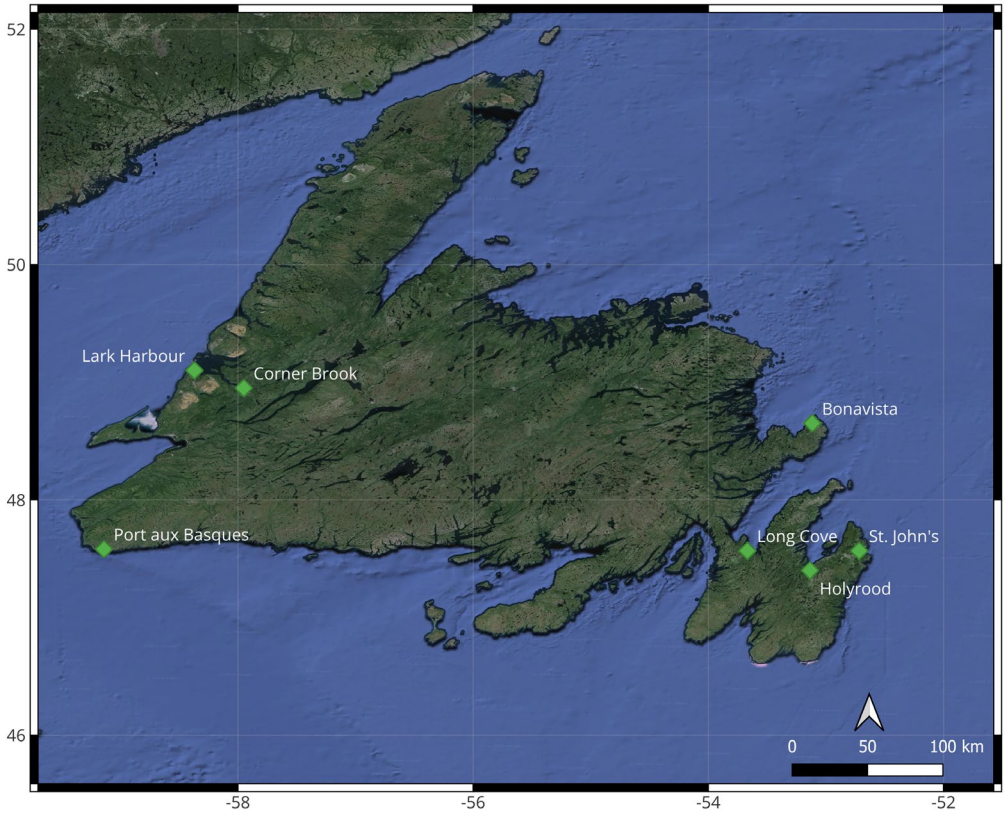


Figure 3.4 DHI $HD_{NL-ERA5}$ water level validation stations

Table 3.3 DHI $HD_{NL\text{-}ERA5}$ water level validation stations

Station	Longitude / Latitude	Time Range
Holyrood	-53.135°/47.400°	2017/07/10 – 2018/04/30
Long Cove	-53.667°/47.566°	2005/10/04 – 2005/11/17
Bonavista	-53.115°/48.651°	2005/10/26 – 2022/11/01
St. John's	-52.716°/47.566°	1989/01/01 – 2022/10/31
Port aux Basques	-59.139°/47.580°	1980/01/01 – 2022/12/31
Corner Brook	-57.95°/48.95°	1990-07-01 – 1990-09-09
Lark Harbour	-58.37°/49.10°	1980-01-01 – 1988-04-21

To obtain an objective and quantitative measure of how well the model data compared to the observed data, several statistical parameters, so-called quality indices (QI's), are calculated. A number of validation plots are presented from Figure 3.5 to Figure 3.11, encompassing timeseries comparisons with basic statistics for water level residual (WL_{Res}) and scatter plot comparisons for WL_{Res}. Table 3.4 summarizes the comparison metrics, such as bias, root mean square error (RMSE) and correlation coefficient for all stations[6]. Details on the definition of each metric is provided in Appendix A.

Table 3.4 DHI $HD_{NL\text{-}ERA5}$ summary of quality indices

Stations	$WL_{Residual}$		
	BIAS (m)	RMSE (m)	CC
Holyrood	0.03	0.10	0.72
Long Cove	0.05	0.11	0.71
Bonavista	0.05	0.09	0.82
St. John's	0.04	0.09	0.81
Port aux Basques	0.01	0.07	0.84
Corner Brook	0.03	0.08	0.64
Lark Harbour	0.04	0.09	0.81

Overall, the water level residual is well represented by the model, with small biases (from 0.02 m at Port aux Basques to 0.05 m at Long Cove) and satisfactory correlation coefficients (from 0.71 at Long Cove to 0.82 at Bonavista). It is highlighted that the Long Cove and Holyrood stations are located inside Trinity Bay and Conception Bay, respectively, for which the higher resolution HD hindcasts, which were developed for the community-level assessment during phase 1 of this project are more suited.

The scatter plots presented in Figure 3.5 to Figure 3.11 indicate that the model effectively captures positive surge levels but tends to underestimate negative surge levels. In coastal flood hazard mapping, the primary emphasis lies in predicting high water levels and positive storm surge events rather than low water levels. Although the model may not perform as strongly for negative surges, it is important to emphasize that this aspect is less crucial and that the model remains highly suitable for providing information for flood risk assessments.

[6] The BIAS is the mean difference between the modelled and observed data. A positive value indicates that the simulated water level is in average higher than the measurements. RMSE is the root-mean-square of the difference, and the Correlation Coefficient is a non-dimensional measure reflecting the degree to which the variation of the first variable is reflected linearly in the variation of the second variable. A value close to 0 indicates very limited or no (linear) correlation between the two data sets, while a value close to 1 indicates a very high or perfect correlation.

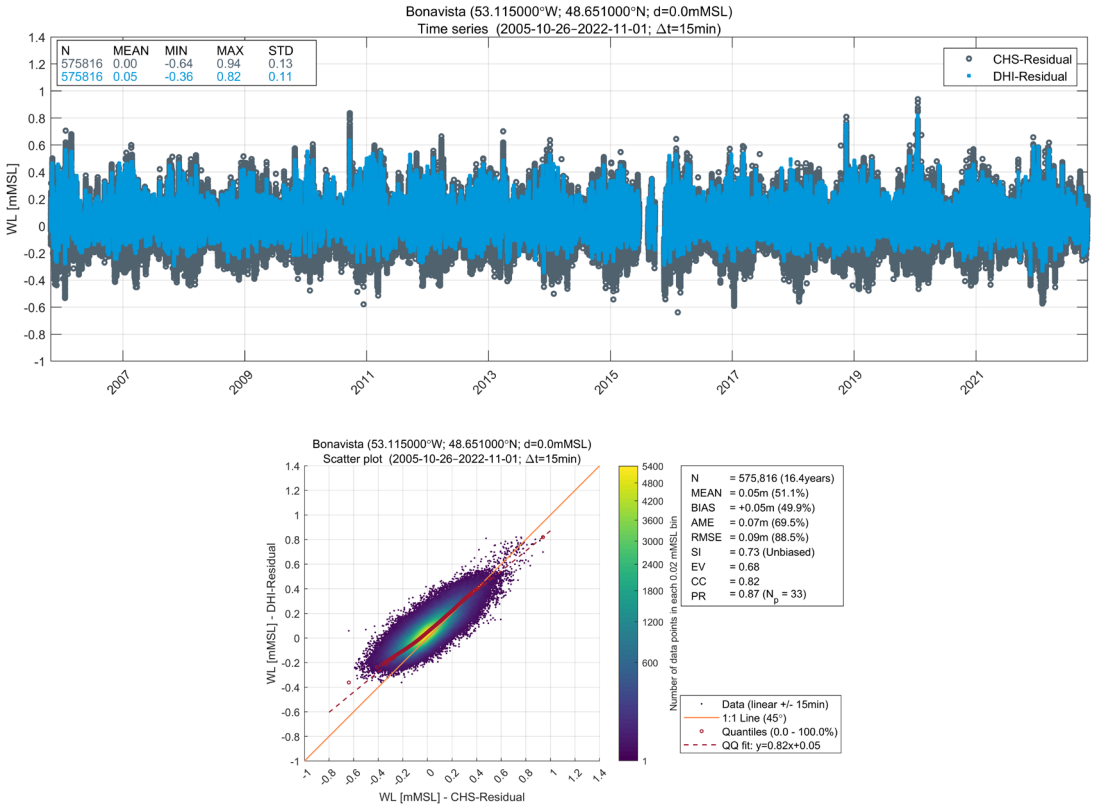


Figure 3.5 Comparison between measured (CHS-Residual) and modelled (DHI-Residual) water level residual at Bonavista

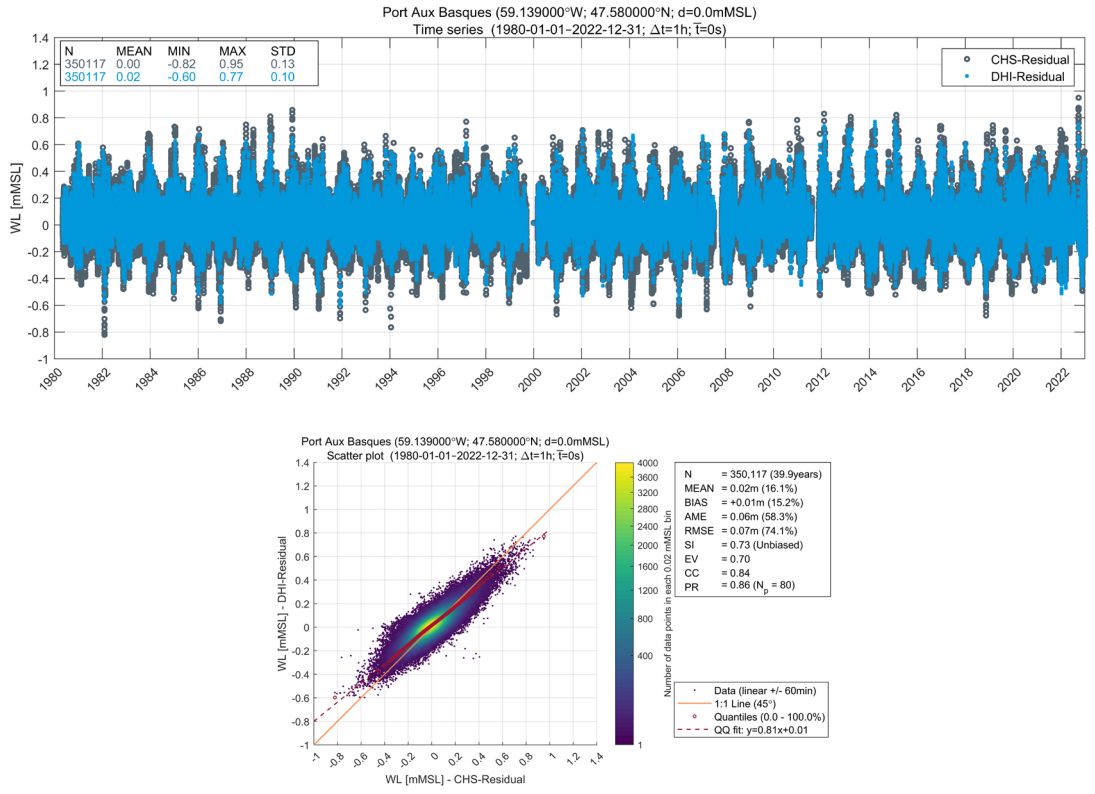


Figure 3.6 Comparison between measured (CHS-Residual) and modelled (DHI-Residual) water level residual at Port aux Basques

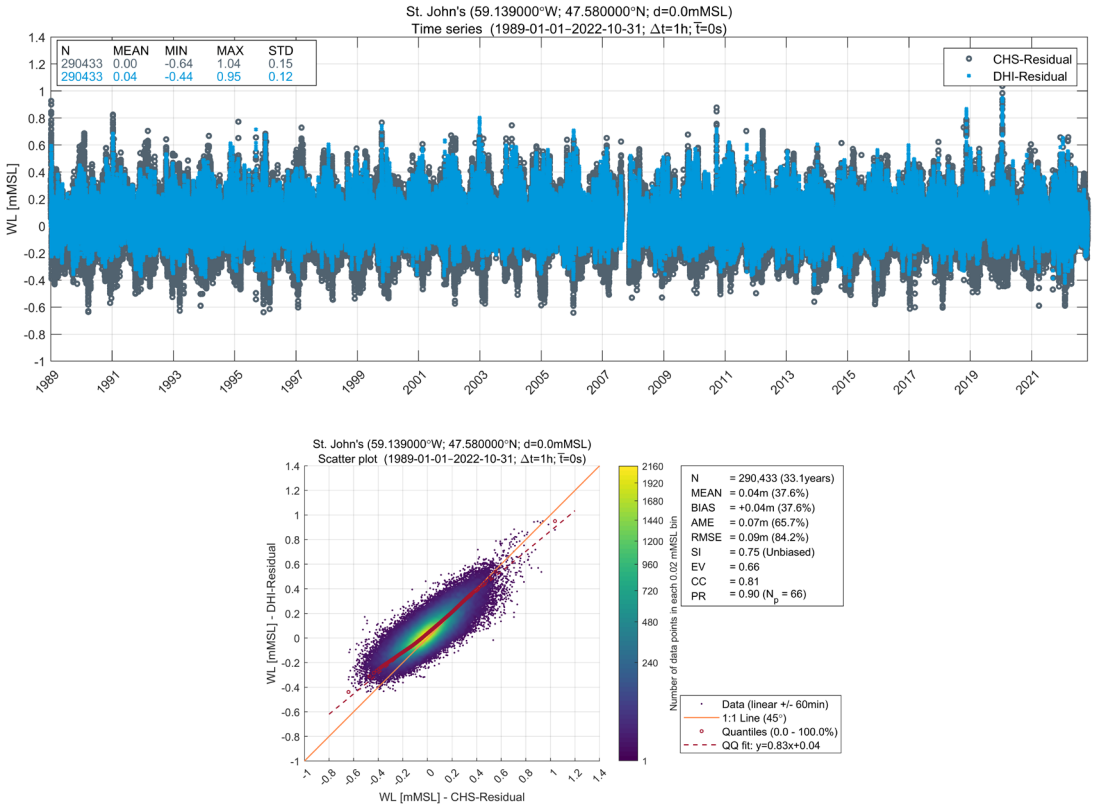


Figure 3.7 Comparison between measured (CHS-Residual) and modelled (DHI-Residual) water level residual at St. John's

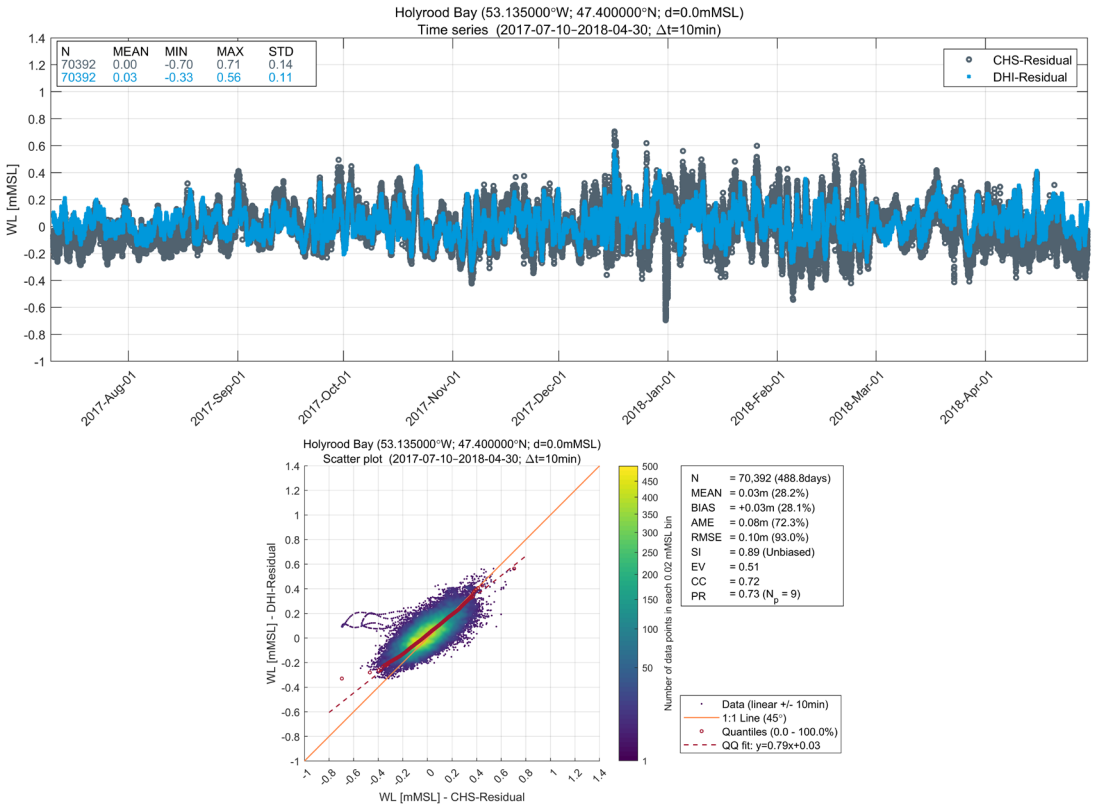


Figure 3.8 Comparison between measured (CHS-Residual) and modelled (DHI-Residual) water level residual at Holyrood Bay

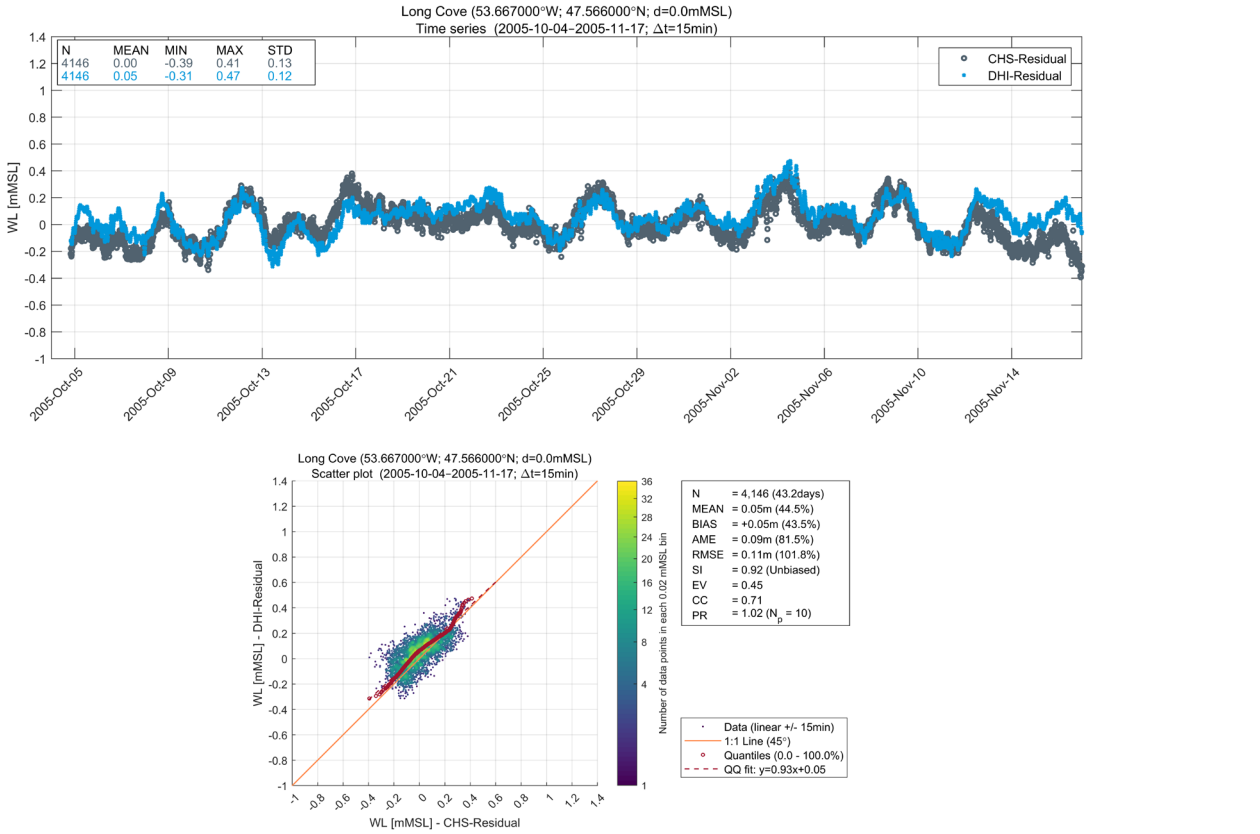


Figure 3.9 Comparison between measured (CHS-Residual) and modelled (DHI-Residual) water level residual at Long Cove

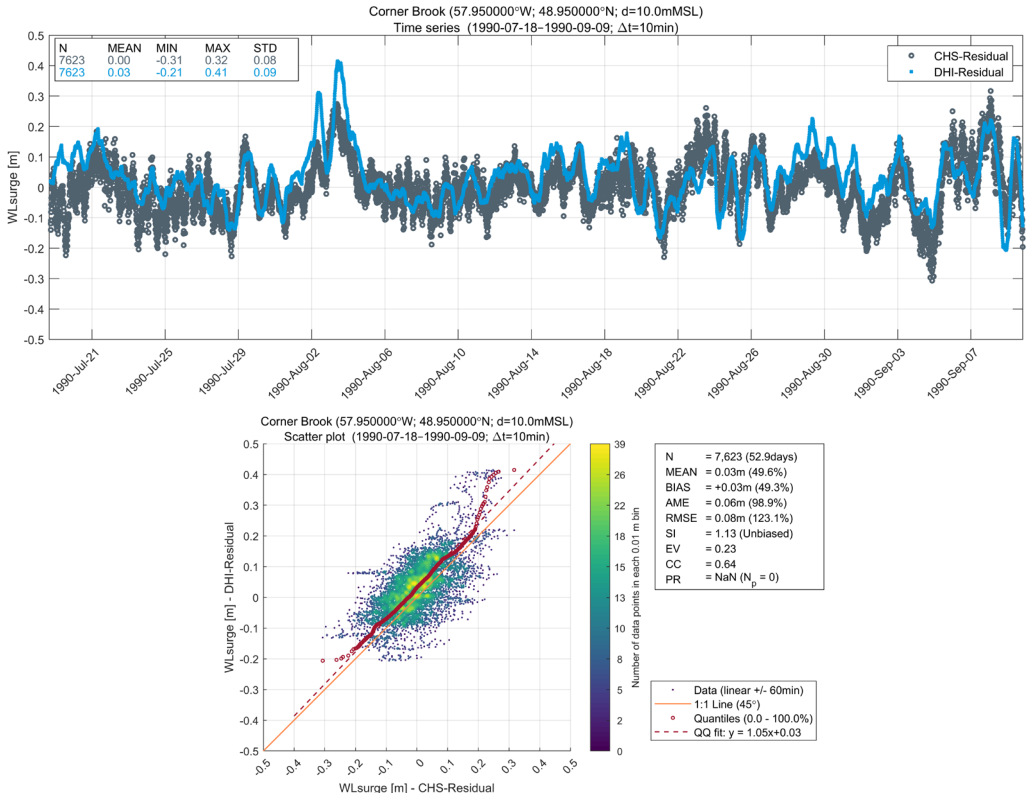


Figure 3.10 Comparison between measured (CHS-Residual) and modelled (DHI-Residual) water level residual at Corner Brook

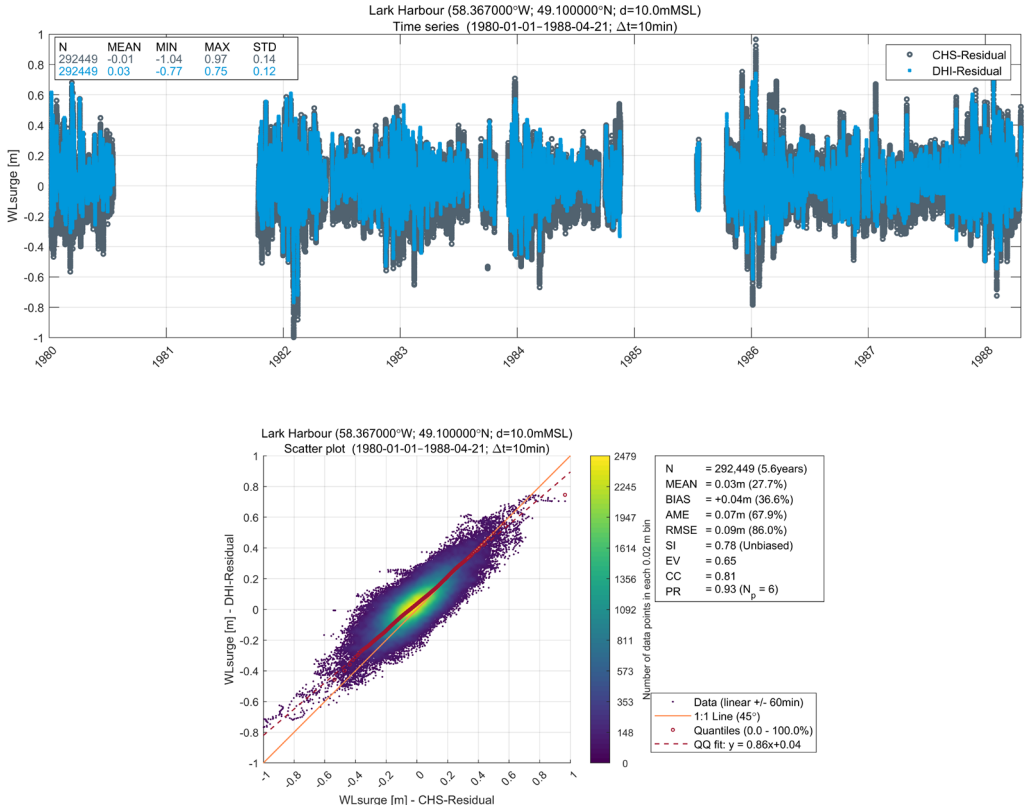


Figure 3.11 Comparison between measured (CHS-Residual) and modelled (DHI-Residual) water level residual at Lark Harbour

Additionally, Figure 3.12 presents a comparison focusing on the DHI $HD_{NL\text{-}ERA5}$ representation of the water level residual from two hurricanes that hit Newfoundland in recent years: Hurricanes Fiona (September 2022) and Igor (September 2010) at Port aux Basques and St. John's, respectively. Overall, the effect of those hurricanes on the water level residuals are well captured by the DHI $HD_{NL\text{-}ERA5}$ model. However, the peak of both events is slightly underestimated, which can be due to limitations of the ERA5 wind and atmospheric pressure fields – hurricanes are generally underestimated in the global reanalyses, such as ERA5 – and to other processes which may contribute to the total water level (such as wave effects) which are not included in the storm surge model. Preliminary sensitivity tests using a coupled hydrodynamic and wave model (not shown in this report) indicate that wave setup was a significant contributor to the surge levels during hurricane Fiona.

Considering the complexity of hurricane wind and pressure fields and the uncertainties involved in simulating such events, it is recommended to use the Atlas' results cautiously in regions significantly affected by hurricane-induced storm surge. In such cases, additional analyses are advised, with some recommended approaches outlined in Section 6.3.

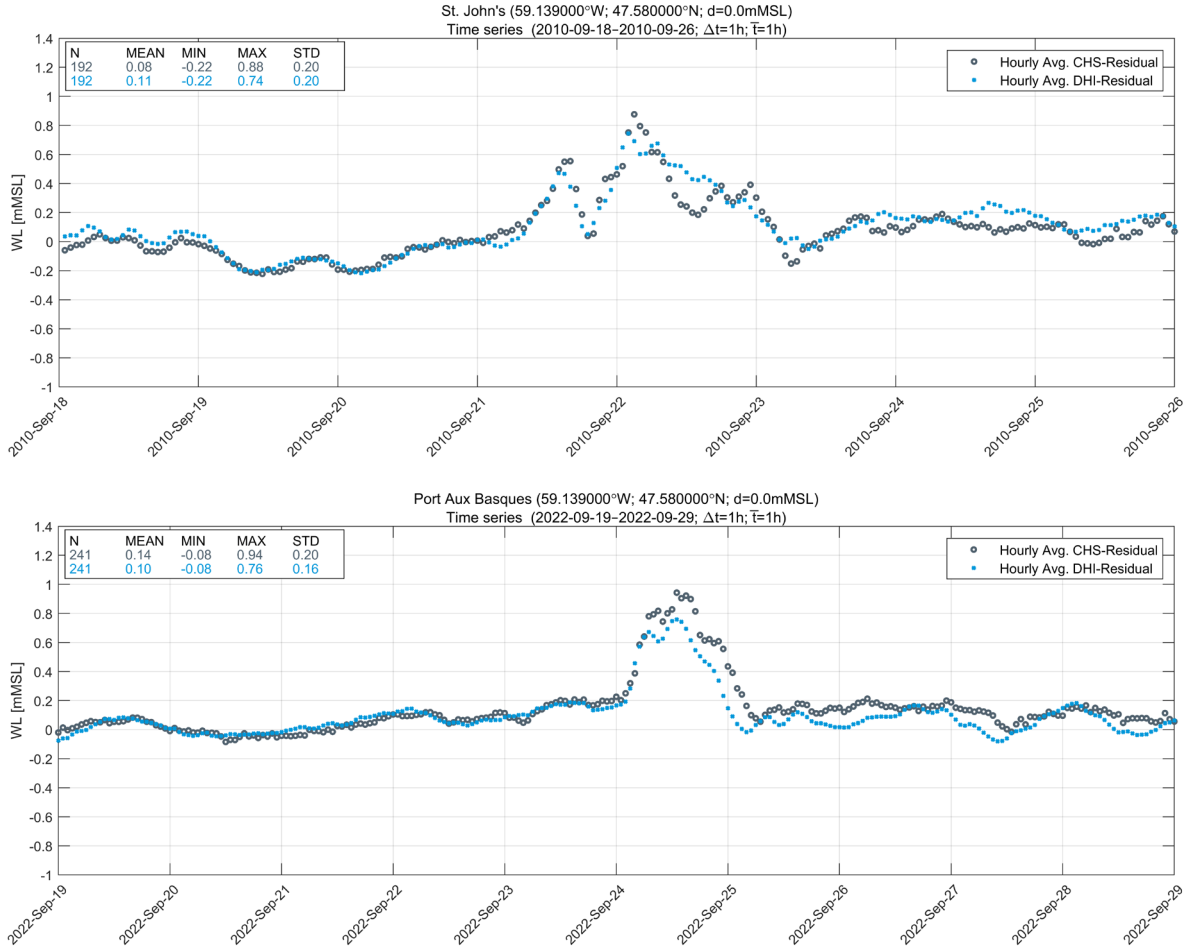


Figure 3.12 Surge water levels time series for hurricanes Igor (2010) and Fiona (2022)
Comparison between measured (CHS-Residual) and modelled (DHI-Residual) hourly-averaged water level residual at St. John's & Port aux Basques.

3.3 Wave Model

To simulate the wave climate hindcast and climate change future projections, the DHI MIKE Metocean Simulator (MIKE MS) was applied. MIKE MS follows the scientific basis defined by Camus et al. [9] [10] [11] and consists of a hybrid modelling approach that combines process-based models and statistical methods. This approach allows for increasing the number of ensemble members without excessive computational costs and is briefly described in the following section.

A general description of the MIKE Metocean Simulator is provided in Section 3.3.1, while the specific model setup used in the wave model for the NL Atlas is presented in Section 3.3.2. The wave model validation is discussed in Section 3.3.3, including comparisons with local wave measurements and other hindcast products.

3.3.1 MIKE Metocean Simulator

The MIKE MS is intended to downscale the offshore wave climate to coastal areas in a cost-effective way while maintaining a satisfactory accuracy. Figure 3.13 presents a schematic representation of the MIKE MS process illustrating each of the steps described below:

1. Provision of boundary and forcing data (control vector) for the whole period of simulation. The control vector can include wave partitions bulk parameters timeseries at multiple points along the model boundary; space and time varying wind x- and y- components; and space and time varying water level.

2. Selection of a subset of sea states (events) - to be dynamically downscaled in the subsequent step - from the entirety of extracted parameters across all boundaries and the domain involves a two-step process:
    a. Utilizing Principal Component Analysis (PCA), the dimensionality of the input data is reduced through linear combinations. The user has the flexibility to specify the number of principal components (PCAs) that effectively encapsulate the total variance present in the input data.
    b. Subsequently, the Maximum Dissimilarity Algorithm (MDA) comes into play, identifying and selecting the most dissimilar events within the PCA space. This strategic selection ensures that the downscaled model captures a diverse range of variability in metocean parameters, optimizing the representativeness of the chosen subset for dynamic downscaling.
    c. An example of a Significant Wave Height timeseries and the scatter of Peak Wave Period and Mean Wave Direction with a selection of events, shown relative to the input timeseries are shown in Figure 3.14.
3. Dynamical downscaling the selected sub-set of events using a state-of-the-art wave propagation model to calculate wave propagation to nearshore areas.
    a. At this step, the user can edit and calibrate the wave model configuration parameters, allowing for test runs to be completed as verification of the model setup before running the full set of events.
    b. All the selected events are simulated using the MIKE21 FM Spectral Wave model, and the associated outputs are stored at the desired output locations.
4. Reconstruction of the full time series of wave parameters at each output grid point using a radial basis function (RBF) interpolator.
5. Validation of the results by comparing to wave measurements.

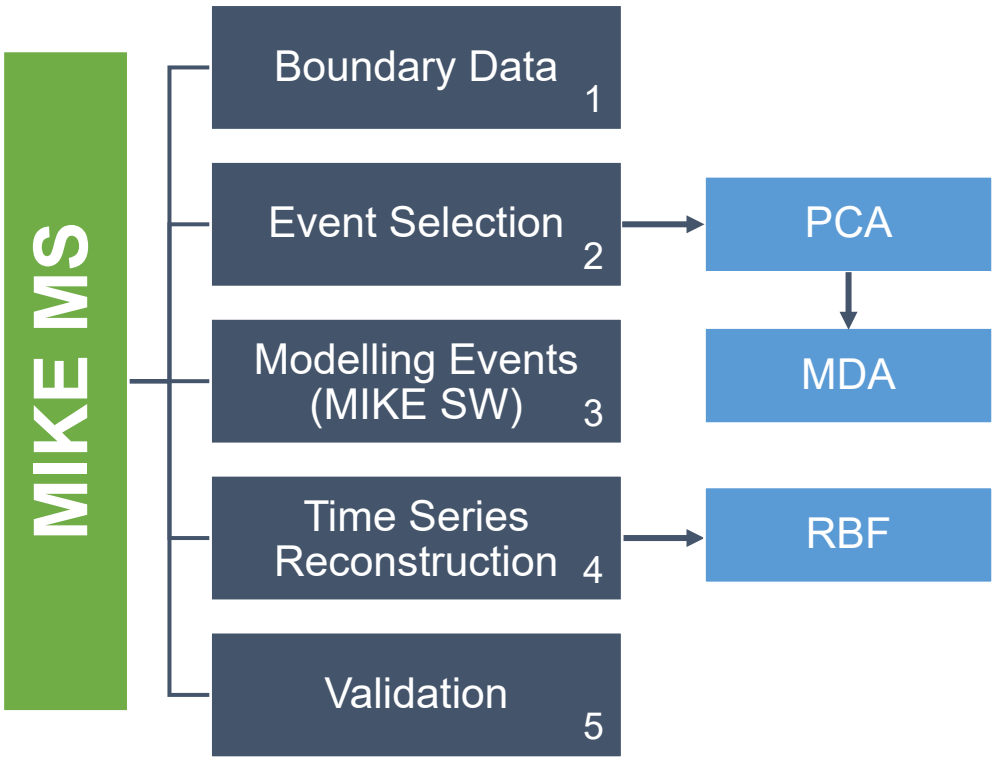


Figure 3.13 Schematic representation of the MIKE MS modelling process

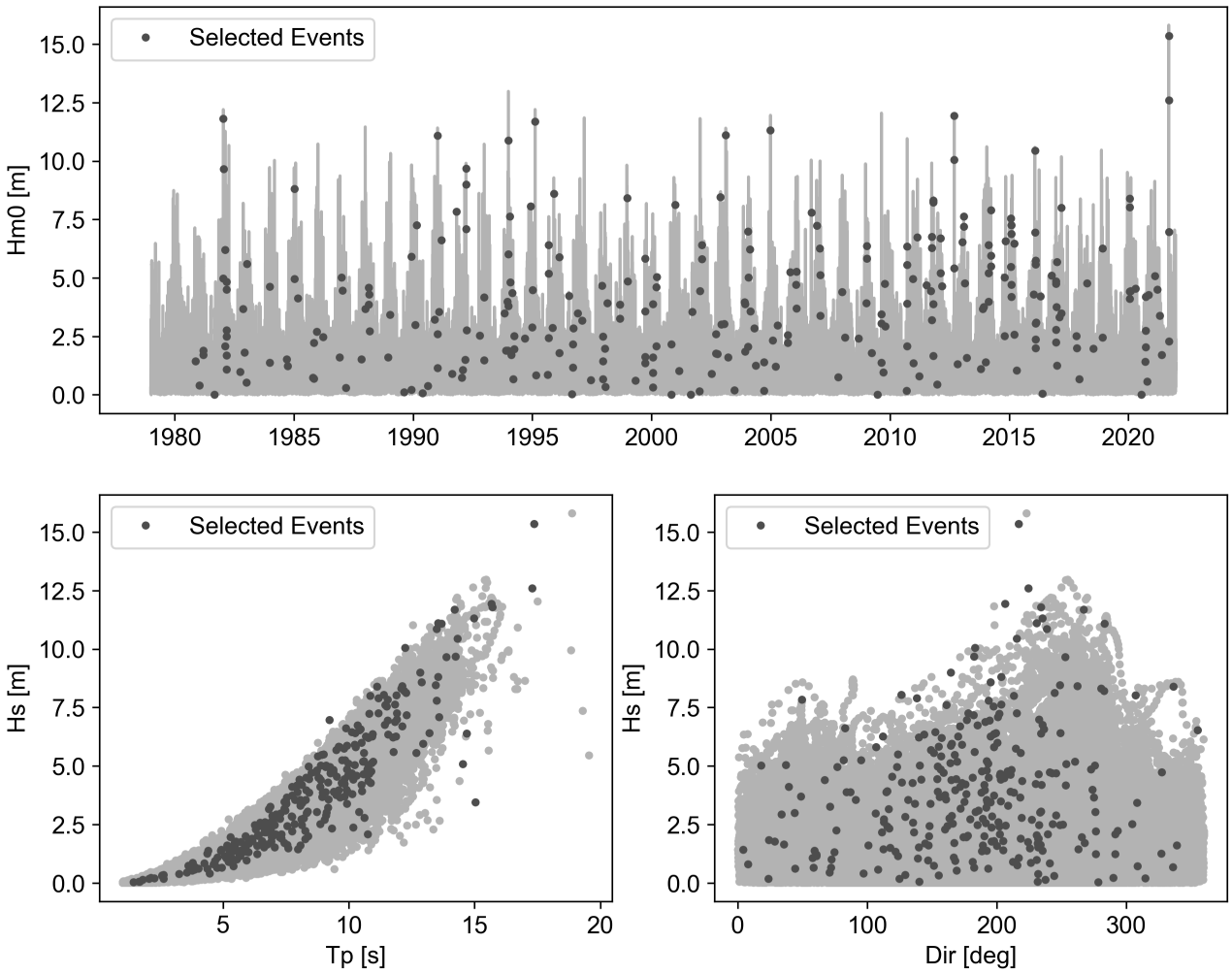


Figure 3.14 Example of the selected events after completion of the PCA and the MDA steps
(Step 2 in the MIKE MS flow chart in Figure 3.13)

3.3.2 Model Setup

A set of twelve sub-regional wave model domains were developed covering the entire province's coastline and extending up to 200 km offshore (Figure 3.15). The unstructured meshes using triangular elements have a horizontal resolution varying from 10 km to 1.5 km near the shoreline around Newfoundland and from 10 km to 2.5 km around Labrador (Figure 3.15). The domain extension and mesh resolution were carefully selected to strike a balance between capturing the relevant dynamics from the global wave and wind models and focusing on the specific nearshore areas of interest. The bathymetry was obtained from the Canadian Hydrographic Service Non-Navigational (NONNA) Bathymetric Data.

Table 3.5 summarizes the models forcings and boundary conditions. For the assessment of historical conditions, the models were forced with (i) wind and pressure fields from the global ECMWF-ERA5 model hindcast [2], (ii) tides from the DTU10 global tide model [3] [12] and (iii) water level residuals from the DHI $HD_{NL\text{-}ERA5}$ storm surge model described in Section 3.2, all varying in space and time. The model open boundaries are forced by the wave partitions bulk parameters: sea and swell significant wave height (H_{m0}), peak wave period (T_p) and mean wave direction (MWD) from the DHI Global Wave Model [13].

For the future climate assessment, the models were forced with two CMIP6 global climate models (GCM): EC-Earth3 and ACCESS-CM2 for the SSP5.8.5 scenario. Offshore wave conditions were derived from the GCM-forced wind-wave climate models by Meucci et al. (2013) [14]. A description of the climate projection models and why these models were selected for this investigation is provided in Section 3.4.

Similar to the input used in the surge model, historical sea ice cover is based on a combination of weekly ice charts from the Canadian Ice Services (CIS) for the coastal areas and satellite-derived ice concentration from the National Snow and Ice Data Center (NSIDC) for the offshore region, where ice charts are not available. For the climate change projections, ice concentration from the GCMs was used. The processing of developing the ice concentration input to the models is described in Section 3.2.1. The impact of the sea ice cover is integrated in the wave model as spatially and temporally varying specified sea ice concentration. For the wave model, the sea ice concentration was applied as a post-processing step: the wave energy is set to 0 in areas where the ice concentration is larger than a specified critical concentration (0.33).

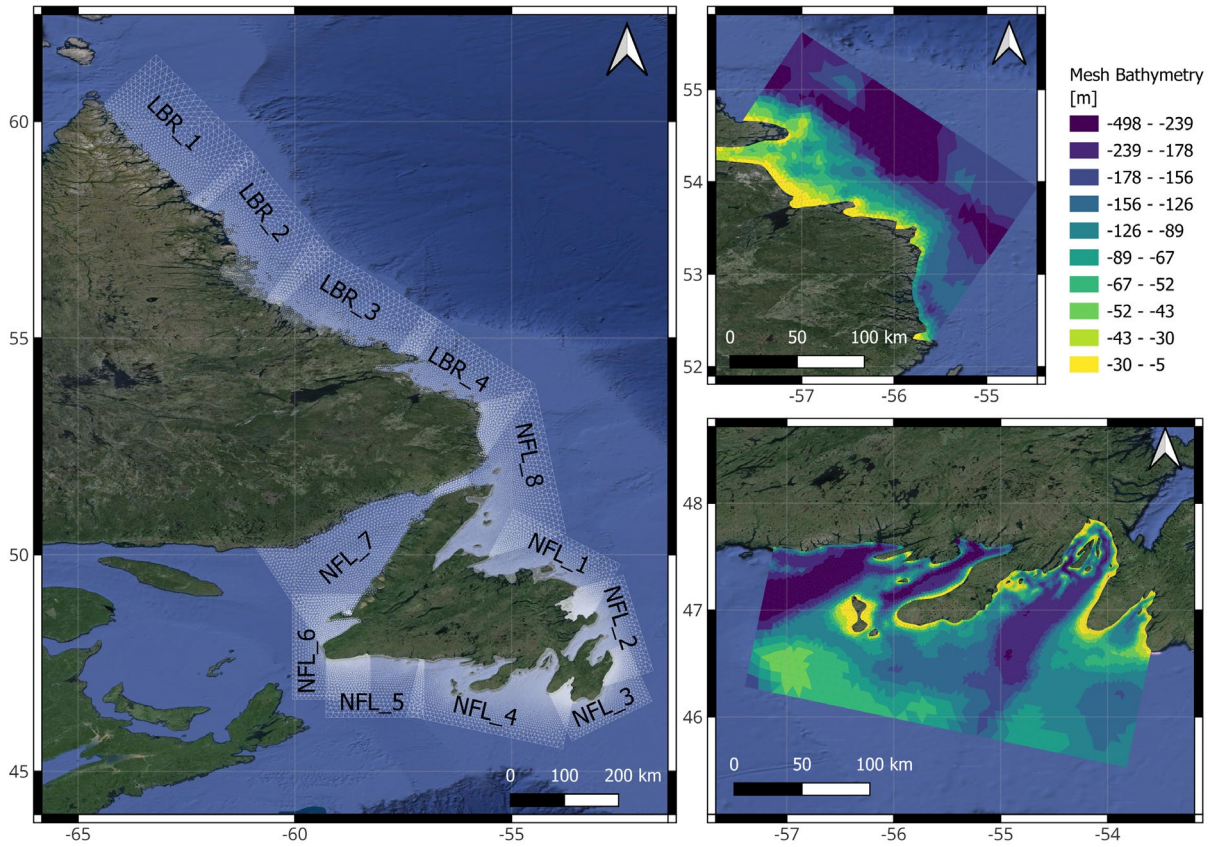


Figure 3.15 Subdomains of the wave model (left) Examples of the model bathymetry for subdomains NFL_4 and LBR_4 (right)

Table 3.5 Wave model forcings and boundary conditions for the hindcast and climate change projections simulations

	Hindcast	Climate Change Projections (SSP5-8.5)
	ECMWF ERA5	ACCESS-CM2 EC-Earth3
	DHI Global Wave Model	CSIRO WW3-ACCESS-CM2 CSIRO WW3-EC-Earth3
	Astronomical Tide (DTU10) NL Atlas Storm Surge Model (Hindcast)	AR6 NASA SLR NL Atlas Storm Surge Model (Projections)
	Composite (CIS Ice Charts + NSIDC)	ACCESS-CM2 EC-Earth3

Table 3.6 DHI MIKE MS wave model setup

Setting	Description
Mesh Resolution	~10 km offshore ~1.5 km nearshore – **Newfoundland subdomains** ~10 km offshore ~2.5 km nearshore – **Labrador subdomains**
Simulation Period	1980 – 2022 (42 years) – **HINDCAST** 1984 – 2014 (30 years) – **CLIMATE CHANGE BASELINE** 2015 – 2100 (85 years) – **CLIMATE CHANGE PROJECTIONS**
Outputs	Hourly H_{m0}, T_p, MWD – **HINDCAST** 3-Hourly H_{m0}, T_p, MWD – **CLIMATE CHANGE BASELINE AND PROJECTIONS**
Spin-up Time	12 hours prior to the selected event
Events Selection	Principal Component Analysis (PCA): 15 principal components, explaining > 95% of the natural variability. Maximum Dissimilarity Algorithm (MDA) to select discrete events
Number of MIKE SW Events	300 – **HINDCAST AND CLIMATE CHANGE BASELINE** 500 – **CLIMATE CHANGE PROJECTIONS**
MIKE SW Basic Equations	Fully spectral instationary
MIKE SW Time Step (Adaptative)	0.01-300 s with a maximum time-step factor of 32
Spectral Discretisation	25 frequencies with logarithmic increment factor of 1.13 and f_{min} of 0.039 Hz (i.e., periods of 1–25 s), 24 directions of 15°
Energy Transfer	Quadruplet-wave interaction included
Air/Water Density Ratio	Specified density, constant in space and time: 1.23725 kg/m^3
Wave Breaking	Included, Specified Gamma, γ=0.8, α= 1
Bottom Friction	Nikuradse, roughness, kn: 0.005 m
White Capping	Formulation [15], Cdis = 1.33, DELTA dis =0.25

3.3.3 Wave Model Validation

Measurements from various wave buoys throughout Newfoundland were compiled to assess the MIKE MS wave models. Available wave parameters include significant wave height (H_{m0}), peak wave period (T_p) and mean wave direction (MWD) representative of the full wave spectra. These parameters were obtained from SmartAtlantic [16] and Ocean Networks Canada [17] for wave buoys at St. John's, Bonavista, Placentia Bay Mouth, Placentia Bay Head, Fortune Bay, and Port aux Basques. The location of these stations is presented in Figure 3.16. A summary of key characteristics of these datasets is provided in Table 3.7.

Due to the limited number of in-situ wave measurements, the model validation was expanded by comparing the model results against other hindcast products: (i) the MSC50 Wind and Wave Climate Hindcast [18] [19], which is a well-established hindcast product for Atlantic Canada and (ii) the ECMWF-ERA5 wave model, which has the same forcing as the MIKE MS model.

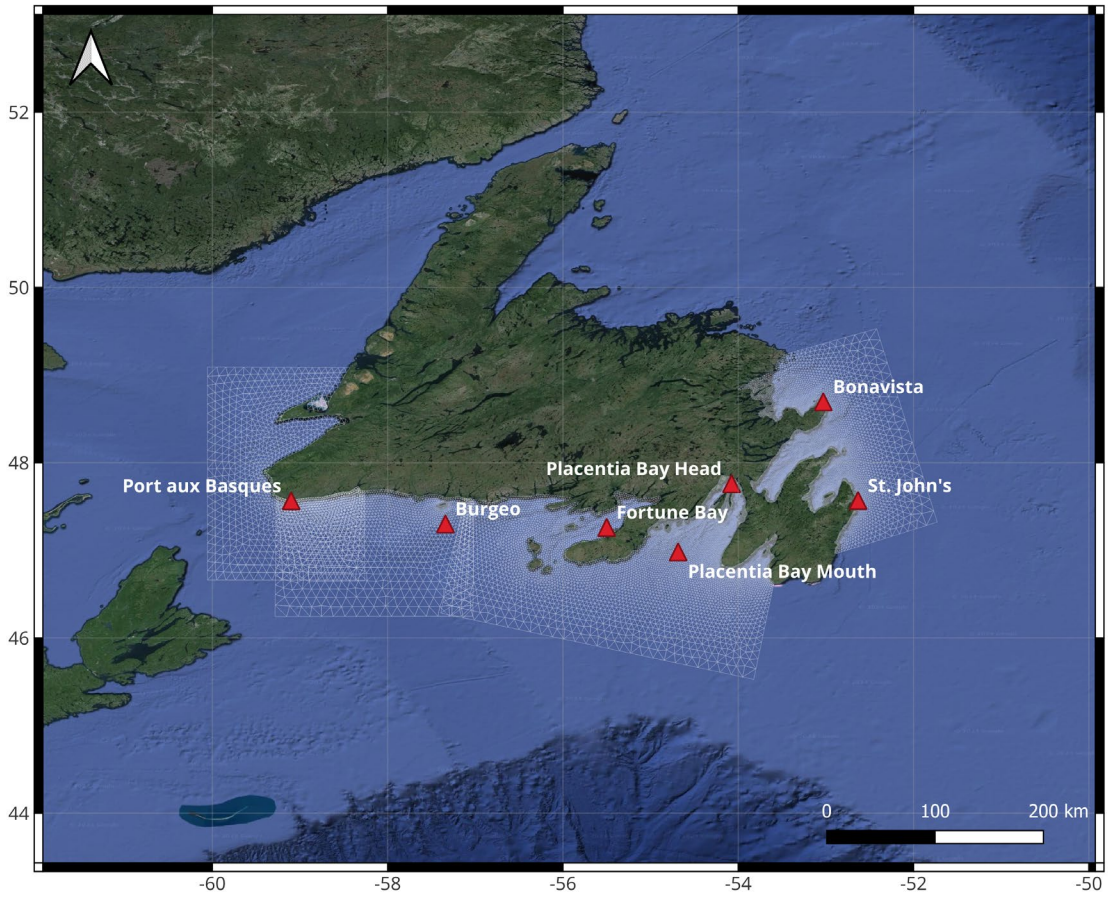


Figure 3.16 Location of wave buoys for the validation of the wave model

Comparison of the model results with measurements are presented from Figure 3.17 to Figure 3.22. Table 3.8 summarizes the comparison metrics, such as bias, root mean square error (RMSE) and correlation index for all stations. Details on the definition of each metric is provided in Appendix A.

The models exhibit strong performance in representing significant wave height (H_{m0}) with minor biases and high correlation coefficients across locations. They also accurately capture the distribution of mean wave direction. While the point-by-point comparison for simulated versus measured peak wave period is less satisfactory, the overall wave climate is well represented. The variable nature of peak wave period, particularly in regions with frequent bi-modal sea states, contributes to fluctuations. Despite this, general statistics of T_p indicate a well-represented local wave climate.

Particular attention was given to evaluate model performance during cyclonic events, especially given the devastating impacts of hurricane Fiona in Port aux Basques in 2022. It should be noted that wind speeds during cyclonic events, such as post-tropical storms and hurricanes, are generally underestimated in the global reanalyses, such as ERA5, especially in the North Atlantic [20]. Currently, no bias correction has been applied to the atmospheric forcing, potentially leading to an underestimation of wave conditions during these events.

Evaluations of the model's performance (specifically at Port aux Basques) against measurements and anecdotal information from hurricanes Dorian in 2019 and Fiona in 2022 suggest that the model can reasonably simulate these storms. Additional comparison of model results to the MSC50 reanalysis dataset [19] for earlier historical events, such as hurricane Bertha in 1990, shows significant lower wave conditions during this specific event compared to the MSC50 results. The difference could be explained by the ERA5 model's insufficient representation of the event, stemming from its resolution not being capable of adequately depicting the complexity of this region, especially during cyclonic events. It should be noted that the the MIKE MS model shows significantly higher wave heights for another notable extreme

(non-cyclonic) storm event in January 2000 compared to the MSC50 dataset. These comparisons are further elaborated in the following sections of this report.

Due to the absence of measurements for these specific storm events, evaluating the accuracy of the models becomes challenging. However, it is important to note that despite the considerably improved resolution in the Atlas wave model for this area (1.5 km near the coast), its accuracy is still contingent on the resolution of the wind fields utilized to drive the models. Therefore, caution is advised when using these results for assessing hurricane-generated waves in the southwest region of Newfoundland.

Table 3.7 Wave buoys stations used to compare the wave model results

Station	Domain	Parameters	Long/Lat	Time Range
Bonavista	NFL_2	H_{m0}, T_p, MWD	-53.029°/48.694°	2017/06/22 – 2017/12/24
St. Johns	NFL_2	H_{m0}, T_p, MWD	-52.632°/47.566°	2018/08/31 – 2020/12/31
Placentia Mouth	NFL_4	H_{m0}, T_p, MWD	-54.685°/46.980°	2018/02/27 – 2020/12/31
Placentia Head	NFL_4	H_{m0}, MWD	-54.075°/47.758°	2018/02/27 – 2018/04/07
Fortune Bay	NFL_4	H_{m0}, T_p, MWD	-55.500°/47.260°	2019/07/17 – 2019/12/19
Port aux Basques	NFL_6	H_{m0}, T_p, MWD	-59.100°/47.563°	2014/11/28 – 2020/11/12[7]
Burgeo (MEDS C44235)	NFL_5	H_{m0}, T_p	-57.4°/47.3°	2010-06-11 – 2011-05-13

Table 3.8 Comparison Metrics Summary

Stations	H_{m0}			T_p		
	BIAS (m)	RMSE (m)	CC	BIAS (s)	RMSE (s)	CC
Port aux Basques	0.29	0.74	0.78	0.27	2.16	0.53
Burgeo (MEDS C44235)	-0.07	0.39	0.94	0.5	1.83	0.64
Placentia Bay Mouth	0.11	0.46	0.92	0.01	1.90	0.63
Placentia Bay Head	0	0.17	0.87	N/A	N/A	N/A
Fortune Bay	-0.07	0.3	0.91	1.26	2.65	0.36
St. John's	0.21	0.54	0.87	0.02	1.87	0.67
Bonavista	0.34	0.54	0.86	-0.27	1.97	0.57

Comparison with Wave Buoys

Model performance was assessed at various locations around the province, where wave buoy measurements are available. No wave measurements were available along the Labrador coast.

It is important to highlight that the measurements contain various gaps and instances of questionable data integrity. Although best efforts were made to complete a basic pre-processing of the measurements to eliminate outliers and potentially unreliable data, it is noted that there are likely still some erroneous data points remaining. The absence of the original, unprocessed data complicates the determination of whether additional data points should have been eliminated or if some were suitable for comparison. These outliers and erroneous points can impact the calculation of the quality indices and validation metrics. Nonetheless, this issue does not compromise the quality of the models presented.

[7] Data quality concerns arise after 2019-02-16, particularly regarding peak wave period (T_p). For T_p, only information up to this date was utilized.

For some stations extensive measurement periods were removed from the comparison due to unreliable data quality. For example, at Port aux Basques, after 16 February 2019, there was a notable surge in outliers, and the peak wave period values appeared to be unrealistic. Despite quality control efforts (enabling the analysis with Hurricane Dorian in September 2019), the validation metrics are significantly affected during this period. Furthermore, T_p data from this station had to be entirely omitted.

Several validation figures are presented from Figure 3.17 to Figure 3.22, encompassing (i) timeseries comparison with basic statistics for significant wave height (H_{m0}) and peak wave period (T_p), (ii) scatter plot comparison for H_{m0} and T_p, and (iii) a dual rose plot for assessing the joint mean wave direction (MWD) and H_{m0} distributions. Details on the definition of the various quality indices shown in the figures are provided in Appendix A.

Overall, H_{m0} is well represented by the models, with small biases (from -0.07 m at Fortune Bay to 0.34 m at Bonavista) and good correlation coefficients (from 0.78 at Port aux Basques to 0.92 at Placentia Bay Mouth). The model also demonstrates strong skill in representing the mean wave direction distribution, with the correct representation of the main incoming wave directions. The evaluation of simulated versus measured peak wave period yields less than satisfactory results when considering a point-by-point comparison; however, the model still provides a good representation of the wave period distribution considering the overall wave climate. The lower agreement in a point-by-point comparison is partly attributed to the inherent nature of the variable—being linked to the frequency at a specific point in the wave energy spectrum, as opposed to a parameter that considers the spectrum's integral or an averaged quantity. Regions with frequent bi-modal sea states, where swell waves coincide with locally-generated sea waves, often exhibit significant fluctuations in peak wave period, as evident in the comparison plots. A more suitable parameter for an equitable comparison would be the mean wave period which is currently not available from the measurements. Notwithstanding, the comparison of general statistics of T_p, indicate that the characteristics of the local wave climate is well represented.

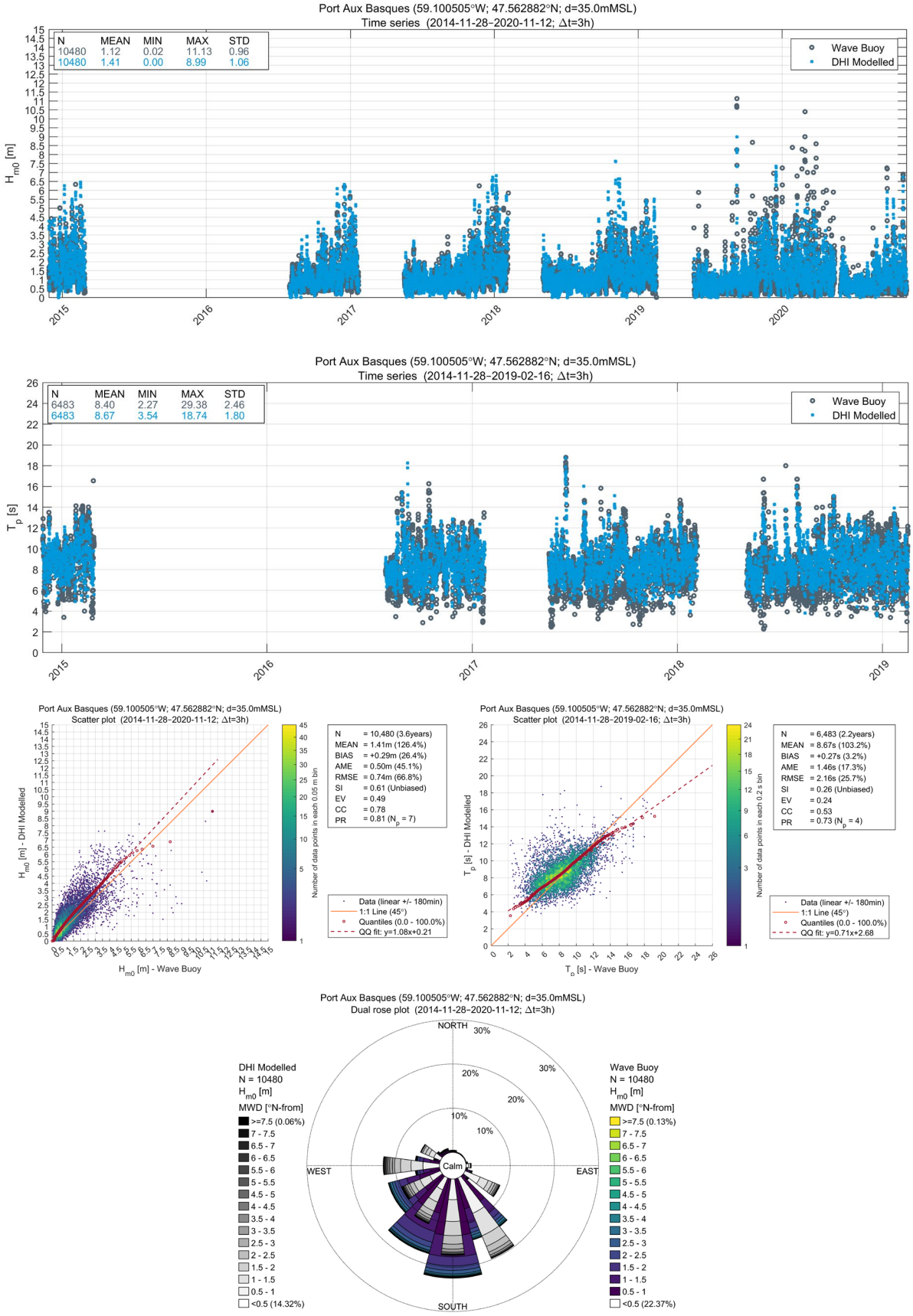


Figure 3.17 Wave Model Validation – Port aux Basques

Significant Wave Height (H_{m0}) and Peak Wave Period (T_p) timeseries and scatter plots comparison. Bottom: dual rose plot illustrating the joint Mean Wave Direction (MWD) and H_{m0} distribution.

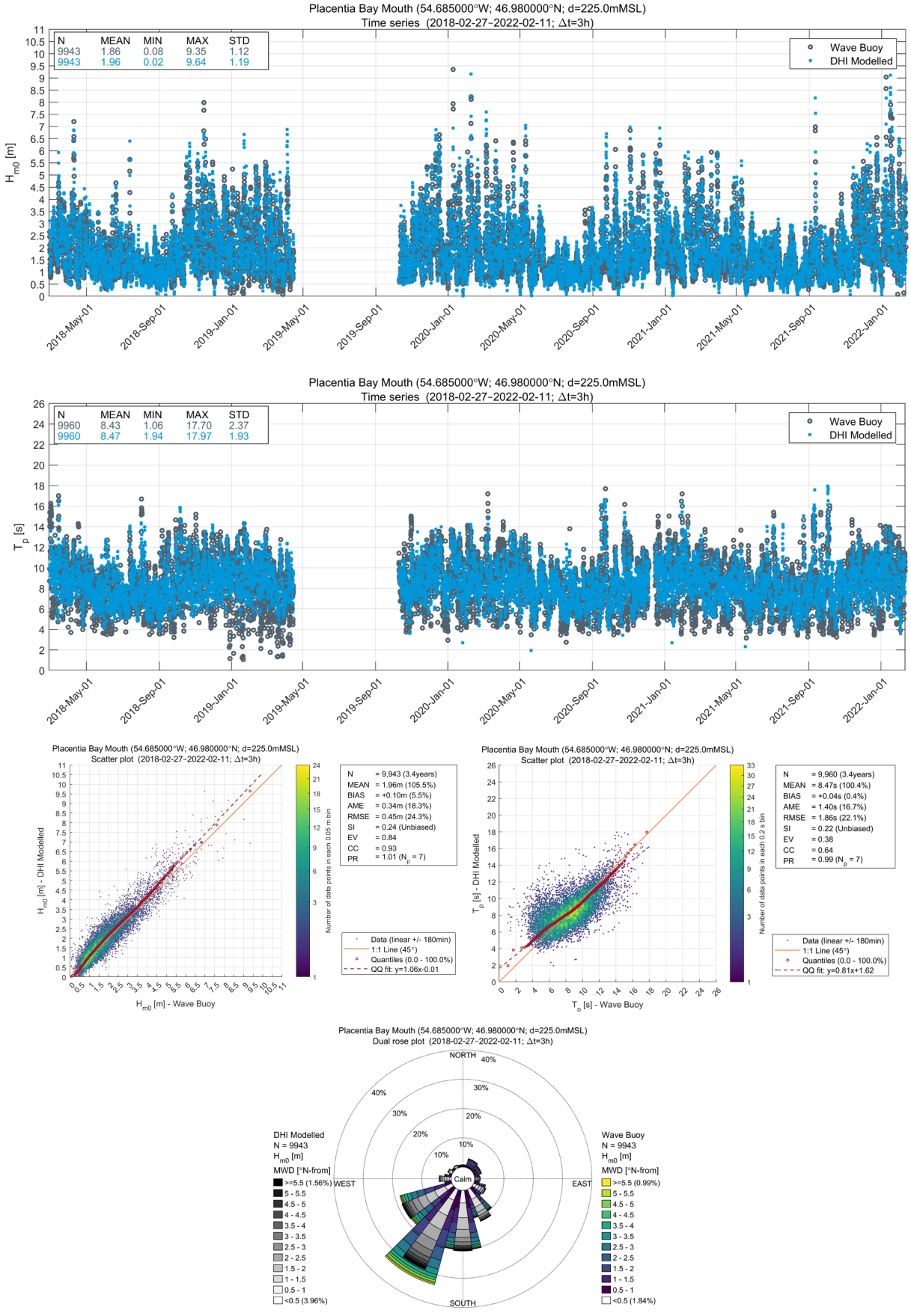


Figure 3.18 Wave Model Validation – Placentia Bay Mouth

Significant Wave Heigh (H_{m0}) and Peak Period (T_p) timeseries and scatter plots comparison. Bottom: dual rose plot illustrating the joint Mean Wave Direction (MWD) and H_{m0} distribution.

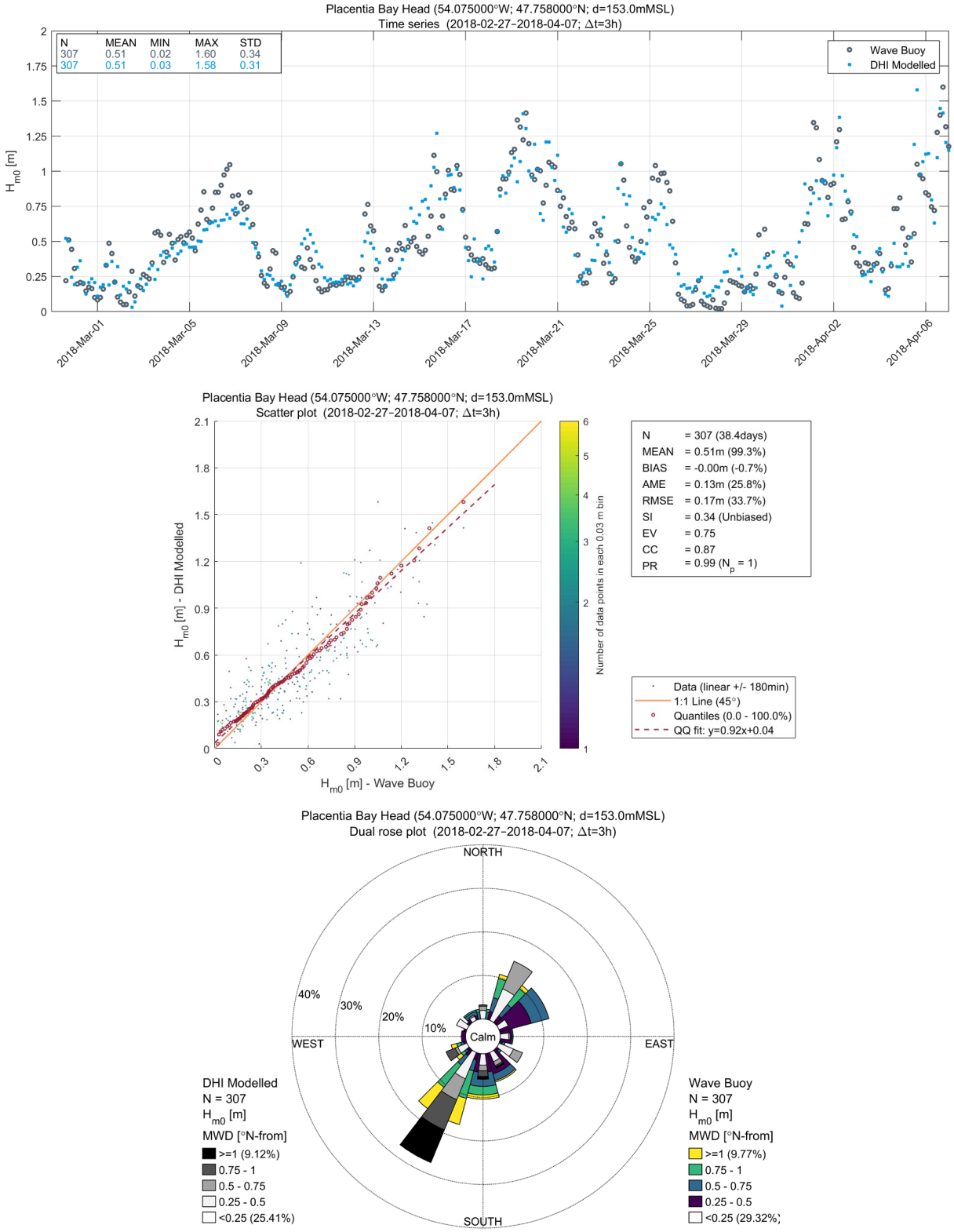


Figure 3.19 Wave Model Validation – Placentia Bay Head

Significant Wave Heigh (H_{m0}) timeseries and scatter plots comparison. Bottom: dual rose plot illustrating the joint Mean Wave Direction (MWD) and H_{m0} distribution.

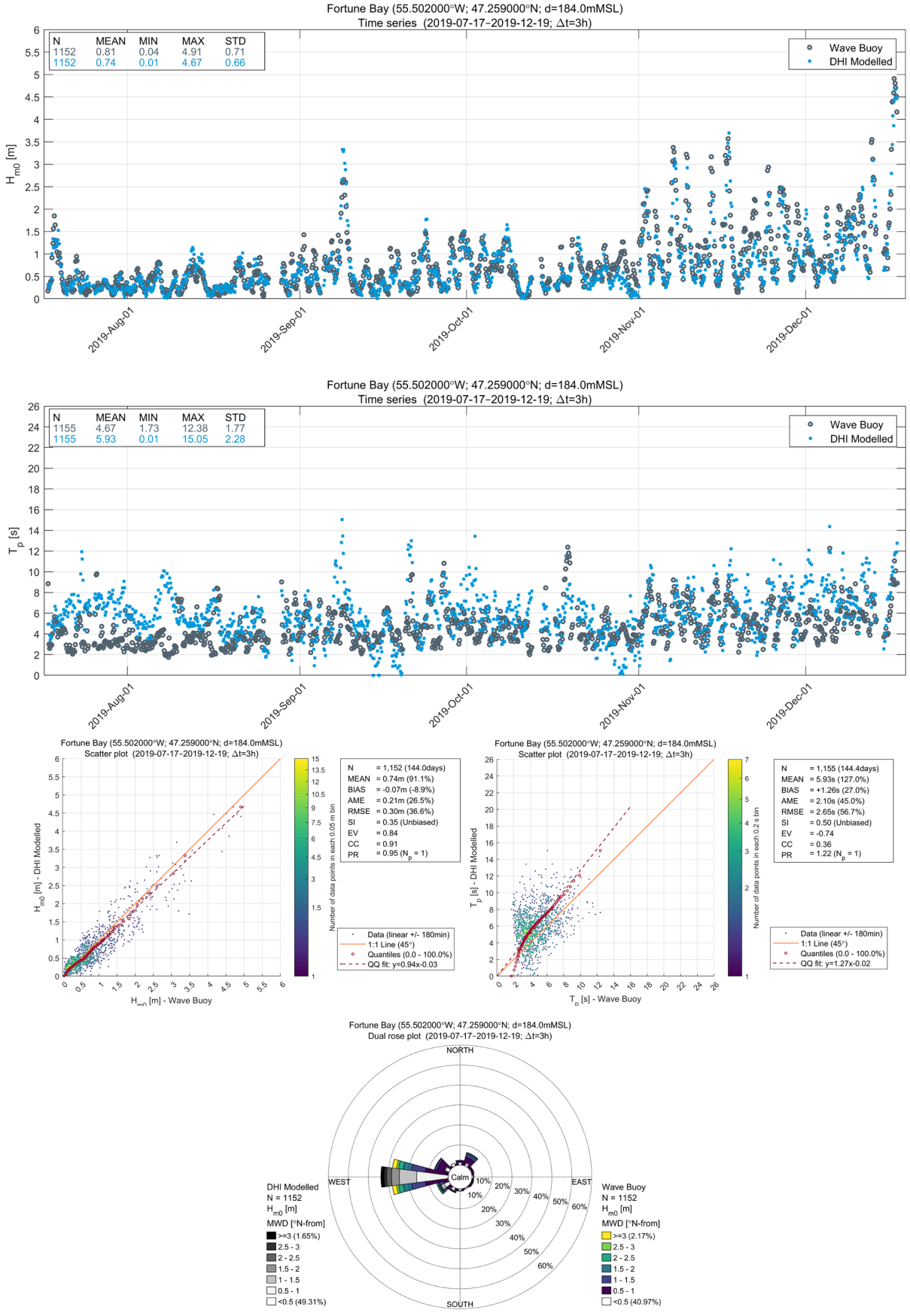


Figure 3.20 Wave Model Validation – Fortune Bay

Significant Wave Heigh (H_{m0}) and Peak Period (T_p) timeseries and scatter plots comparison. Bottom: dual rose plot illustrating the joint Mean Wave Direction (MWD) and H_{m0} distribution.

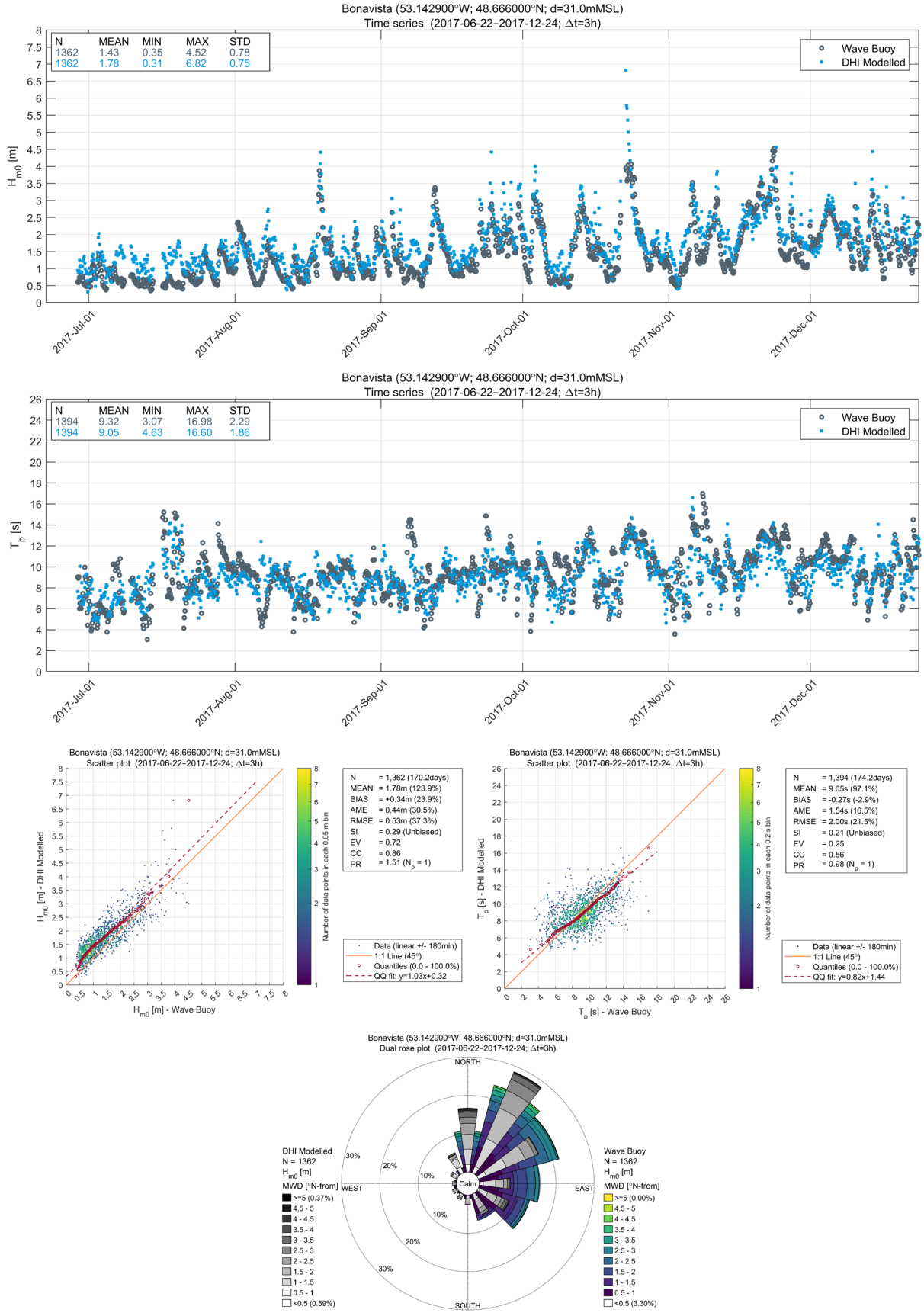


Figure 3.21 Wave Model Validation – Bonavista

Significant Wave Heigh (H_{m0}) and Peak Period (T_p) timeseries and scatter plots comparison. At bottom, dual rose plot assessing the joint Mean Wave Direction and H_{m0} distribution.

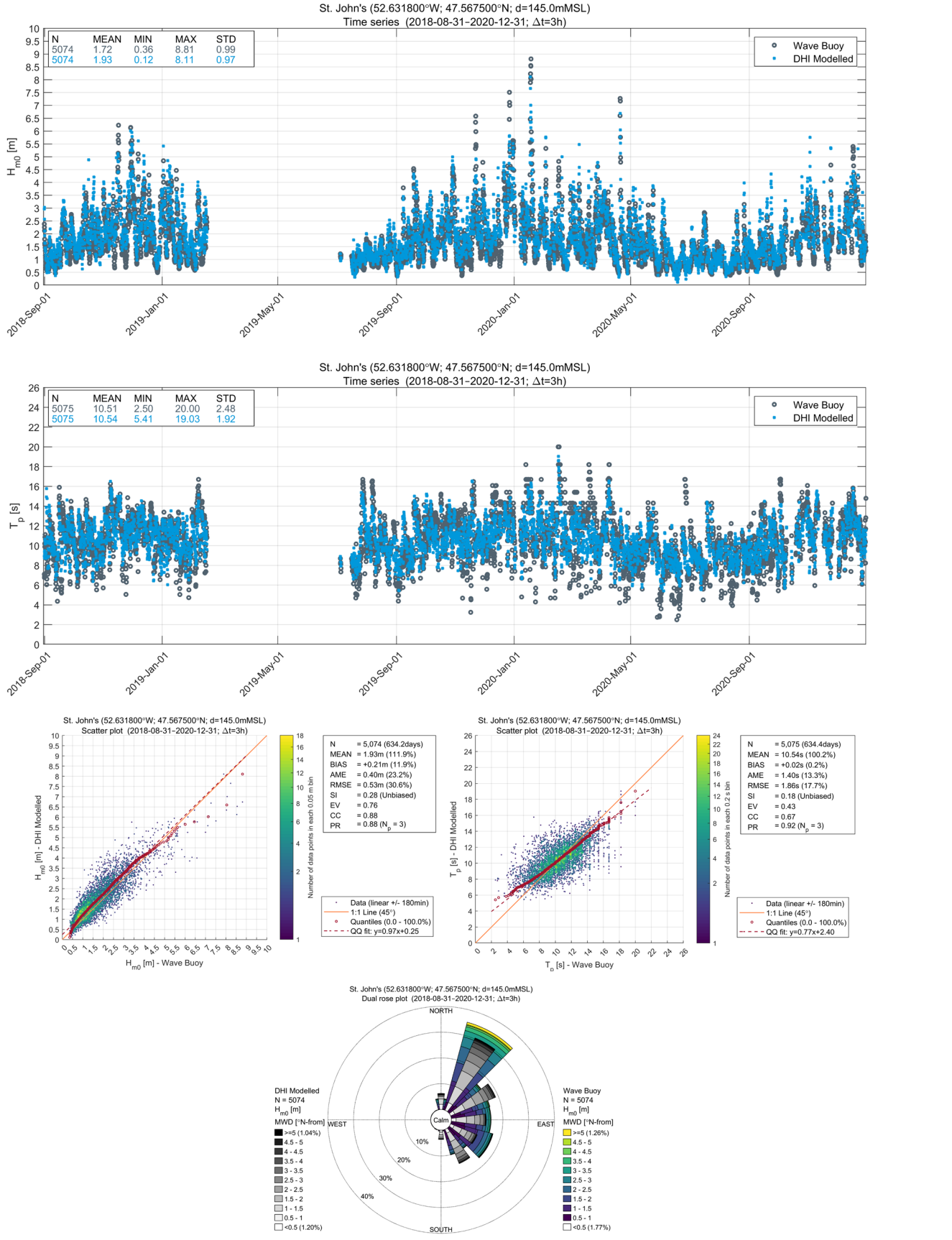


Figure 3.22 Wave Model Validation – St. John's

Significant Wave Heigh (H_{m0}) and Peak Period (T_p) timeseries and scatter plots comparison. At bottom, dual rose plot assessing the joint Mean Wave Direction and H_{m0} distribution.

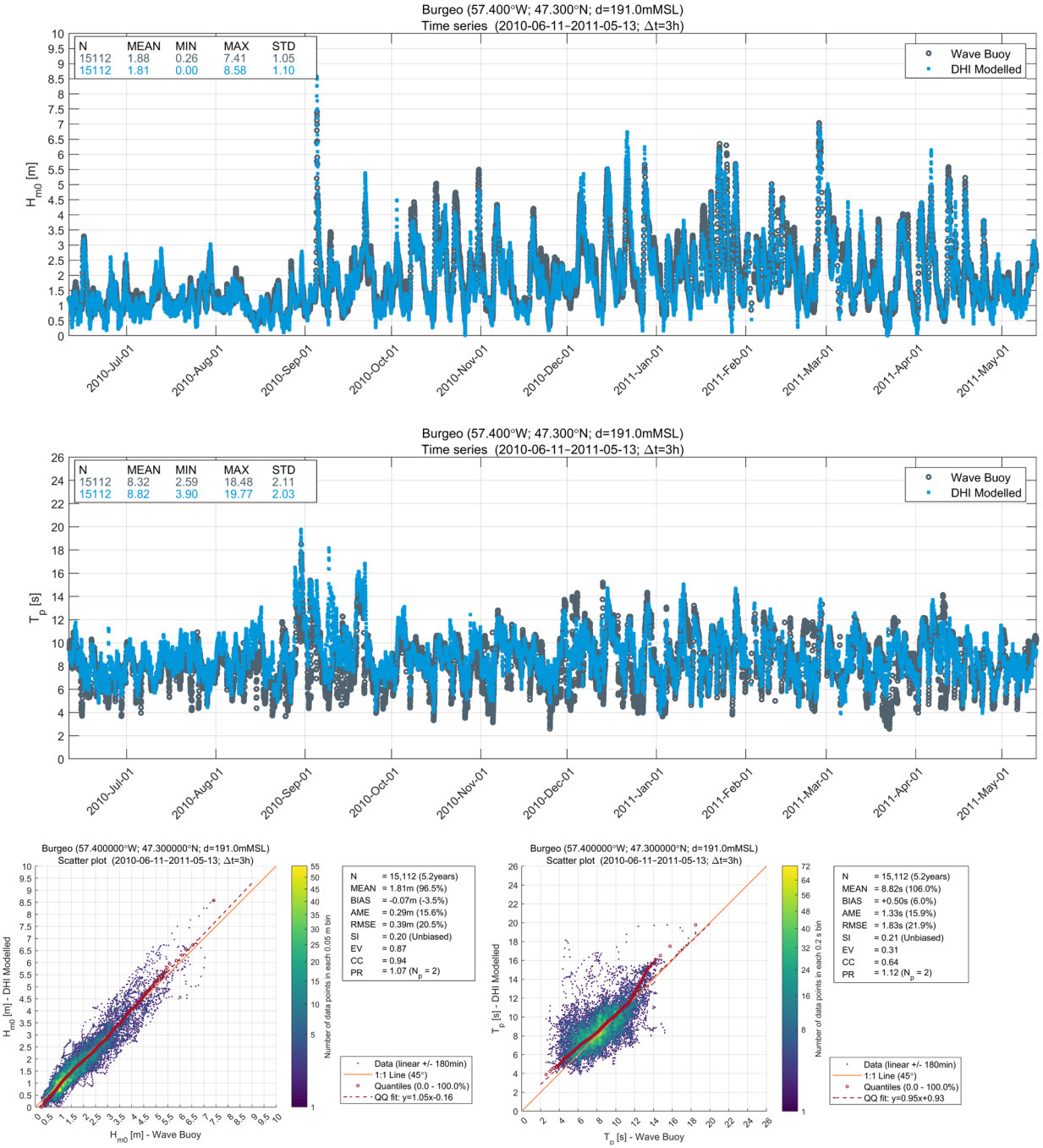


Figure 3.23 Wave Model Validation – Burgeo (MEDS C44235)
Significant Wave Heigh (H_{m0}) and Peak Period (T_p) timeseries and scatter plots comparison.

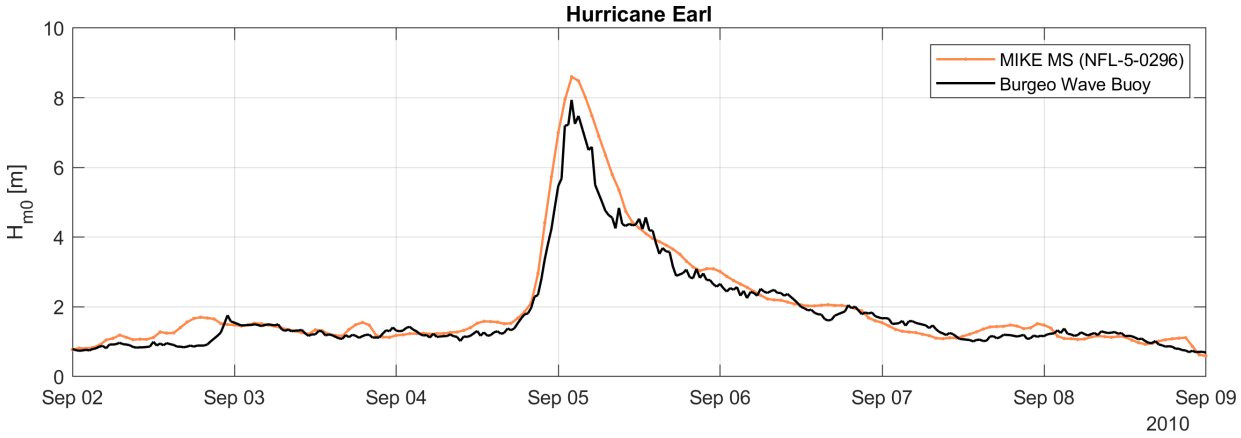


Figure 3.24 Wave Model Validation – Burgeo (MEDS C44235) – Hurricane Earl (Sep 2010)
Significant Wave Height (H_{m0}) time series depicting the Hurricane Earl (Sep-2010) as represented by the Atlas (orange) and measured by a wave buoy (grey).

Comparison with Other Hindcast Products

Due to the limited number of in-situ wave measurements, the model validation was expanded by comparing the model results against other hindcast products: (i) the MSC50 Wind and Wave Climate Hindcast [18] [19], which is a well-established hindcast product for Atlantic Canada and (ii) the ECMWF-ERA5 wave model, which has the same forcing as the MIKE MS model. Comparisons were performed at locations around Newfoundland and Labrador (locations shown in Figure 3.25 and Table 3.9).

The MSC50 Wind and Wave Climate Hindcast comprises of wind and wave time series from 1954 to 2018 covering the Canadian East Coast with time interval of one hour and spatial resolution of 0.1 degree (~7x11 km) from Nova Scotia to the north of Newfoundland and time steps of 3-hourly and spatial resolution of 0.5 degree (~32x55 km) along Labrador. This dataset is the industry-standard for assessments which require long term wave data, such as extreme value analyses, due to higher resolution compared to global models and because it incorporates regional characteristics, such as regional ice charts. The ECMWF-ERA5 wave hindcast provides hourly time series of various wave parameters from 1940 to present with a spatial resolution of 0.5 degree[8].

[8] Note that the native ERA5 resolution is approximately 40 km but model output is interpolated to a regular 0.5 degree grid.

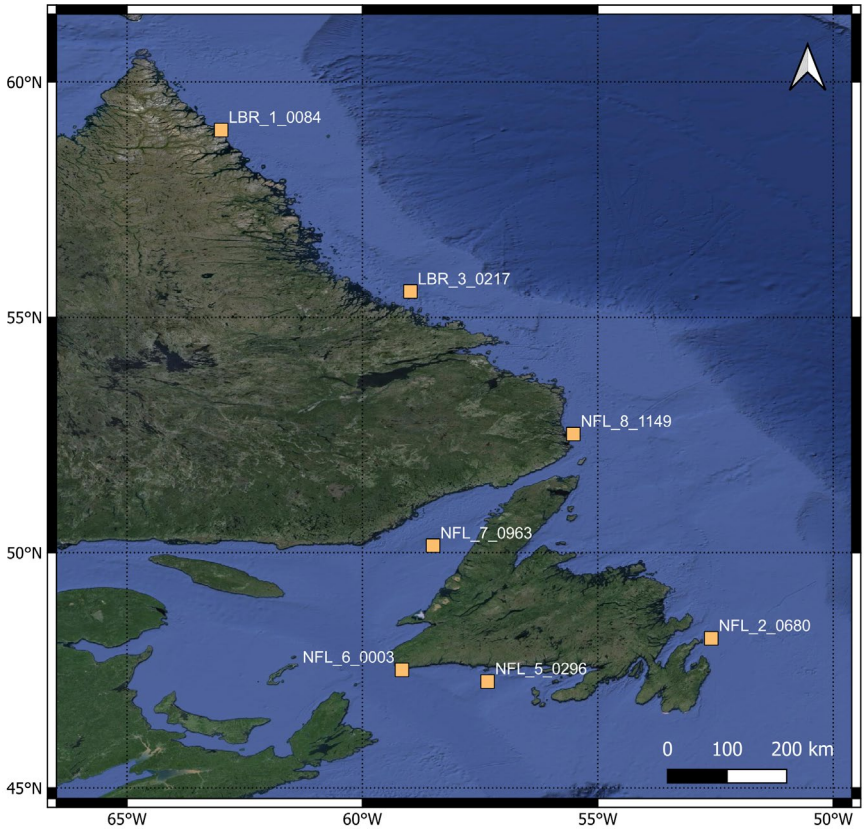


Figure 3.25 Locations used for comparison with other hindcast products

Table 3.9 Locations used for comparison with other hindcast products.

Location	MIKE MS		MSC50		ERA5	
	Lon	Lat	Lon	Lat	Lon	Lat
LBR_1_0084	-63.00	58.98	-63.00	59.00	-63.00	59.00
LBR_3_0217	-58.98	55.55	-59.00	55.50	-59.00	55.50
NFL_2_0680	-52.59	48.18	-52.60	48.20	-52.50	48.00
NFL_5_0296	-57.34	47.26	-57.40	47.30	-57.50	47.50
NFL_6_0003	-59.16	47.51	-59.10	47.50	-59.00	47.50
NFL_7_0963	-58.50	50.15	-58.50	50.20	-58.50	50.00
NFL_8_1149	-55.52	52.52	-55.50	52.50	-55.50	52.50

A time series of significant wave height for the overlapping period between the three models is shown in Figure 3.26. Overall, there is good agreement between the different models. Seasonal variability and overall trends are well represented. Figure 3.27 shows scatter plots comparing the MIKE MS wave model results against MSC50 and ERA5 for different locations for the ice-free period. Some differences are observed in the duration of the storm events and timing of occurrence of the peak of storm which can cause some spreading in the comparison figures.



Figure 3.26 Time series of significant wave height based for the overlapping period (1980-2018) between MIKE MS, MSC50 and ERA5 for various locations around Newfoundland and Labrador

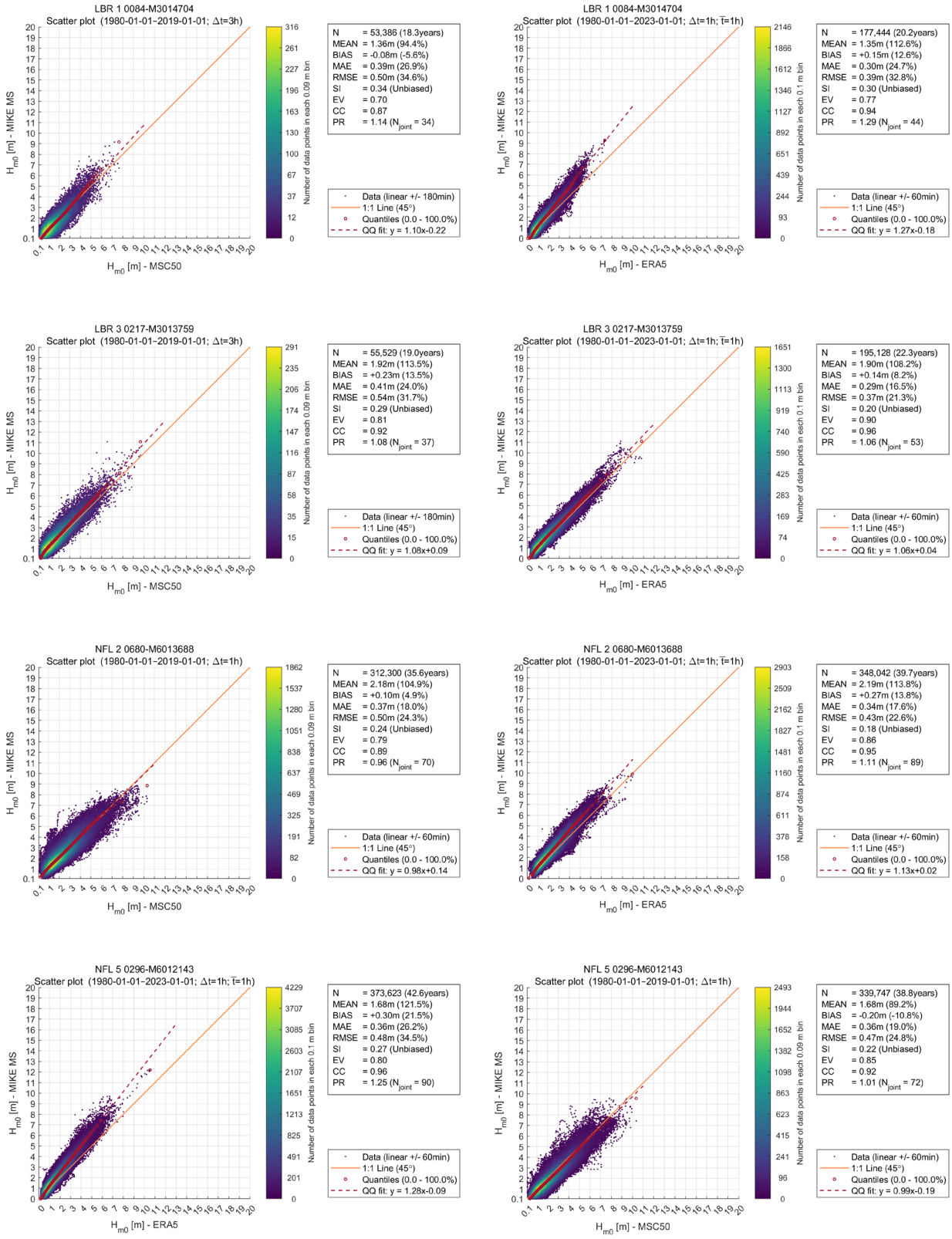


Figure 3.27 Scatter plots comparing MIKE MS results with MSC50 hindcast (left) and ERA5 (right) for various locations around Newfoundland and Labrador
Periods with ice coverage were removed from the comparison.

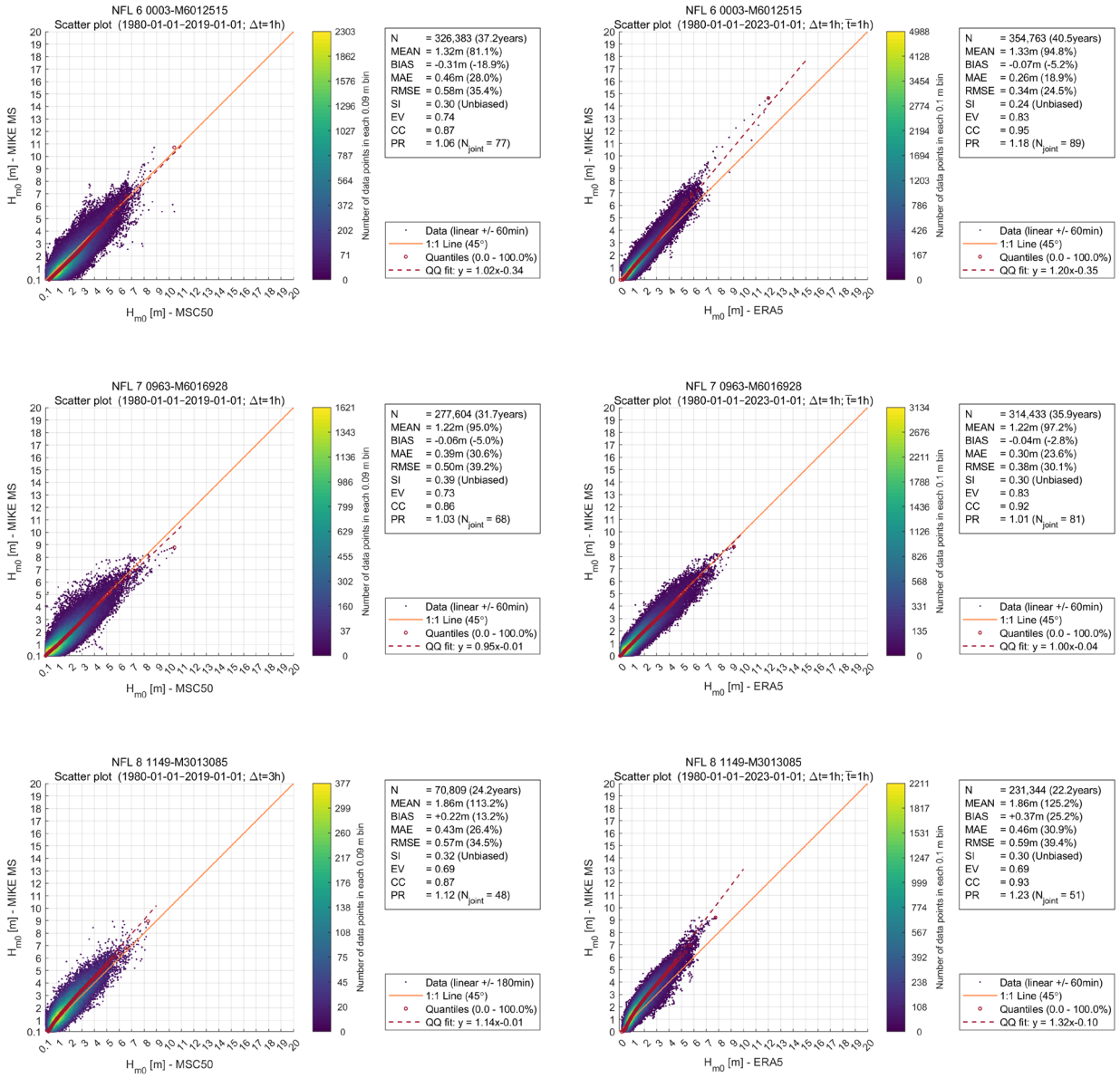


Figure 3.28 Scatter plots comparing MIKE MS results with MSC50 hindcast (left) and ERA5 (right) for various locations around Newfoundland and Labrador
Periods with ice coverage were removed from the comparison.

To further evaluate the performance of the MIKE MS wave model in simulating extreme events, some relevant extreme events were selected. As shown in Figure 3.24, the model successfully reproduced wave conditions during hurricane Earl in 2010, which is the only significant hurricane event for which reliable measurements are available. Comparison of this event with the other hindcast products reveals that the MIKE MS wave model had better performance for this specific event (Figure 3.29).

Another specific event that underwent a more detailed analysis is Hurricane Bertha, which passed near Port aux Basques in August 1990 (Figure 3.30). This event stands out as one of the most intense storm occurrences within the shared timeframe between the models (1980-2018) and holds significance for extreme value analysis. In this event, MSC50 calculates significant wave heights reaching 10.4 m, whereas the MIKE MS model indicates a peak of 6.4 m, and ERA5 estimates the height to be 5.4 m. The difference could be explained by the ERA5 wind model's insufficient representation of the event, stemming from its resolution not being capable of adequately depicting the complexity of this region, especially during cyclonic events. Despite the considerably improved resolution in the MIKE MS model

for this area (1.5 km near the coast), its accuracy is still contingent on the resolution of the wind fields utilized to drive the model.

Conversely, the MIKE MS model shows significantly higher wave heights for another notable extreme storm event in January 2000 compared to the MSC50 dataset (10.7 m from MIKE MS, 8.8 m from MSC50 and 7.8 m from ERA5, Figure 3.31). Due to the absence of measurements for these specific storm events, evaluating the accuracy of the models becomes challenging.

It should be cautioned that wind fields (and consequently wave conditions) during hurricane events are highly complex and oftentimes, depending on the location and characteristics of the storm event, global atmospheric models, such as ERA5 do not have sufficient resolution to accurately simulate those events. Despite having a higher resolution, the MSC50 wind fields can also fall short in accurately representing these events, as demonstrated by comparisons with the Burgeo wave buoy (MEDS C44235) during hurricane Earl. In areas where hurricane-generated waves are critical, caution is advised when using the results of the Atlas, and any other regional products, without conducting additional analysis.

However, it is important to mention that two significant hurricane events on the South-West coast of Newfoundland occurred post-2018, beyond the MCS50 dataset's coverage. These events can significantly impact the shape of the extreme value distributions in this region, leading to increased return values and should be considered in the analysis[9]. Recommendations for improving the representation and consideration of hurricane conditions in local assessments are discussed in section 6.

The MIKE MS models used in this atlas have higher resolution than the other existing hindcast products and have undergone validation against local measurements, demonstrating sufficient accuracy to depict historical conditions around Newfoundland and Labrador, including extreme events.

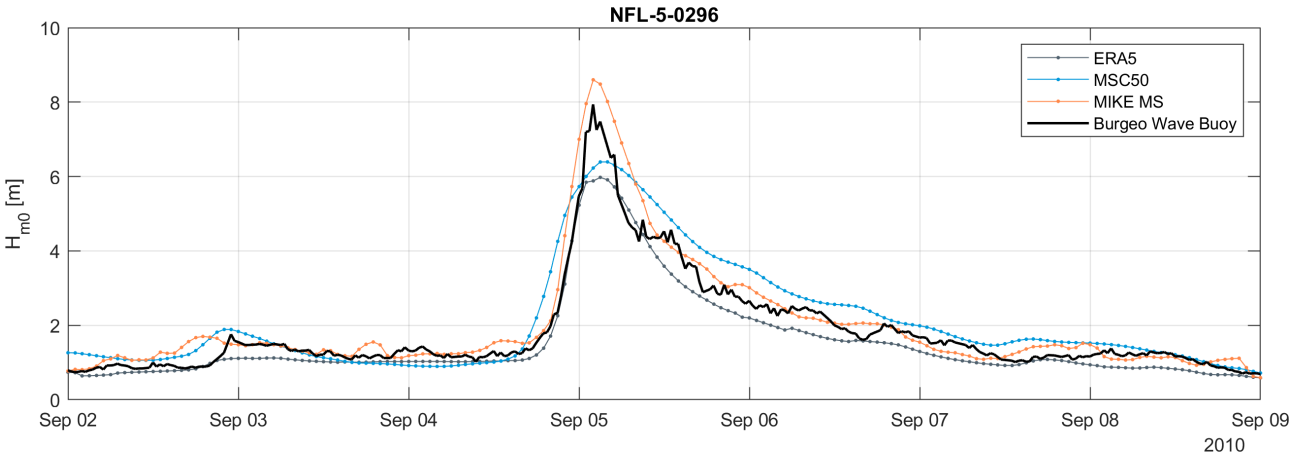


Figure 3.29 Comparison of significant wave height at Burgeo wave buoy (MEDS C44235) during Hurricane Earl in 2010

[9] Several comparisons of Extreme Value Analysis results using the MCS50 dataset (1954-2018) and the Atlas dataset (1980-2022) were conducted and shows that the NL Atlas produces higher return values than using the MSC50 dataset alone. This can vary for other regions and thus it is of utmost importance to rely on expert judgement.

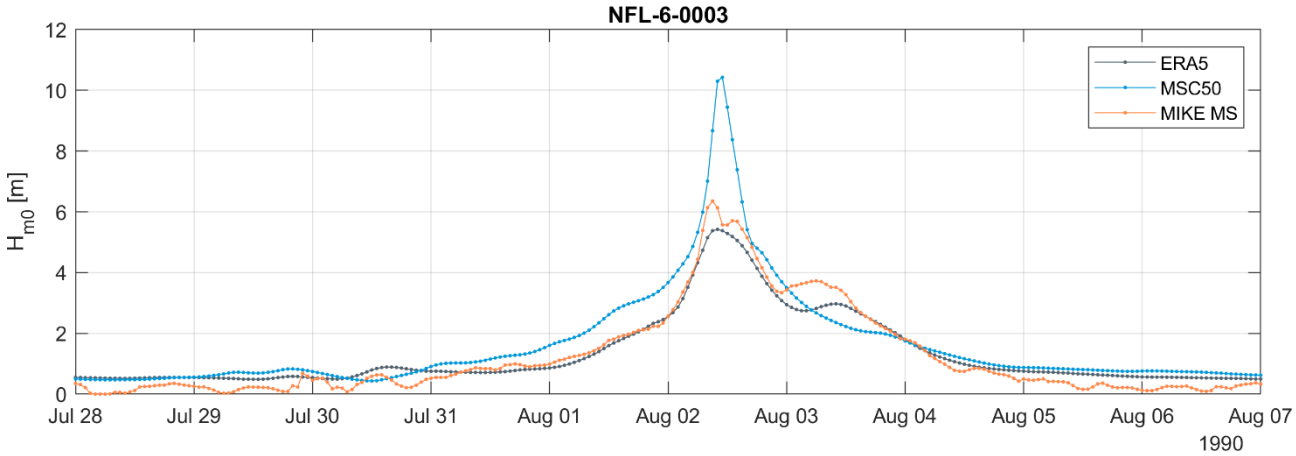


Figure 3.30 Comparison of significant wave height at Port aux Basques during Hurricane Bertha in 1990

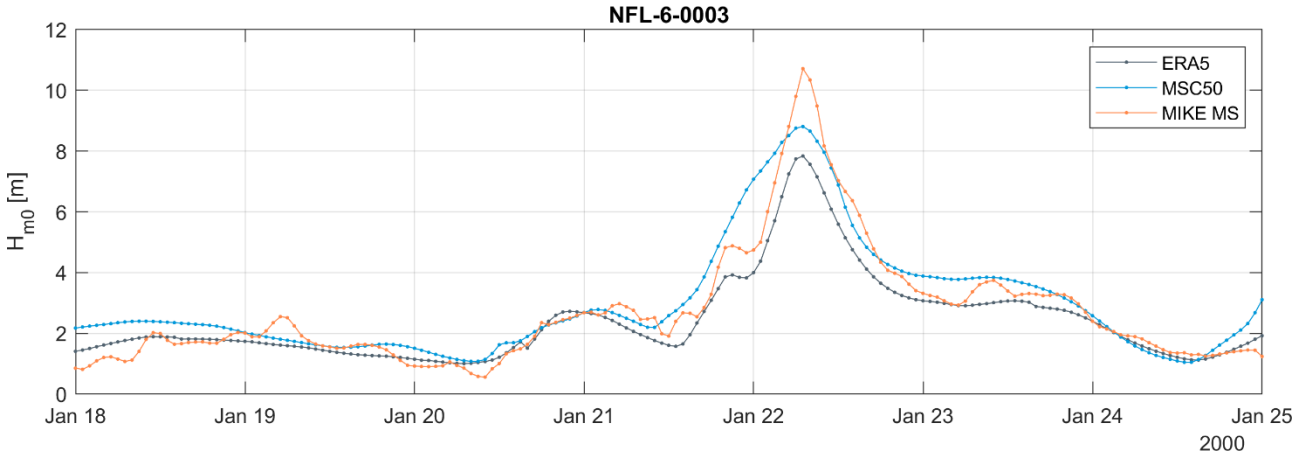


Figure 3.31 Comparison of significant wave height at Port aux Basques during the January 2000 storm

3.4 Climate Projections

To evaluate potential changes to the storm surge and wave climates around Newfoundland and Labrador, two Global Climate Models (GCM) were used to force the storm surge and wave models described in Sections 3.2 and 3.3. The selected models are the EC-Earth3 and ACCESS-CM2 from the Coupled Model Intercomparison Project (Phase 6) (CMIP6).

These models were chosen as they constituted the sole CMIP6 global wave climate projections accessible at the time of the project. Details on model performance with respect to wave conditions are provided in Meucci et al (2023) [14]. It is worth emphasizing that, moving forward, the Atlas has the potential for expansion to include a broader model ensemble as additional global wave climate projections become available. The methodology and approach outlined here can be applied universally, allowing the surge and wave models to be forced with diverse global climate models. Expanding the number of climate projections would enhance the robustness of the results.

Furthermore, regional sea level changes from an ensemble of models from the Intergovernmental Panel on Climate Change (IPCC) 6th Assessment Report (AR6) were used [1]. This data was downloaded from the NASA Sea Level Projection Tool [21].

For this study, the Shared Socioeconomic Pathway 5-8.5 (SSP5-8.5) scenario was used. The Shared Socioeconomic Pathways (SSP) scenarios used in the IPCC AR6 represent a range of plausible scenarios of future socioeconomic development and greenhouse gas emissions. SSP5-8.5 assumes a future with high economic growth and a continued reliance on fossil fuels, with little international cooperation on climate change and no additional climate policy. SSP5-8.5 is the usual choice for climate risk assessments and engineering design because it represents a high-end emissions scenario that can be used to explore the potential impacts of a future where emissions continue to rise at a high rate. It is also considered a useful reference point for evaluating the costs and benefits of different mitigation and adaptation strategies. While some have criticized the scenario for being too pessimistic, it is still an important tool for exploring the potential risks and uncertainties of climate change and for informing policy decisions.

Wind speed and direction, atmospheric mean sea level pressure and sea-ice concentration were obtained from the World Climate Research Programme, CMIP6 website [22] for the ACCESS-CM2 and EC-EARTH3 global climate models (GCMs). Additionally, wave conditions were obtained from the Commonwealth Scientific and Industrial Research Organisation (CSIRO) CMIP6 global wind-wave 21st century climate projections phase 1 [23]. This dataset encompasses 3-hourly outputs from wave climate simulations at 0.5-degree global grid resolution using WaveWatch III model. This model is forced by surface wind and sea-ice concentration fields from the GCMs.

Climate projections come with notable uncertainties, as discussed in Section 5. It is essential to exercise caution when interpreting the outcomes of these simulations. The two projections provided in the NL Atlas of Storm Surge and Wave Climates, while valuable, represents an initial effort in the direction of constructing a more comprehensive and reliable climate projection resource. To achieve a deeper understanding of real trends and uncertainties, there is a need for an expanded ensemble of models. Such an ensemble would contribute to refining climate projections, offering a more nuanced and encompassing perspective on potential climate scenarios.

4 Extreme Value Analysis

This chapter describes the extreme value analysis (EVA) performed on the significant wave height and storm surge.

Extreme Value Analysis (EVA) of wave and surge conditions is crucial for comprehending and mitigating the impact of extreme natural events. EVA results, often displayed through metrics like return periods (T_r) and/or Annual Exceedance Probability (AEP), allow stakeholders to derive design conditions, set risk tolerances, prioritize mitigation efforts, and allocate resources effectively, to safeguard coastal communities against the impacts of extreme wave and surge events.

One key metric often associated with EVA outputs is the Annual Exceedance Probability (AEP). AEP represents the likelihood of a particular wave or surge event exceeding a certain threshold in any given year. In practical terms, a 1% AEP corresponds to an event that has a 1% chance of occurring or being exceeded in a given year. Conversely, the return period is a statistical measure representing the average time interval between the recurrence of a specific extreme event. It is the inverse of the Annual Exceedance Probability. For instance, an event with a 100-year return period has a 1 in 100 chance of occurring in a given year (1% AEP). A longer return period corresponds to a lower AEP, indicating a rarer and more severe event, while a shorter return period is associated with a higher AEP, representing a more frequent occurrence.

4.1 Methodology

Extreme values with conditioned long return periods are estimated by fitting a probability distribution to historical data. Several distributions, data selection and fitting techniques are available for estimation of extremes, and the estimated extremes are often rather sensitive to the choice of method. However, it is not possible to choose a preferred method only on its superior theoretical support or widespread acceptance within the industry. Hence, it is common practice to test several approaches and make the final decision based on goodness of fit.

The extreme value analyses involve the following steps:

1. Extraction of independent identically distributed events by requiring that events are separated by at least 36 hours, and that the value between events had dropped to below 70% of the minor of two consecutive events. The extraction is conducted individually for omni and directional subsets respectively.
2. Fitting of extreme value distribution to all events above a certain threshold (the Peak-Over-Threshold method), individually for omni and directional subsets. The distribution type can be exponential, truncated Weibull or 2-parameter Weibull to excess. Distribution parameters are estimated either by maximum likelihood or least-square methods; see Appendix B for details.
3. Constraining of subseries to ensure consistency with the omni/all-year distribution; see Appendix B for details.
4. Bootstrapping to estimate the uncertainty due to sampling error; see Appendix B for details.

Figure 4.1 shows an example of EVA based on 43 years of hindcast data and a truncated Weibull distribution fitted to the average annual peak using least-squares.

To define the most appropriate EVA parameters to be used in this study a sensitivity analysis was performed. First, an extensive sensitivity analysis was performed for selected locations, using all distribution types and various thresholds. Then, the most promising distribution types were applied to all locations with varying threshold criteria (e.g. average number of peaks per year). The best distribution type and threshold criteria were determined based on goodness of fit (e.g. reduction of the root mean square error – RMSE) and robustness of the estimates (e.g. how sensitive the estimative is depending on the threshold applied). A summary of the sensitivity analysis is presented in Figure 4.2.

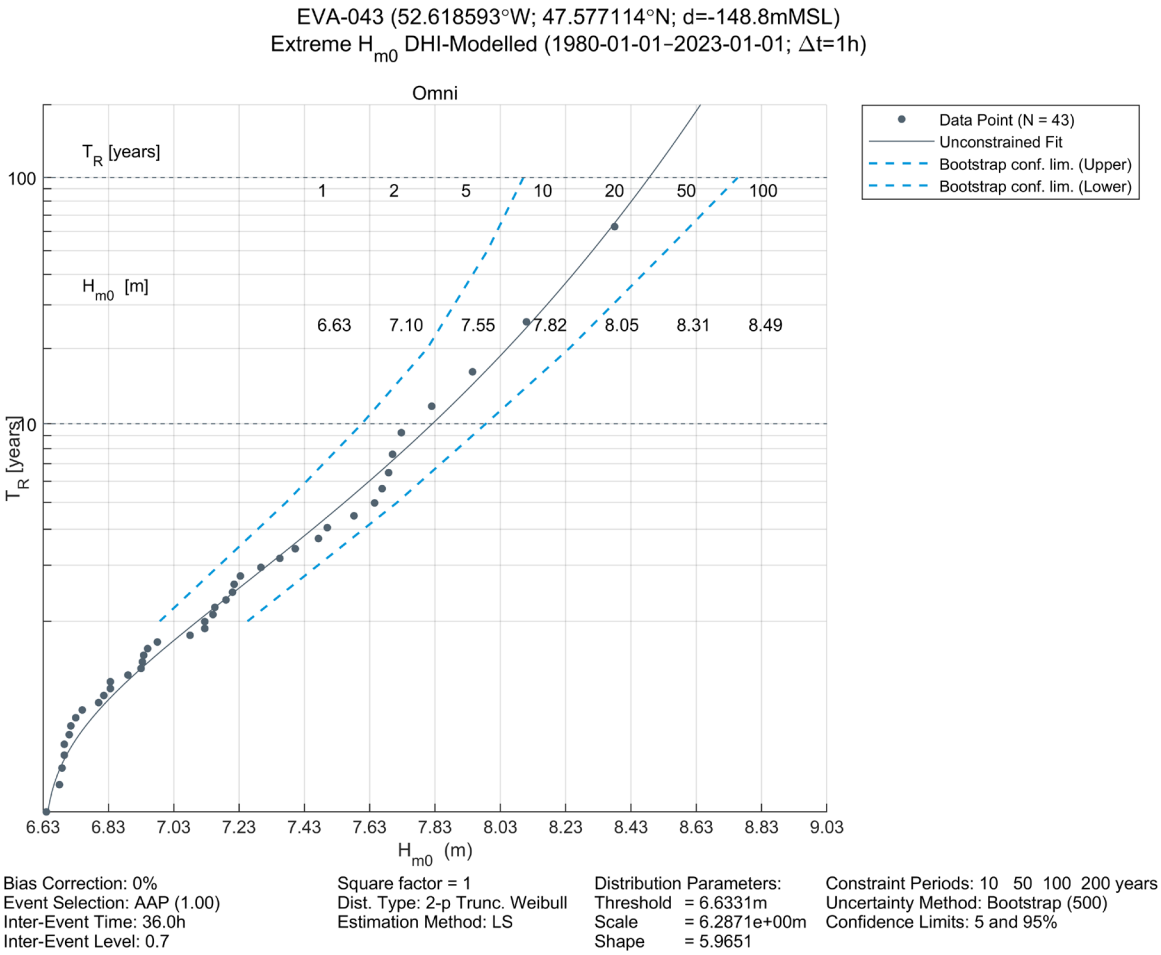


Figure 4.1 Example of Extreme Value Analysis of H_{m0}
Based on Weibull distribution fitted to the average annual peaks using least-squares.

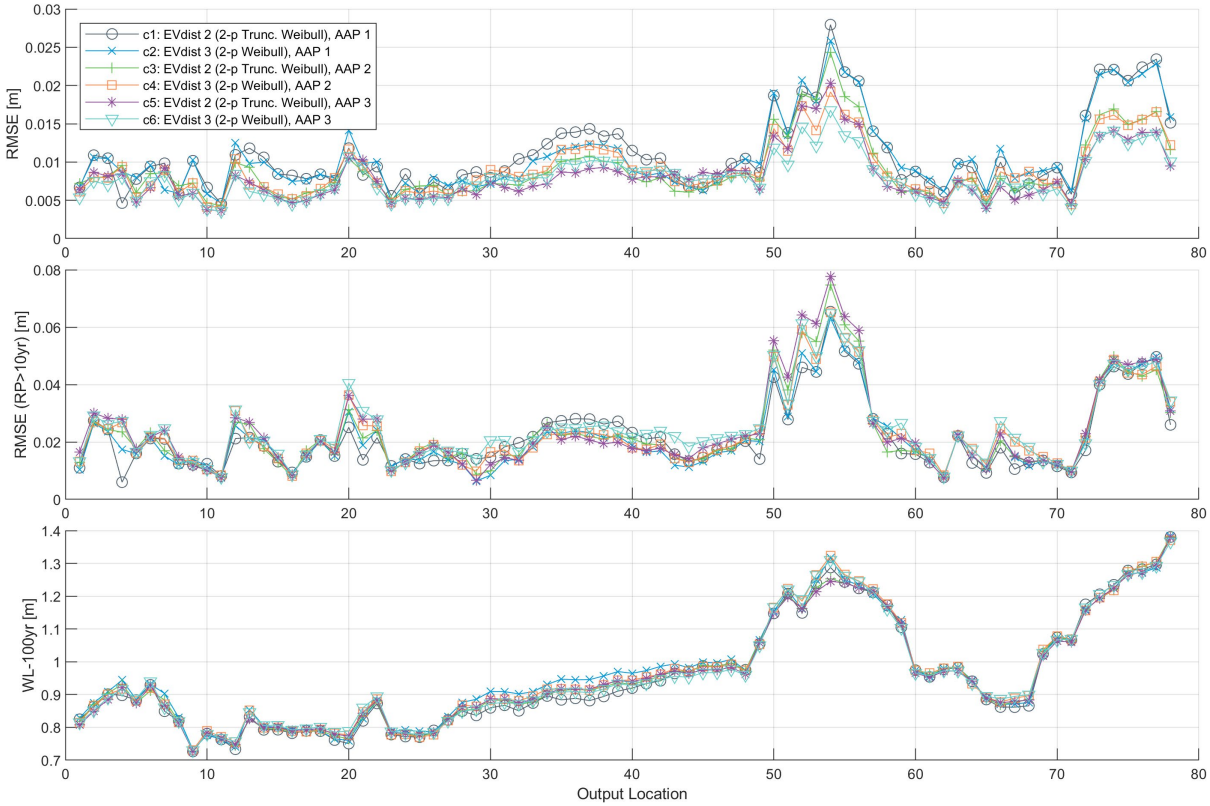


Figure 4.2 **Summary of the Sensitivity Analysis of the EVA Parameters**
Top panel shows the root mean square error (RMSE) for all analysed return periods, middle panel shows the RMSE for return periods above 10 years, and bottom panel shows the estimated 100-year water level.

4.2 Results

Table 4.1 summarizes the results of the extreme value analyses for 20-year and 100-year return periods for all stations. Figures of the time series, selected peaks and extreme value distribution fitting for each station are provided in Appendix C.

Table 4.1 **Summary of Extreme Value Analyses Results for 20-year and 100-year Return Periods**
Water level residual (WL_{Res}), omni-directional significant wave height (H_{m0}) and associated peak wave period ($T_{p,50\%}$) based on the 50% quantile estimation.

	T_R 20-year			T_R 100-year		
	WL_{Res} [m]	H_{m0} [m]	Ass. $T_{p,50\%}$ [s]	WL_{Res} [m]	H_{m0} [m]	Ass. $T_{p,50\%}$ [s]
Point_1	0.7	7.8	13.9	0.8	8.9	14.6
Point_2	0.8	8.3	13.9	0.9	9.7	14.6
Point_3	0.8	9.2	14.5	0.9	10.6	15.3
Point_4	0.7	8.9	13.9	0.9	10.0	14.5
Point_5	0.8	8.3	14.2	0.9	9.3	14.6
Point_6	0.8	8.2	14.0	0.9	9.0	14.3
Point_7	0.8	8.2	13.6	0.9	9.3	13.9
Point_8	0.7	4.5	12.1	0.8	5.0	12.6
Point_9	0.7	7.0	14.1	0.7	7.9	14.7
Point_10	0.7	7.4	13.7	0.8	8.4	14.3
Point_11	0.7	7.0	13.0	0.8	7.9	13.7
Point_12	0.7	5.0	11.5	0.7	5.5	11.9

	T_R 20-year			T_R 100-year		
	WL_{Res} [m]	H_{m0} [m]	Ass. $T_{p,50\%}$ [s]	WL_{Res} [m]	H_{m0} [m]	Ass. $T_{p,50\%}$ [s]
Point_13	0.7	3.5	10.3	0.9	4.2	10.5
Point_14	0.7	6.0	12.3	0.8	6.7	12.8
Point_15	0.7	7.3	12.6	0.8	8.0	12.9
Point_16	0.7	6.0	12.6	0.8	6.8	12.9
Point_17	0.7	7.3	13.3	0.8	8.2	13.7
Point_18	0.7	7.9	13.3	0.8	8.8	13.7
Point_19	0.7	8.6	13.9	0.8	9.3	14.2
Point_20	0.7	8.9	14.3	0.8	9.8	14.7
Point_21	0.7	8.1	13.7	0.8	8.8	14.1
Point_22	0.7	7.8	14.0	0.9	8.3	14.3
Point_23	0.7	6.6	12.1	0.8	7.1	12.2
Point_24	0.7	6.1	11.3	0.8	6.7	11.5
Point_25	0.7	5.7	12.8	0.8	6.0	13.0
Point_26	0.7	5.1	11.8	0.8	5.5	12.0
Point_27	0.7	7.3	14.6	0.8	8.2	15.4
Point_28	0.7	6.5	13.7	0.9	6.9	13.9
Point_29	0.7	4.6	14.0	0.9	5.1	14.5
Point_30	0.8	3.2	6.5	0.9	3.7	6.8
Point_31	0.8	3.2	7.7	0.9	3.7	8.1
Point_32	0.8	5.4	14.1	0.9	5.8	14.5
Point_33	0.8	5.2	13.3	0.9	5.7	13.8
Point_34	0.8	6.5	11.7	0.9	7.0	11.9
Point_35	0.8	5.1	12.9	1.0	5.5	13.1
Point_36	0.8	5.0	12.9	0.9	5.5	13.1
Point_37	0.8	4.6	13.6	1.0	5.0	14.1
Point_38	0.8	3.2	9.8	1.0	3.7	10.0
Point_39	0.8	2.6	9.2	1.0	3.0	9.9
Point_40	0.8	7.5	14.9	1.0	8.1	15.4
Point_41	0.8	7.4	14.7	1.0	8.0	15.2
Point_42	0.8	8.0	14.6	1.0	8.7	15.1
Point_43	0.8	8.1	14.0	1.0	8.5	14.3
Point_44	0.8	7.7	11.9	1.0	8.2	12.0
Point_45	0.9	7.6	11.4	1.0	8.5	11.6
Point_46	0.8	7.9	11.6	1.0	8.8	11.8
Point_47	0.9	7.4	11.4	1.0	8.3	11.6
Point_48	0.8	8.1	11.6	1.0	8.9	11.8
Point_49	0.9	9.1	17.0	1.1	10.7	18.3
Point_50	1.0	9.3	15.9	1.2	10.6	16.9
Point_51	1.0	5.1	14.4	1.2	5.7	15.2
Point_52	1.0	8.7	16.2	1.2	9.6	17.1
Point_53	1.0	6.4	12.6	1.3	7.2	13.2
Point_54	1.1	2.9	6.4	1.3	3.2	6.6
Point_55	1.0	7.7	14.0	1.2	8.2	14.4
Point_56	1.0	7.9	13.9	1.2	8.5	14.4
Point_57	1.0	8.8	14.5	1.2	9.6	15.0

	T_R 20-year			T_R 100-year		
	WL_{Res} [m]	H_{m0} [m]	Ass. $T_{p,50\%}$ [s]	WL_{Res} [m]	H_{m0} [m]	Ass. $T_{p,50\%}$ [s]
Point_58	1.0	8.8	14.7	1.2	9.5	15.3
Point_59	0.9	8.5	14.9	1.1	9.5	15.7
Point_60	0.8	6.1	12.0	1.0	6.5	12.4
Point_61	0.8	5.0	11.7	1.0	5.3	12.2
Point_62	0.8	3.0	9.9	1.0	3.1	10.0
Point_63	0.8	6.3	11.7	1.0	6.8	11.9
Point_64	0.8	9.1	13.6	0.9	10.2	14.3
Point_65	0.8	9.1	15.2	0.9	10.3	16.0
Point_66	0.8	9.1	14.9	0.9	10.4	15.6
Point_67	0.8	8.8	13.3	0.9	10.3	14.0
Point_68	0.8	9.3	13.6	0.9	10.8	14.3
Point_69	0.9	7.6	13.6	1.0	8.0	14.1
Point_70	0.9	5.2	13.1	1.1	5.5	13.7
Point_71	0.9	9.1	12.9	1.1	9.5	13.3
Point_72	1.0	7.8	12.3	1.2	8.6	12.8
Point_73	1.0	7.2	12.2	1.2	8.0	12.8
Point_74	1.1	6.8	12.2	1.2	7.5	12.8
Point_75	1.1	7.0	12.0	1.3	7.6	12.5
Point_76	1.1	6.7	12.2	1.3	7.4	12.7
Point_77	1.1	7.0	12.0	1.3	7.6	12.6
Point_78	1.2	7.2	11.9	1.4	7.8	12.3

4.3 Sources of Uncertainty

The extreme values are estimated quantities and therefore all associated with uncertainty. The uncertainty arises from several sources, detailed below. While some sources, such as sampling error, can be quantified, others are more challenging to measure. This section aims to describe these sources cautioning the user that these should be taken into consideration when interpreting the EVA results. It should be noted that the confidence limits presented in the figures in Appendix C, represent only the uncertainty due to sampling error and not the other sources of uncertainty.

Measurement/Model Uncertainty

The contents of the database for the extreme value analysis are associated with uncertainty. This type of uncertainty is preferably mitigated at the source – e.g., by correction of biased model data and removal of obvious outliers in data series. The model uncertainty can be quantified if simultaneous good quality measurements are available for a reasonably long overlapping period. Validation of model results and associated uncertainties is presented in Section 3.

True Extreme Value Distribution is Unknown

The distribution of extremes is theoretically unknown for levels above the levels contained in the extreme value database. There is no justification for the assumption that a parametric extreme value distribution fitted to observed/modelled data can be extrapolated beyond the observed levels. However, it is common practice to do so, and this obviously is a source of uncertainty in the derived extreme value estimates. This uncertainty, increasing with decreasing occurrence probability of the event in question, is not quantifiable but the metocean expert may minimise it by using experience and knowledge when deciding on an appropriate extreme value analysis approach. Proper inclusion of other information than direct measurements and model results may also help to minimise this type of uncertainty.

Uncertainty Due to Sampling Error

The number of observed/modelled extreme events is limited. This gives rise to sampling error which can be quantified by statistical methods such as Monte Carlo simulations or bootstrap resampling. The results of such an analysis are termed the confidence limits. The confidence limits (see Appendix B) should **not** be mistaken for the total uncertainty in the extreme value estimate.

Settings of the Analysis (Judgement)

Any EVA involves the need to define the various settings of the analysis (threshold, distribution, and fitting method), which introduces subjectivity to the analysis. The sensitivity of these settings can be assessed by comparing the resulting extreme values, and the goodness of fit can, to some extent, be objectively assessed by statistical measures. However, standard practice typically includes manual inspection of the fitted distributions. The tail of the distribution, representing the values corresponding to longer return periods, can be notably influenced by the analysis settings and parametrization. Hence, the final settings, and thus results, relies on the experience and preference of the metocean expert conducting the analysis ('engineering judgement').

5 Considerations on Climate Projections

It should be noted that climate change projections carry significant uncertainty due to, among other things, the complex and nonlinear nature of the Earth's climate system, making it difficult to accurately model and predict future climate conditions. Projections are also subject to uncertainties in future emissions, feedback mechanisms, and other factors that can influence future climate change. Limited historical data to inform climate models, difficulty in attributing impacts, and challenges in communicating scientific findings to stakeholders add to the uncertainty.

Climate change assessments are typically conducted to provide an overview and understanding of potential future climate scenarios, its impacts, and potential response options, helping to inform decisions on climate policy, sustainable design, and adaptation planning.

The high uncertainty associated with projections is an integral part of these assessments and it is important to keep this in mind when communicating the results to the public. It is important to consult with experts which understand these concepts before conveying information to a broad audience. This ensures accuracy, clarity, and alignment with the intended message, contributing to the overall effectiveness and reliability of the Atlas.

Interpreting the results of individual climate projection models requires an understanding of the sources and magnitude of uncertainties associated with each model. Ideally, the assessment should use a multi-model ensemble approach, which combines the projections of multiple models to provide a more comprehensive understanding of potential future climate conditions.

The NL Atlas of Storm Surge and Wave Climates provides results from two Global Climate Models (GCM) and should be considered as a first step towards developing a more comprehensive and robust climate projection product, with a larger ensemble of models.

Figure 5.1 and Figure 5.2 provide an example of the projected changes in the 99th percentile of storm surge and significant wave height by end-of-century for SSP5-8.5. It can be noted that, although both climate models consistently predict an increase in average wave conditions and surge levels along the Labrador coast, linked to reduced ice cover, trends around Newfoundland are less evident with significant differences between the two GCMs simulations. This example results emphasize the importance of a multi-model ensemble approach to capture the inherent variability in climate change projections.

The results provided in the Atlas should be treated as indicative of potential future climate change scenarios and is meant primarily to offer illustrative guidance to develop regional adaptation strategies. The model results should not be directly applied in engineering design. It is envisioned that model outcomes can support regional planning, education and capacity building, and other strategic objectives for the Province of Newfoundland and Labrador.

For example, in the context of coastal infrastructure planning and design, while these results should not be employed to establish the exact elevation of a wharf, they can be utilized to initiate discussions about the possible need for updating the wharf design in the next two decades and/or for adding additional safety factors to present design work in areas where an increase in wave height or surge levels are expected. The data offers insights and indications about potential future scenarios, empowering planners to make proactive provisions for addressing these aspects in the future. This proactive approach prevents surprises down the road and allows planners to anticipate and address potential challenges based on the indications provided by the data.

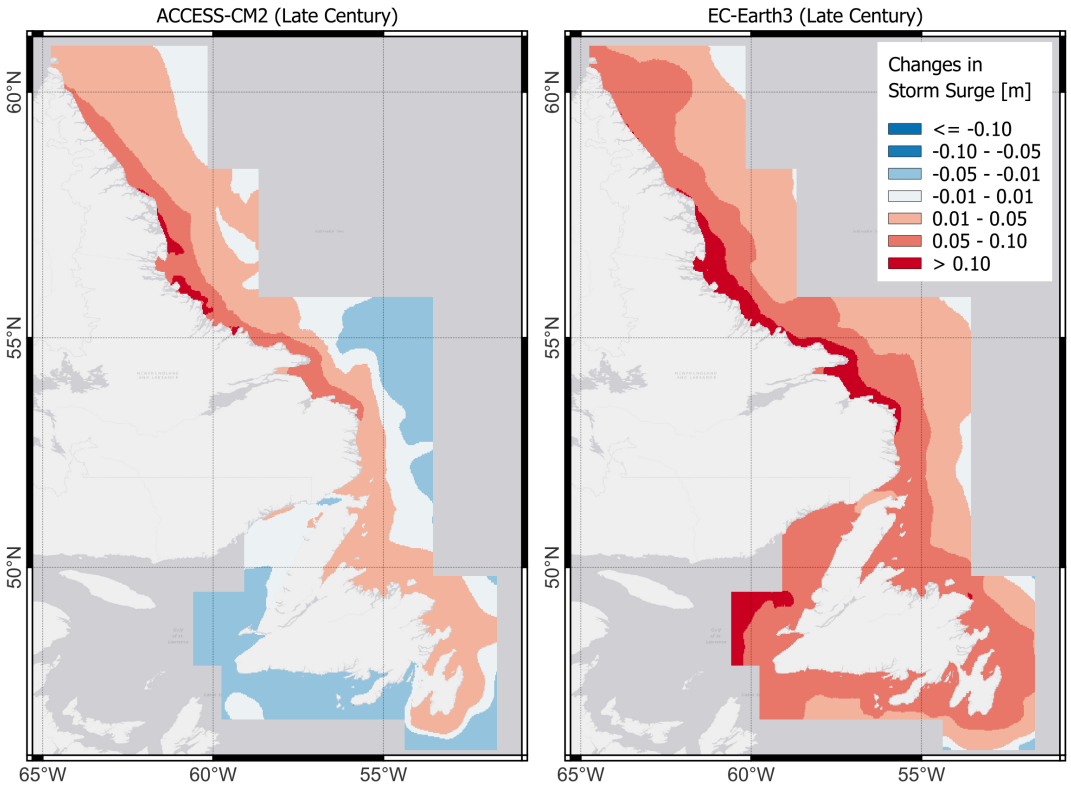


Figure 5.1 **Projected changes in the 99th percentile of storm surges by end-of-century compared to the baseline (1984-2014 to 2070–2100) for SSP5-8.5**

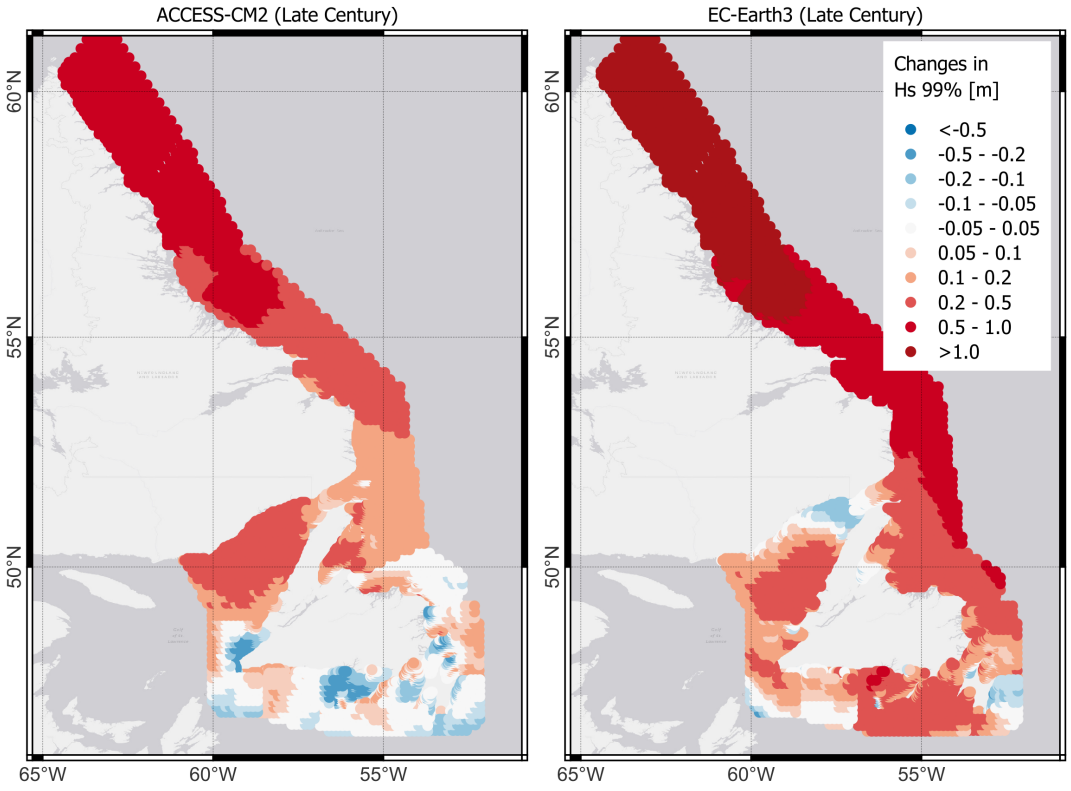


Figure 5.2 **Projected changes in the 99th percentile of significant wave height by end-of-century compared to the baseline (1984-2014 to 2071–2100) for SSP5-8.5**

6 Discussion

The following section delineates various applications of the Atlas, provides recommendations for an adequate utilization of the dataset and highlights limitations to consider of when interpreting and using the data. Regional planning, high-level vulnerability assessments, public information and awareness, downscaling to detailed community level assessments incorporating climate change impacts are examples of use cases for the Atlas. Ensuring that the Atlas is employed for its intended purposes and making thoughtful modifications and adaptations can enhance its effectiveness in specific contexts.

6.1 Typical Use Cases

The Newfoundland and Labrador Atlas of Storm Surge and Wave Climates provides useful insights for various stakeholders involved in coastal management, planning, and risk mitigation. The datasets contained in the Atlas can be used in a range of applications at a regional level, as well as adapted to be used at a local level, following recommendations to consider (see Section 6.3), and overcome the limitations described in Section 6.2. Outlined below are examples of use cases and application of the datasets.

Regional Planning and High-Level Vulnerability Assessment

The Atlas can be directly used as a foundational resource for high-level planning by offering comprehensive insights into the patterns and characteristics of storm surges and waves at a regional level. Utilizing statistical maps and time series distributed at a relatively high resolution along the coastline, planners and decision-makers can identify sections of the province that are particularly vulnerable to the impacts of extreme events, develop policies to establish zones requiring considerations for resilience against coastal hazard and prioritize areas for further study and intervention.

Furthermore, the Atlas can support the assessment of coastal vulnerability due to climate change. The maps of projected changes in storm surge and wave conditions (see for example Figure 5.1 and Figure 5.2) can be used to identify regions that are projected to become increasingly vulnerable due to sea level rise, reductions in seasonal sea ice coverage, greater storm surges and more severe wave action. This aspect of the Atlas is relevant for planning long-term interventions and enabling stakeholders to preemptively address the anticipated challenges posed by climate change.

General Public Information and Understanding

The Atlas can be a relevant resource in supporting general public communication on present and future risks posed by storm surges and waves. This can materialise, for example, in the form of targeted campaigns that utilize the Atlas' data to inform the public about coastal risks and the importance of preparedness and resilience or community workshops and public forums to discuss the results from the Atlas, encouraging community input and fostering a collaborative approach to coastal hazard mitigation.

Furthermore, by correlating data and analyses from recent extreme weather events with the comprehensive information provided in the Atlas, individuals can gain insights into the likelihood of an event as soon as it happens. This connection not only aids in a basic assessment of the storm but also enhances public comprehension of the broader impacts of climate change on their immediate environments. The practical use of the Atlas in educating the community contributes significantly to building a more informed public, capable of appreciating the complexities and potential consequences of coastal phenomena and climate change.

Downscaling for Community-Level Assessments

The Atlas covers the entire Newfoundland & Labrador province's coastline with relatively fine spatial resolution at a regional scale. One of the main objectives of this dataset is to offer boundary conditions for community-specific modelling endeavors, and it is the intention that the information presented in the

Atlas is downscaled using numerical modelling methods to derive detailed nearshore conditions using locally obtained bathymetric data, coastline delineation and site-specific surveys, as applicable.

The Atlas provides future projected changes to wave and storm surge climate, which can be incorporated into the local community high-resolution modeling in several ways. For example, an informed user can simulate additional discrete extreme wave scenarios incorporating a percentage of increase/decrease in the wave energy at the boundaries accounting for the climate change effects.

Allowance for Climate Change Impacts into Community-Level Assessments

The Atlas can also serve as an initial reference point for integrating climate change impacts into assessments at the community level for early design phases and high-level assessment. The projected changes to storm surge and wave conditions presented in the Atlas can be employed as an initial estimate to establish a safety factor or vertical allowance during the preliminary design and assessment stages of coastal infrastructure projects. While this resource should not substitute detailed design analyses, its application provides an essential starting point. By offering insight into the potential future changes to storm surge and wave conditions, the Atlas aids in the development of more sustainable preliminary designs, thereby enhancing the preparedness of coastal communities against the adverse effects of climate change.

6.2 Limitations

This Atlas and associated datasets were developed within the specific context of the project "*Climate Change Flood Risk Mapping Study for Ferryland, Brigus, Heart's Delight, Winterton and Hant's Harbour*" and are bound by the defined scope. As such, these findings may have inherent limitations that should be considered when interpreting and using the data:

- The accurate representation of hydrodynamic and wave transformation processes is bound to the model resolution. In areas of complex geometries, such as behind islands and within bays, wave conditions and storm surge might not be accurately represented. Therefore, model results might not be available within these areas and it is strongly advised to rely on expert judgment in order to assess the suitability and relevance of the results presented in the Atlas for a particular area.
- The assessment of extreme wave heights is based on extreme value analyses of the 43-year hindcast (1980-2022) which include recent (extreme) storm events, such as hurricane Fiona from September 2022 and hurricane Dorian from September 2019. These severe events led to a significant change on the extreme value distribution in the southwest of Newfoundland, increasing return values (or conversely, reducing return periods of extreme events). There is limited data availability during extreme hurricane events to derive definite conclusions with respect to the Atlas' accuracy during these events. Although the models seem to provide a good representation of recent hurricane events (based on comparison with limited data and anecdotal information), specific storms at certain locations seem to be underestimated. This is possibly due to limitations of the ERA5 wind fields and wave boundary conditions.
- Similarly, the storm surge model potentially underestimates the peak surge levels during hurricane events. This underestimation can be attributed to limitations in the ERA5 wind and atmospheric pressure data, as hurricanes are generally underestimated in global reanalyses like ERA5. Moreover, the storm surge model does not account for other processes contributing to rises in local water level, such as wave effects, which can be a significant contributor to the total surge levels during hurricane events. Thus, it is strongly advised to rely on expert judgement to evaluate the suitability and relevance of the hindcast results presented in the Atlas for particular sites and applications, especially in areas affected by post-tropical storms and hurricanes.
- It should be noted that future scenarios can vary broadly (see Section 3), with dozens of global and regional climate models that each present numerous future emission scenarios. Therefore, the results presented by DHI should be treated as indicative of potential future climate change scenarios and is meant primarily to offer illustrative guidance to develop regional adaptation strategies. The model results should not be directly applied in engineering design.

- Since the Global Climate Models results have not undergone bias correction, the climate projections in this Atlas should only be used for comparing them to the baseline period of the same model. It is recommended to utilize the datasets offered in the Atlas exclusively for comparative purposes, such as calculating percentage changes from the baseline and identifying overall trends. Direct manipulation of absolute numbers, such as conducting extreme value analysis or deriving flood construction levels directly from the dataset, is discouraged.
- Regular updates to the Atlas are essential to ensure its relevance and accuracy over time. As new information becomes available, it is imperative to update the climate models to reflect the latest data and scientific advancements, such as applying Regional Climate Models (RCM), once those become available. This proactive approach will enhance the Atlas' ability to provide reliable climate projections, benefiting various sectors that rely on climate data for decision-making. Looking ahead, expanding the scope by running additional climate models to create an ensemble can further strengthen the Atlas' robustness. Utilizing an ensemble approach will allow us to better understand uncertainties and improve the reliability of future climate projections, contributing significantly to our efforts in adapting to the challenges of a changing climate.

6.3 Recommendations

The Atlas offers a wide range of applications, and it is necessary to recognize its potential while appreciating its limitations. Ensuring that the Atlas is employed for its intended purposes and making careful modifications and adaptations can significantly enhance its effectiveness. Several strategies for improving the use of the Atlas and overcoming some limitations are recommended below. These strategies are both tailored for specific applications as well as universally applicable across all use cases.

Validation with Local Observations

Validating the accuracy and reliability of downscaled models, as well as the Atlas regional outputs, with local observational data, where available, or even anecdotal evidence when data is not available is important to ensure that the models reflect local conditions and can be trusted for their use cases. The comparison with measured data not only affirms the model reliability but also supports the calibration and improvement of the models to better represent the local conditions.

Maintaining a critical eye when using a regional dataset such as the Atlas is important and the comparison with local observations can provide valuable insights into potential enhancements for the application of the dataset in specific and precise contexts. Informed users could engage in a meticulous post-processing of the dataset (by applying correction factors, for instance), provided there is robust evidence from reliable local data sources indicating that such modifications will improve its usability and accuracy in the defined context.

In addition to keeping a critical eye when using model results, it is also important to be vigilant when anomalies arise in measured data. These recorded deviations from the regular behaviour might be accurate. However, having access to raw unprocessed measured data and understanding the post-processing done (removal of outliers, averaging) can improve this referential dataset and avoid misleading events to be considered in the analysis.

Understanding and Assessment of Local Processes

When using the regional Atlas to inform community level-assessments, it is recommended to evaluate the local processes at play and their potential impact on the local hydrodynamic and wave conditions. This background information is needed to support the development of local models suitable for each area, which should have a sufficient spatial resolution to resolve local bathymetry features and structures, while also incorporating additional and relevant physical processes that are not included in the Atlas, such as wave setup and river discharge.

For extreme events, it is recommended to examine specific events and locations individually, with support from local measurements, to accurately assess the potential contribution from wave setup and other local processes to the total water level.

Integration and Comparison with Other Regional Datasets

It is important to recognize the Atlas as another regional dataset, akin to others like MSC50. As such, it should be considered an additional asset for benchmarking, enhancing the accuracy when determining offshore boundary conditions for downscaling studies. Although a comparison between the Atlas and other hindcast products for selected locations is provided in Section 3.3.3, it is recommended to undertake this comparative analysis on a project-basis, evaluating the strengths and limitations of each dataset for a certain project or application and selecting which one is best employed. This also includes expanding the analysis to additional parameters, such as wave period and wave direction, which can be relevant for certain areas or purposes. An alternative approach is merging the different datasets to generate a longer time series for analysis, as discussed below.

Use of Composite Time Series

The Atlas' wave time series could be strategically combined with other hindcast datasets, such as MSC50 (available from 1954 to 2018), to forge a longer and more comprehensive composite time series, spanning from 1954 to 2022. This approach has the benefit of combining a longer historical series with more recent extreme events, such as hurricanes Dorian (2019) and Fiona (2022), which are captured by the Atlas. Using this composite dataset for Extreme Value Analysis (EVA) can significantly improve the estimation of extreme wave conditions to inform the downscaling of wave conditions to community-level studies, offering a more reliable basis for planning, assessment and design of coastal infrastructure.

Dedicated Hurricane Modelling

There is limited data availability during extreme hurricane events to derive definite conclusions with respect to the Atlas' accuracy during these events. While the wave model closely matched the data measured at the Burgeo wave buoy during hurricane Earl, it showed potential underestimations for events like hurricane Bertha when compared to MSC50. The storm surge model appears to underestimate the peak storm surge during hurricane events, based on comparison at Port aux Basques during hurricane Fiona and at St. John's during hurricane Igor. This variability highlights the models' dependence on the specific characteristics and locations of each storm, suggesting the need for additional analyses in local assessments to ensure comprehensive storm representation.

For community-level and detailed assessments in areas affected by hurricanes, the use of specialized models is recommended, such as creating parametric wind fields with tools like the MIKE Cyclone Toolbox or using high-resolution atmospheric models like the Weather Research & Forecasting Model (WRF). However, hurricane modelling is intrinsically complex and sensitive to numerous factors, from the wind field parameters to hydrodynamic and wave model calibrations. Given the scarcity of measurements during hurricanes, accurately setting these parameters is challenging and requires experience.

Engagement with Experts

Collaborating with coastal scientists, researchers, and consultants in the development of downscaled models and deeper analysis of the Atlas datasets offers significant advantages. These experts bring a wealth of knowledge and experience that can be leveraged to enhance the use of the Atlas. Their involvement ensures that the results are not only scientifically rigorous but also relevant to address the unique challenges of individual communities.

Community Engagement

Involving local stakeholders when applying the Atlas for community-level assessments is essential for ensuring that the studies reflect the local conditions accurately. This engagement facilitates the integration of local knowledge and datasets, enriching the scientific analysis. Moreover, it ensures that the outcomes of these studies are communicated in a clear, accessible manner, making them more useful and actionable for local decision-makers and community members alike. This inclusive approach promotes a shared understanding and collective action towards enhancing coastal resilience.

7 Closing

The Newfoundland & Labrador Atlas of Storm Surge and Wave Climates is a comprehensive dataset which can be leveraged to address present- and future- flood risk planning and management activities. It includes detailed maps, charts, tables, and time series data, consolidating a vast array of information to support the assessment of coastal flooding hazards.

The regional numerical models developed specifically to cover the entire province's coastline were applied to reconstruct more than 40 years of storm surge and wave conditions, as well as simulating climate change projections for a selected SSP scenario and based on two GCMs.

As a regional dataset with relatively fine resolution along the entire province's coastline, the Atlas main value is to provide boundary conditions for community-specific, high-resolution modeling. For that, it is important that users rely on expert judgement and acknowledge the Atlas limitations and recommendations. The Atlas wave and storm surge regional hindcasts covers the period from 1980 to 2022, including two of the most recent severe hurricane events (Fiona and Dorian) which grants additional value when considering Extreme Value Analysis exercises.

Moreover, the Atlas results can be leveraged as is for several purposes such as (i) high-level identification of sections of the province that are more prone to the impacts of extreme events, (ii) general public communication and education regarding the effect of extreme wave and storm surge events along the province, as well as the impacts of climate change, (iii) quick and preliminary assessment of the recurrence of new storm surge and extreme wave events, by relating them with the Atlas EVA results, and (iv) high-level planning to anticipate the need for revisiting the design conditions of coastal structures considering the future projected changes in wave and storm surge climates.

Considering the increasing recurrence of severe hurricane events observed recently in the province, it will be relevant to plan for periodic updates of the Atlas to include new extreme events in the modelled timeseries and statistical derived products. It is also important to acknowledge the inherent uncertainties in climate projections and to consider the Atlas as a first step to develop a more complete and robust climate projection product, with a larger ensemble of models and climate change scenarios.

8 References

[1] Fox-Kemper, B., H. T. Hewitt, C. Xiao, G. Aðalgeirsdóttir, S. S. Drijfhout, T. L. Edwards, N. R. Golledge, M. Hemer, R. E. Kopp, G. Krinner, A. Mix, D. Notz, S. Nowicki, I. S. Nurhati, L. Ruiz, J.-B. Sallée, A. B. A. Slangen and Y. Yu, "Ocean, Cryosphere and Sea Level Change," in *Climate Change 2021: The Physical Science Basis. Contribution of Working Group I to the Sixth Assessment Report of the Intergovernmental Panel on Climate Change*, Cambridge University Press, 2021.

[2] ECMWF, "ERA5 hourly data on single levels from 1940 to present," [Online]. Available: https://cds.climate.copernicus.eu/cdsapp#!/dataset/reanalysis-era5-single-levels?tab=overview.

[3] Y. Cheng and O. B. Andersen, "Improvement in global ocean tide model in shallow water regions," in *Poster, SV 45 (1-68)*, 2010.

[4] Canadian Ice Services, "Ice Archive," [Online]. Available: https://iceweb1.cis.ec.gc.ca/Archive/page1.xhtml?lang=en.

[5] N. B. Bernier and K. R. Thompson, "Tide-surge interaction off the east coast of Canada and northeastern United States," *Journal of Geophysical Research: Oceans,* vol. 112, no. C6, 2007.

[6] CHS, "Canadian Hydrographic Service Non-Navigational (NONNA) Bathymetric Data," [Online]. Available: https://data.chs-shc.ca/dashboard/map.

[7] "GEBCO - The General Bathymetric Chart of the Oceans," [Online]. Available: https://www.gebco.net/.

[8] DHI, "MIKE C-MAP," [Online]. Available: https://www.mikepoweredbydhi.com/products/mike-c-map.

[9] P. Camus, F. J. Mendez and R. Medina, "A hybrid efficient method to downscale wave climate to coastal areas," *Coastal Engineering,* vol. 58, no. 9, pp. 851-862, 2011.

[10] P. Camus, F. J. Mendez, R. Medina, A. Tomas and C. Izaguirre, "High resolution downscaled ocean waves (DOW) reanalysis in coastal areas," *Coastal Engineering,* pp. 72, 56-68, 2013.

[11] P. Camus, F. J. Mendez, R. Medina and A. S. Cofiño, "Analysis of clustering and selection algorithms for the study of multivariate wave climate," *Coastal Engineering,* vol. 58, no. 6, pp. 453-462, 2011.

[12] "Global Ocean Tide Model," [Online]. Available: https://www.space.dtu.dk/english/research/scientific_data_and_models/global_ocean_tide_model.

[13] DHI, "Metocean on Demand MOODv2 Web App," [Online]. Available: https://www.metocean-on-demand.com/.

[14] A. Meucci, I. R. Young, M. Hemer, C. Trenham and I. G. Watterson, "140 years of global ocean wind-wave climate derived from CMIP6 ACCESS-CM2 and EC-Earth3 GCMs: Global trends, regional changes, and future projections," *Journal of Climate,* pp. 36(6): 1605-1631, 2023.

[15] J. Bidlot, P. Janssen and S. Abdalla, "A Revised Formulation of Ocean Wave Dissipation and Its Model Impact," ECMWF Technical Memorandum No. 509, 2007.

[16] "SmartAtlantic," [Online]. Available: https://www.smartatlantic.ca/.

[17] "Ocean Networks Canada," [Online]. Available: https://www.oceannetworks.ca/.

[18] V. R. Swail, V. J. Cardone, M. Ferguson, D. J. Gummer, E. L. Harris, E. A. Orelup and A. T. & Cox, “The MSC50 wind and wave reanalysis,” in *Proceedings of the 9th International Workshop on Wave Hindcasting and Forecasting*, Victoria, BC, Canada, 2006.

[19] DFO, “MSC50 Wind and Wave Climate Hindcast,” [Online]. Available: https://www.meds-sdmm.dfo-mpo.gc.ca/isdm-gdsi/waves-vagues/MSC50-eng.html.

[20] R. M. Campos, C. B. Gramcianinov, R. de Camargo and P. L. da Silva Dias, “Assessment and calibration of ERA5 severe winds in the Atlantic Ocean using satellite data,” *Remote Sensing,* pp. 14(19), 4918, 2022.

[21] “NASA Sea Level Projection Tool,” [Online]. Available: https://sealevel.nasa.gov/ipcc-ar6-sea-level-projection-tool.

[22] “WCRP Coupled Model Intercomparison Project (Phase 6),” [Online]. Available: https://esgf-node.llnl.gov/projects/cmip6/.

[23] CSIRO, “CMIP6 global wind-wave 21st century climate projections phase 1,” [Online]. Available: https://data.csiro.au/collection/csiro:53176.

Appendix A Quality Indices

DHI Model Quality Indices (QI's)

Contents

1 Model Quality Indices..... 2

Revisions

Date	Description	Initials
2024-01-08	Version 1.3; Renamed AME to MAE.	PDG
2023-12-07	Version 1.2; Definition of PR updated.	PDG
2022-11-24	Version 1.1; Table formatting updated.	SJA
2021-08-13	Version 1.0	PDG

Nomenclature

Abbreviation	Explanation
QI	Quality Index
POT	Peak-Over-Threshold

1 Model Quality Indices

To obtain an objective and quantitative measure of how well the model data compared to the observed data, several statistical parameters, so-called quality indices (QI's), are calculated.

Prior to the comparisons, the model data is synchronised to the time stamps of the observations so that both time series had equal length and overlapping time stamps. For each valid observation, measured at time t, the corresponding model value is found using linear interpolation between the model time steps before and after t. Only observed values that had model values within ± the representative sampling or averaging period of the observations are included (e.g., for 10-min observed wind speeds measured every 10 min compared to modelled values every hour, only the observed value every hour is included in the comparison).

The comparisons of the synchronised observed and modelled data are illustrated in (some of) the following figures:

- Time series plot including general statistics
- Scatter plot including quantiles, QQ-fit and QI's (density-colored dots)
- Histogram of occurrence vs. magnitude or direction
- Histogram of bias vs. magnitude
- Histogram of bias vs. direction
- Dual rose plot (overlapping roses)
- Peak event plot including joint (coinciding) individual peaks

The quality indices are described below, and their definitions are listed in Table 1.1. Most of the quality indices are based on the entire dataset, and hence the quality indices should be considered averaged measures and may not be representative of the accuracy during rare conditions.

The MEAN represents the mean of modelled data, while the bias is the mean difference between the modelled and observed data. MAE is the mean of the absolute difference, and RMSE is the root-mean-square of the difference. The MEAN, BIAS, MAE and RMSE are given as absolute values and relative to the average of the observed data in percent in the scatter plot.

The scatter index (SI) is a non-dimensional measure of the difference calculated as the unbiased root-mean-square difference relative to the mean absolute value of the observations. In open water, an SI below 0.2 is usually considered a small difference (excellent agreement) for significant wave heights. In confined areas or during calm conditions, where mean significant wave heights are generally lower, a slightly higher SI may be acceptable (the definition of SI implies that it is negatively biased (lower) for time series with high mean values compared to time series with lower mean values (and same scatter/spreading), although it is normalised).

EV is the explained variation and measures the proportion [0 - 1] to which the model accounts for the variation (dispersion) of the observations.

The correlation coefficient (CC) is a non-dimensional measure reflecting the degree to which the variation of the first variable is reflected linearly in the variation of the second variable. A value close to 0 indicates very limited or no (linear) correlation between the two data sets, while a value close to 1 indicates a very high or perfect correlation. Typically, a CC above 0.9 is considered a high correlation (good agreement) for wave heights. It is noted that CC is 1 (or -1) for any two fully linearly correlated variables, even if they are not 1:1. However, the slope and intercept of the linear relation may be different from 1 and 0, respectively, despite CC of 1 (or -1).

The QQ line slope and intercept are found from a linear fit to the data quantiles in a least-square sense. The lower and uppermost quantiles are not included on the fit. A regression line slope different from 1 may indicate a trend in the difference.

The peak ratio (PR) is the average ratio of the N_{peak} highest joint (coinciding) model and measured events. The peaks are found individually for each dataset through a declustering technique, such as fx two (2) Average-Annual-Peaks (AAP) and an inter-event time (IET) of 36 hours. Subsequently, the joint peaks are found by identifying events within half the IET (ie 18 hours) of each other. A general/average underestimation of the modelled peaks results in a PR < 1, while an overestimation results in a PR > 1.

An example of a peak plot is shown in Figure 1.1. 'X' represents the observed peaks (x-axis), while 'Y' represents the modelled peaks (y-axis), based on the POT methodology, both represented by circles ('o') in the plot. The joint (coinciding) peaks, defined as any X and Y peaks within ±36 hours[1] of each other (i.e., less than or equal to the number of individual peaks), are represented by crosses ('x'). Hence, the joint peaks ('x') overlap with the individual peaks ('o') only if they occur at the same time exactly. Otherwise, the joint peaks ('x') represent an additional point in the plot, which may be associated with the observed and modelled individual peaks ('o') by searching in the respective X and Y-axis directions, see example with red lines in Figure 1.1. It is seen that the 'X' peaks are often underneath the 1:1 line, while the 'Y' peaks are often above the 1:1 line.

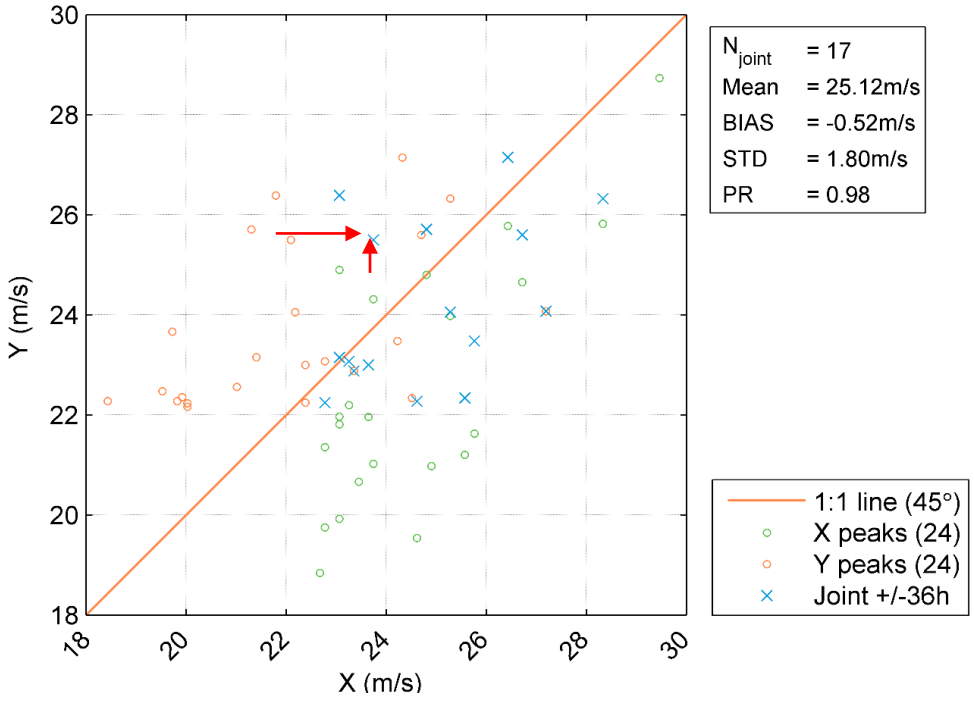


Figure 1.1 Example of peak event plot (wind speed)

[1] 36 hours is chosen arbitrarily as representative of an average storm duration. Often the measured and modelled peaks are within 1-2 hours of each other.

Table 1.1 Definitions of model quality indices (X = Observation, Y = Model)

Abbreviation	Description	Definition
N	Number of data (synchronised)	–
MEAN	Mean of Y data Mean of X data	$\frac{1}{N}\sum_{i=1}^{N} Y_i \equiv \overline{Y}$, $\frac{1}{N}\sum_{i=1}^{N} X_i \equiv \overline{X}$
STD	Standard deviation of Y data Standard deviation of X data	$\sqrt{\frac{1}{N-1}\sum_{i=1}^{N}(Y-\overline{Y})^2}$, $\sqrt{\frac{1}{N-1}\sum_{i=1}^{N}(X-\overline{X})^2}$
BIAS	Mean difference	$\frac{1}{N}\sum_{i=1}^{N}(Y-X)_i = \overline{Y}-\overline{X}$
MAE	Mean absolute difference	$\frac{1}{N}\sum_{i=1}^{N}(\lvert Y-X\rvert)_i$
RMSE	Root-mean-square difference	$\sqrt{\frac{1}{N}\sum_{i=1}^{N}(Y-X)_i^{\,2}}$
SI	Scatter index (unbiased)	$\frac{\sqrt{\frac{1}{N}\sum_{i=1}^{N}(Y-X-\mathrm{BIAS})_i^{\,2}}}{\frac{1}{N}\sum_{i=1}^{N}\lvert X_i\rvert}$
EV	Explained variance	$\frac{\sum_{i=1}^{N}(X_i-\overline{X})^2-\sum_{i=1}^{N}[(X_i-\overline{X})-(Y_i-\overline{Y})]^2}{\sum_{i=1}^{N}(X_i-\overline{X})^2}$
CC	Correlation coefficient	$\frac{\sum_{i=1}^{N}(X_i-\overline{X})(Y_i-\overline{Y})}{\sqrt{\sum_{i=1}^{N}(X_i-\overline{X})^2\sum_{i=1}^{N}(Y_i-\overline{Y})^2}}$
QQ	Quantile-Quantile (line slope and intercept)	Linear least square fit to quantiles
PR	Peak ratio (of N_{peak} highest – joint – events)	$PR = \frac{\sum_{i=1}^{N_{peak}}\frac{Y_i}{X_i}}{N_{peak}}$

Appendix B EVA Methodology

DHI Extreme Value Analysis (EVA)

Contents

1 DHI Extreme Value Analysis (EVA) 2

1.1 Summary of Approach 2
1.2 Long-Term Distributions 3
1.3 Individual Wave and Crest Height 3
1.4 Subset Extremes 5
1.5 Uncertainty Assessment 6
1.6 Confidence Limits 7
1.7 Joint Probability Analyses (JPA) 7
1.8 References 9

Revisions

Date	Description	Initials
2021-08-13	Version 1.0	PDG

Nomenclature

Abbreviation	Explanation
C	Individual crest level [m]
C_{max}	Maximum (highest) individual crest level [m]
C_{mp}	Most probable maximum individual crest level in a storm event [m]
H_{m0}	Zeroth moment significant wave height [m]
H	Individual (trough-crest) wave height [m]
H_{max}	Maximum (highest) individual (trough-crest) wave height [m]
H_{mp}	Most probable maximum individual wave height in a storm event [m]
T_R	Return period [years]

1 DHI Extreme Value Analysis (EVA)

This document describes the DHI Extreme Value Analysis (EVA).

1.1 Summary of Approach

Extreme values with conditioned long return periods are estimated by fitting a probability distribution to historical data. Several distributions, data selection and fitting techniques are available for estimation of extremes, and the estimated extremes are often rather sensitive to the choice of method. However, it is not possible to choose a preferred method only on its superior theoretical support or widespread acceptance within the industry. Hence, it is common practice to test several approaches and make the final decision based on goodness of fit.

The typical extreme value analyses involved the following steps:

1. Extraction of independent identically-distributed events by requiring that events are separated by at least 36 hours (or similar), and that the value between events had dropped to below 70% (or similar) of the minor of two consecutive events. The extraction is conducted individually for omni and directional/seasonal subsets respectively.
2. Fitting of extreme value distribution to the extracted events, individually for omni and directional/seasonal subsets. Distribution parameters are estimated either by maximum likelihood or least-square methods. The following analysis approaches are used (see Section 1.2 for details):
   - Fitting the Gumbel distribution to annual maxima.
   - Fitting a distribution to all events above a certain threshold (the Peak-Over-Threshold method). The distribution type can be exponential, truncated Weibull or 2-parameter Weibull to excess.
3. Constraining of subseries to ensure consistency with the omni/all-year distribution; see Section 1.4 for details.
4. Bootstrapping to estimate the uncertainty due to sampling error; see Section 1.6 for details.
5. Values of other parameters conditioned on extremes of one variable are estimated using the methodology proposed in [1] (Heffernan & Tawn).

Figure 1.1 shows an example of EVA based on 38 years of hindcast data and a Gumbel distribution fitted to the annual maxima using max. likelihood.

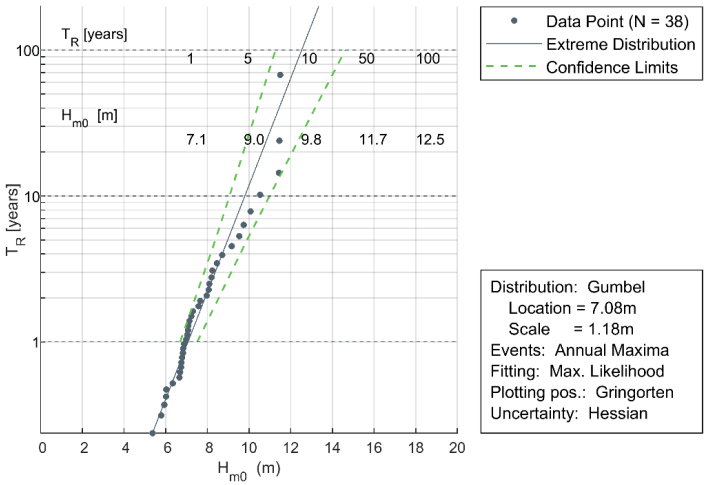


Figure 1.1 Example of traditional extreme value analysis of H_{m0}
A Gumbel distribution fitted to the annual maxima using maximum likelihood.

1.2 Long-Term Distributions

The following probability distributions are often used in connection with extreme value estimation:
2-parameter Weibull distribution
Truncated Weibull distribution
Exponential distribution

- Gumbel distribution

The 2-parameter Weibull distribution is given by:

$$P(X < x) = 1 - \exp\left(-\left(\frac{x}{\beta}\right)^{\alpha}\right) \quad (1.1)$$

with distribution parameters α (shape) and β (scale). The 2-parameter Weibull distribution used in connection with Peak-Over-Threshold (POT) analysis is fitted to the excess of data above the threshold, i.e., the threshold value is subtracted from data prior to fitting.

The 2-parameter *truncated* Weibull distribution is given by:

$$P(X < x) = 1 - \frac{1}{P_0}\exp\left(-\left(\frac{x}{\beta}\right)^{\alpha}\right) \quad (1.2)$$

with distribution parameters α (shape) and β (scale) and the exceedance probability, P_0, at the threshold level, γ, given by:

$$P_0 = \exp\left(-\left(\frac{\gamma}{\beta}\right)^{\alpha}\right) \quad (1.3)$$

The 2-parameter truncated Weibull distribution is used in connection with Peak-Over-Threshold analysis, and as opposed to the non-truncated 2-p Weibull, it is fitted directly to data, i.e., the threshold value is **not** subtracted from data prior to fitting.

The exponential distribution is given by:

$$P(X < x) = 1 - \exp\left(-\left(\frac{x-\mu}{\beta}\right)\right), \quad x \geq \mu \quad (1.4)$$

with distribution parameters β (scale) and μ (location). Finally, the Gumbel distribution is given by:

$$P(X < x) = \exp\left(-\exp\left(\frac{\mu - x}{\beta}\right)\right) \quad (1.5)$$

with distribution parameters β (scale) and μ (location).

1.3 Individual Wave and Crest Height

Short-Term Distributions

The short-term distributions of individual wave heights and crests conditional on H_{m0} are assumed to follow the distributions proposed by Forristall, (Forristall G. Z., 1978) and (Forristall G. Z., 2000). The Forristall wave height distribution is based on Gulf of Mexico measurements, but experience from the North Sea has shown that these distributions may have a more general applicability. The Forristall wave and crest height distributions are given by:

$$P(X > x \mid H_{m0}) = \exp\left(-\left(\frac{x}{\alpha H_{m0}}\right)^{\beta}\right) \quad (1.6)$$

where the distribution parameters, α and β, are as follows:

Forristall wave height: α = 0.681 β = 2.126

Forristall crest height (3D): $\alpha = 0.3536 + 0.2568 \cdot S_1 + 0.0800 \cdot Ur$

$\beta = 2 - 1.7912 \cdot S_1 - 0.5302 \cdot Ur + 0.284 \cdot Ur^2$

$$S_1 = \frac{2\pi}{g}\frac{H_{m0}}{T_{01}^2} \quad \text{and} \quad U_r = \frac{H \cdot L^2}{d^3}$$

For this type of distribution, the distribution of the extremes of a given number of events, N, (waves or crests) converges towards the Gumbel distribution conditional on the most probable value of the extreme event, H_{mp} (or C_{mp} for crests):

$$P(h_{\max} \mid H_{mp}) = \exp\left(-\exp\left(-\ln N\left(\left(\frac{h_{\max}}{H_{mp}}\right)^{\beta} - 1\right)\right)\right) \qquad (1.7)$$

1.3.1 Individual Waves (Modes)

The extreme individual wave and crest heights are derived using the storm mode approach, (Tromans, P.S. and Vanderschuren, L., 1995). The storm modes, or most probable values of the maximum wave or crest in the storm (H_{mp} or C_{mp}), are obtained by integrating the short-term distribution of wave heights conditional on H_{m0} over the entire number of sea states making up the storm. In practice, this is done by following these steps:

1. Storms are identified by peak extraction from the time series of significant wave height. Individual storms are taken as portions of the time series with H_{m0} above 0.7 times the storm peak, H_{m0}.
2. The wave (or crest) height distribution is calculated for each sea state above the threshold in each individual storm. The short-term distribution of H (or C) conditional on H_{m0}, $P(h|H_{m0})$, is assumed to follow the empirical distributions by Forristall (see Section 1.3). The wave height probability distribution is then given by the following product over the n sea states making up the storm:

$$P(H_{\max} < h) = \prod_{j=1}^{n_{seastates}} P(h \mid H_{m0,j})^{N_{waves,j}} \qquad (1.8)$$

with the number of waves in each sea state, N_{waves}, being estimated by deriving the mean zero-crossing period of the sea state. The most probable maximum wave height (or mode), H_{mp}, of the storm is given by:

$$P(H_{\max} < h) = \frac{1}{e} \qquad (1.9)$$

This produces a database of historical storms each characterised by its most probable maximum individual wave height which is used for further extreme value analysis.

1.3.2 Convolution of Short-Term Variability with Long-Term Storm Density

The long-term distribution of individual waves and crests is found by convolution of the long-term distribution of the modes (subscript $_{mp}$ for most probable value) with the distribution of the maximum conditional on the mode given by:

$$P(H_{\max}) = \int_0^\infty P(h_{\max} \mid H_{mp}) \cdot p(H_{mp}) dH_{mp}$$
$$= \int_0^\infty \exp\left(-\exp\left(-\ln N \left(\left(\frac{h}{H_{mp}} \right)^\beta - 1 \right) \right) \right) \cdot p(H_{mp}) dH_{mp} \quad (1.10)$$

The value of N, which goes into this equation, is determined by defining equivalent storm properties for each individual storm. The equivalent storms have constant H_{m0} and a duration such that their probability density function of H_{max} or C_{max} matches that of the actual storm. The density functions of the maximum wave in the equivalent storms are given by:

$$p(H_{\max} \mid H_{m0,eq}, N_{eq}) = \frac{d}{dH} \left[1 - \exp\left(-\left(\frac{H_{\max}}{\alpha \cdot H_{m0,eq}} \right)^\beta \right) \right]^{N_{eq}} \quad (1.11)$$

The β parameter in eq. (1.10) comes from the short-term distribution of individual crests, eq. ((1.6), and is a function of wave height and wave period. Based on previous studies, it has been assessed that the maximum crest heights are not sensitive to β_C for a constant value of 1.88 and hence, it is decided to apply β_C = 1.88. The number of waves in a storm, N, was conservatively calculated from a linear fit to the modes minus one standard deviation.

1.4 Subset Extremes

Estimates of subset (e.g., directional, and monthly) extremes are required for several parameters. To establish these extremes, it is common practice to fit extreme value distributions to data sampled from the population (i.e., the model database) that fulfils the specific requirement e.g., to direction, i.e., the extremes from each direction are extracted and distributions fitted to each set of directional data in turn. By sampling an often relatively small number of values from the data set, each of these directional distributions is subject to uncertainty due to sampling error. This will often lead to the directional distributions being inconsistent with the omnidirectional distribution fitted to the maxima of the entire (omnidirectional) data set. Consistency between directional and omnidirectional distributions is ensured by requiring that the product of the n directional annual non-exceedance probabilities equals the omnidirectional, i.e.:

$$\prod_{i=1}^{n} F_i(x, \hat{\theta}_i)^{N_i} = F_{omni}(x, \hat{\theta}_{omni})^{N_{omni}} \quad (1.12)$$

where N_i is the number of sea states or events for the i'th direction and $\hat{\theta}_i$, the estimated distribution parameter. This is ensured by estimating the distribution parameters for the individual distributions and then minimising the deviation:

$$\delta = \sum_{x_j} \left[-\ln\left(-N_{omni} \ln F_{omni}(x, \hat{\theta}_{omni}) \right) + \ln\left(-\sum_{i=1}^{n} N_i \ln F_i(x_j, \hat{\theta}_i) \right) \right]^2 \quad (1.13)$$

Here x_j are extreme values of the parameter for which the optimisation is carried out, i.e., the product of the directional non-exceedance probabilities is forced to match the omnidirectional for these values of the parameter in question.

The directional extremes presented in this report are given without scaling, that is, a T_{yr} event from direction i will be exceeded once every T years on the average. The same applies for monthly extremes.

A T_{yr} monthly event corresponds to the event that is exceeded once (in that month) every T years, which is the same as saying that it is exceeded once every *T*/12 years (on average) of the climate for that month.

1.4.1 Optimised Directional Extremes

The directional extremes are derived from fits to each subseries data set meaning that a T_R year event from each direction will be exceeded once every T_R years on average. Having e.g., 12 directions, this means that **one** of the directions will be exceeded once every T_R/12 years on average. A 100-year event would thus be exceeded once every 100/12 = 8⅓ years (on average) from **one** of the directions.

For design application, it is often required that the summed (overall) return period (probability) is T_R years. A simple way of fulfilling this would be to take the return value corresponding to the return period T_R times the number of directions, i.e., in this case the 12x100 = 1200-year event for each direction. However, this is often not optimal since it may lead to very high estimates for the strong sectors, while the weak sectors may still be insignificant.

Alternatively, an optimised set of directional extreme values may be produced for design purpose in addition to the individual values of directional extremes described above. The optimised values are derived by increasing (scaling) the individual T_R values of the directions to obtain a summed (overall) probability of T_R years while ensuring that the extreme values of the strong sector(s) become as close to the overall extreme value as possible. In practice, this is done by increasing the T_R of the weak directions more than that of the strong sectors but ensuring that the sum of the inverse directional T_R's equals the inverse of the targeted return period, i.e.:

$$\sum_{i=1}^{n} \frac{1}{T_{R,i}} = \frac{1}{T_{R,\text{omni}}} \qquad (1.14)$$

where n is the number of directional sectors and $T_{R,omni}$ is the targeted overall return period.

1.5 Uncertainty Assessment

The extreme values are estimated quantities and therefore all associated with uncertainty. The uncertainty arises from several sources:

Measurement/Model Uncertainty

The contents of the database for the extreme value analysis are associated with uncertainty. This type of uncertainty is preferably mitigated at the source – e.g., by correction of biased model data and removal of obvious outliers in data series. The model uncertainty can be quantified if simultaneous good quality measurements are available for a reasonably long overlapping period.

True Extreme Value Distribution is Unknown

The distribution of extremes is theoretically unknown for levels above the levels contained in the extreme value database. There is no justification for the assumption that a parametric extreme value distribution fitted to observed/modelled data can be extrapolated beyond the observed levels. However, it is common practice to do so, and this obviously is a source of uncertainty in the derived extreme value estimates. This uncertainty, increasing with decreasing occurrence probability of the event in question, is not quantifiable but the metocean expert may minimise it by using experience and knowledge when deciding on an appropriate extreme value analysis approach. Proper inclusion of other information than direct measurements and model results may also help to minimise this type of uncertainty.

Uncertainty Due to Sampling Error

The number of observed/modelled extreme events is limited. This gives rise to sampling error which can be quantified by statistical methods such as Monte Carlo simulations or bootstrap resampling. The results of such an analysis are termed the confidence limits. The confidence limits (see Section 1.6) should **not** be mistaken for the total uncertainty in the extreme value estimate.

Settings of the Analysis (Judgement)

Any EVA involves the need to define the various settings of the analysis (threshold, distribution, and fitting method), which introduces subjectivity to the analysis. The sensitivity of these settings can be assessed by comparing the resulting extreme values, and the goodness of fit can, to some extent, be objectively assessed by statistical measures. However, standard practice typically includes manual inspection of the fitted distributions. Hence, the final settings, and thus results, relies on the experience and preference of the metocean expert conducting the analysis ('engineering judgement'). The tail of the distributions (the values of long the return periods) can be particularly sensitive to the settings of the analysis.

1.6 Confidence Limits

The confidence limits of extreme estimates are established from a bootstrap analysis or a Monte Carlo simulation.

The bootstrap analysis estimates the uncertainty due to sampling error. The bootstrap consists of the following steps:

1. Construct a new set of extreme events by sampling randomly with replacement from the original data set of extremes
2. Carry out an extreme value analysis on the new set to estimate T-year events

An empirical distribution of the T-year event is obtained by looping steps 1 and 2 many times. The percentiles are read from the resulting distribution.

In the Monte Carlo simulation, the uncertainty is estimated by randomly generating many samples that have the same statistical distribution as the observed sample.

The Monte Carlo simulation can be summarised in the following steps:

1. Randomly generating a sample consisting of N data points, using the estimated parameters of the original distribution. If the event selection is based on a fixed number of events, N is set equal to the size of original data set of extremes. If the event selection is based on a fixed threshold, the sample size N is assumed to be Poisson-distributed.
2. From the generated sample, the parameters of the distribution are estimated, and the T-year return estimates are established.

Steps 1 and 2 are looped numerous times, whereby an empirical distribution of the T-year event is obtained. The quartiles are read from the resulting distribution.

1.7 Joint Probability Analyses (JPA)

Values of other parameters conditioned on extremes of one variable are estimated using the methodology proposed in [1] (Heffernan & Tawn). This method consists in modelling the marginal distribution of each variable separately. The variables are transformed from physical space, X, to standard Gumbel space by the relationship:

$$Y = \mathrm{LN}\left(-\mathrm{LN}\left(F\left(X,\hat{\theta}\right)\right)\right) \qquad (1.15)$$

where $\mathrm{F}\left(\mathrm{X},\hat{\theta}\right)$ denotes the distribution function of the variable, X, with estimated parameters, $\hat{\theta}$. No restriction is given on the marginal model of the variables. A combination of the empirical distribution for the bulk of events and a parametric extreme value distribution function fitted to the extreme tail of data was adopted here. For parameters which may have both a positive and a negative extreme such as the water level conditioned on wave height, both the positive and the negative extreme tail are modelled parametrically.

The dependence structure of the two variables is modelled in standard Gumbel distribution space, conditioning one variable by the other. The model takes the form:

$$(Y_2|Y_1 = y_1) = ay_1 + y_1^b Z \qquad (1.16)$$

with Y_1 being the conditioning variable and Y_2 the conditioned. The residual, Z, is assumed to converge to a normal distribution, G, with increasing y_1. The parameters, $\hat{a}$ and $\hat{b}$, are found from regression and the parameters, $\hat{\mu}$ and $\hat{\sigma}$, of the normal distribution, G, estimated from the residuals, Z:

$$Z = \frac{y_2 - a \cdot y_1}{y_1^b} \qquad (1.17)$$

Figure 1.2 shows an example of the modelled dependence structure for H_{m0} and water level in standard Gumbel space. Figure 1.3 shows the same in physical space. The model is clearly capable of describing the positive association between wave heights and water level for this condition and appears also to capture the relatively large spreading.

The applied joint probability model is event-based. This means that independent events of the conditioning parameter are extracted from the model data. The combined inter-event time and inter-event level criterion described in Section 1.1 is applied to isolate independent events of the conditioning parameter. The conditioned parameter is extracted from the model time series at the point in time of the peak of the conditioning parameter. Time averaging of the conditioned parameter is often carried out prior to data extraction to reduce the influence of phases in the analysis (the fact that the water level may not peak at the same time as the peak wave height for instance).

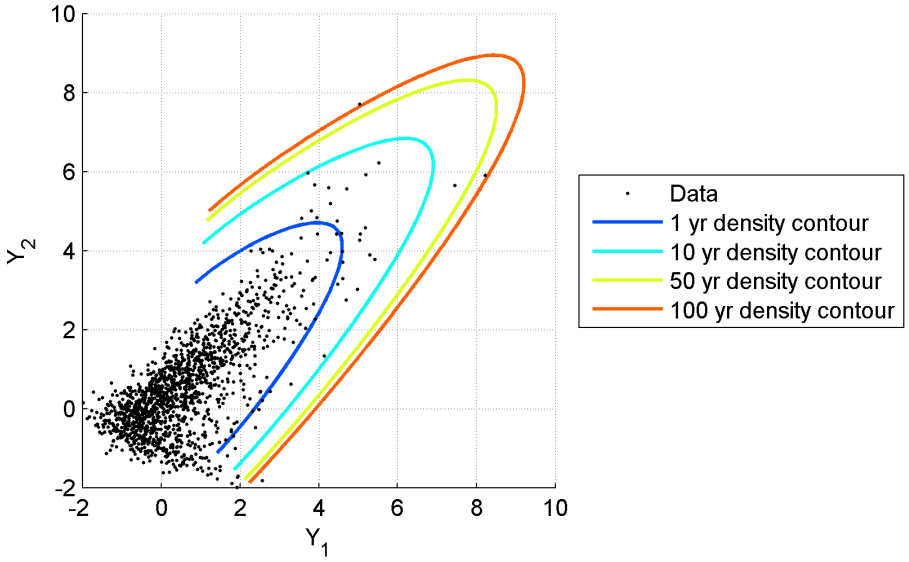


Figure 1.2 Dependence structure of H_{m0} and water level transformed into standard Gumbel space

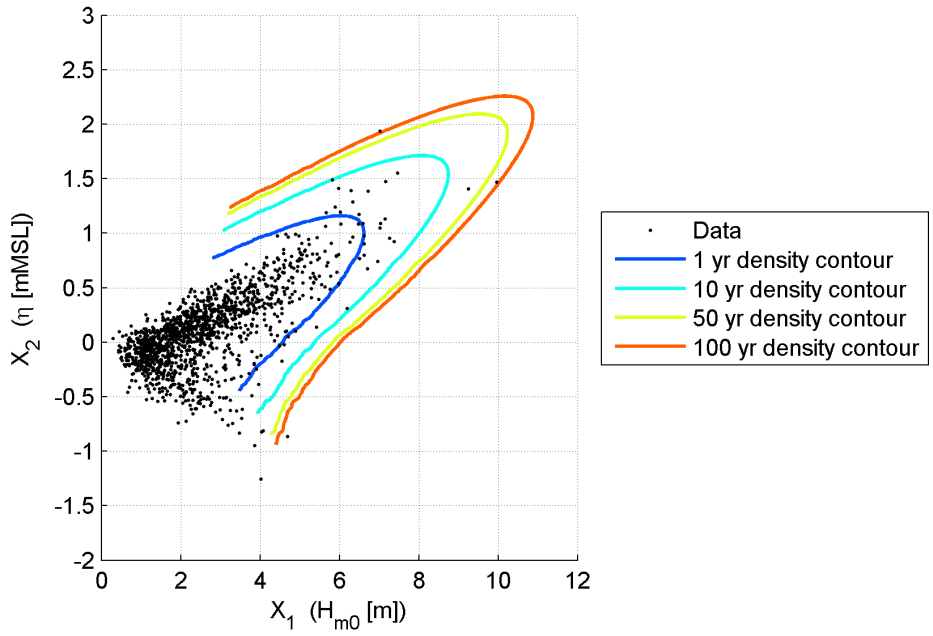


Figure 1.3 Dependence structure of H_{m0} and water level in physical space

1.8 References

[1] J. E. Heffernan and J. A. Tawn, “A conditional approach for multivariate extreme values,” *Journal of the Royal Statistical Society. Series B,* vol. 66, no. 3, pp. 497-546, 2004.

Appendix C EVA Results

Appendix C.1 - Water Level Analysis

EVA-001

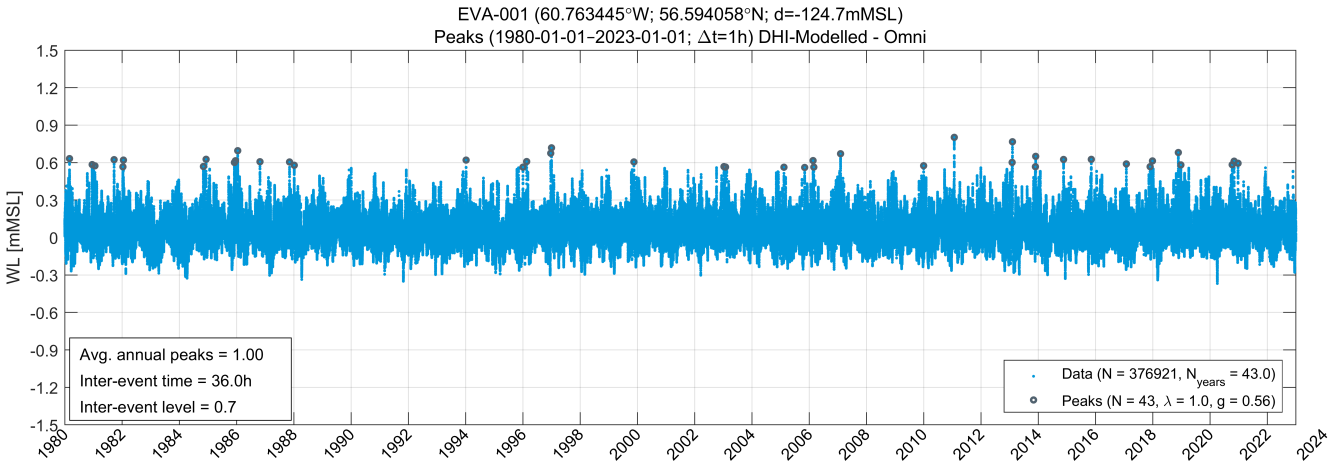


Figure C-1: Time series of water level residual at EVA-001 and selected peaks.

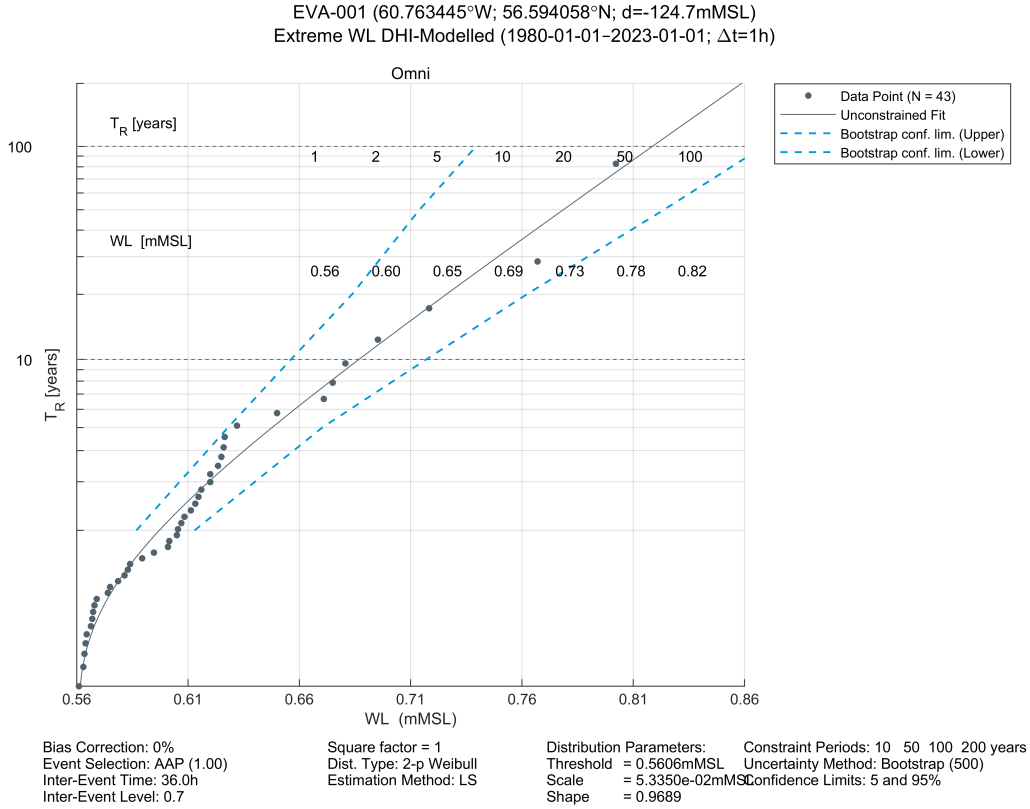


Figure C-2: Extreme value distribution fit at EVA-001.

EVA-002

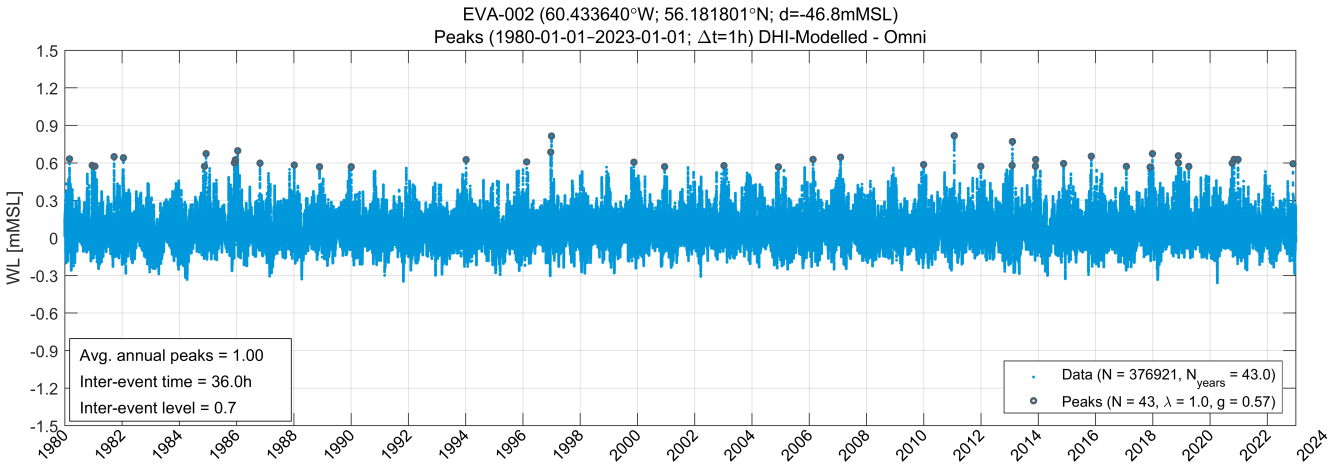


Figure C-3: Time series of water level residual at EVA-002 and selected peaks.

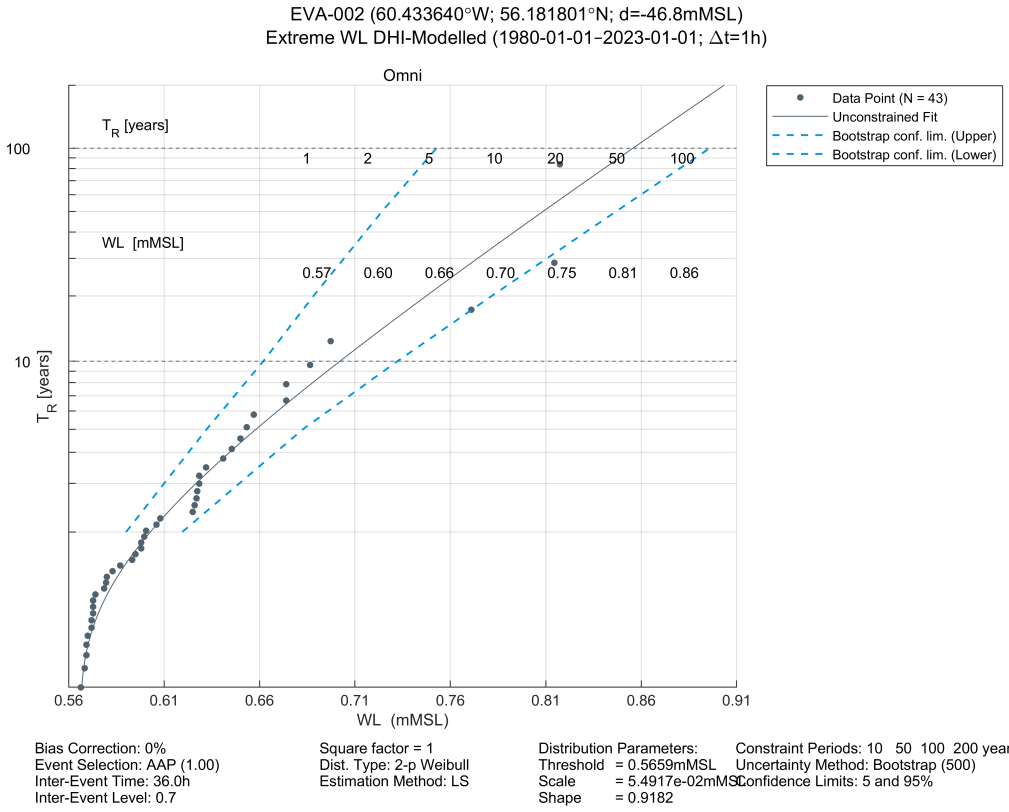


Figure C-4: Extreme value distribution fit at EVA-002.

EVA-003

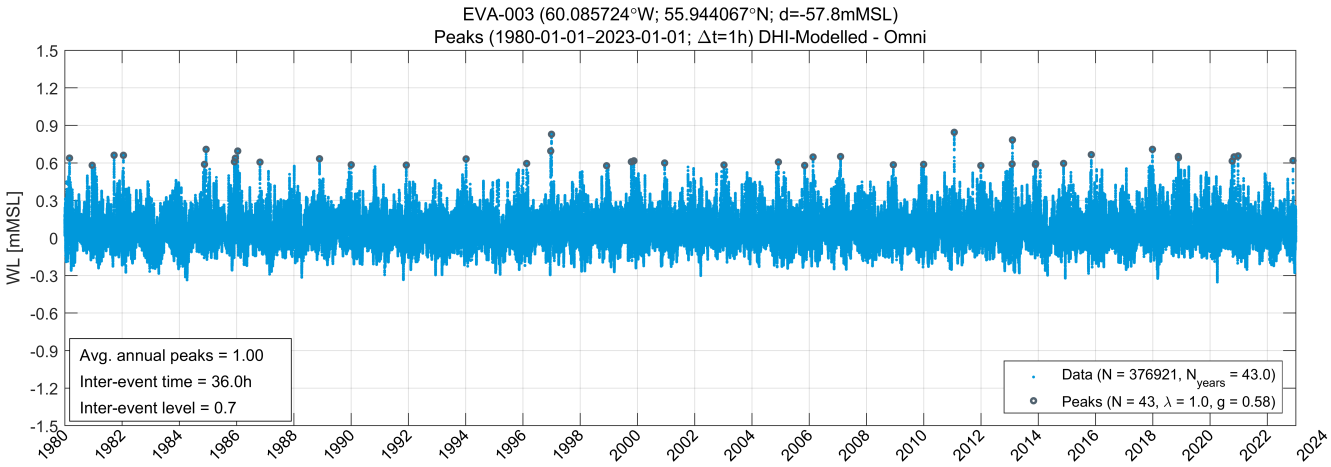


Figure C-5: Time series of water level residual at EVA-003 and selected peaks.

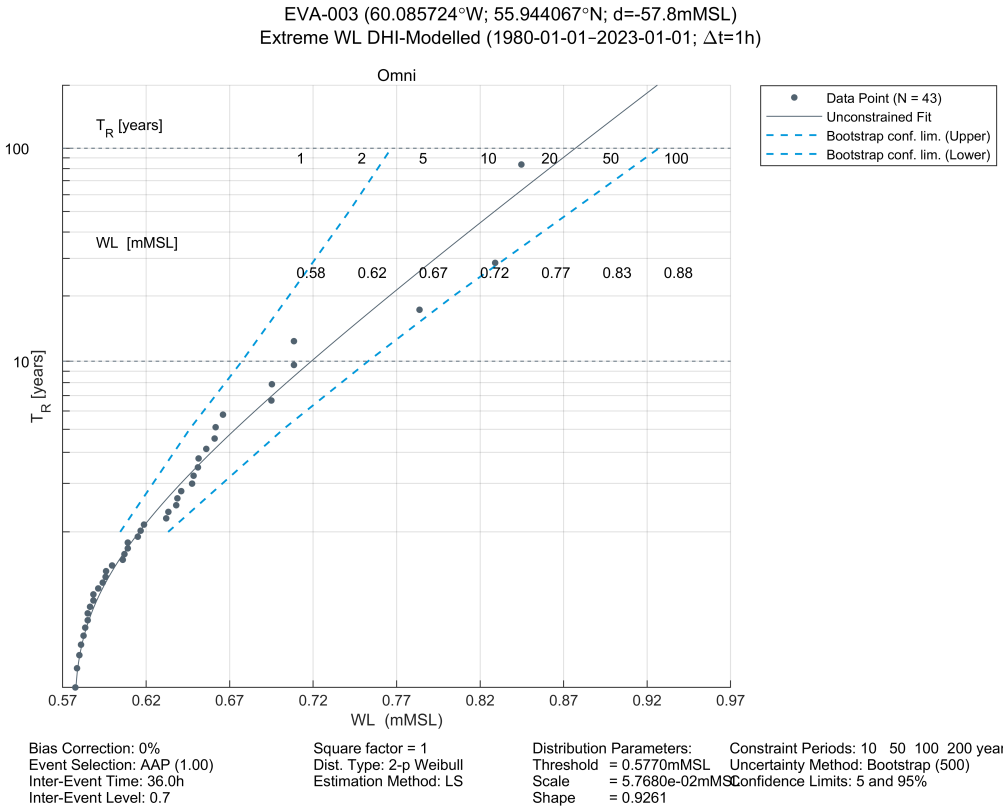


Figure C-6: Extreme value distribution fit at EVA-003.

EVA-004

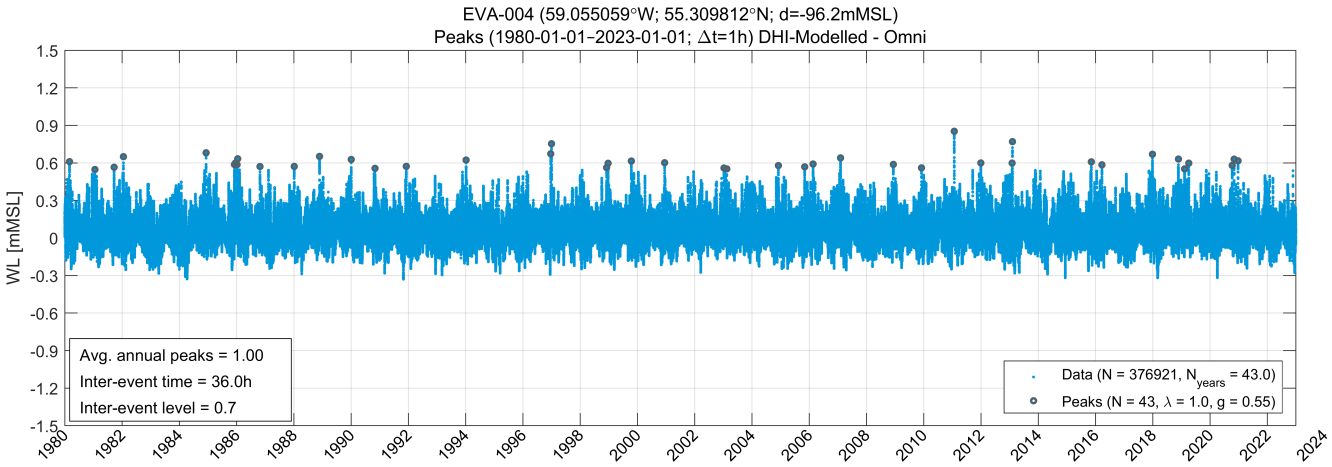


Figure C-7: Time series of water level residual at EVA-004 and selected peaks.

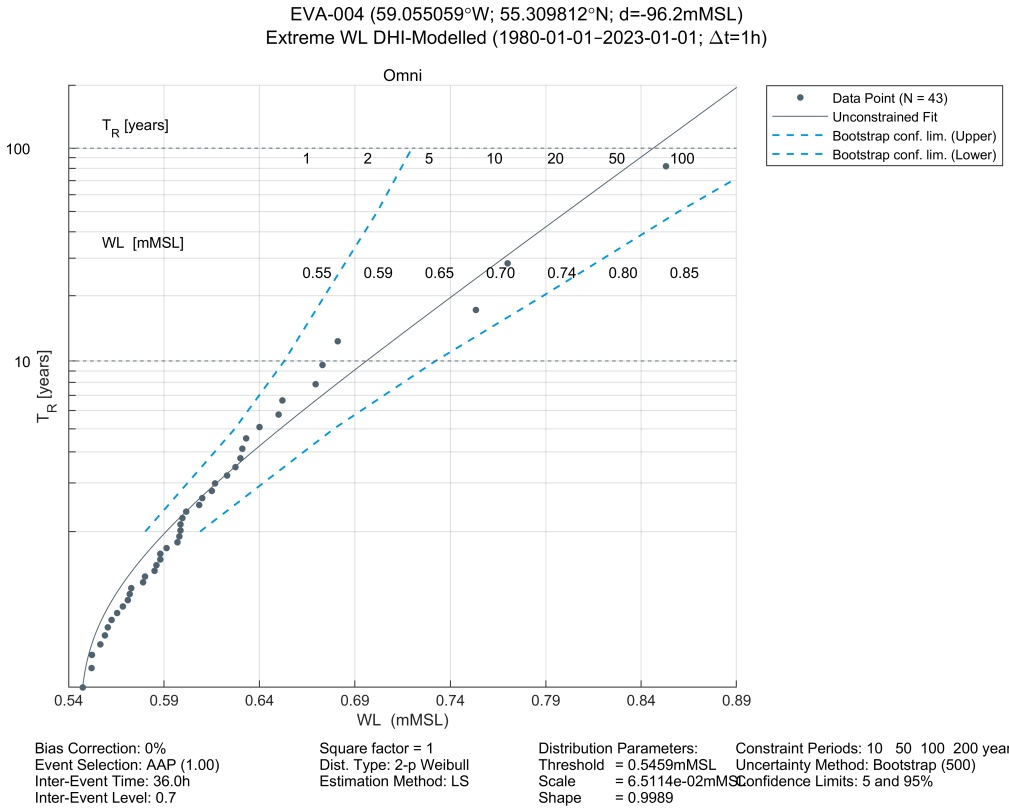


Figure C-8: Extreme value distribution fit at EVA-004.

EVA-005

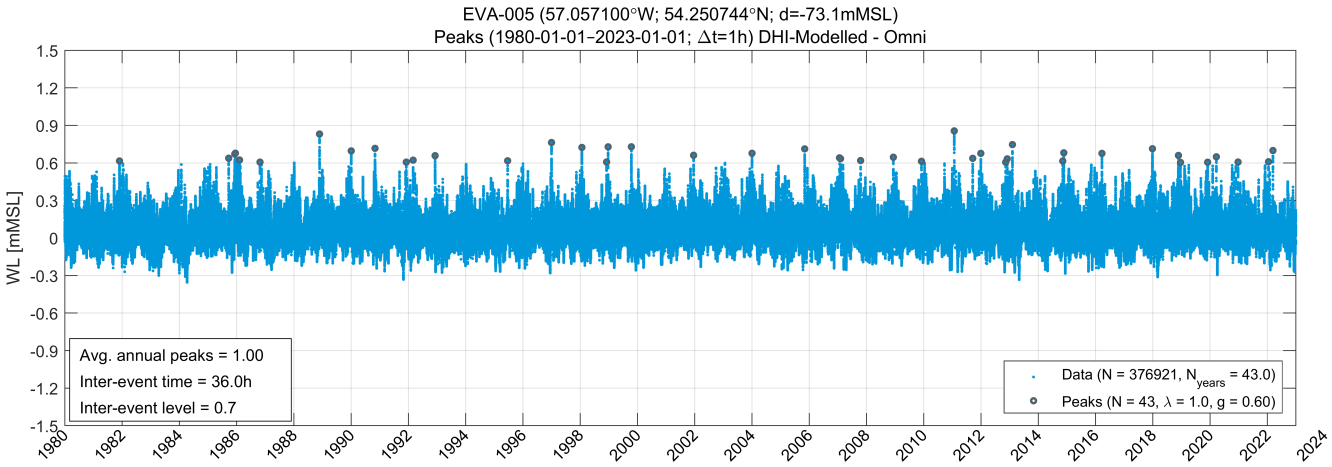


Figure C-9: Time series of water level residual at EVA-005 and selected peaks.

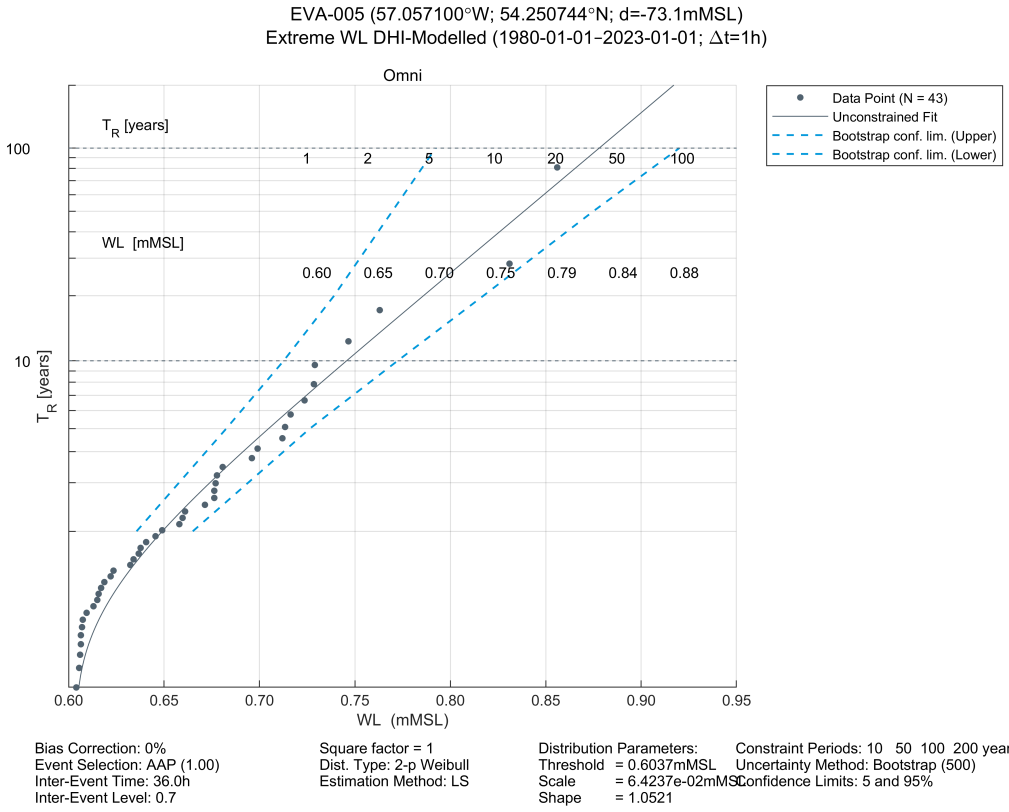


Figure C-10: Extreme value distribution fit at EVA-005.

EVA-006

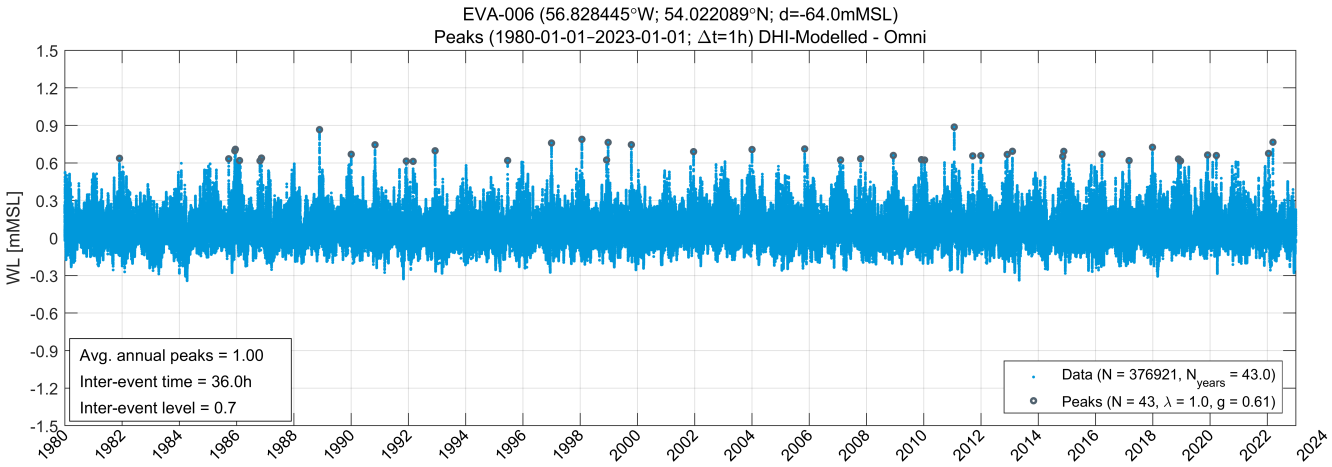


Figure C-11: Time series of water level residual at EVA-006 and selected peaks.

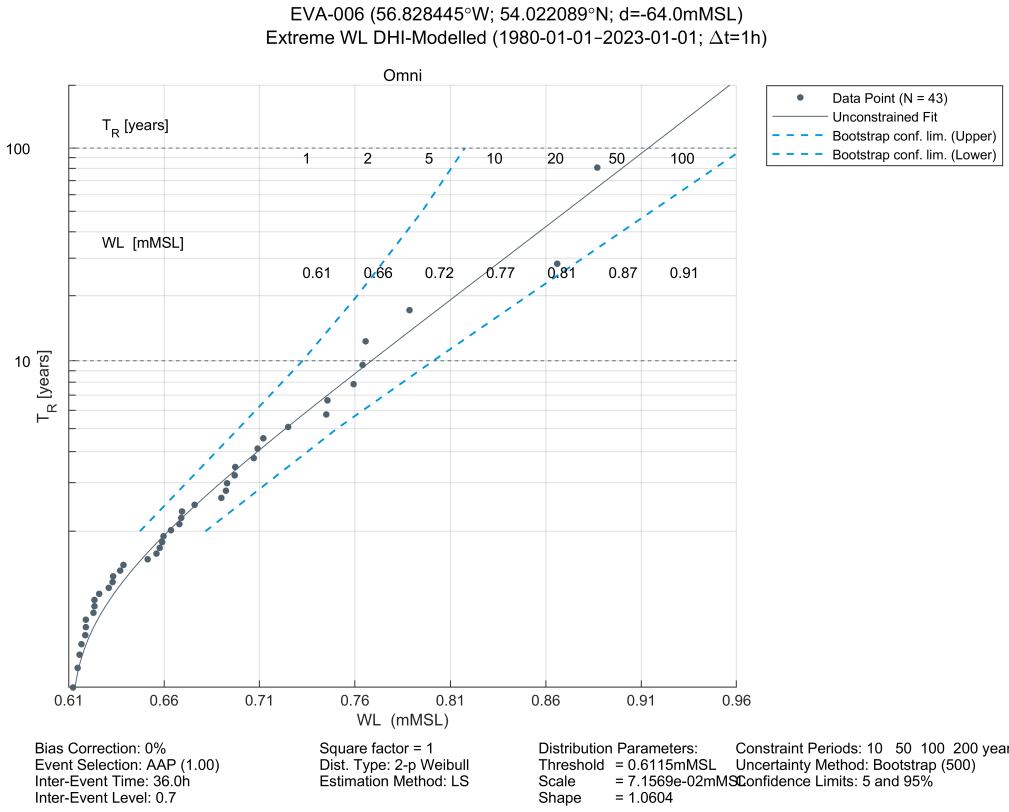


Figure C-12: Extreme value distribution fit at EVA-006.

EVA-007

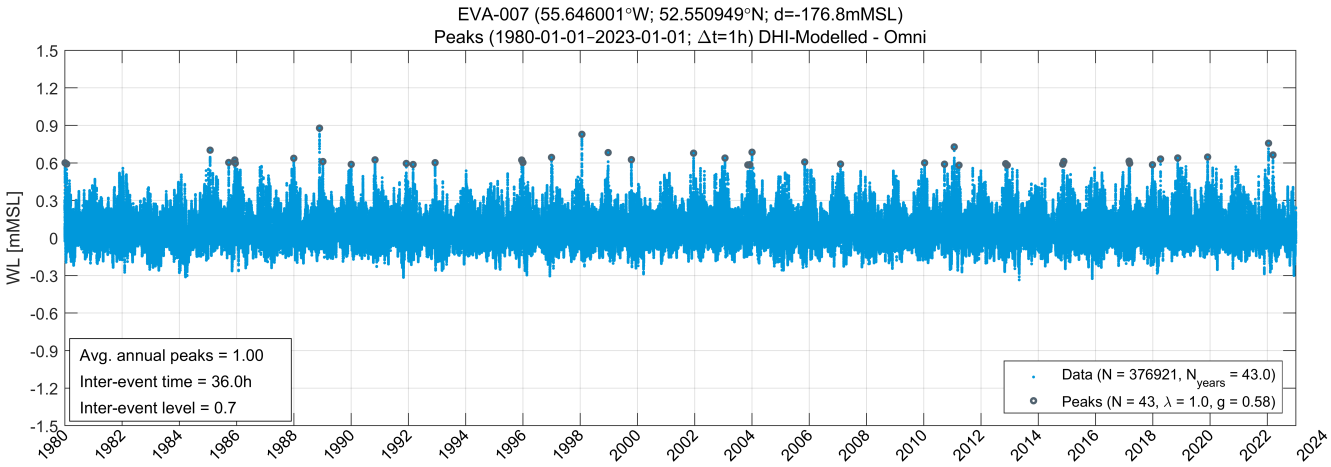


Figure C-13: Time series of water level residual at EVA-007 and selected peaks.

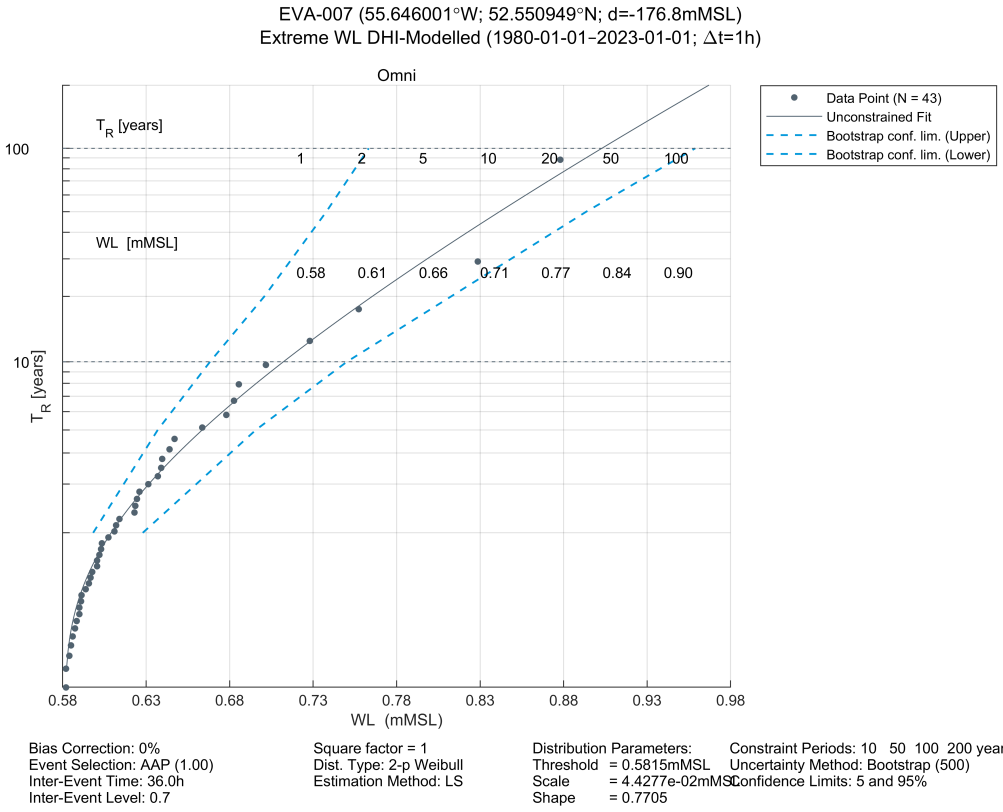


Figure C-14: Extreme value distribution fit at EVA-007.

EVA-008

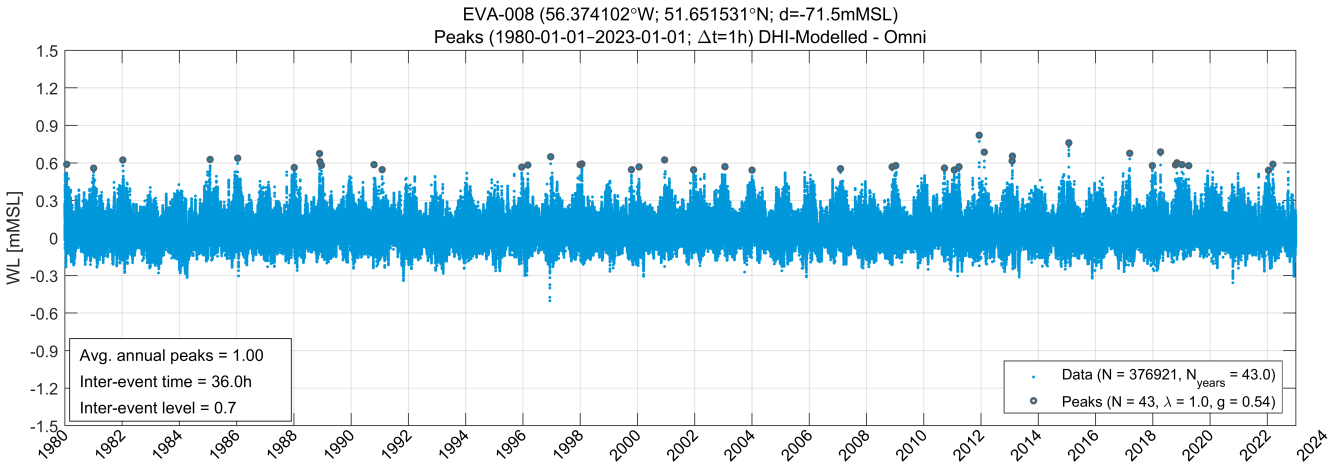


Figure C-15: Time series of water level residual at EVA-008 and selected peaks.

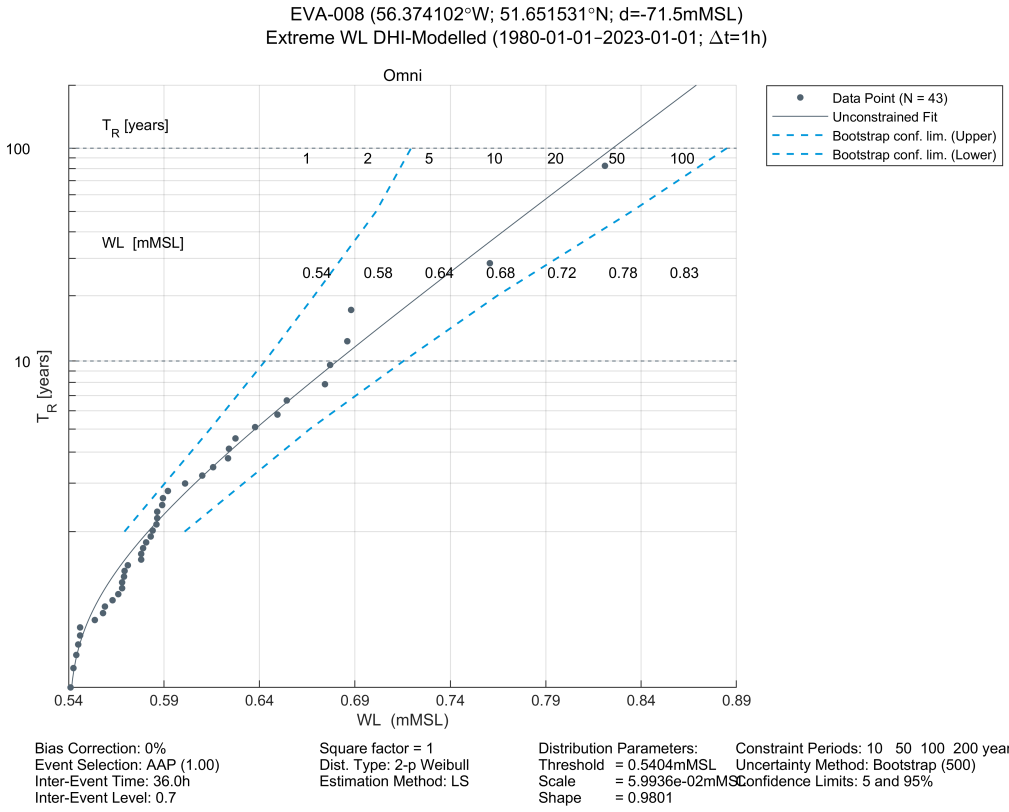


Figure C-16: Extreme value distribution fit at EVA-008.

EVA-009

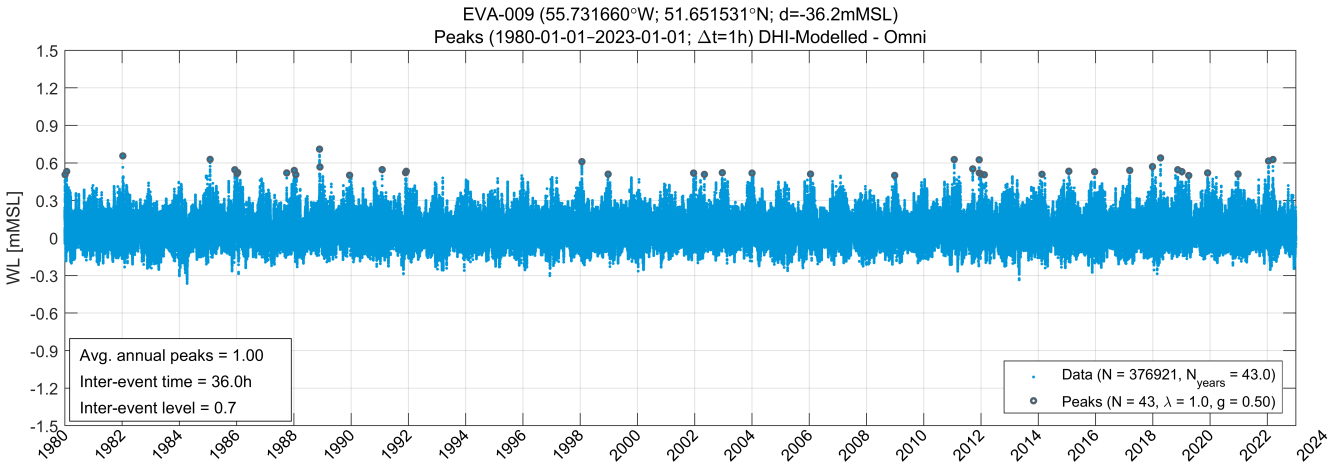


Figure C-17: Time series of water level residual at EVA-009 and selected peaks.

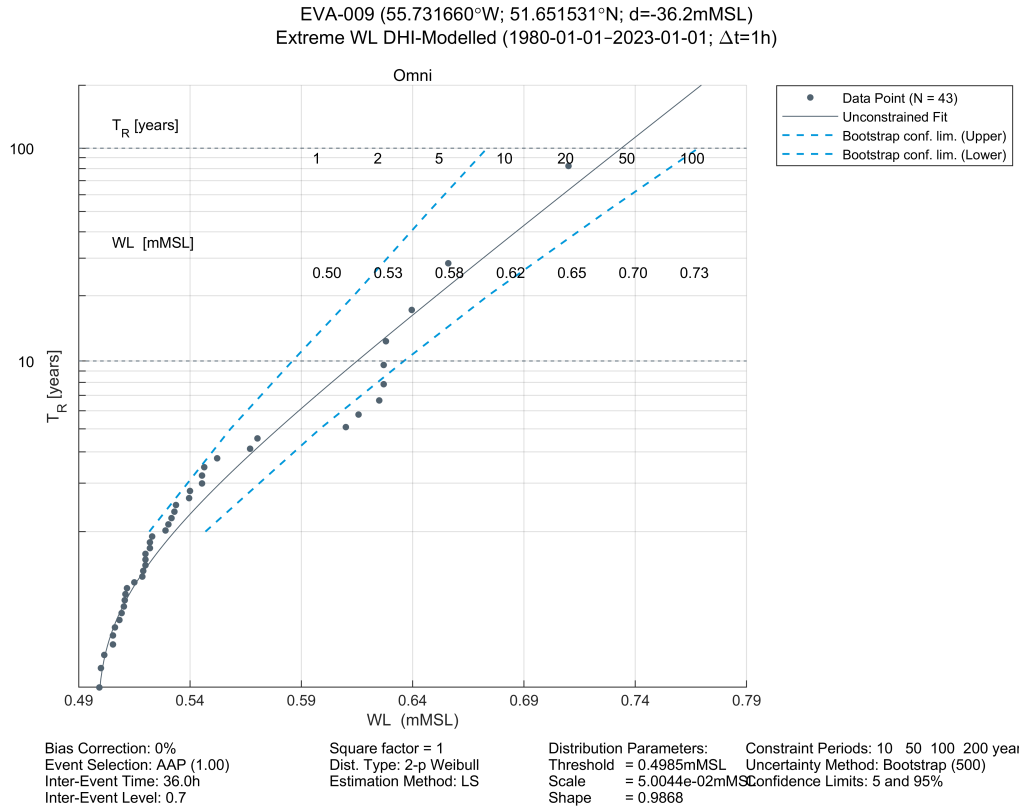


Figure C-18: Extreme value distribution fit at EVA-009.

EVA-010

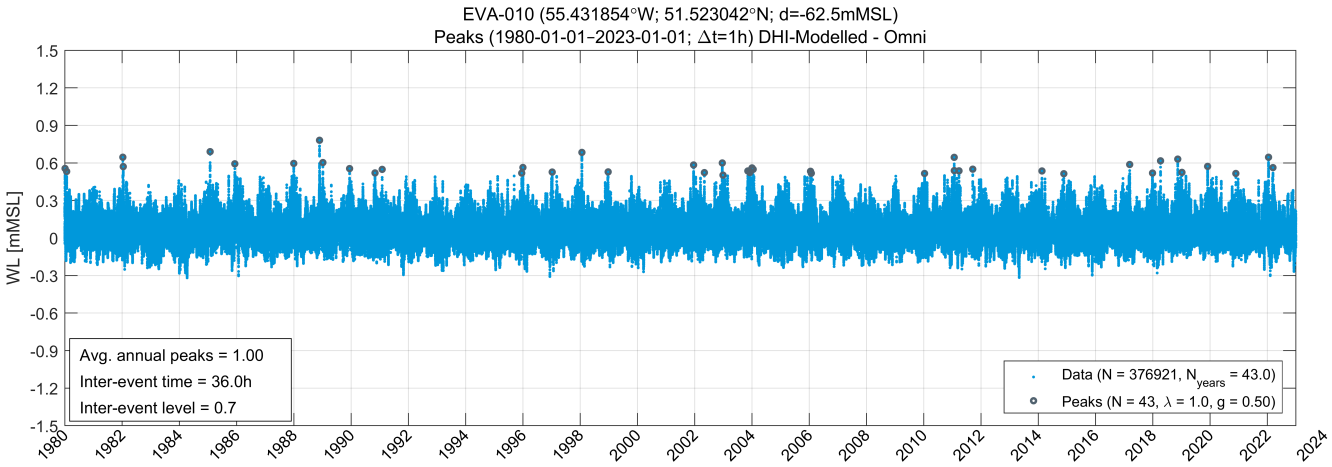


Figure C-19: Time series of water level residual at EVA-010 and selected peaks.

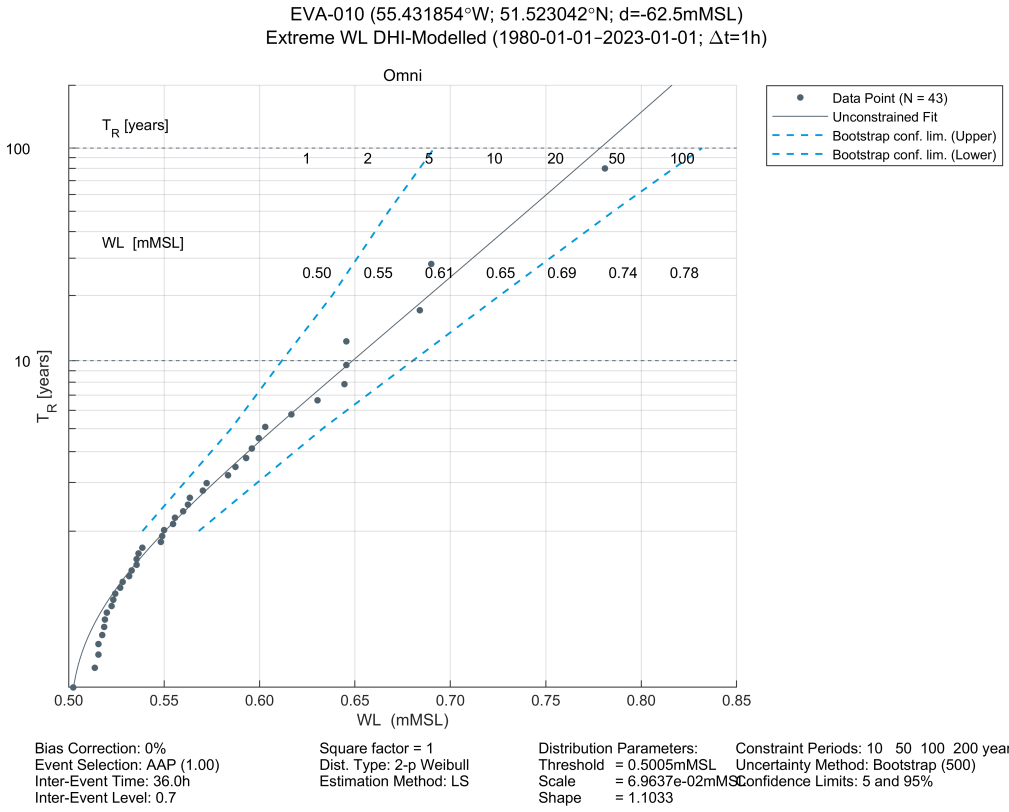


Figure C-20: Extreme value distribution fit at EVA-010.

EVA-011

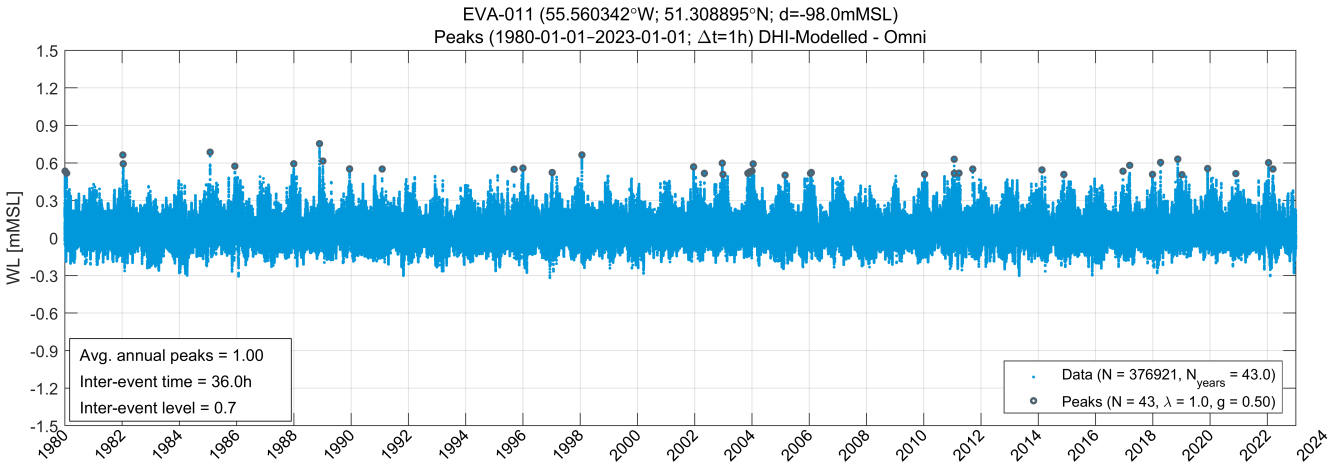


Figure C-21: Time series of water level residual at EVA-011 and selected peaks.

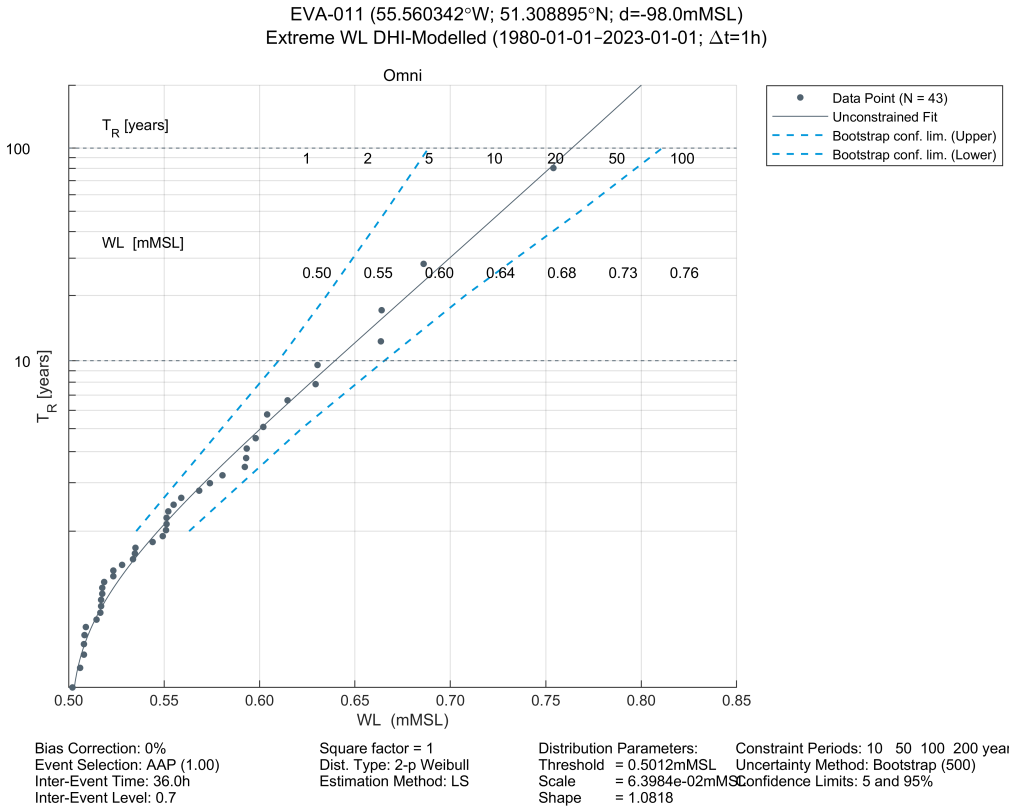


Figure C-22: Extreme value distribution fit at EVA-011.

EVA-012

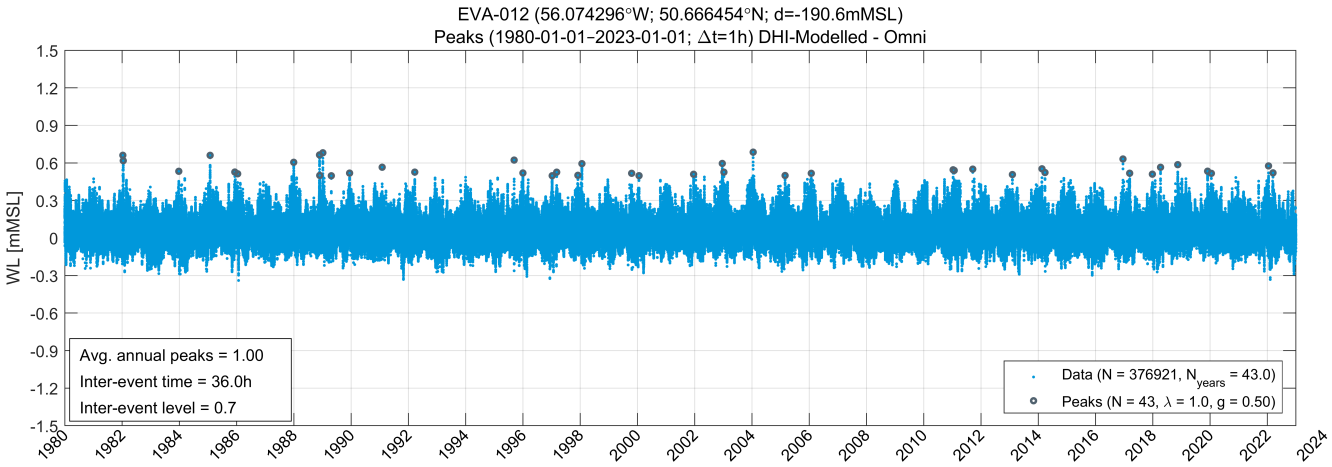


Figure C-23: Time series of water level residual at EVA-012 and selected peaks.

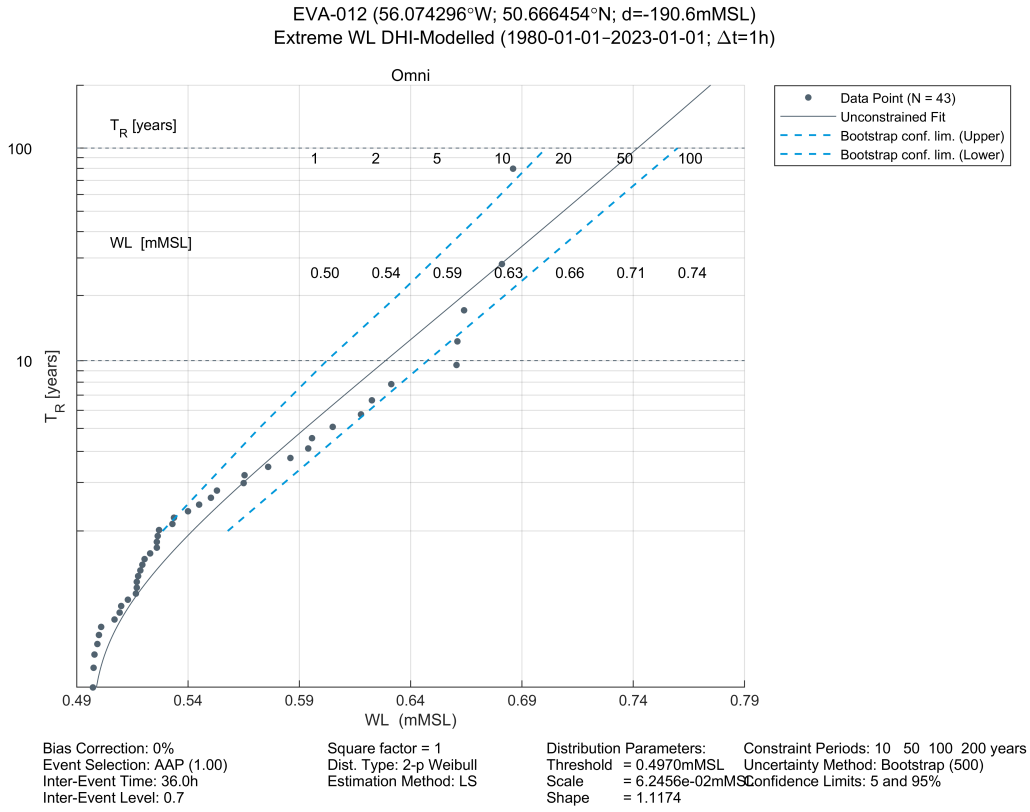


Figure C-24: Extreme value distribution fit at EVA-012.

EVA-013

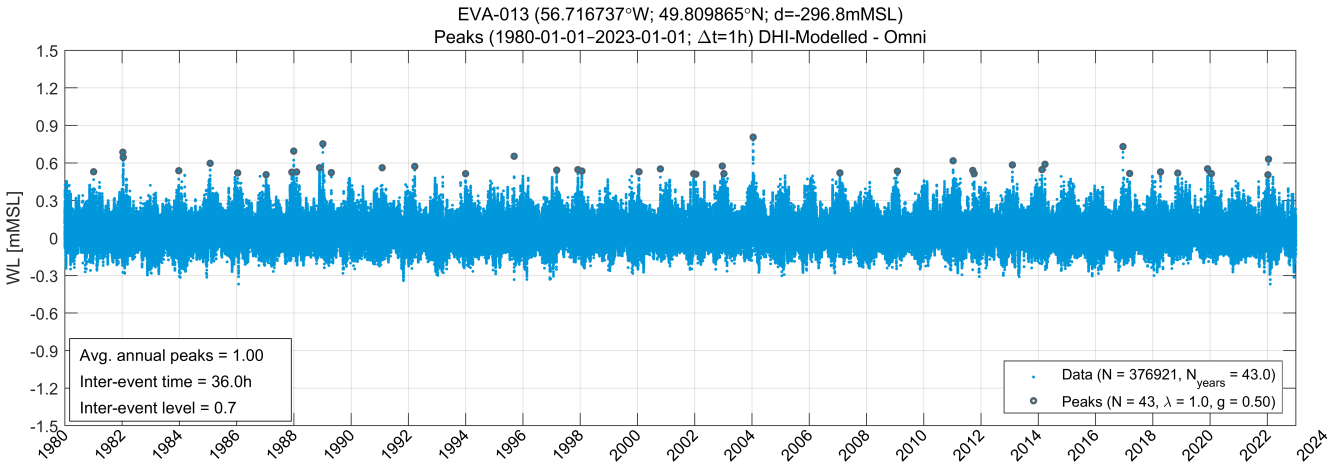


Figure C-25: Time series of water level residual at EVA-013 and selected peaks.

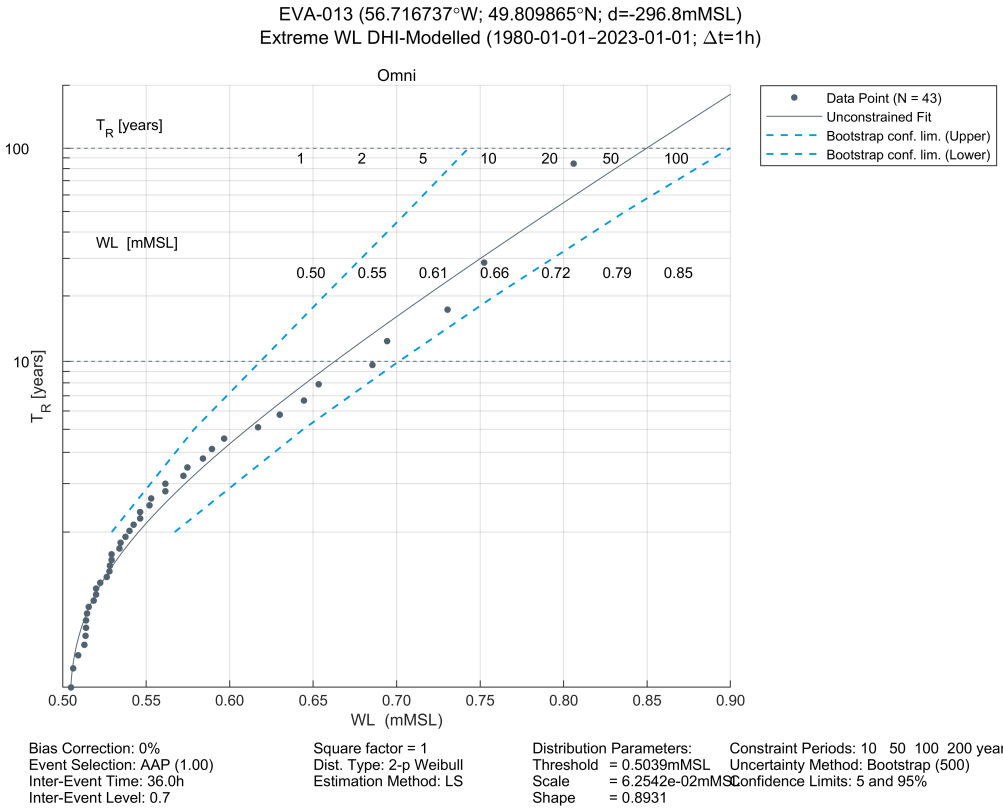


Figure C-26: Extreme value distribution fit at EVA-013.

EVA-014

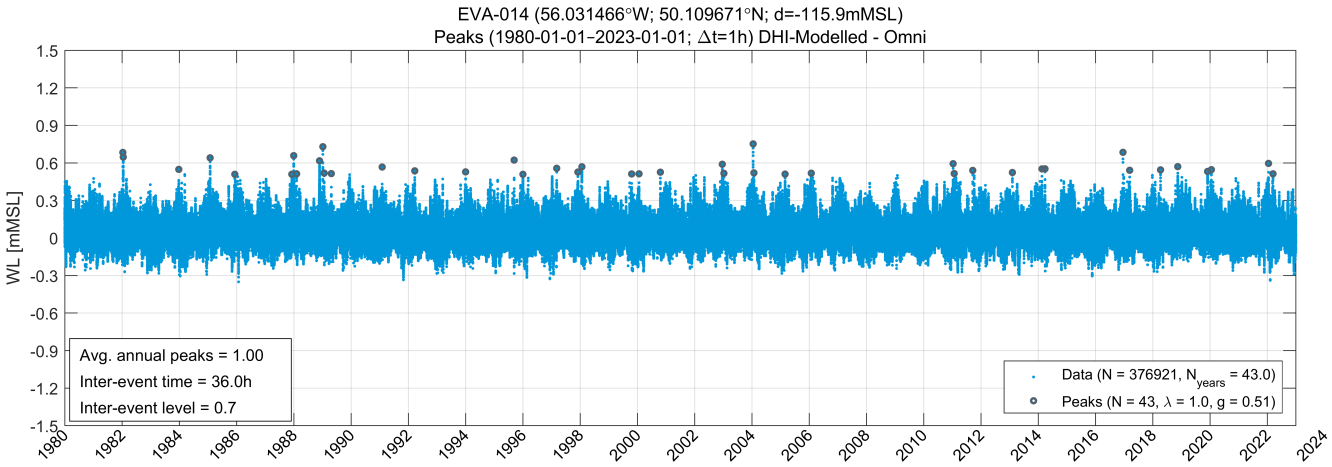


Figure C-27: Time series of water level residual at EVA-014 and selected peaks.

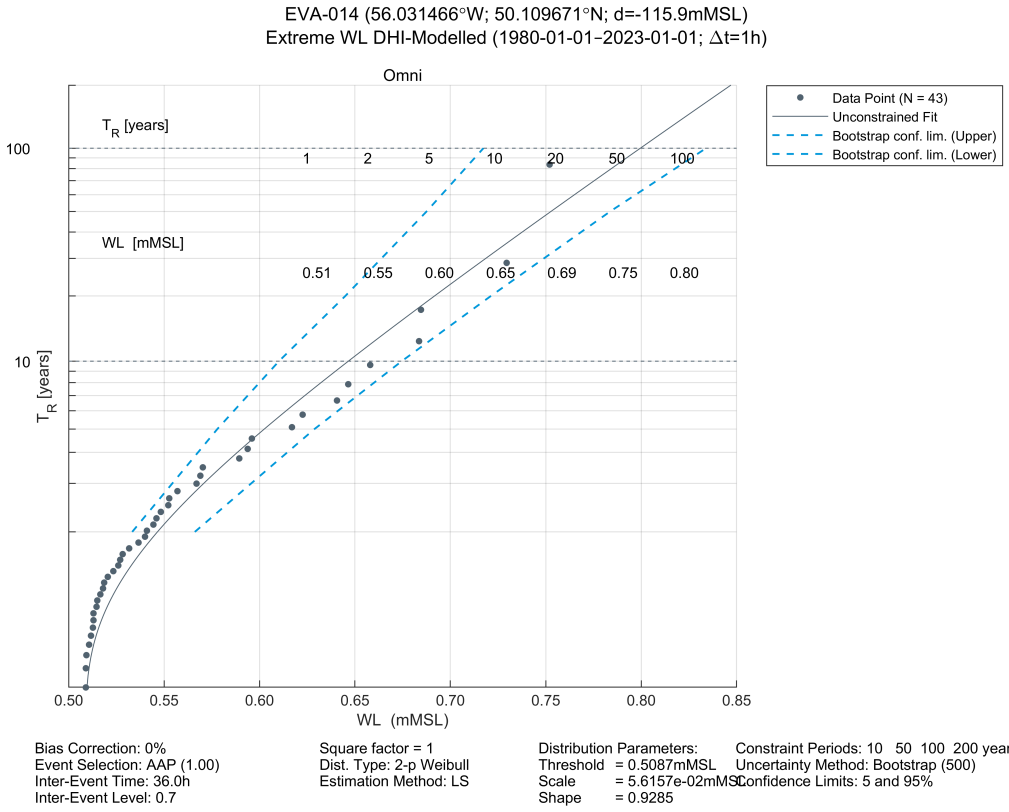


Figure C-28: Extreme value distribution fit at EVA-014.

EVA-015

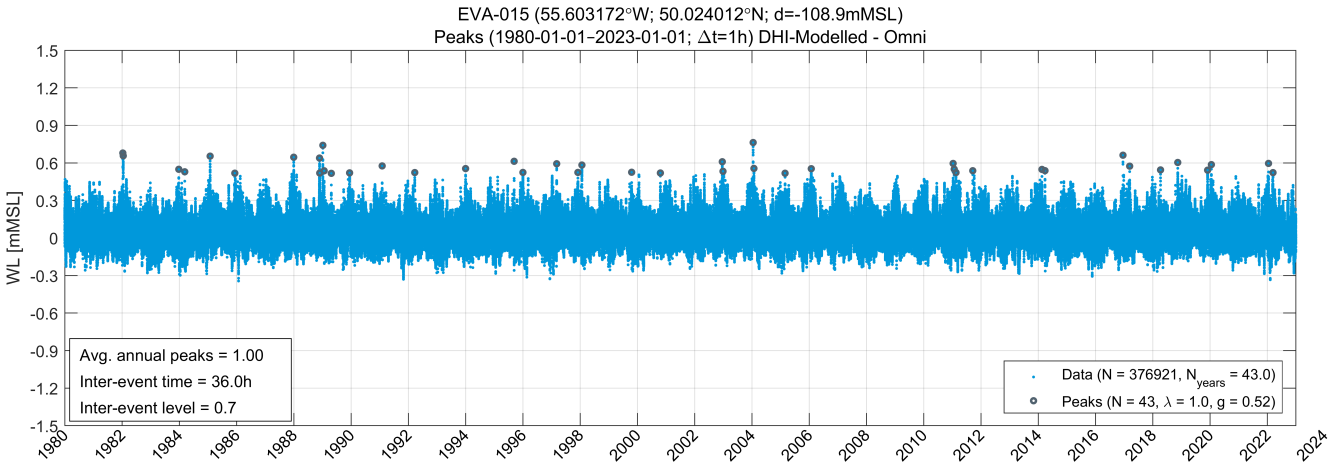


Figure C-29: Time series of water level residual at EVA-015 and selected peaks.

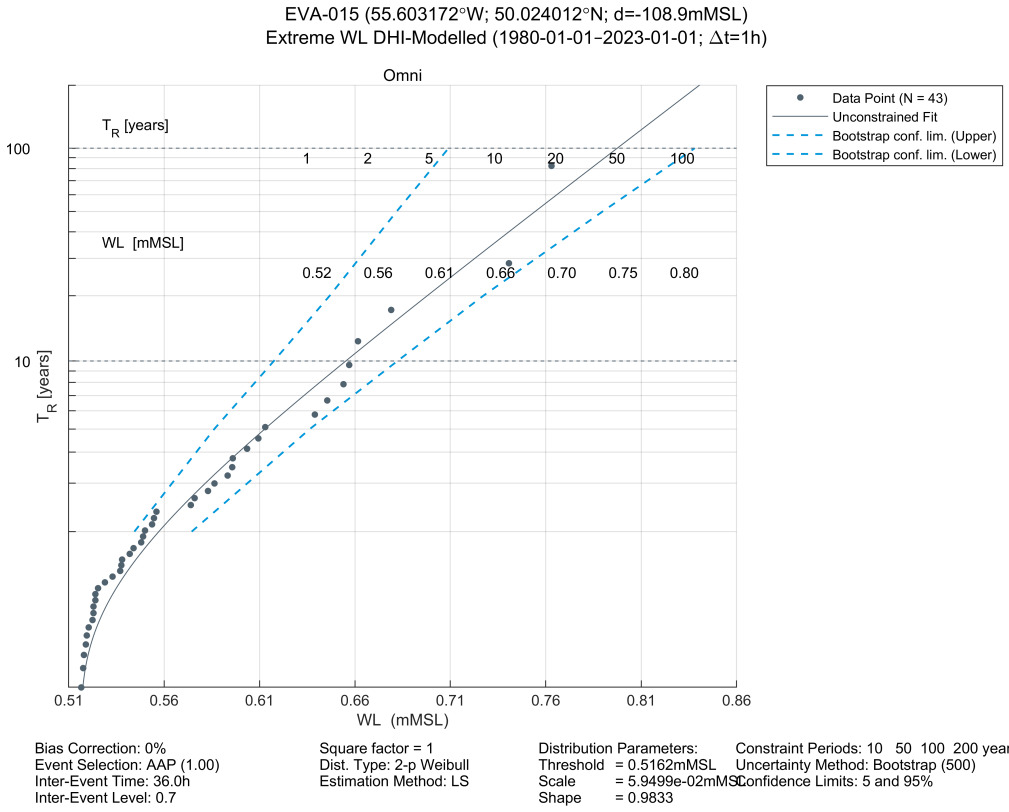


Figure C-30: Extreme value distribution fit at EVA-015.

EVA-016

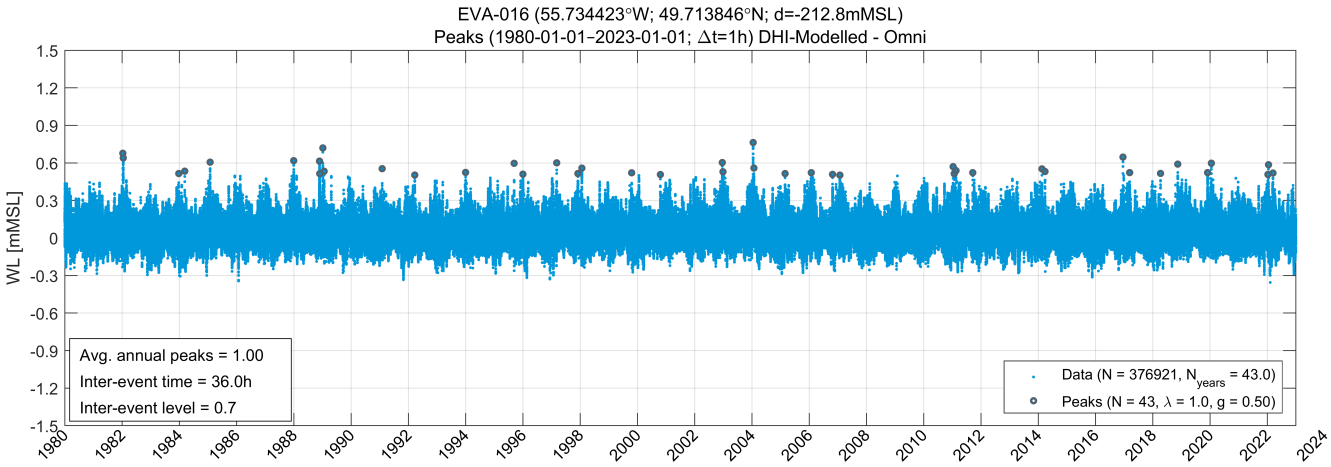


Figure C-31: Time series of water level residual at EVA-016 and selected peaks.

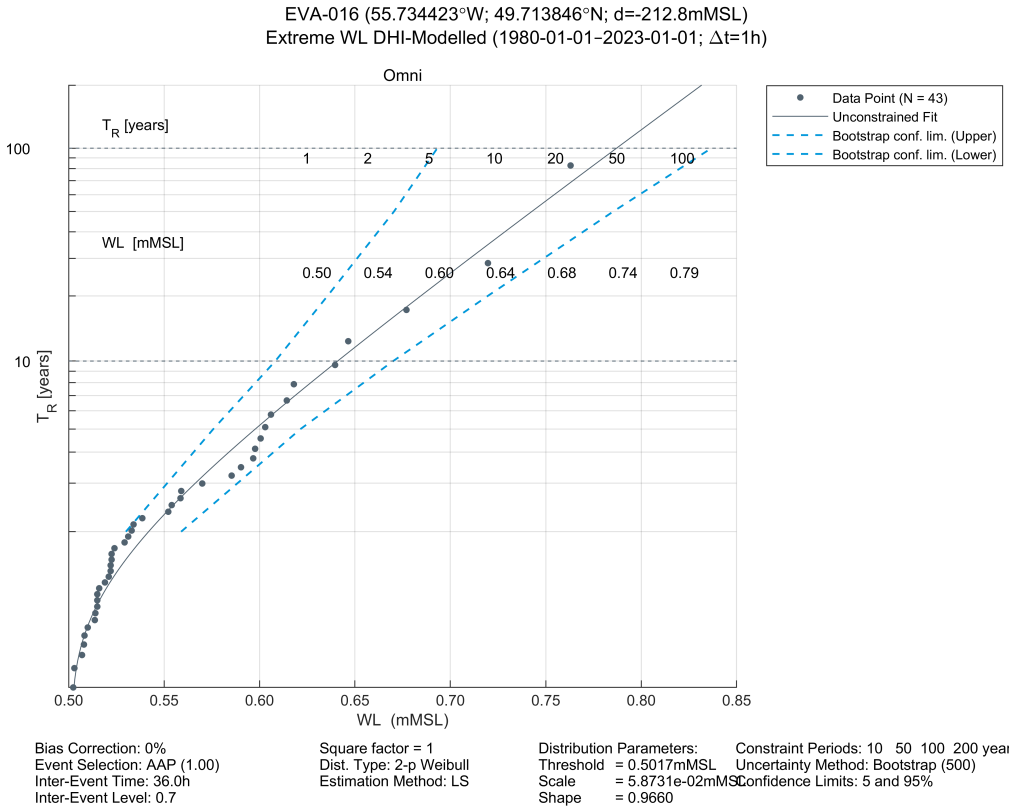


Figure C-32: Extreme value distribution fit at EVA-016.

EVA-017

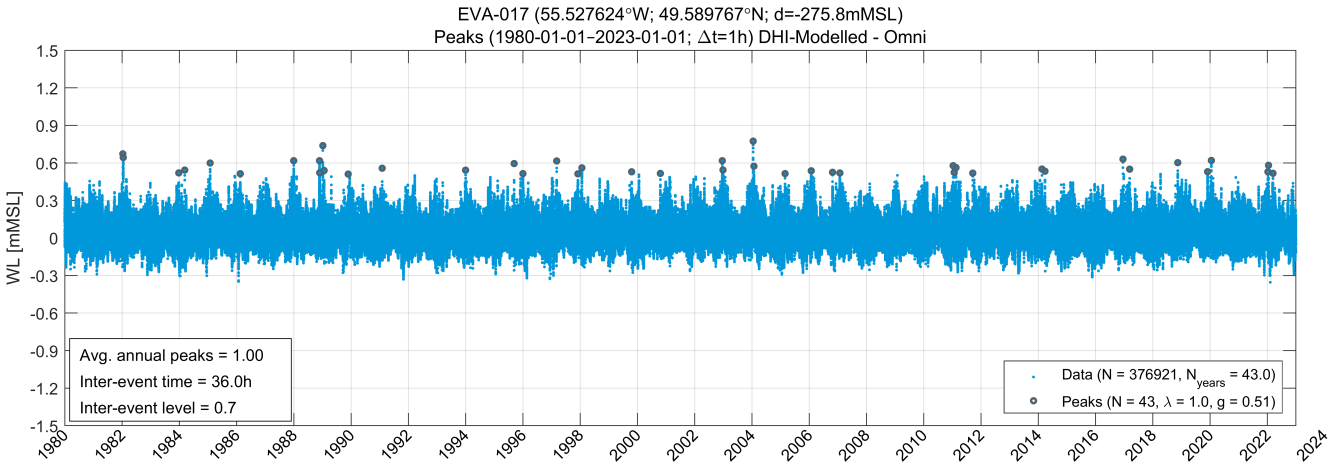


Figure C-33: Time series of water level residual at EVA-017 and selected peaks.

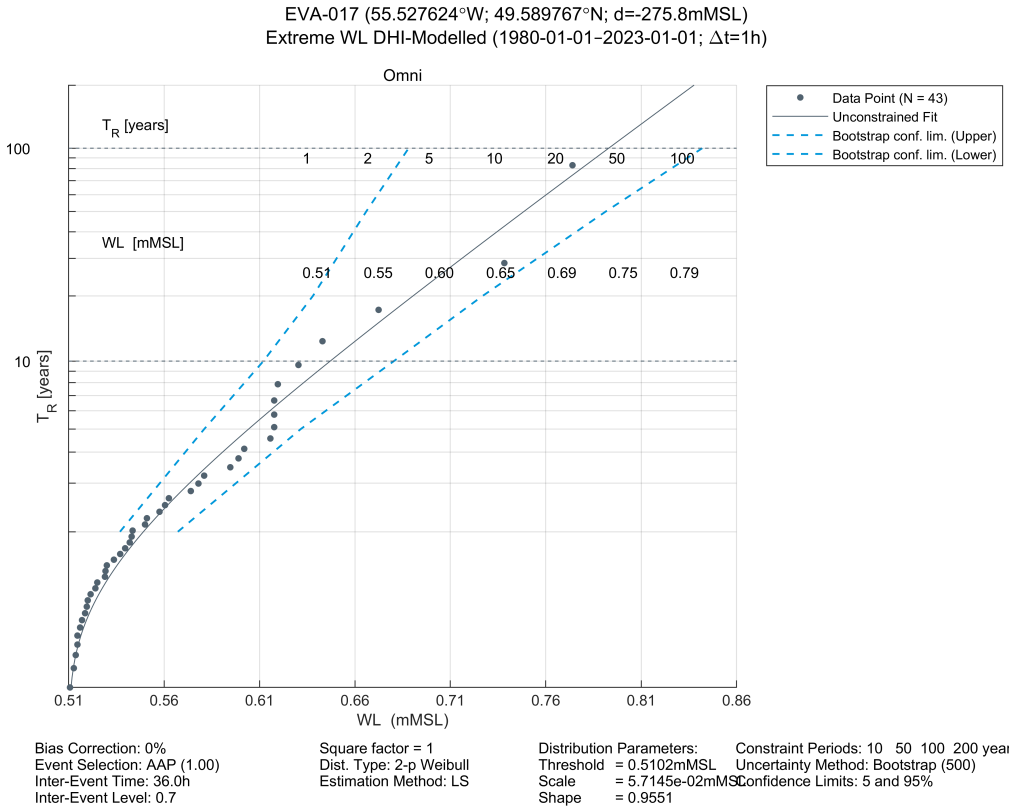


Figure C-34: Extreme value distribution fit at EVA-017.

EVA-018

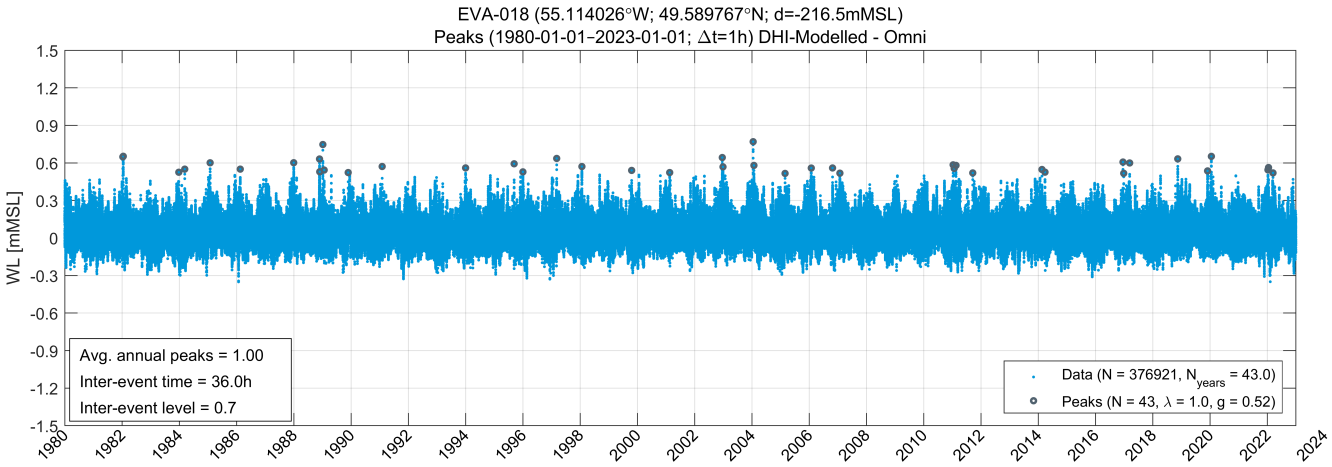


Figure C-35: Time series of water level residual at EVA-018 and selected peaks.

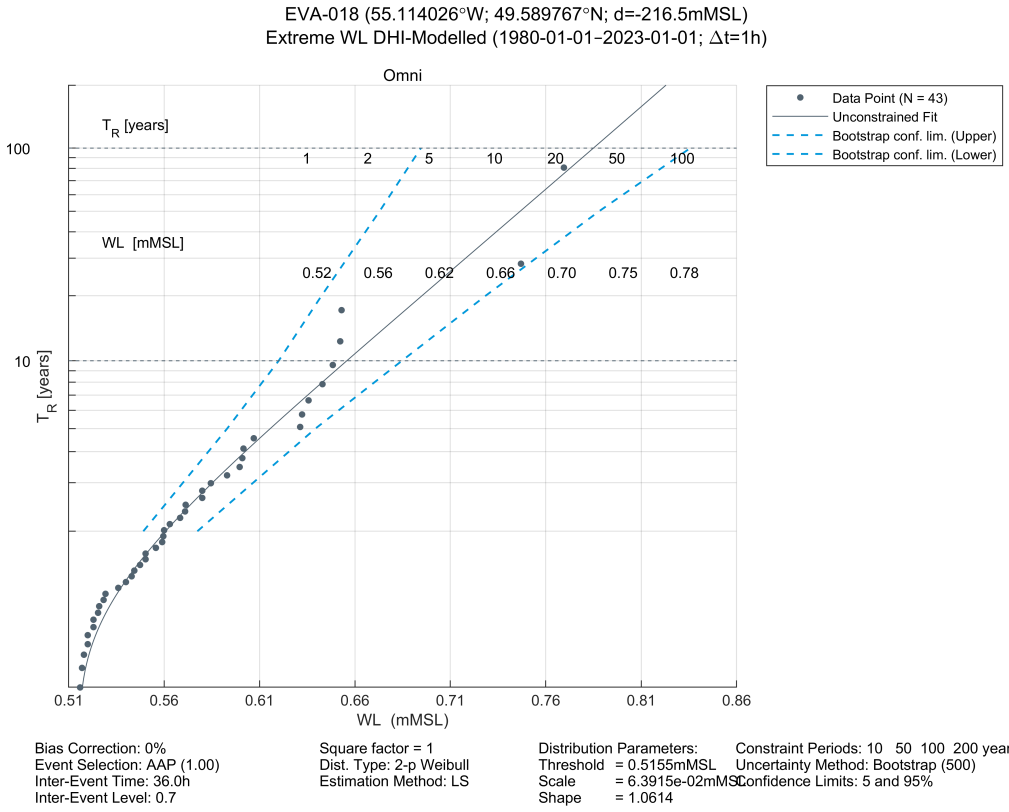


Figure C-36: Extreme value distribution fit at EVA-018.

EVA-019

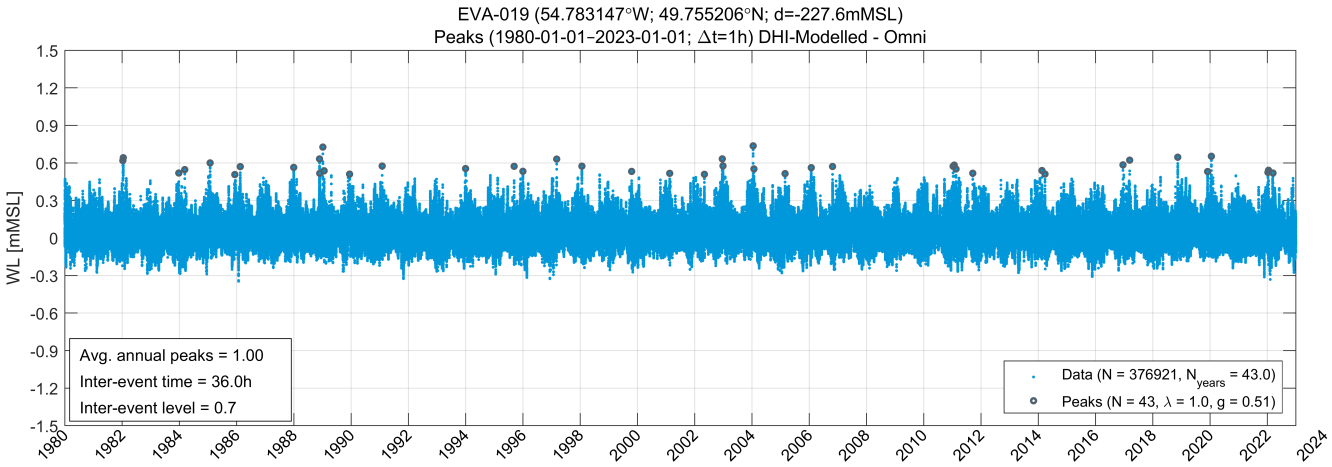


Figure C-37: Time series of water level residual at EVA-019 and selected peaks.

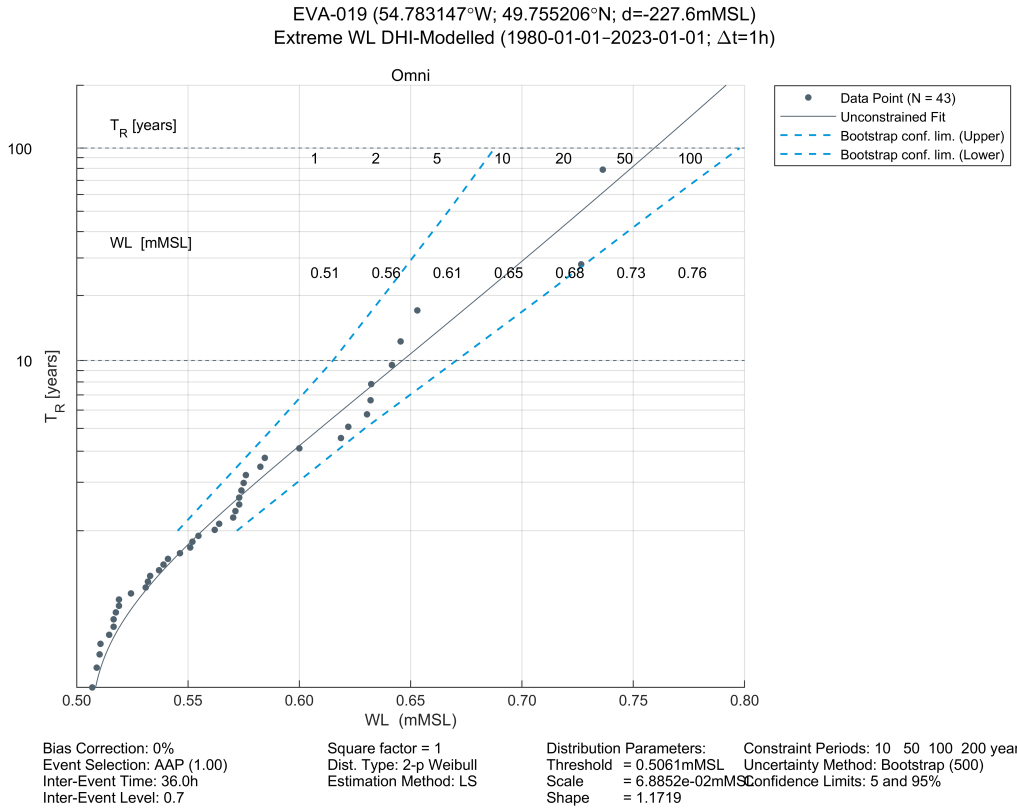


Figure C-38: Extreme value distribution fit at EVA-019.

EVA-020

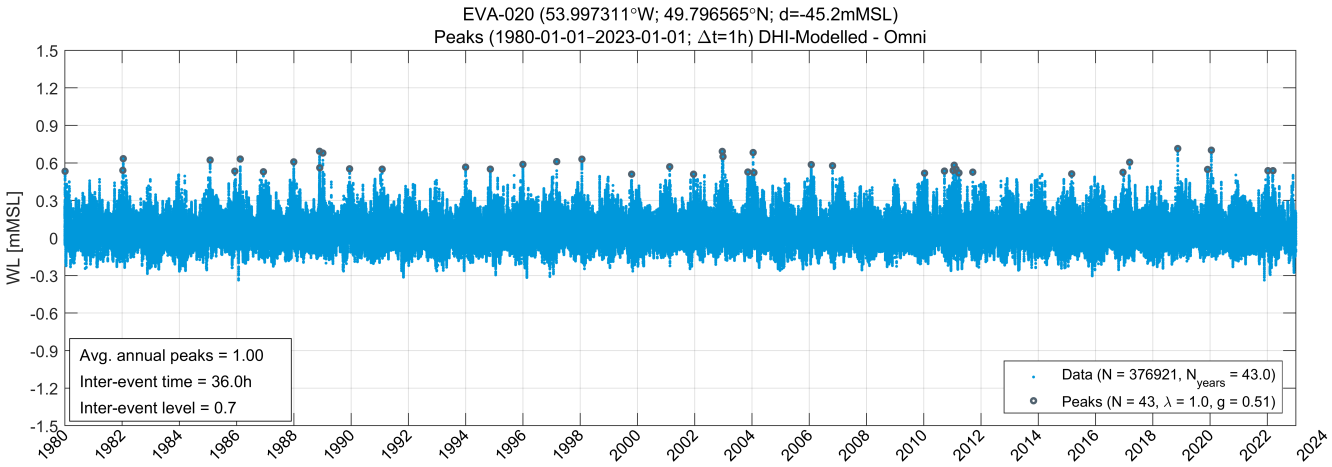


Figure C-39: Time series of water level residual at EVA-020 and selected peaks.

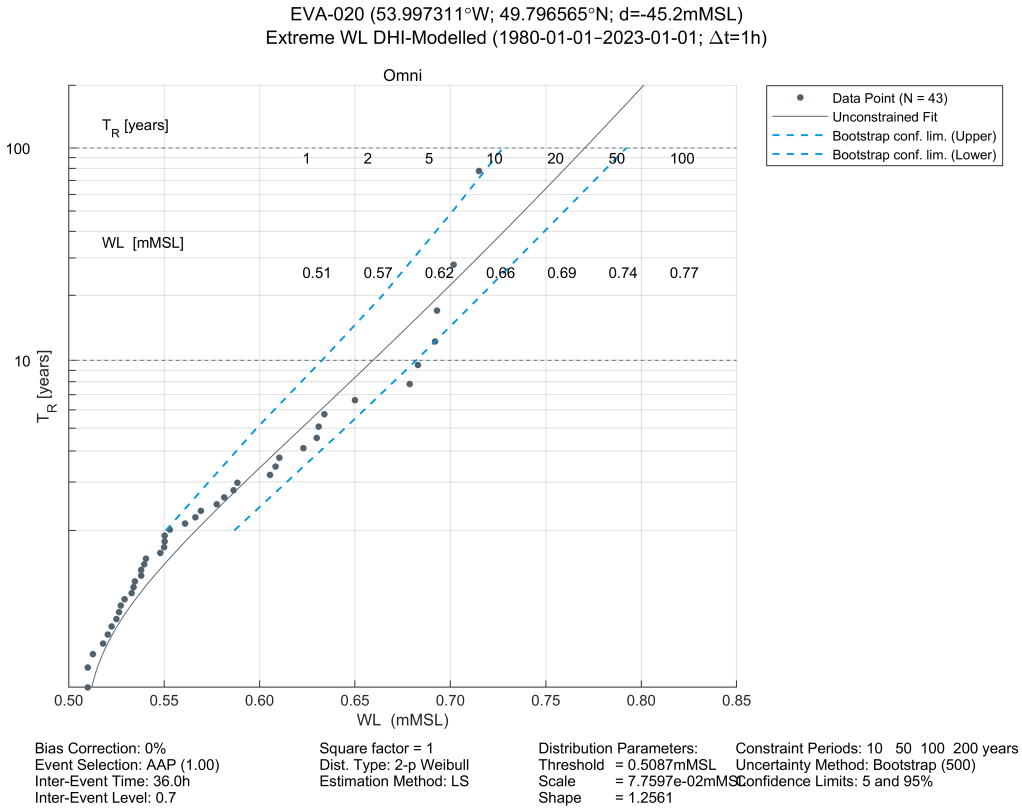


Figure C-40: Extreme value distribution fit at EVA-020.

EVA-021

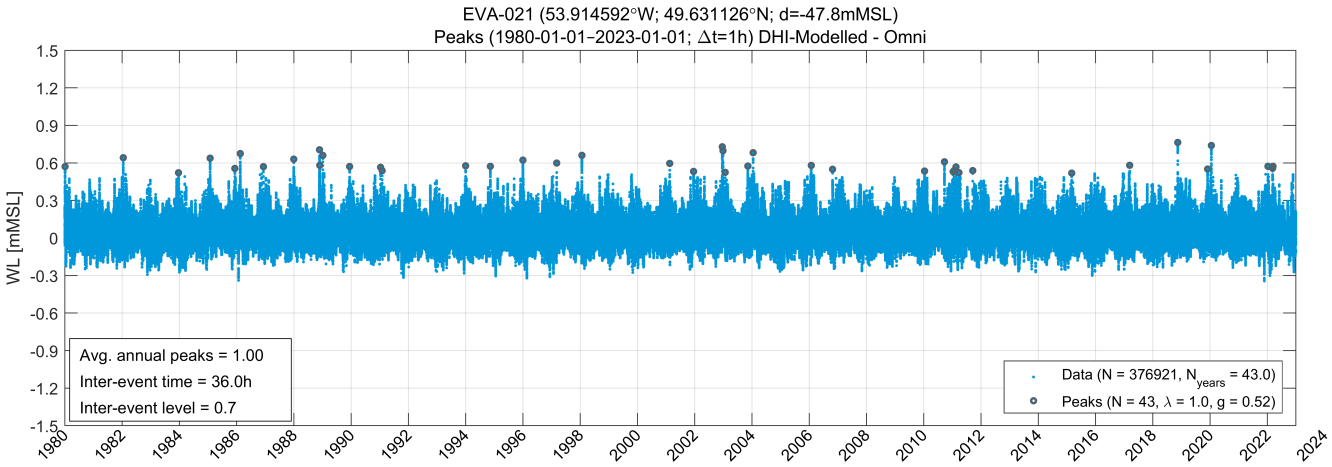


Figure C-41: Time series of water level residual at EVA-021 and selected peaks.

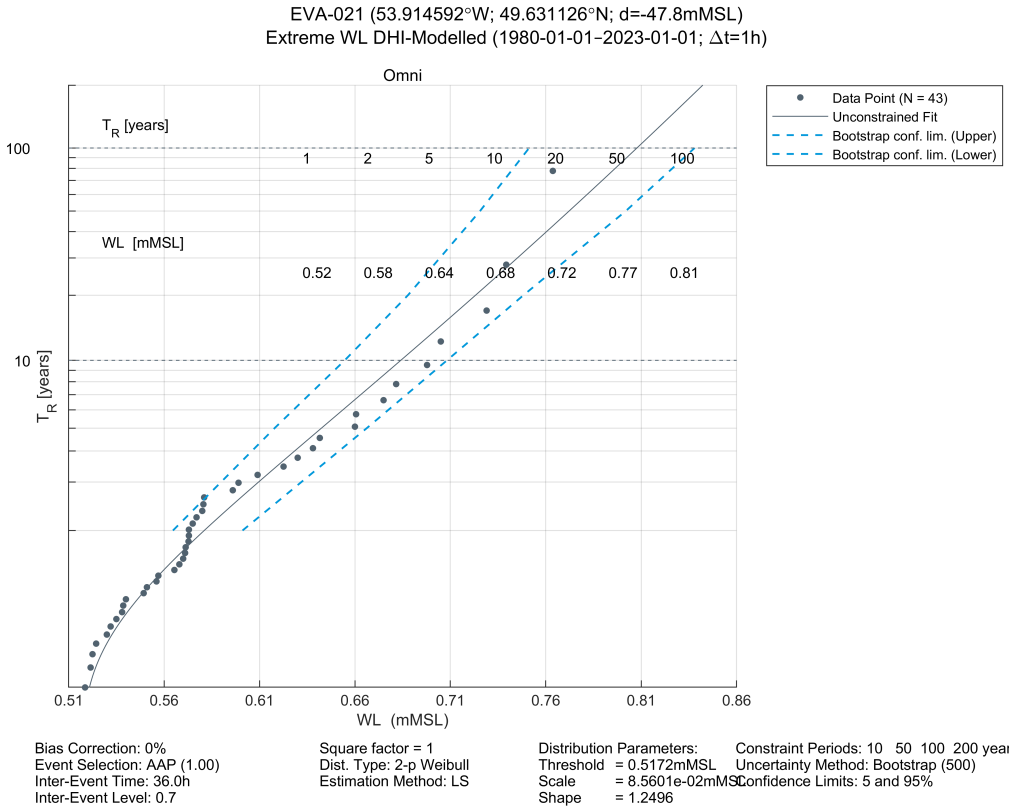


Figure C-42: Extreme value distribution fit at EVA-021.

EVA-022

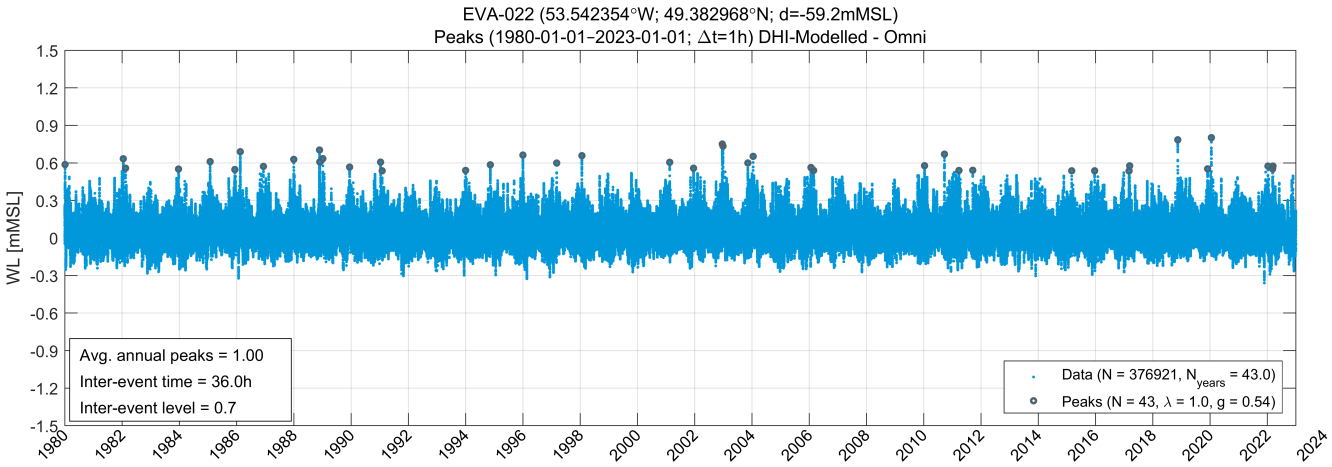


Figure C-43: Time series of water level residual at EVA-022 and selected peaks.

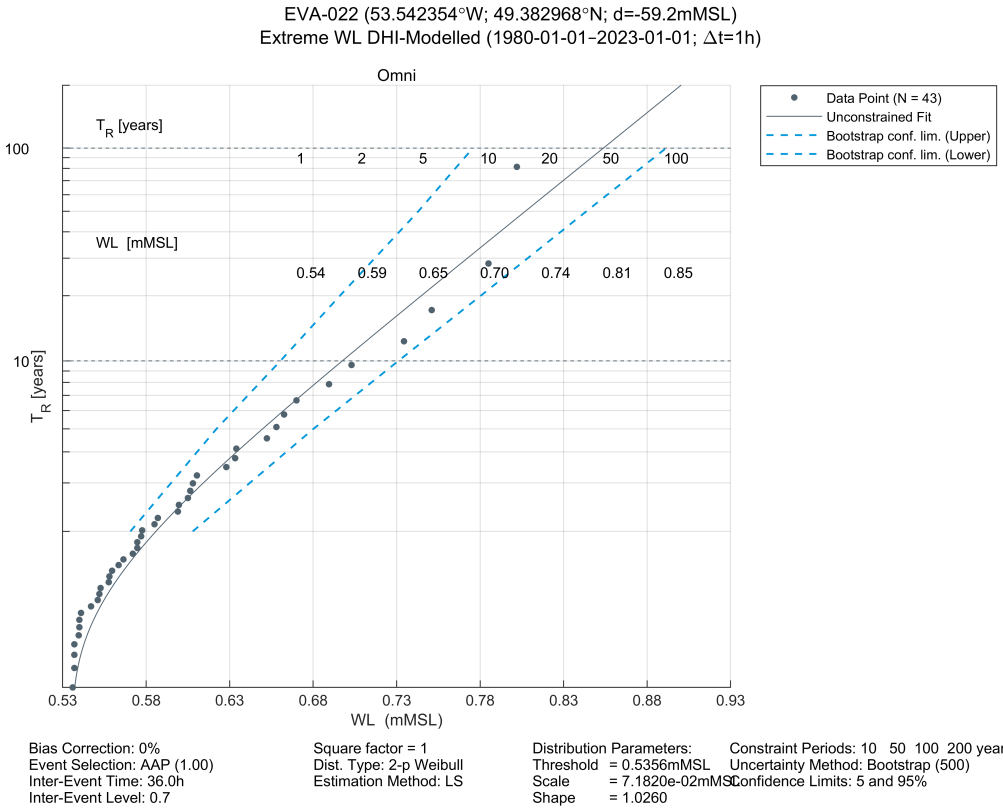


Figure C-44: Extreme value distribution fit at EVA-022.

EVA-023

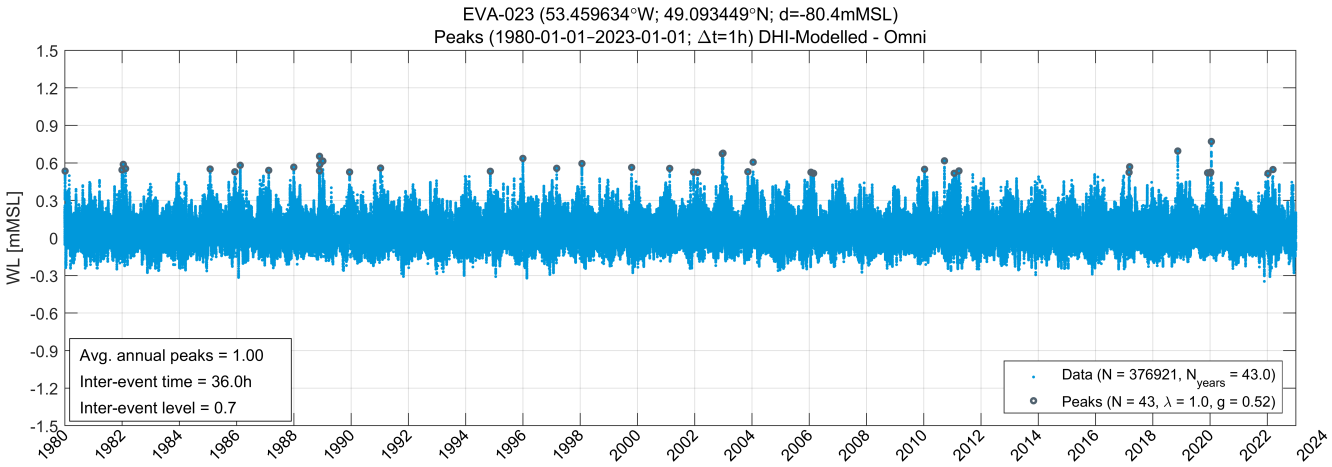


Figure C-45: Time series of water level residual at EVA-023 and selected peaks.

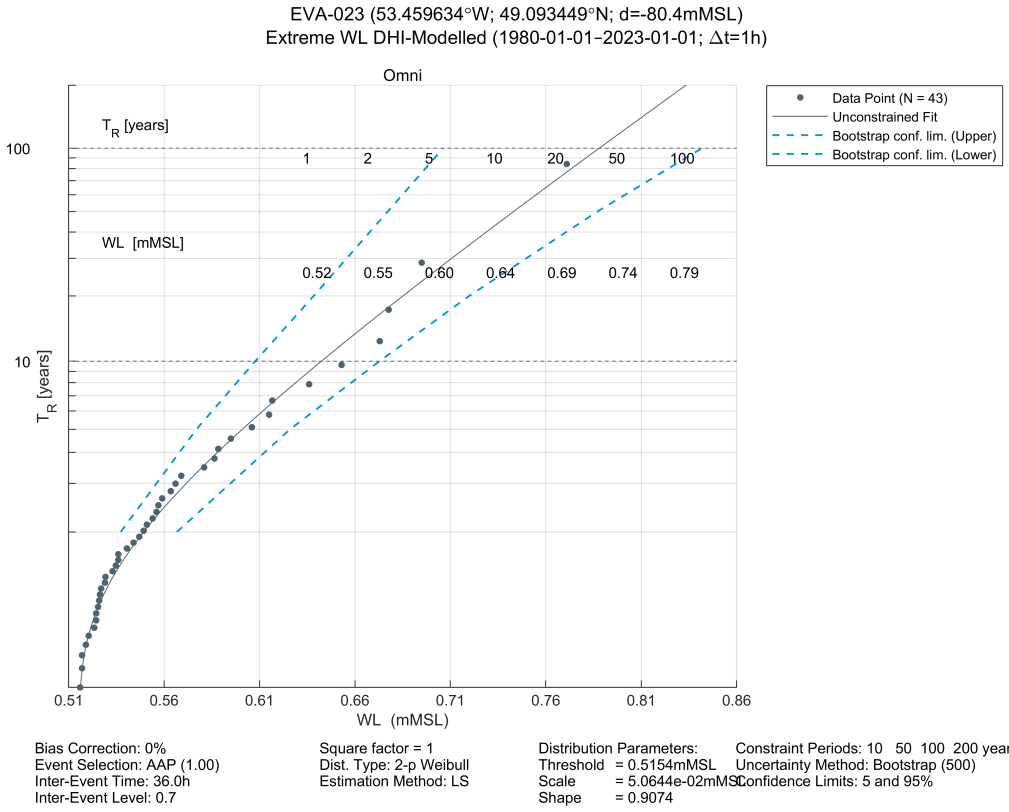


Figure C-46: Extreme value distribution fit at EVA-023.

EVA-024

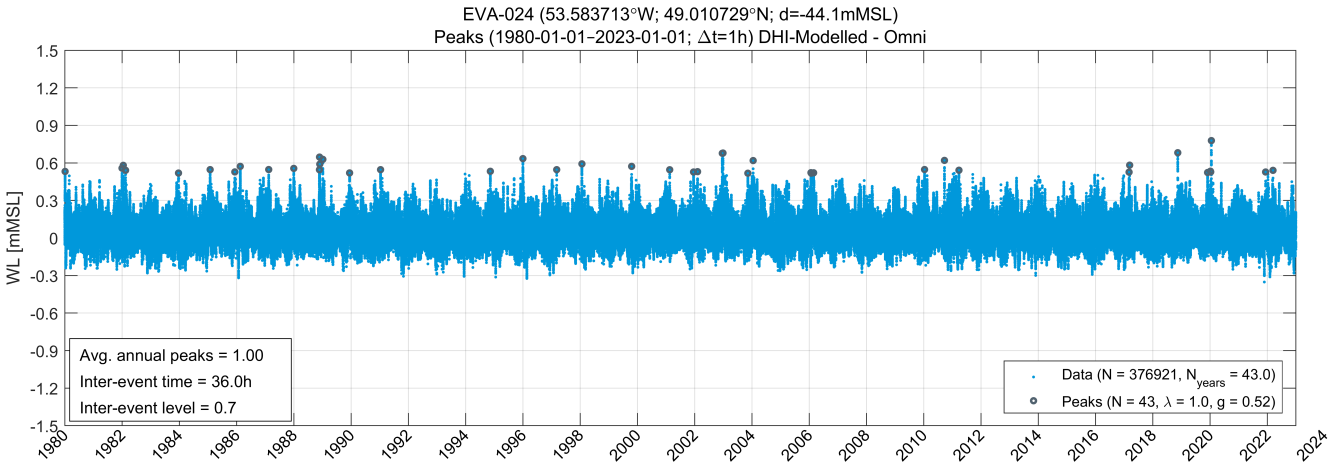


Figure C-47: Time series of water level residual at EVA-024 and selected peaks.

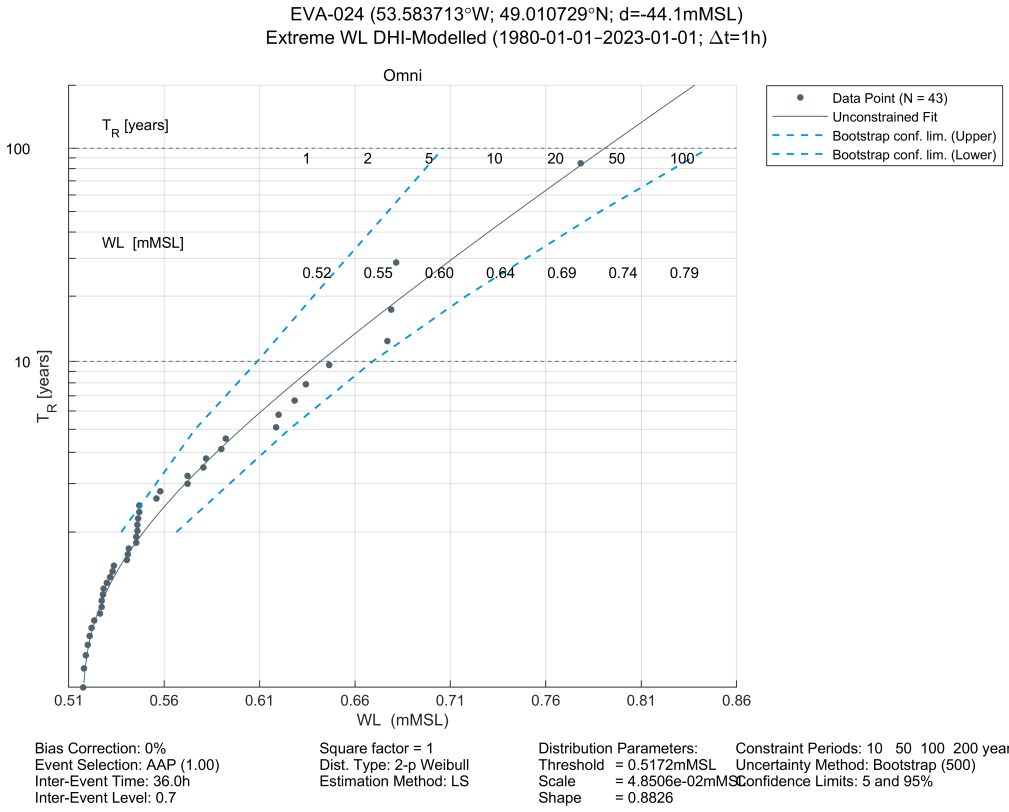


Figure C-48: Extreme value distribution fit at EVA-024.

EVA-025

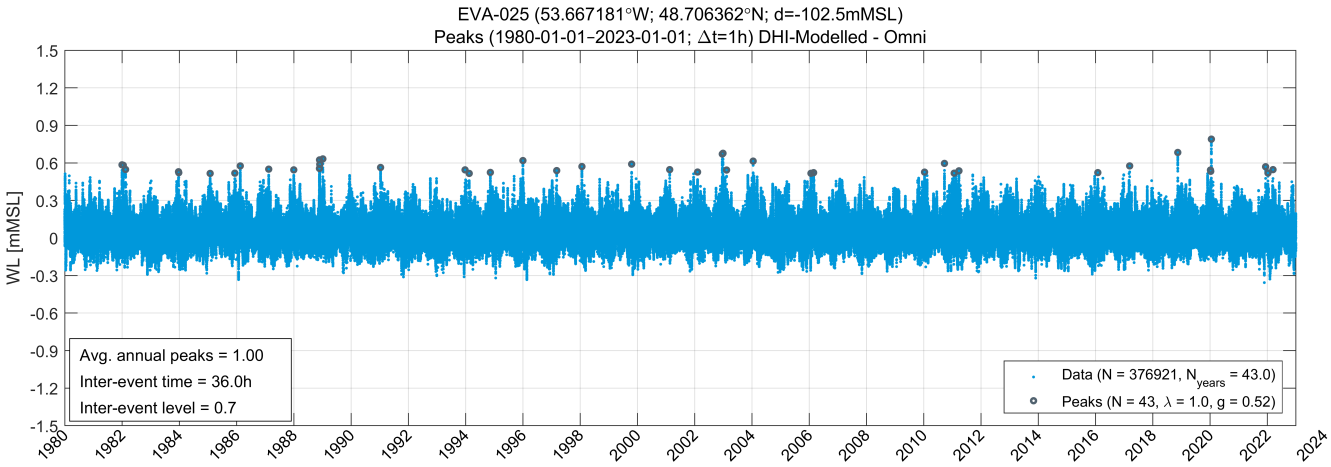


Figure C-49: Time series of water level residual at EVA-025 and selected peaks.

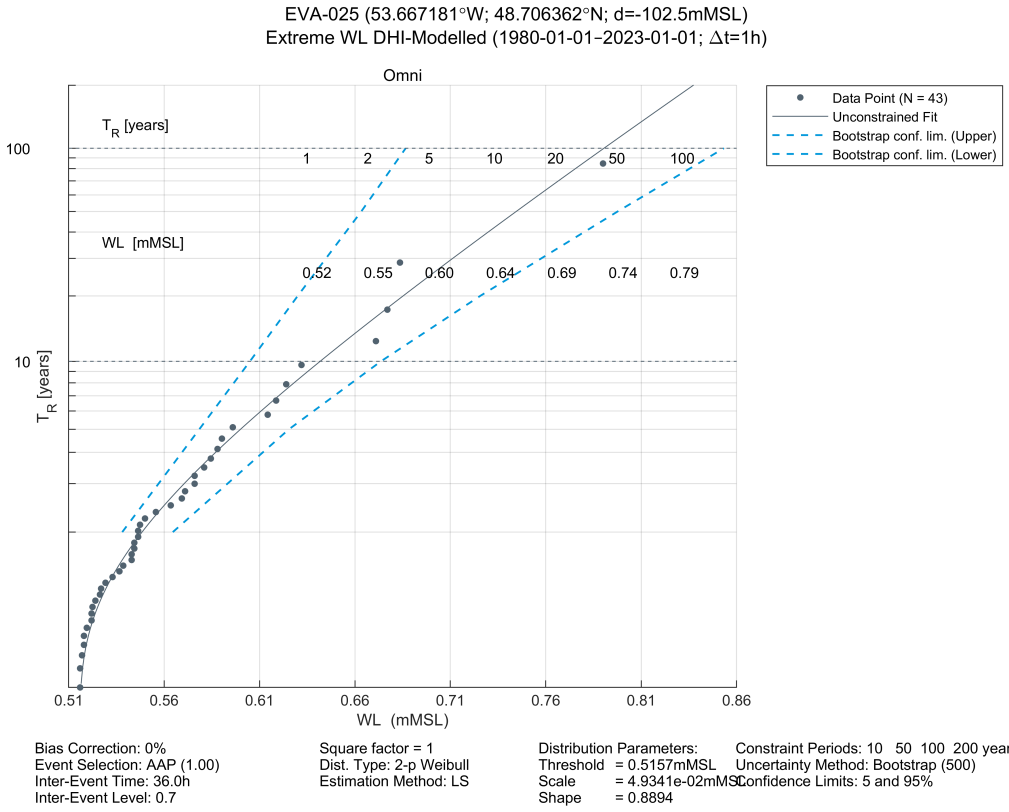


Figure C-50: Extreme value distribution fit at EVA-025.

EVA-026

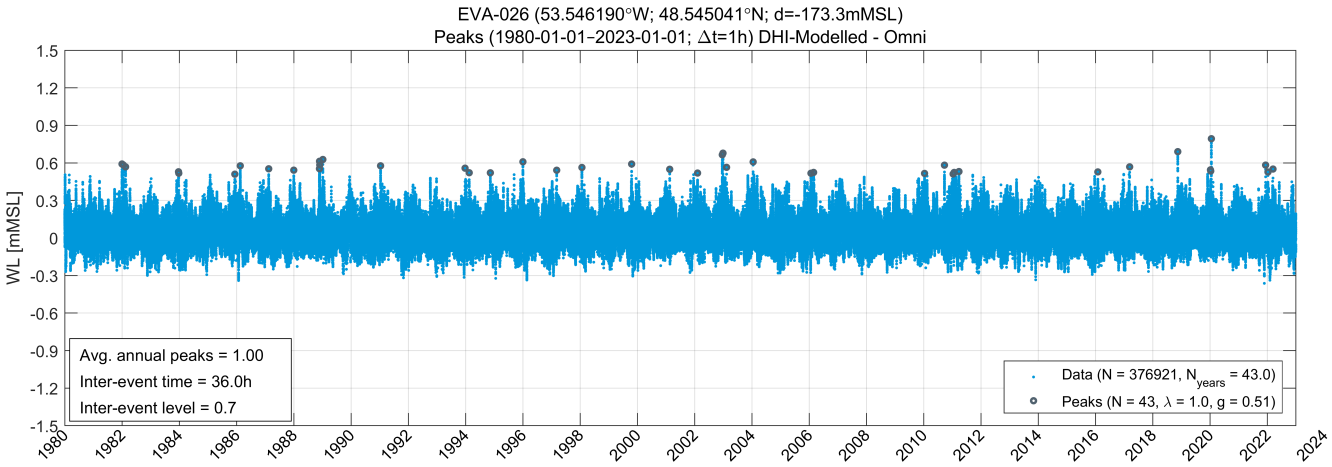


Figure C-51: Time series of water level residual at EVA-026 and selected peaks.

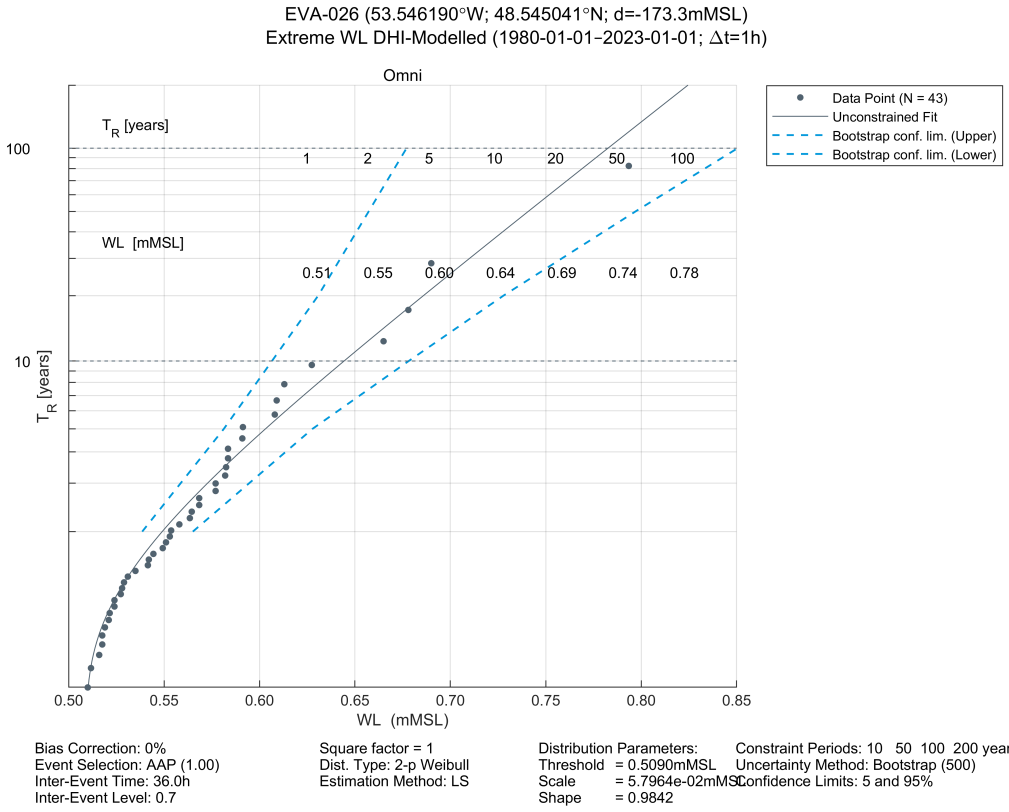


Figure C-52: Extreme value distribution fit at EVA-026.

EVA-027

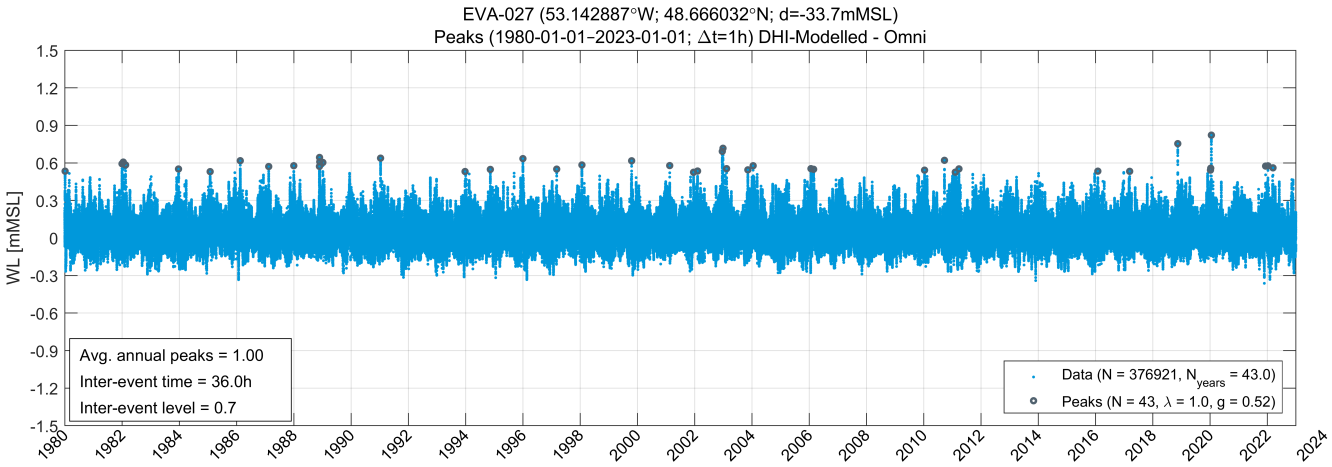


Figure C-53: Time series of water level residual at EVA-027 and selected peaks.

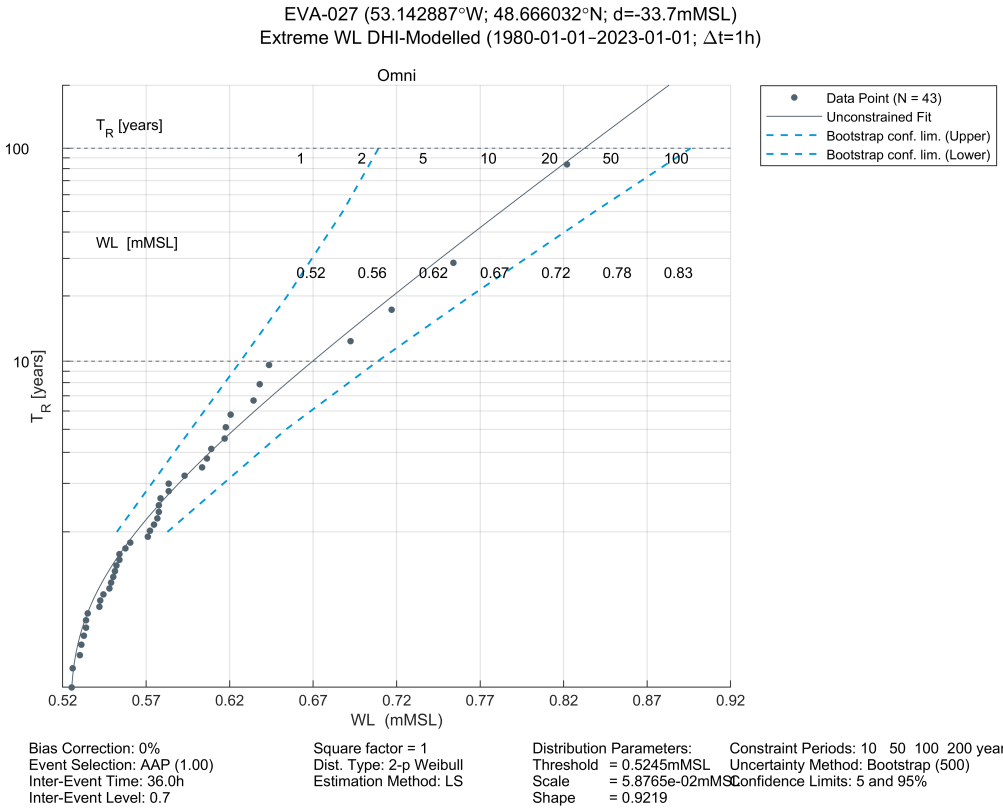


Figure C-54: Extreme value distribution fit at EVA-027.

EVA-028

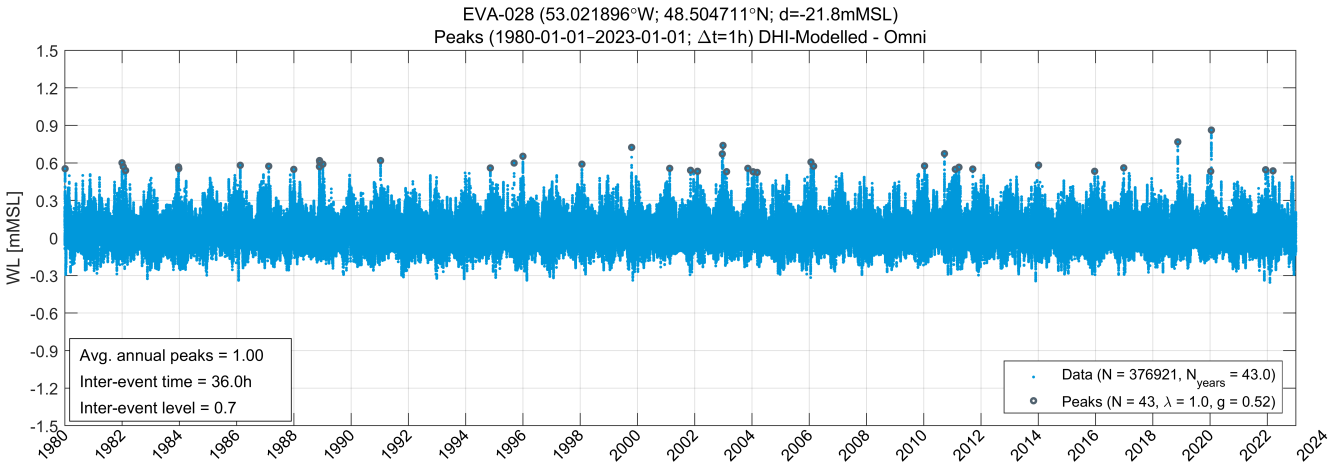


Figure C-55: Time series of water level residual at EVA-028 and selected peaks.

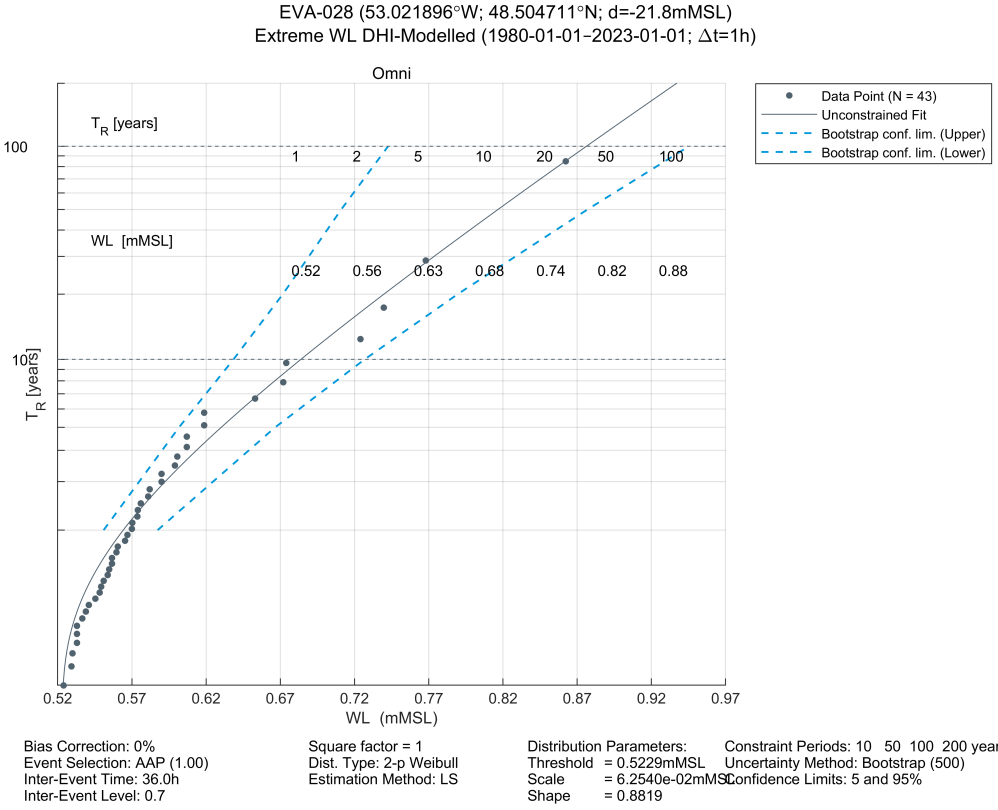


Figure C-56: Extreme value distribution fit at EVA-028.

EVA-029

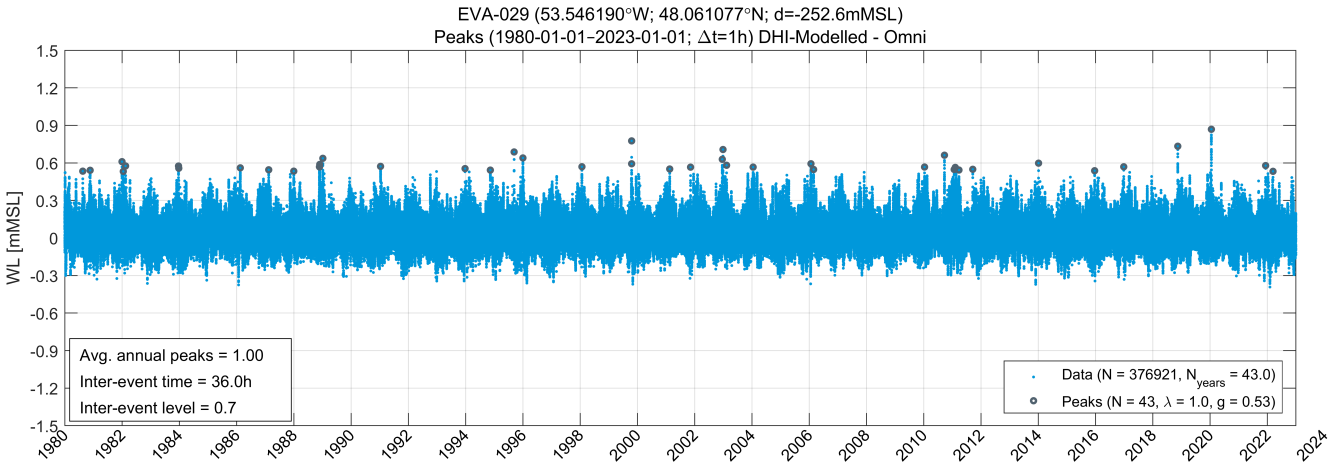


Figure C-57: Time series of water level residual at EVA-029 and selected peaks.

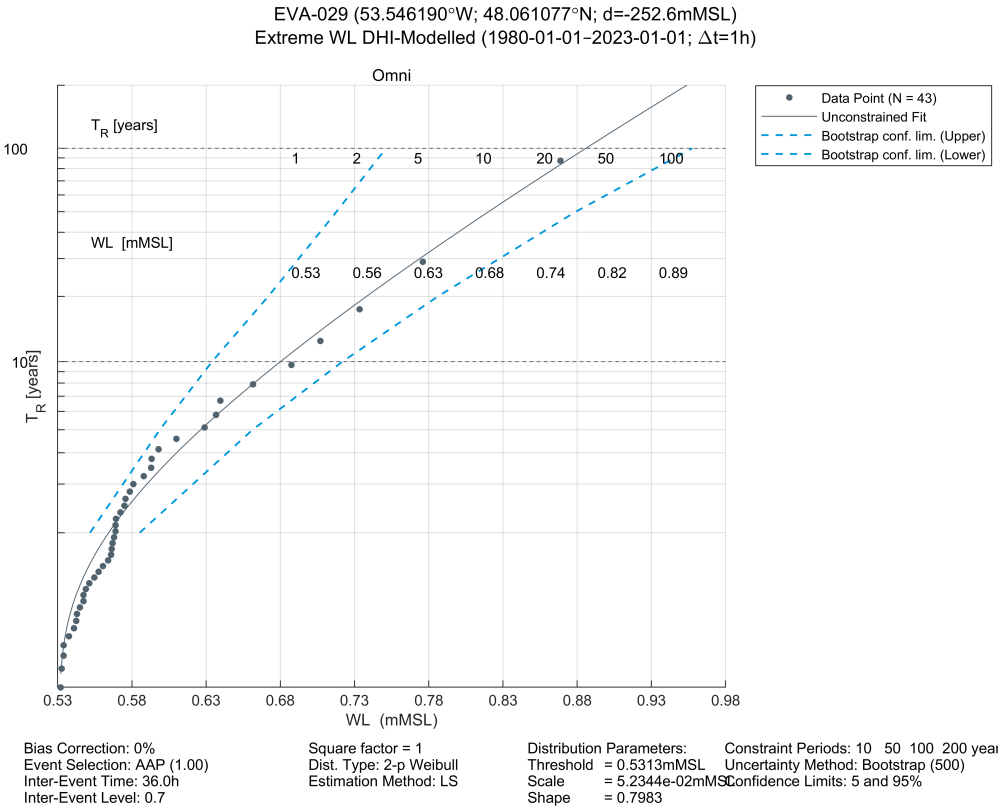


Figure C-58: Extreme value distribution fit at EVA-029.

EVA-030

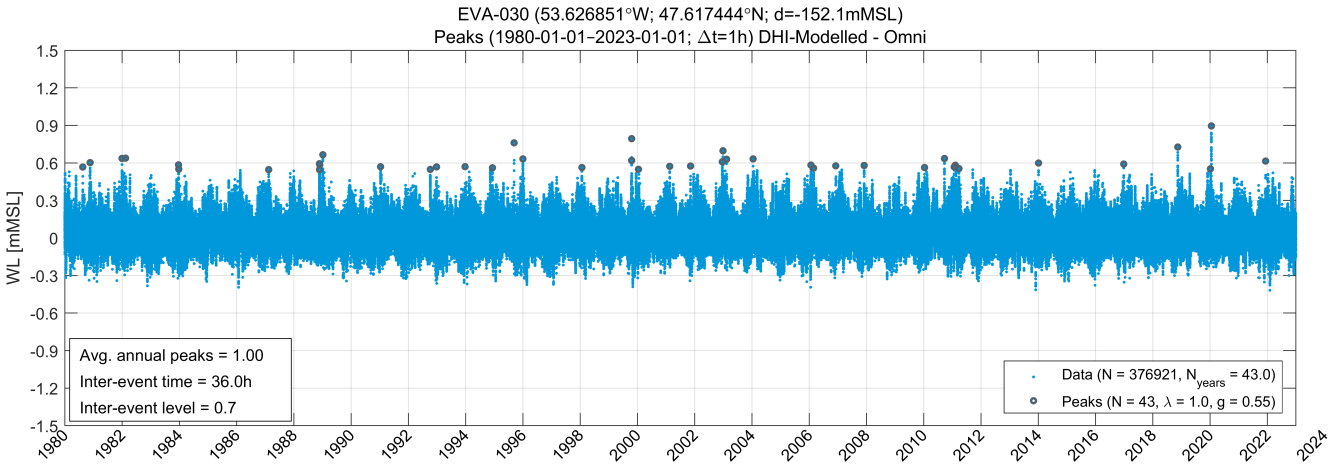


Figure C-59: Time series of water level residual at EVA-030 and selected peaks.

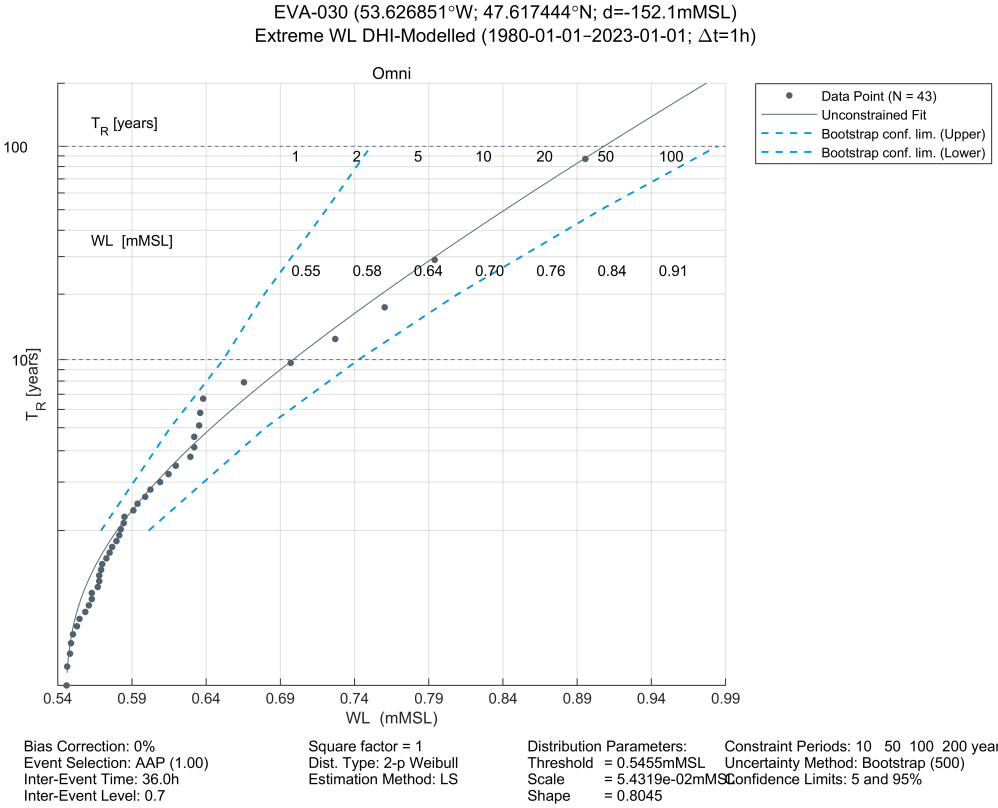


Figure C-60: Extreme value distribution fit at EVA-030.

EVA-031

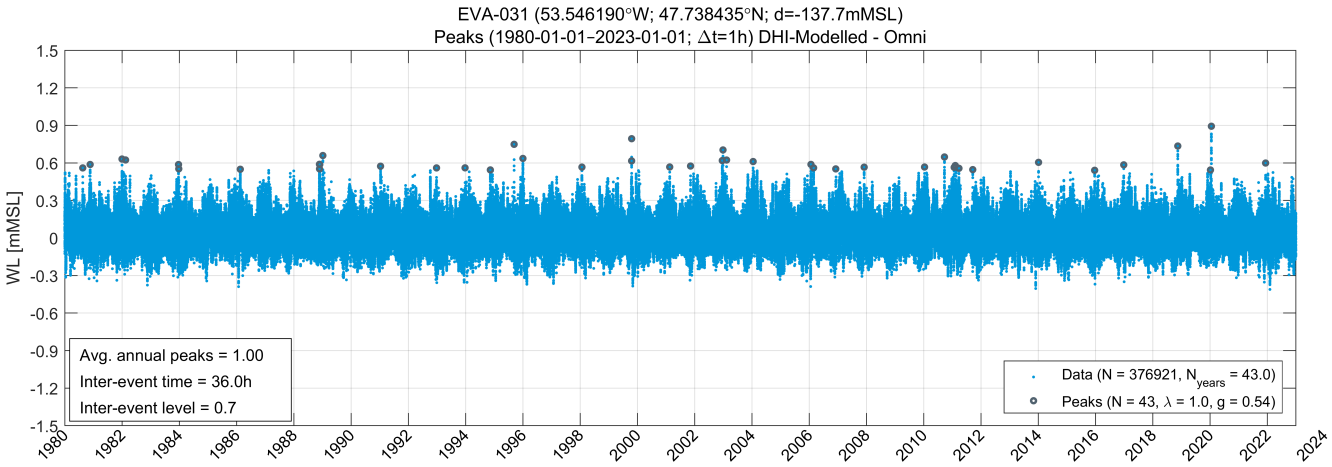


Figure C-61: Time series of water level residual at EVA-031 and selected peaks.

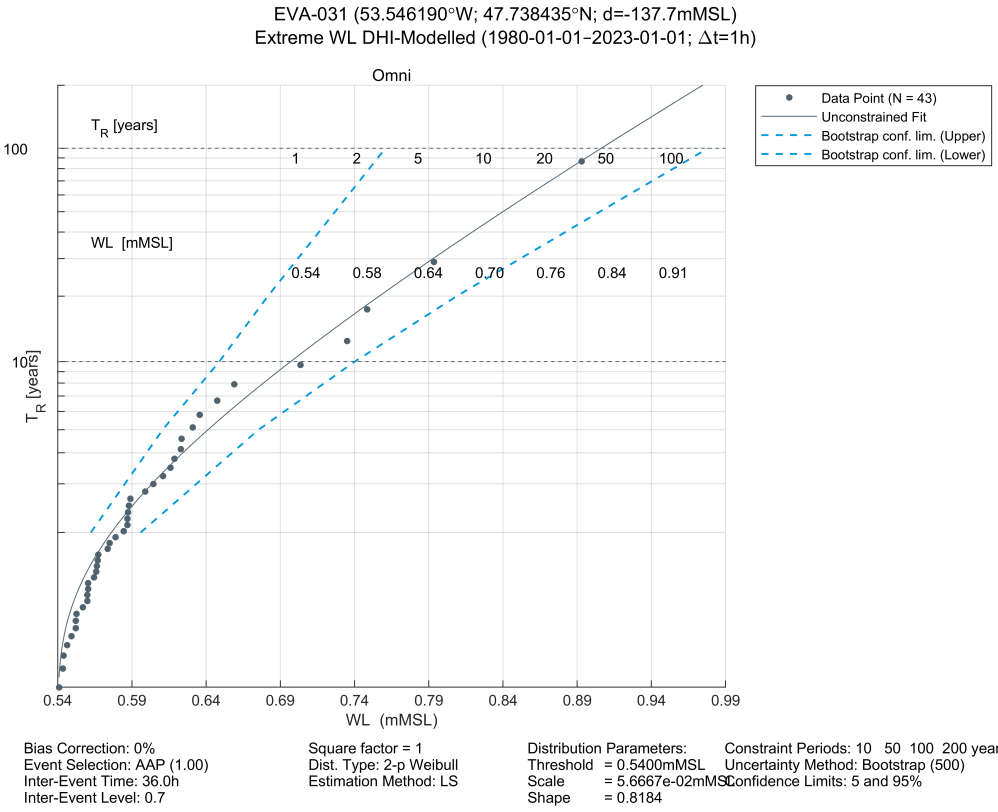


Figure C-62: Extreme value distribution fit at EVA-031.

EVA-032

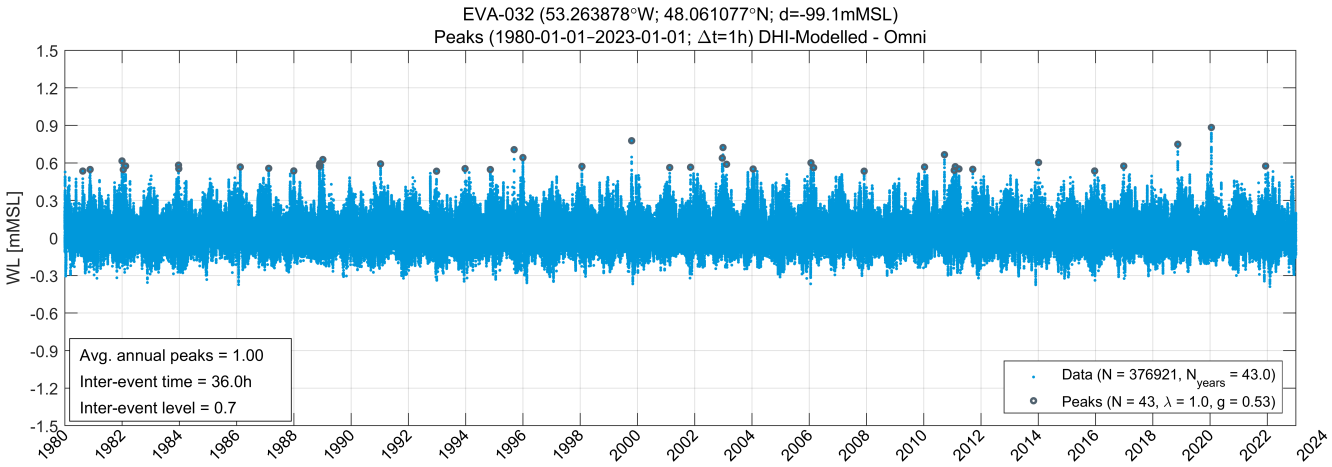


Figure C-63: Time series of water level residual at EVA-032 and selected peaks.

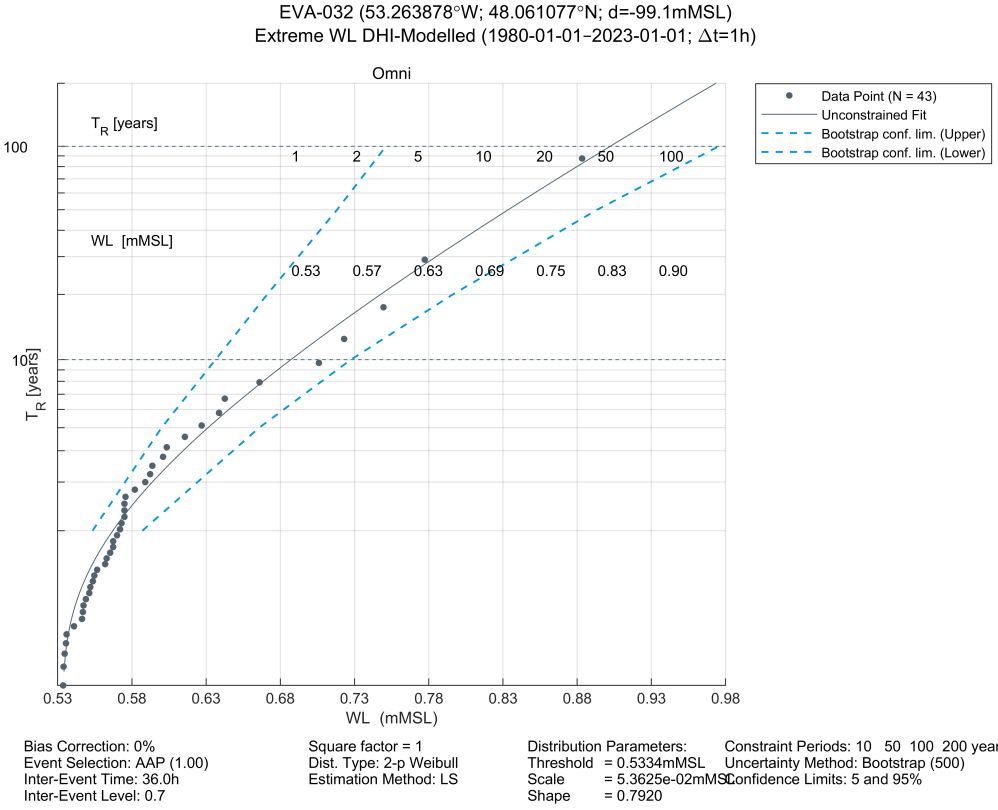


Figure C-64: Extreme value distribution fit at EVA-032.

EVA-033

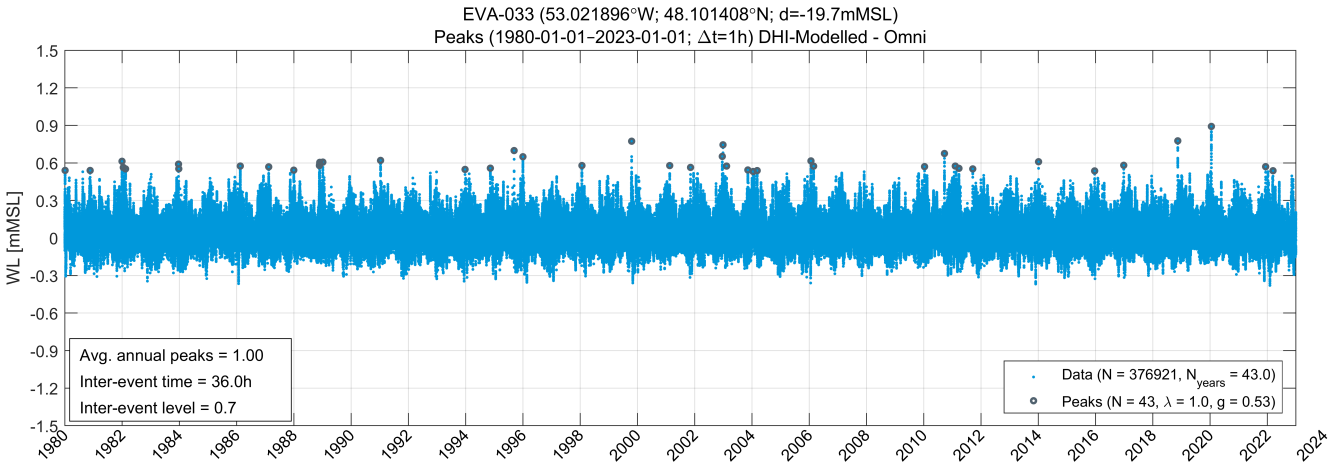


Figure C-65: Time series of water level residual at EVA-033 and selected peaks.

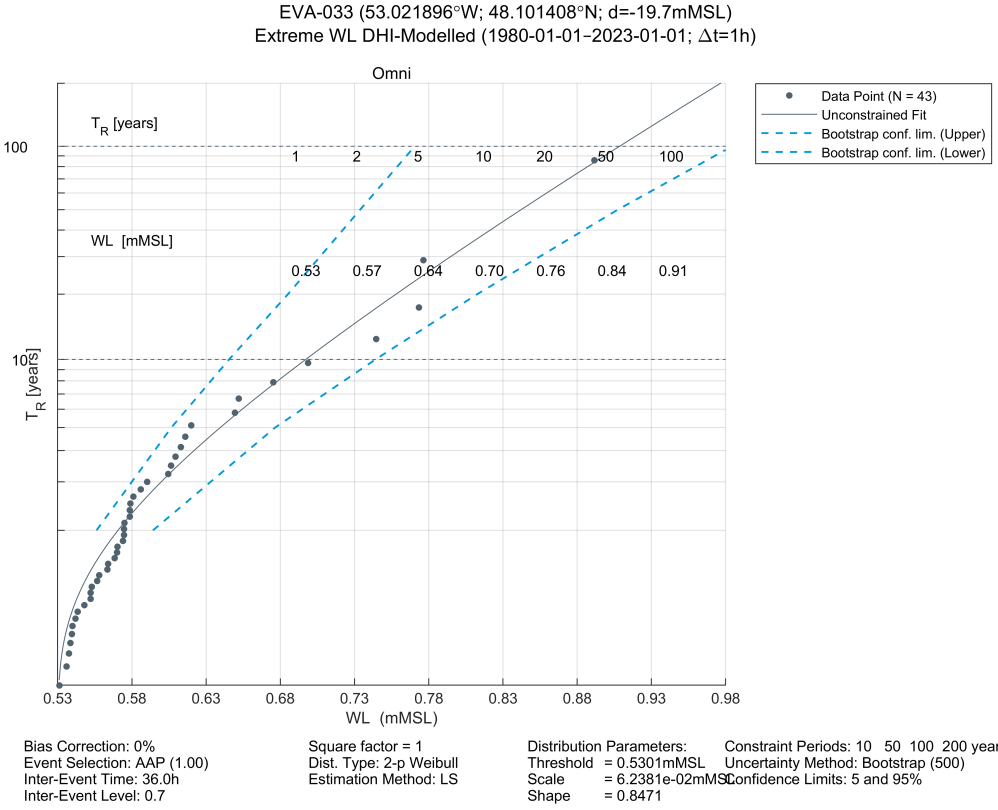


Figure C-66: Extreme value distribution fit at EVA-033.

EVA-034

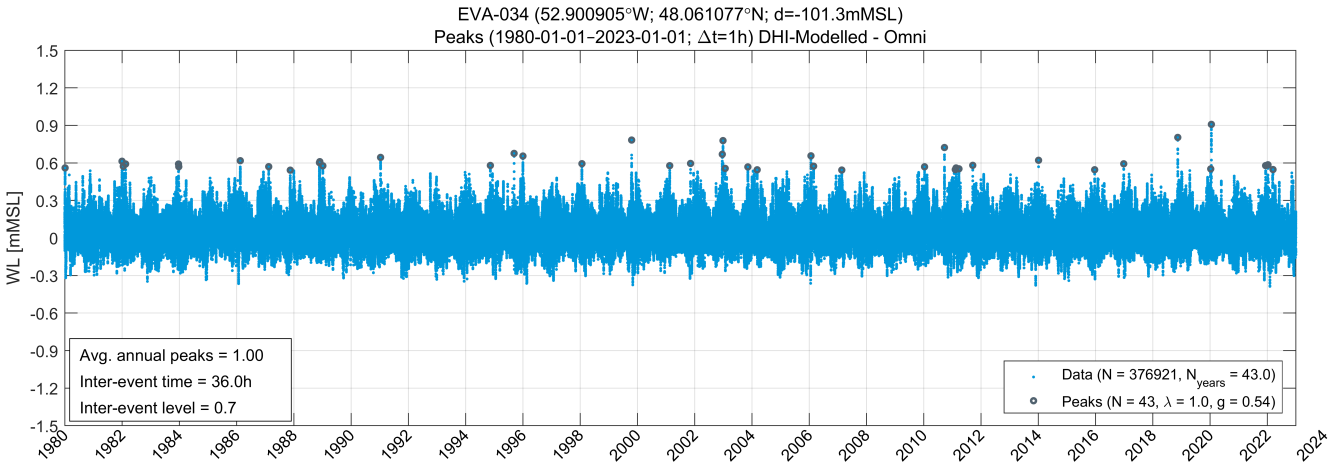


Figure C-67: Time series of water level residual at EVA-034 and selected peaks.

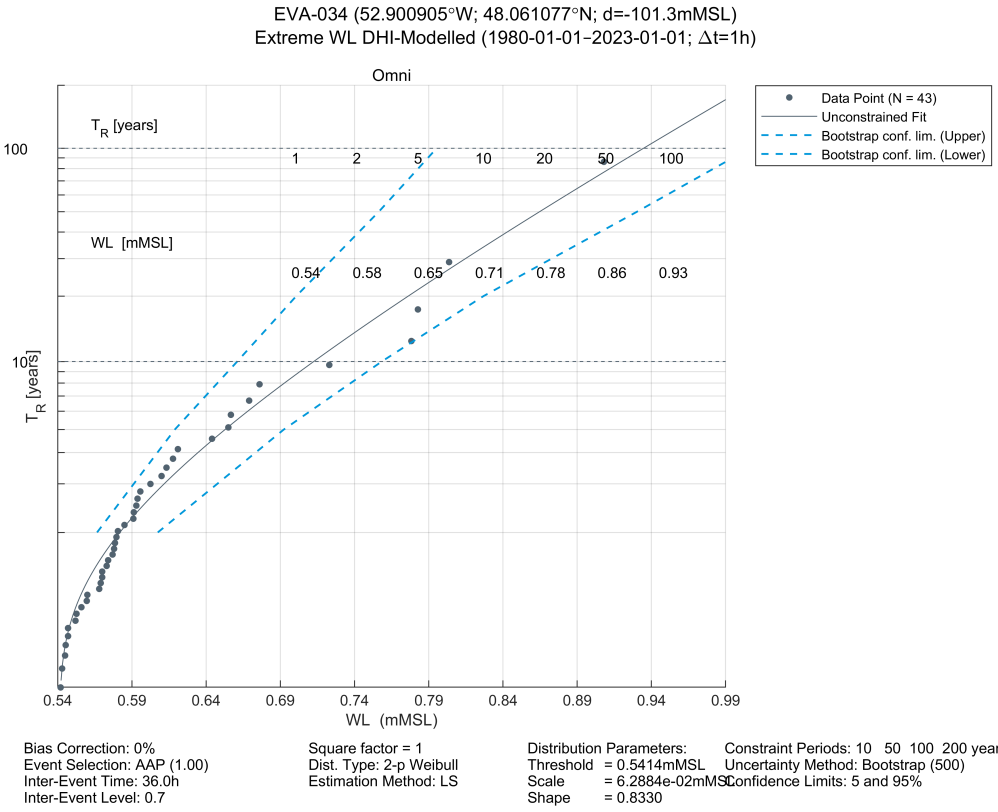


Figure C-68: Extreme value distribution fit at EVA-034.

EVA-035

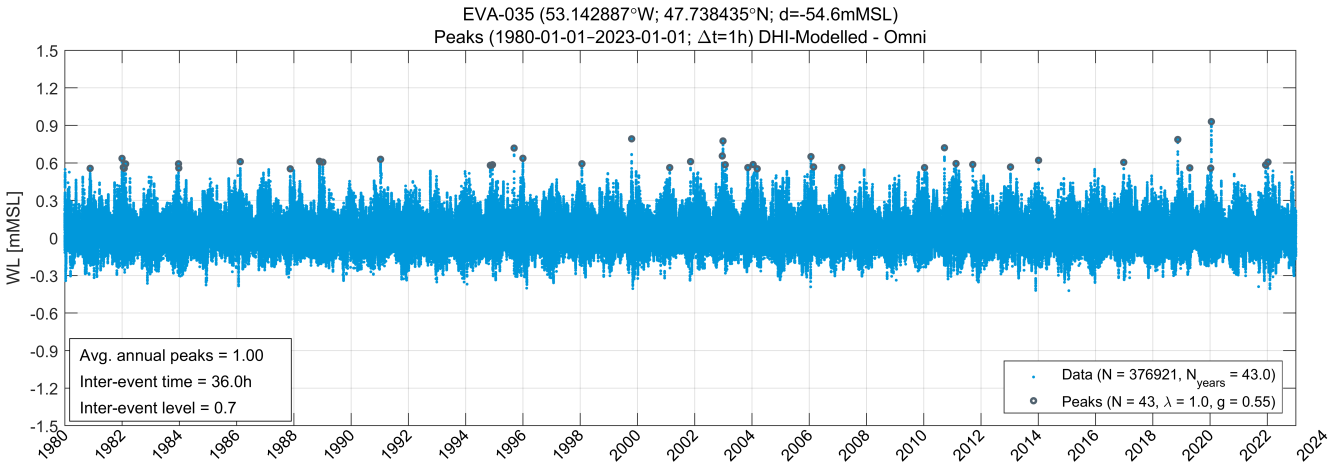


Figure C-69: Time series of water level residual at EVA-035 and selected peaks.

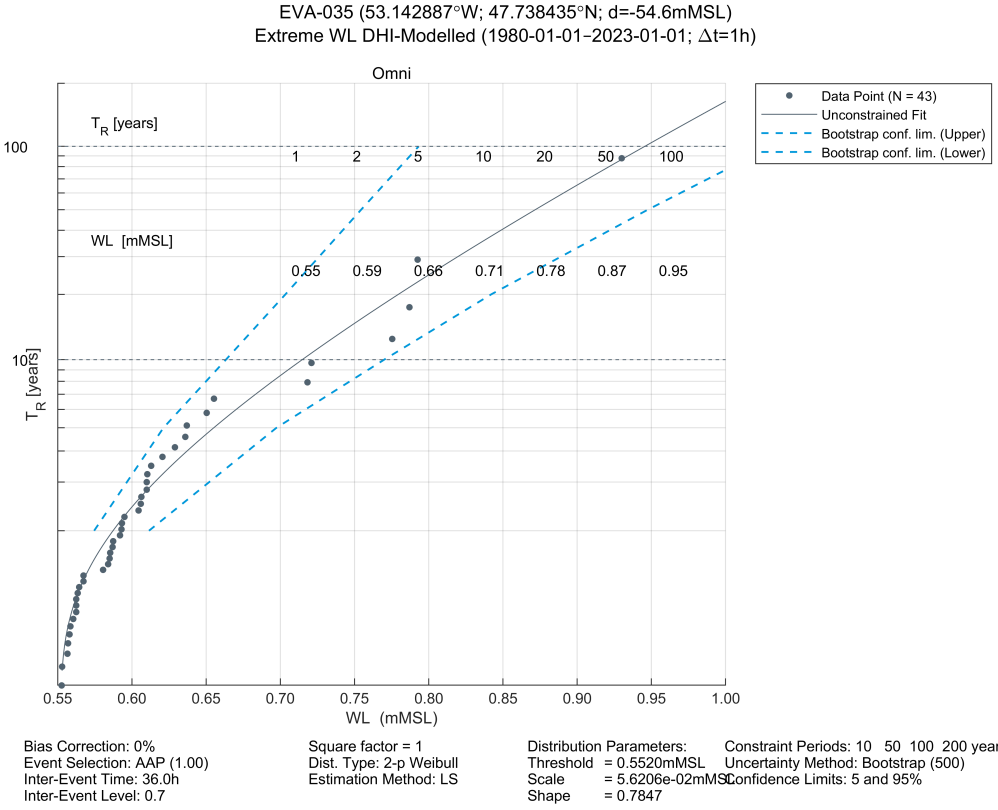


Figure C-70: Extreme value distribution fit at EVA-035.

EVA-036

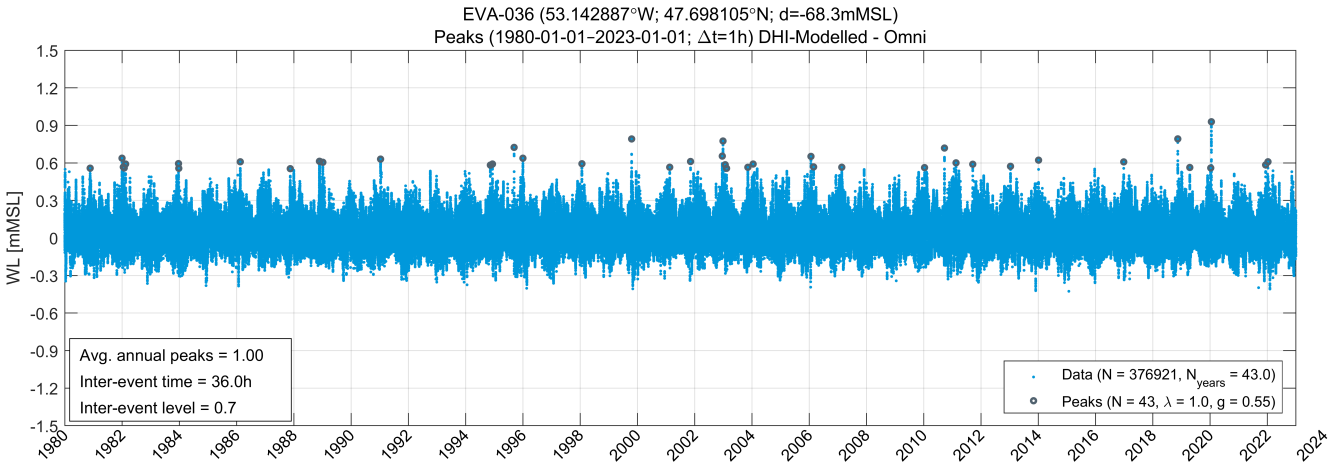


Figure C-71: Time series of water level residual at EVA-036 and selected peaks.

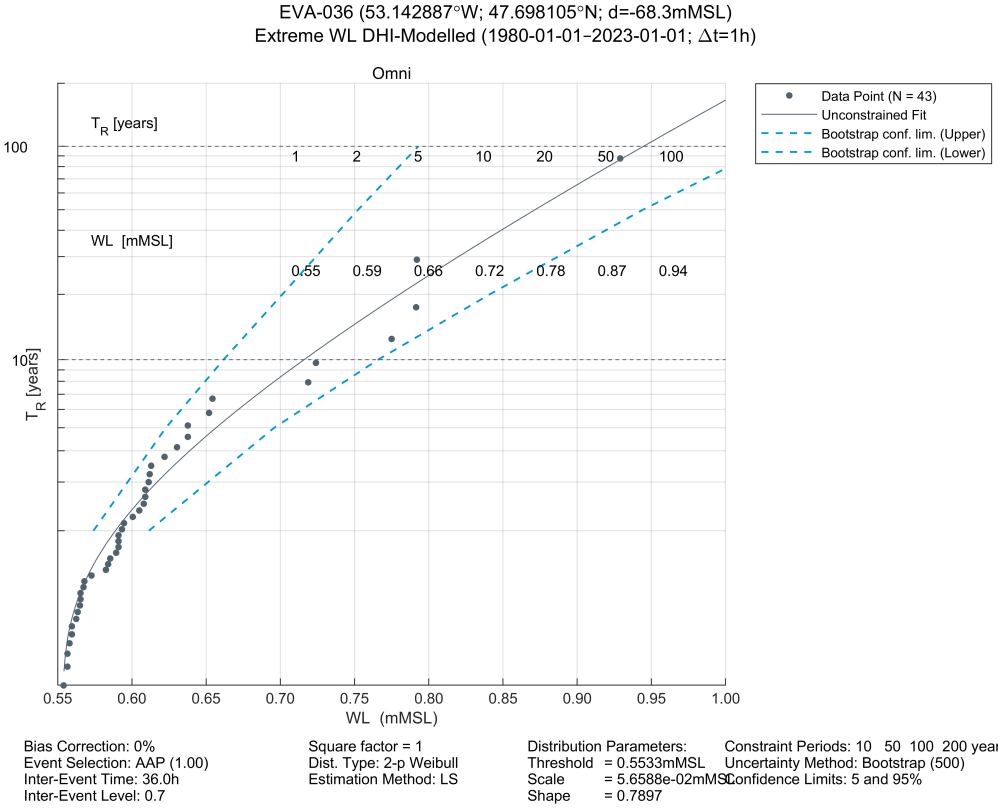


Figure C-72: Extreme value distribution fit at EVA-036.

EVA-037

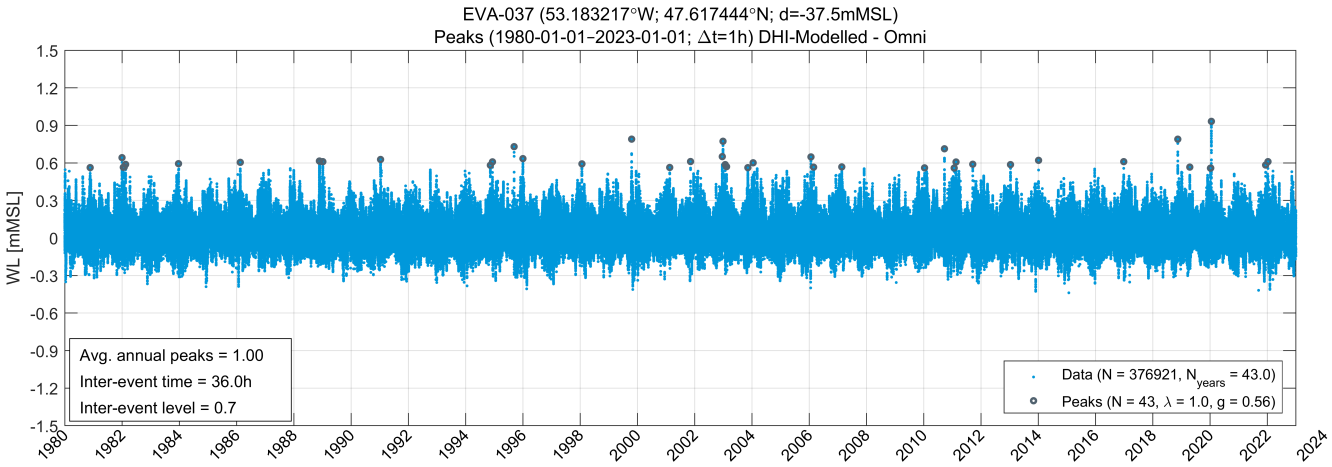


Figure C-73: Time series of water level residual at EVA-037 and selected peaks.

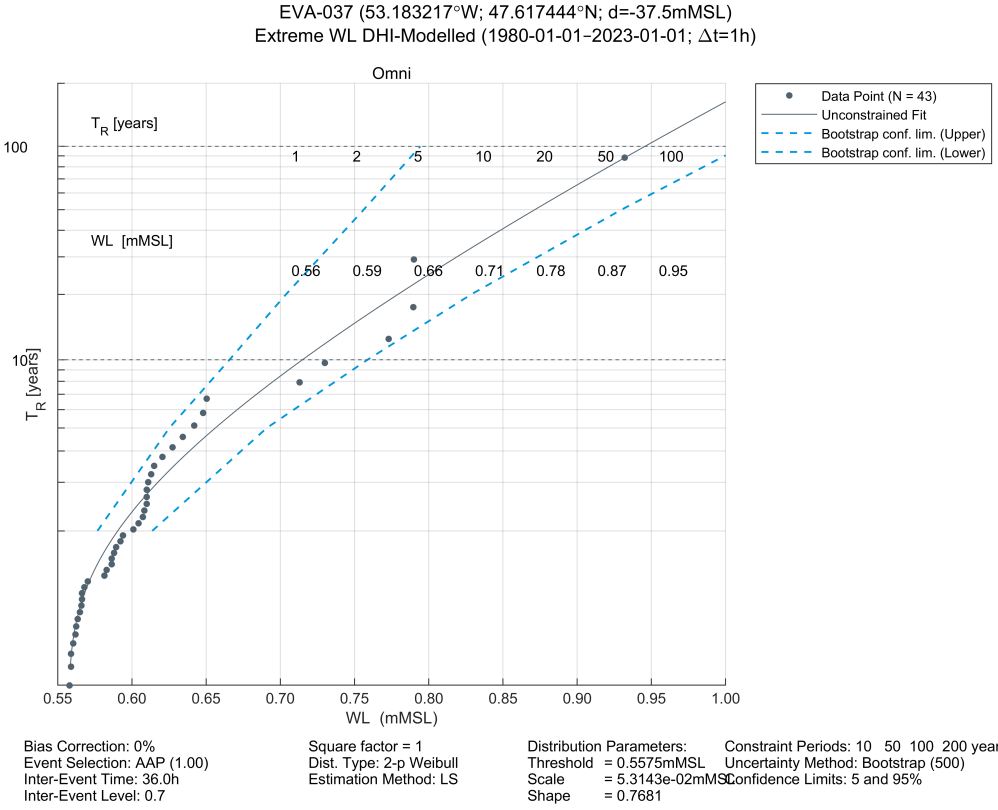


Figure C-74: Extreme value distribution fit at EVA-037.

EVA-038

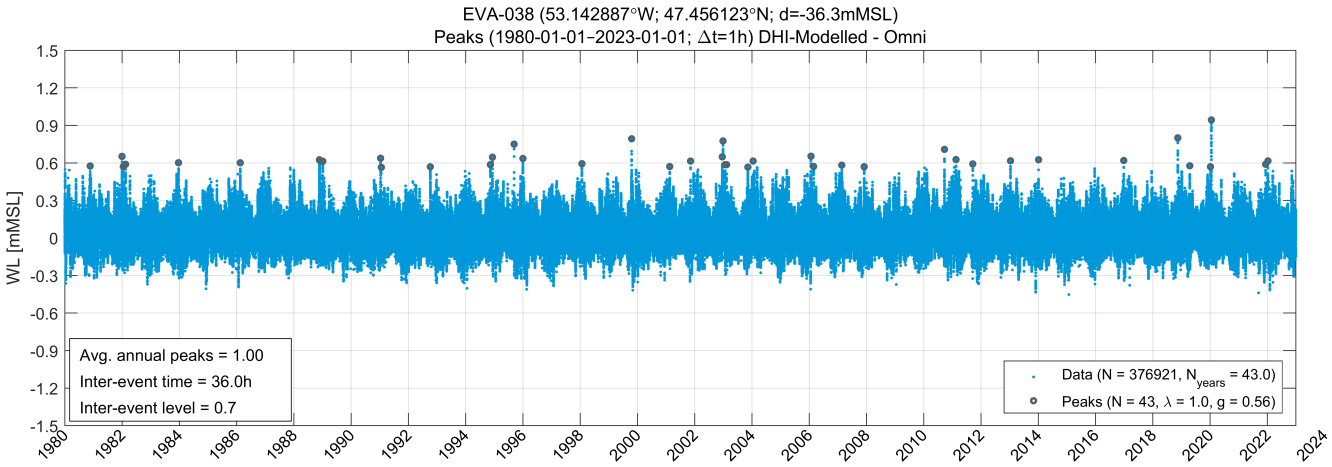


Figure C-75: Time series of water level residual at EVA-038 and selected peaks.

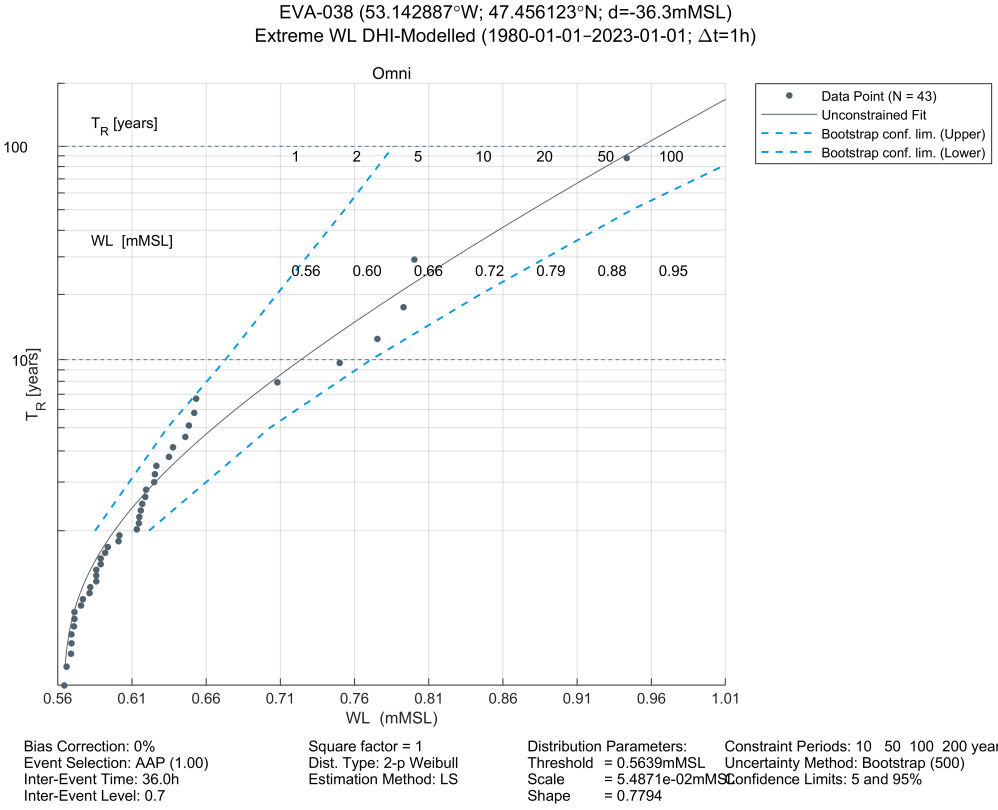


Figure C-76: Extreme value distribution fit at EVA-038.

EVA-039

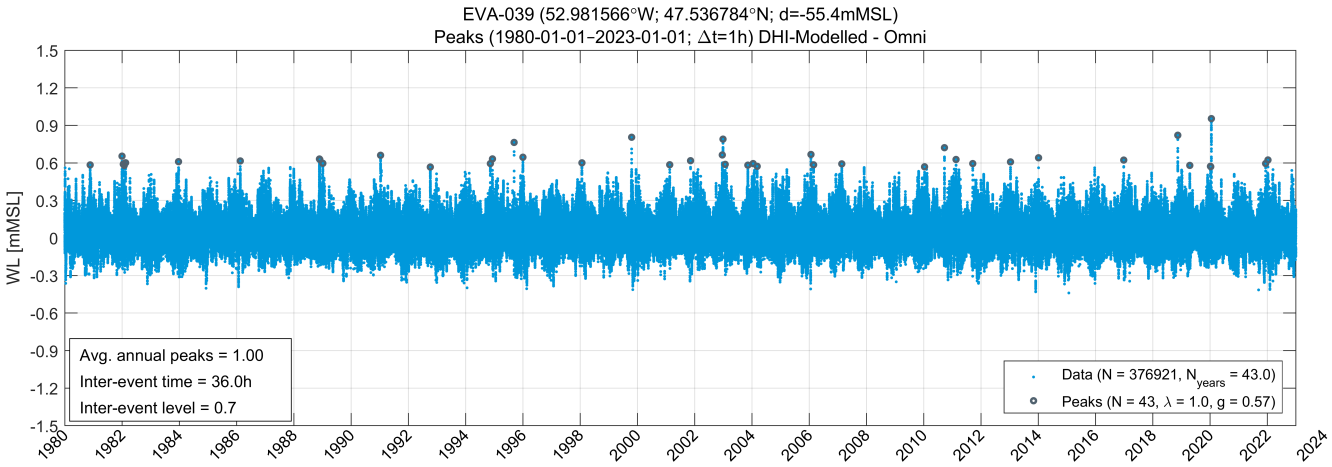


Figure C-77: Time series of water level residual at EVA-039 and selected peaks.

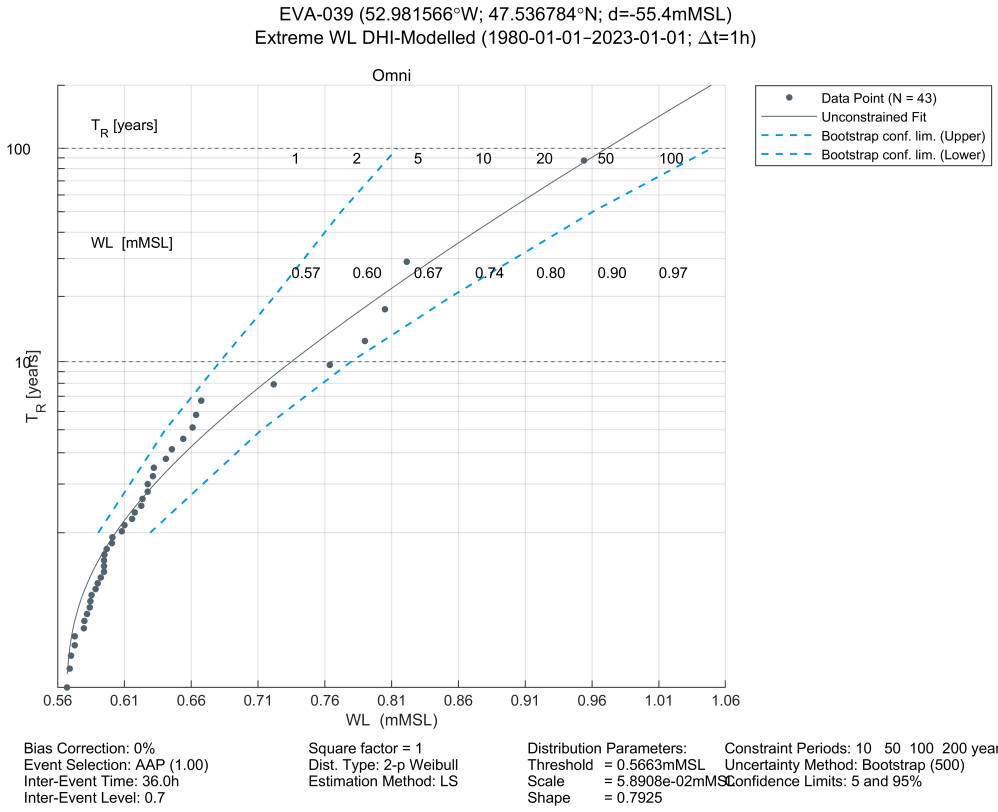


Figure C-78: Extreme value distribution fit at EVA-039.

EVA-040

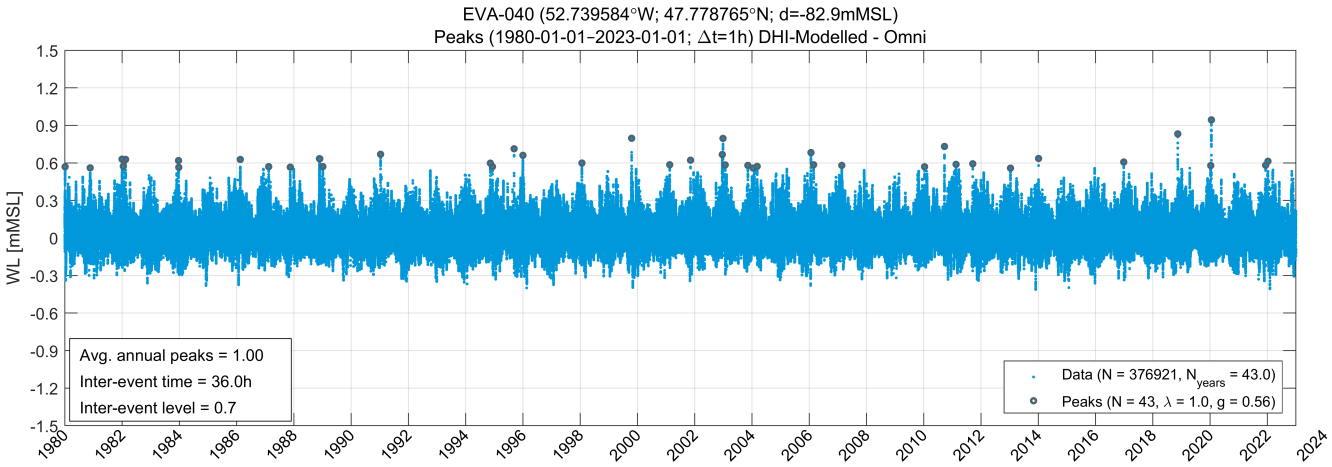


Figure C-79: Time series of water level residual at EVA-040 and selected peaks.

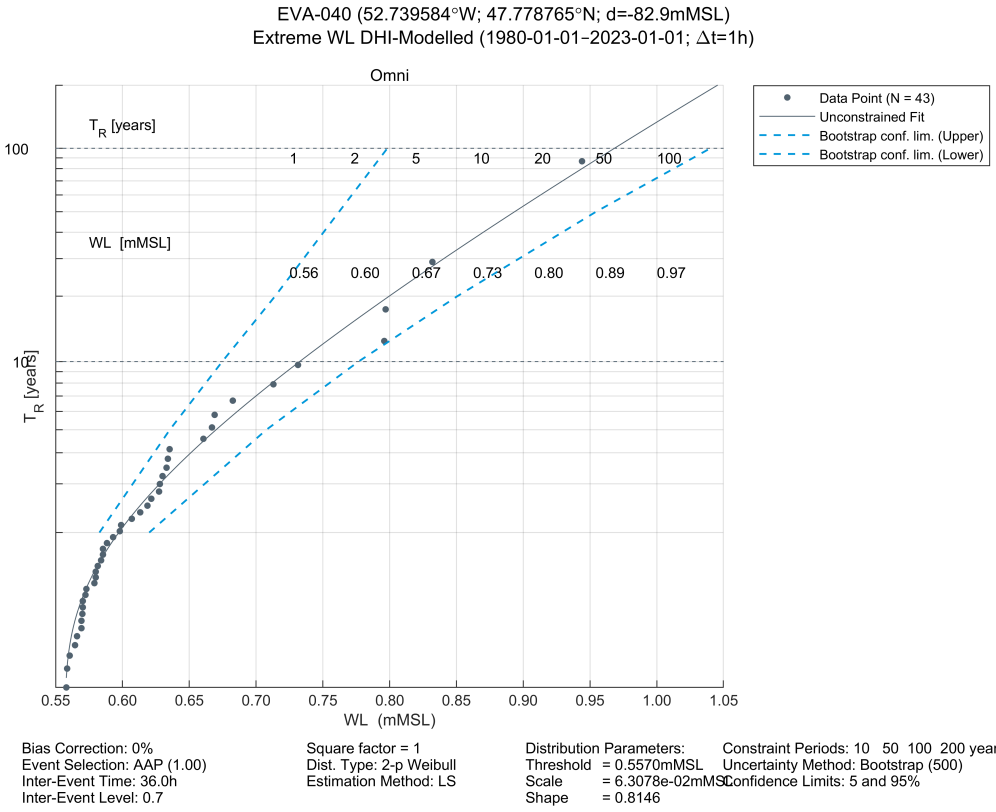


Figure C-80: Extreme value distribution fit at EVA-040.

EVA-041

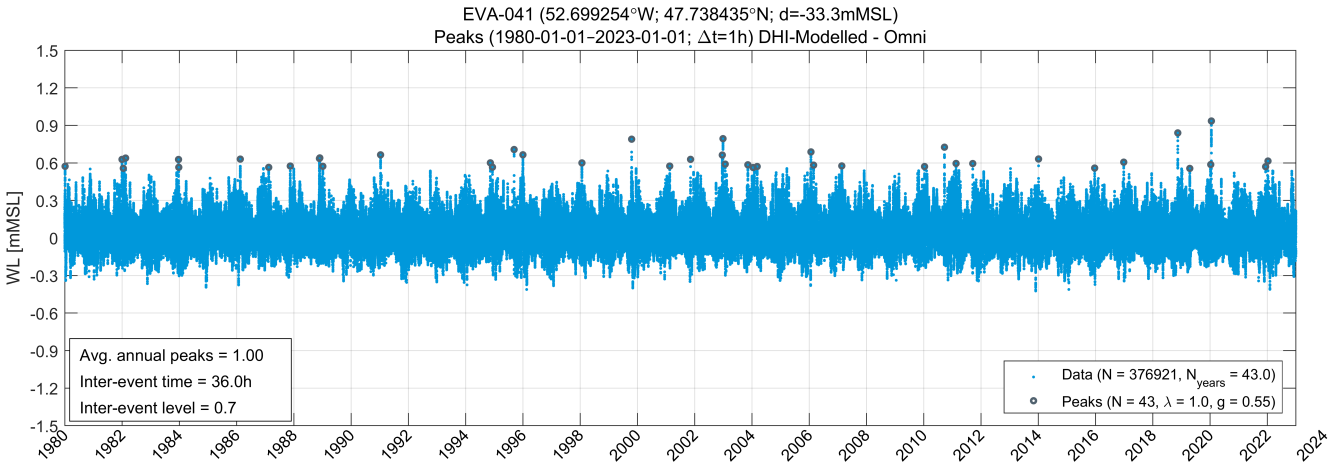


Figure C-81: Time series of water level residual at EVA-041 and selected peaks.

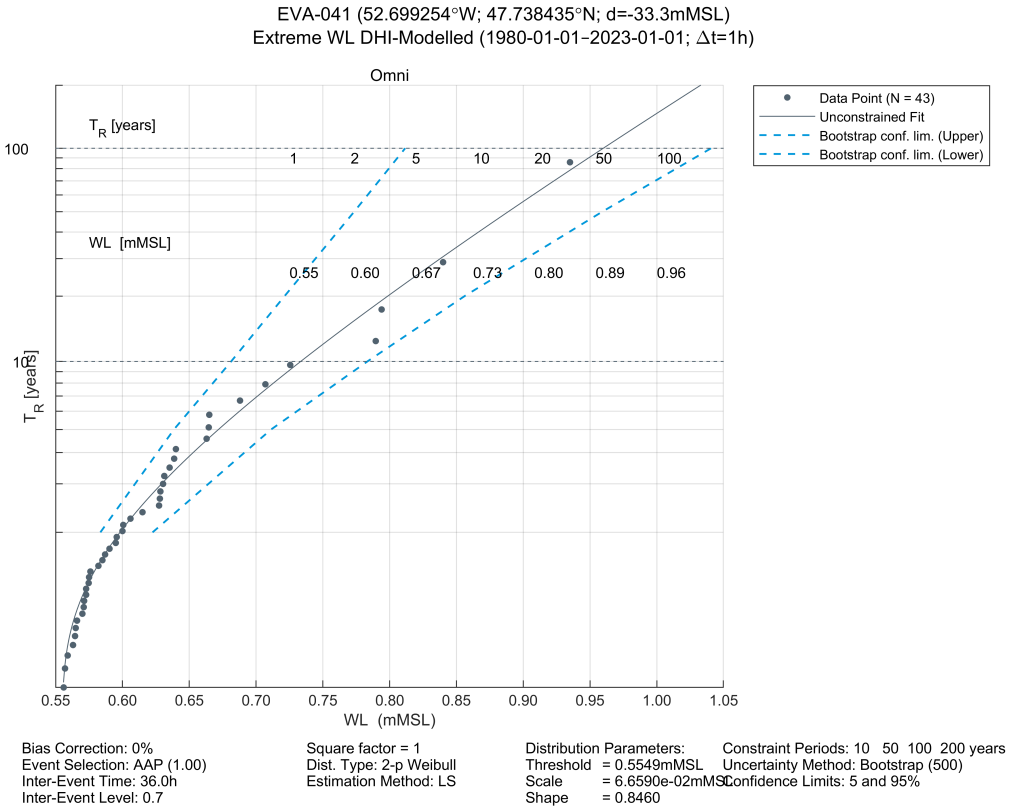


Figure C-82: Extreme value distribution fit at EVA-041.

EVA-042

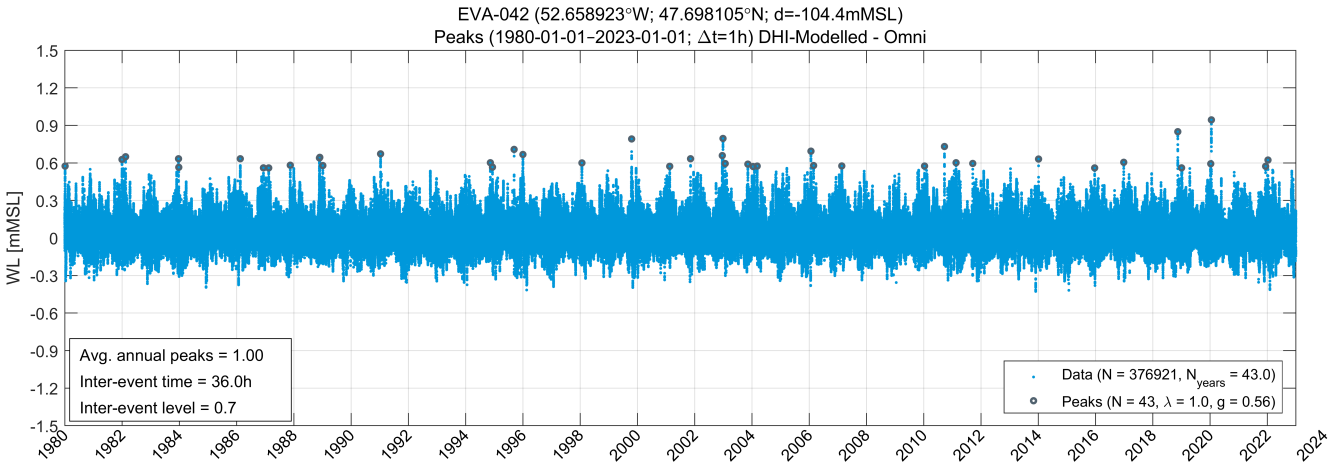


Figure C-83: Time series of water level residual at EVA-042 and selected peaks.

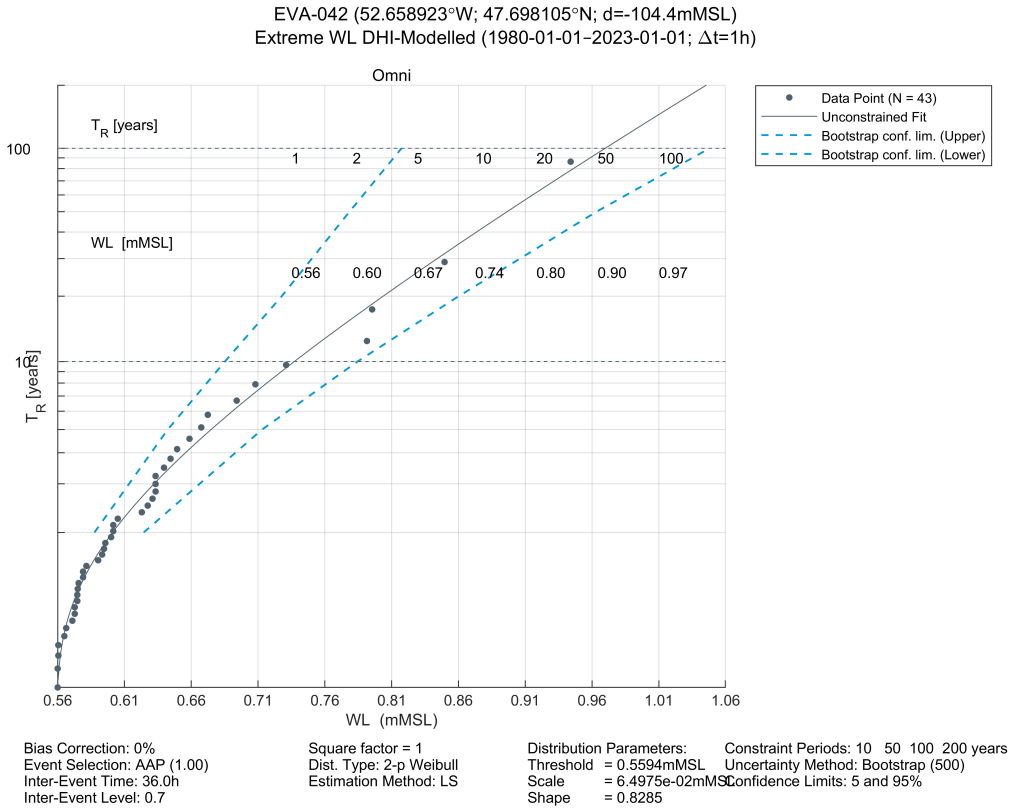


Figure C-84: Extreme value distribution fit at EVA-042.

EVA-043

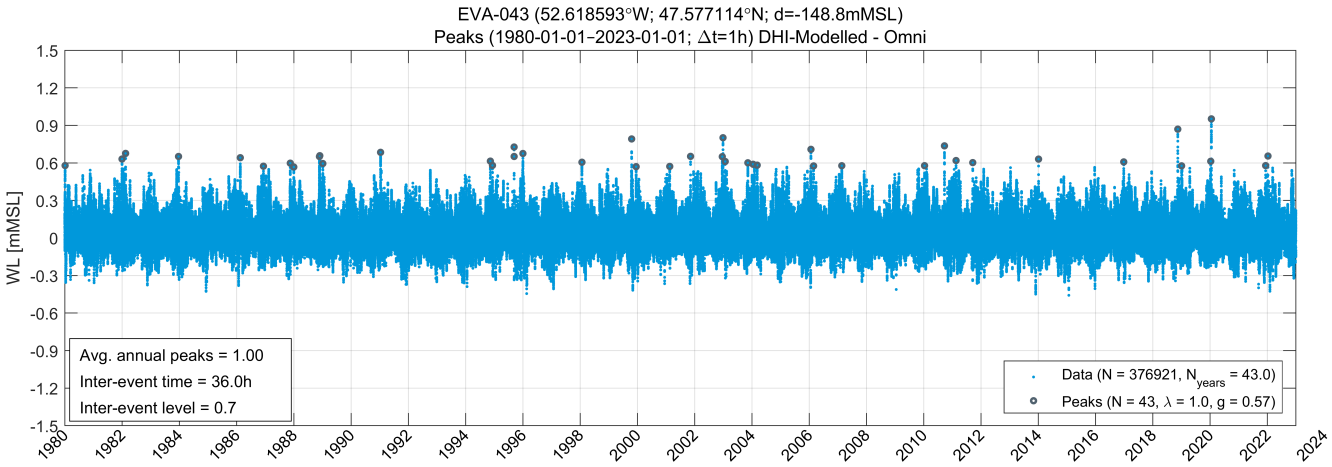


Figure C-85: Time series of water level residual at EVA-043 and selected peaks.

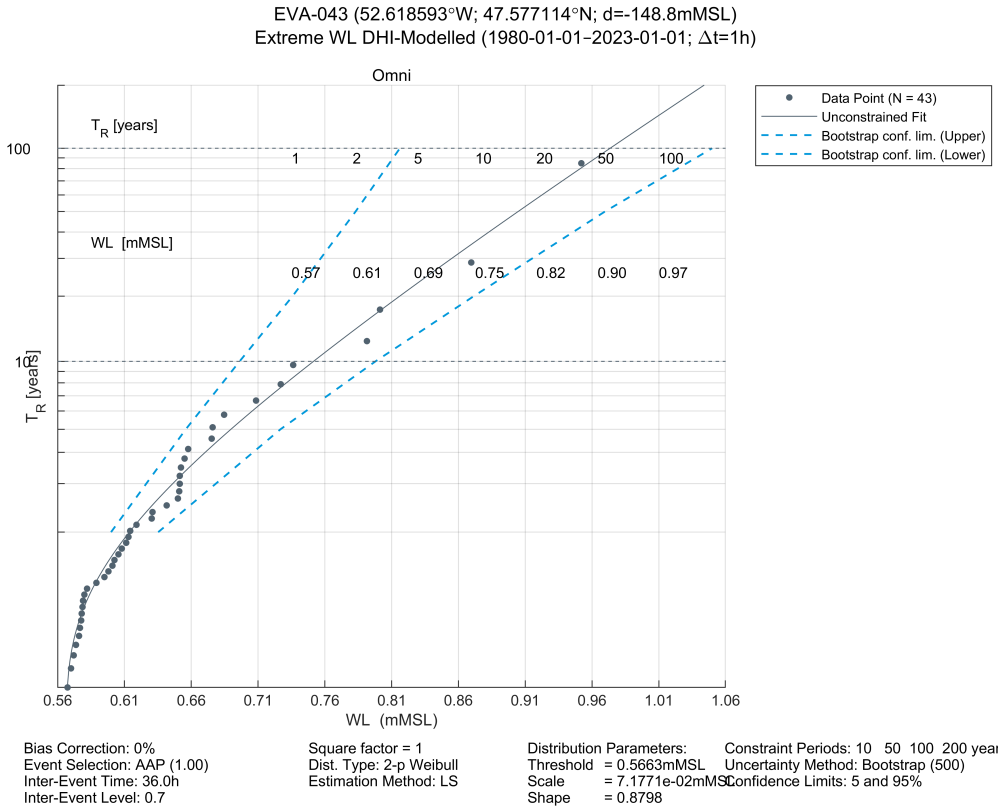


Figure C-86: Extreme value distribution fit at EVA-043.

EVA-044

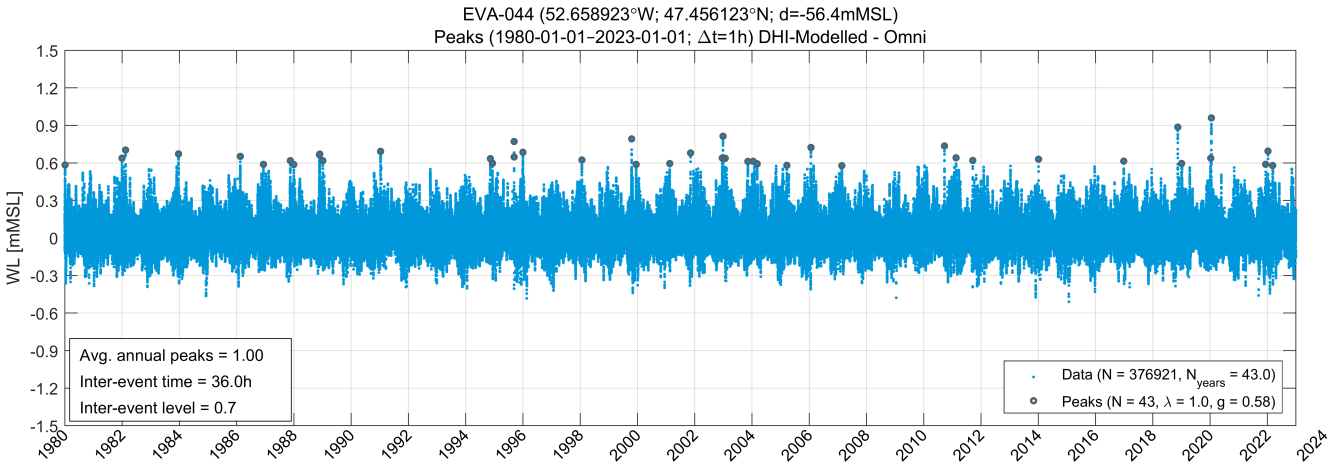


Figure C-87: Time series of water level residual at EVA-044 and selected peaks.

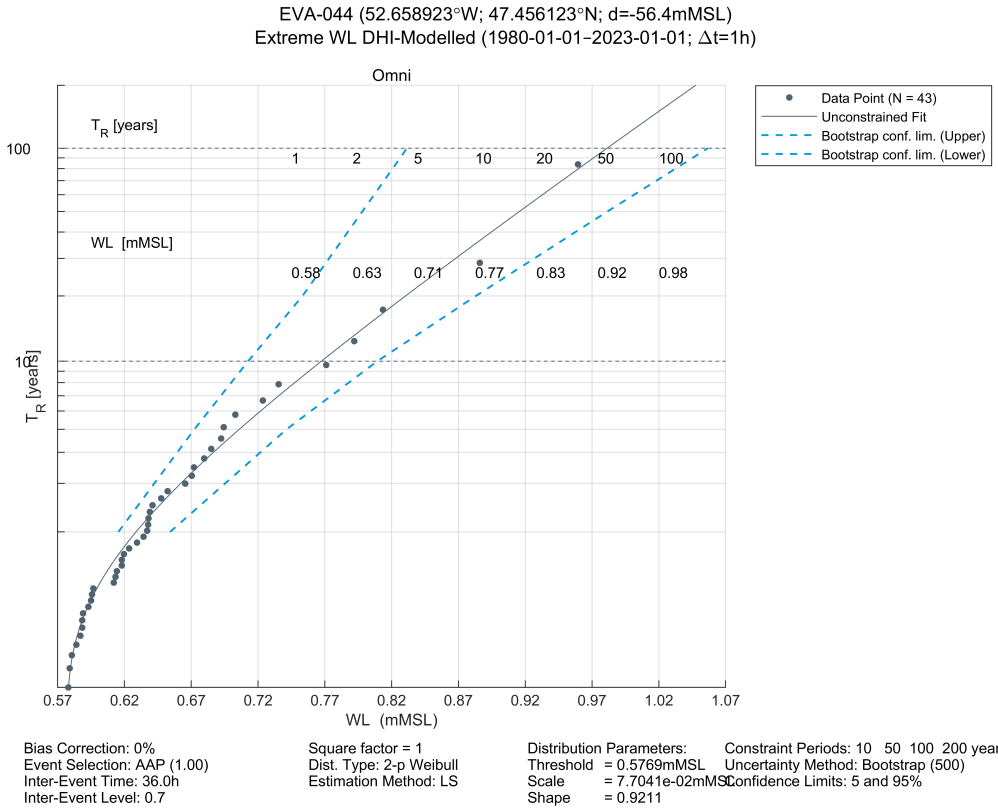


Figure C-88: Extreme value distribution fit at EVA-044.

EVA-045

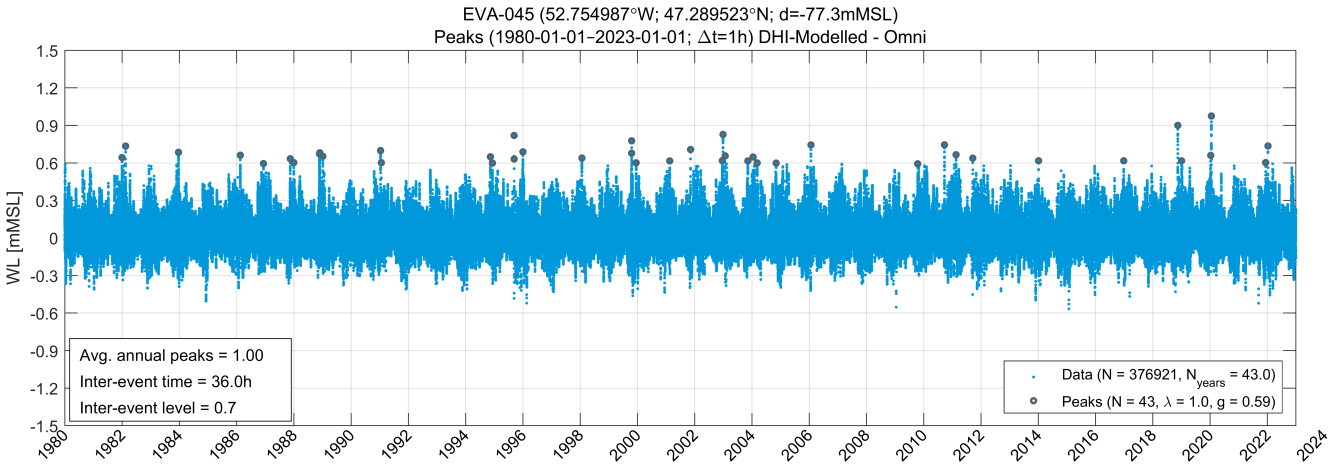


Figure C-89: Time series of water level residual at EVA-045 and selected peaks.

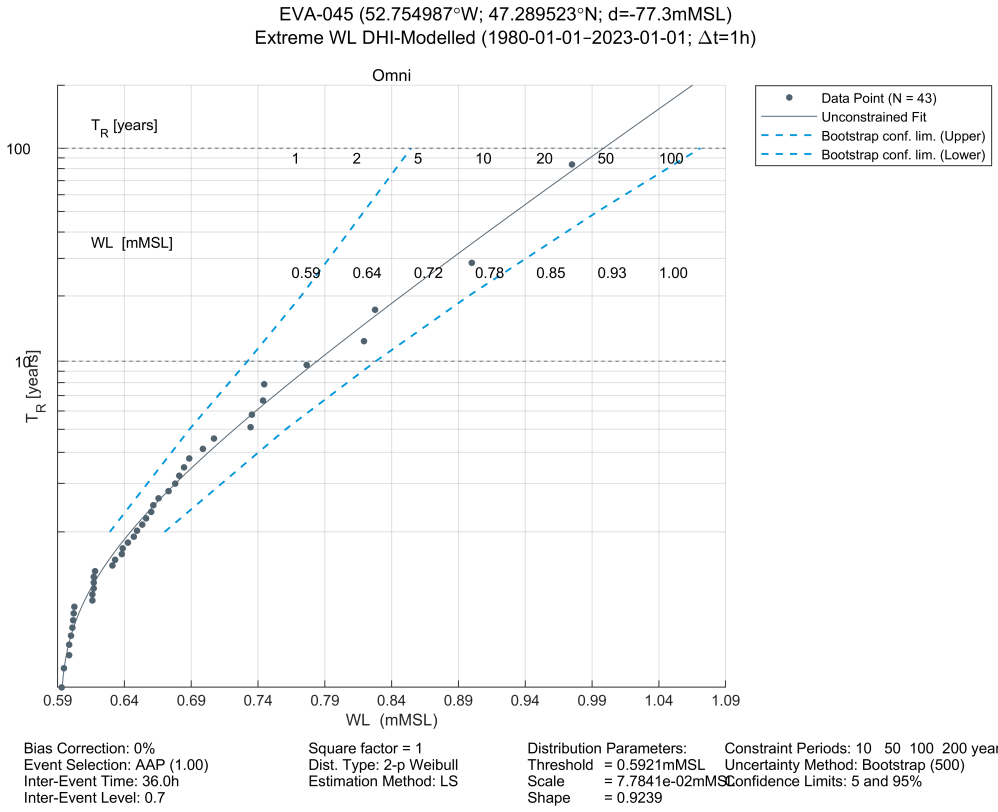


Figure C-90: Extreme value distribution fit at EVA-045.

EVA-046

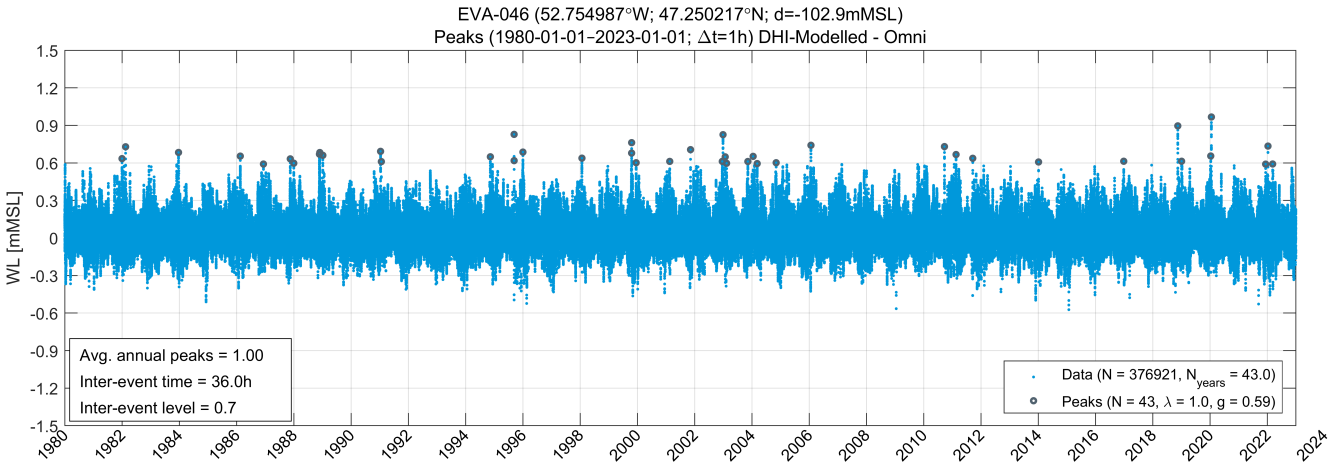


Figure C-91: Time series of water level residual at EVA-046 and selected peaks.

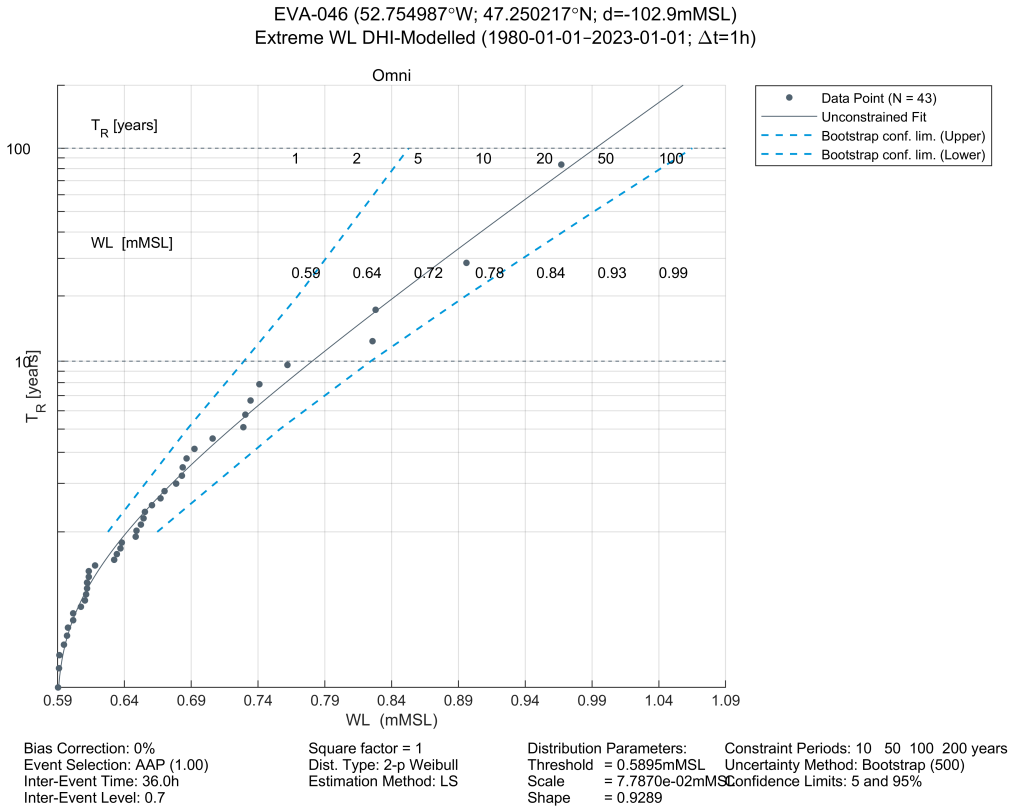


Figure C-92: Extreme value distribution fit at EVA-046.

EVA-047

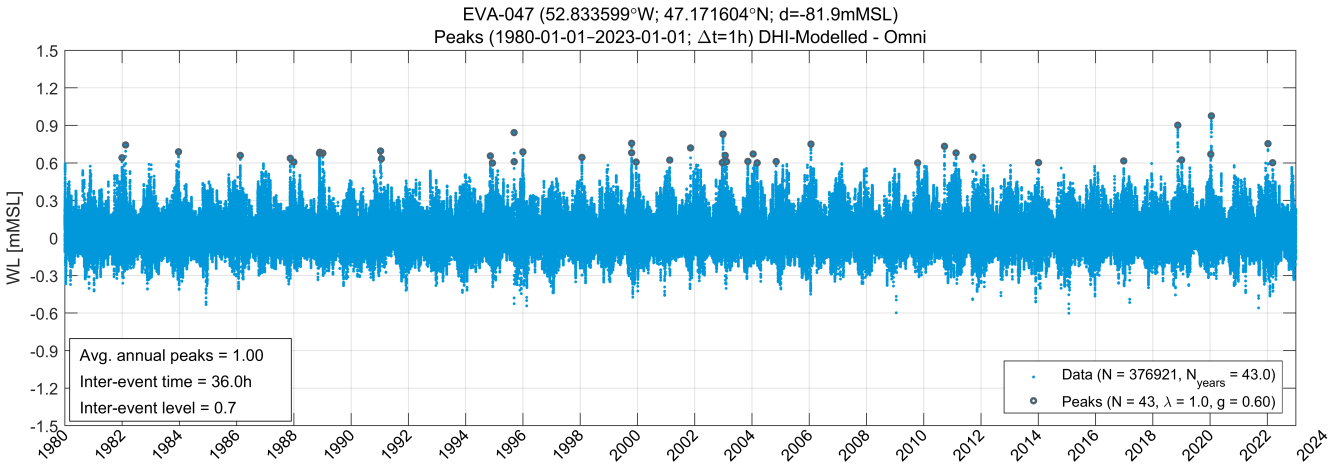


Figure C-93: Time series of water level residual at EVA-047 and selected peaks.

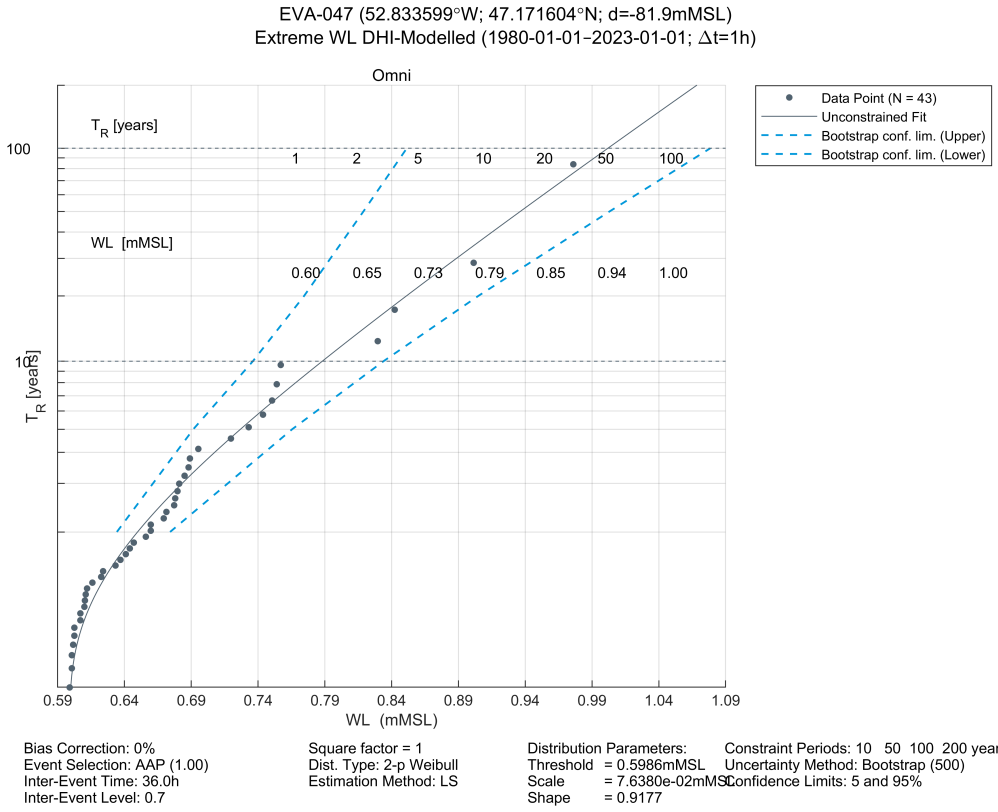


Figure C-94: Extreme value distribution fit at EVA-047.

EVA-048

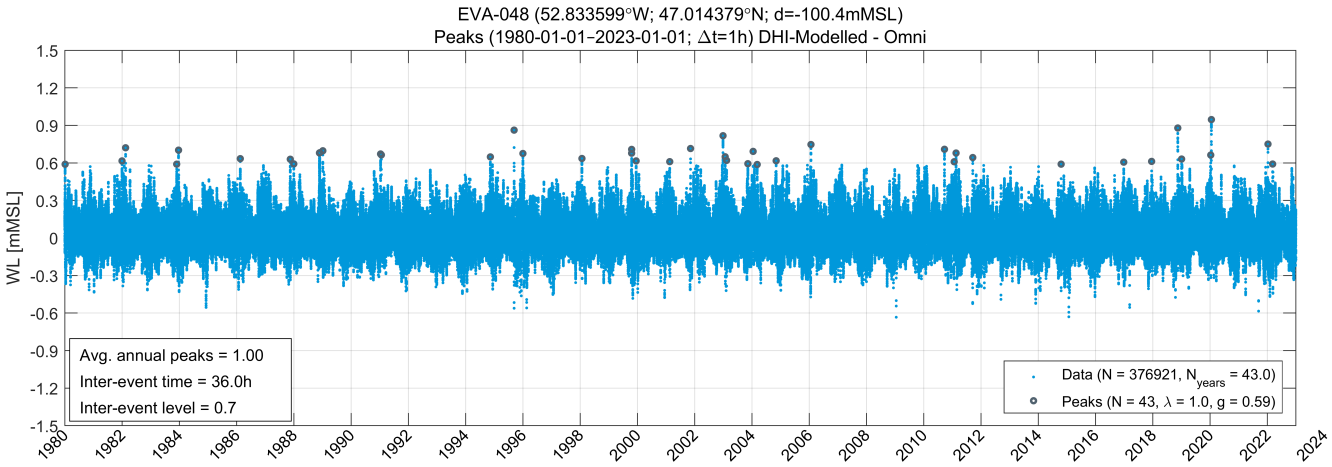


Figure C-95: Time series of water level residual at EVA-048 and selected peaks.

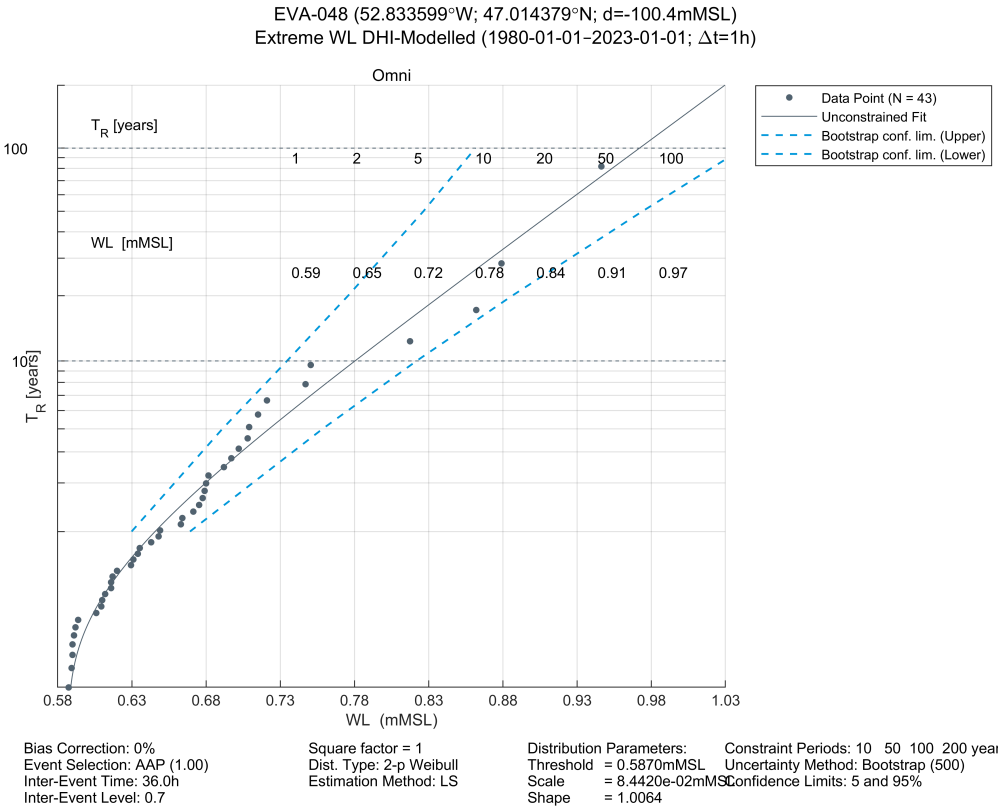


Figure C-96: Extreme value distribution fit at EVA-048.

EVA-049

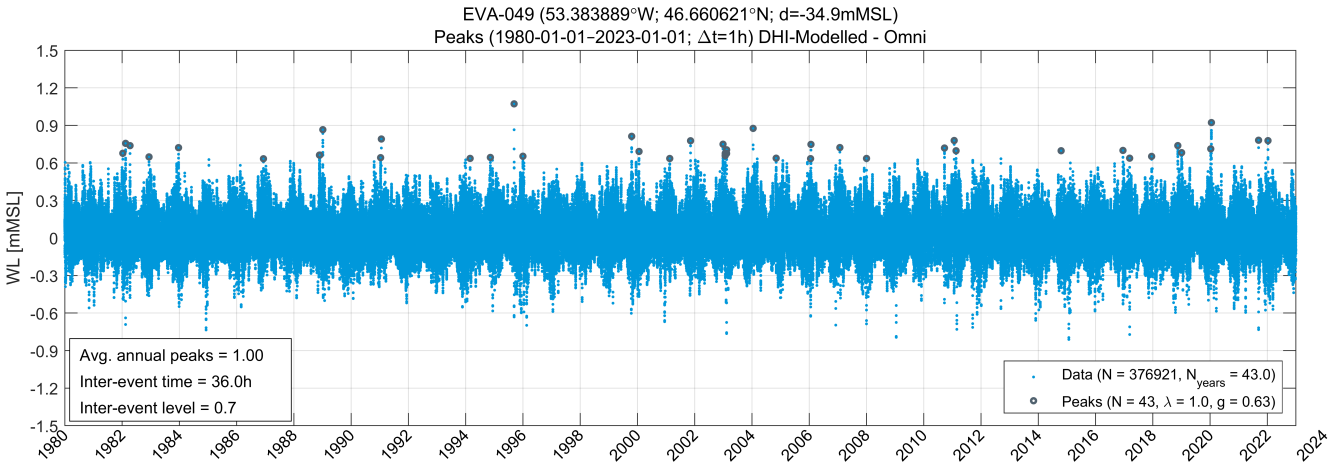


Figure C-97: Time series of water level residual at EVA-049 and selected peaks.

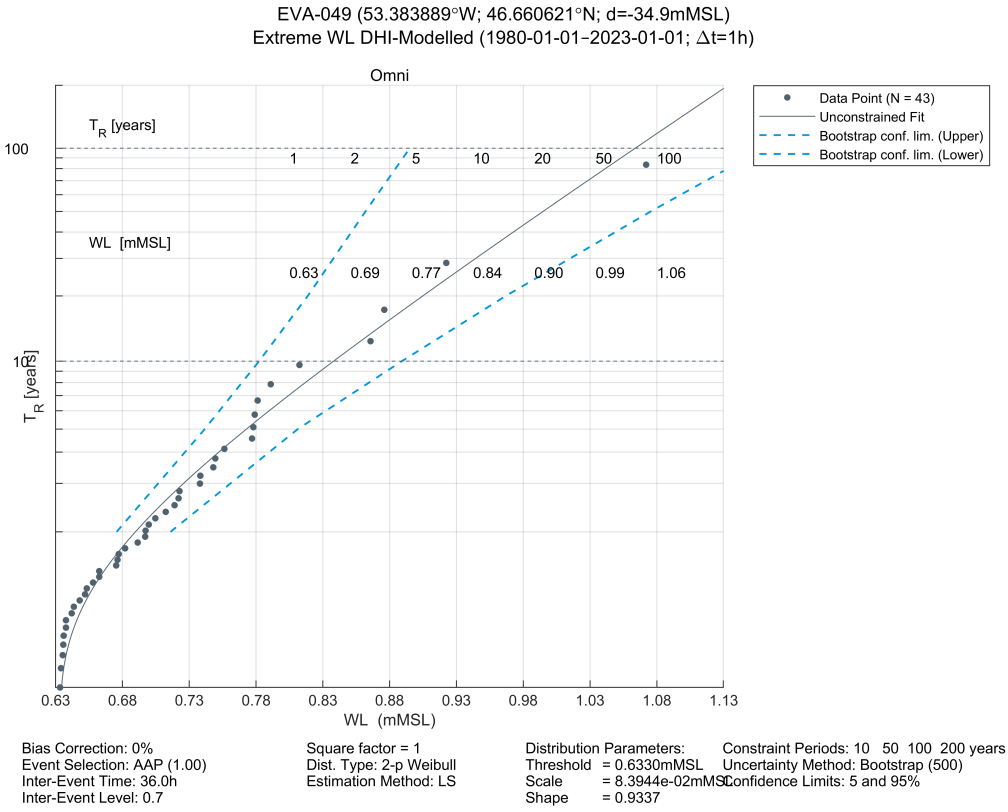


Figure C-98: Extreme value distribution fit at EVA-049.

EVA-050

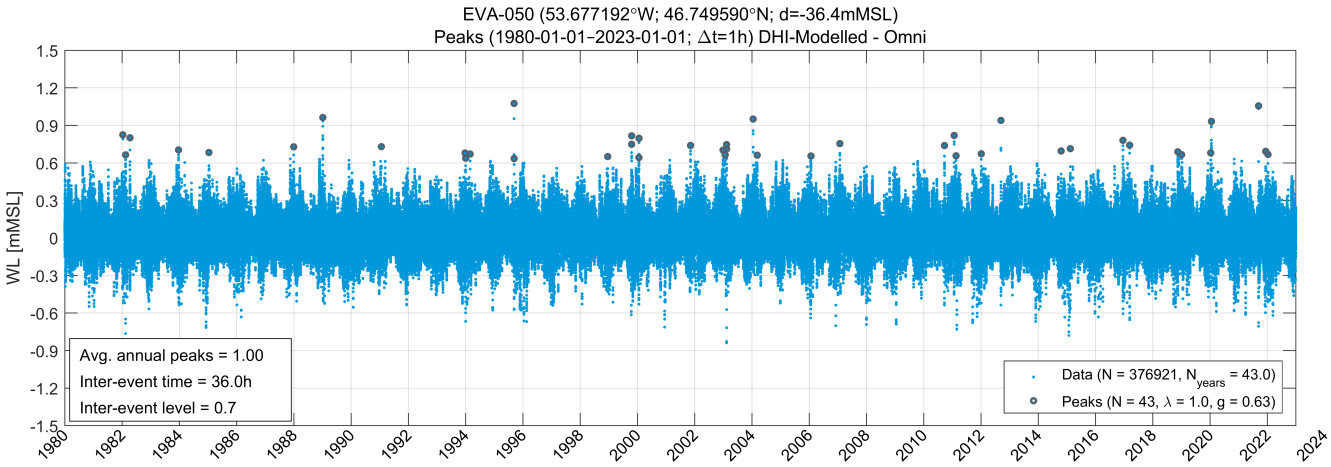


Figure C-99: Time series of water level residual at EVA-050 and selected peaks.

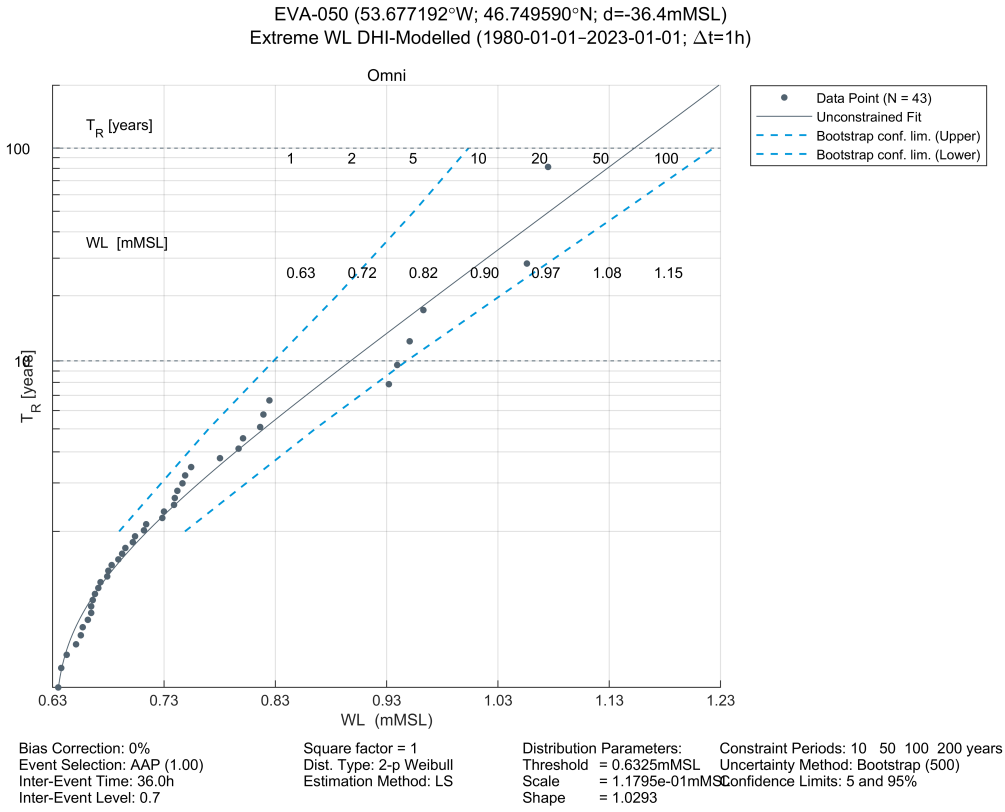


Figure C-100: Extreme value distribution fit at EVA-050.

EVA-051

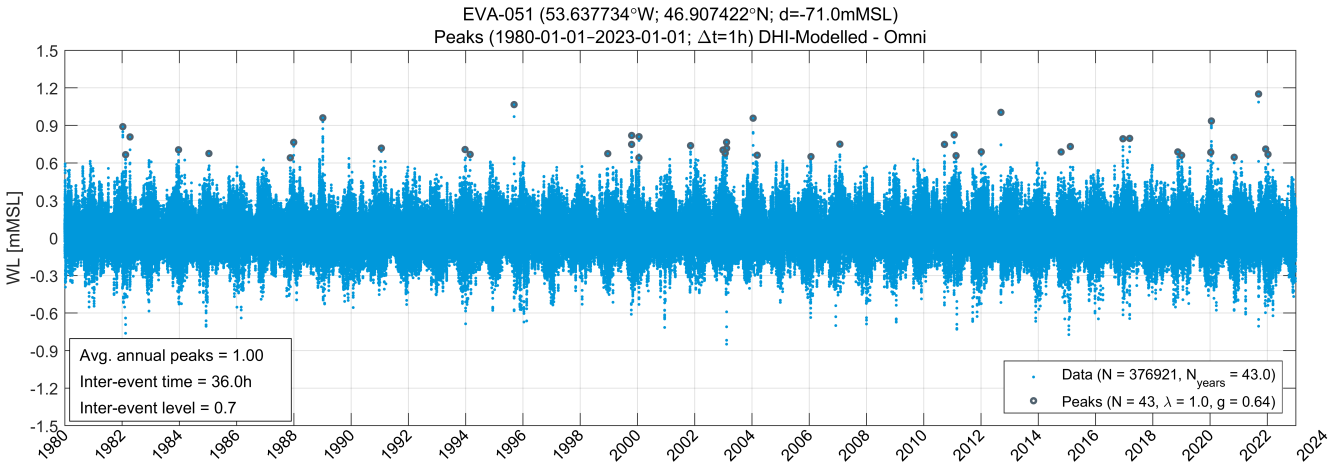


Figure C-101: Time series of water level residual at EVA-051 and selected peaks.

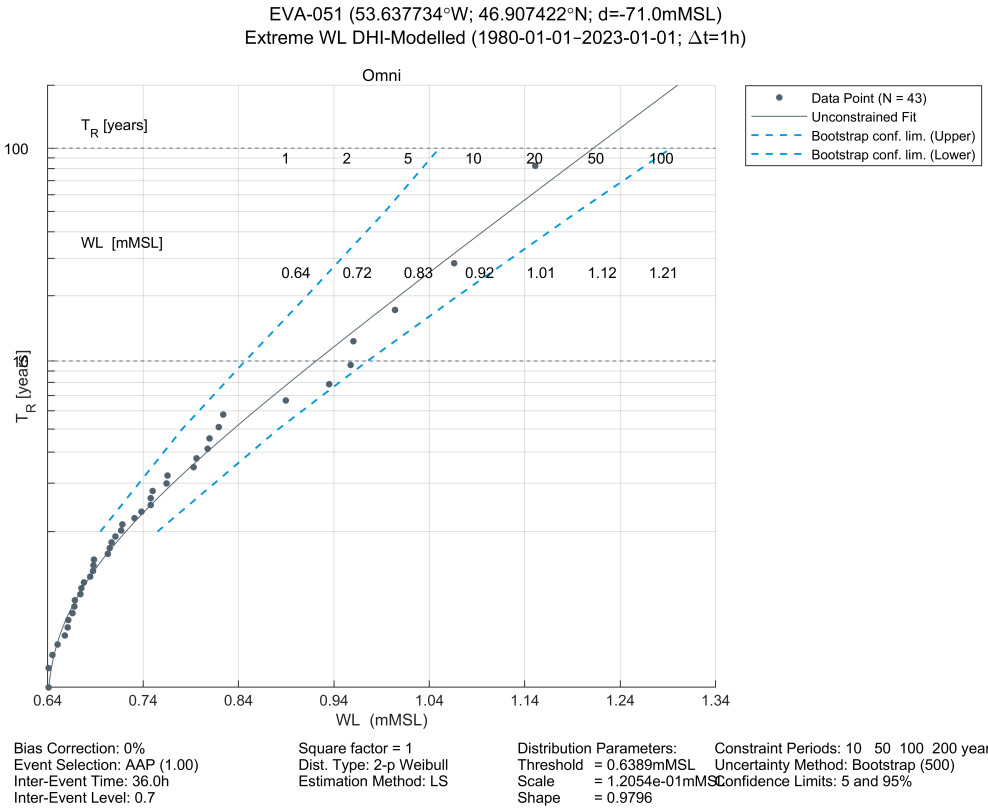


Figure C-102: Extreme value distribution fit at EVA-051.

EVA-052

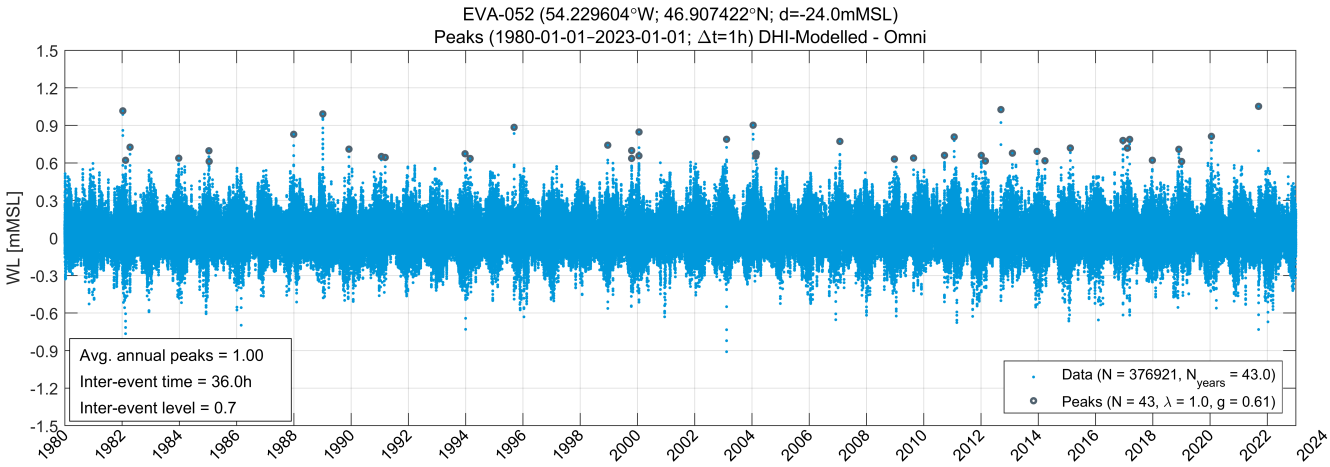


Figure C-103: Time series of water level residual at EVA-052 and selected peaks.

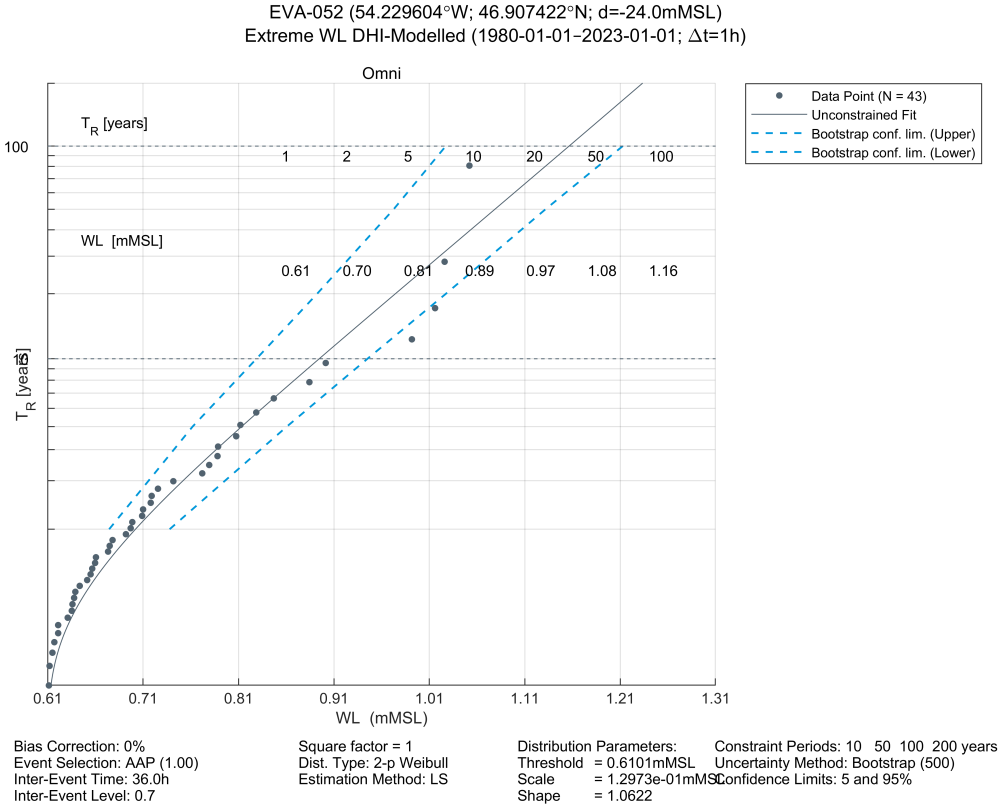


Figure C-104: Extreme value distribution fit at EVA-052.

EVA-053

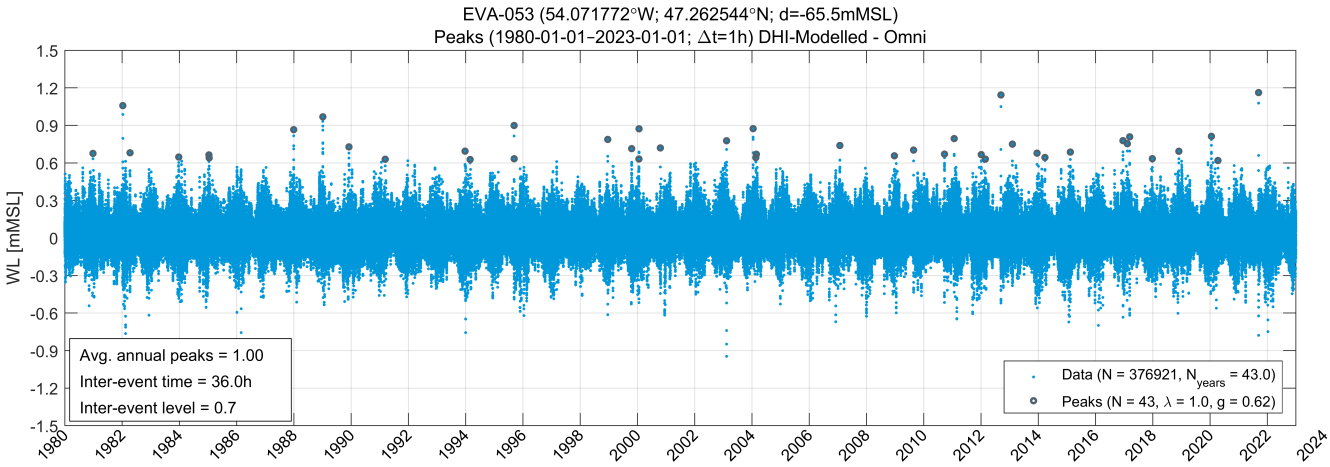


Figure C-105: Time series of water level residual at EVA-053 and selected peaks.

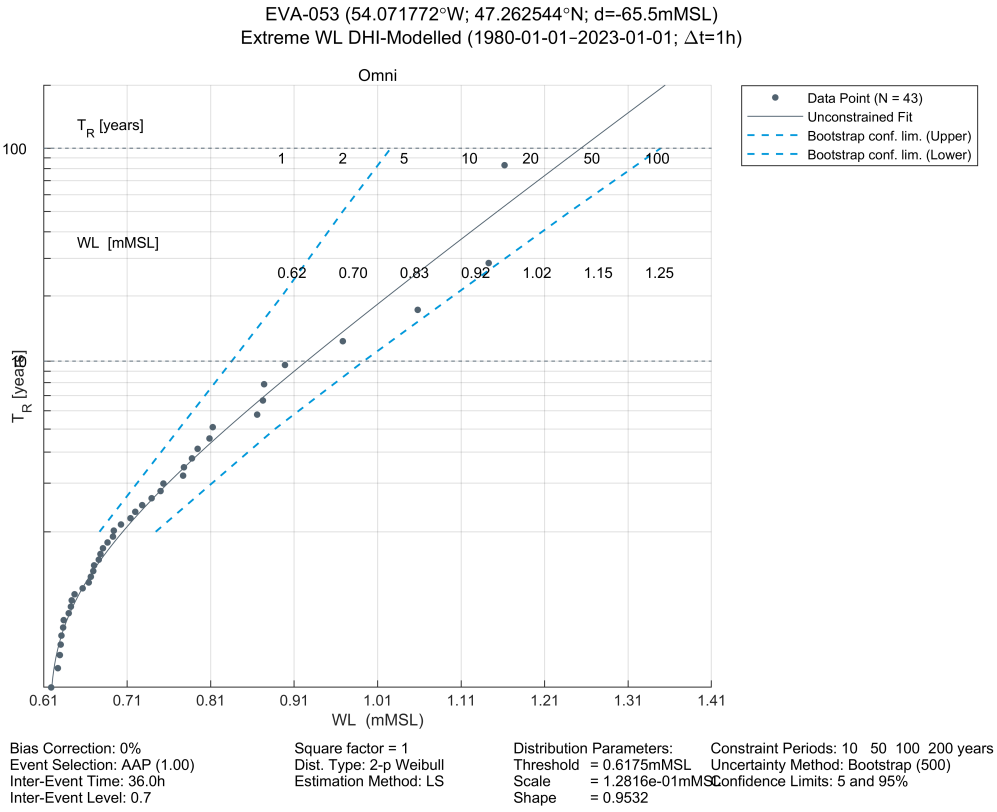


Figure C-106: Extreme value distribution fit at EVA-053.

EVA-054

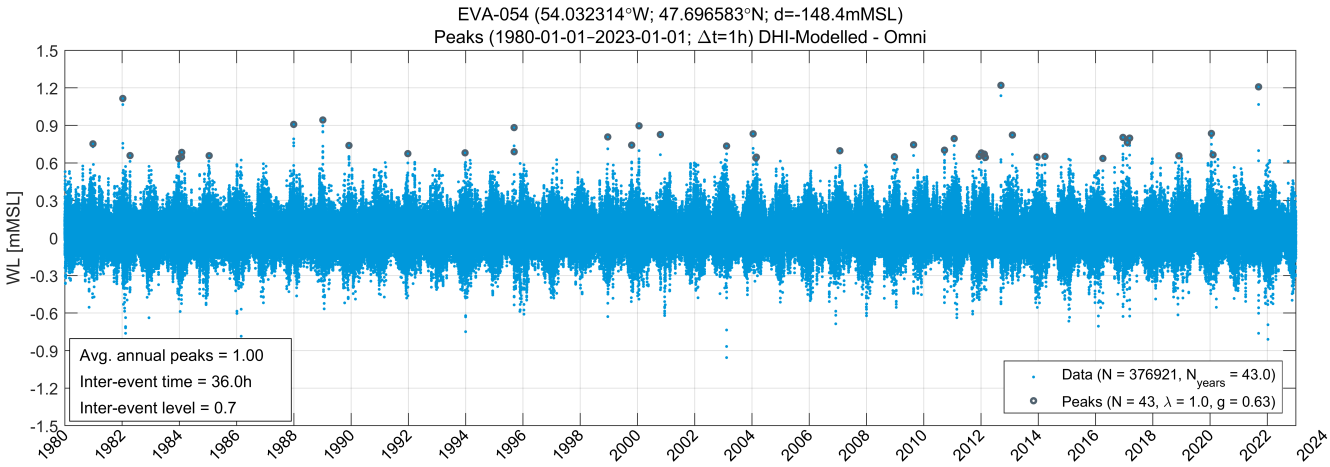


Figure C-107: Time series of water level residual at EVA-054 and selected peaks.

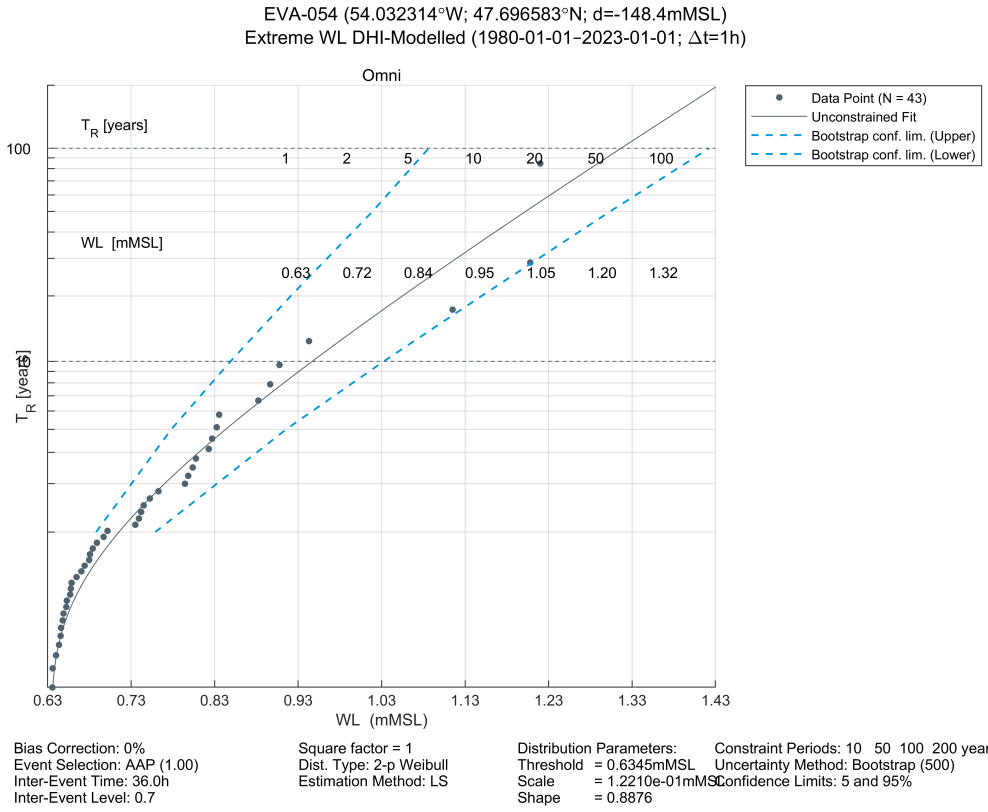


Figure C-108: Extreme value distribution fit at EVA-054.

EVA-055

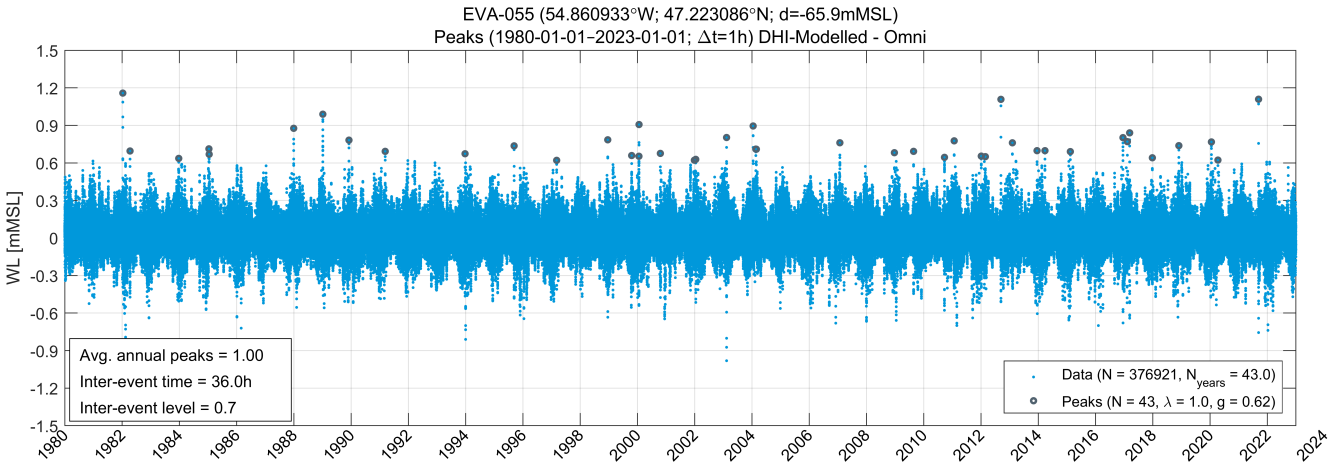


Figure C-109: Time series of water level residual at EVA-055 and selected peaks.

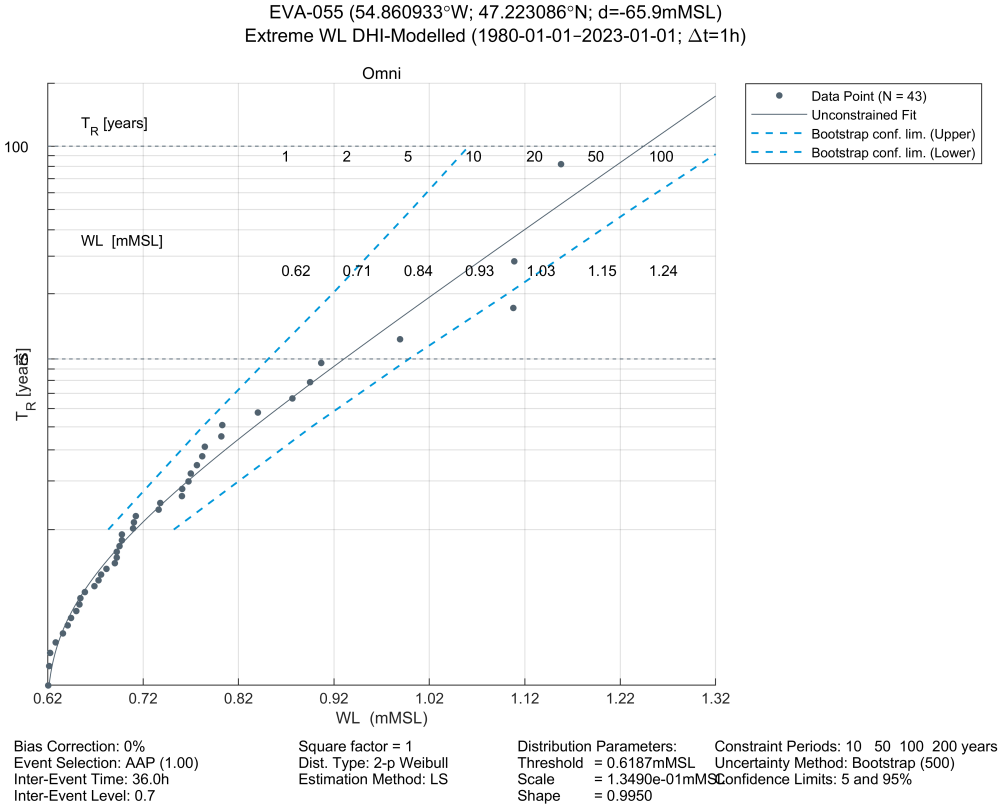


Figure C-110: Extreme value distribution fit at EVA-055.

EVA-056

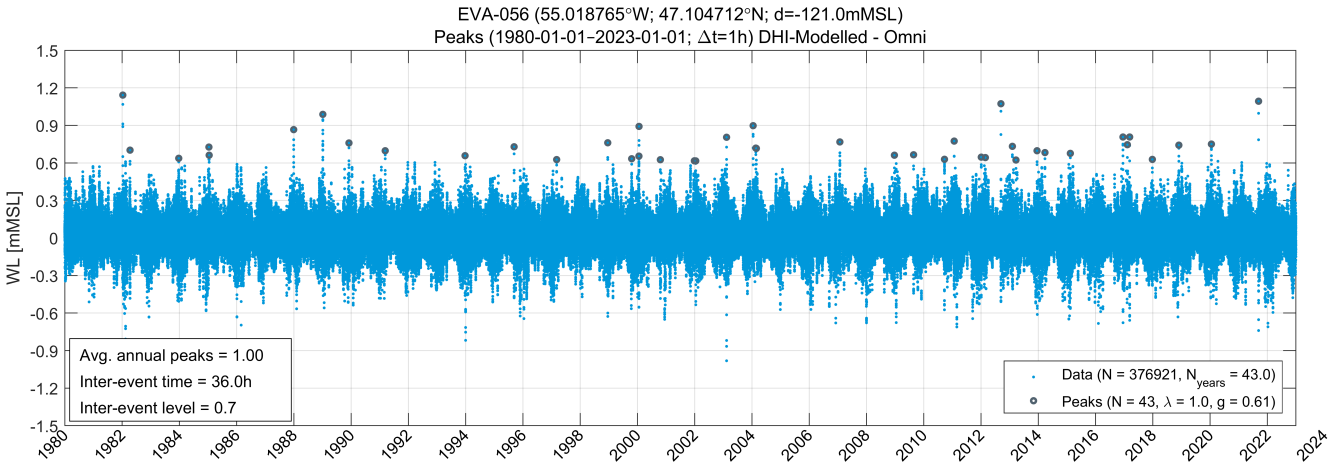


Figure C-111: Time series of water level residual at EVA-056 and selected peaks.

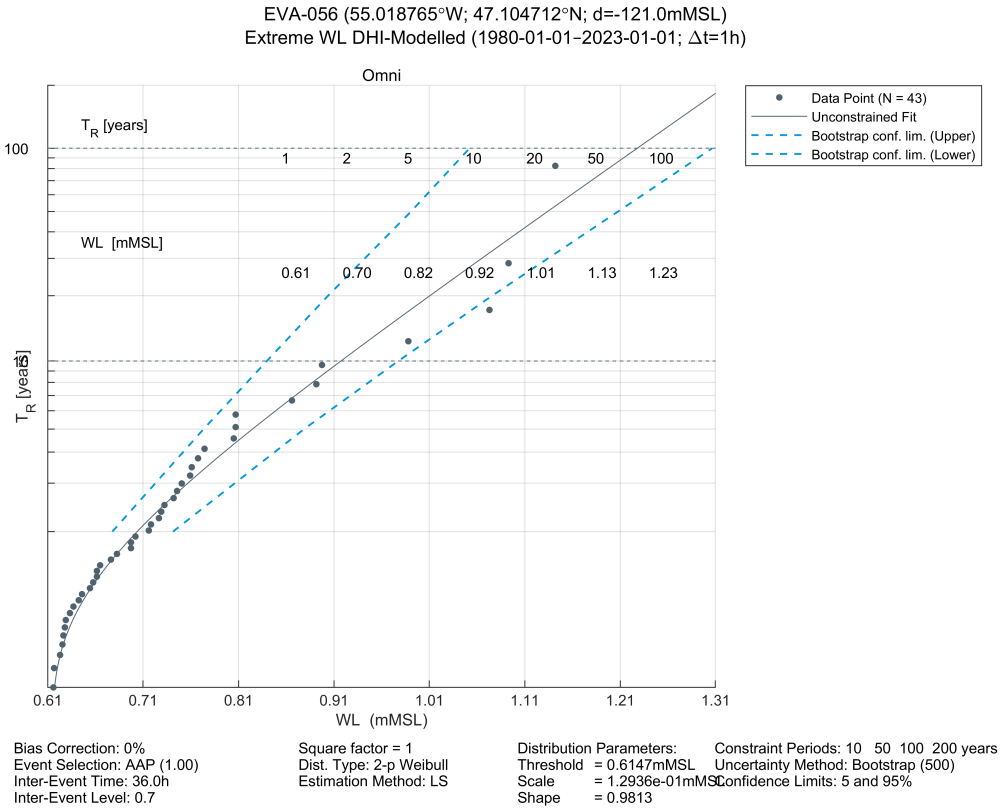


Figure C-112: Extreme value distribution fit at EVA-056.

EVA-057

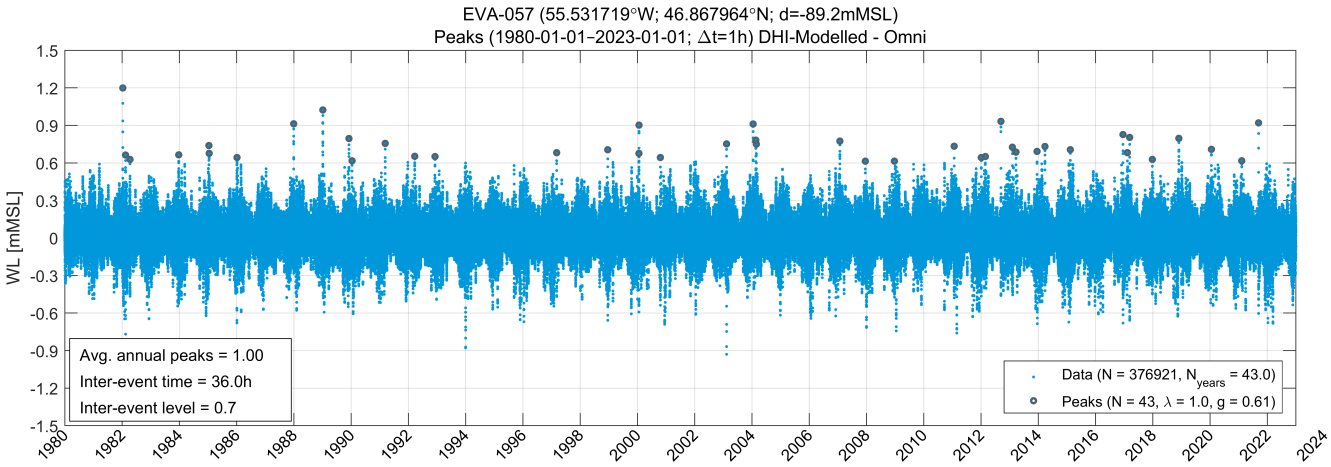


Figure C-113: Time series of water level residual at EVA-057 and selected peaks.

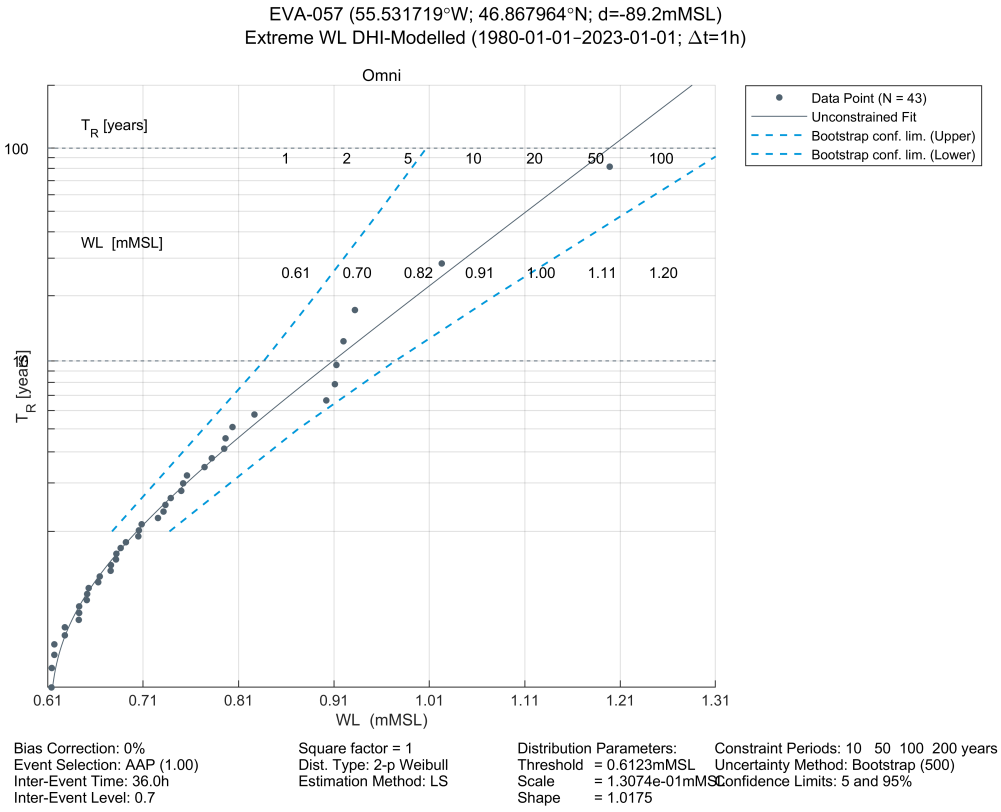


Figure C-114: Extreme value distribution fit at EVA-057.

EVA-058

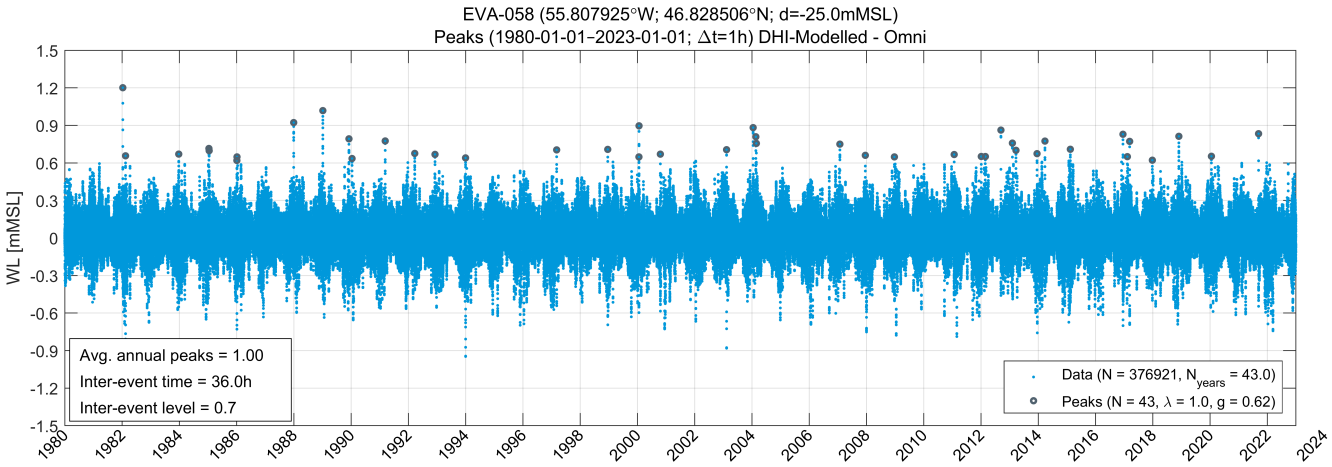


Figure C-115: Time series of water level residual at EVA-058 and selected peaks.

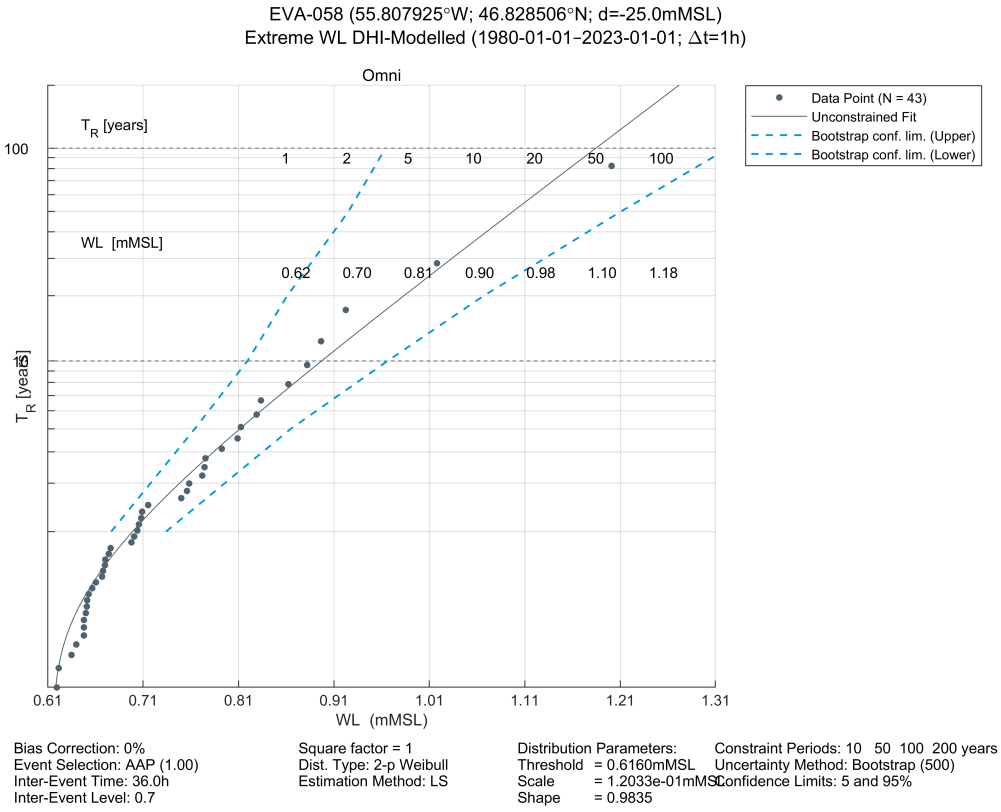


Figure C-116: Extreme value distribution fit at EVA-058.

EVA-059

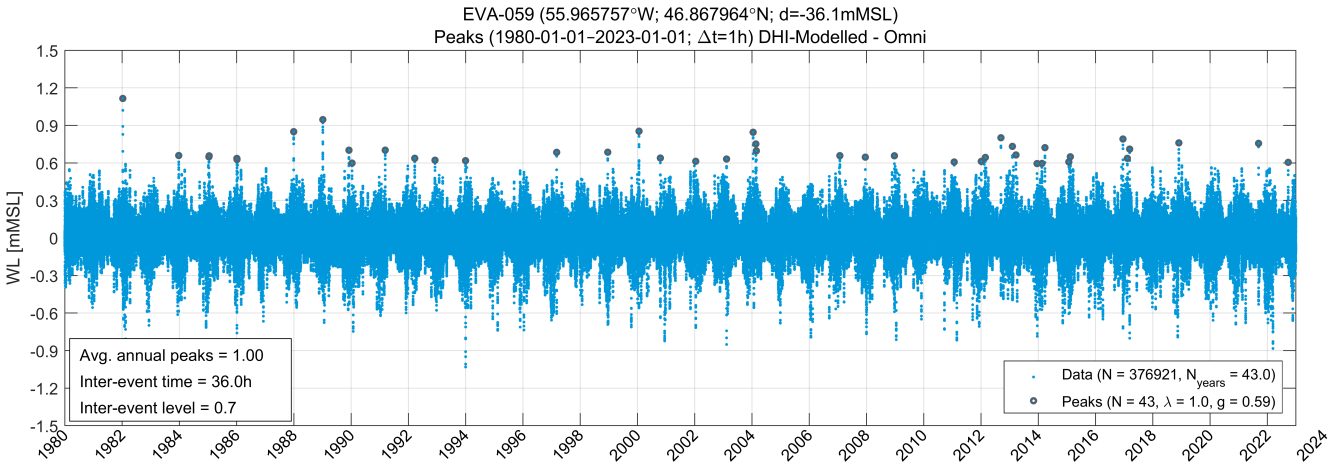


Figure C-117: Time series of water level residual at EVA-059 and selected peaks.

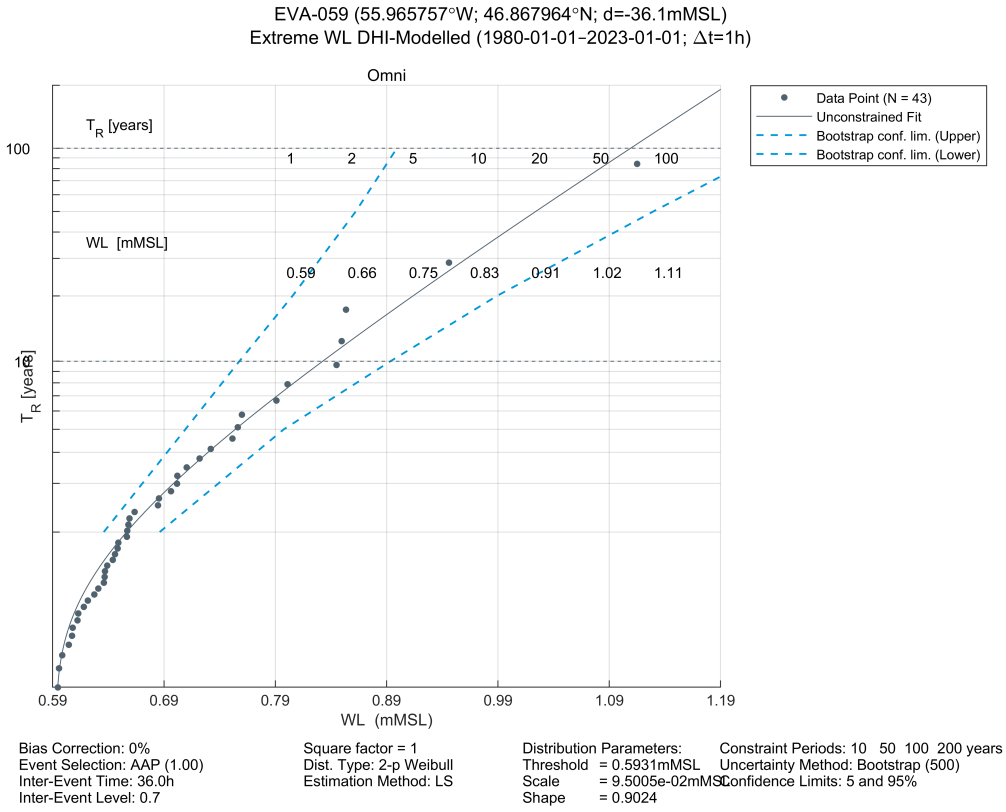


Figure C-118: Extreme value distribution fit at EVA-059.

EVA-060

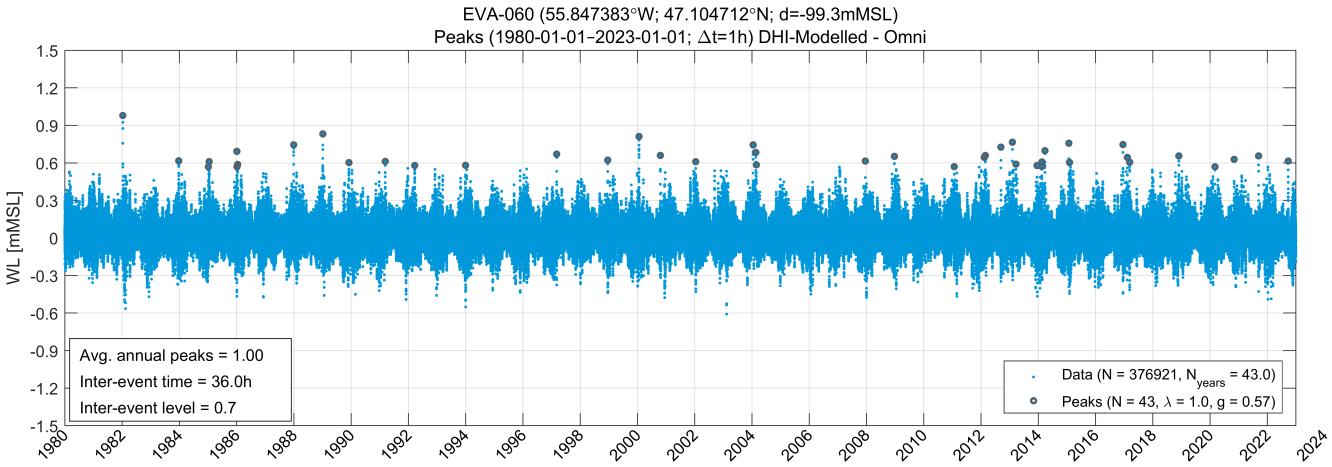


Figure C-119: Time series of water level residual at EVA-060 and selected peaks.

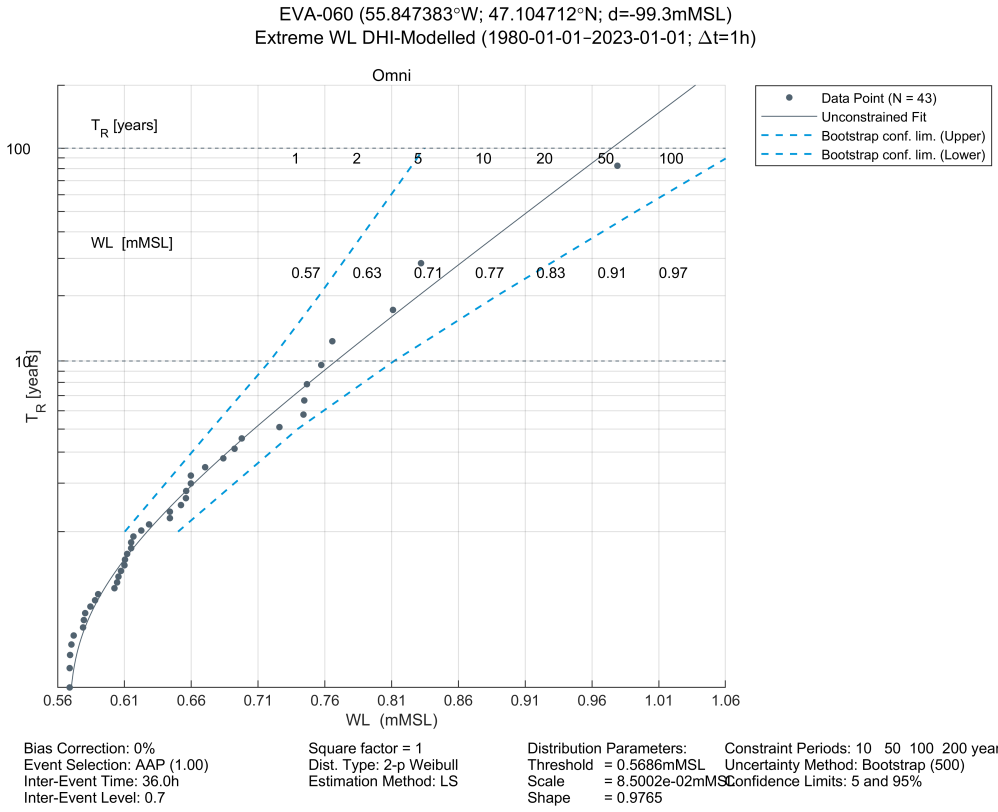


Figure C-120: Extreme value distribution fit at EVA-060.

EVA-061

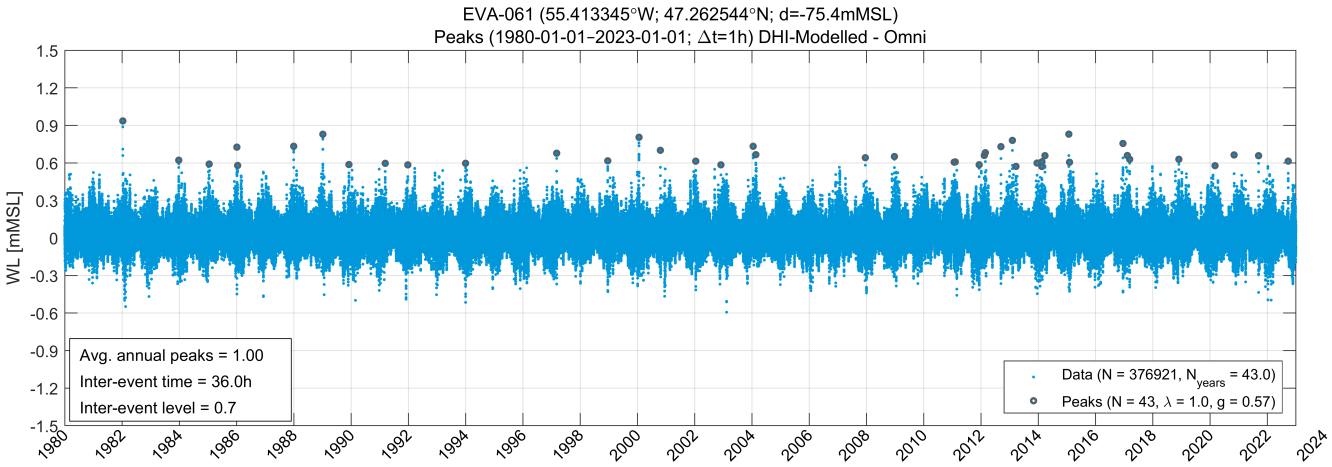


Figure C-121: Time series of water level residual at EVA-061 and selected peaks.

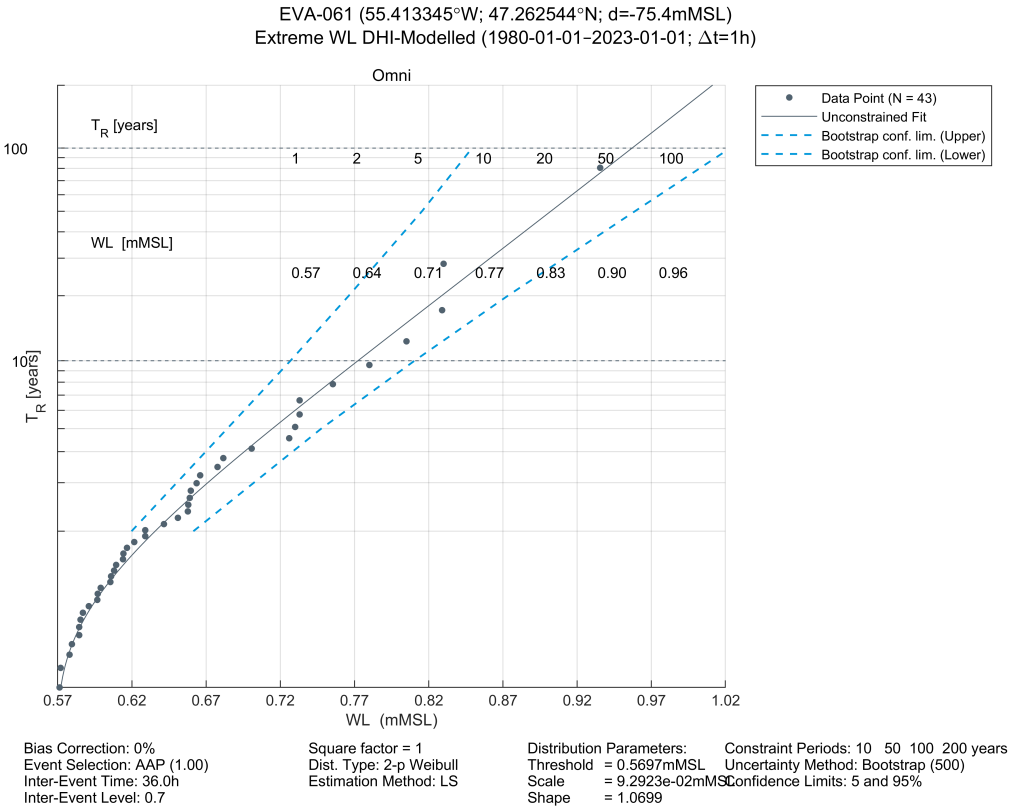


Figure C-122: Extreme value distribution fit at EVA-061.

EVA-062

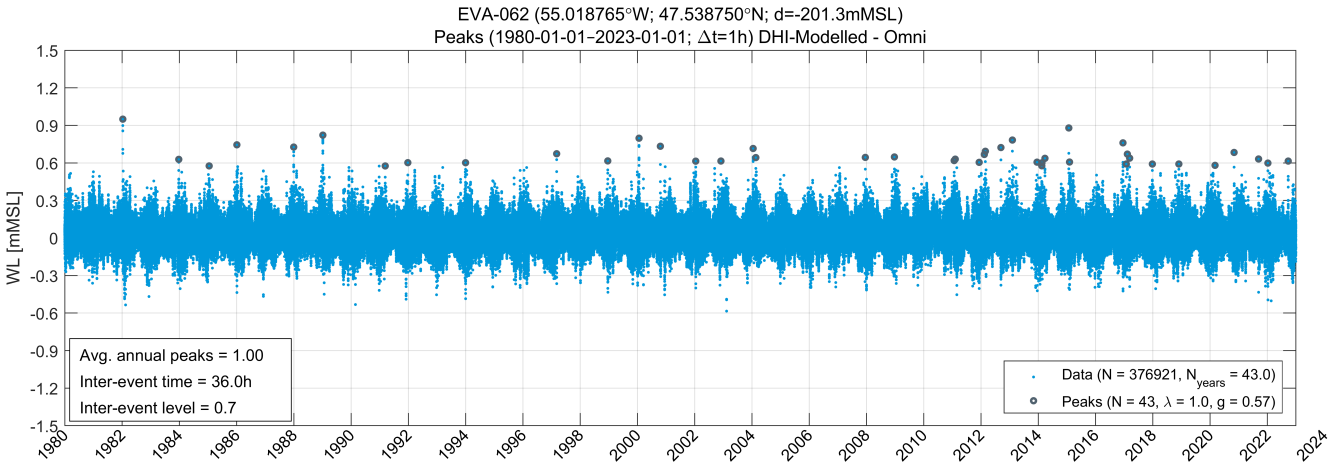


Figure C-123: Time series of water level residual at EVA-062 and selected peaks.

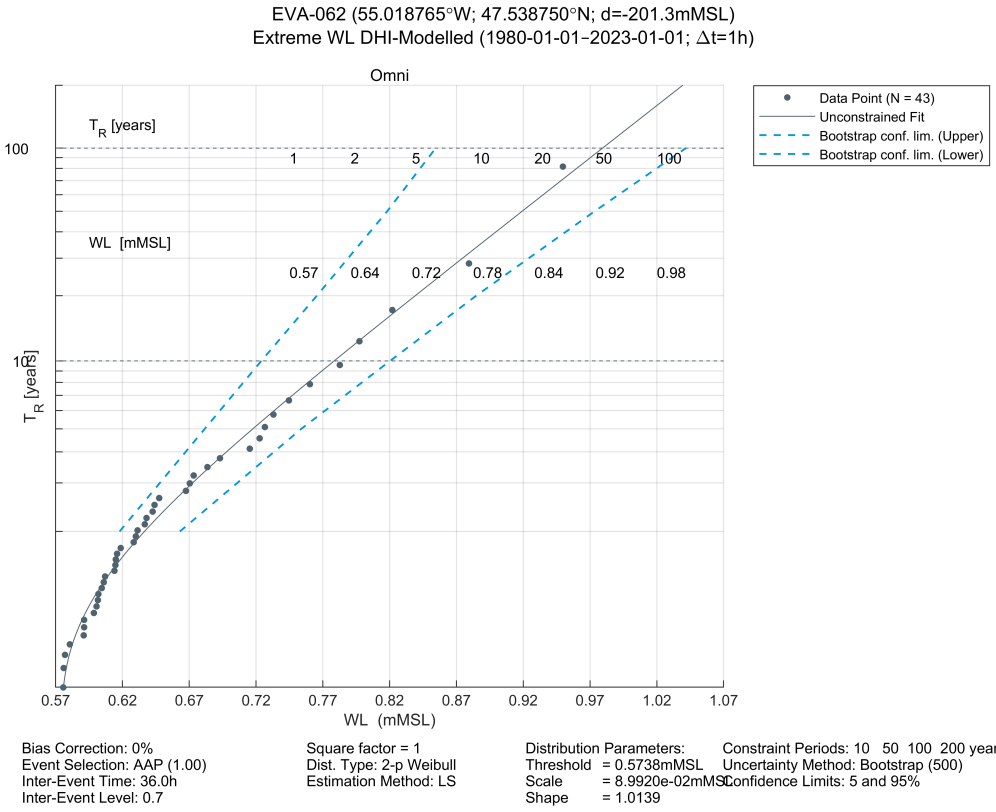


Figure C-124: Extreme value distribution fit at EVA-062.

EVA-063

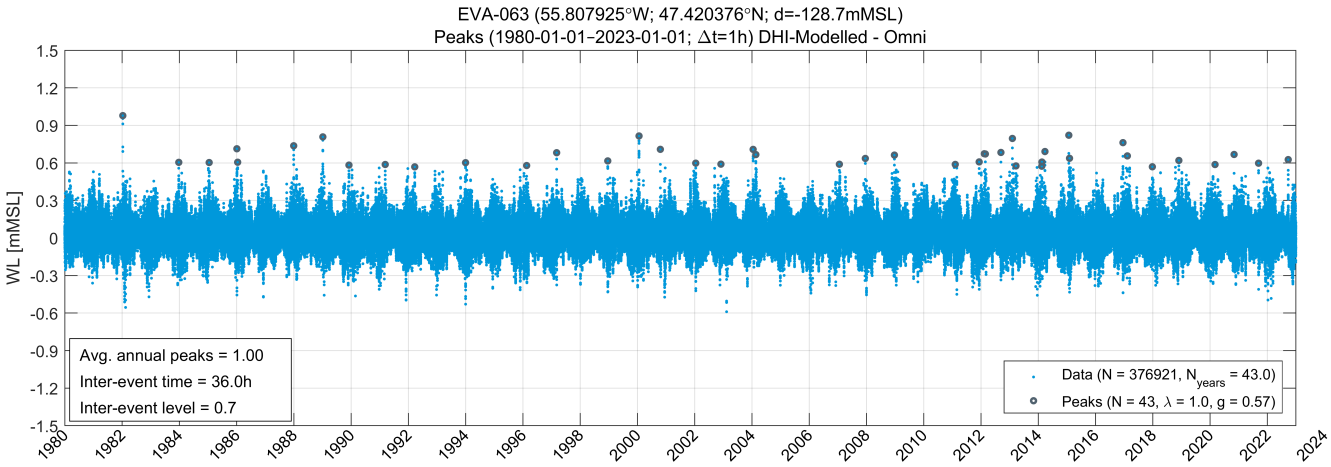


Figure C-125: Time series of water level residual at EVA-063 and selected peaks.

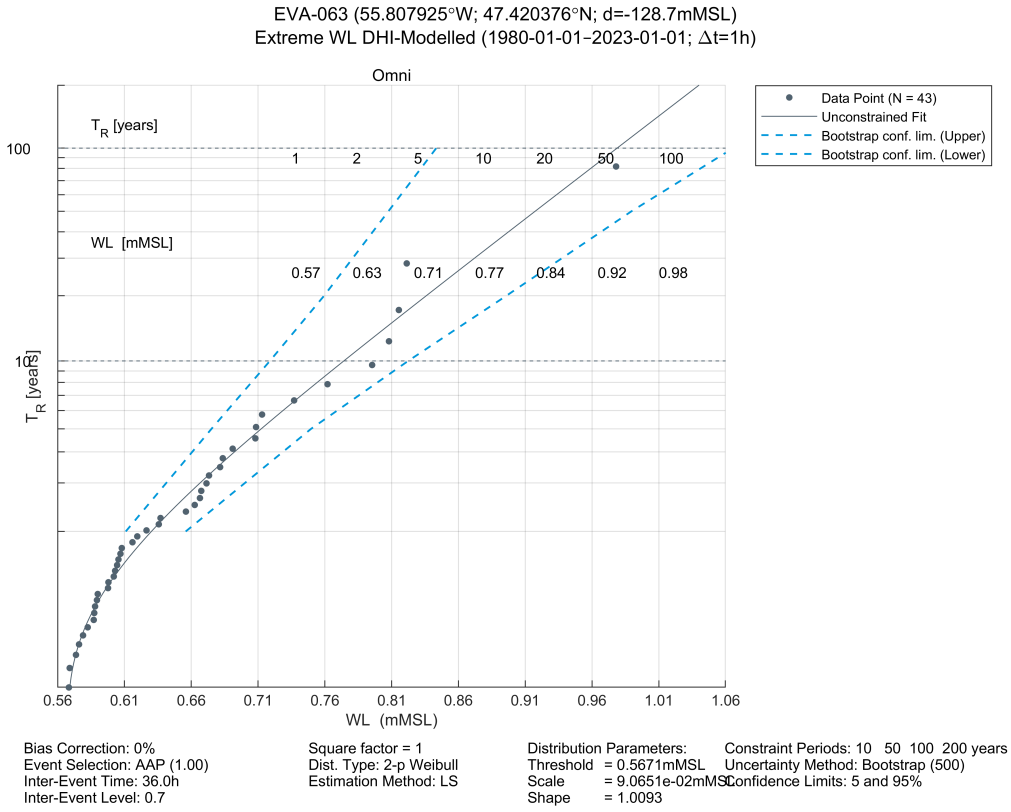


Figure C-126: Extreme value distribution fit at EVA-063.

EVA-064

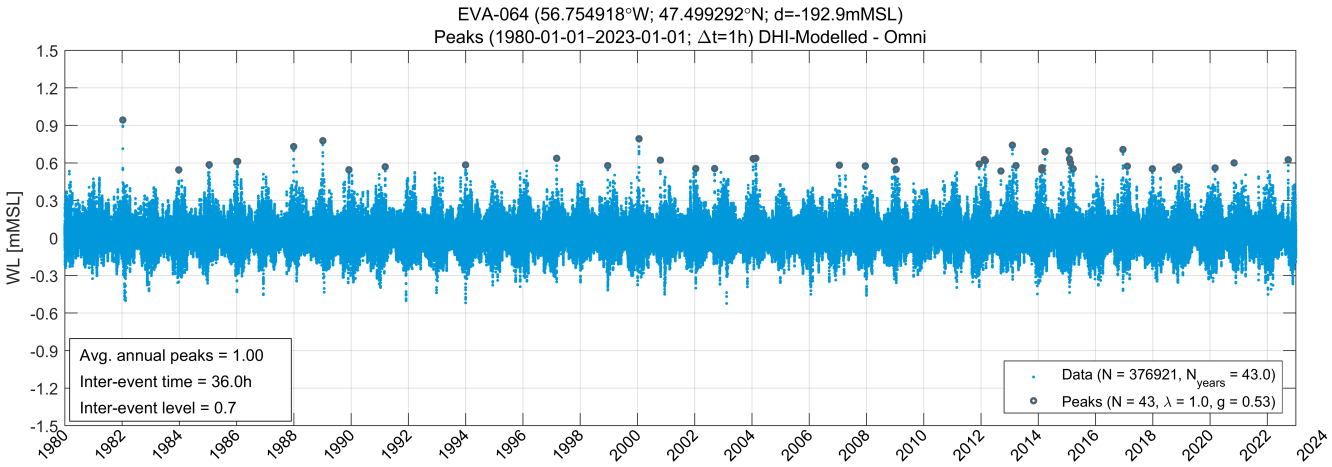


Figure C-127: Time series of water level residual at EVA-064 and selected peaks.

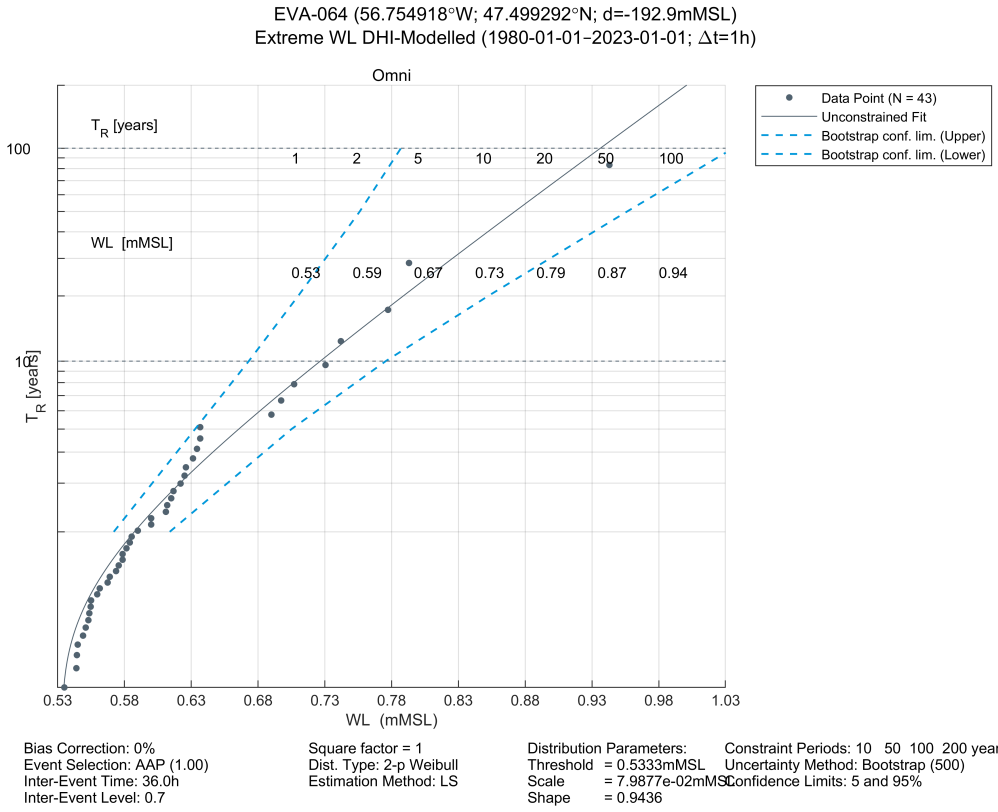


Figure C-128: Extreme value distribution fit at EVA-064.

EVA-065

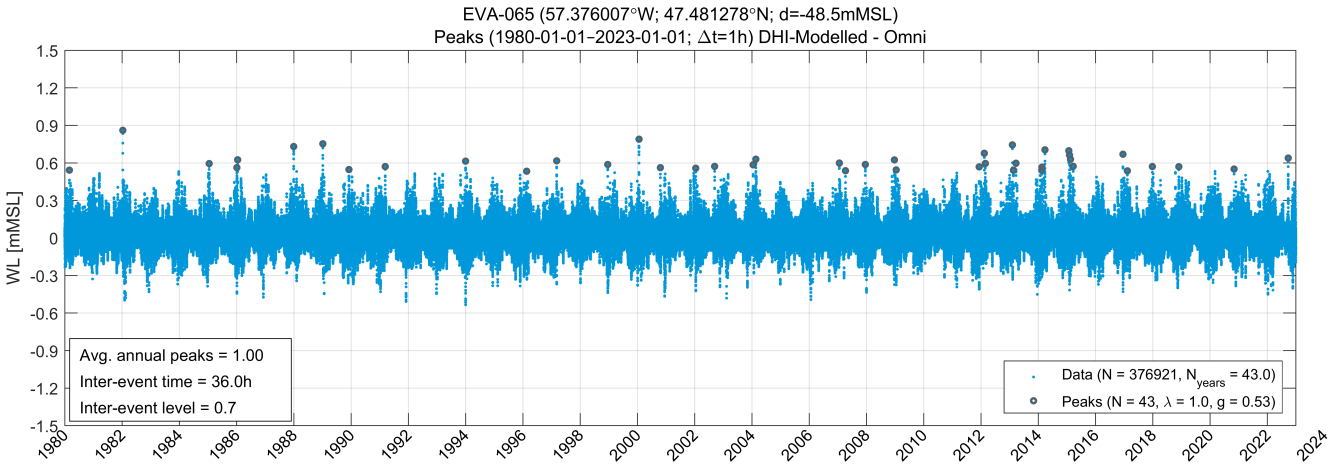


Figure C-129: Time series of water level residual at EVA-065 and selected peaks.

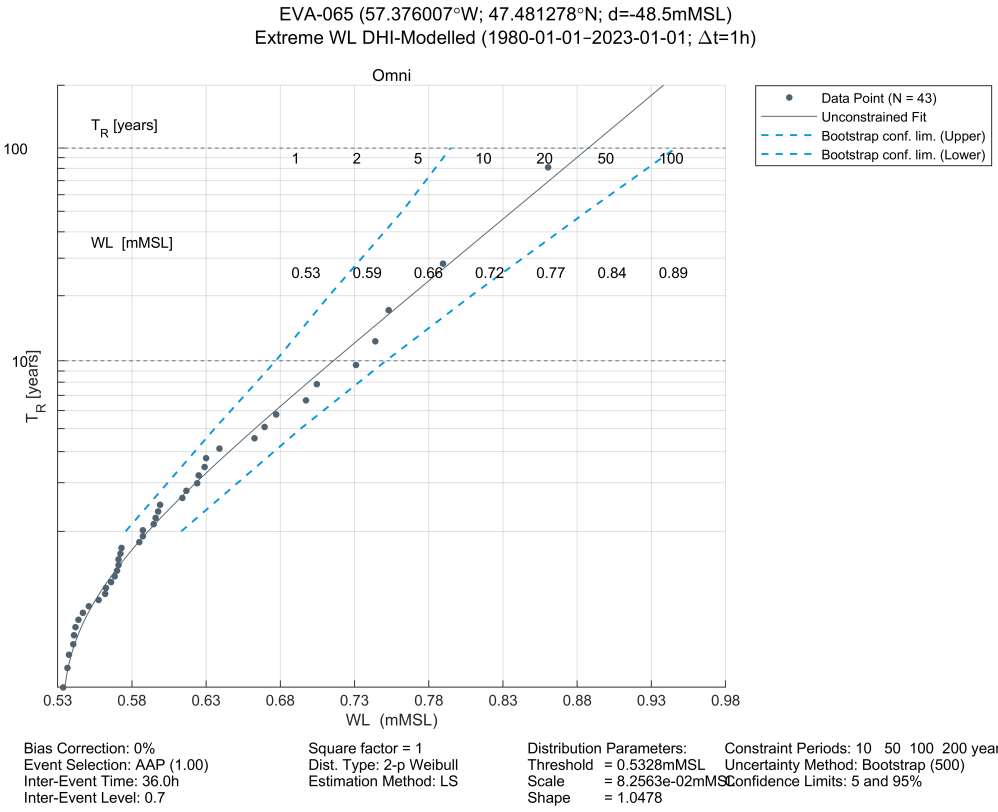


Figure C-130: Extreme value distribution fit at EVA-065.

EVA-066

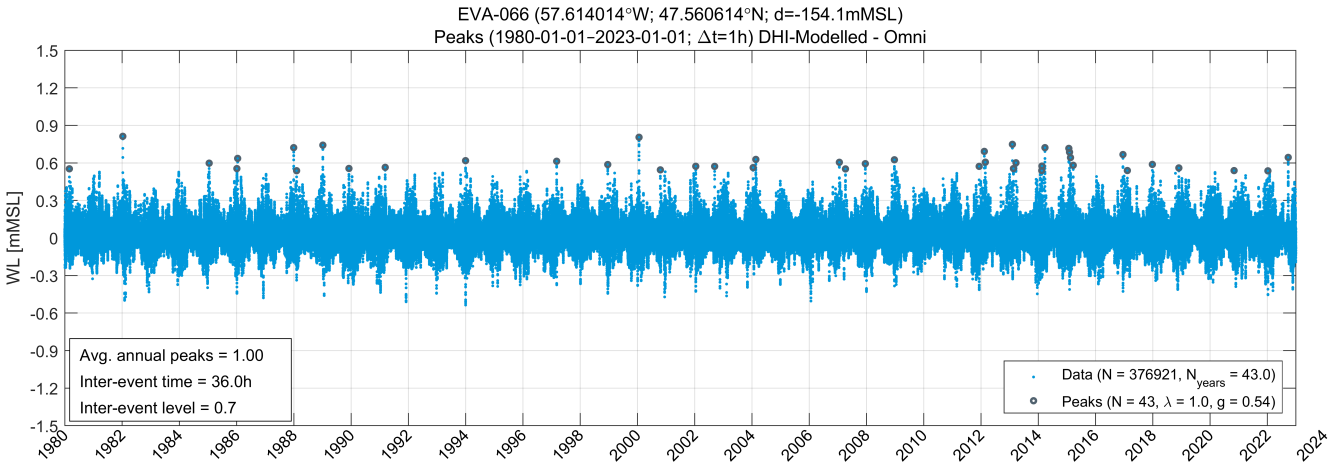


Figure C-131: Time series of water level residual at EVA-066 and selected peaks.

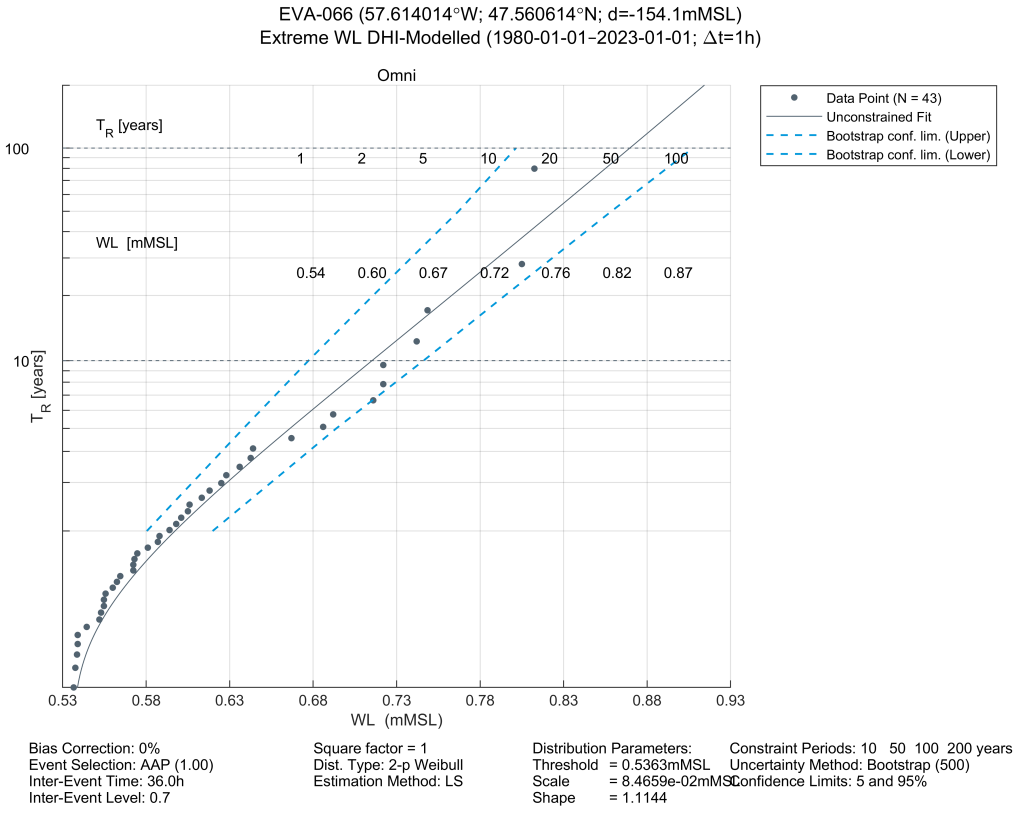


Figure C-132: Extreme value distribution fit at EVA-066.

EVA-067

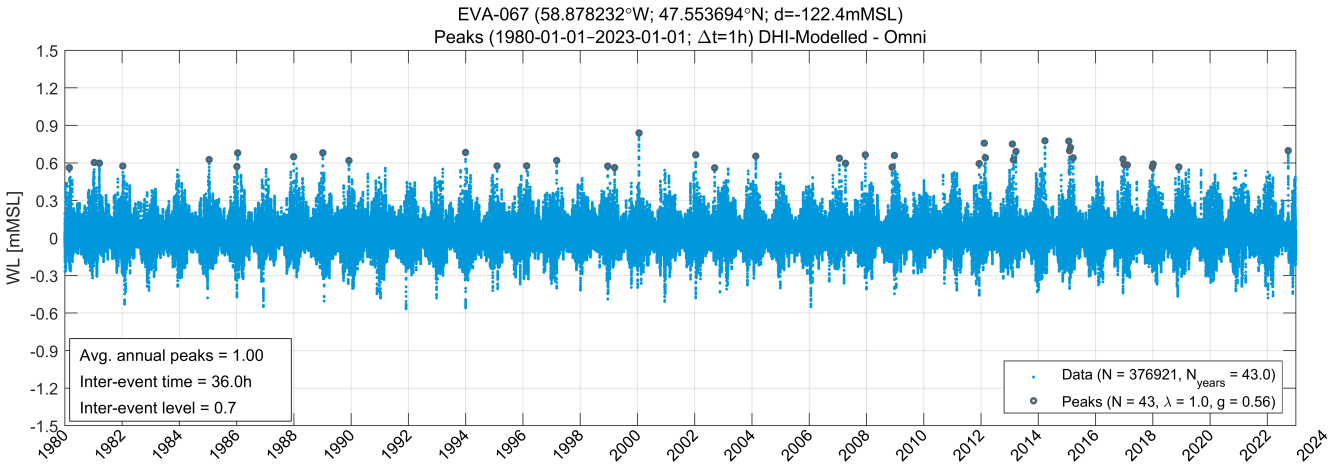


Figure C-133: Time series of water level residual at EVA-067 and selected peaks.

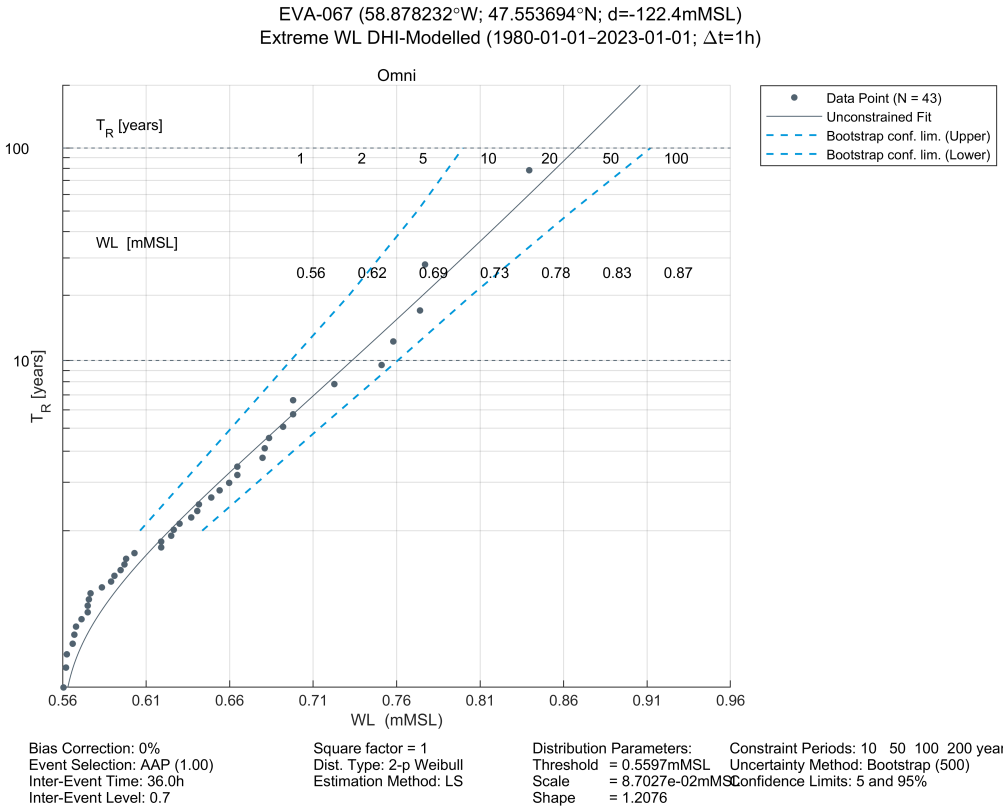


Figure C-134: Extreme value distribution fit at EVA-067.

EVA-068

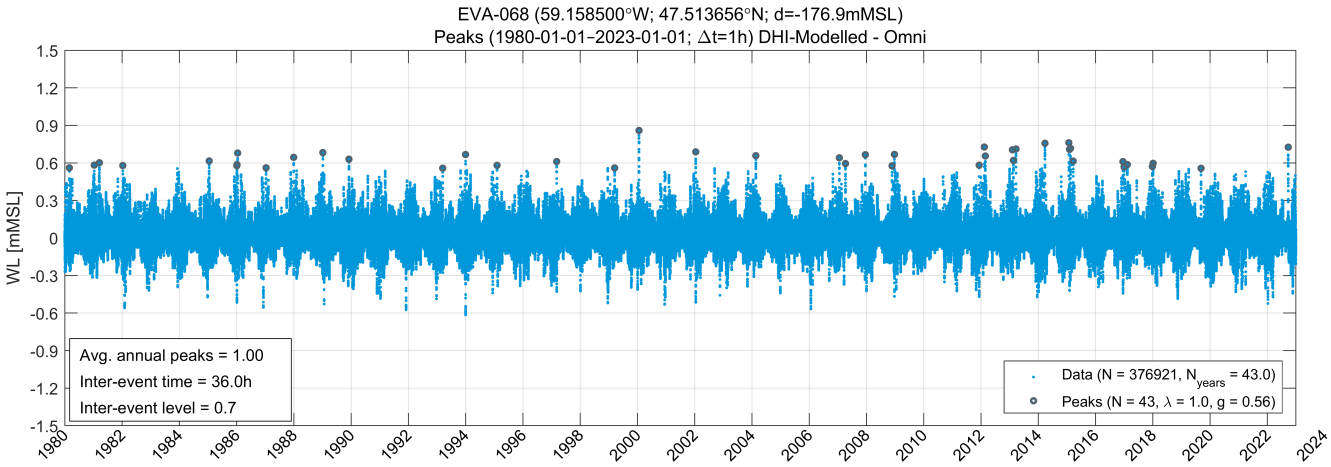


Figure C-135: Time series of water level residual at EVA-068 and selected peaks.

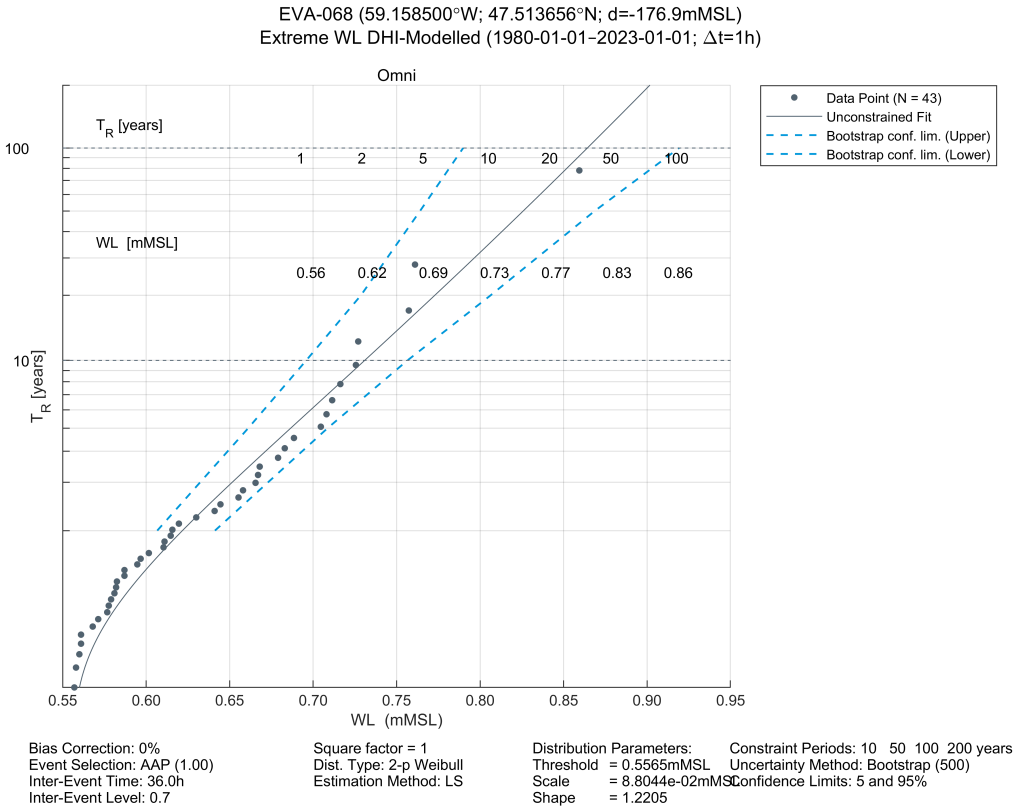


Figure C-136: Extreme value distribution fit at EVA-068.

EVA-069

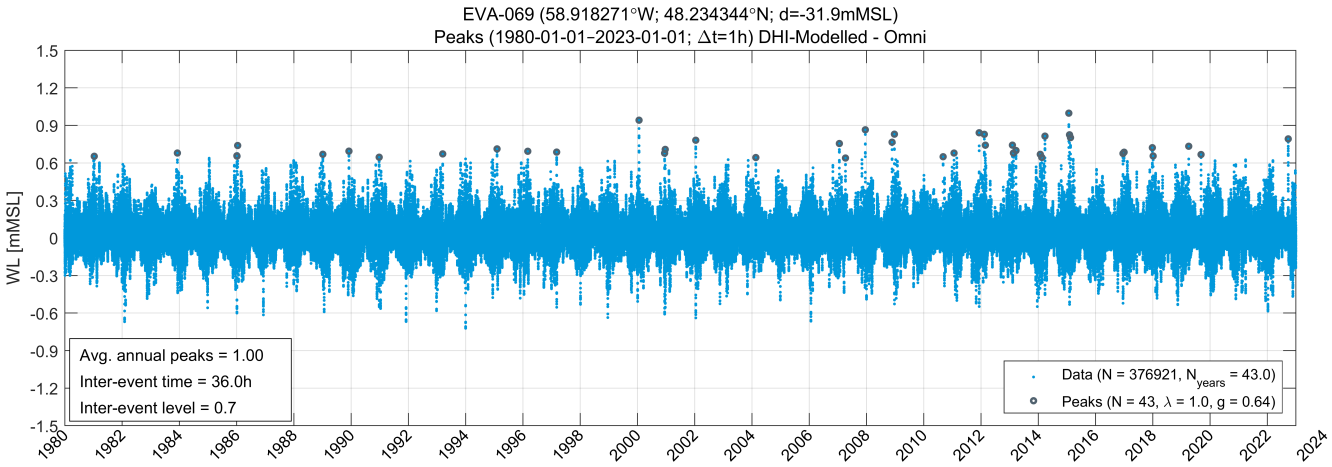


Figure C-137: Time series of water level residual at EVA-069 and selected peaks.

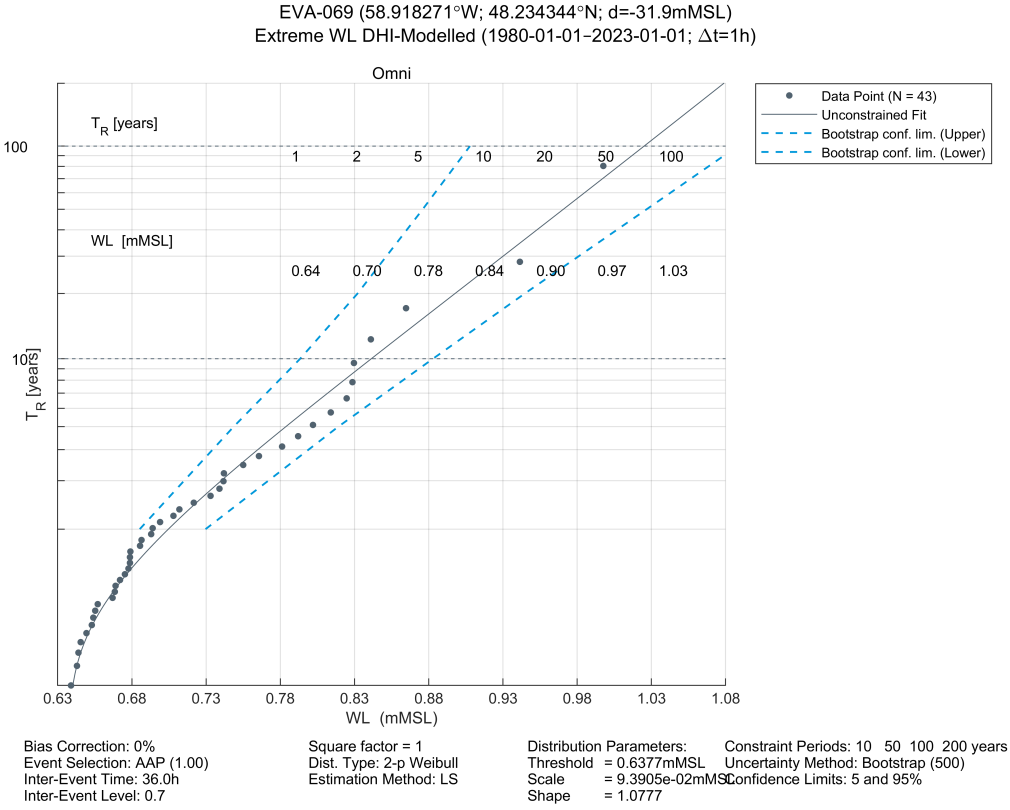


Figure C-138: Extreme value distribution fit at EVA-069.

EVA-070

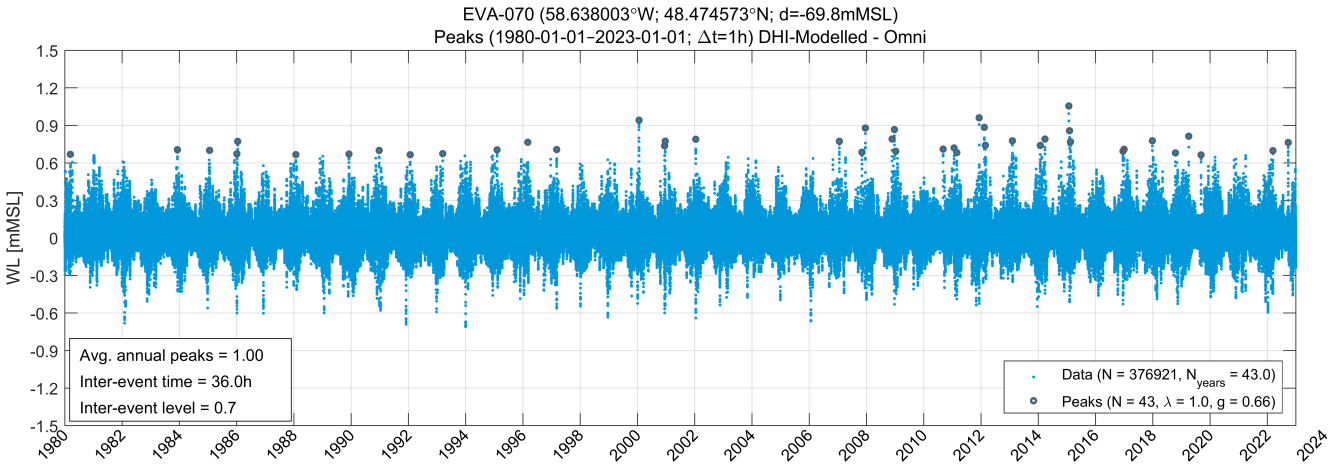


Figure C-139: Time series of water level residual at EVA-070 and selected peaks.

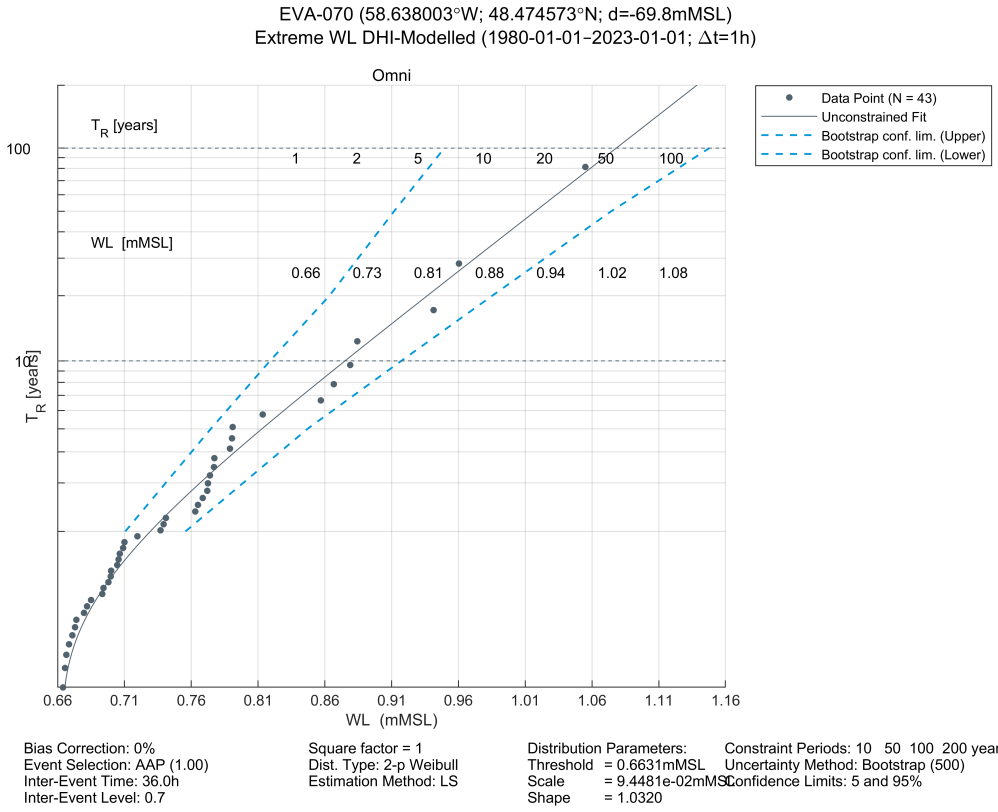


Figure C-140: Extreme value distribution fit at EVA-070.

EVA-071

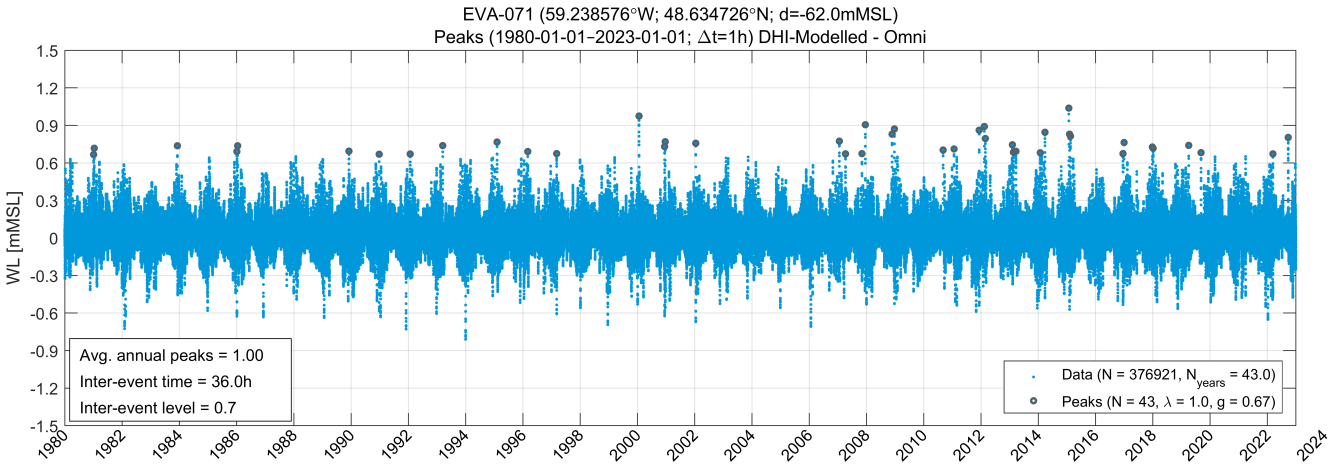


Figure C-141: Time series of water level residual at EVA-071 and selected peaks.

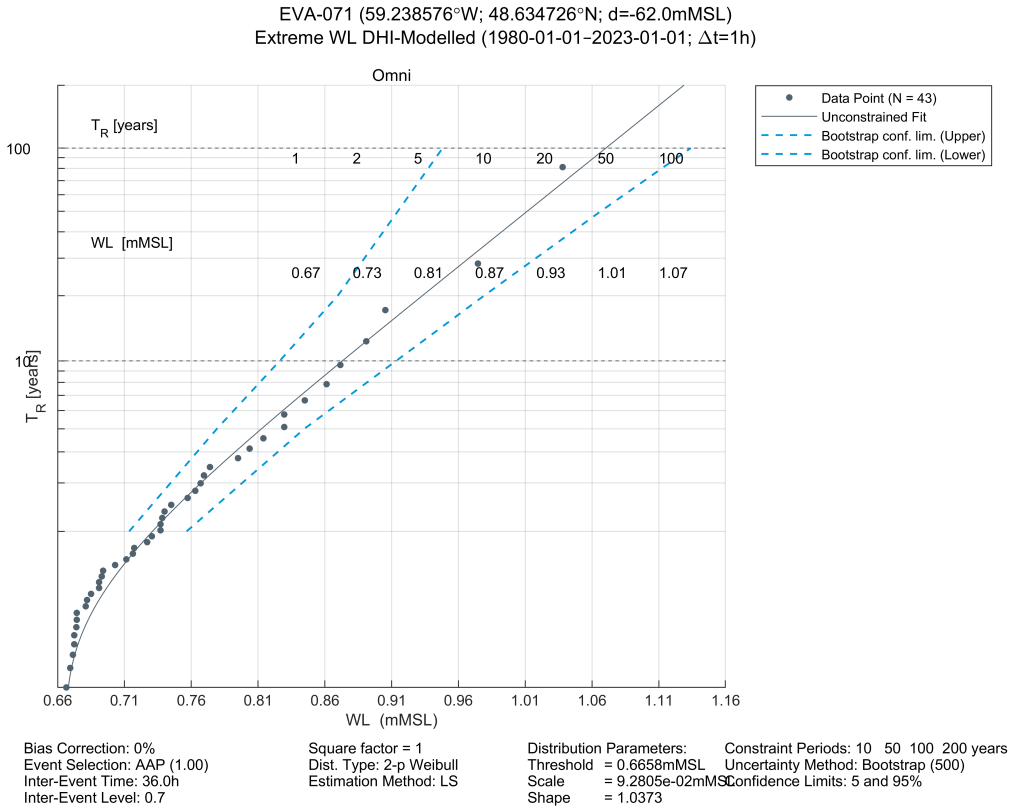


Figure C-142: Extreme value distribution fit at EVA-071.

EVA-072

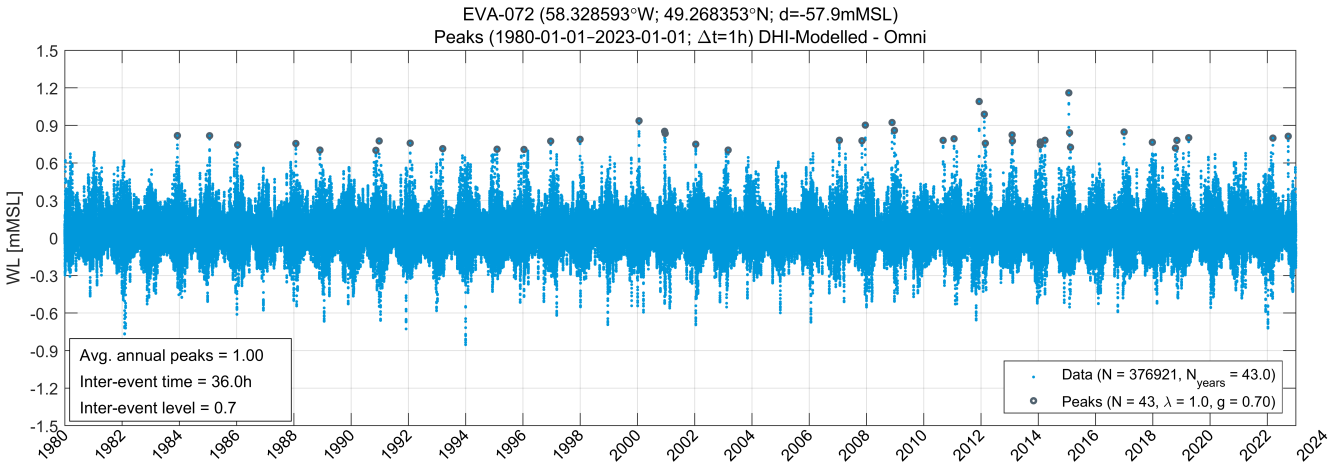


Figure C-143: Time series of water level residual at EVA-072 and selected peaks.

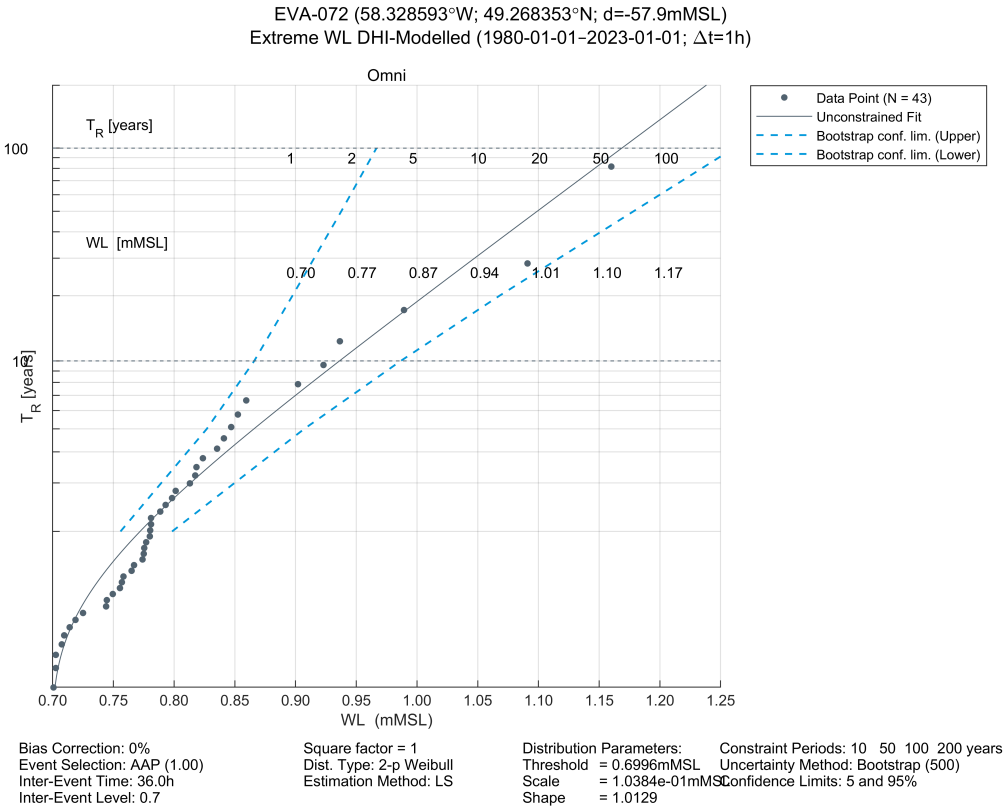


Figure C-144: Extreme value distribution fit at EVA-072.

EVA-073

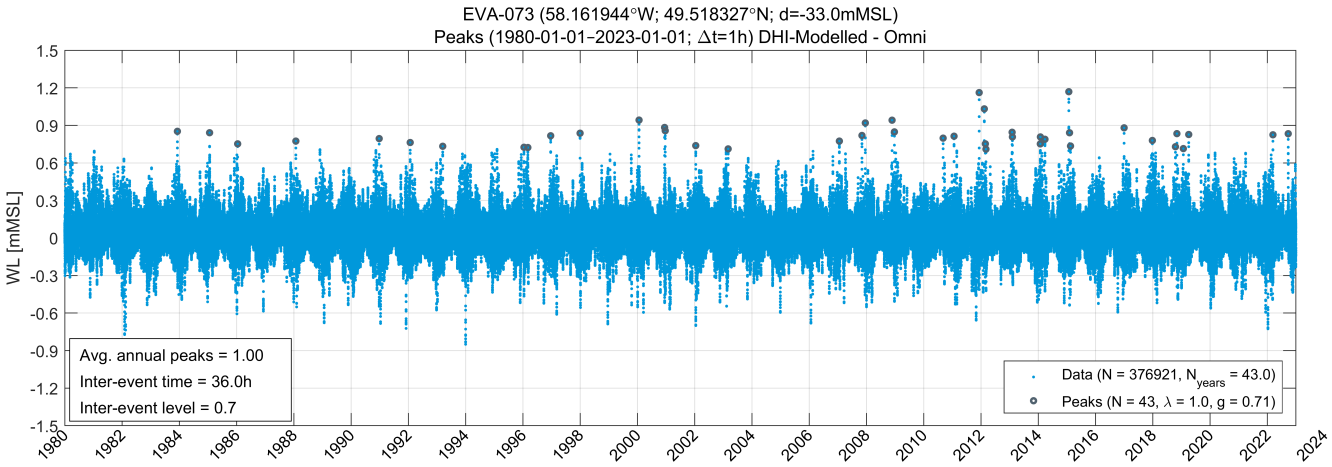


Figure C-145: Time series of water level residual at EVA-073 and selected peaks.

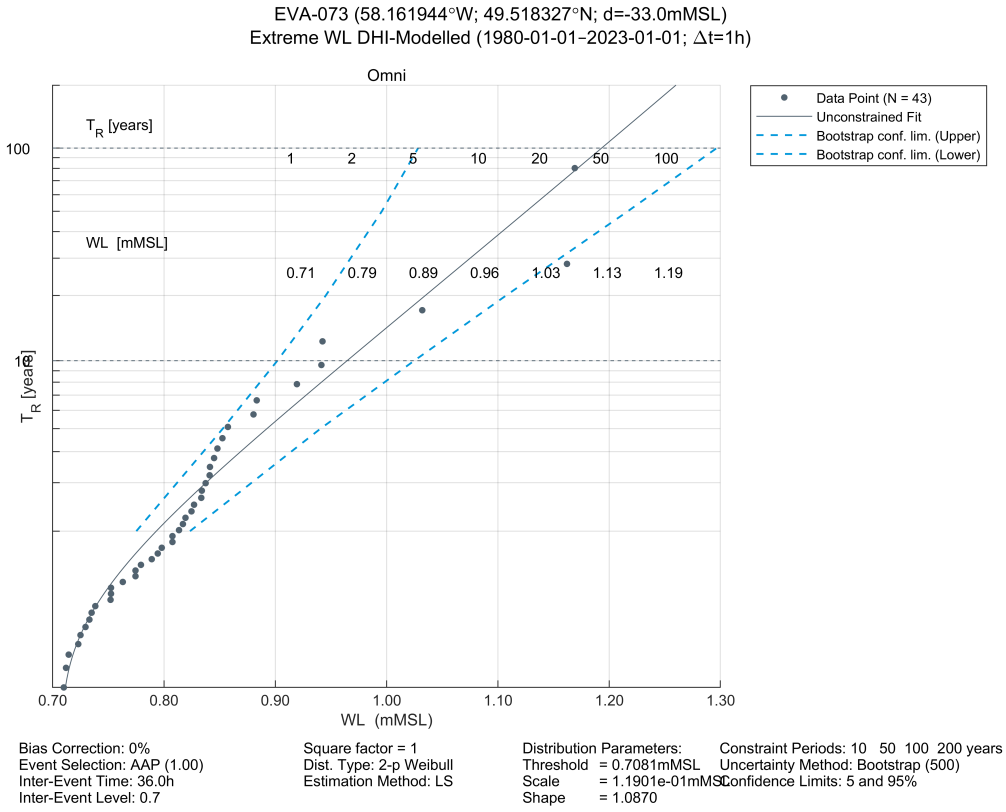


Figure C-146: Extreme value distribution fit at EVA-073.

EVA-074

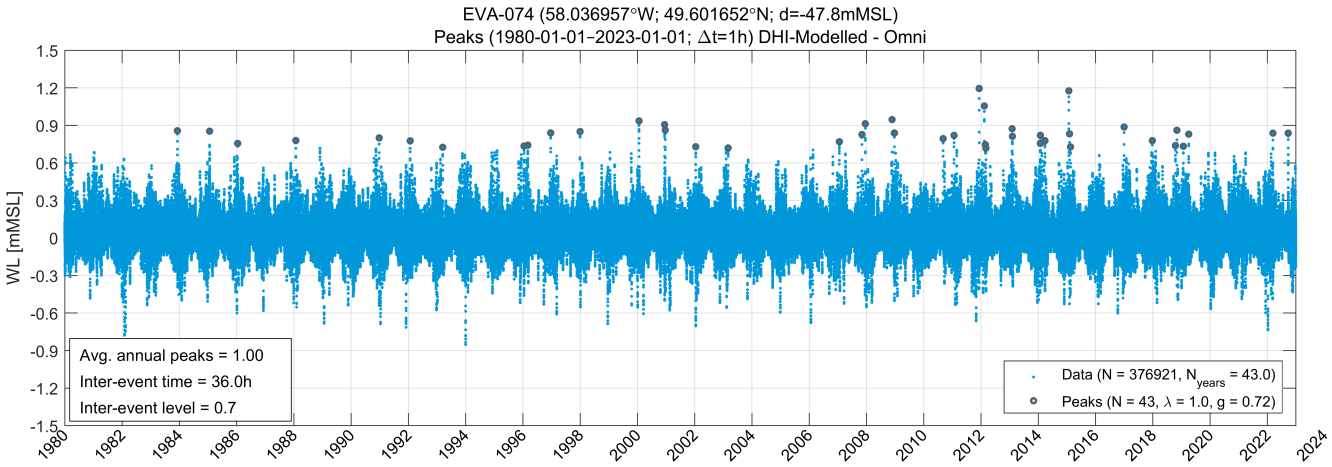


Figure C-147: Time series of water level residual at EVA-074 and selected peaks.

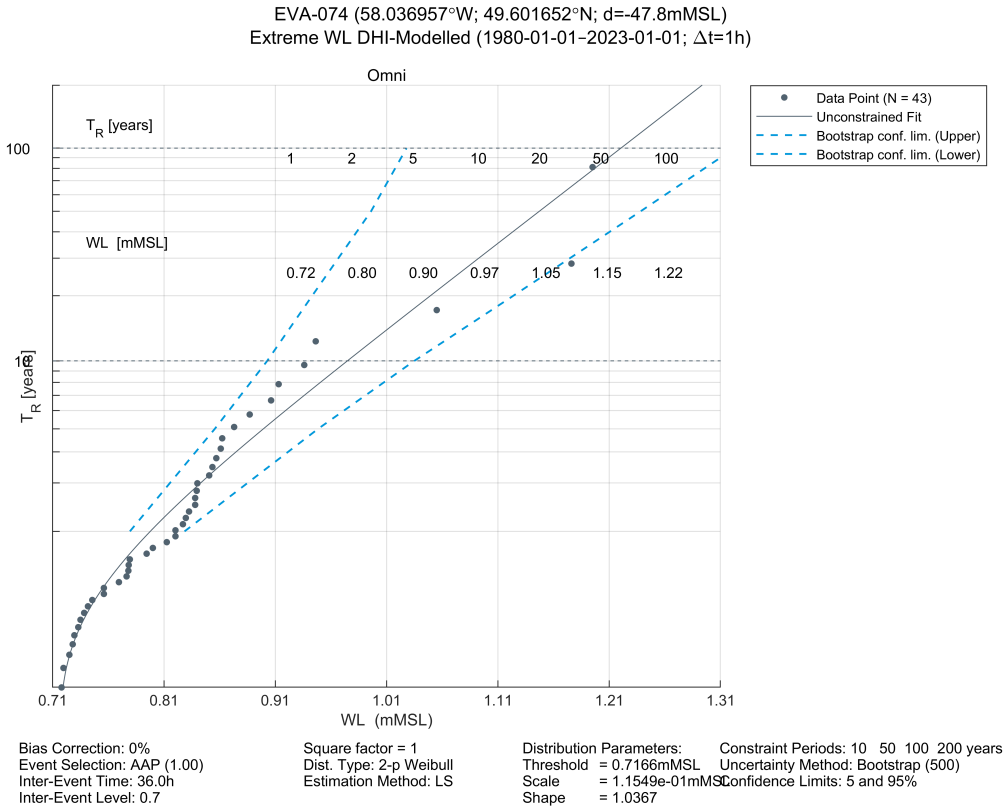


Figure C-148: Extreme value distribution fit at EVA-074.

EVA-075

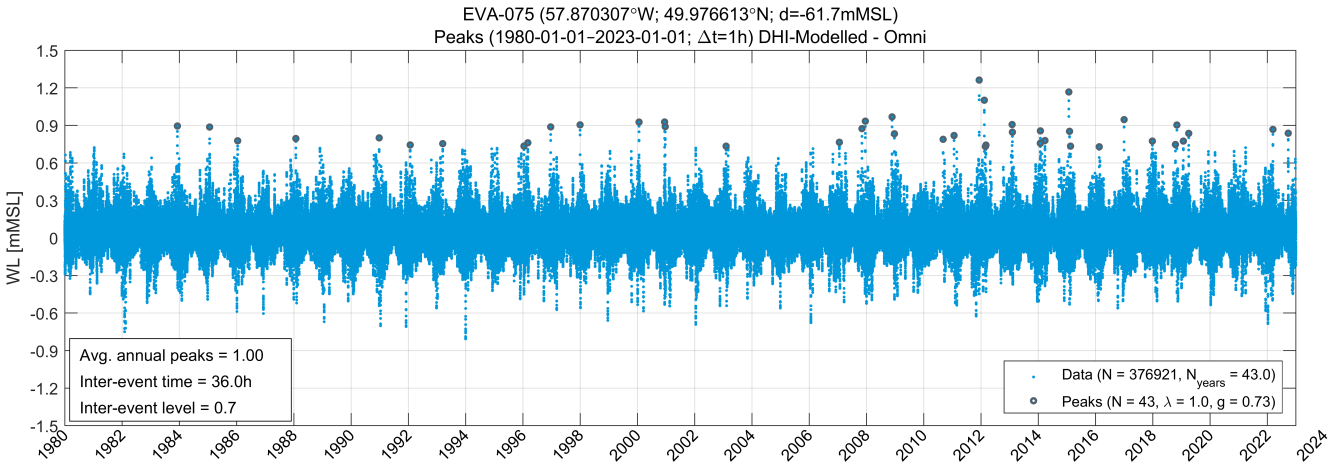


Figure C-149: Time series of water level residual at EVA-075 and selected peaks.

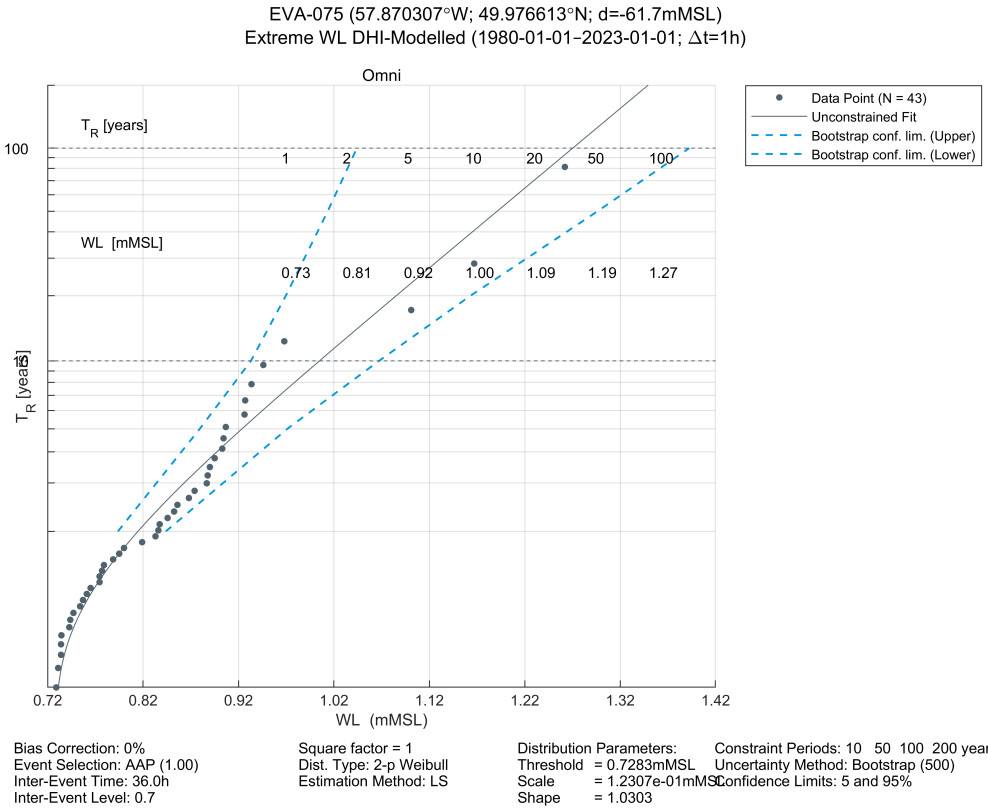


Figure C-150: Extreme value distribution fit at EVA-075.

EVA-076

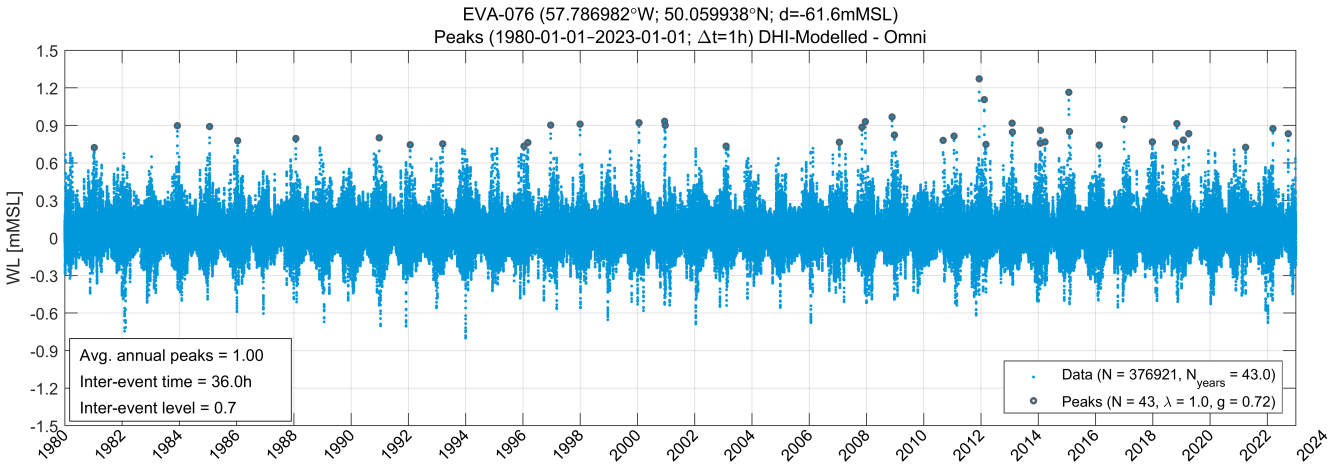


Figure C-151: Time series of water level residual at EVA-076 and selected peaks.

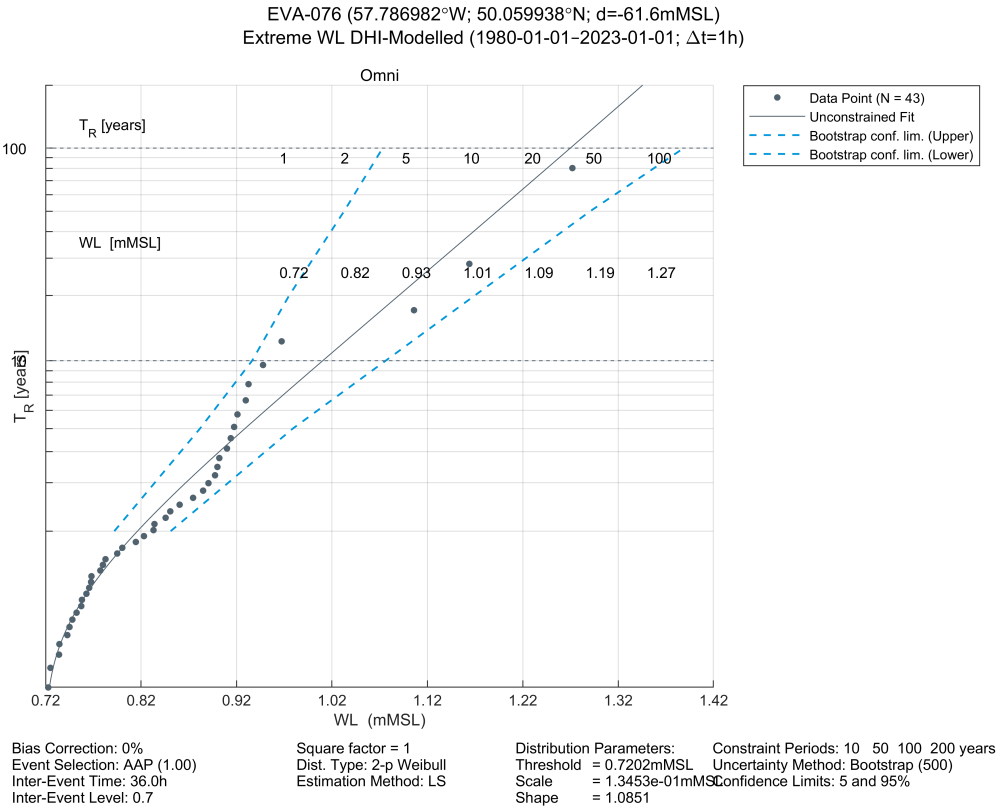


Figure C-152: Extreme value distribution fit at EVA-076.

EVA-077

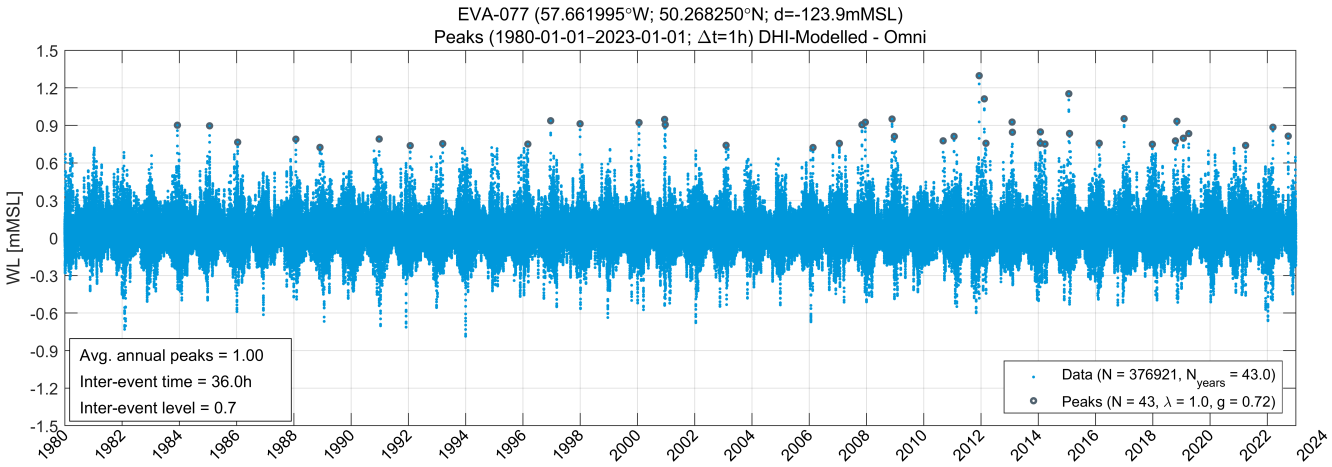


Figure C-153: Time series of water level residual at EVA-077 and selected peaks.

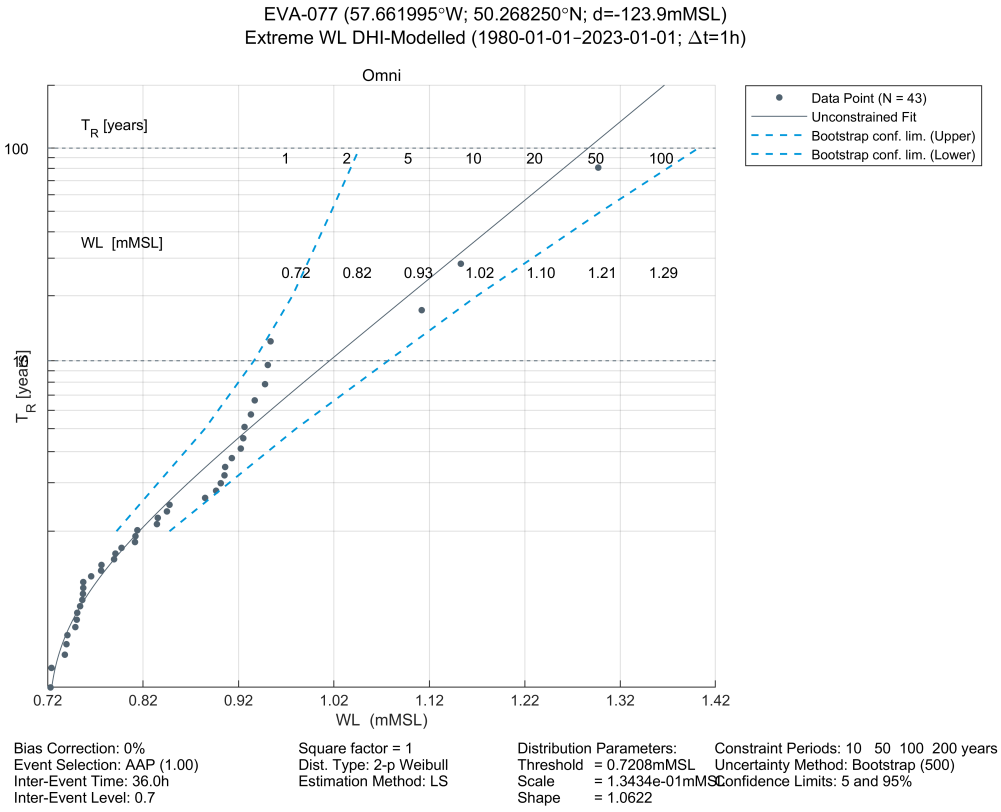


Figure C-154: Extreme value distribution fit at EVA-077.

EVA-078

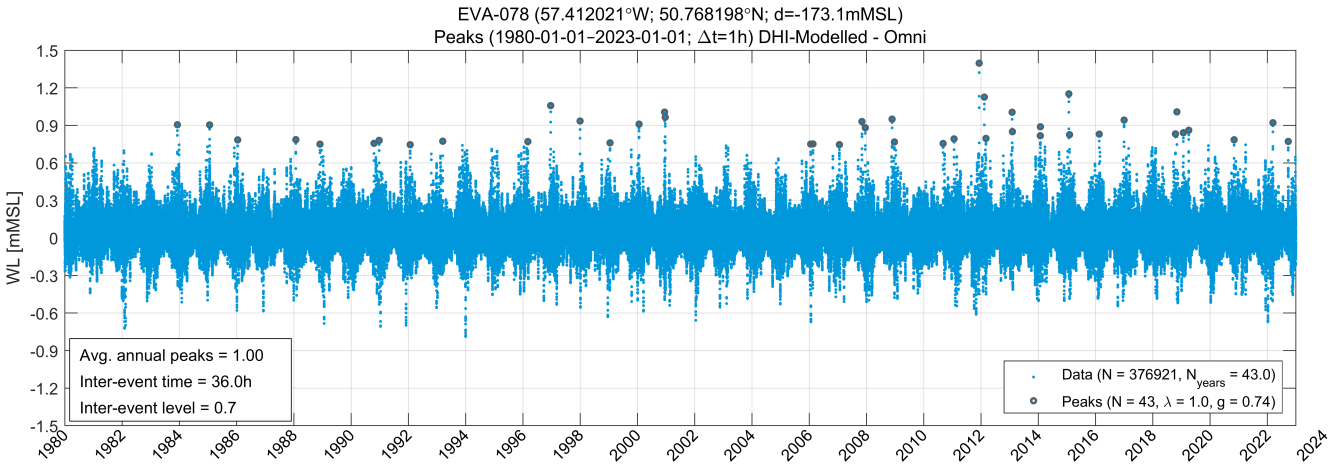


Figure C-155: Time series of water level residual at EVA-078 and selected peaks.

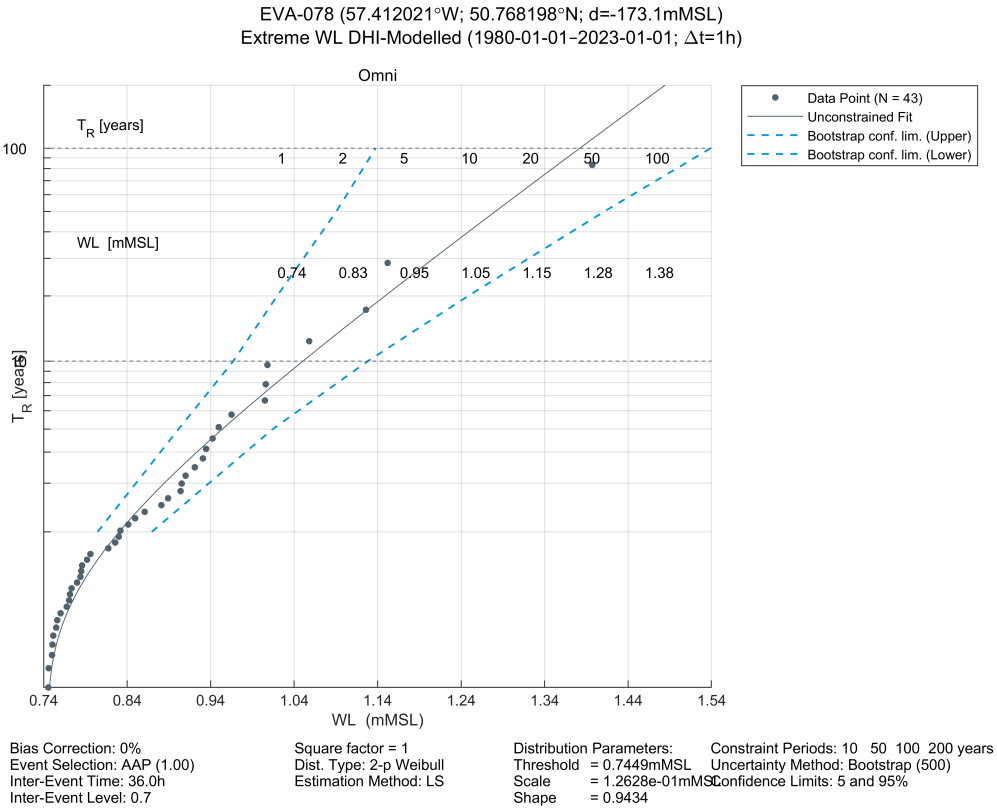


Figure C-156: Extreme value distribution fit at EVA-078.

Appendix C.2 - Omnidirectional Wave Analysis

EVA-001

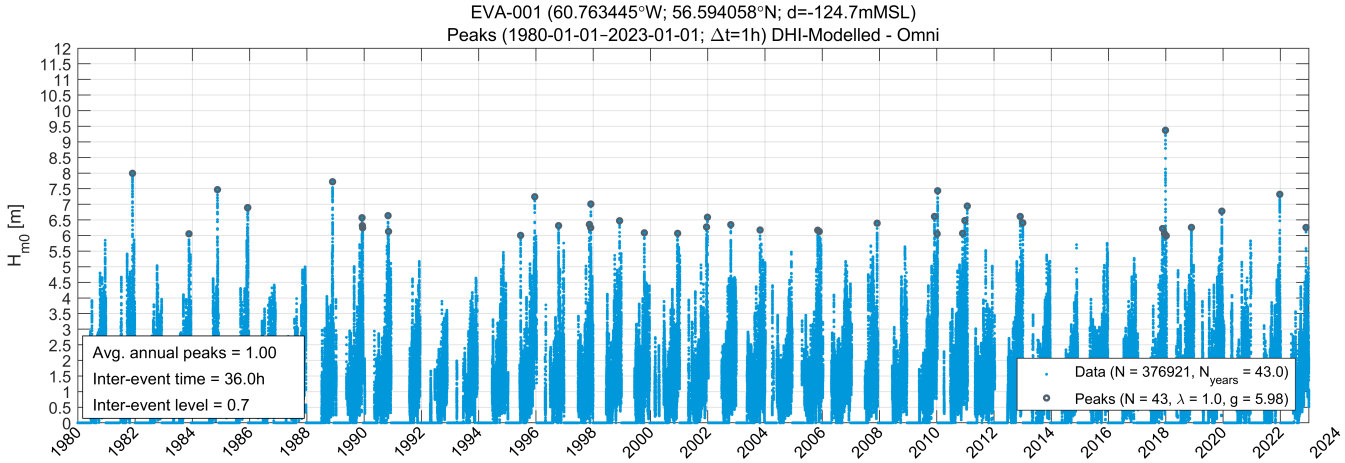


Figure C-157: Time series of significant wave height at EVA-001 and selected peaks.

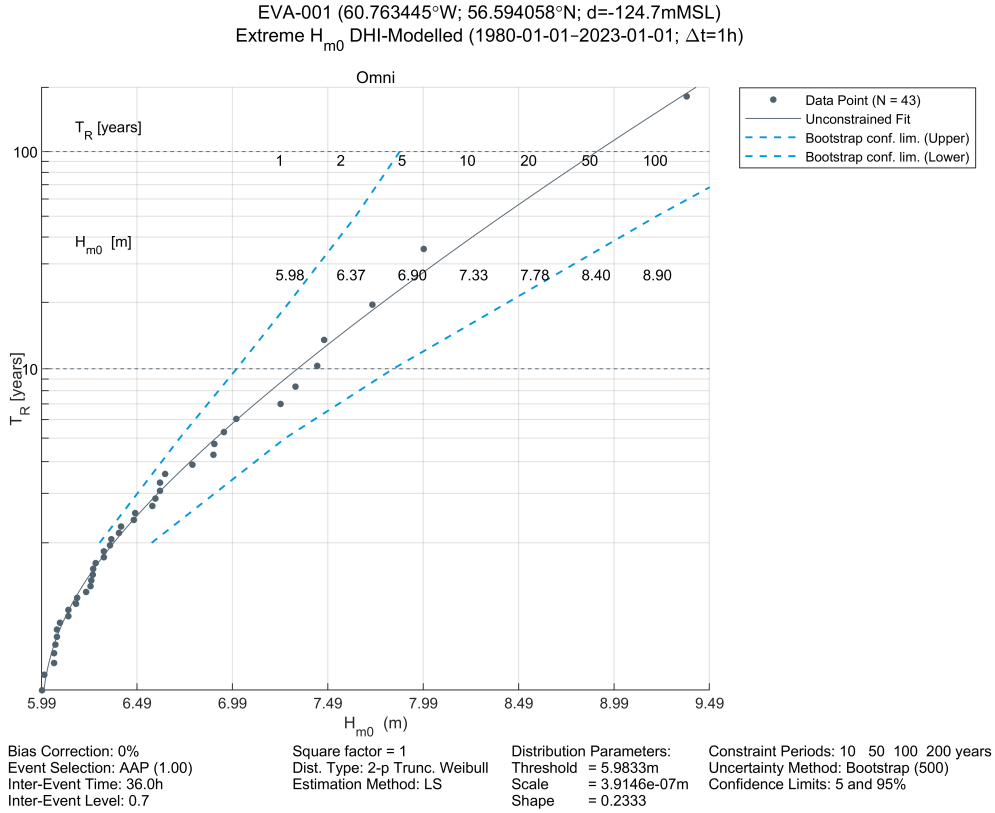


Figure C-158: Extreme value distribution fit at EVA-001.

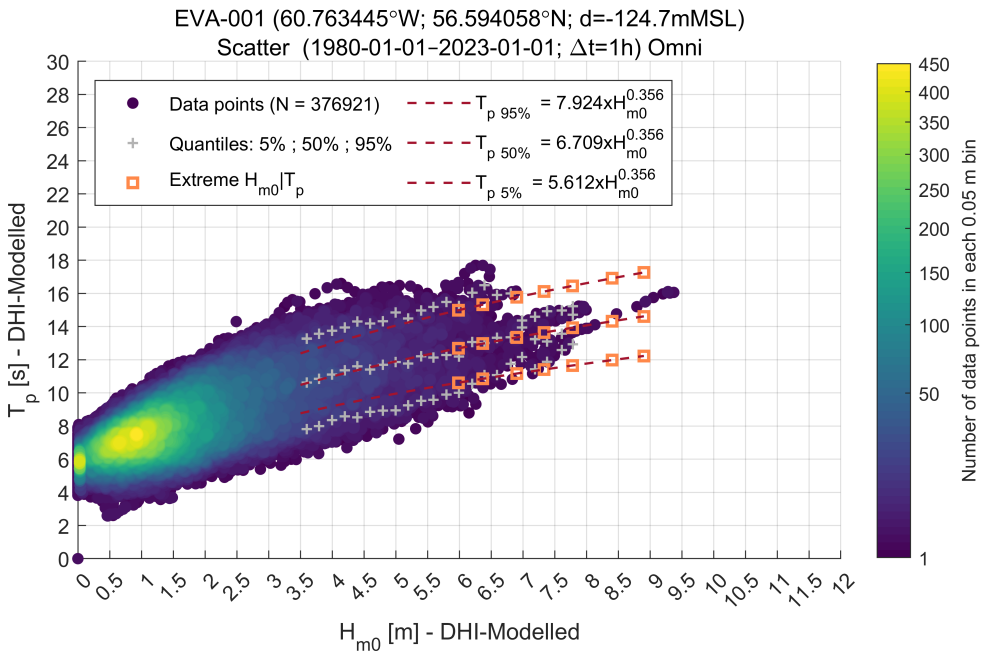


Figure C-159: Scatter plot of Hm0 x Tp at EVA-001 and quantile fit used to derived associated Tp to each extreme Hm0.

EVA-002

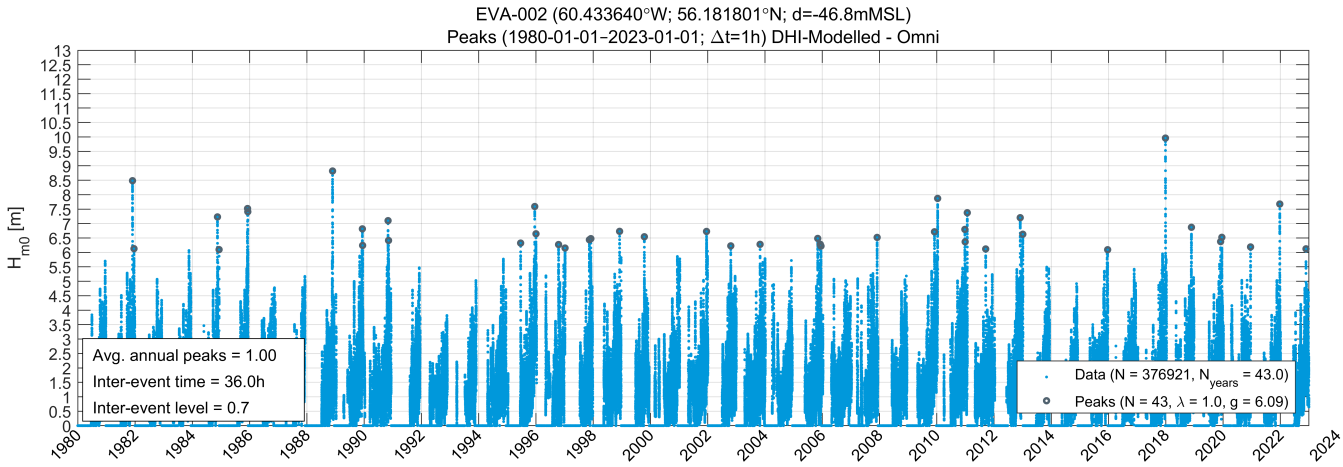


Figure C-160: Time series of significant wave height at EVA-002 and selected peaks.

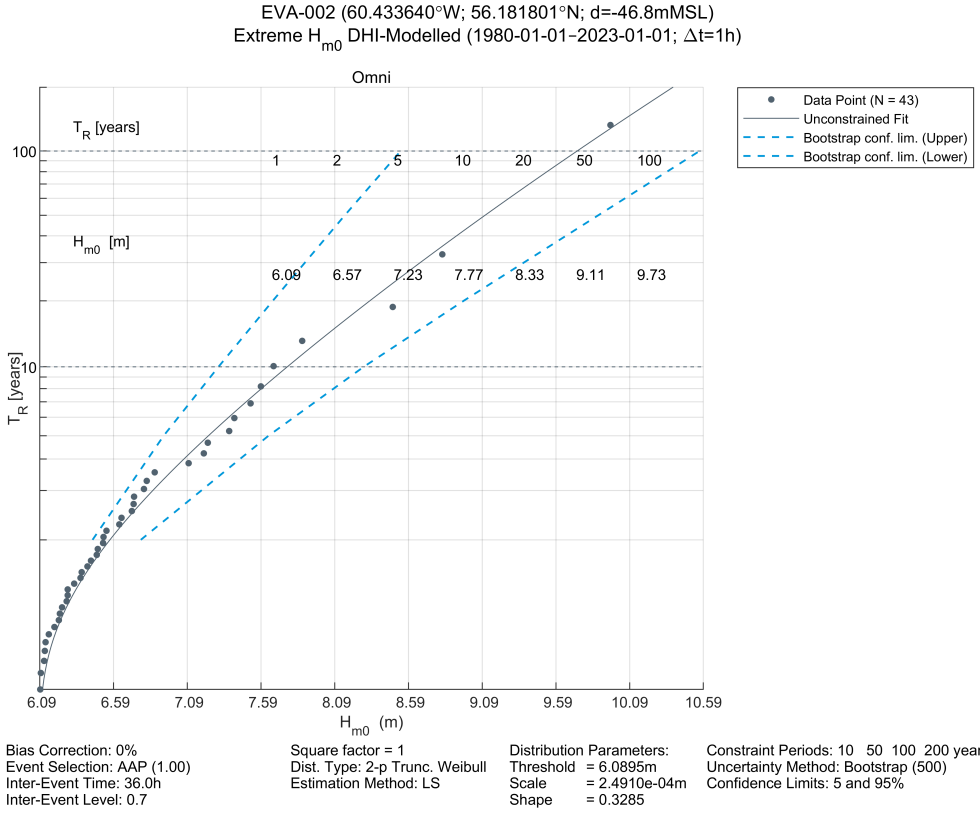


Figure C-161: Extreme value distribution fit at EVA-002.

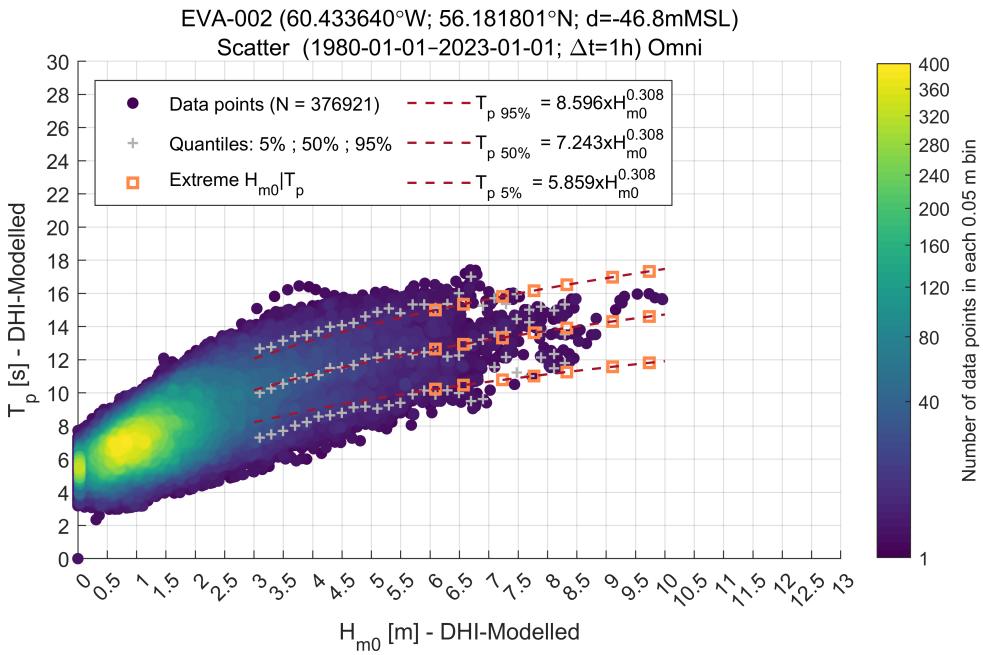


Figure C-162: Scatter plot of Hm0 x Tp at EVA-002 and quantile fit used to derived associated Tp to each extreme Hm0.

EVA-003

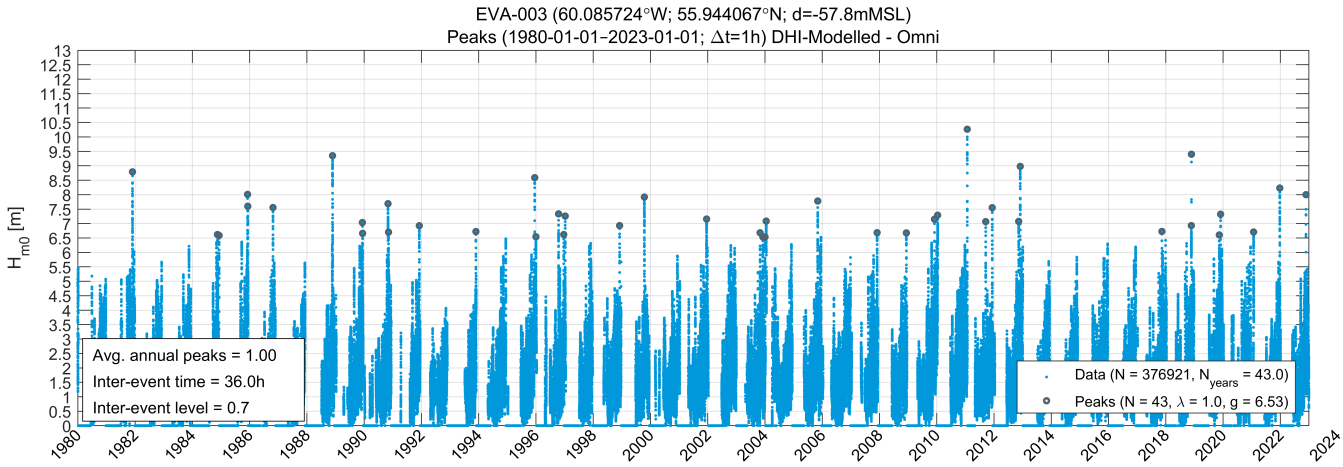


Figure C-163: Time series of significant wave height at EVA-003 and selected peaks.

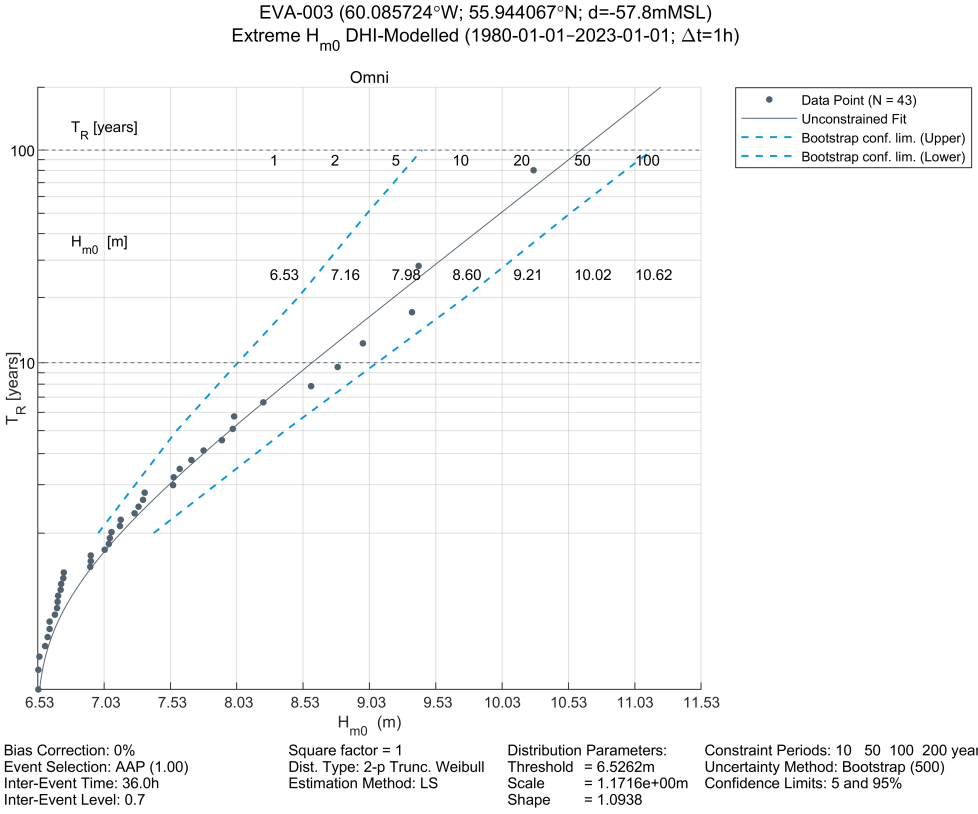


Figure C-164: Extreme value distribution fit at EVA-003.

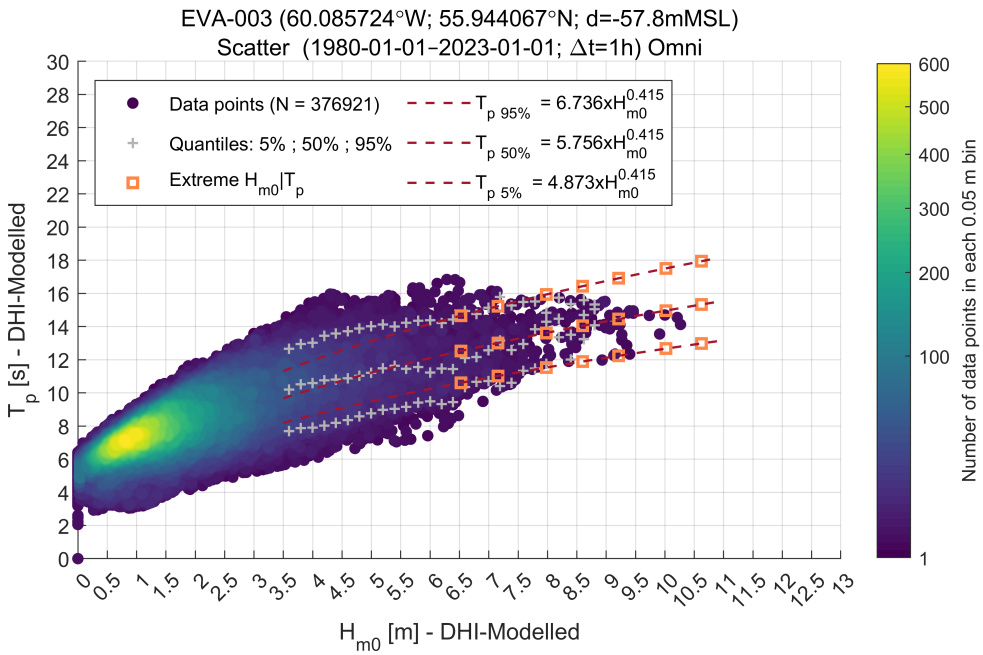


Figure C-165: Scatter plot of Hm0 x Tp at EVA-003 and quantile fit used to derived associated Tp to each extreme Hm0.

EVA-004

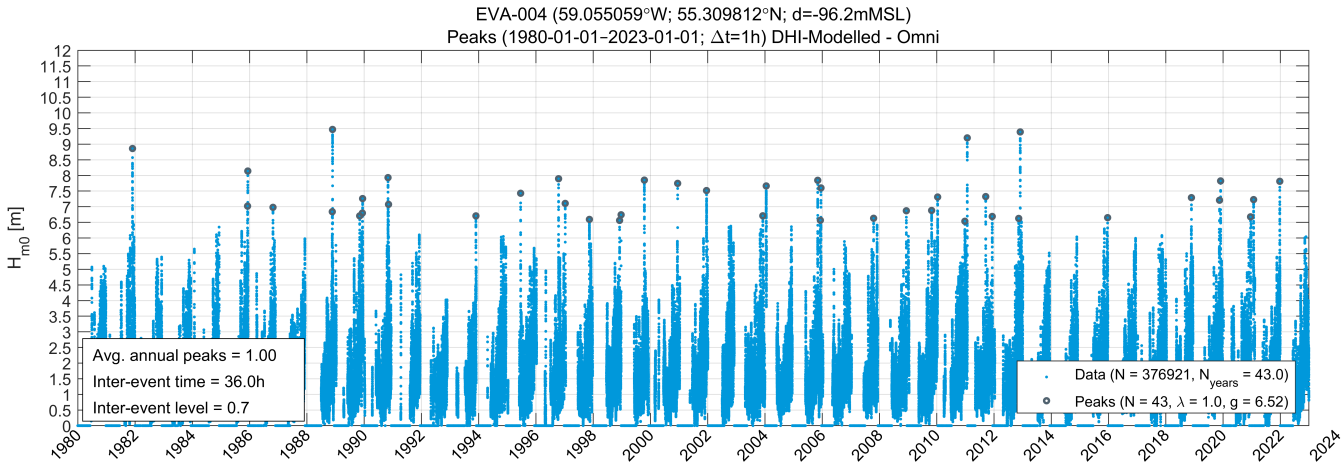


Figure C-166: Time series of significant wave height at EVA-004 and selected peaks.

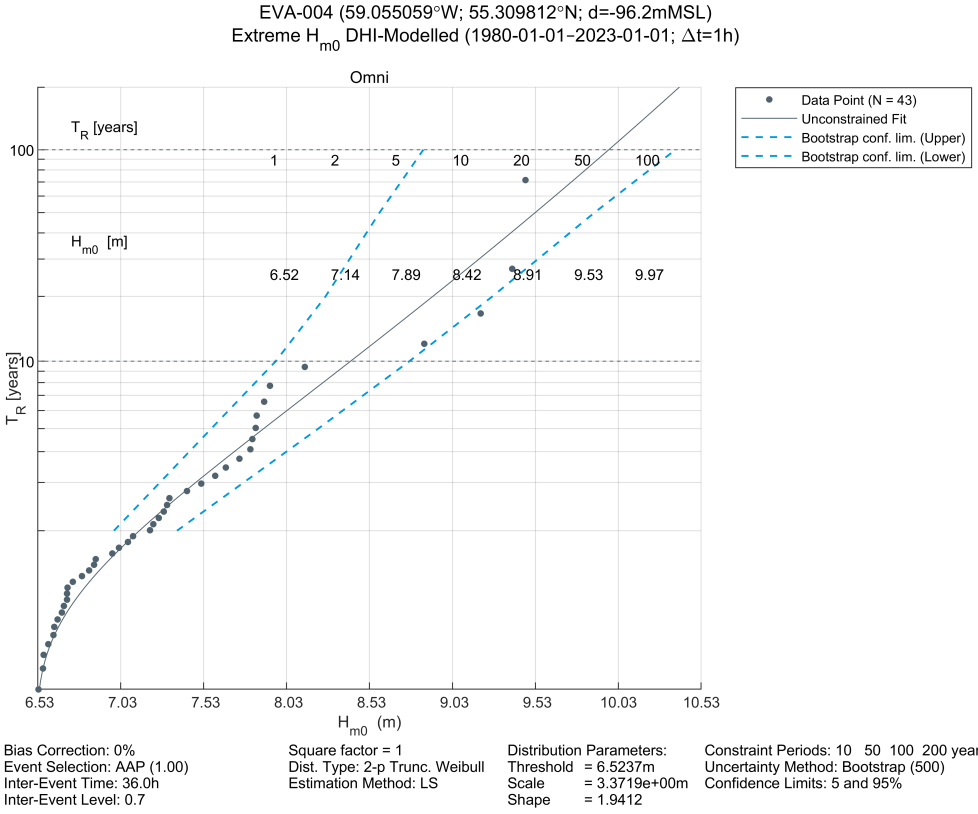


Figure C-167: Extreme value distribution fit at EVA-004.

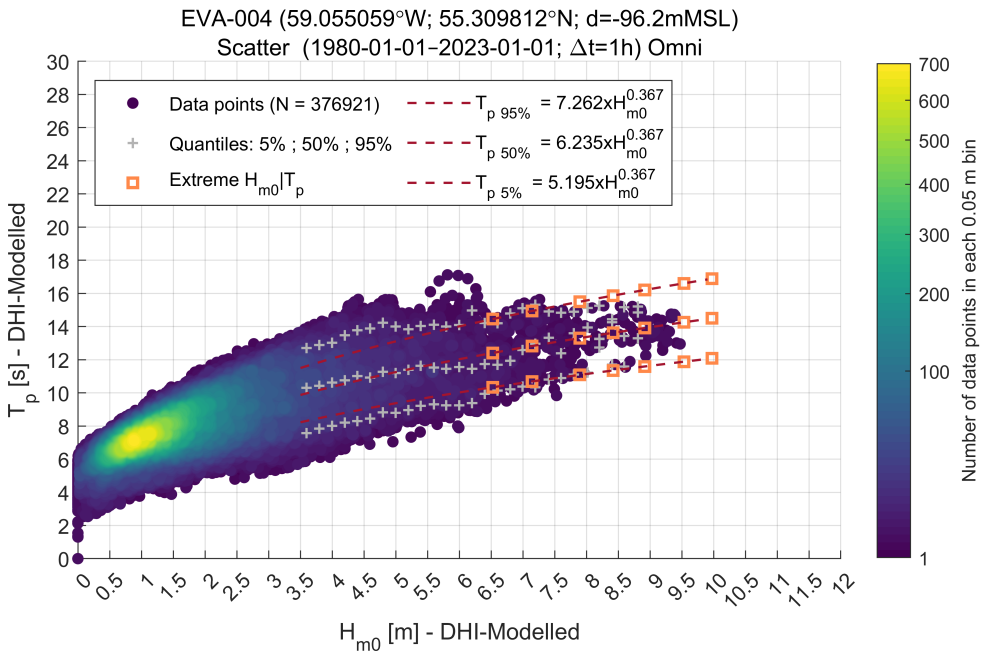


Figure C-168: Scatter plot of Hm0 x Tp at EVA-004 and quantile fit used to derived associated Tp to each extreme Hm0.

EVA-005

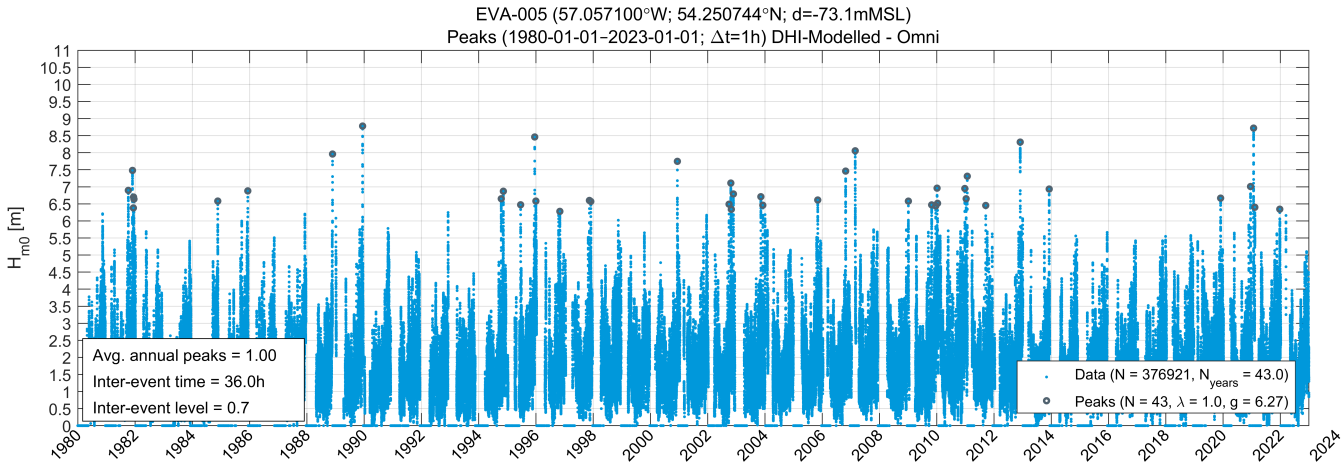


Figure C-169: Time series of significant wave height at EVA-005 and selected peaks.

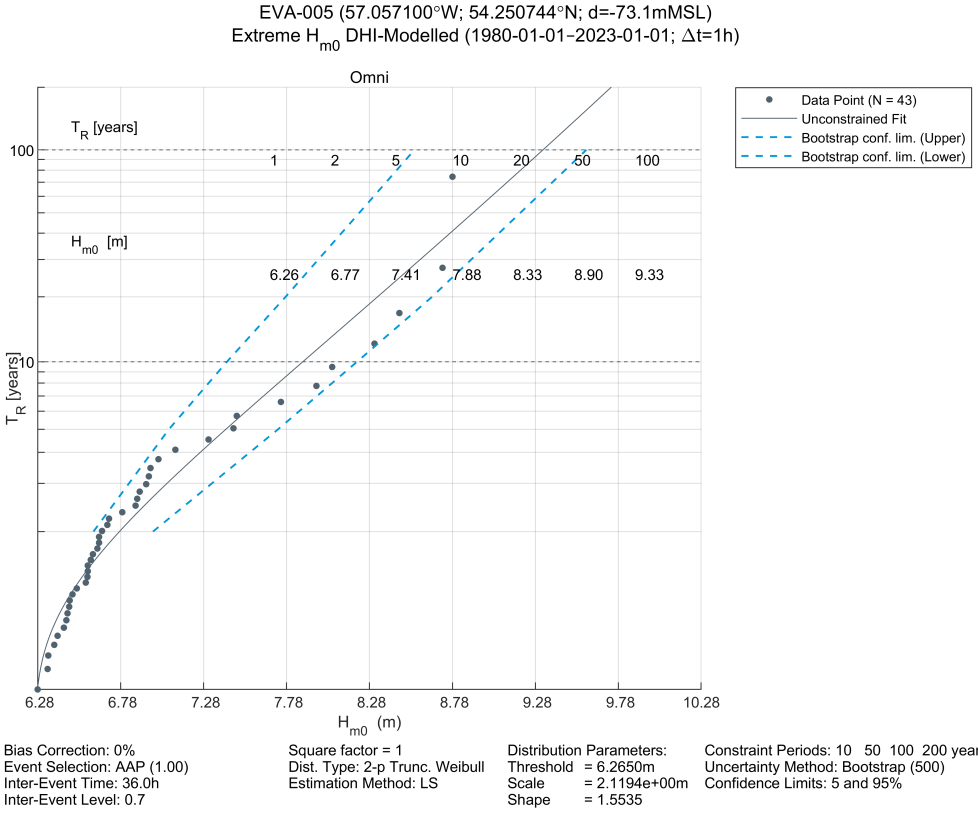


Figure C-170: Extreme value distribution fit at EVA-005.

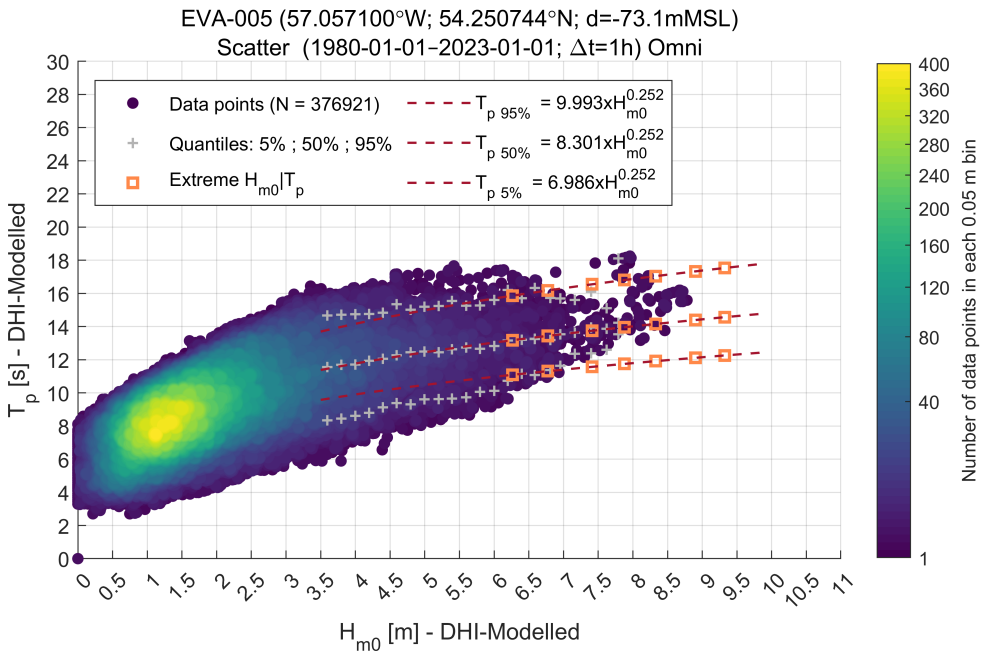


Figure C-171: Scatter plot of Hm0 x Tp at EVA-005 and quantile fit used to derived associated Tp to each extreme Hm0.

EVA-006

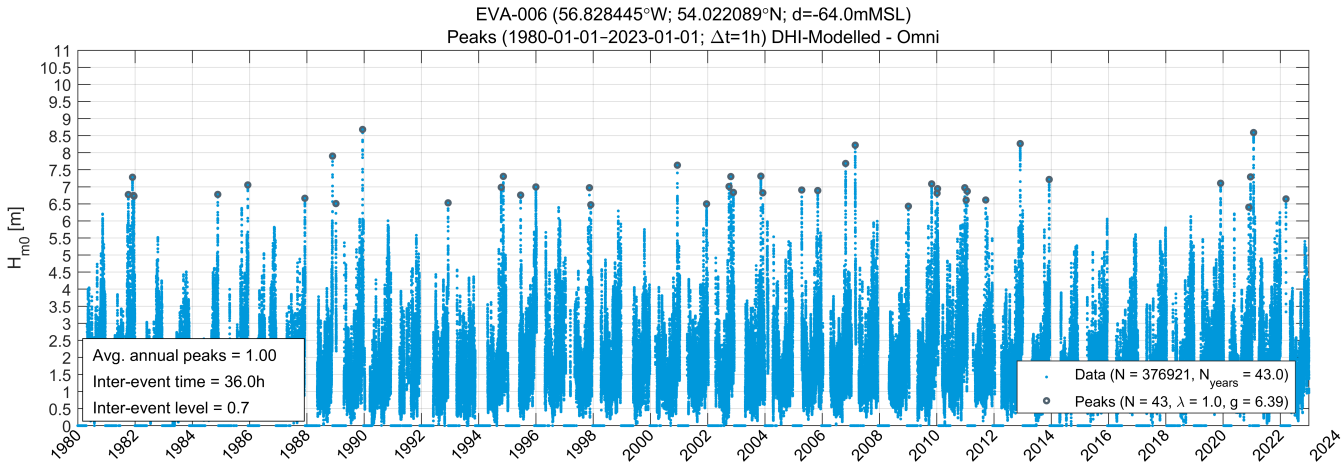


Figure C-172: Time series of significant wave height at EVA-006 and selected peaks.

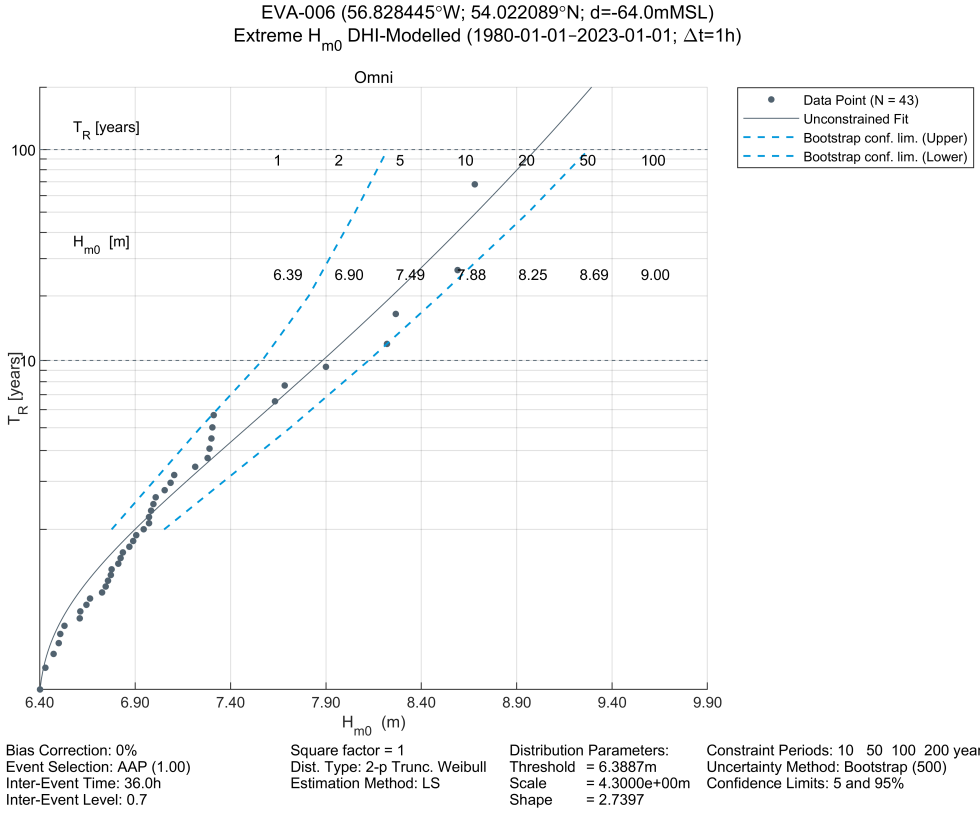


Figure C-173: Extreme value distribution fit at EVA-006.

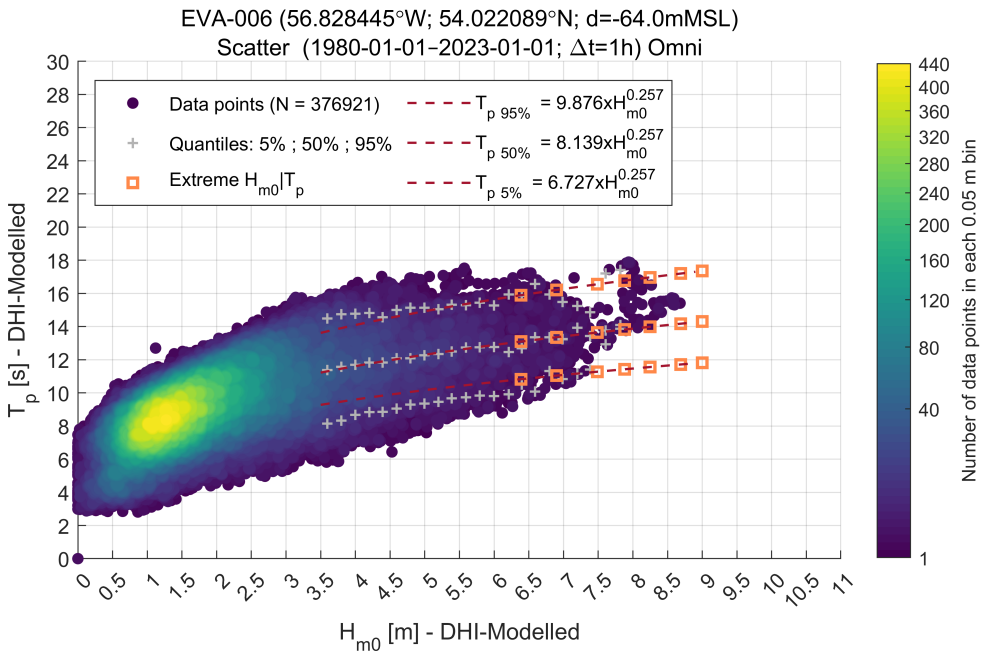


Figure C-174: Scatter plot of Hm0 x Tp at EVA-006 and quantile fit used to derived associated Tp to each extreme Hm0.

EVA-007

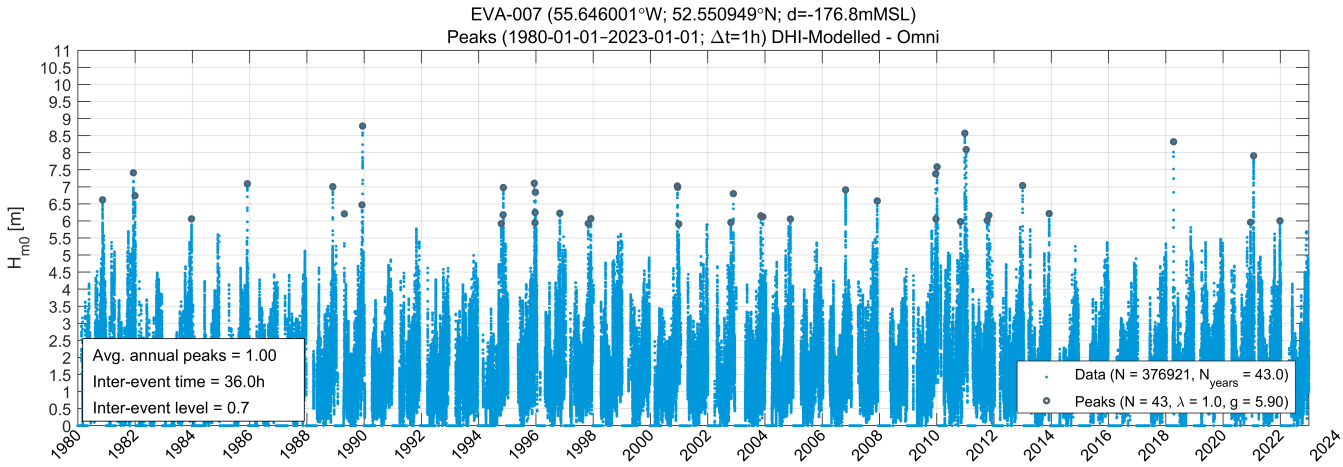


Figure C-175: Time series of significant wave height at EVA-007 and selected peaks.

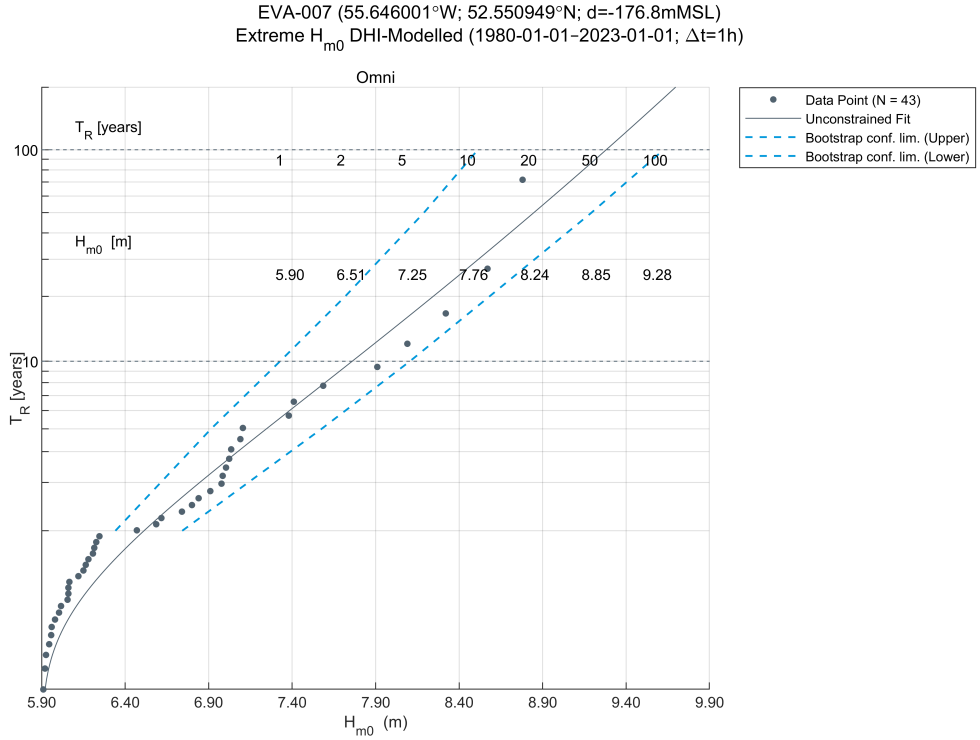


Figure C-176: Extreme value distribution fit at EVA-007.

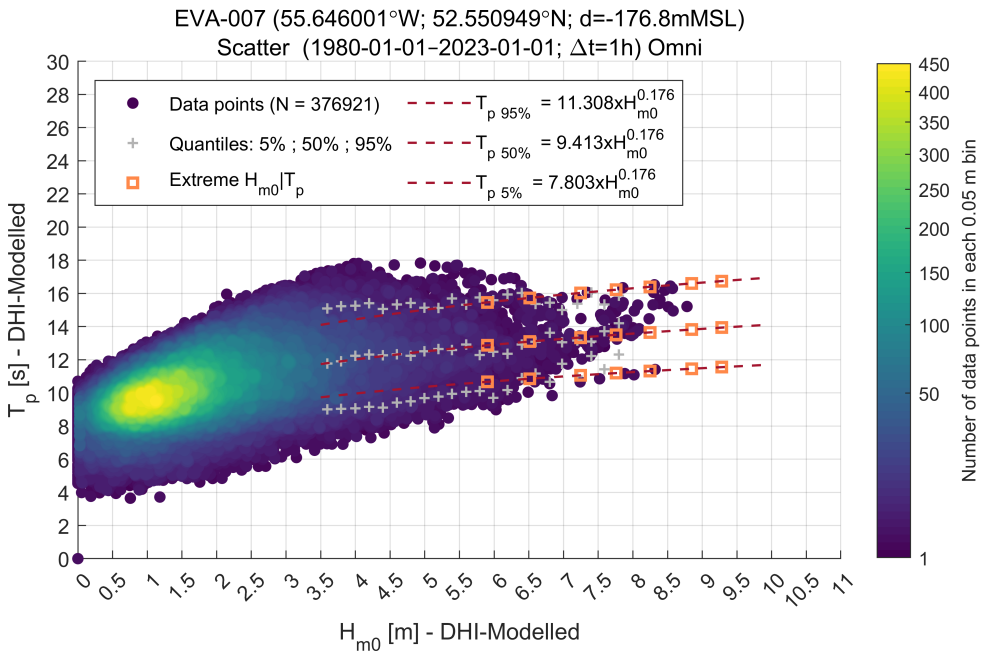


Figure C-177: Scatter plot of Hm0 x Tp at EVA-007 and quantile fit used to derived associated Tp to each extreme Hm0.

EVA-008

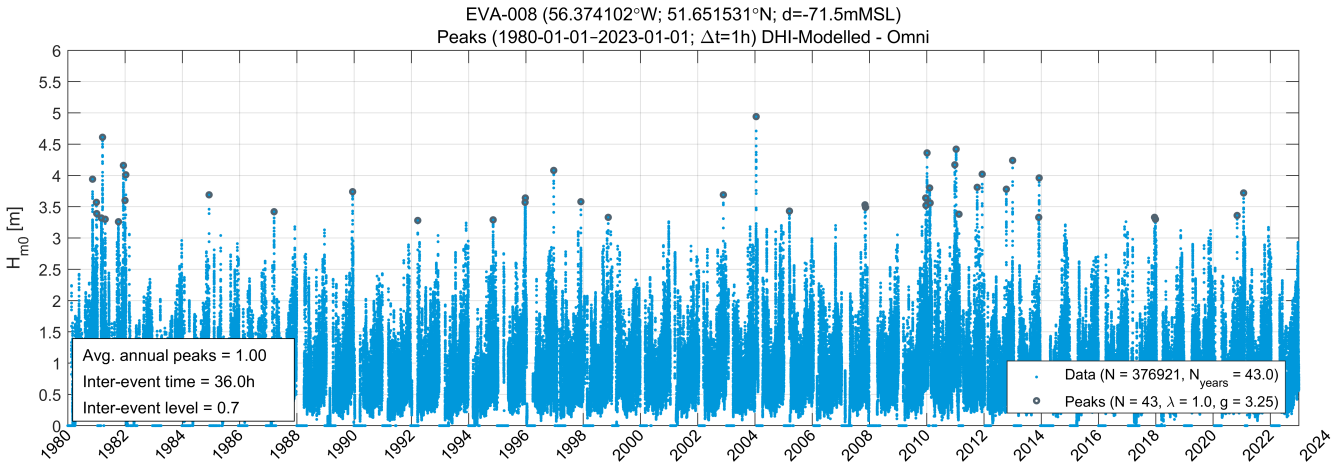


Figure C-178: Time series of significant wave height at EVA-008 and selected peaks.

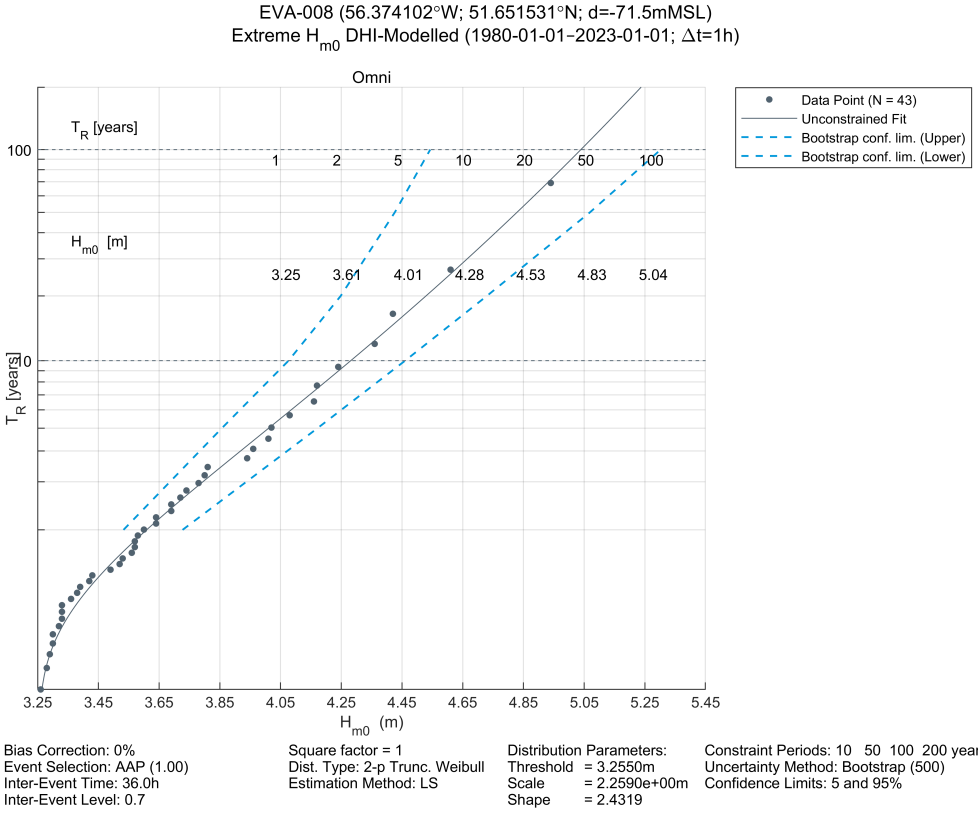


Figure C-179: Extreme value distribution fit at EVA-008.

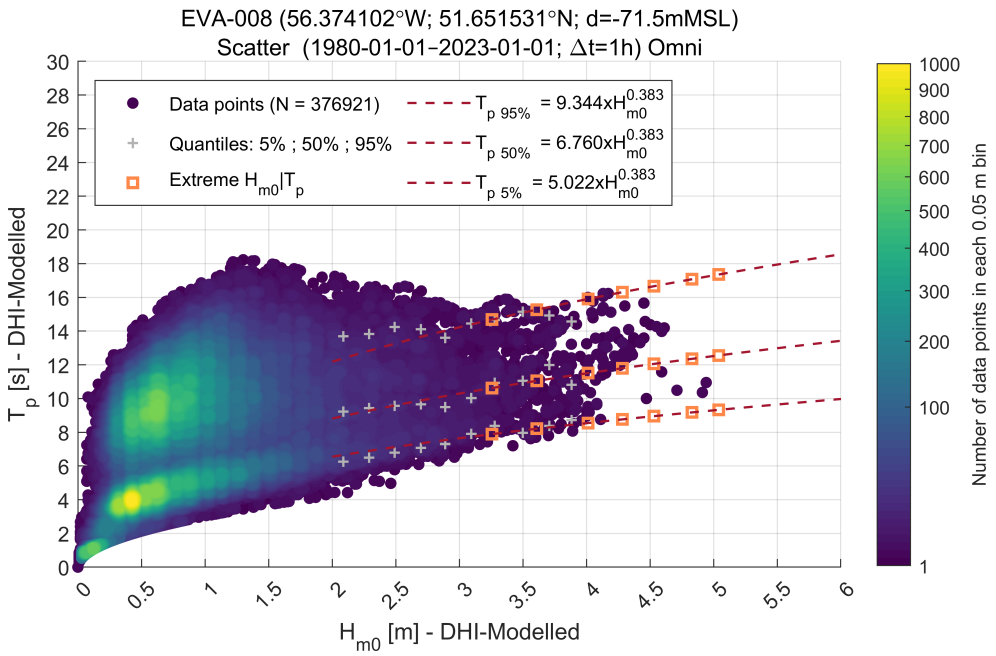


Figure C-180: Scatter plot of Hm0 x Tp at EVA-008 and quantile fit used to derived associated Tp to each extreme Hm0.

EVA-009

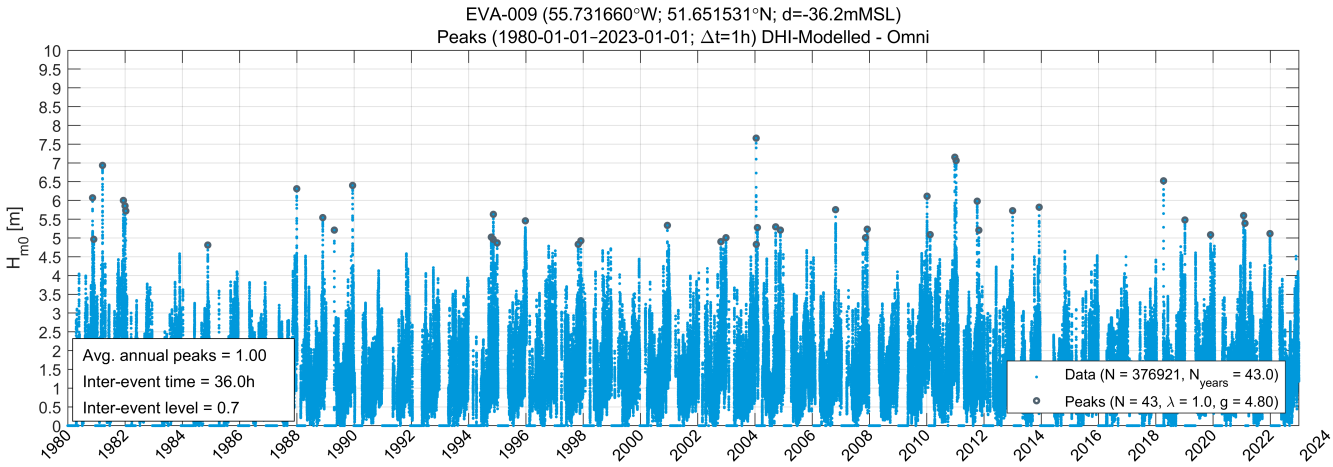


Figure C-181: Time series of significant wave height at EVA-009 and selected peaks.

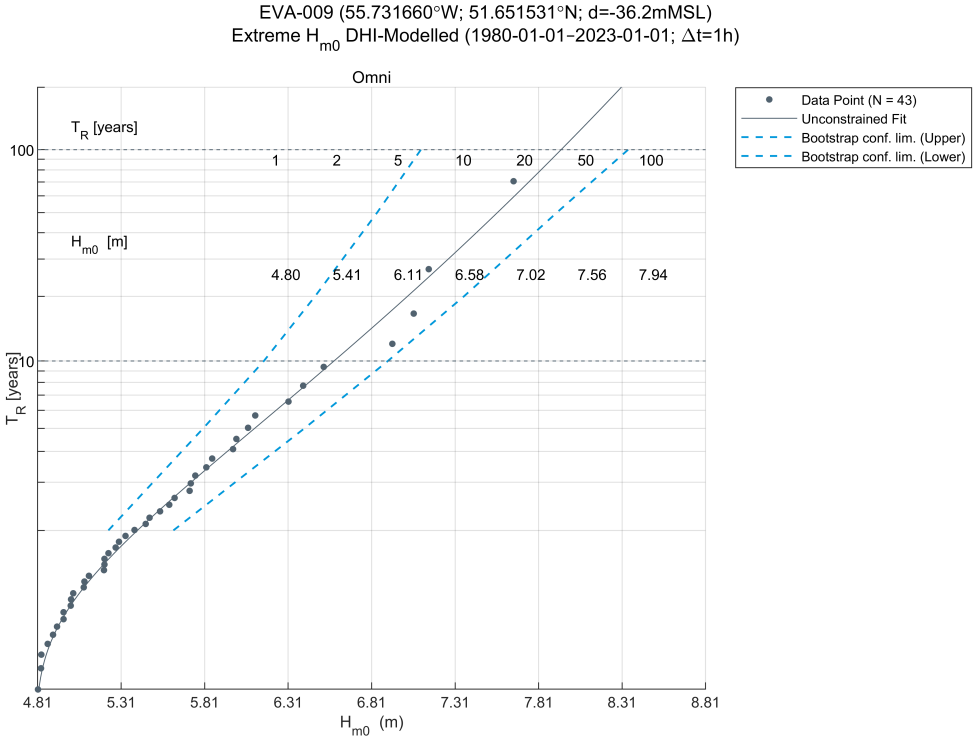


Figure C-182: Extreme value distribution fit at EVA-009.

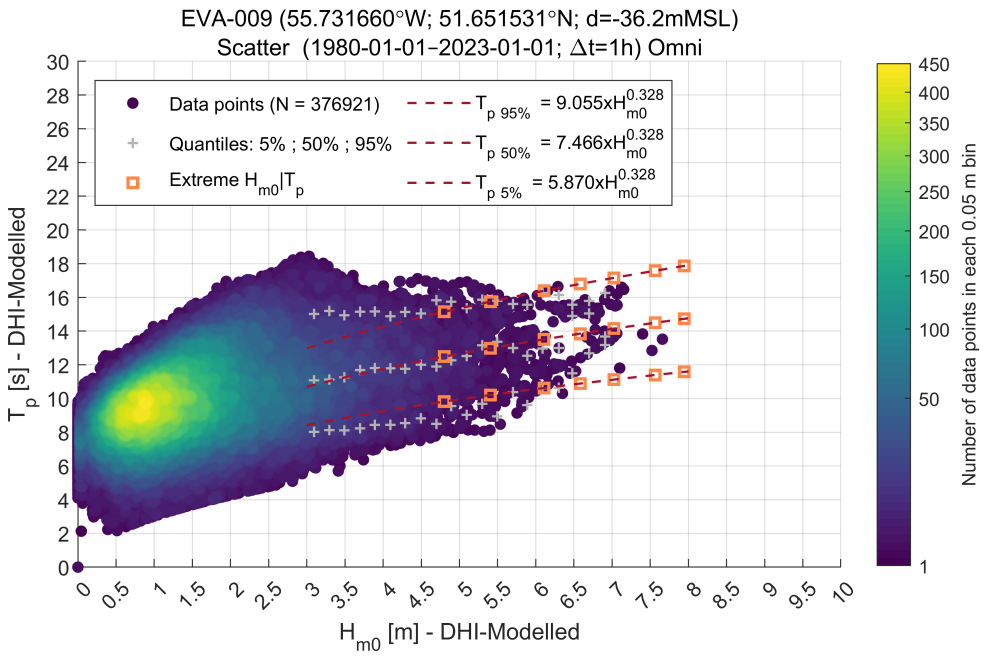


Figure C-183: Scatter plot of Hm0 x Tp at EVA-009 and quantile fit used to derived associated Tp to each extreme Hm0.

EVA-010

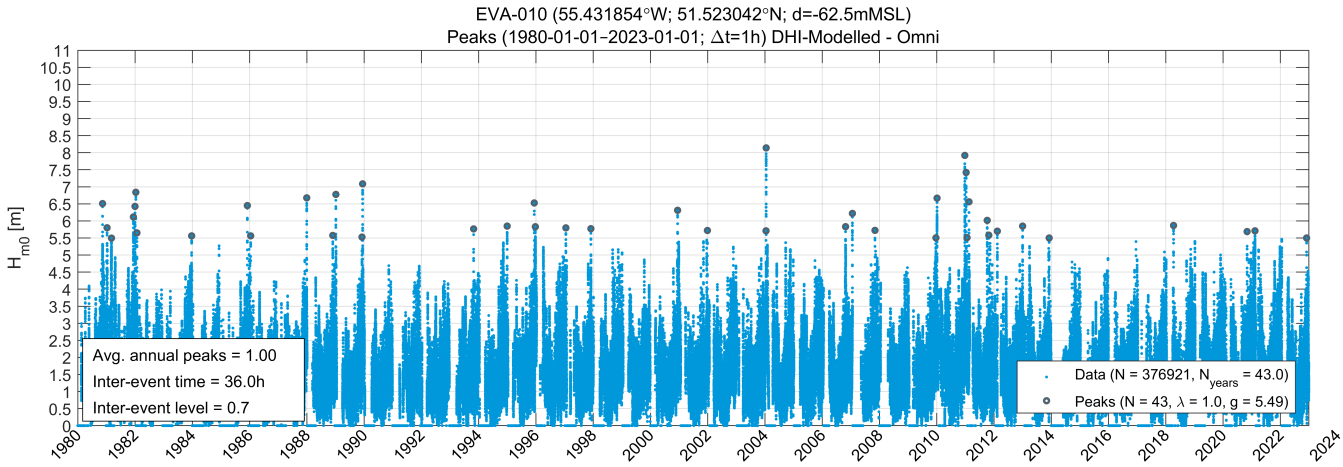


Figure C-184: Time series of significant wave height at EVA-010 and selected peaks.

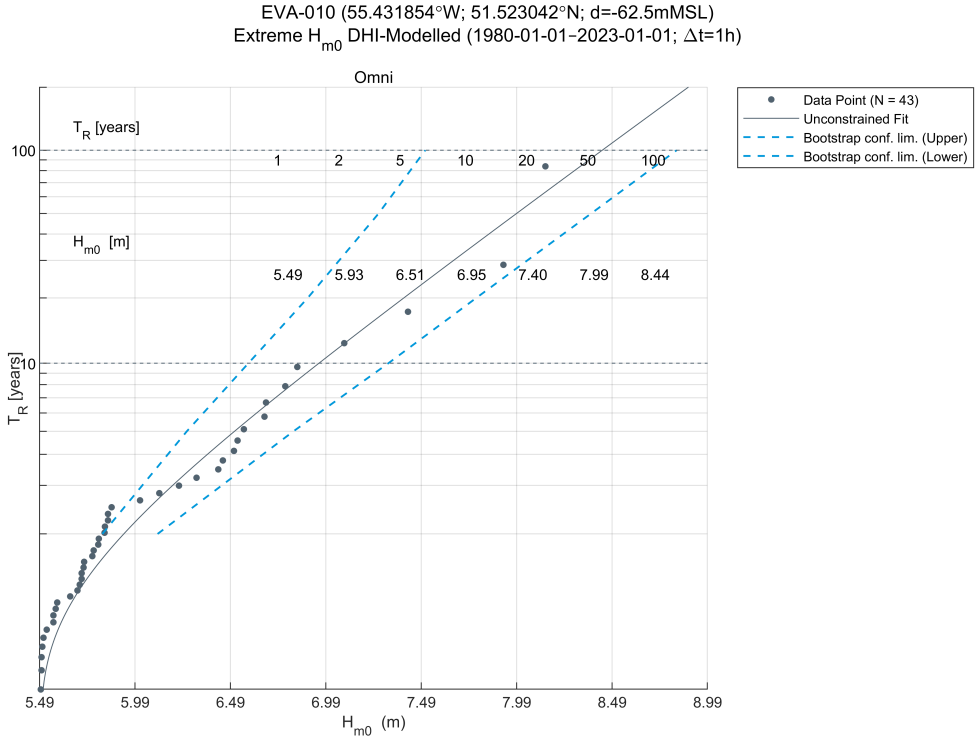


Figure C-185: Extreme value distribution fit at EVA-010.

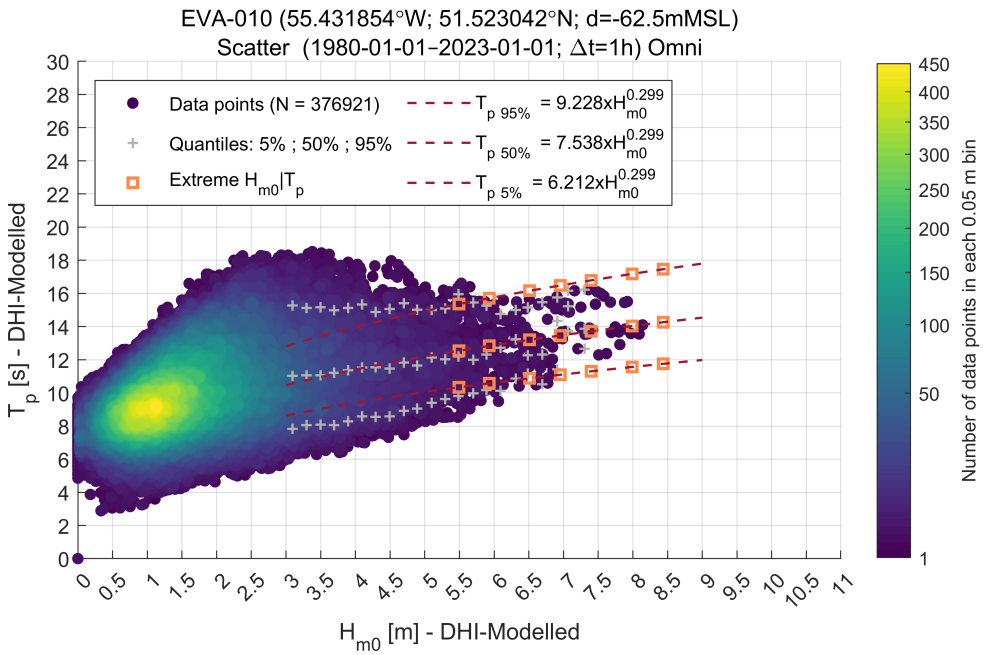


Figure C-186: Scatter plot of Hm0 x Tp at EVA-010 and quantile fit used to derived associated Tp to each extreme Hm0.

EVA-011

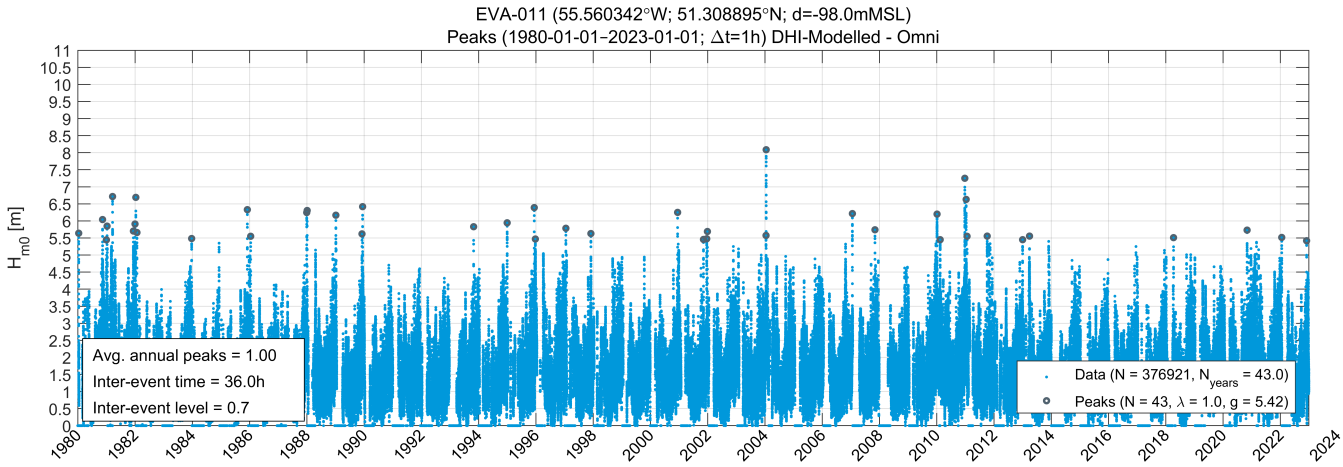


Figure C-187: Time series of significant wave height at EVA-011 and selected peaks.

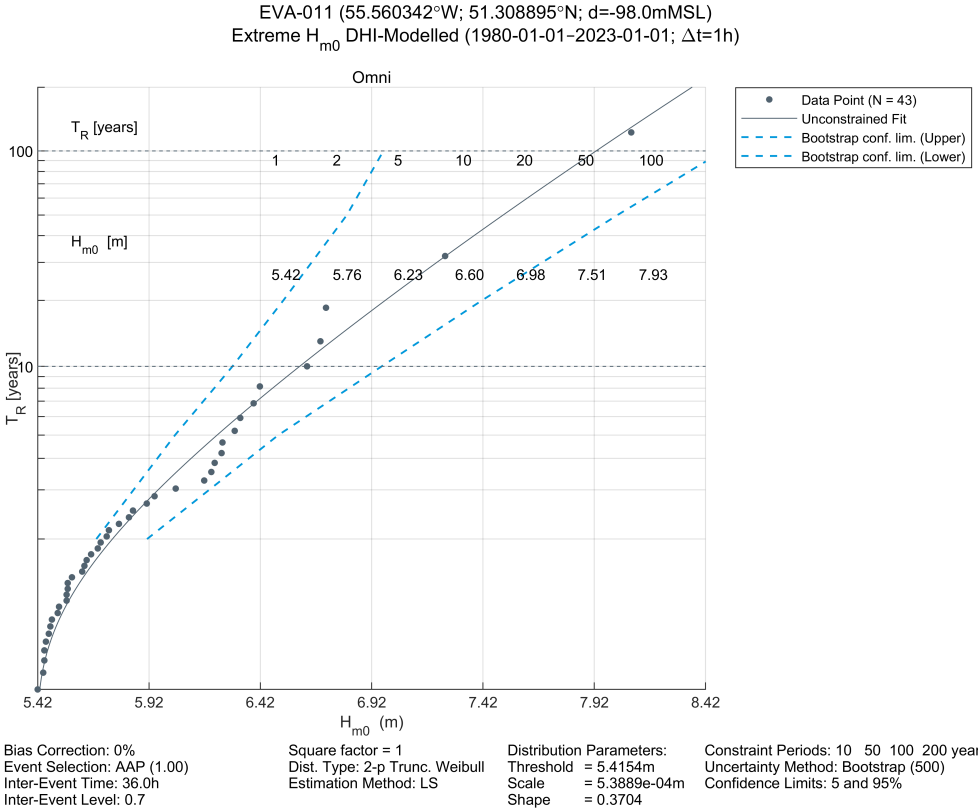


Figure C-188: Extreme value distribution fit at EVA-011.

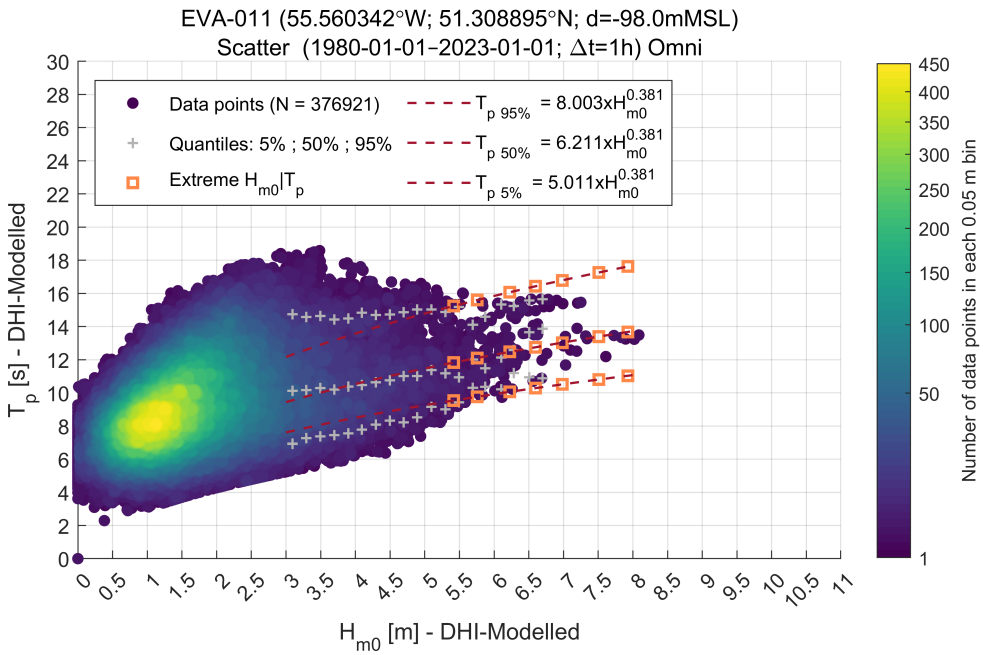


Figure C-189: Scatter plot of Hm0 x Tp at EVA-011 and quantile fit used to derived associated Tp to each extreme Hm0.

EVA-012

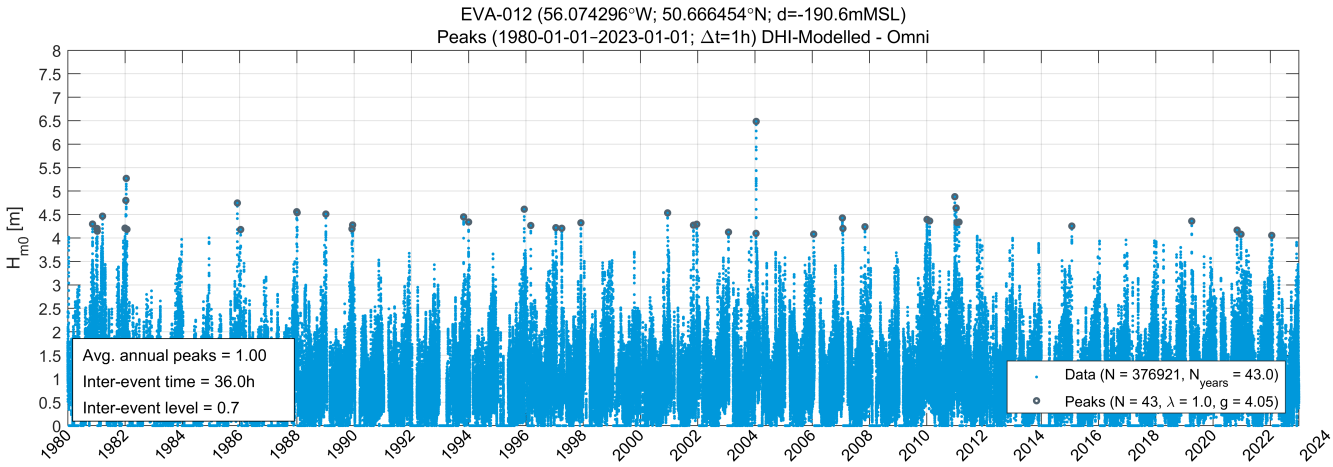


Figure C-190: Time series of significant wave height at EVA-012 and selected peaks.

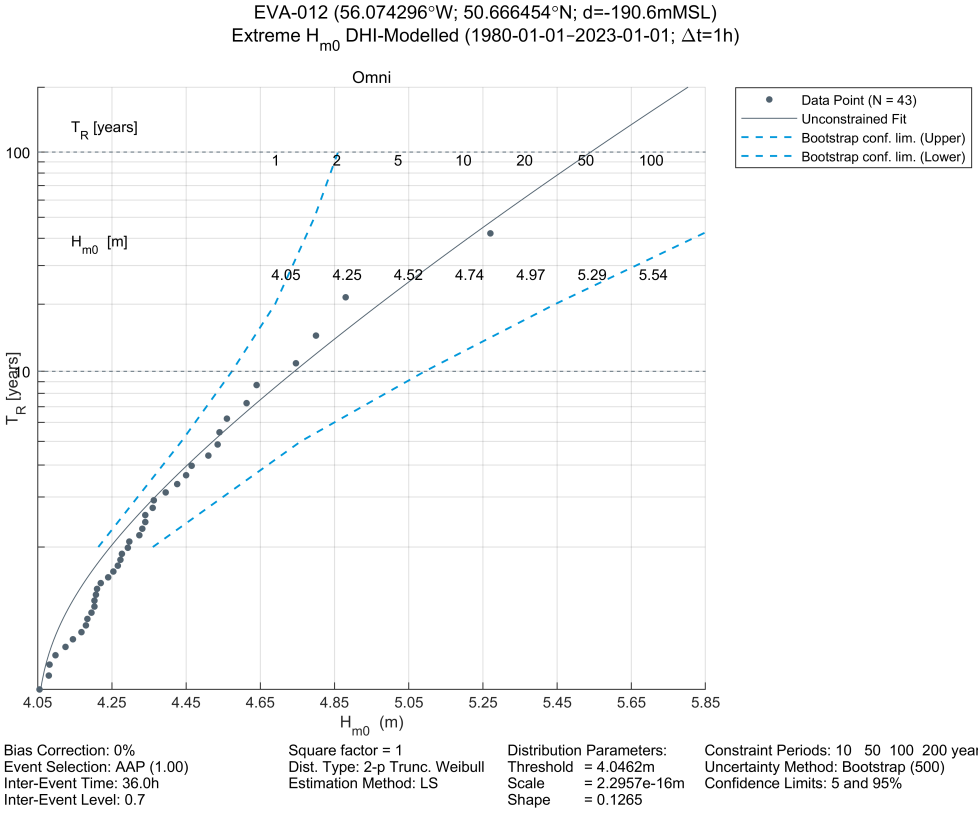


Figure C-191: Extreme value distribution fit at EVA-012.

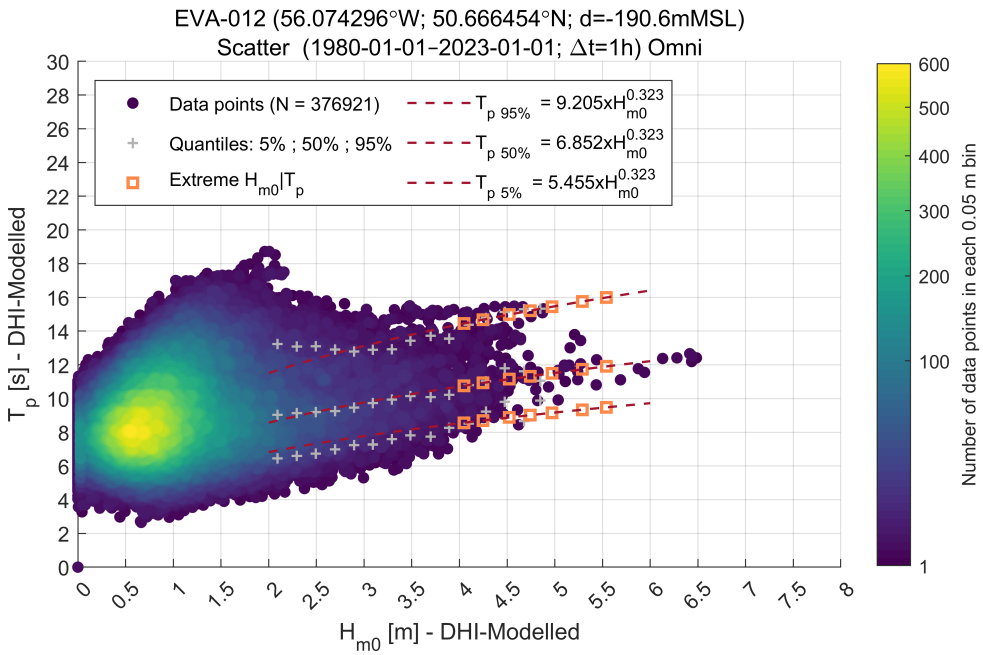


Figure C-192: Scatter plot of Hm0 x Tp at EVA-012 and quantile fit used to derived associated Tp to each extreme Hm0.

EVA-013

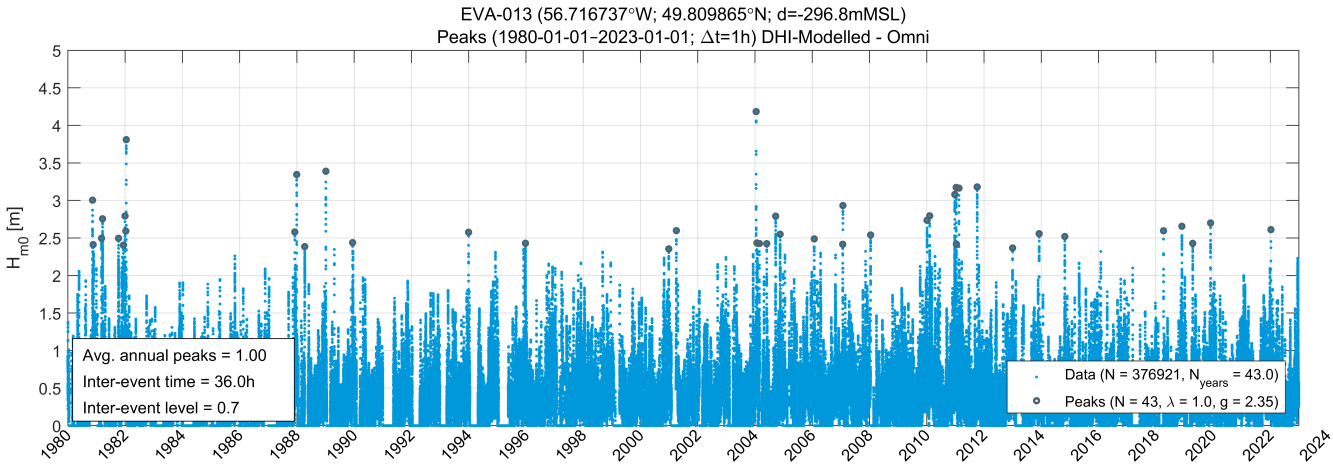


Figure C-193: Time series of significant wave height at EVA-013 and selected peaks.

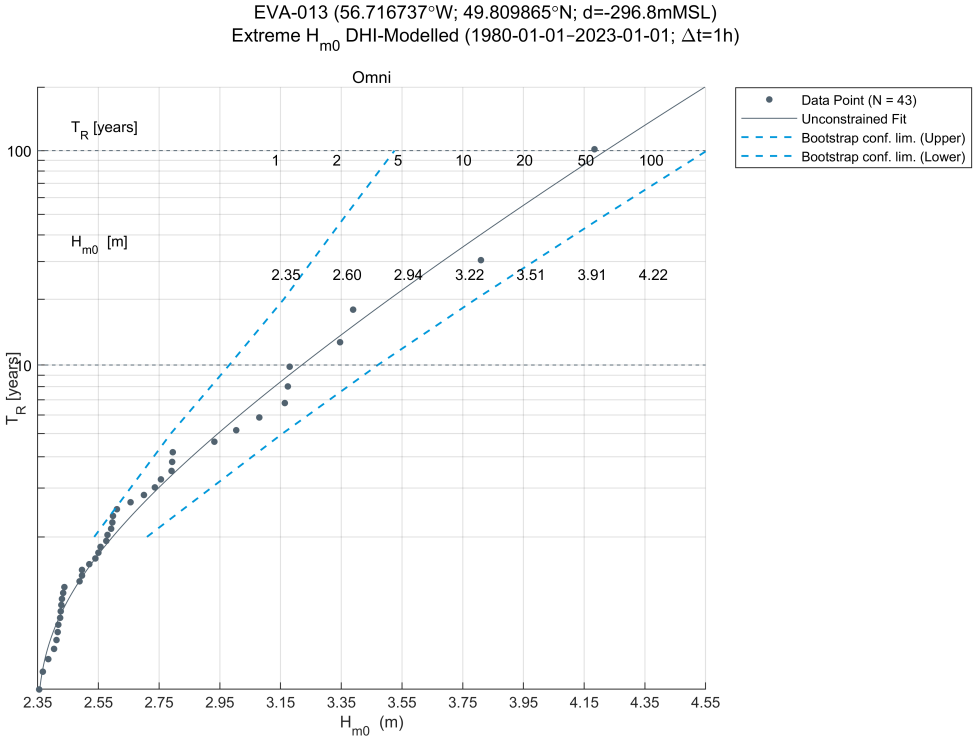


Figure C-194: Extreme value distribution fit at EVA-013.

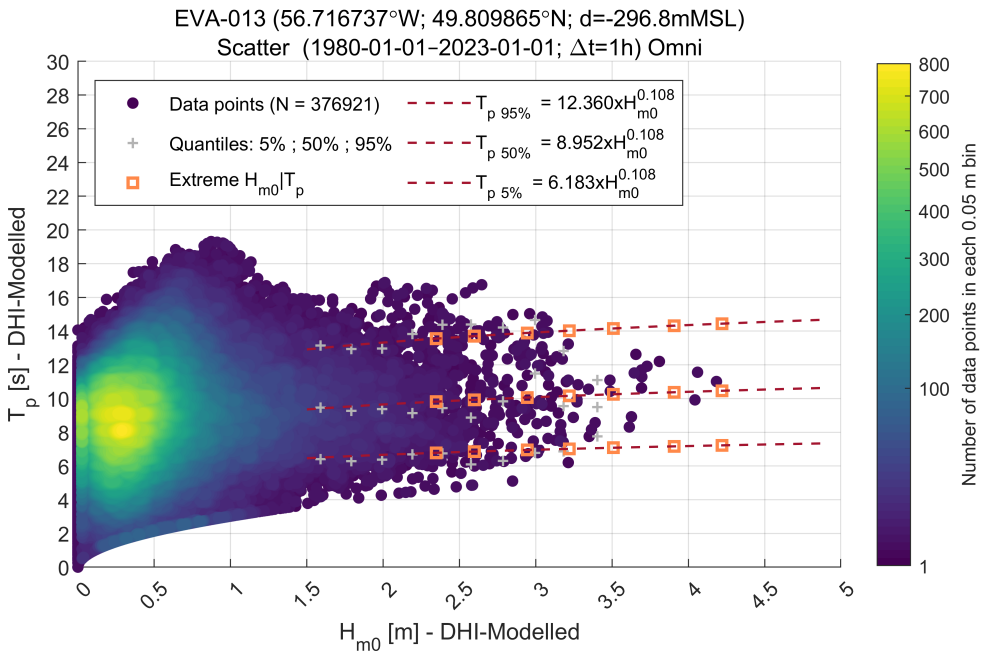


Figure C-195: Scatter plot of Hm0 x Tp at EVA-013 and quantile fit used to derived associated Tp to each extreme Hm0.

EVA-014

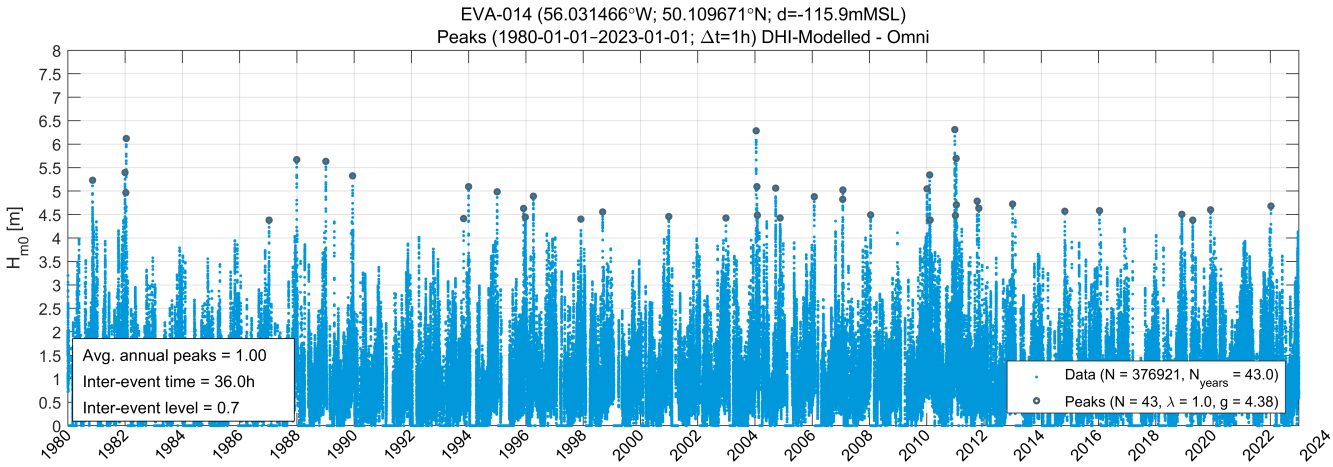


Figure C-196: Time series of significant wave height at EVA-014 and selected peaks.

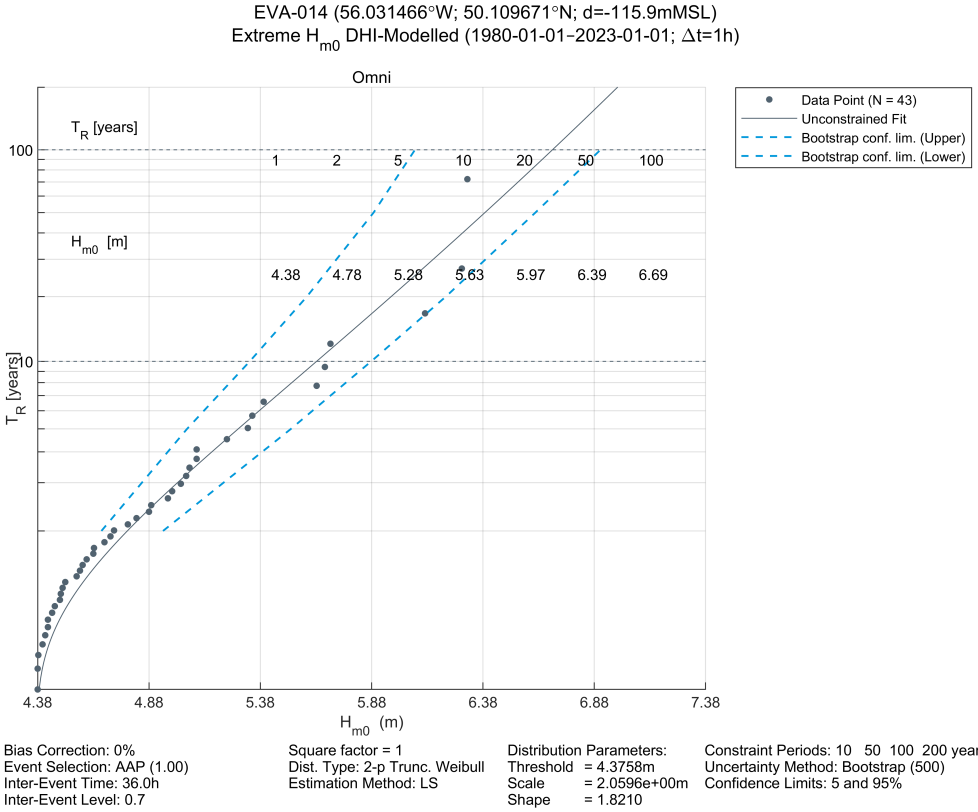


Figure C-197: Extreme value distribution fit at EVA-014.

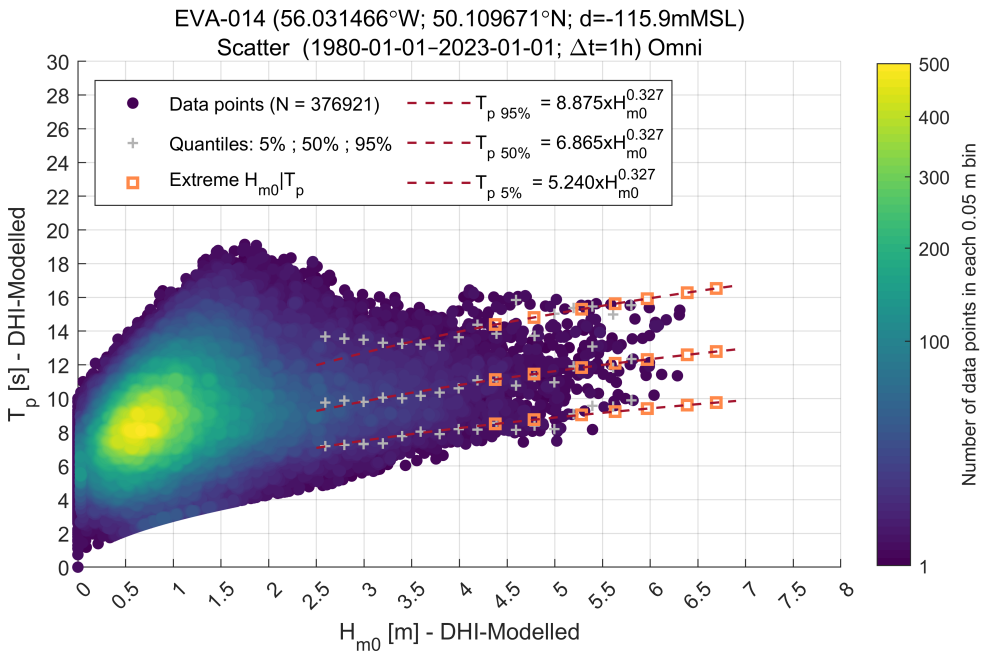


Figure C-198: Scatter plot of Hm0 x Tp at EVA-014 and quantile fit used to derived associated Tp to each extreme Hm0.

EVA-015

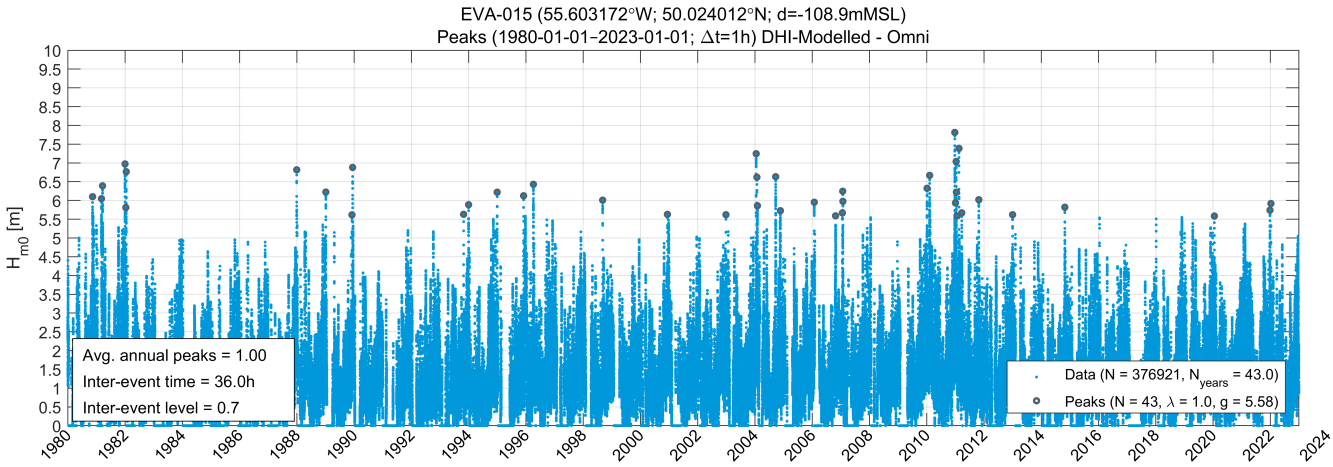


Figure C-199: Time series of significant wave height at EVA-015 and selected peaks.

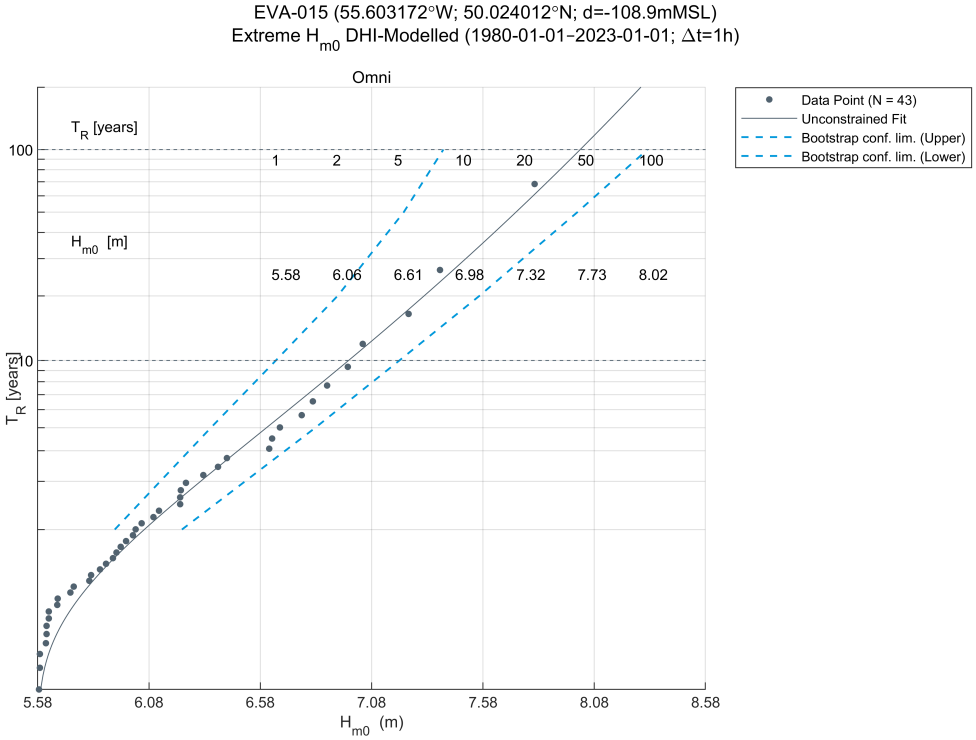


Figure C-200: Extreme value distribution fit at EVA-015.

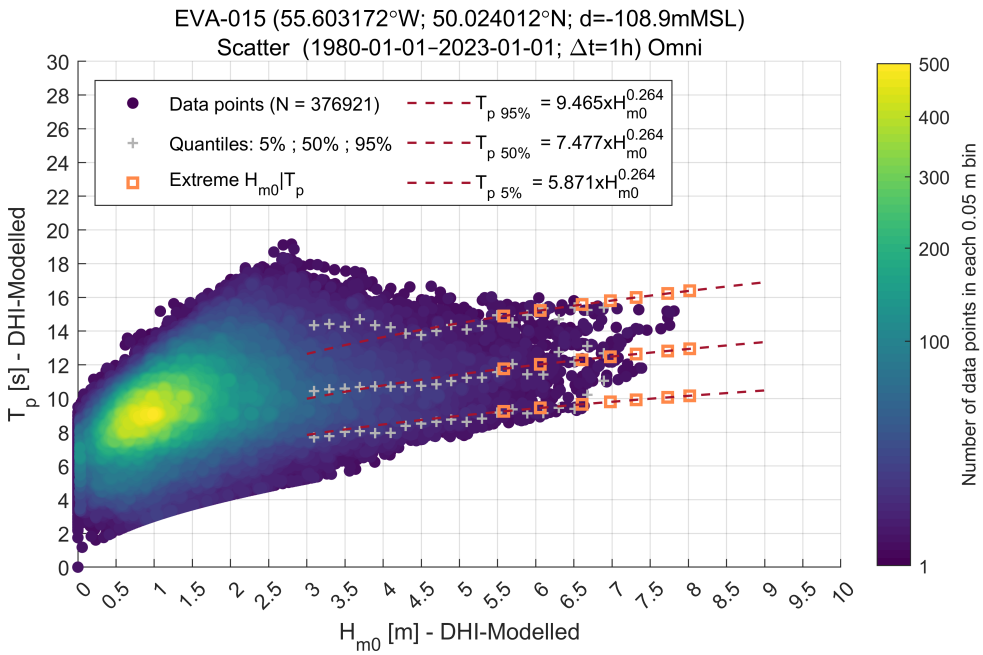


Figure C-201: Scatter plot of Hm0 x Tp at EVA-015 and quantile fit used to derived associated Tp to each extreme Hm0.

EVA-016

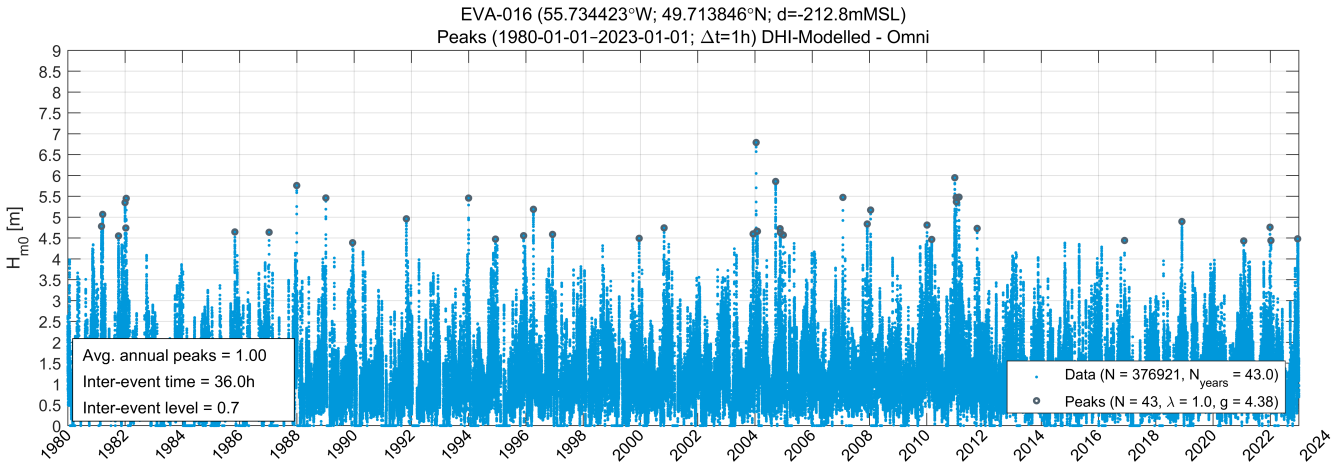


Figure C-202: Time series of significant wave height at EVA-016 and selected peaks.

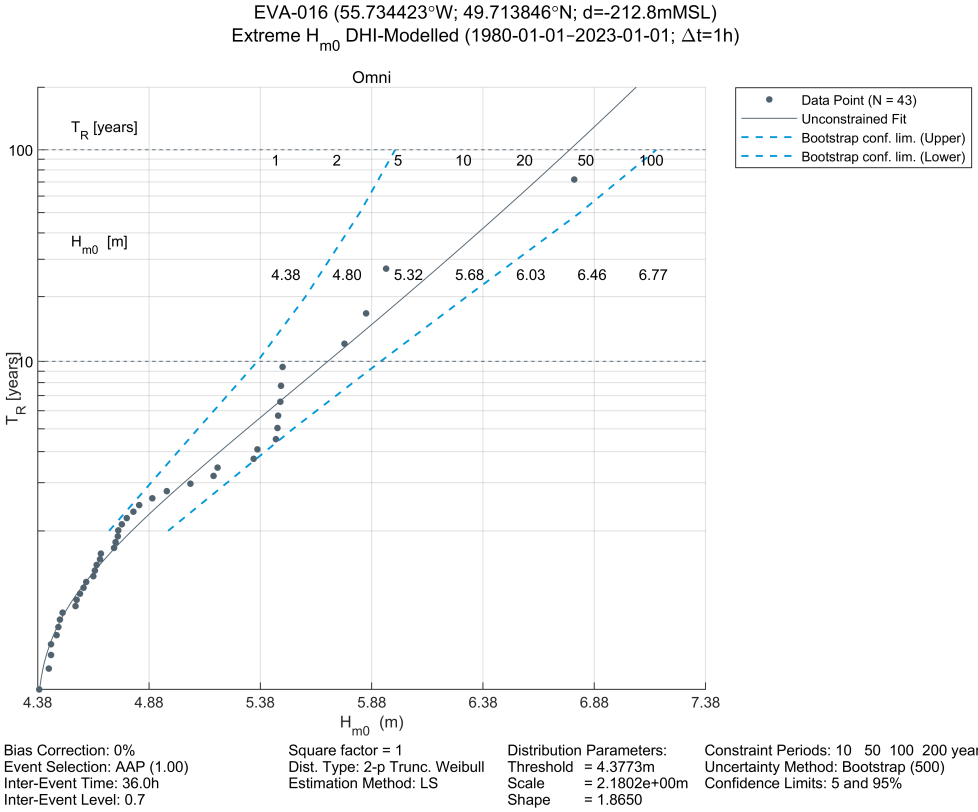


Figure C-203: Extreme value distribution fit at EVA-016.

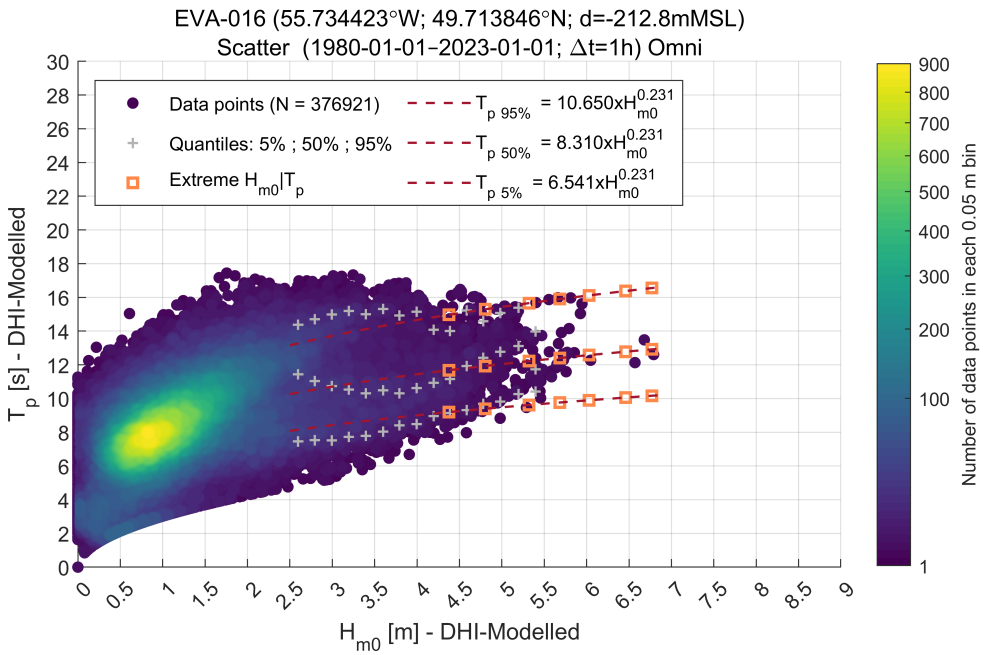


Figure C-204: Scatter plot of Hm0 x Tp at EVA-016 and quantile fit used to derived associated Tp to each extreme Hm0.

EVA-017

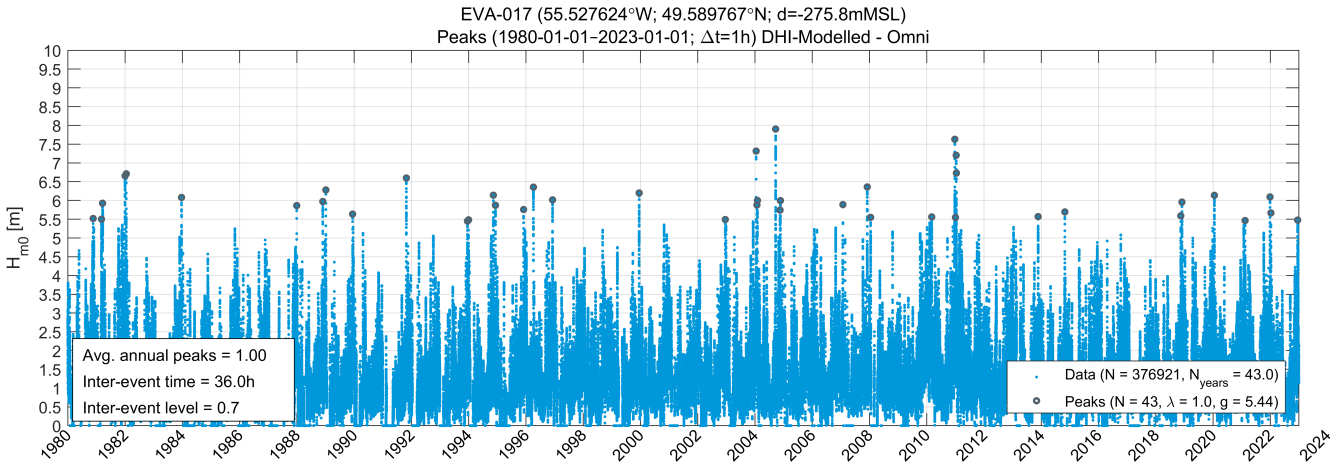


Figure C-205: Time series of significant wave height at EVA-017 and selected peaks.

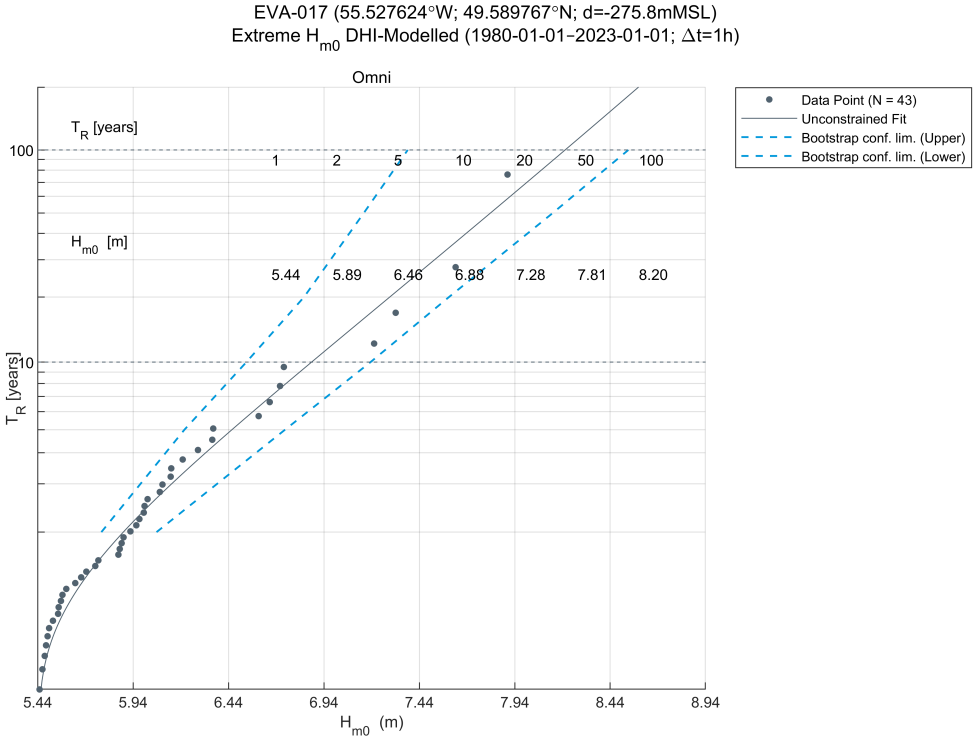


Figure C-206: Extreme value distribution fit at EVA-017.

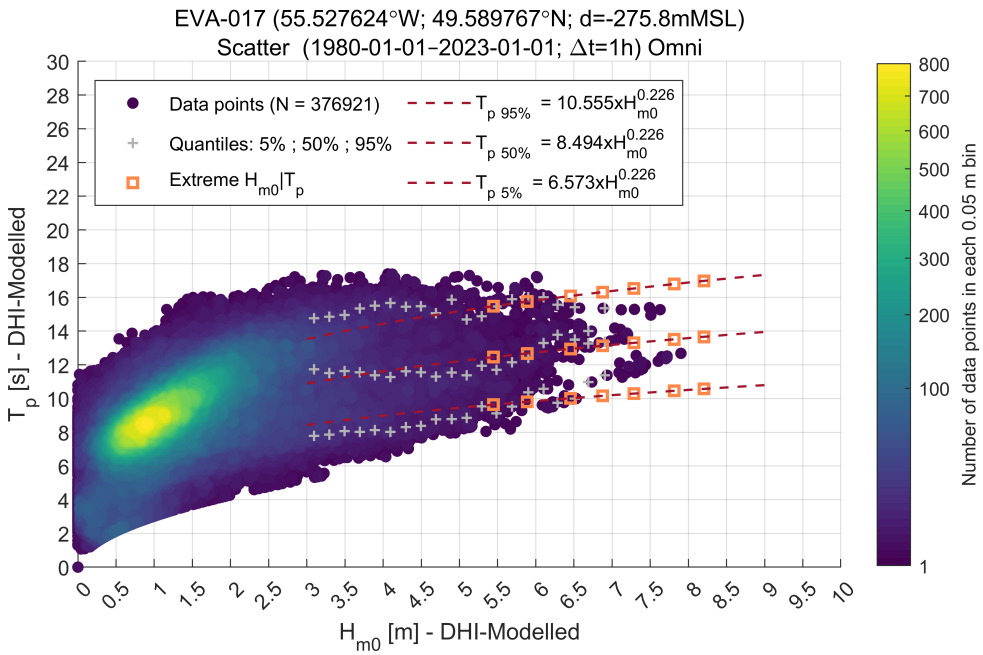


Figure C-207: Scatter plot of Hm0 x Tp at EVA-017 and quantile fit used to derived associated Tp to each extreme Hm0.

EVA-018

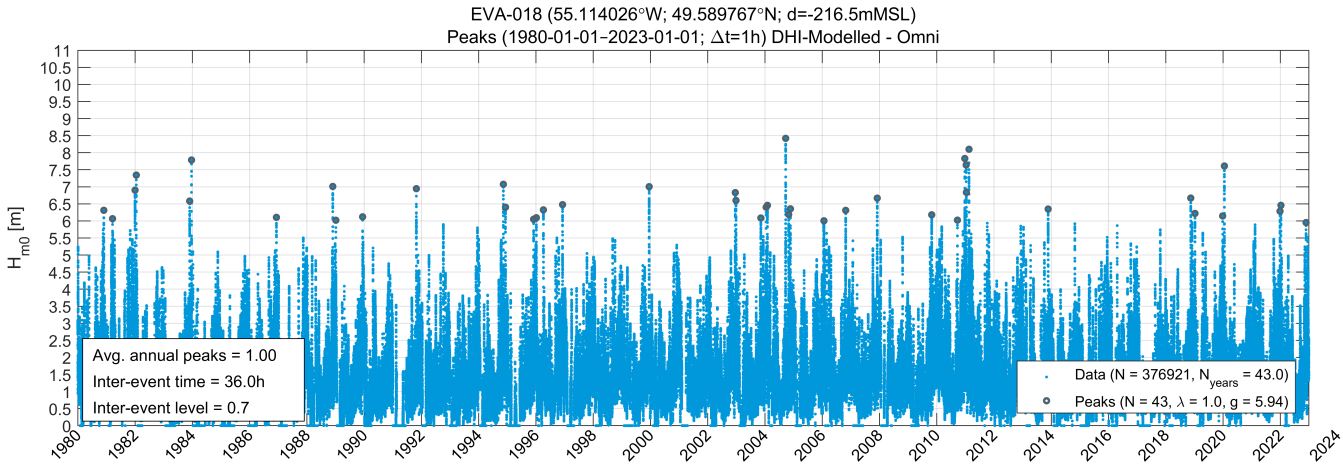


Figure C-208: Time series of significant wave height at EVA-018 and selected peaks.

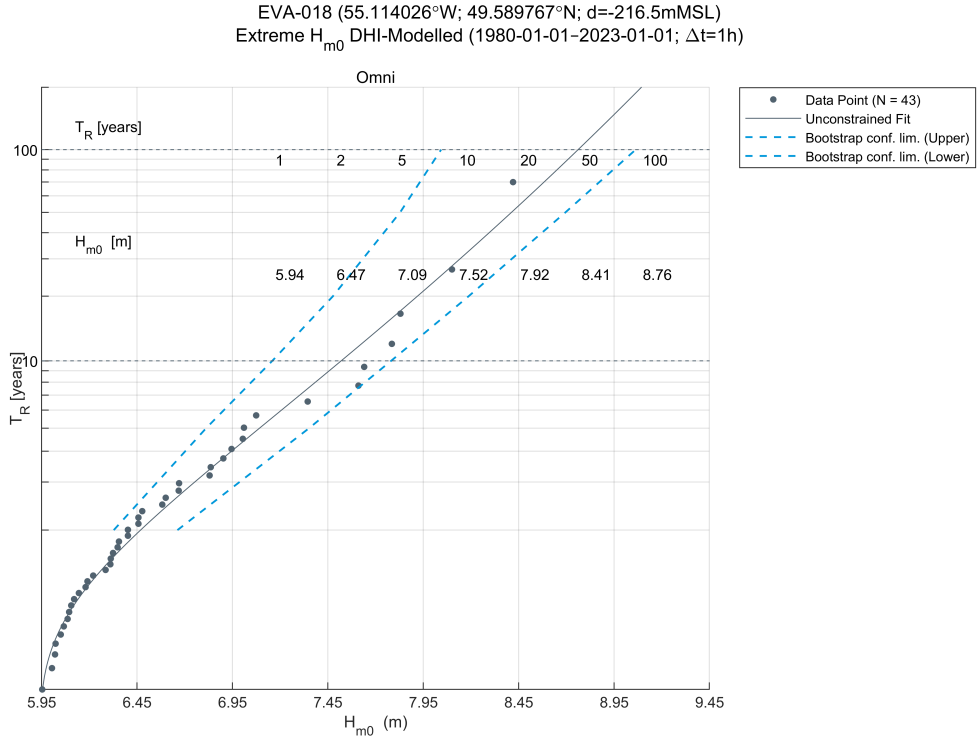


Figure C-209: Extreme value distribution fit at EVA-018.

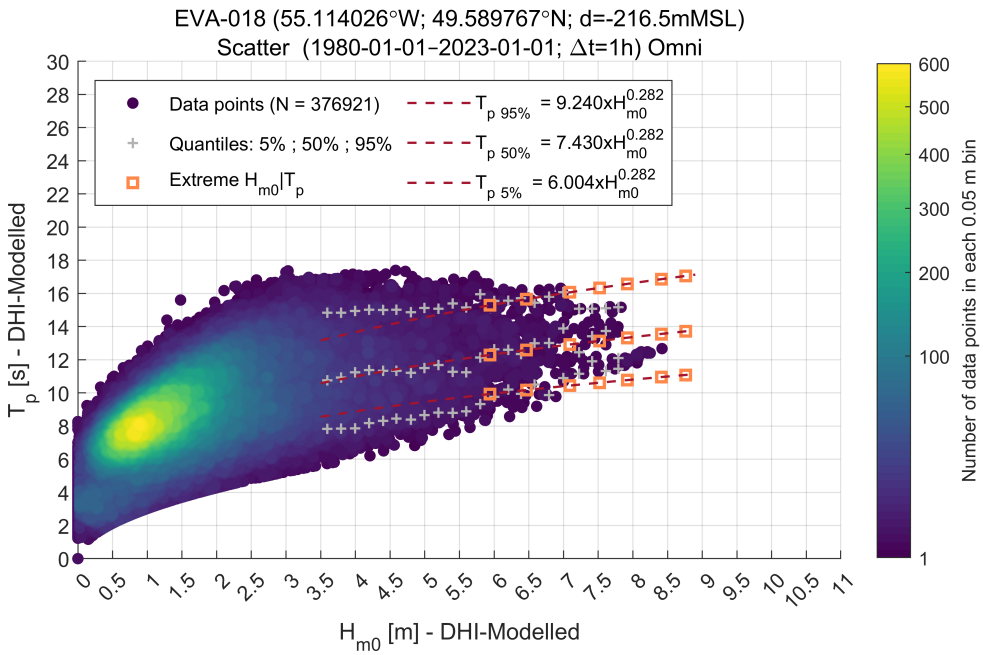


Figure C-210: Scatter plot of Hm0 x Tp at EVA-018 and quantile fit used to derived associated Tp to each extreme Hm0.

EVA-019

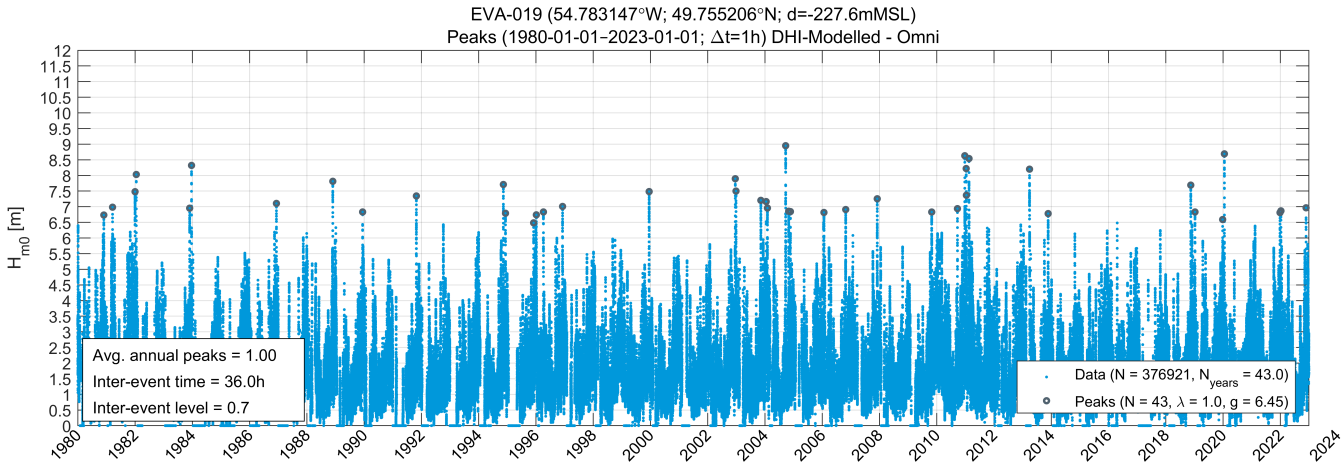


Figure C-211: Time series of significant wave height at EVA-019 and selected peaks.

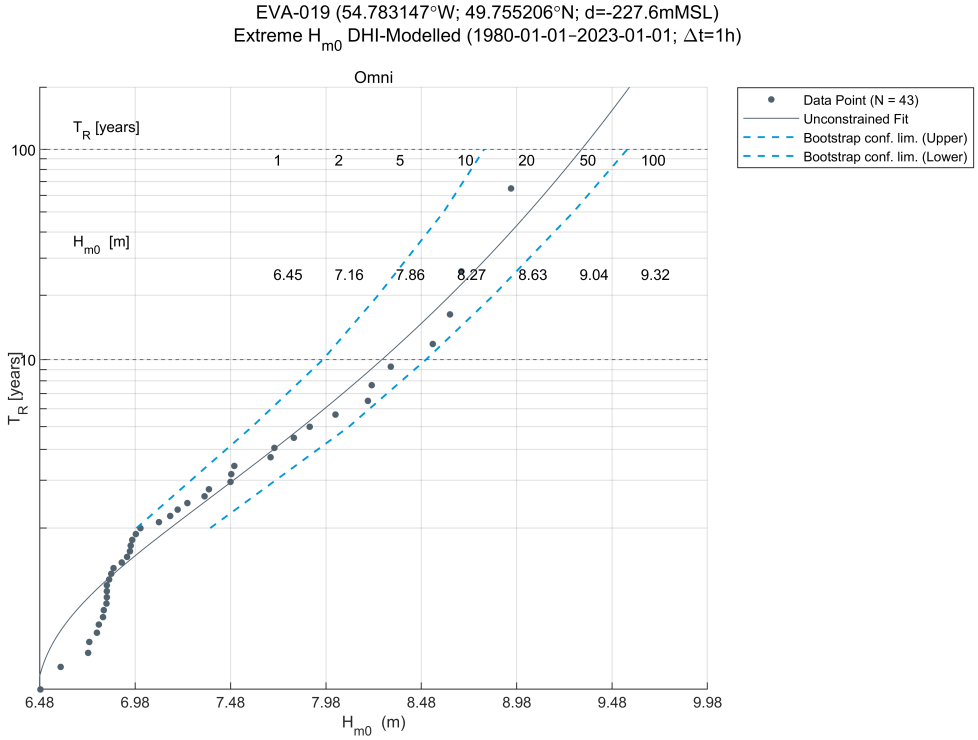


Figure C-212: Extreme value distribution fit at EVA-019.

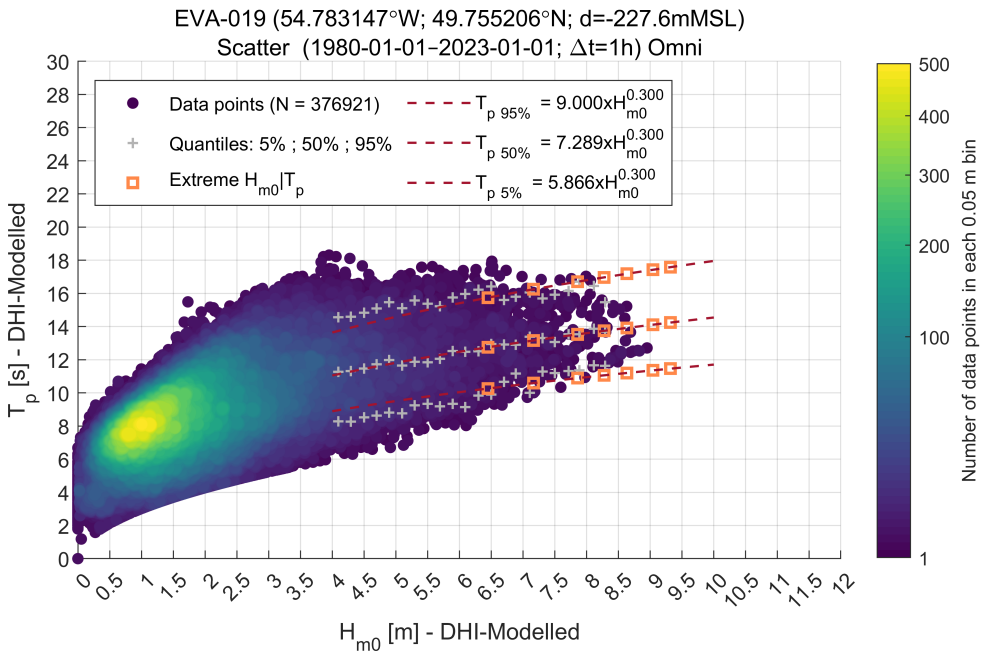


Figure C-213: Scatter plot of Hm0 x Tp at EVA-019 and quantile fit used to derived associated Tp to each extreme Hm0.

EVA-020

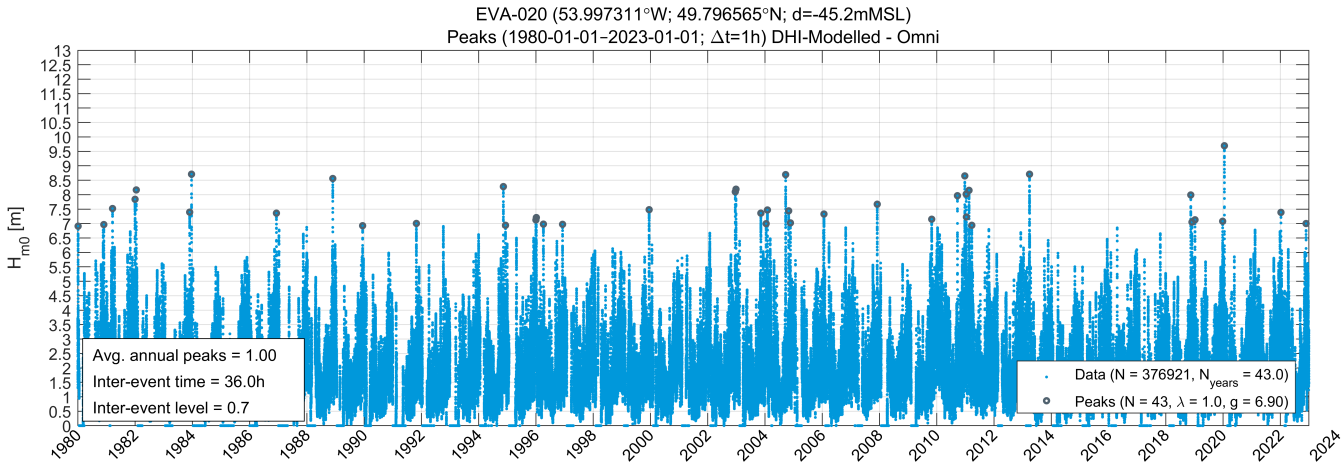


Figure C-214: Time series of significant wave height at EVA-020 and selected peaks.

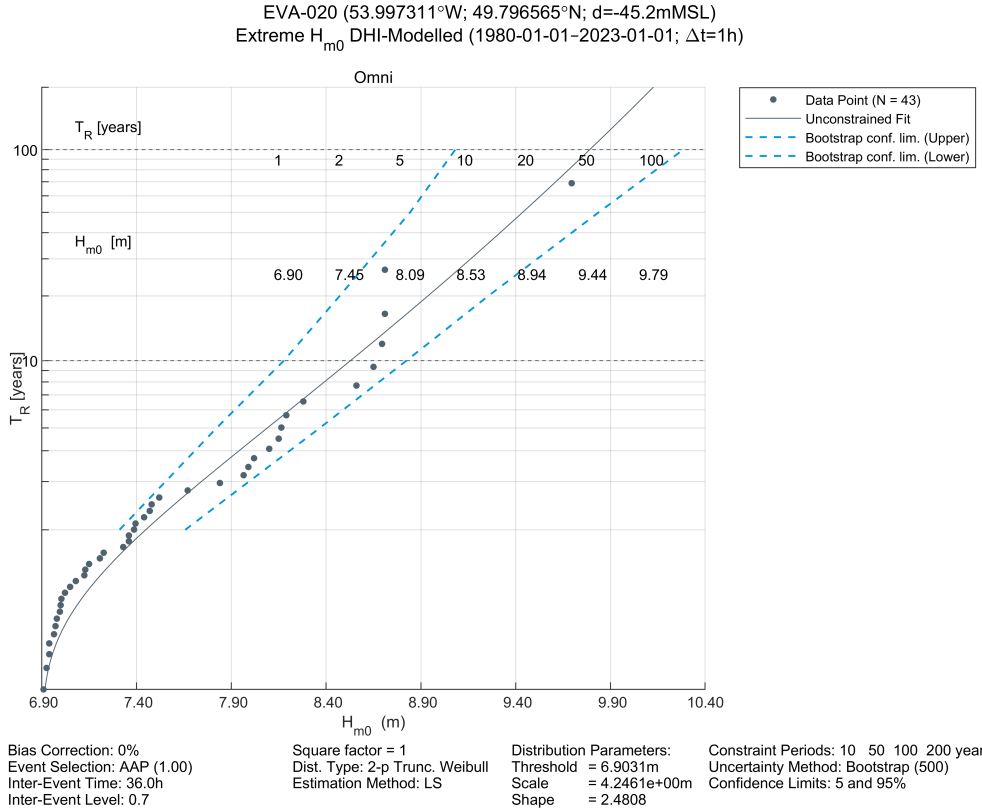


Figure C-215: Extreme value distribution fit at EVA-020.

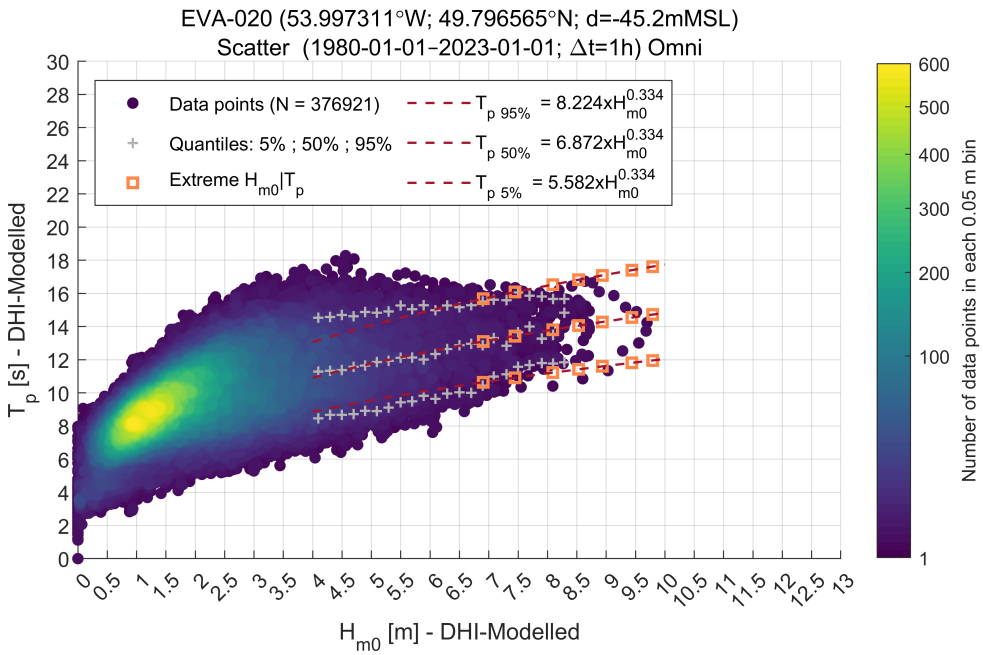


Figure C-216: Scatter plot of Hm0 x Tp at EVA-020 and quantile fit used to derived associated Tp to each extreme Hm0.

EVA-021

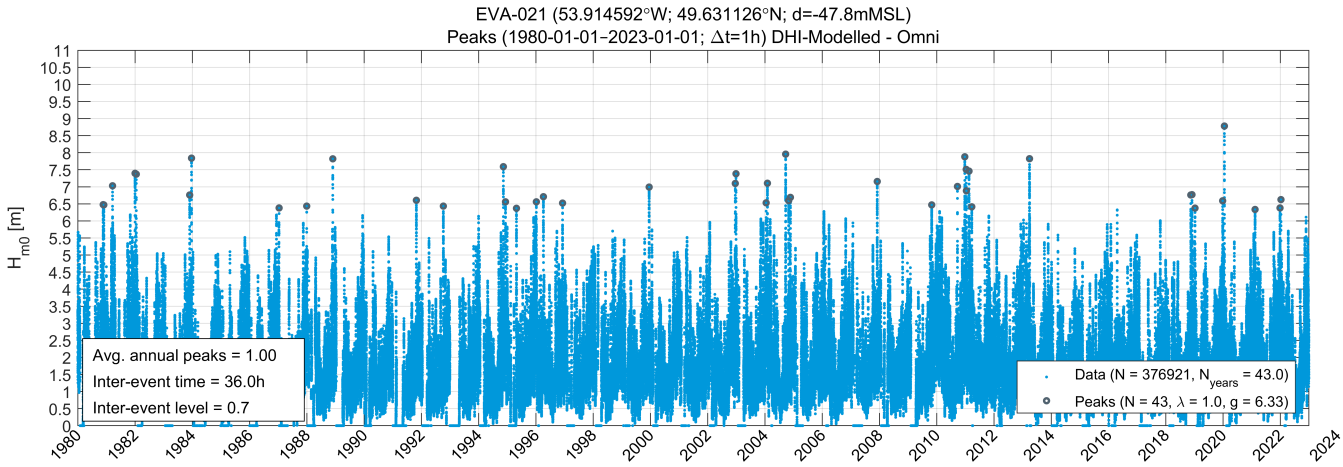


Figure C-217: Time series of significant wave height at EVA-021 and selected peaks.

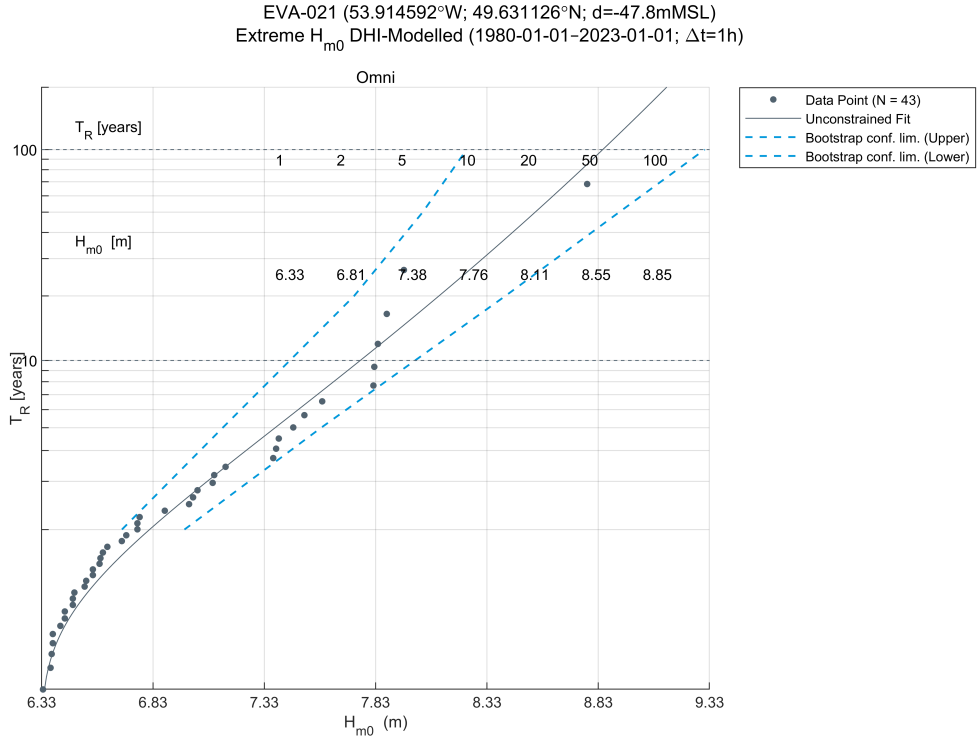


Figure C-218: Extreme value distribution fit at EVA-021.

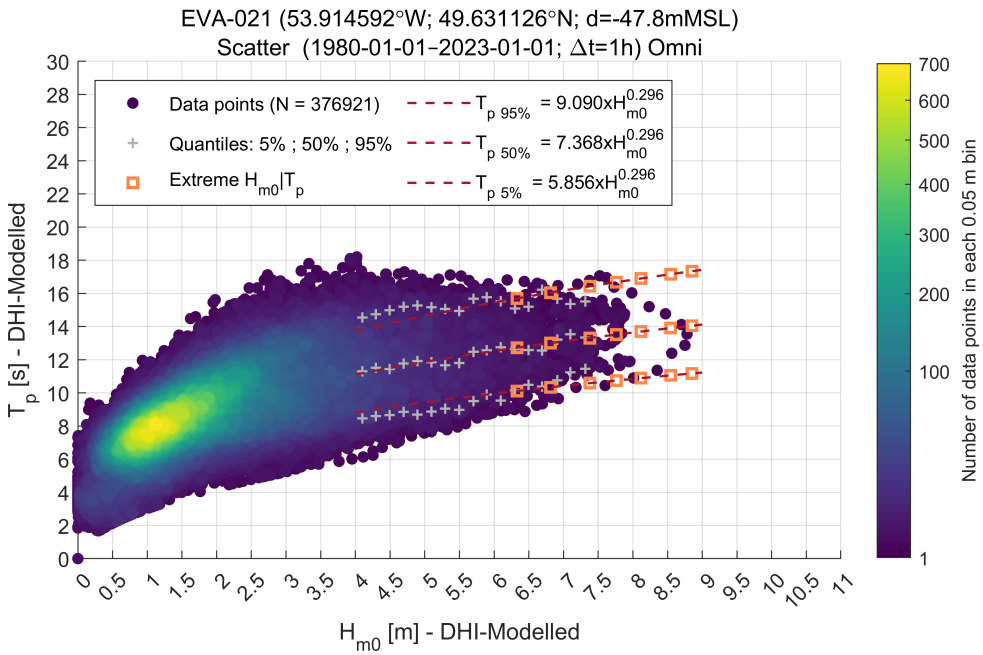


Figure C-219: Scatter plot of Hm0 x Tp at EVA-021 and quantile fit used to derived associated Tp to each extreme Hm0.

EVA-022

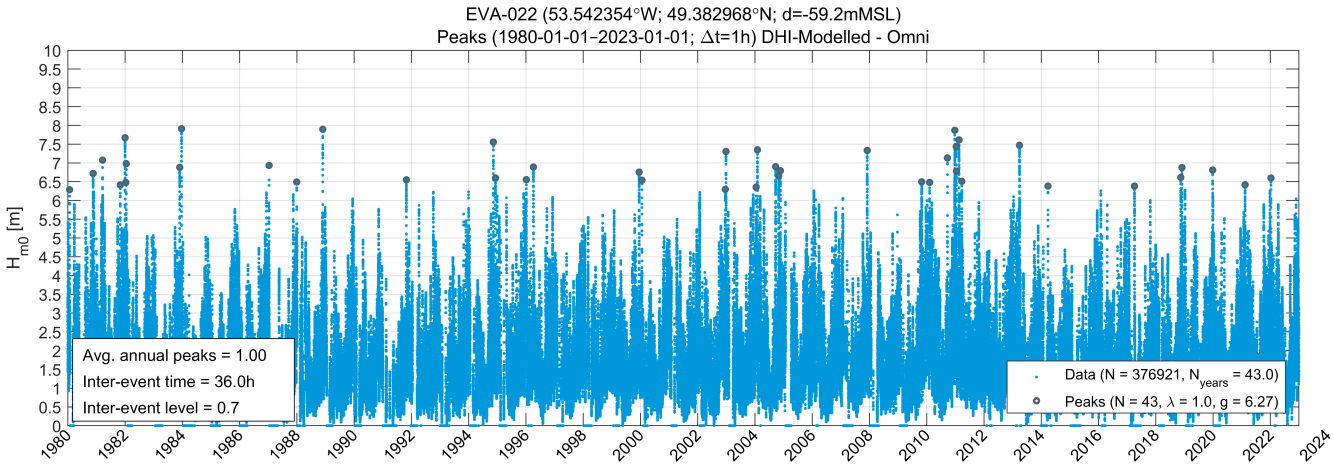


Figure C-220: Time series of significant wave height at EVA-022 and selected peaks.

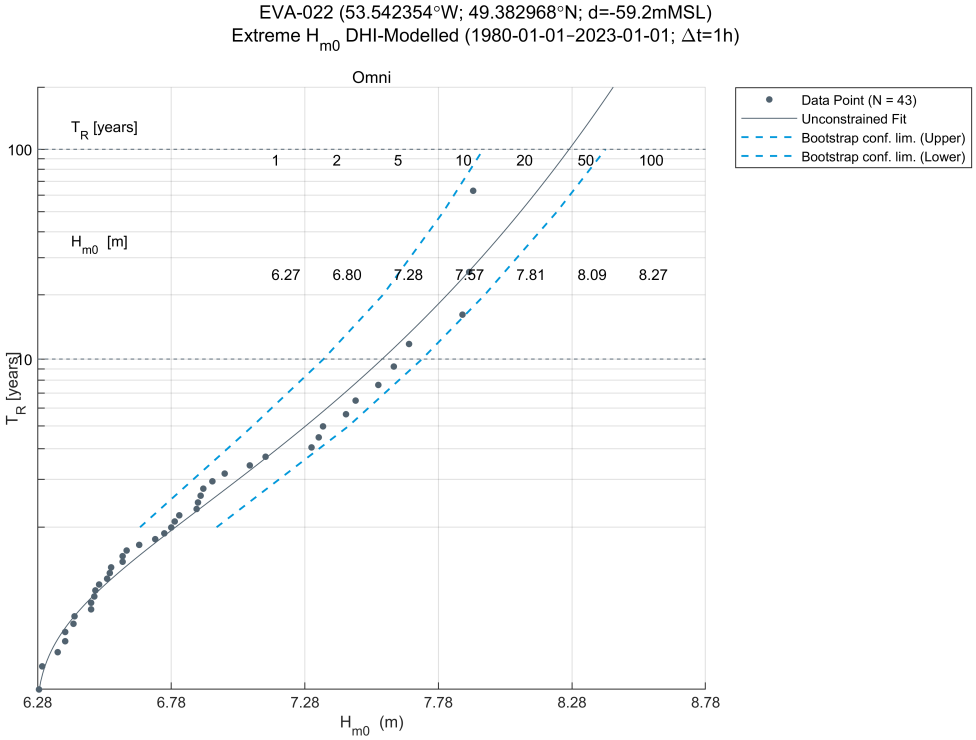


Figure C-221: Extreme value distribution fit at EVA-022.

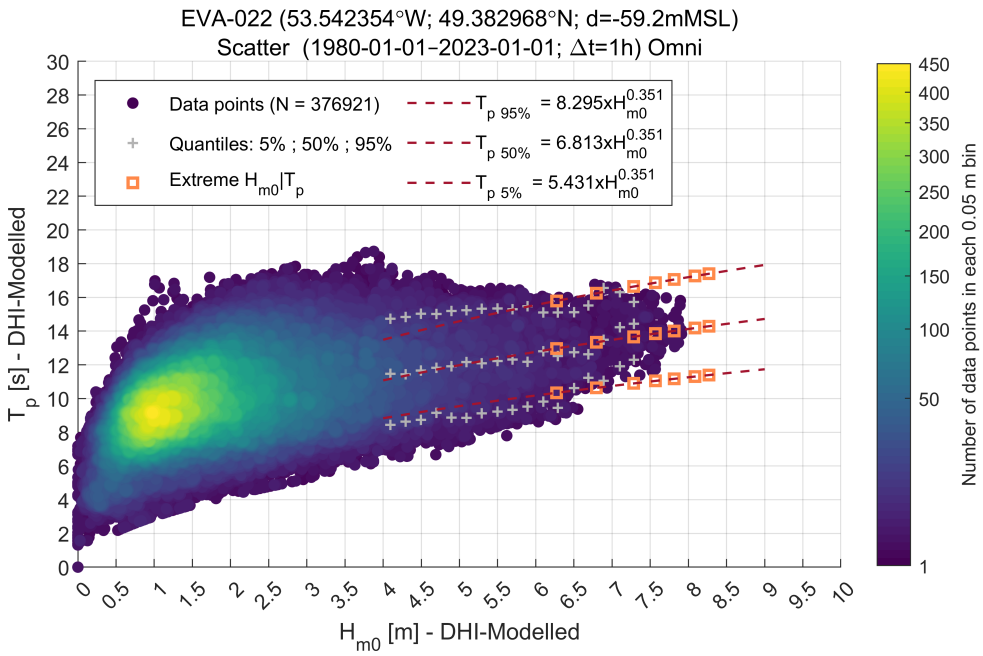


Figure C-222: Scatter plot of Hm0 x Tp at EVA-022 and quantile fit used to derived associated Tp to each extreme Hm0.

EVA-023

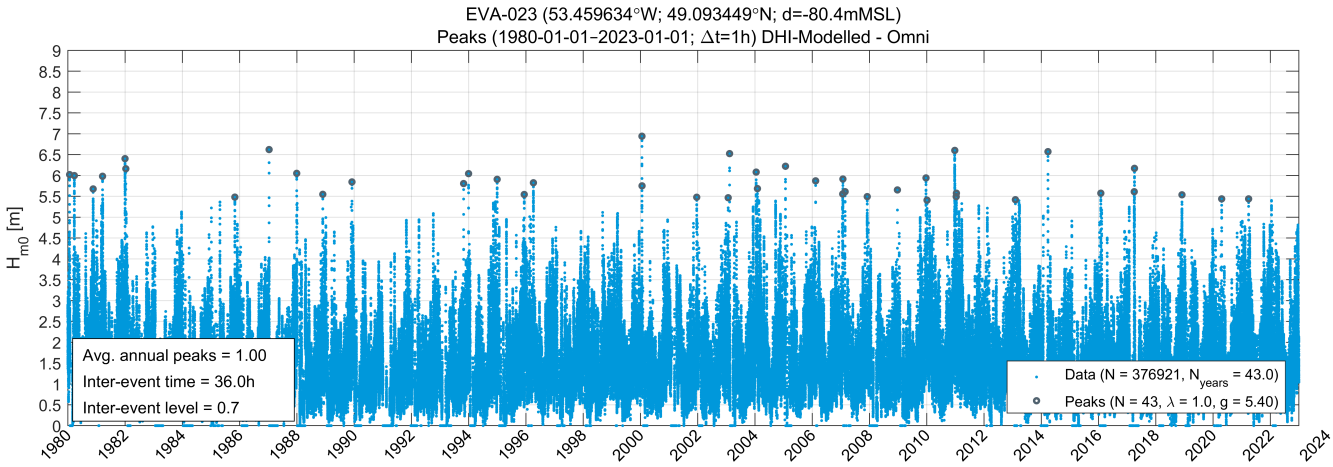


Figure C-223: Time series of significant wave height at EVA-023 and selected peaks.

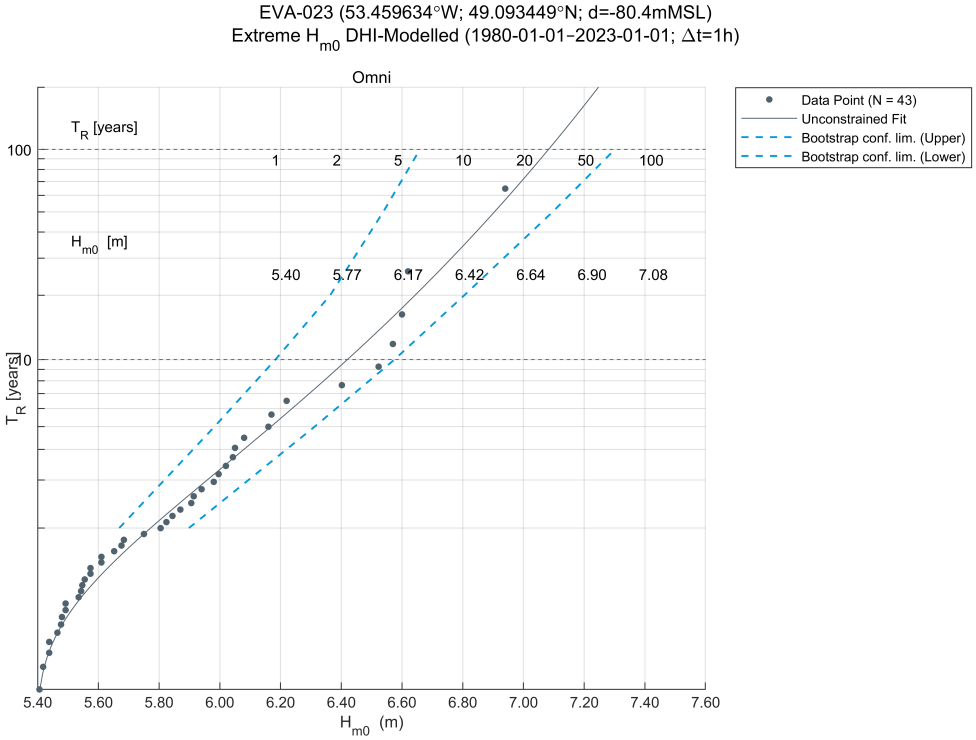


Figure C-224: Extreme value distribution fit at EVA-023.

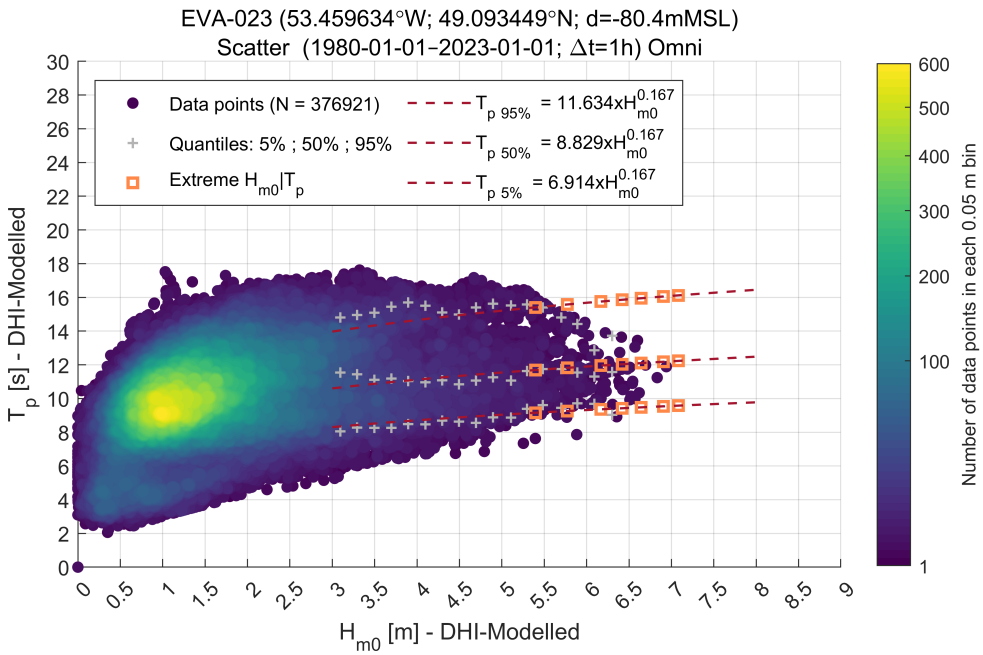


Figure C-225: Scatter plot of Hm0 x Tp at EVA-023 and quantile fit used to derived associated Tp to each extreme Hm0.

EVA-024

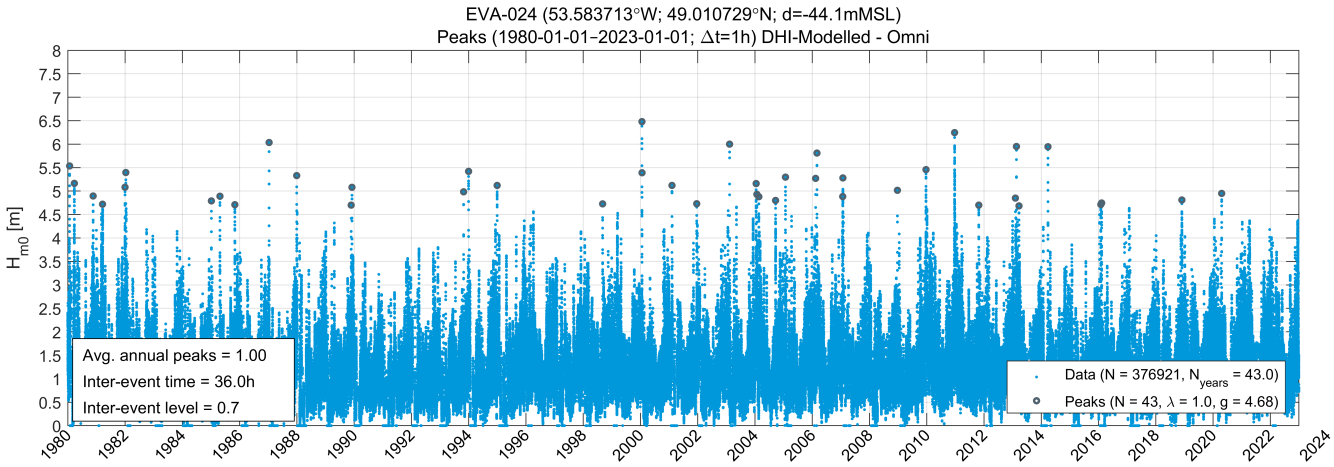


Figure C-226: Time series of significant wave height at EVA-024 and selected peaks.

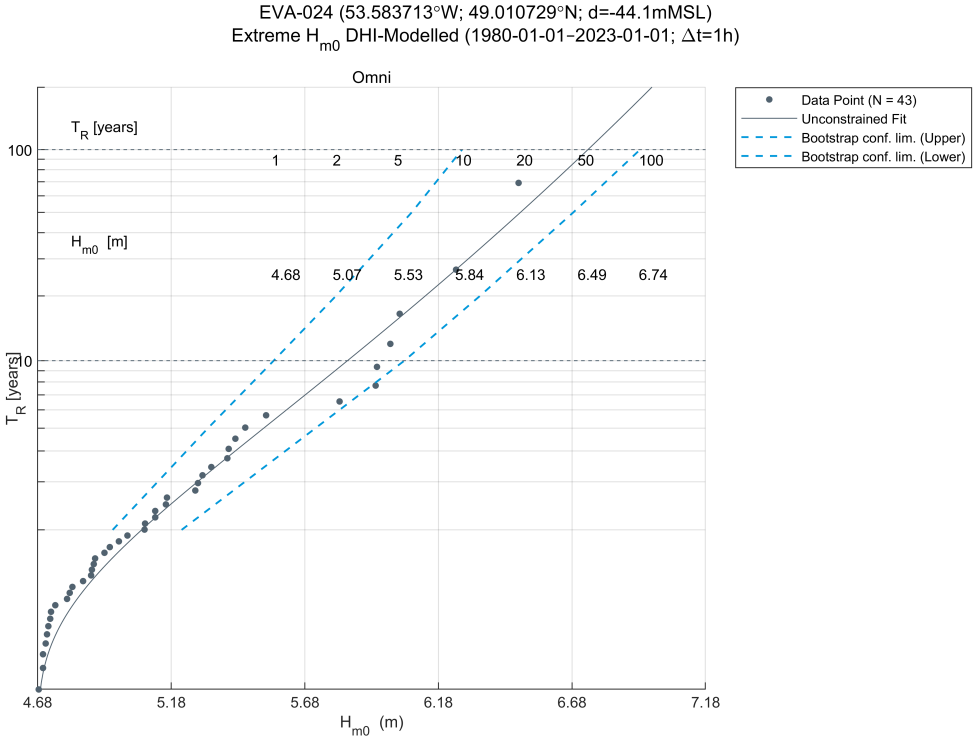


Figure C-227: Extreme value distribution fit at EVA-024.

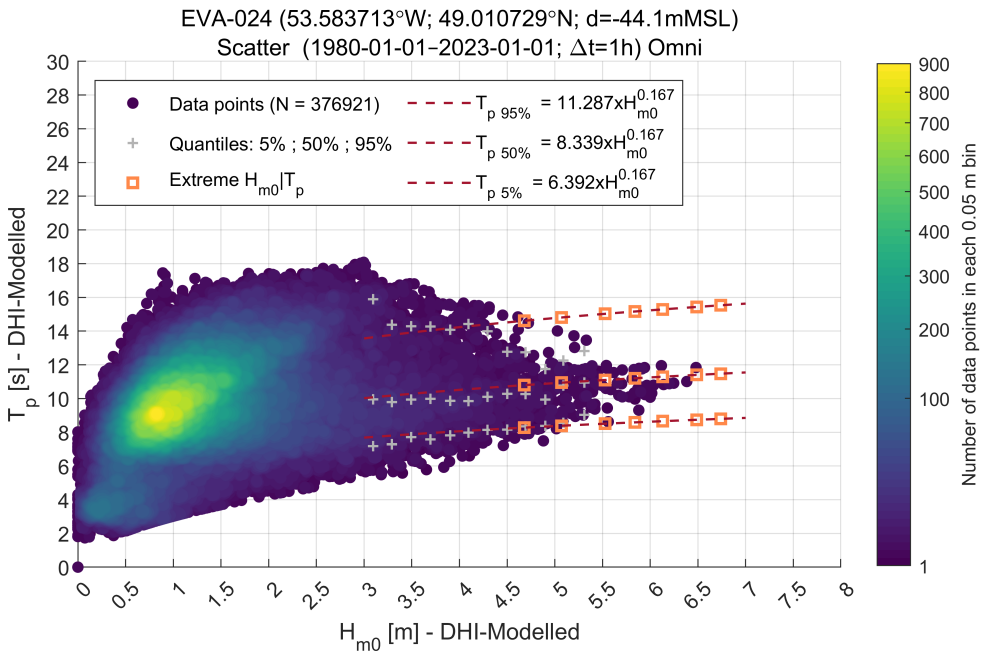


Figure C-228: Scatter plot of Hm0 x Tp at EVA-024 and quantile fit used to derived associated Tp to each extreme Hm0.

EVA-025

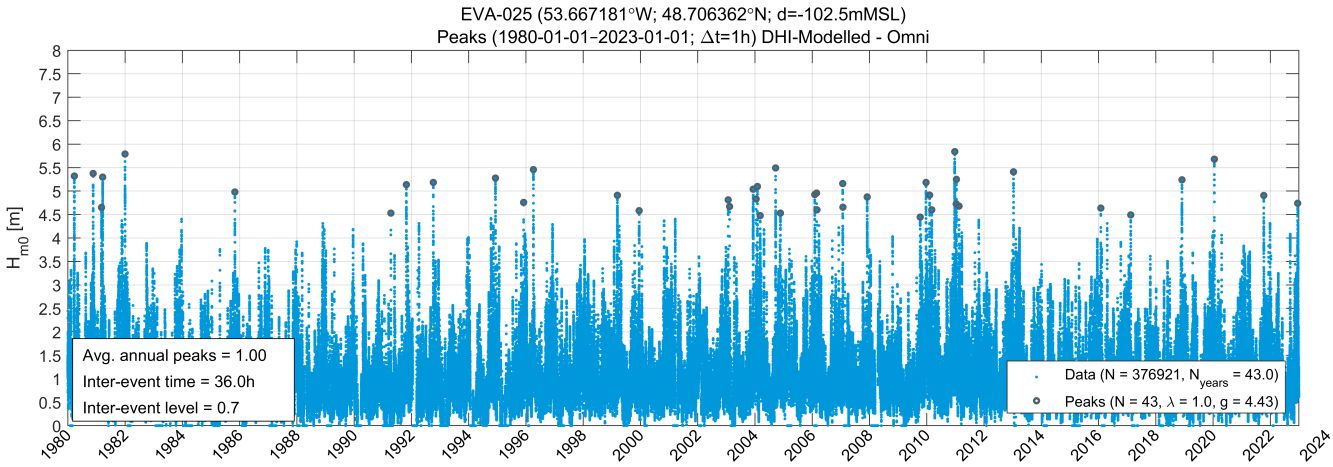


Figure C-229: Time series of significant wave height at EVA-025 and selected peaks.

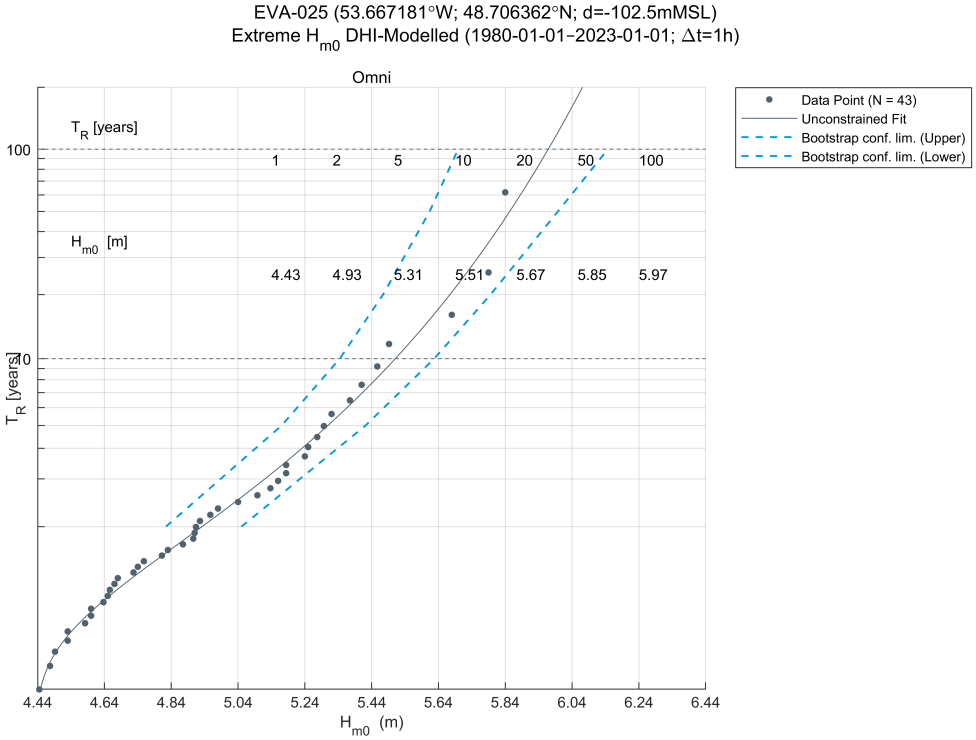


Figure C-230: Extreme value distribution fit at EVA-025.

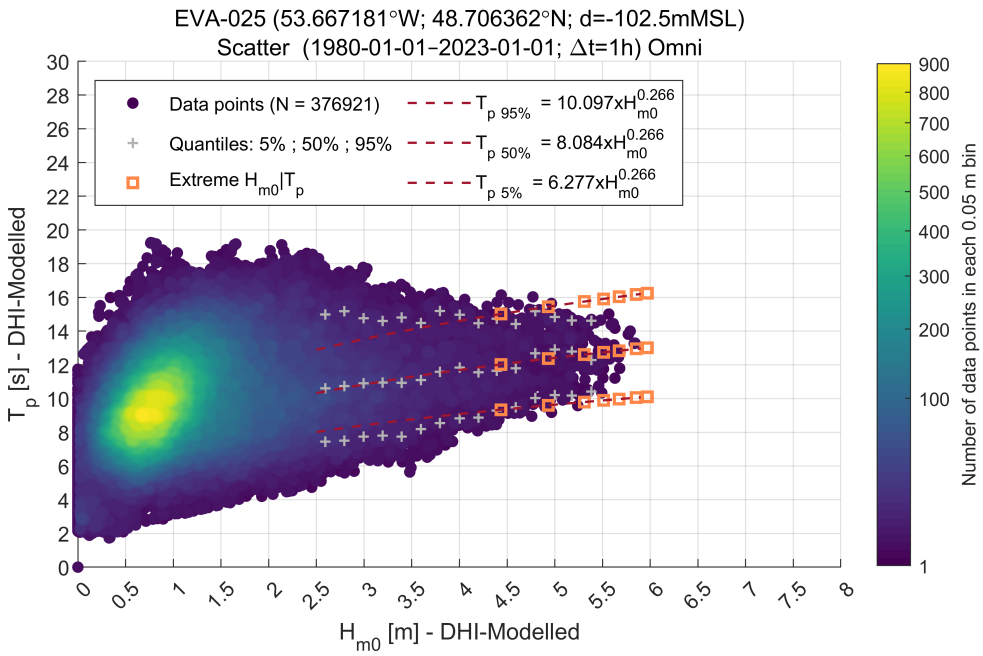


Figure C-231: Scatter plot of Hm0 x Tp at EVA-025 and quantile fit used to derived associated Tp to each extreme Hm0.

EVA-026

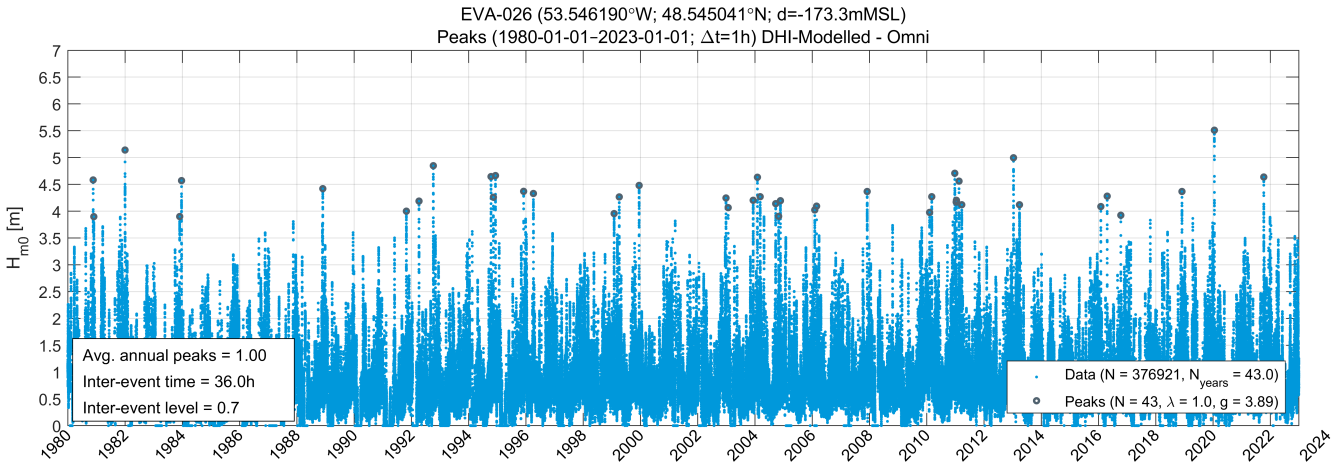


Figure C-232: Time series of significant wave height at EVA-026 and selected peaks.

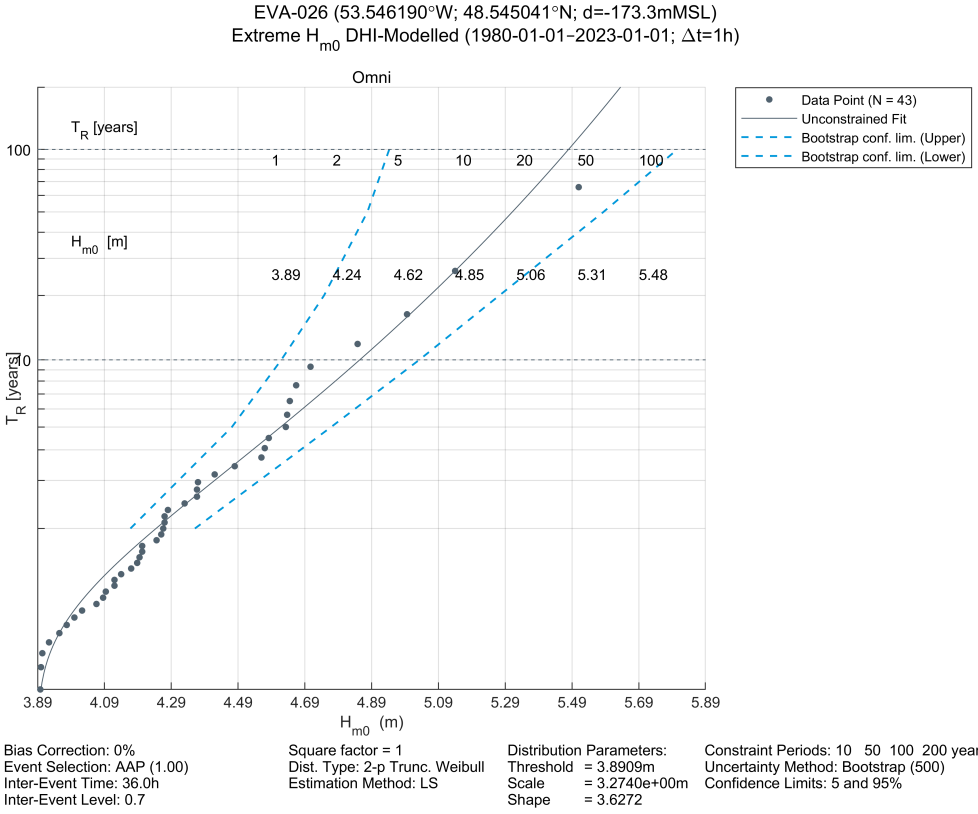


Figure C-233: Extreme value distribution fit at EVA-026.

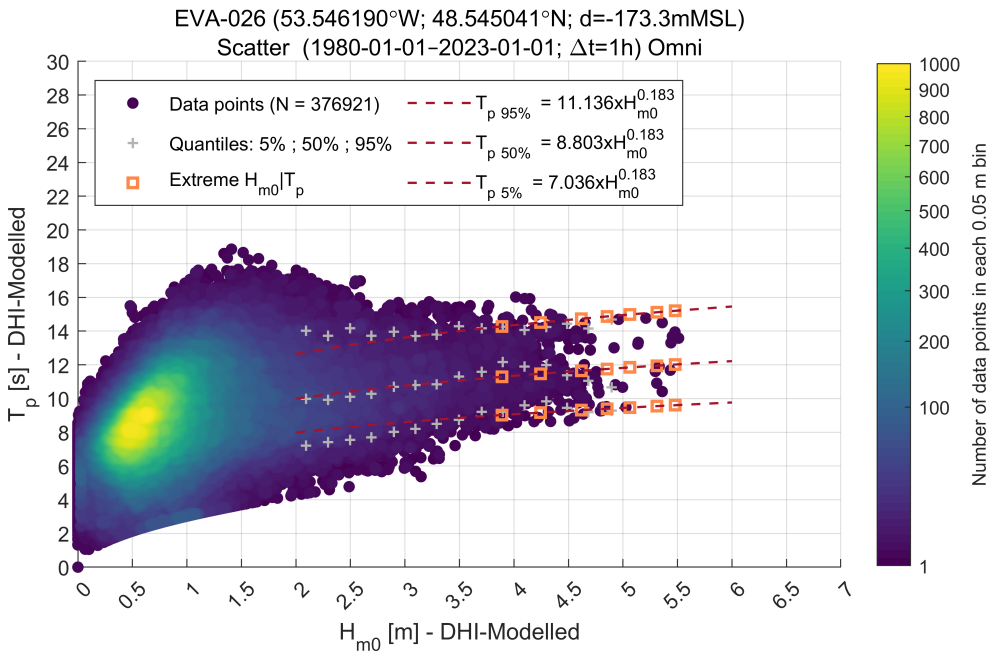


Figure C-234: Scatter plot of Hm0 x Tp at EVA-026 and quantile fit used to derived associated Tp to each extreme Hm0.

EVA-027

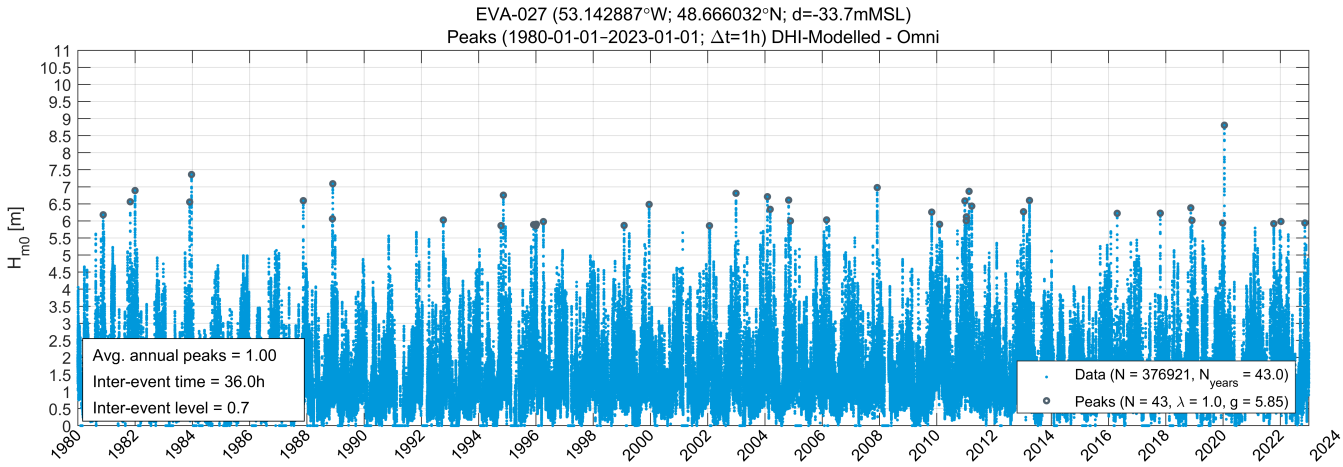


Figure C-235: Time series of significant wave height at EVA-027 and selected peaks.

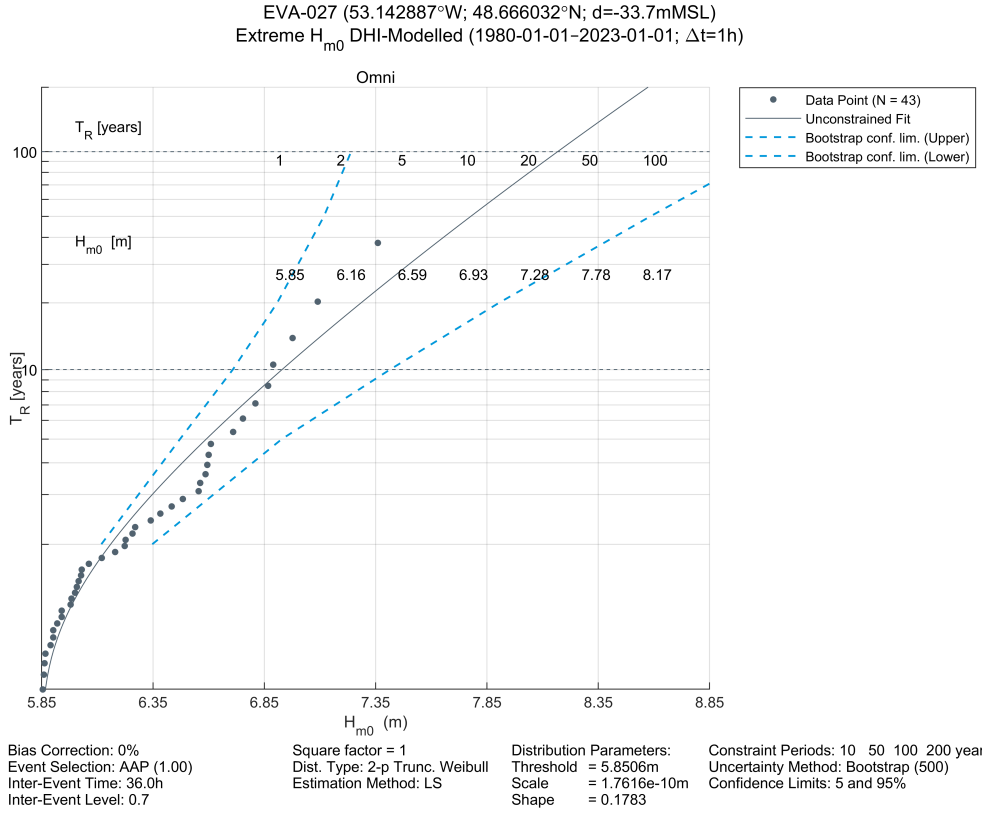


Figure C-236: Extreme value distribution fit at EVA-027.

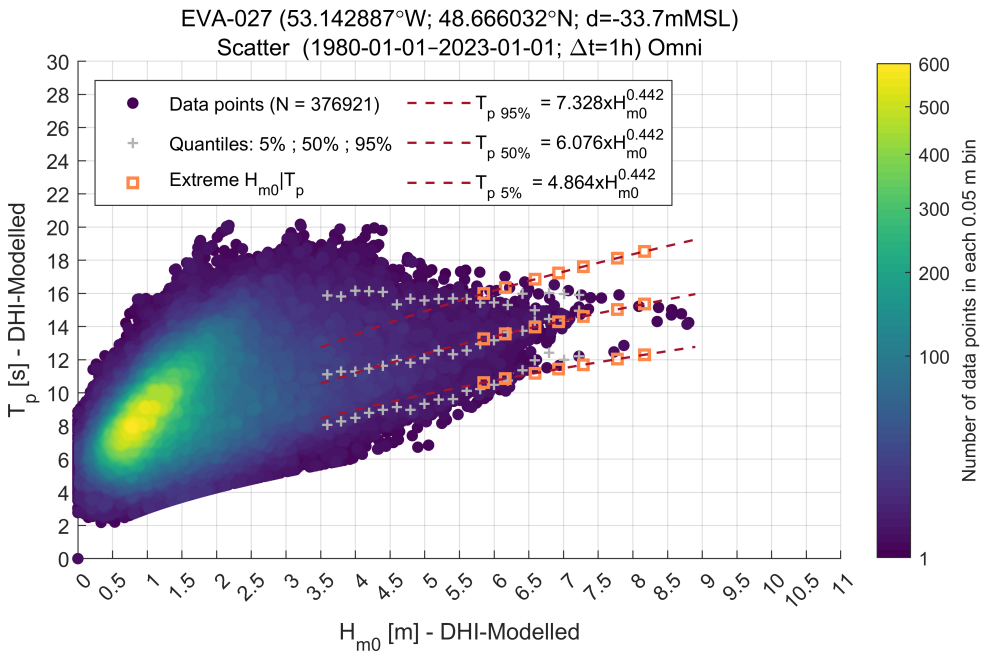


Figure C-237: Scatter plot of Hm0 x Tp at EVA-027 and quantile fit used to derived associated Tp to each extreme Hm0.

EVA-028

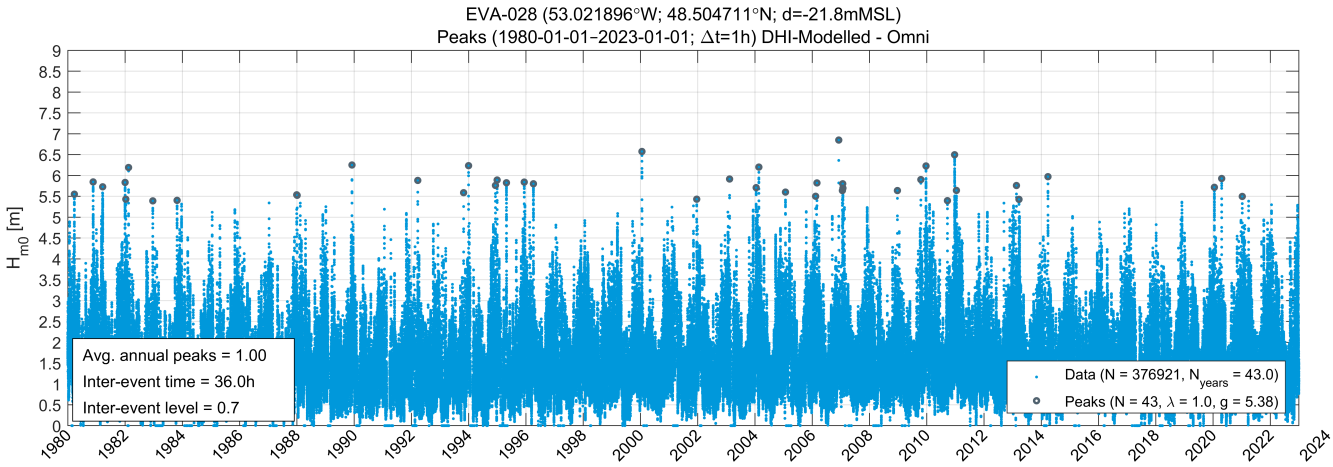


Figure C-238: Time series of significant wave height at EVA-028 and selected peaks.

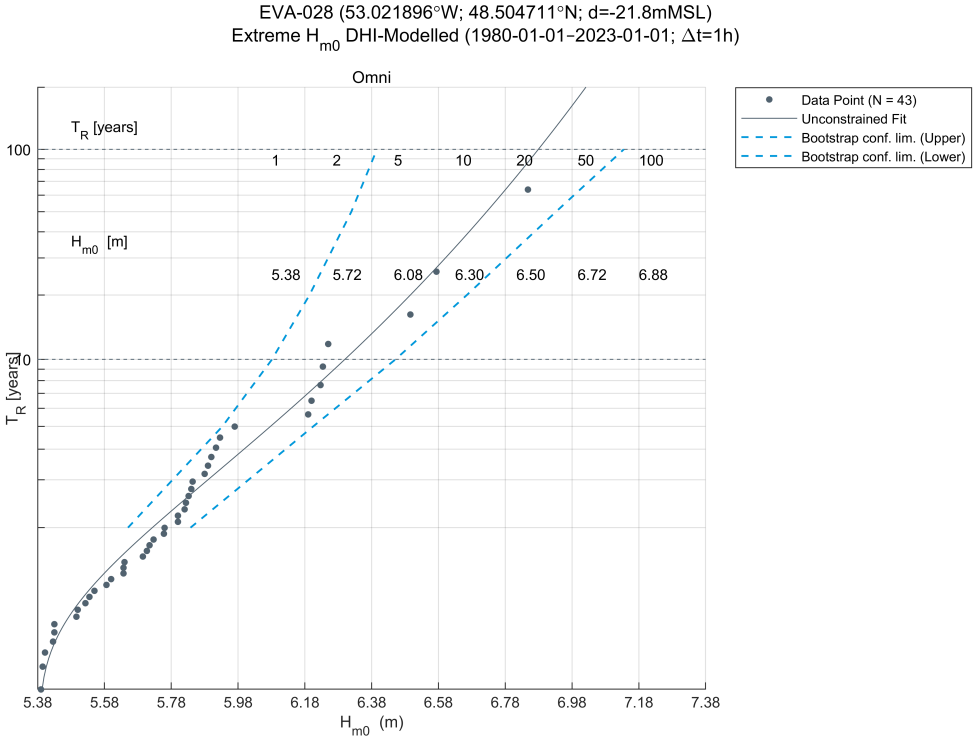


Figure C-239: Extreme value distribution fit at EVA-028.

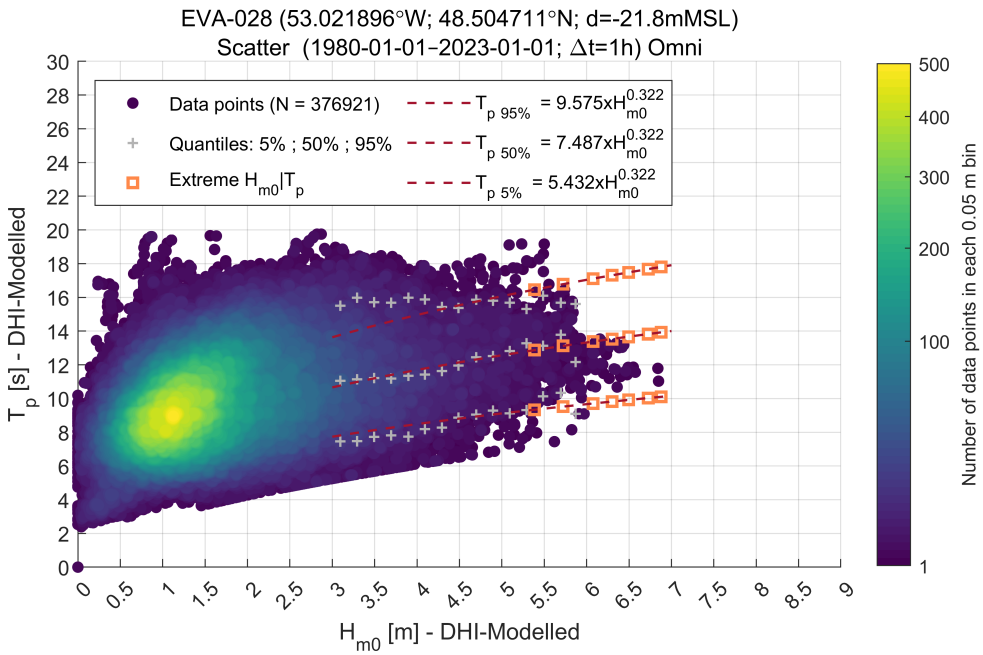


Figure C-240: Scatter plot of Hm0 x Tp at EVA-028 and quantile fit used to derived associated Tp to each extreme Hm0.

EVA-029

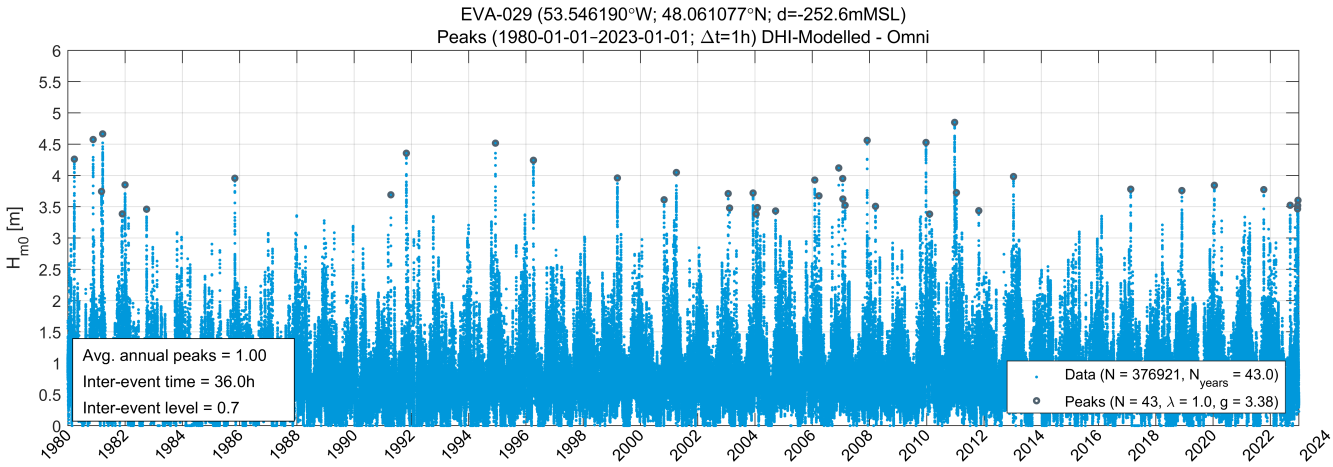


Figure C-241: Time series of significant wave height at EVA-029 and selected peaks.

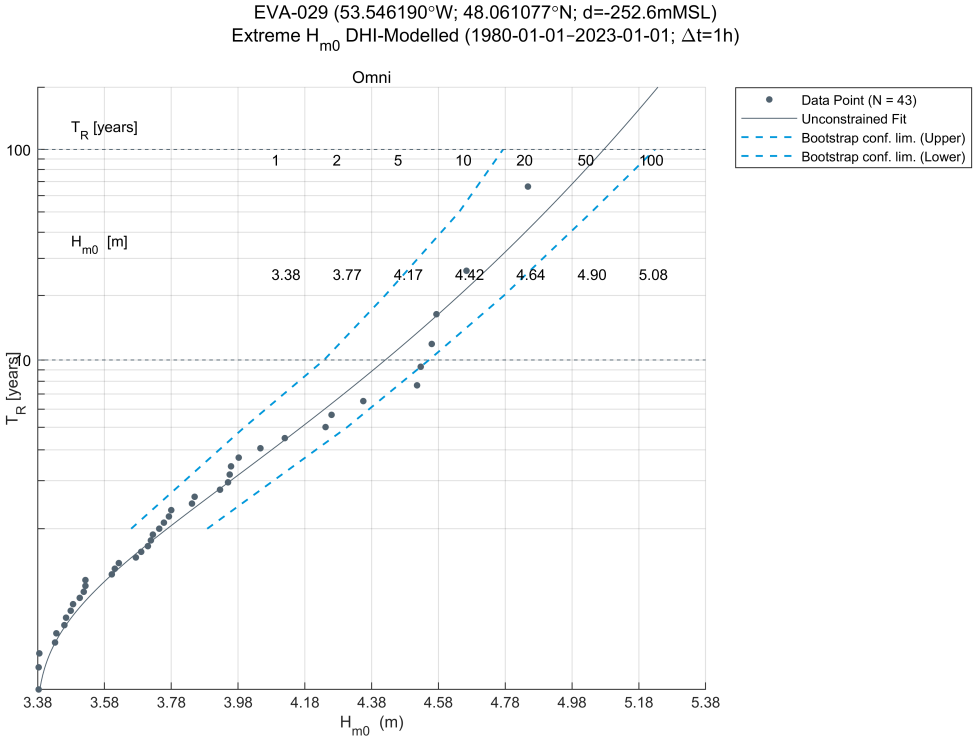


Figure C-242: Extreme value distribution fit at EVA-029.

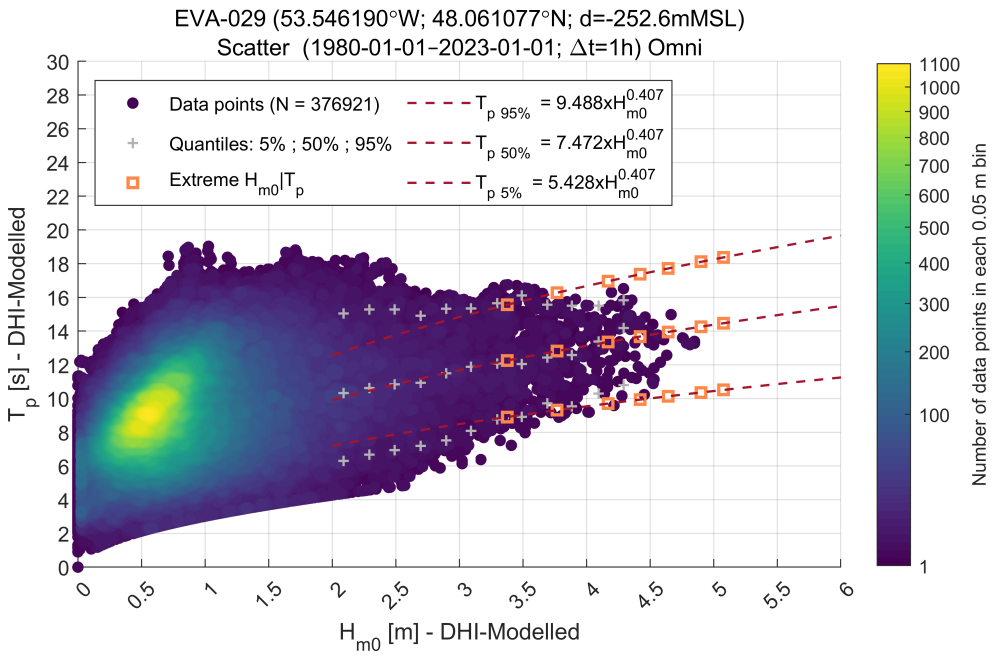


Figure C-243: Scatter plot of Hm0 x Tp at EVA-029 and quantile fit used to derived associated Tp to each extreme Hm0.

EVA-030

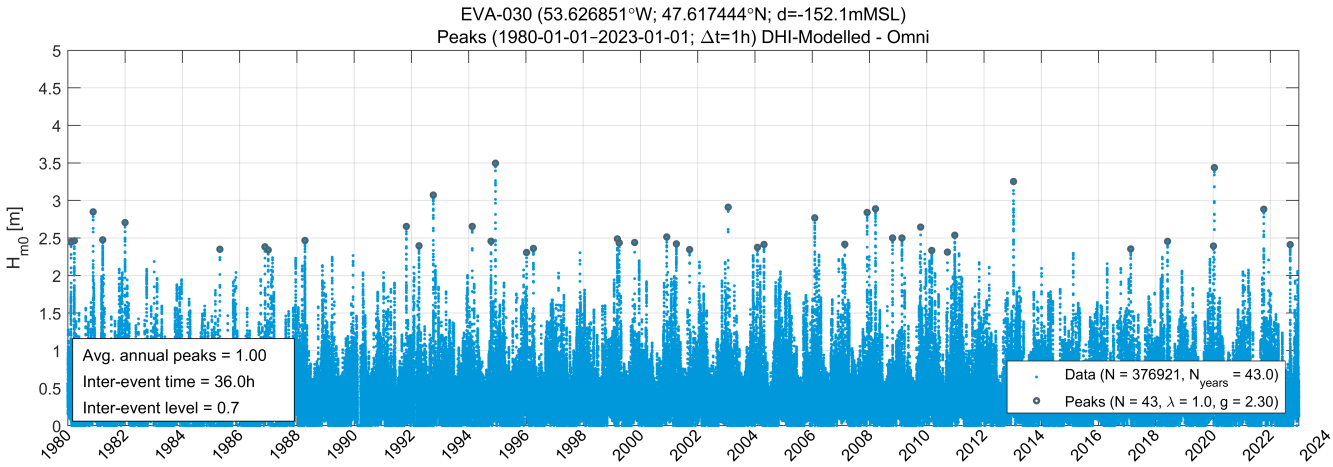


Figure C-244: Time series of significant wave height at EVA-030 and selected peaks.

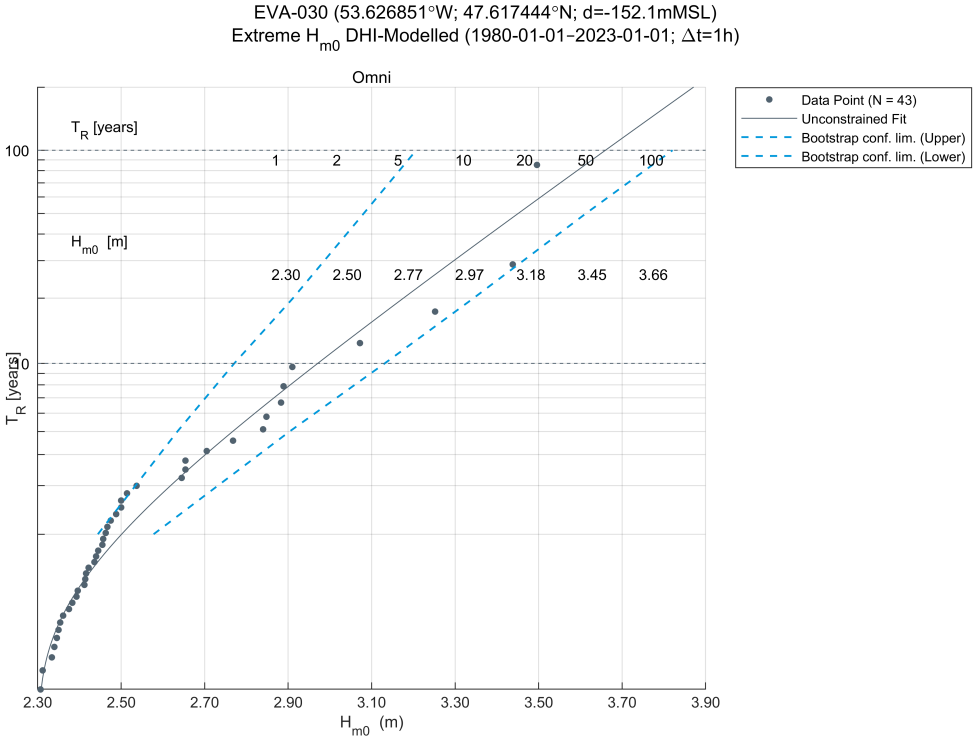


Figure C-245: Extreme value distribution fit at EVA-030.

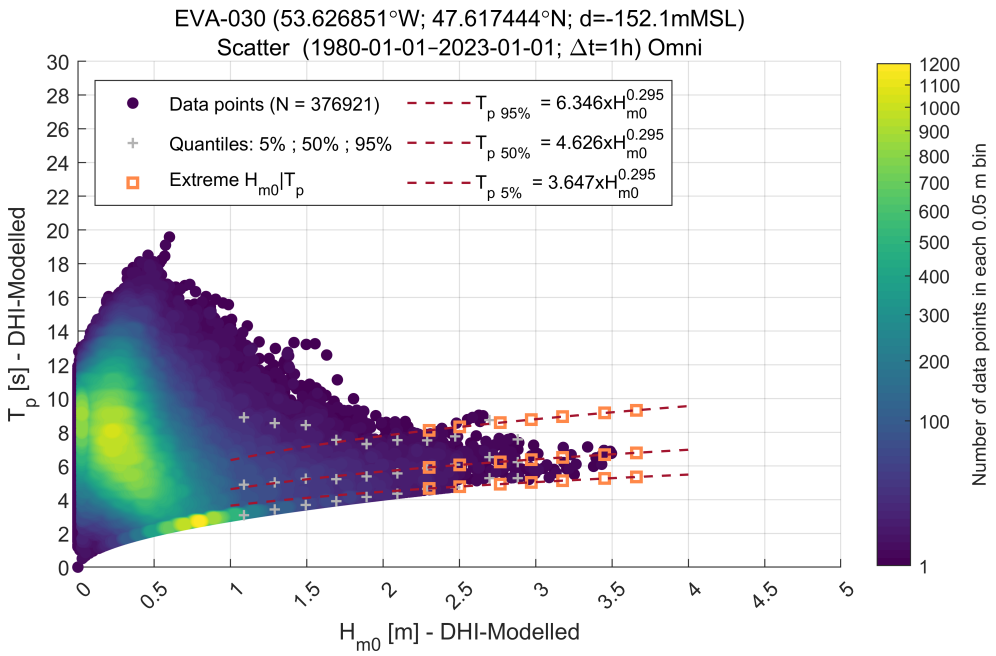


Figure C-246: Scatter plot of Hm0 x Tp at EVA-030 and quantile fit used to derived associated Tp to each extreme Hm0.

EVA-031

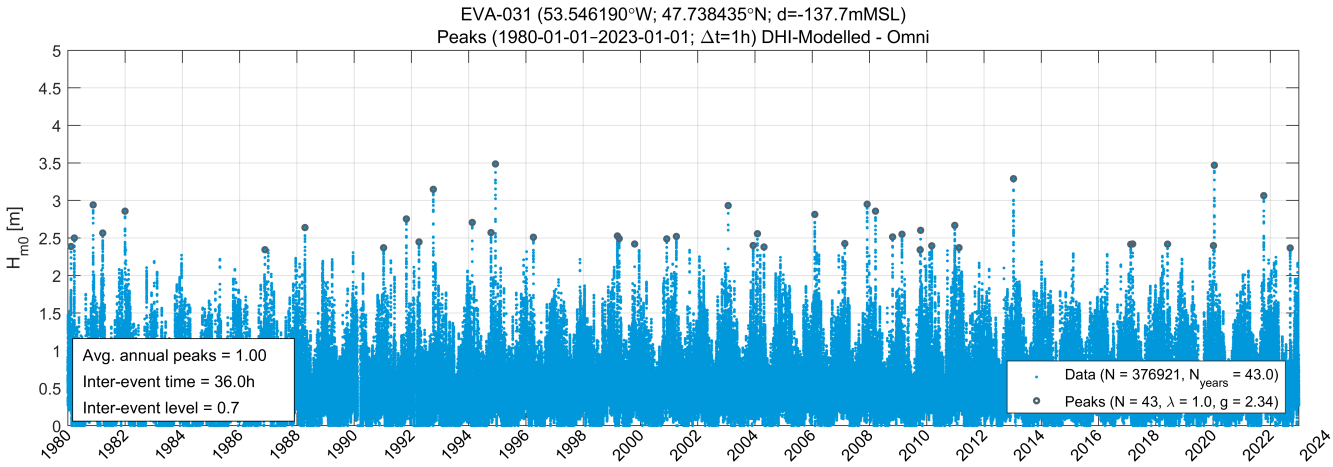


Figure C-247: Time series of significant wave height at EVA-031 and selected peaks.

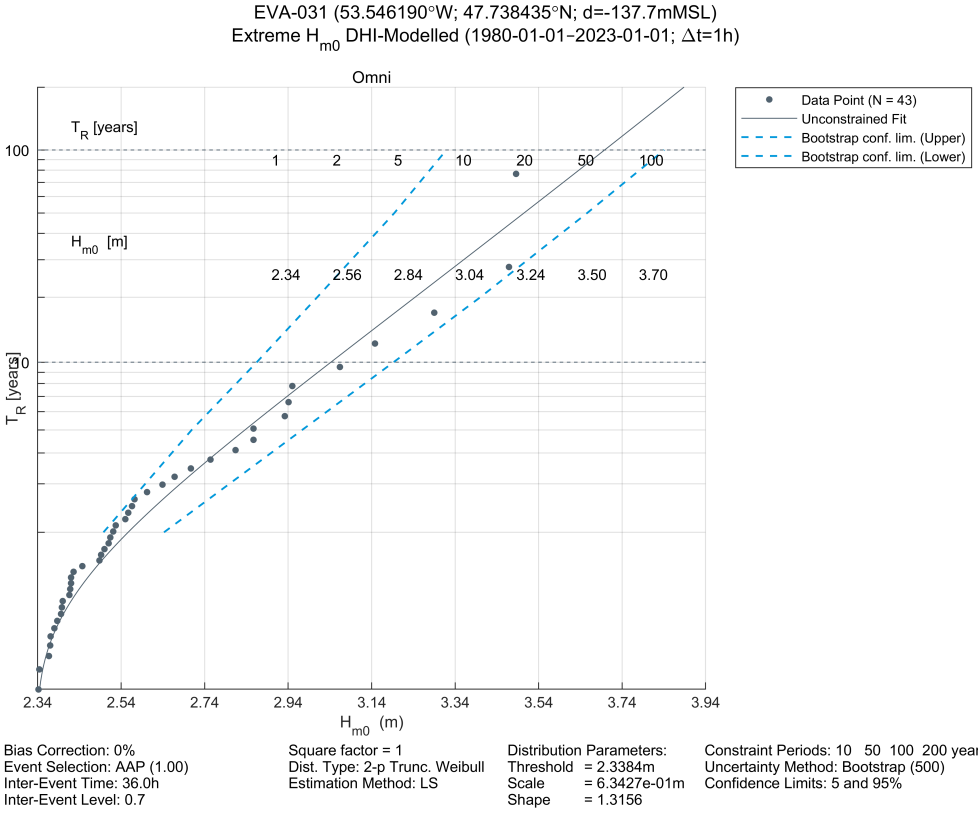


Figure C-248: Extreme value distribution fit at EVA-031.

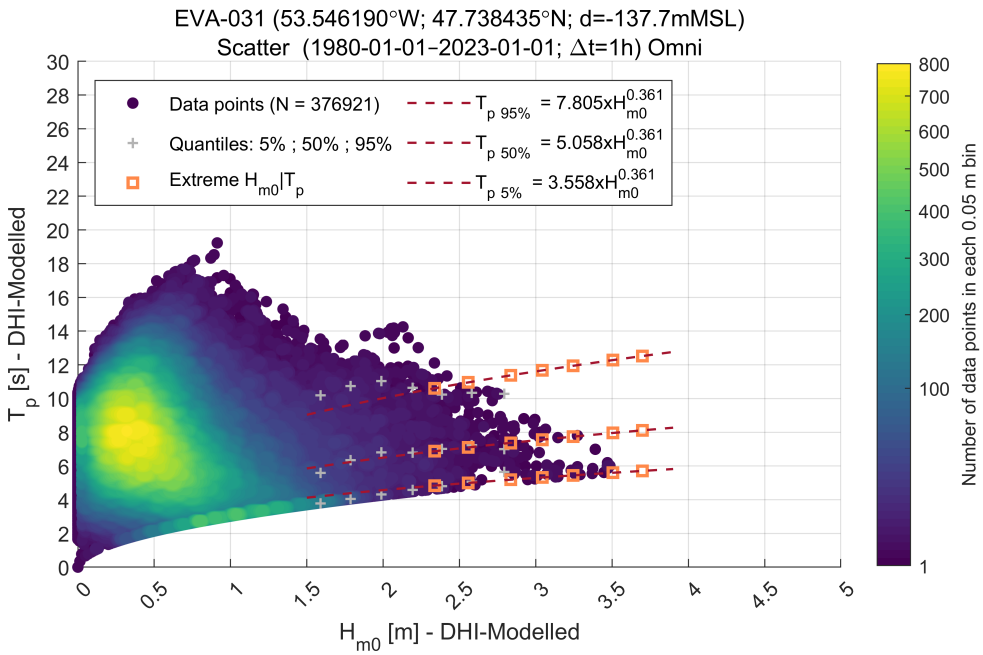


Figure C-249: Scatter plot of Hm0 x Tp at EVA-031 and quantile fit used to derived associated Tp to each extreme Hm0.

EVA-032

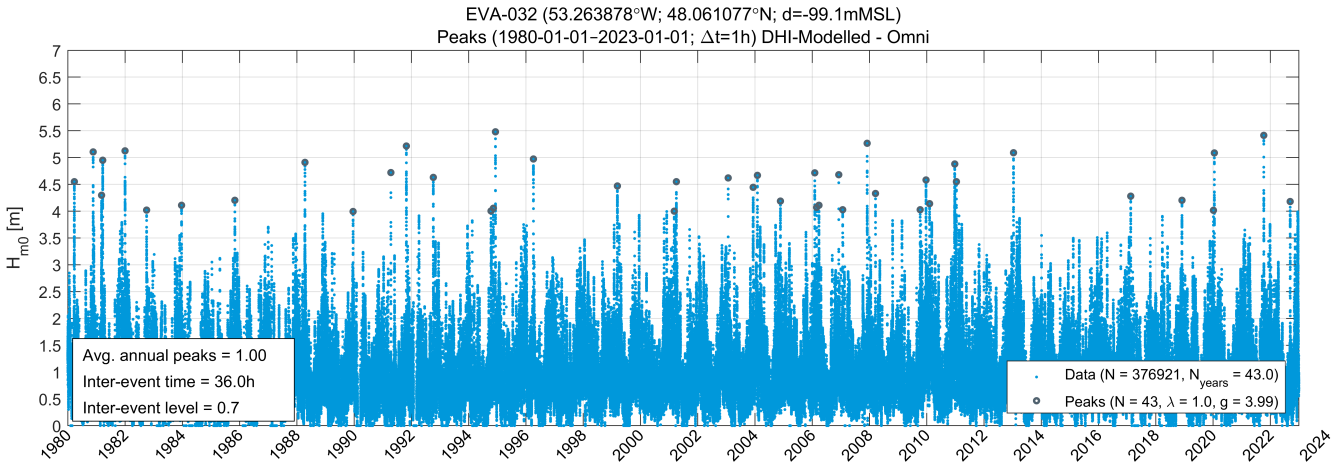
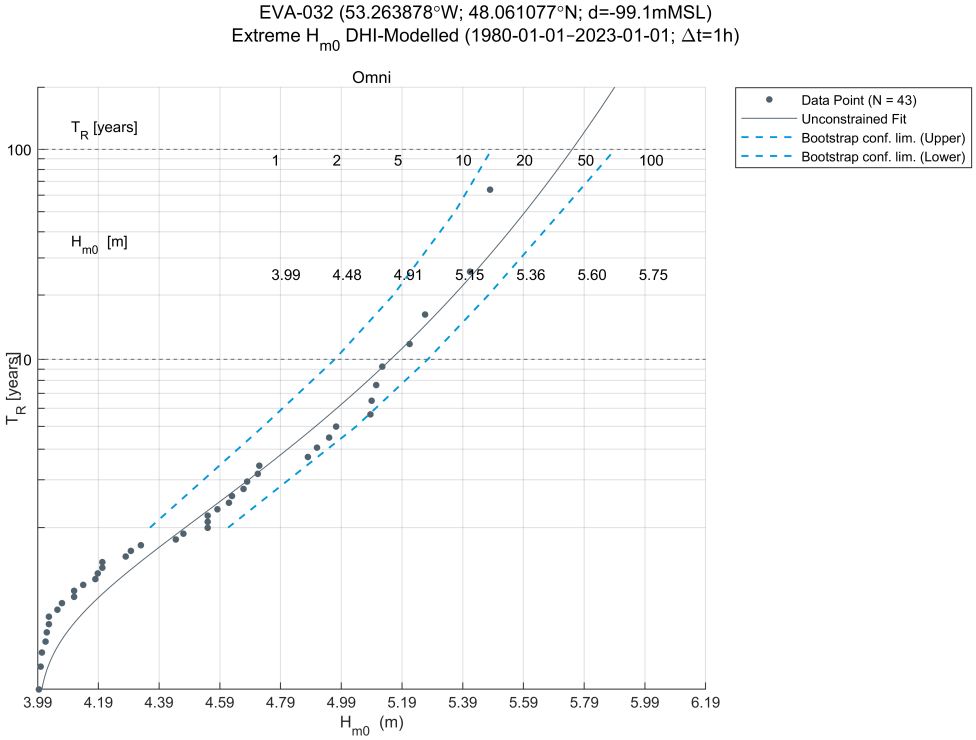


Figure C-250: Time series of significant wave height at EVA-032 and selected peaks.



Bias Correction: 0%
Event Selection: AAP (1.00)
Inter-Event Time: 36.0h
Inter-Event Level: 0.7

Square factor = 1
Dist. Type: 2-p Trunc. Weibull
Estimation Method: LS

Distribution Parameters:
Threshold = 3.9907m
Scale = 4.0639e+00m
Shape = 4.9211

Constraint Periods: 10 50 100 200 years
Uncertainty Method: Bootstrap (500)
Confidence Limits: 5 and 95%

Figure C-251: Extreme value distribution fit at EVA-032.

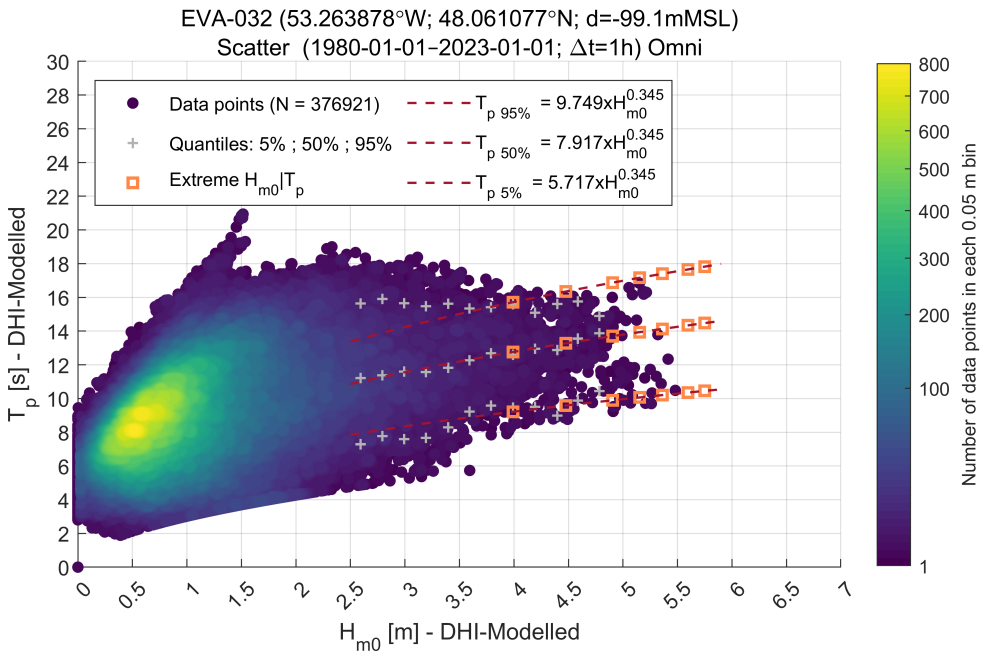


Figure C-252: Scatter plot of Hm0 x Tp at EVA-032 and quantile fit used to derived associated Tp to each extreme Hm0.

EVA-033

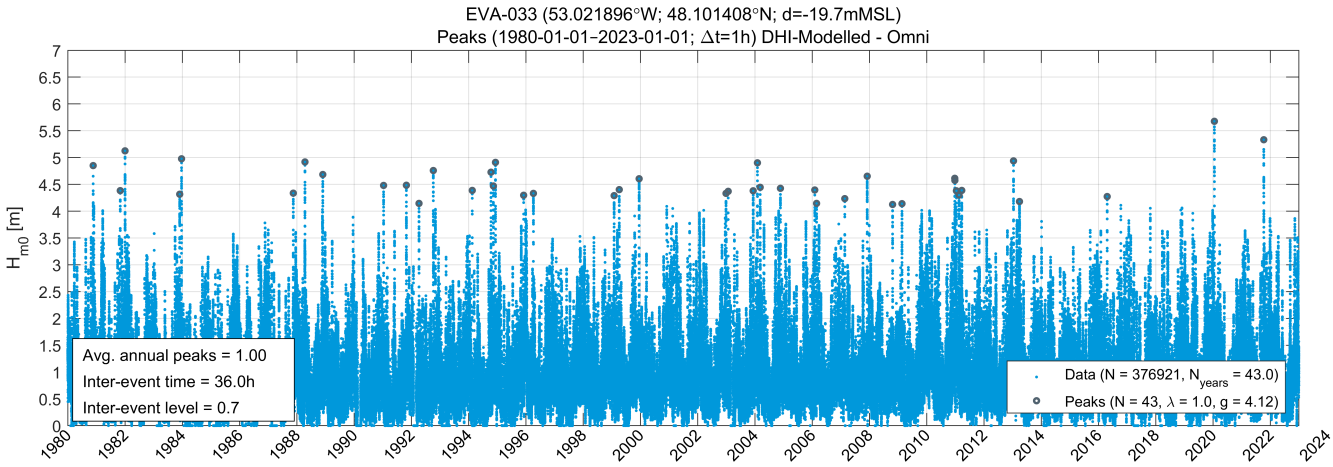


Figure C-253: Time series of significant wave height at EVA-033 and selected peaks.

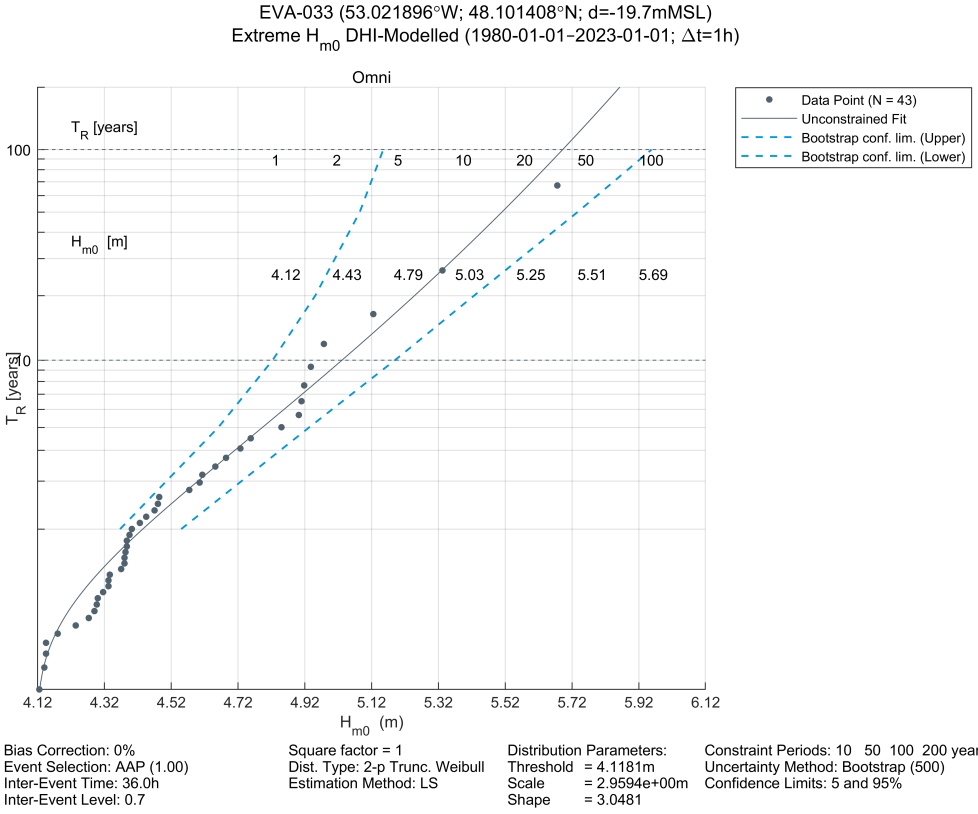


Figure C-254: Extreme value distribution fit at EVA-033.

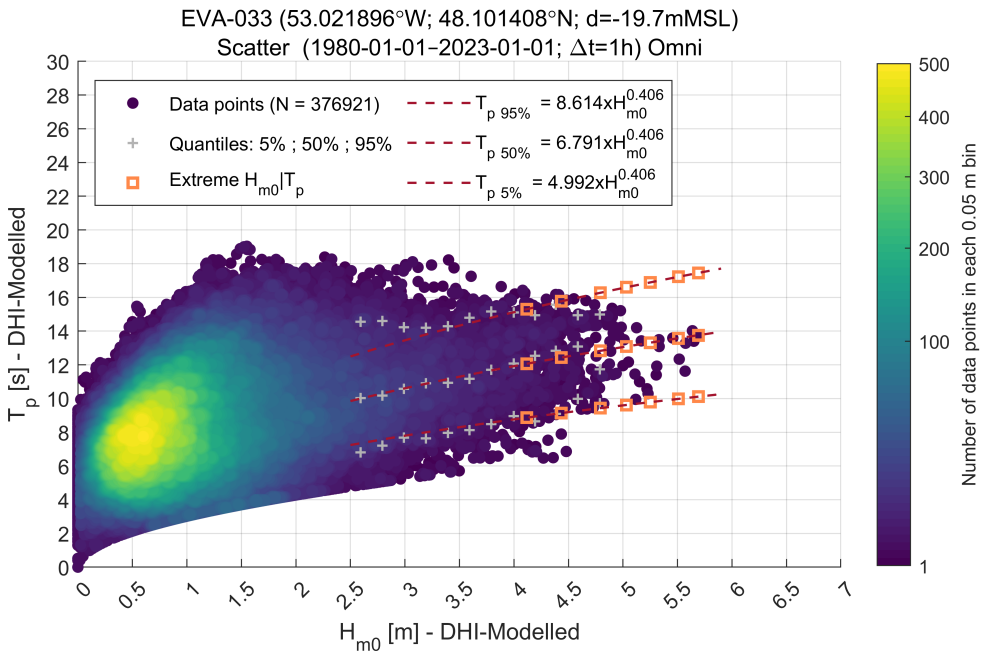


Figure C-255: Scatter plot of Hm0 x Tp at EVA-033 and quantile fit used to derived associated Tp to each extreme Hm0.

EVA-034

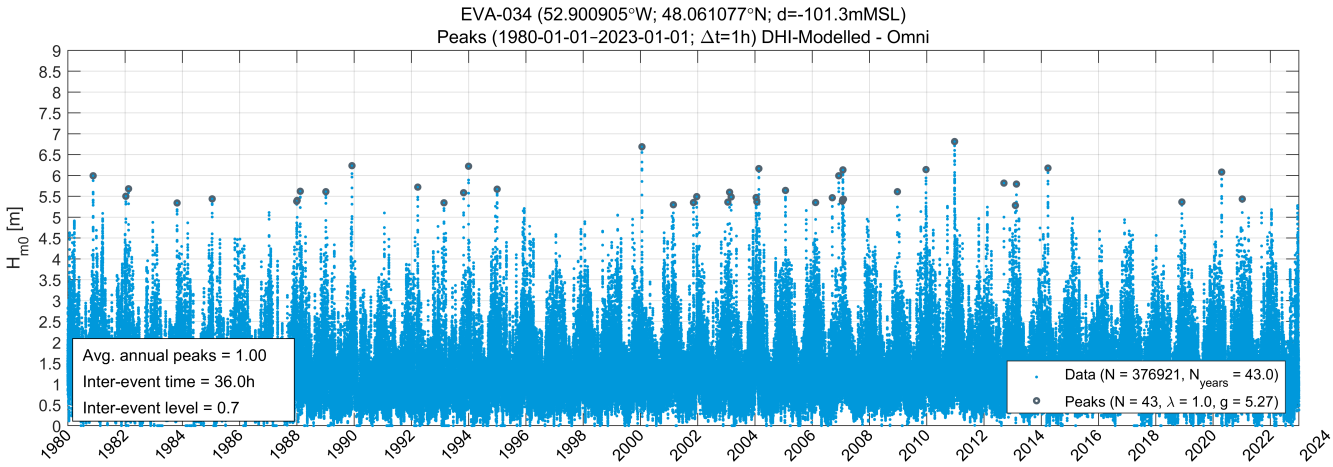


Figure C-256: Time series of significant wave height at EVA-034 and selected peaks.

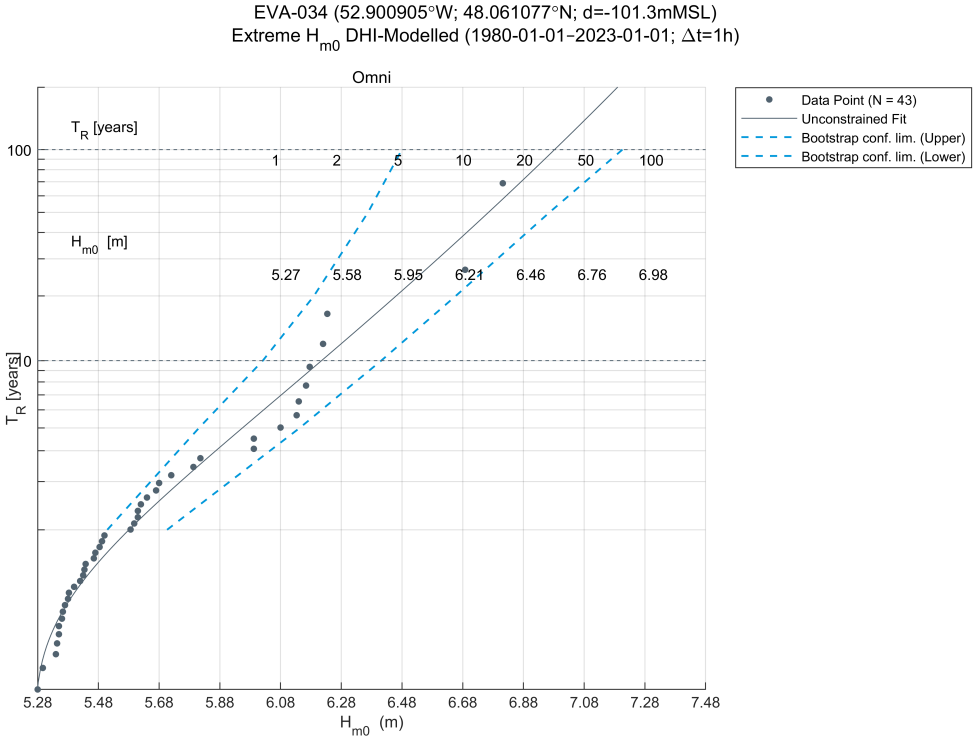


Figure C-257: Extreme value distribution fit at EVA-034.

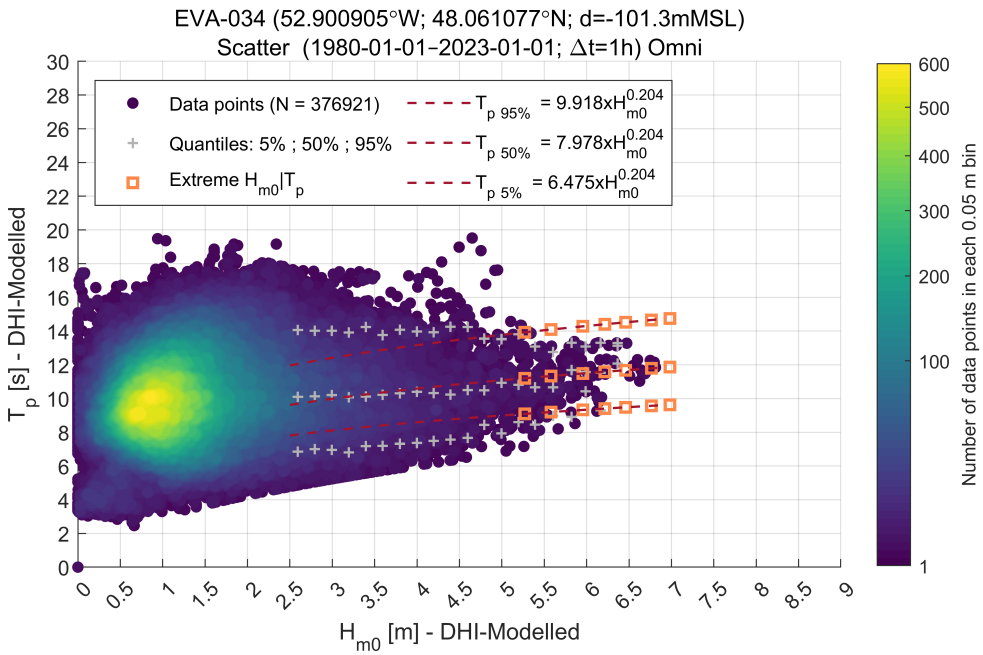


Figure C-258: Scatter plot of Hm0 x Tp at EVA-034 and quantile fit used to derived associated Tp to each extreme Hm0.

EVA-035

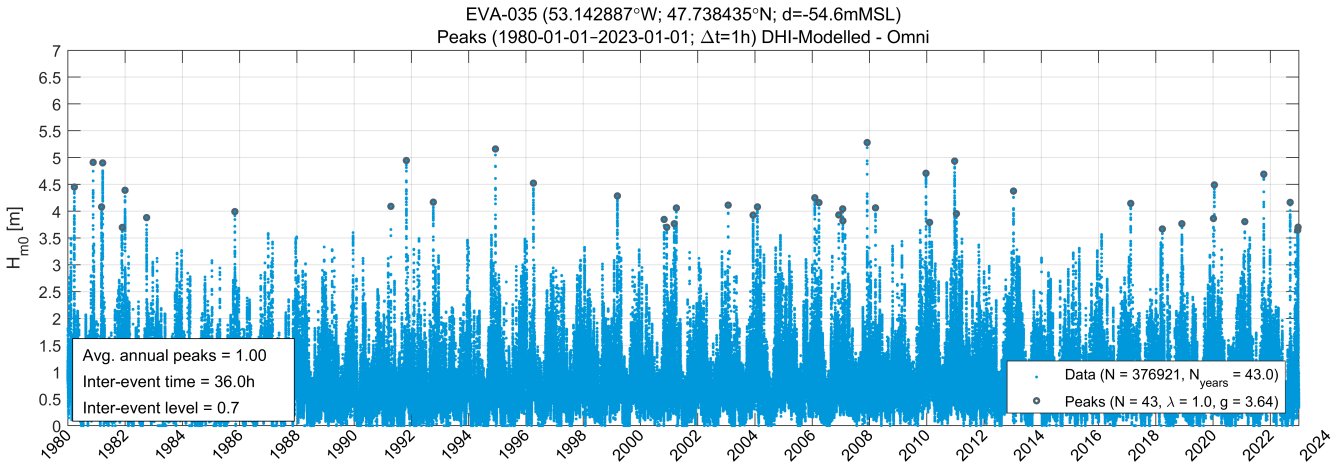


Figure C-259: Time series of significant wave height at EVA-035 and selected peaks.

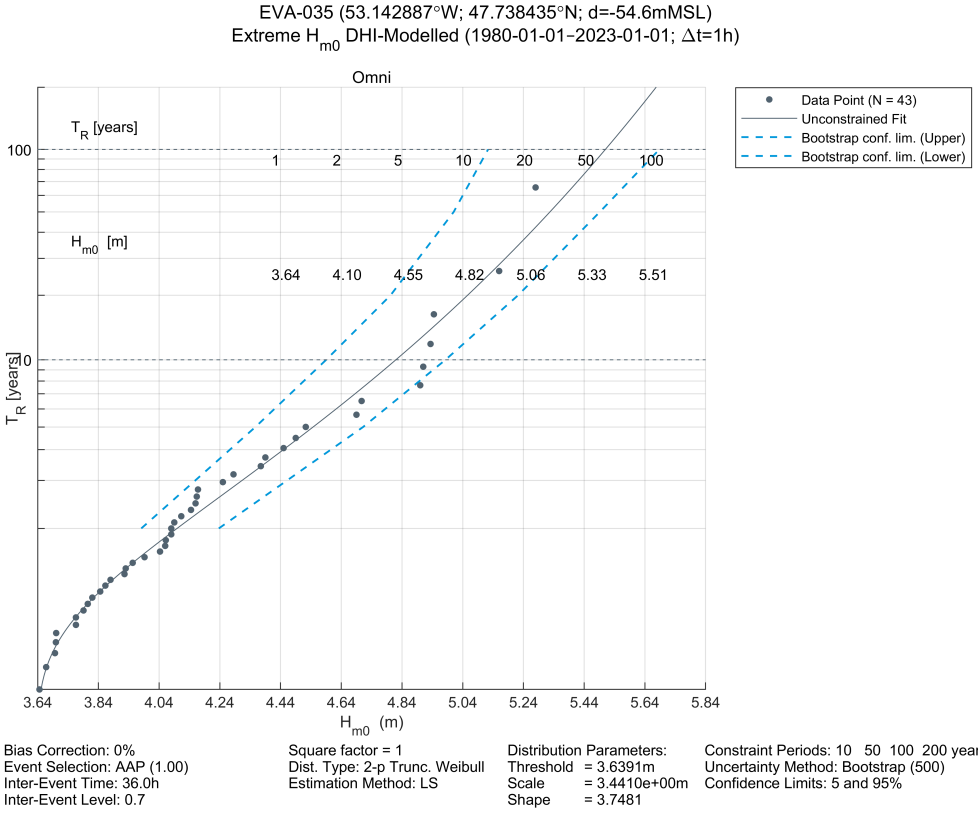


Figure C-260: Extreme value distribution fit at EVA-035.

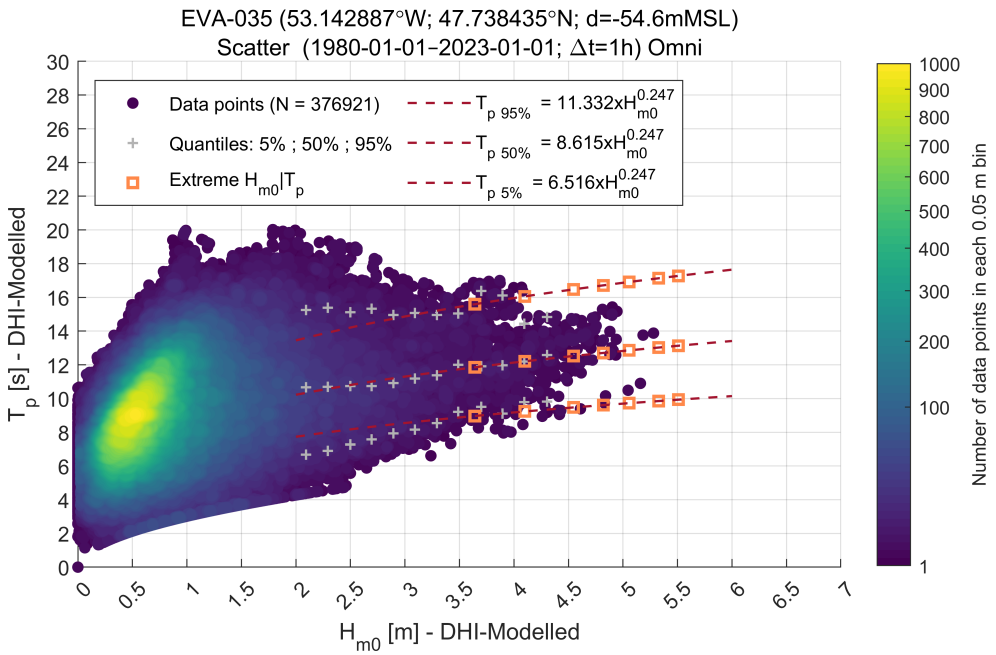


Figure C-261: Scatter plot of Hm0 x Tp at EVA-035 and quantile fit used to derived associated Tp to each extreme Hm0.

EVA-036

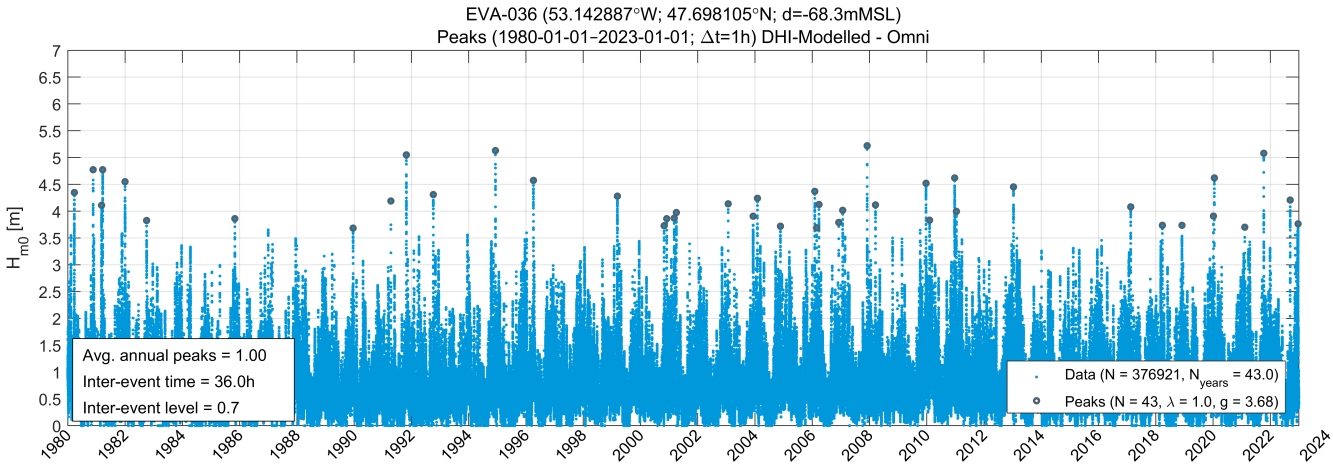


Figure C-262: Time series of significant wave height at EVA-036 and selected peaks.

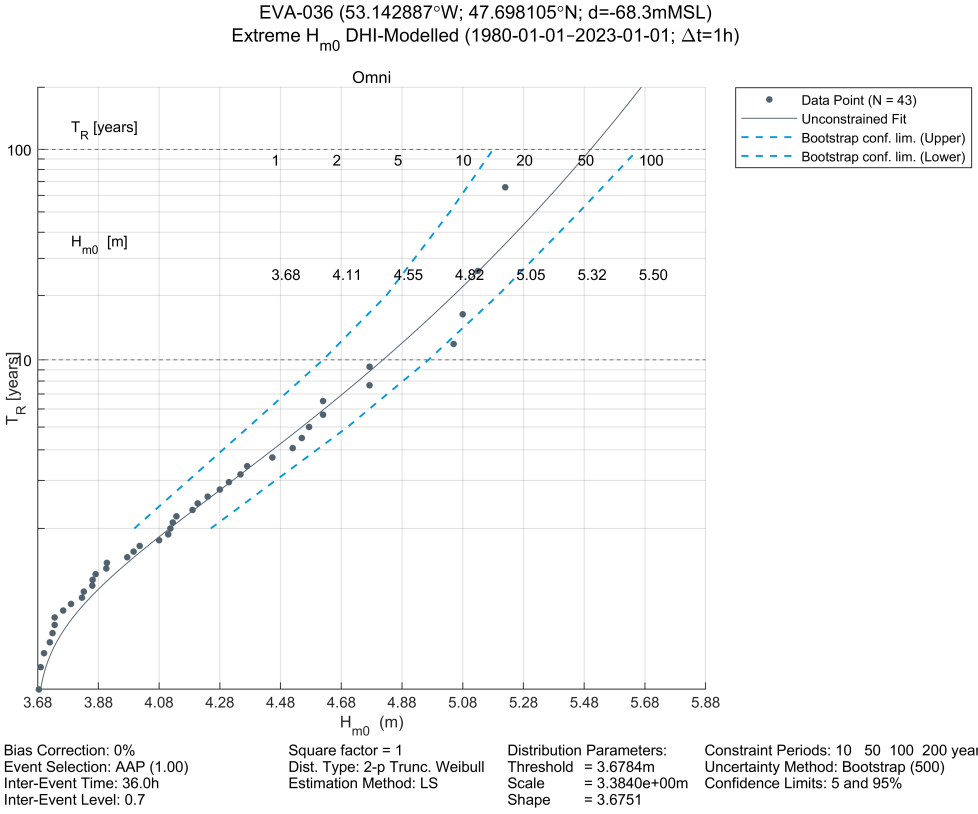


Figure C-263: Extreme value distribution fit at EVA-036.

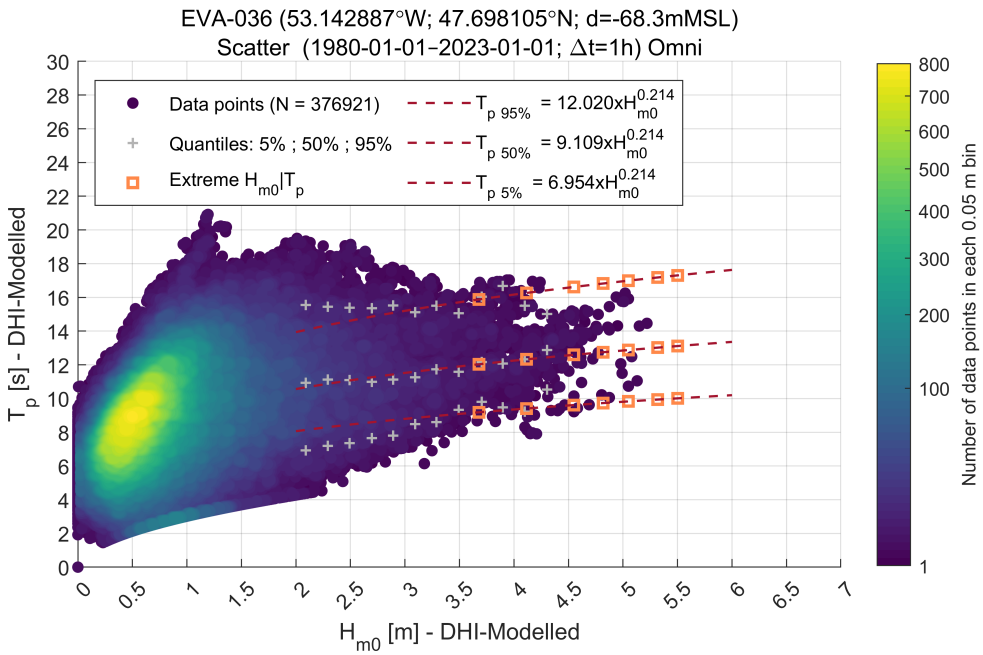


Figure C-264: Scatter plot of Hm0 x Tp at EVA-036 and quantile fit used to derived associated Tp to each extreme Hm0.

EVA-037

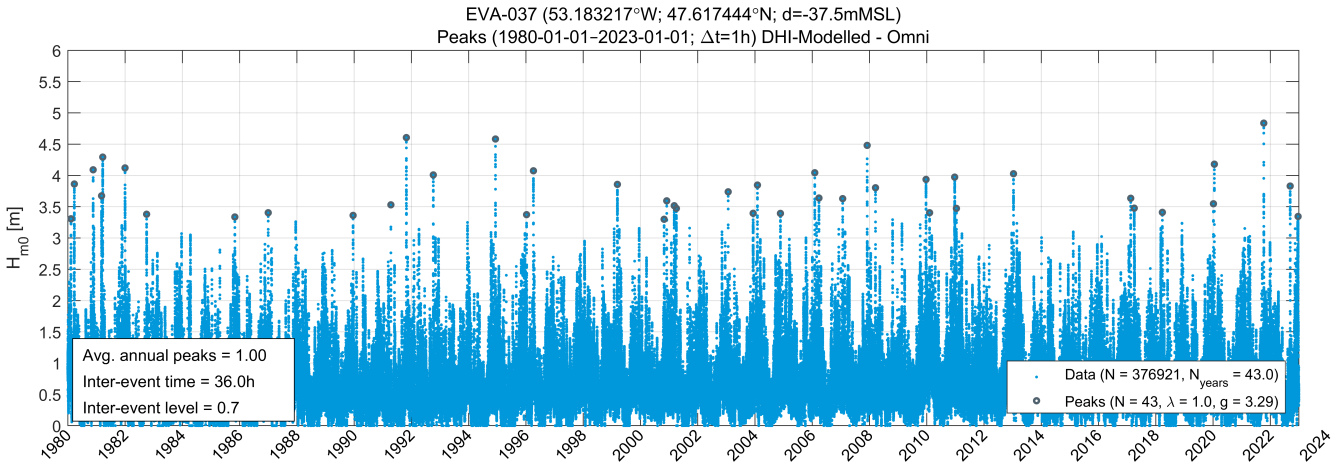


Figure C-265: Time series of significant wave height at EVA-037 and selected peaks.

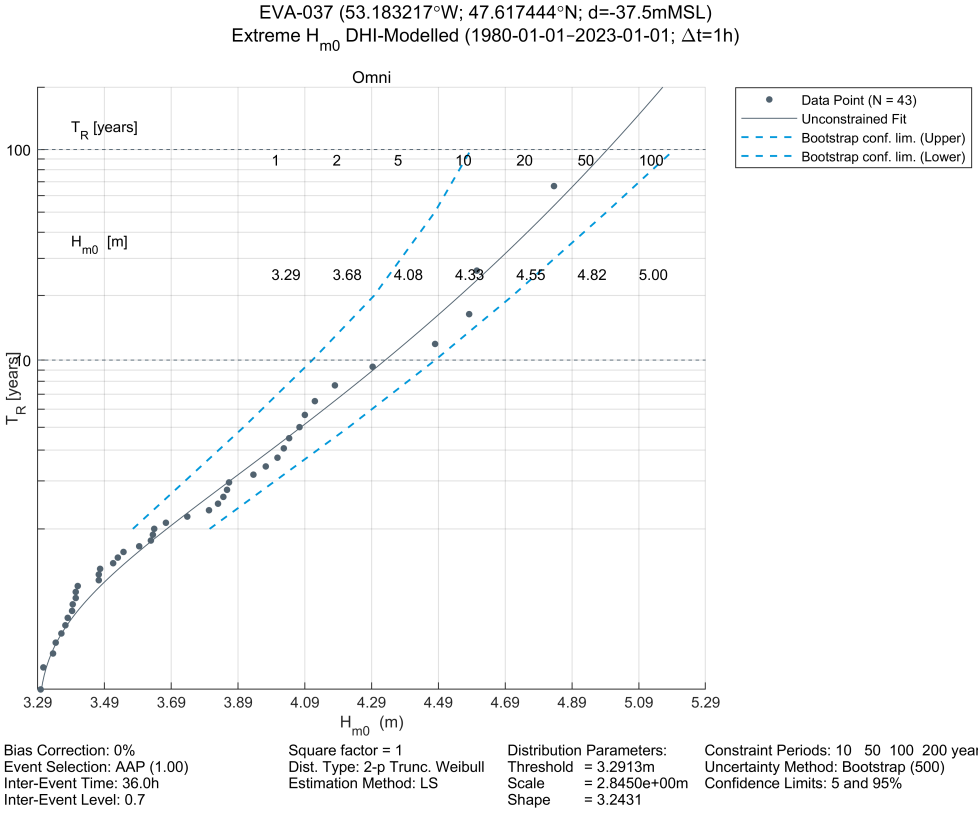


Figure C-266: Extreme value distribution fit at EVA-037.

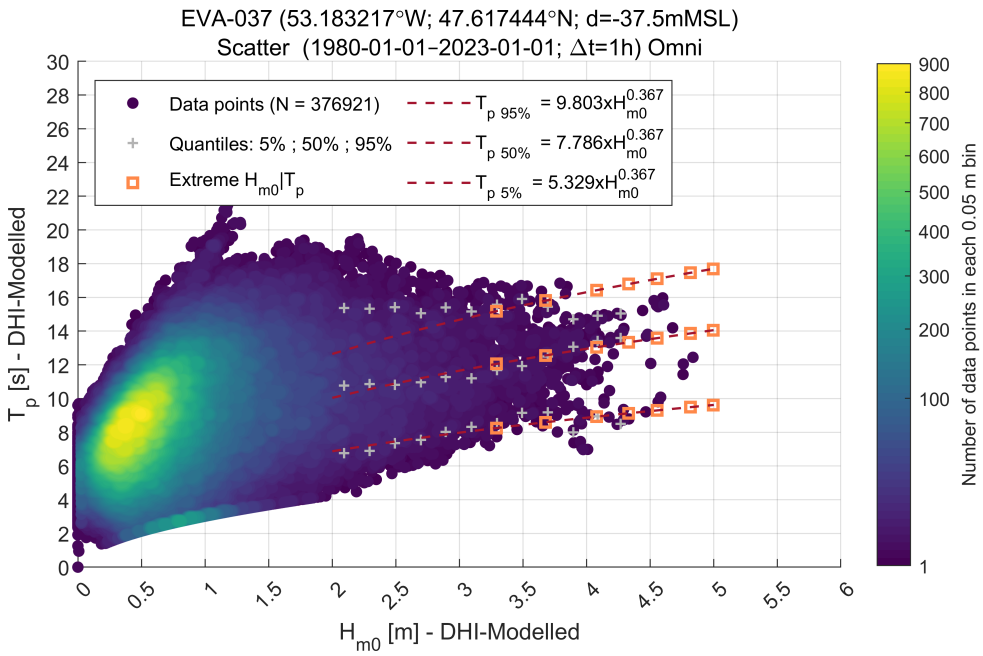


Figure C-267: Scatter plot of Hm0 x Tp at EVA-037 and quantile fit used to derived associated Tp to each extreme Hm0.

EVA-038

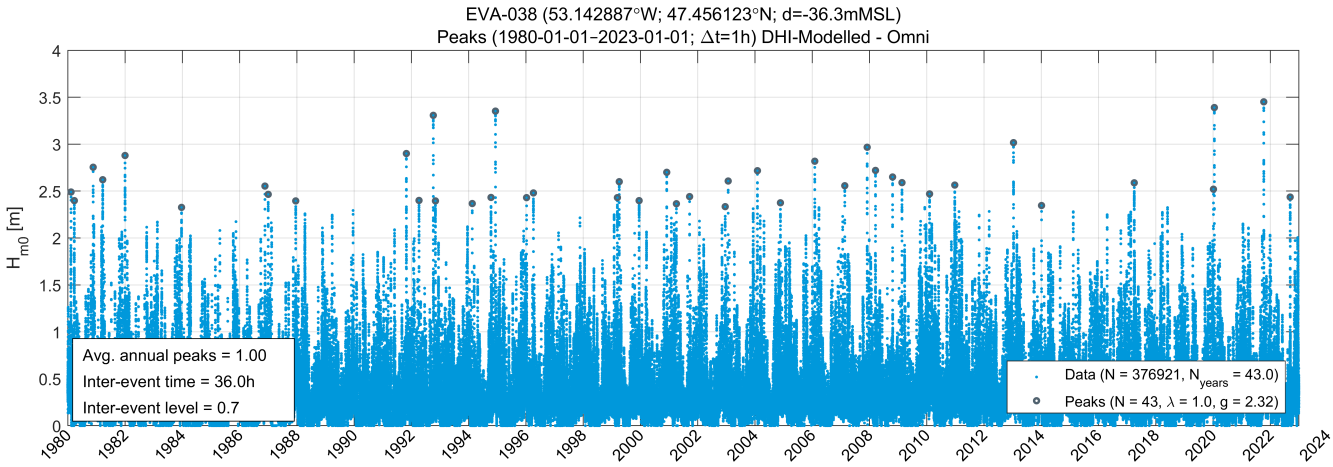


Figure C-268: Time series of significant wave height at EVA-038 and selected peaks.

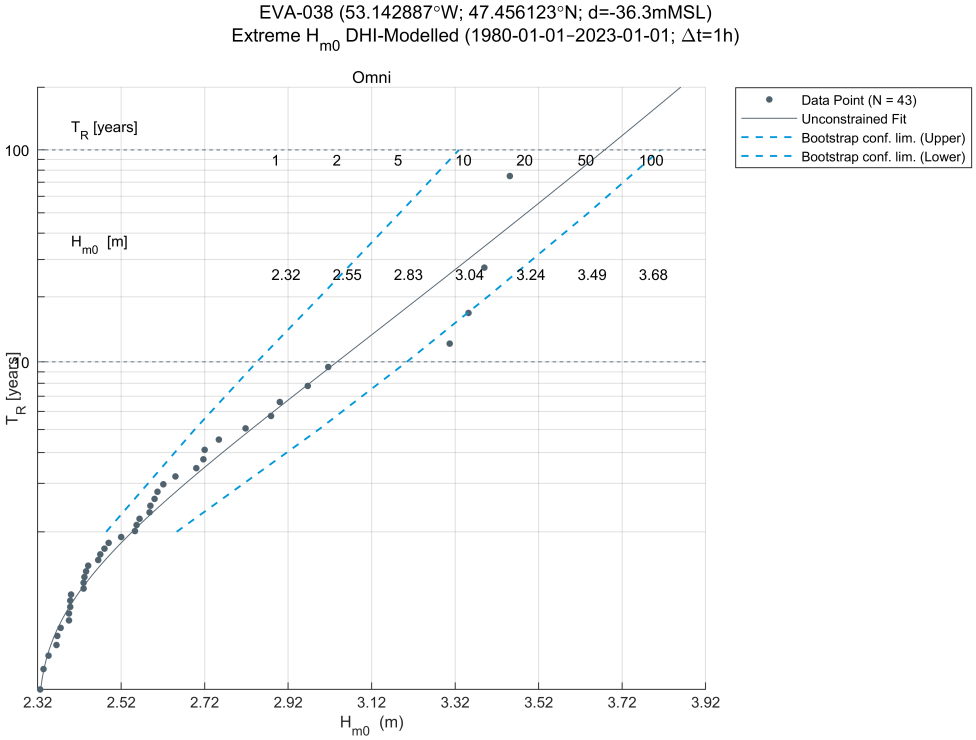


Figure C-269: Extreme value distribution fit at EVA-038.

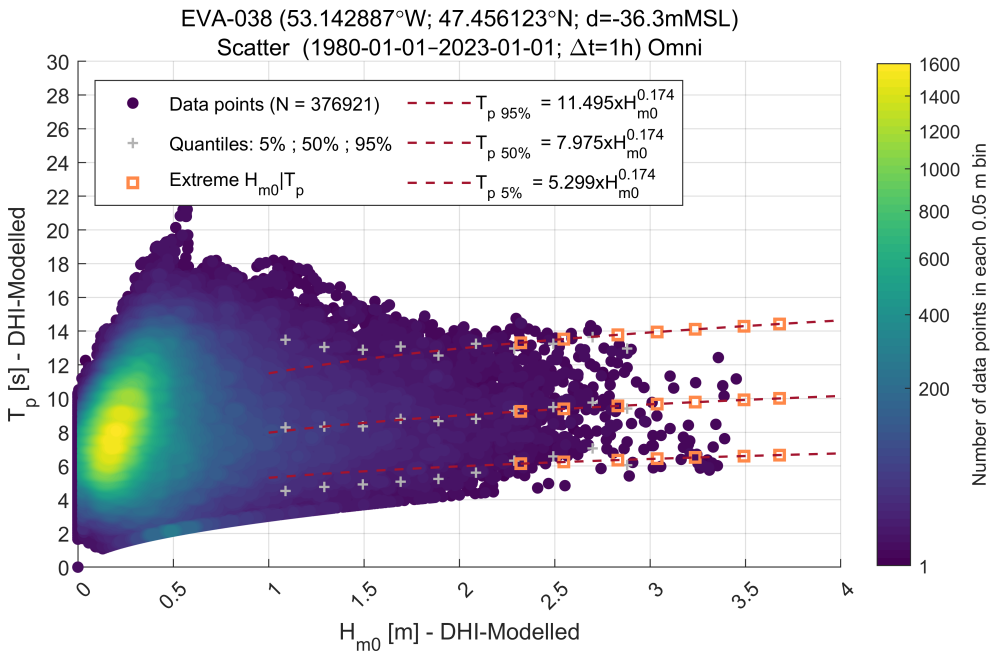


Figure C-270: Scatter plot of Hm0 x Tp at EVA-038 and quantile fit used to derived associated Tp to each extreme Hm0.

EVA-039

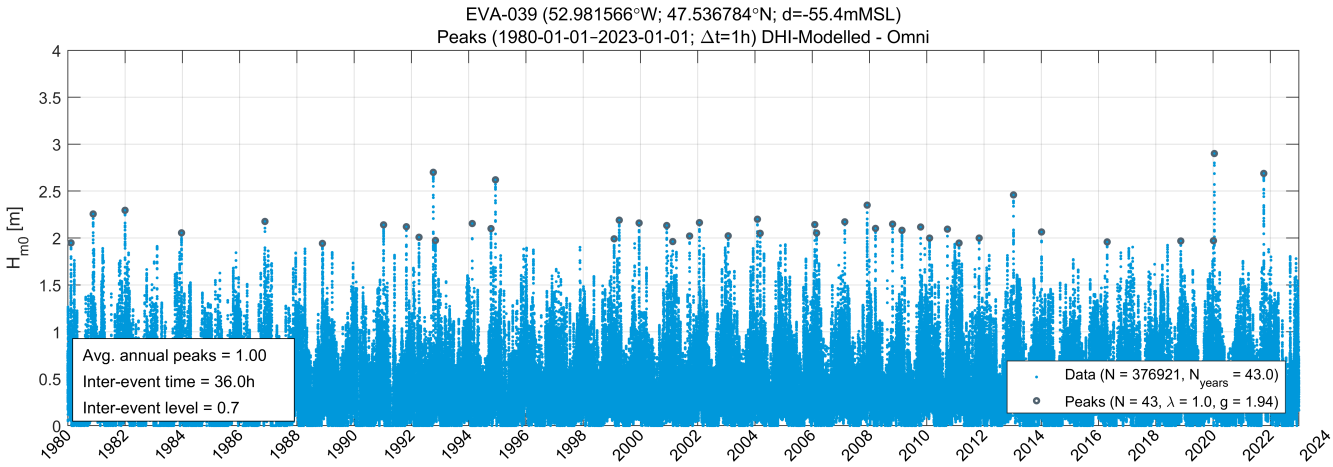


Figure C-271: Time series of significant wave height at EVA-039 and selected peaks.

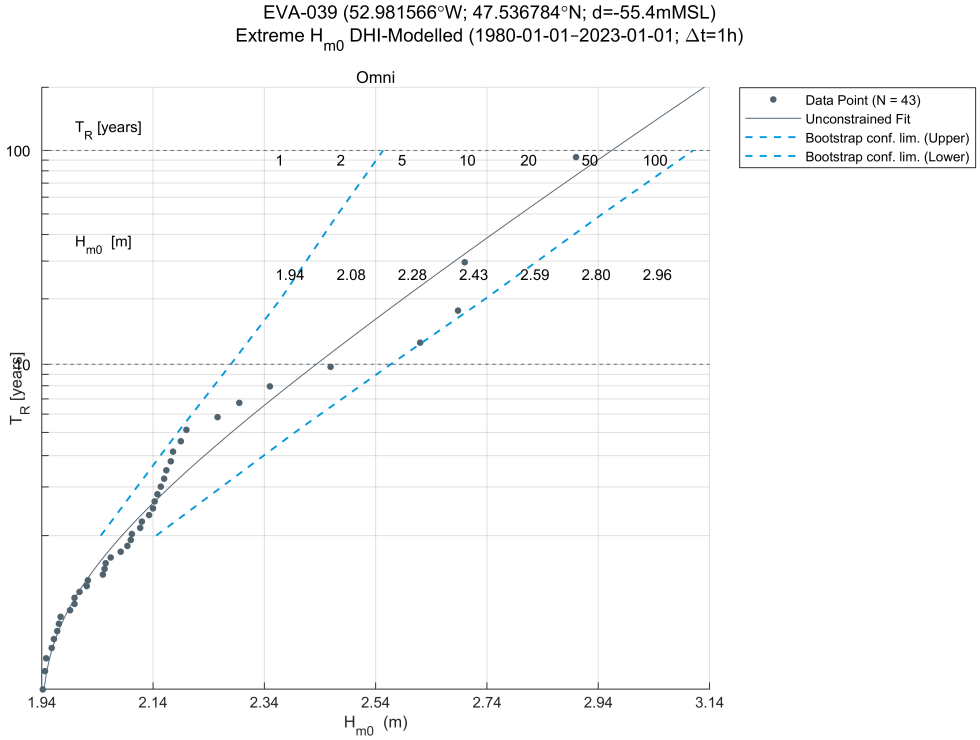


Figure C-272: Extreme value distribution fit at EVA-039.

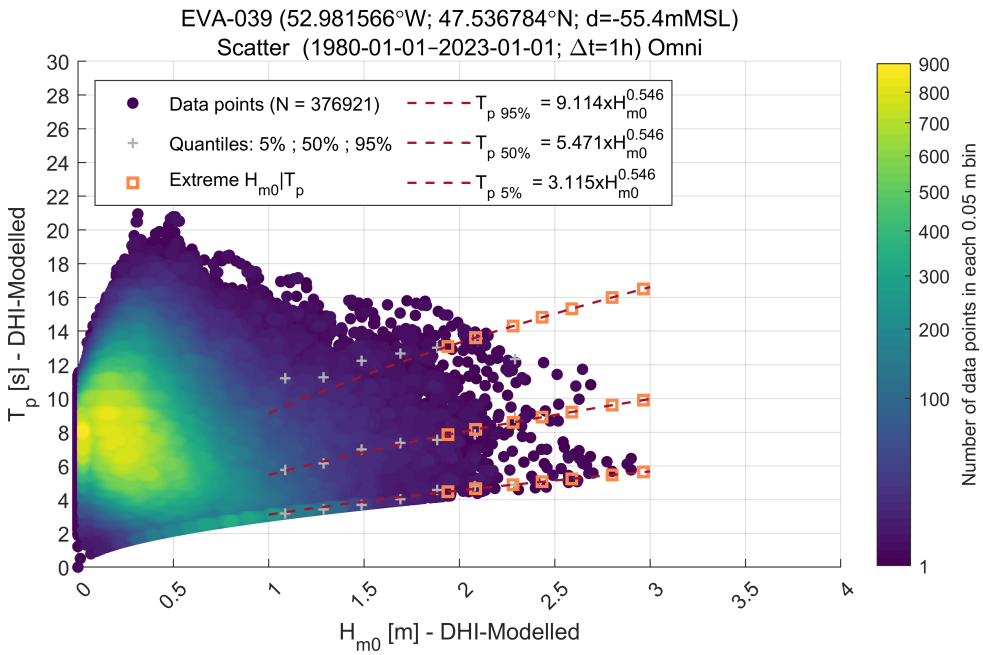


Figure C-273: Scatter plot of Hm0 x Tp at EVA-039 and quantile fit used to derived associated Tp to each extreme Hm0.

EVA-040

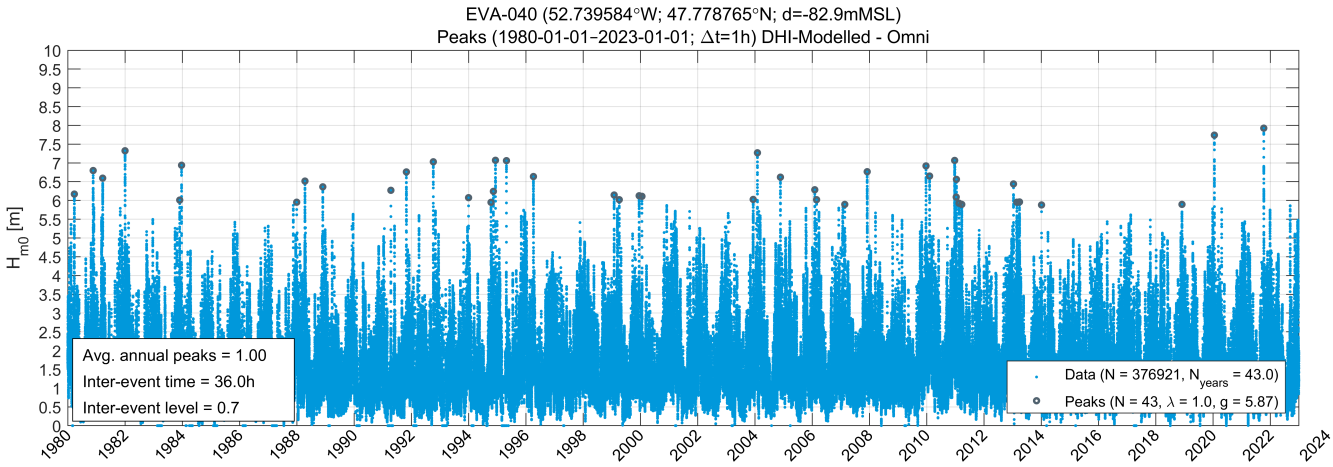


Figure C-274: Time series of significant wave height at EVA-040 and selected peaks.

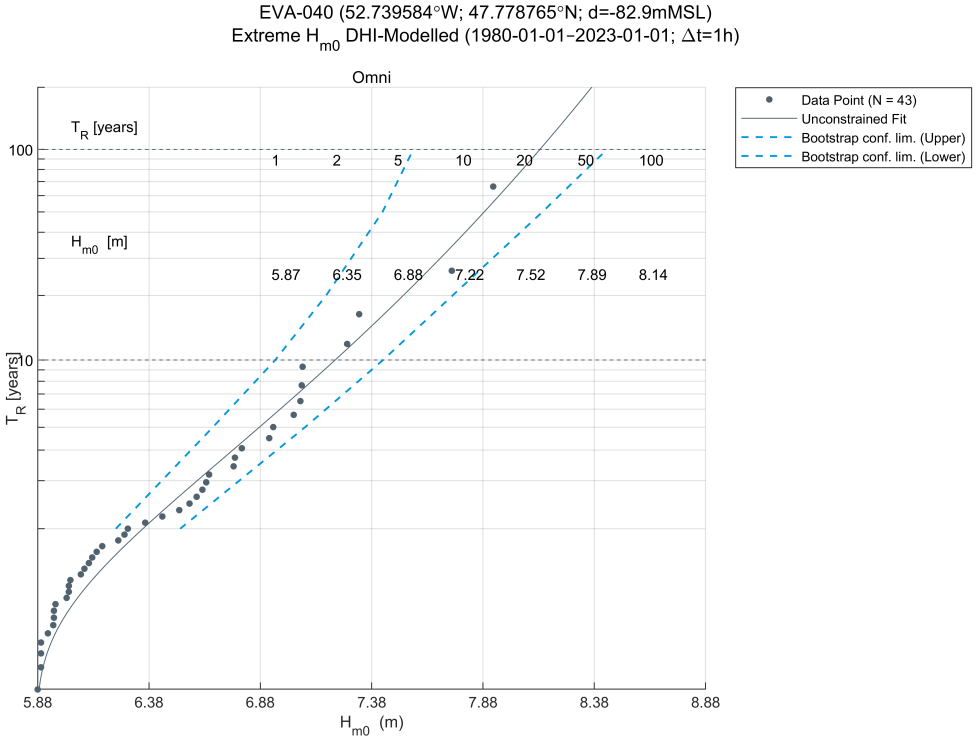


Figure C-275: Extreme value distribution fit at EVA-040.

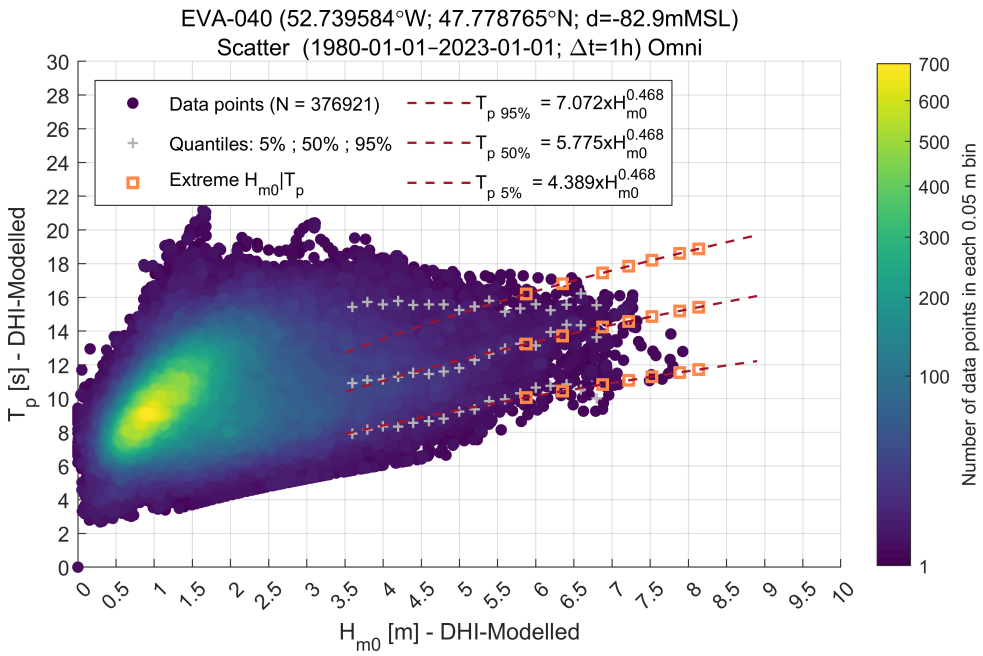


Figure C-276: Scatter plot of Hm0 x Tp at EVA-040 and quantile fit used to derived associated Tp to each extreme Hm0.

EVA-041

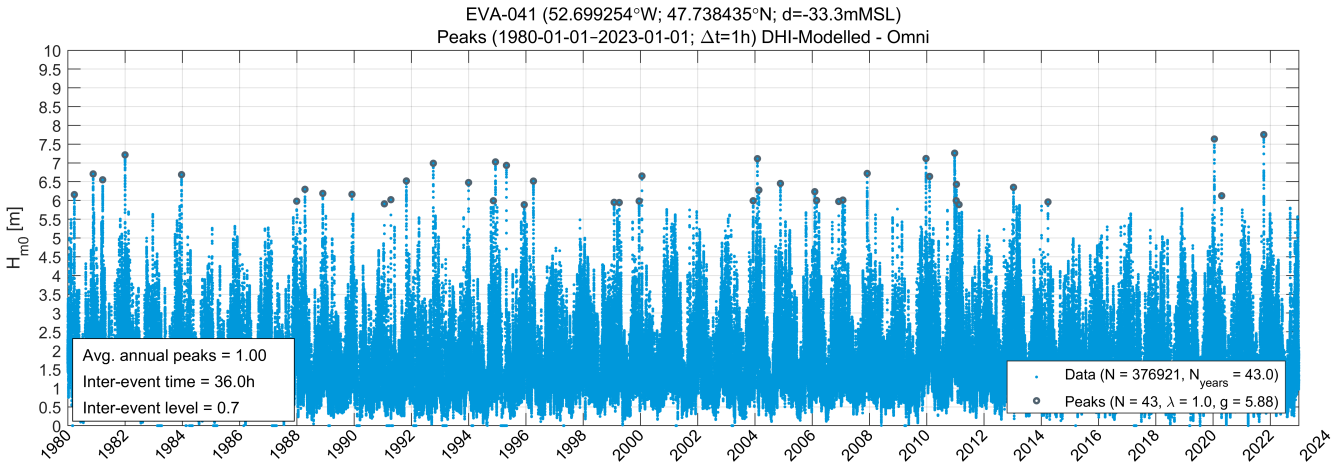


Figure C-277: Time series of significant wave height at EVA-041 and selected peaks.

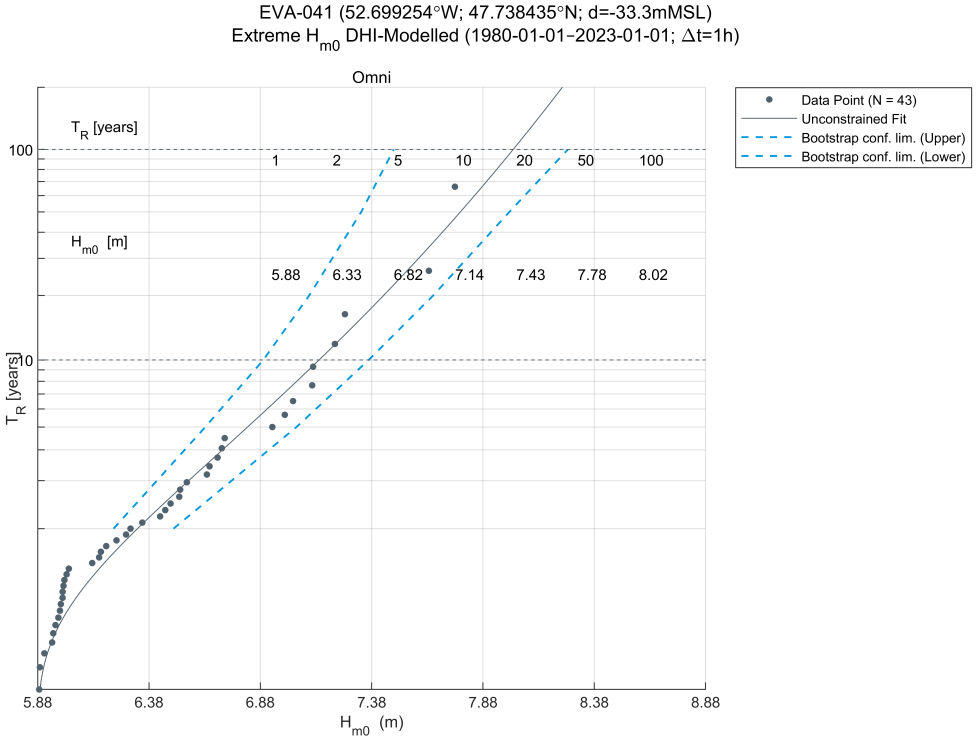


Figure C-278: Extreme value distribution fit at EVA-041.

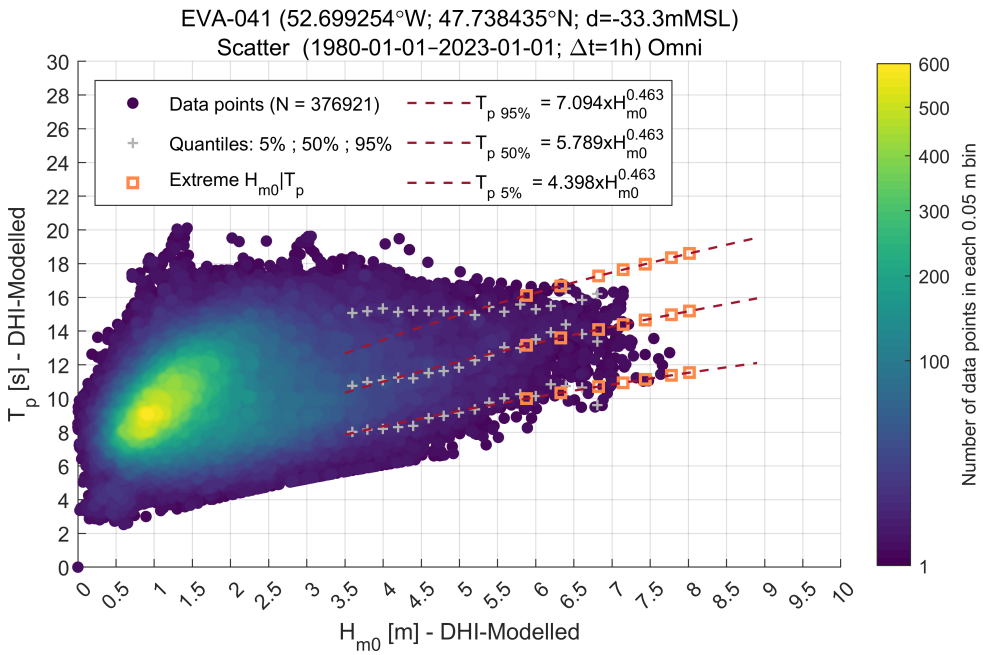


Figure C-279: Scatter plot of Hm0 x Tp at EVA-041 and quantile fit used to derived associated Tp to each extreme Hm0.

EVA-042

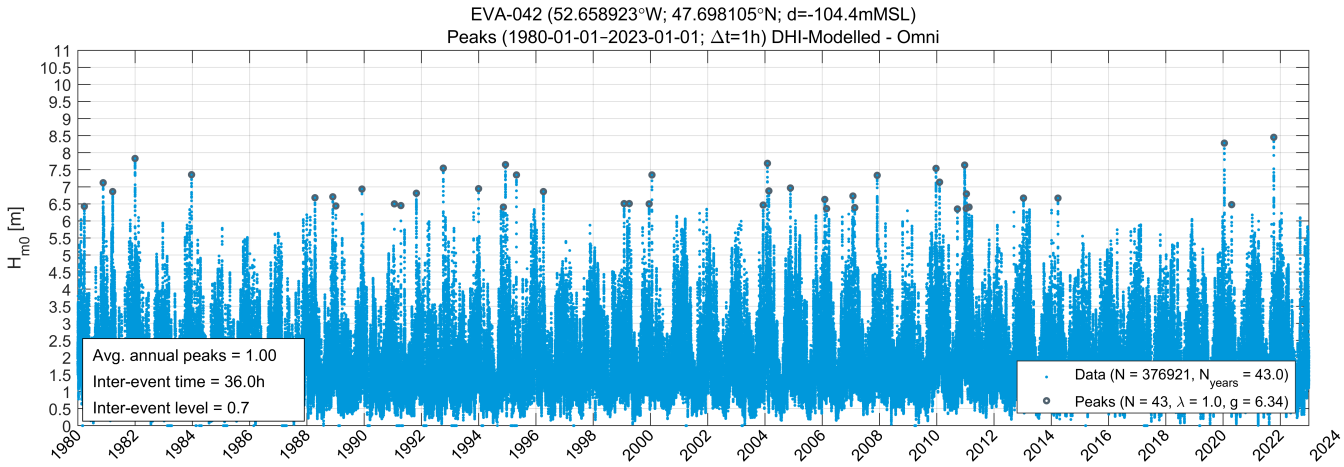


Figure C-280: Time series of significant wave height at EVA-042 and selected peaks.

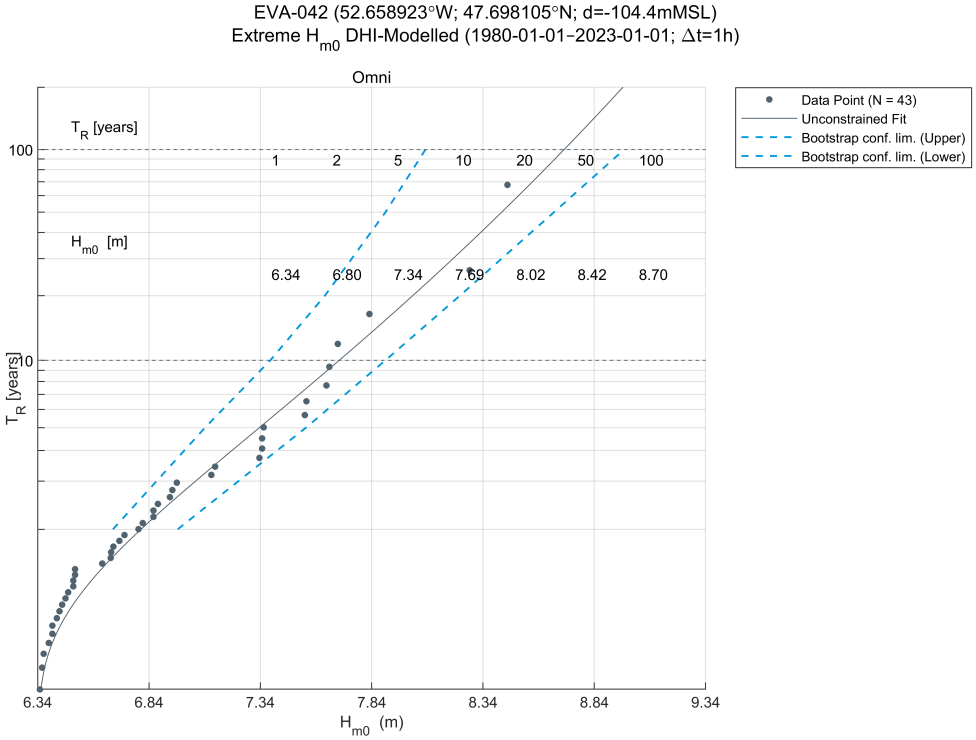


Figure C-281: Extreme value distribution fit at EVA-042.

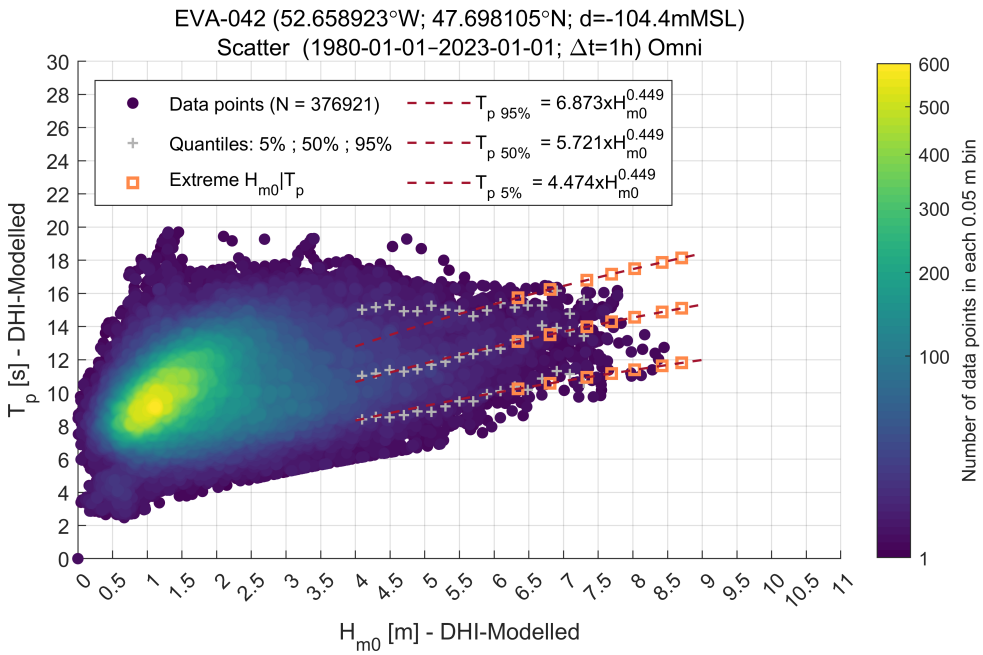


Figure C-282: Scatter plot of Hm0 x Tp at EVA-042 and quantile fit used to derived associated Tp to each extreme Hm0.

EVA-043

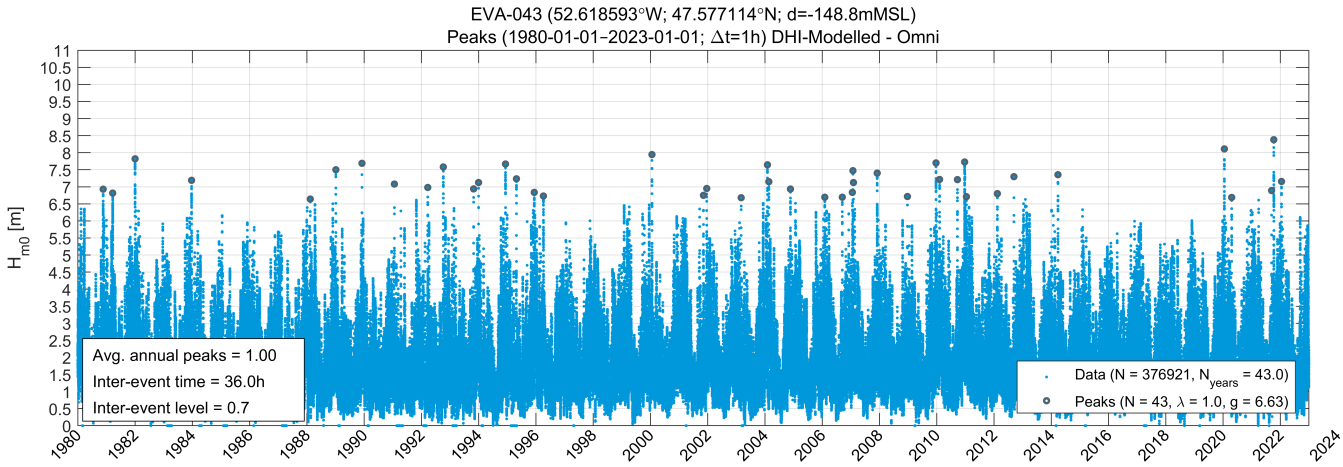


Figure C-283: Time series of significant wave height at EVA-043 and selected peaks.

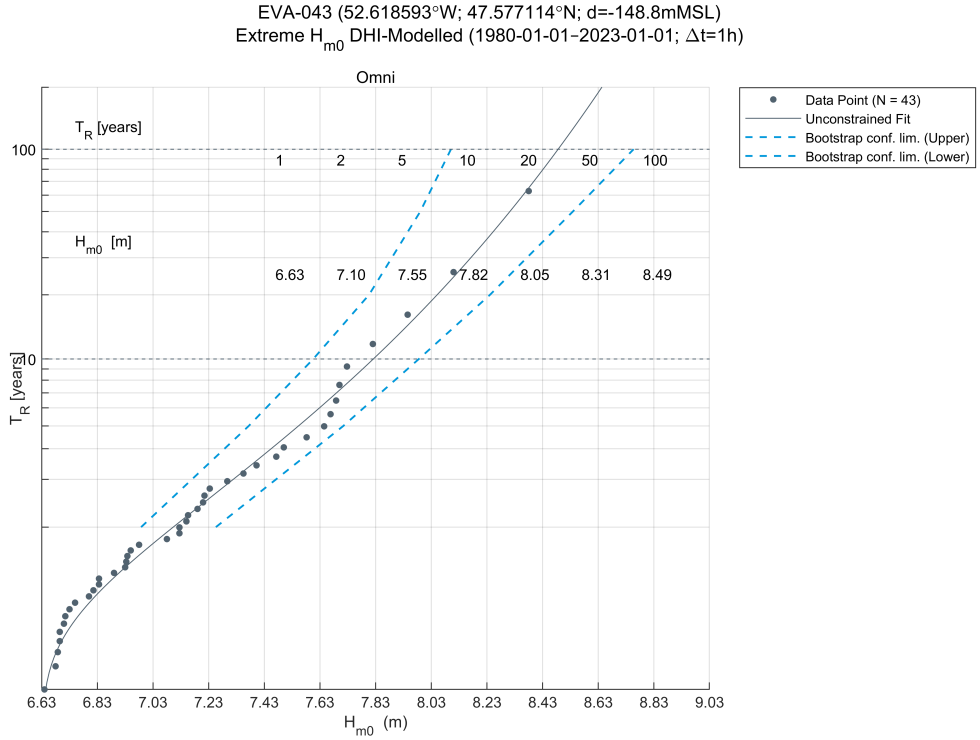


Figure C-284: Extreme value distribution fit at EVA-043.

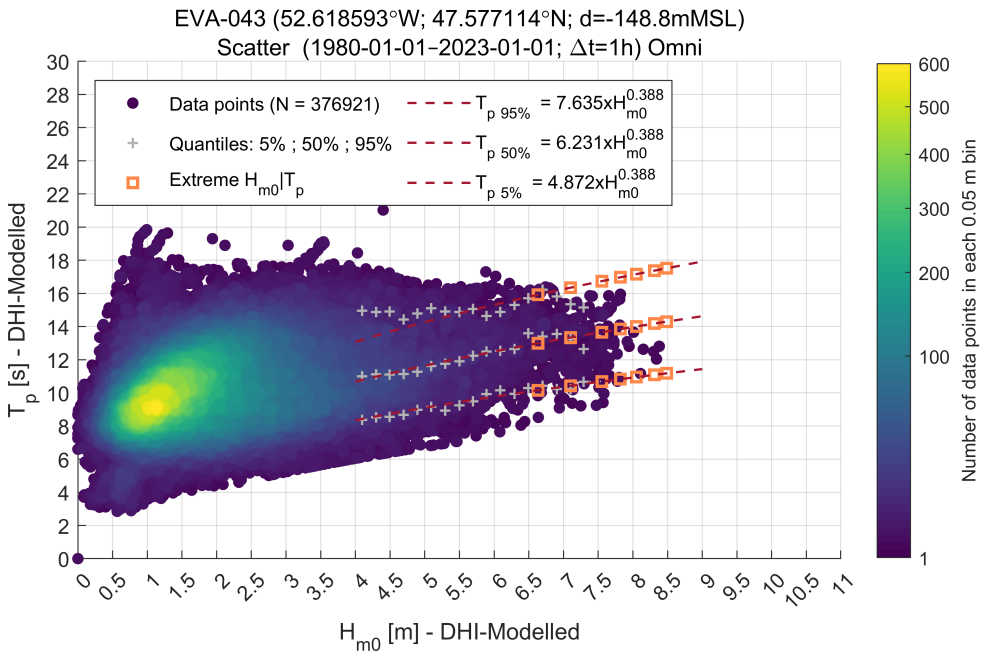


Figure C-285: Scatter plot of Hm0 x Tp at EVA-043 and quantile fit used to derived associated Tp to each extreme Hm0.

EVA-044

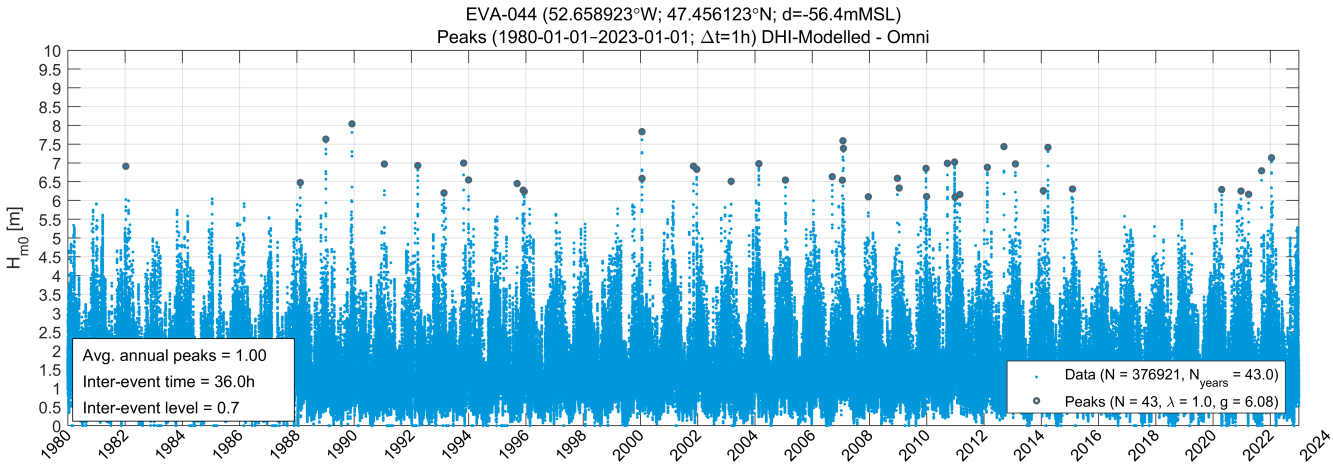


Figure C-286: Time series of significant wave height at EVA-044 and selected peaks.

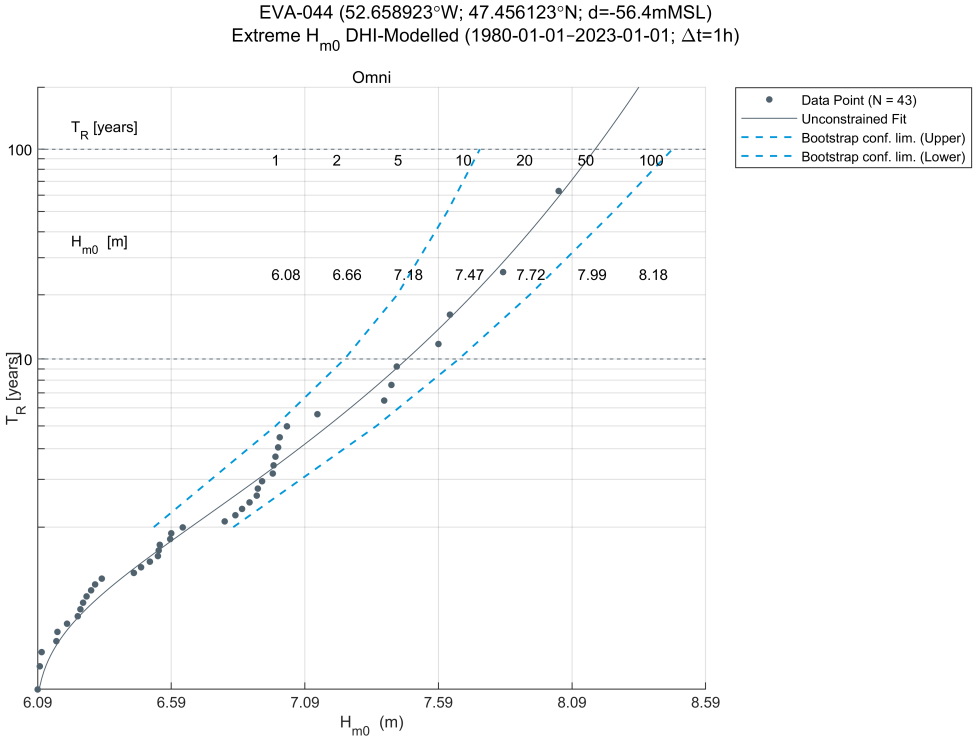


Figure C-287: Extreme value distribution fit at EVA-044.

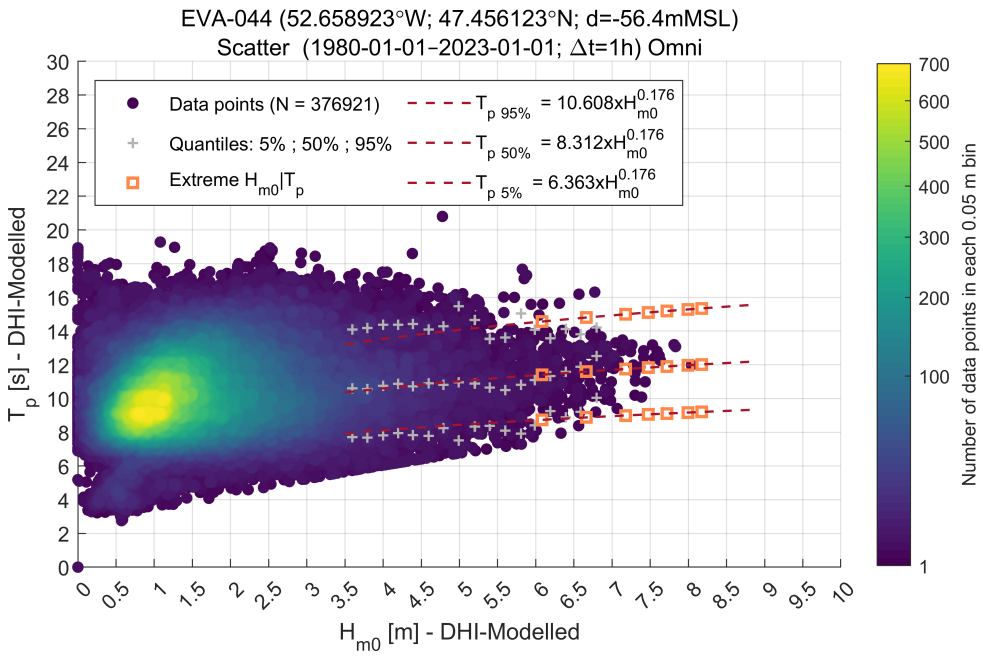


Figure C-288: Scatter plot of Hm0 x Tp at EVA-044 and quantile fit used to derived associated Tp to each extreme Hm0.

EVA-045

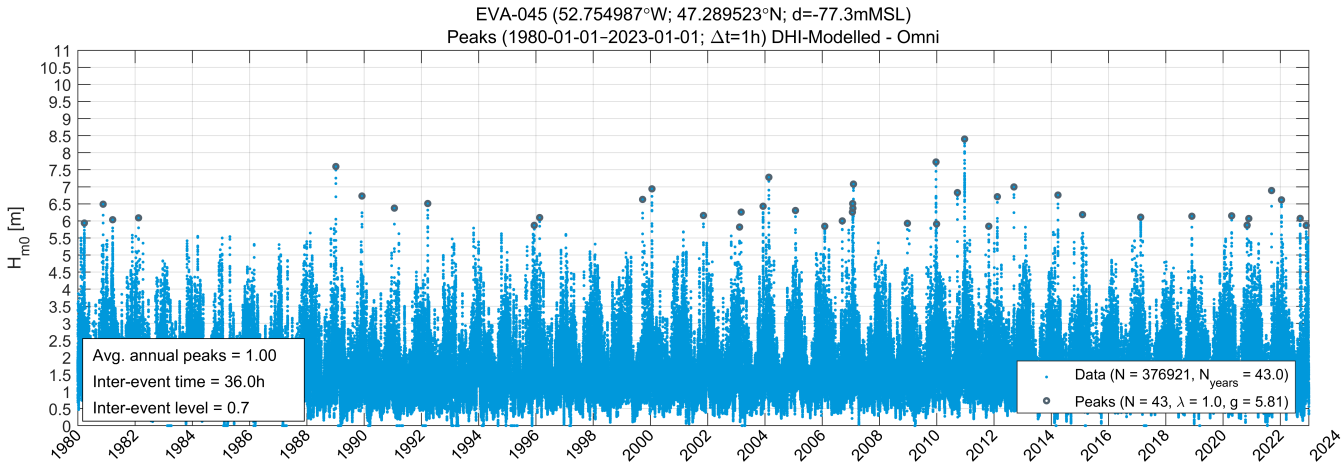


Figure C-289: Time series of significant wave height at EVA-045 and selected peaks.

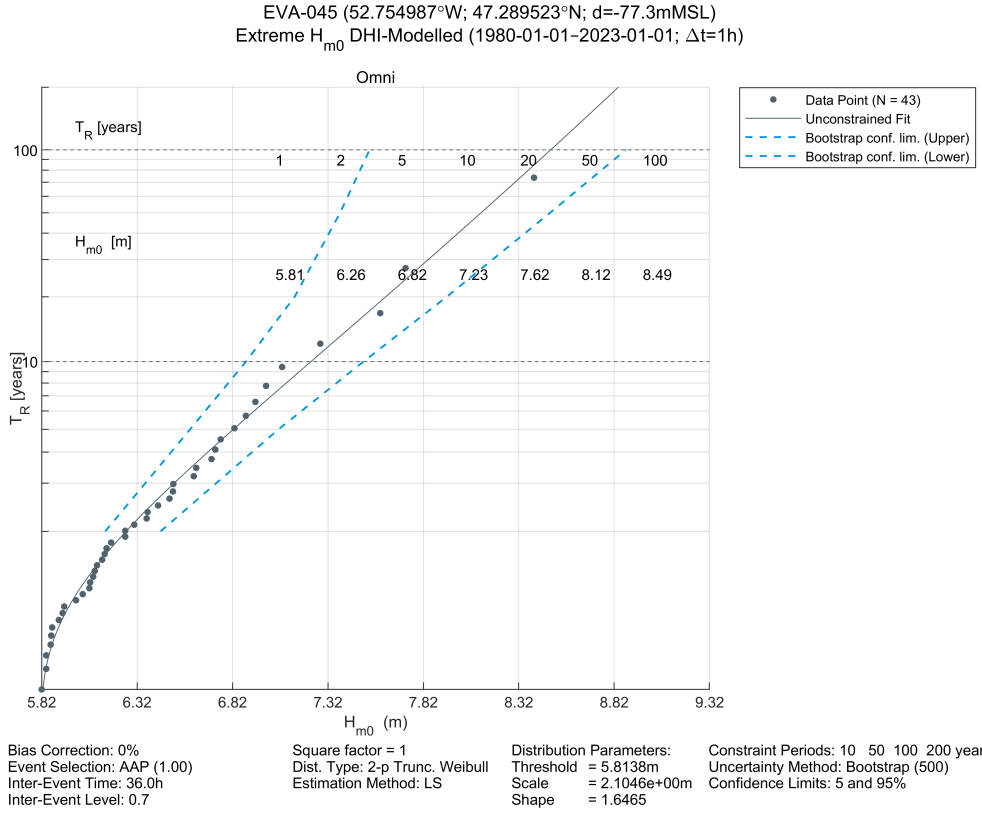


Figure C-290: Extreme value distribution fit at EVA-045.

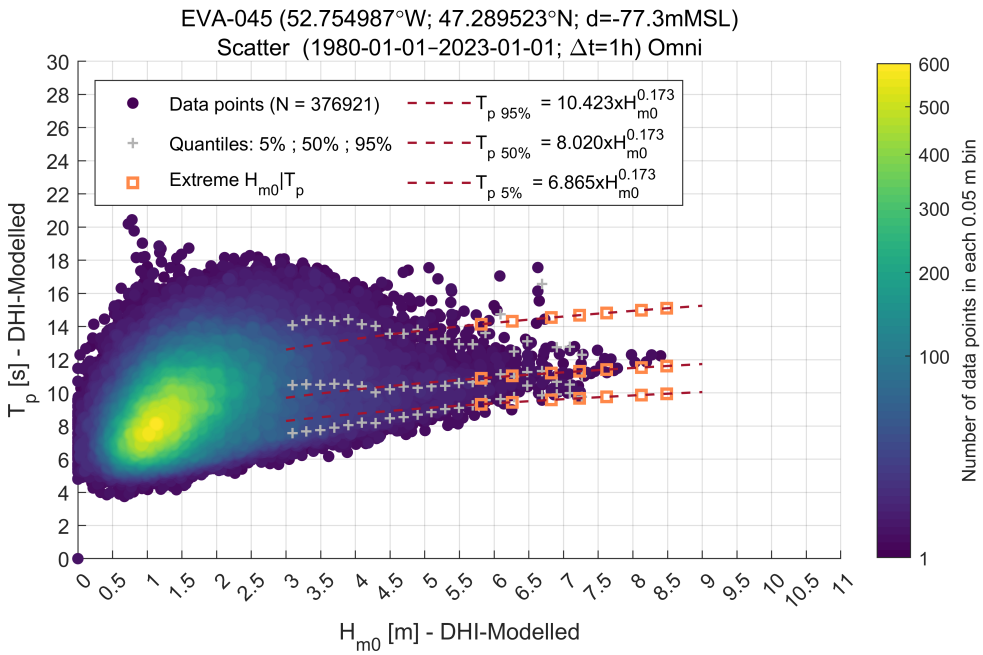


Figure C-291: Scatter plot of Hm0 x Tp at EVA-045 and quantile fit used to derived associated Tp to each extreme Hm0.

EVA-046

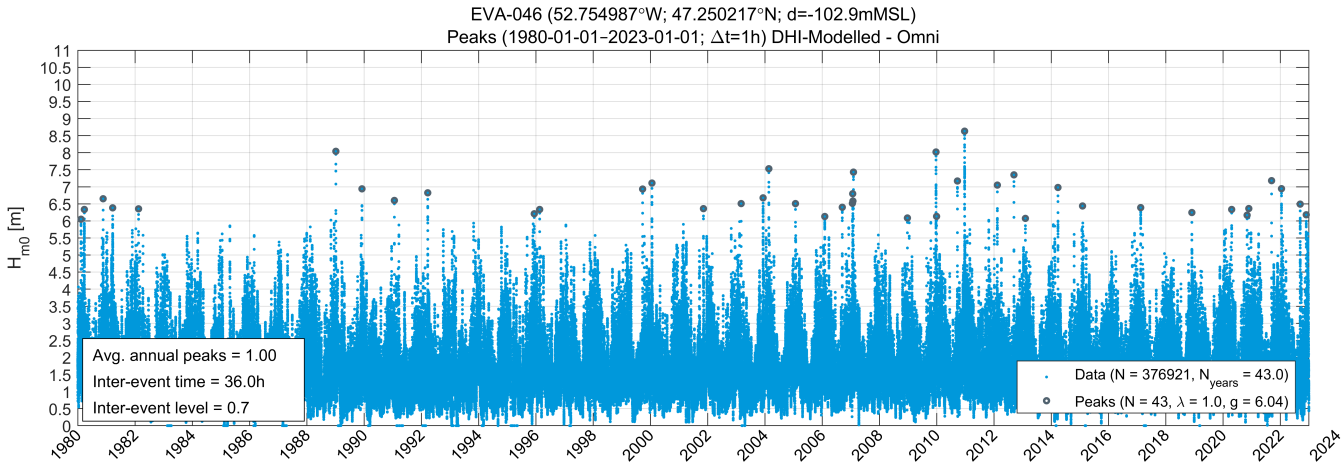


Figure C-292: Time series of significant wave height at EVA-046 and selected peaks.

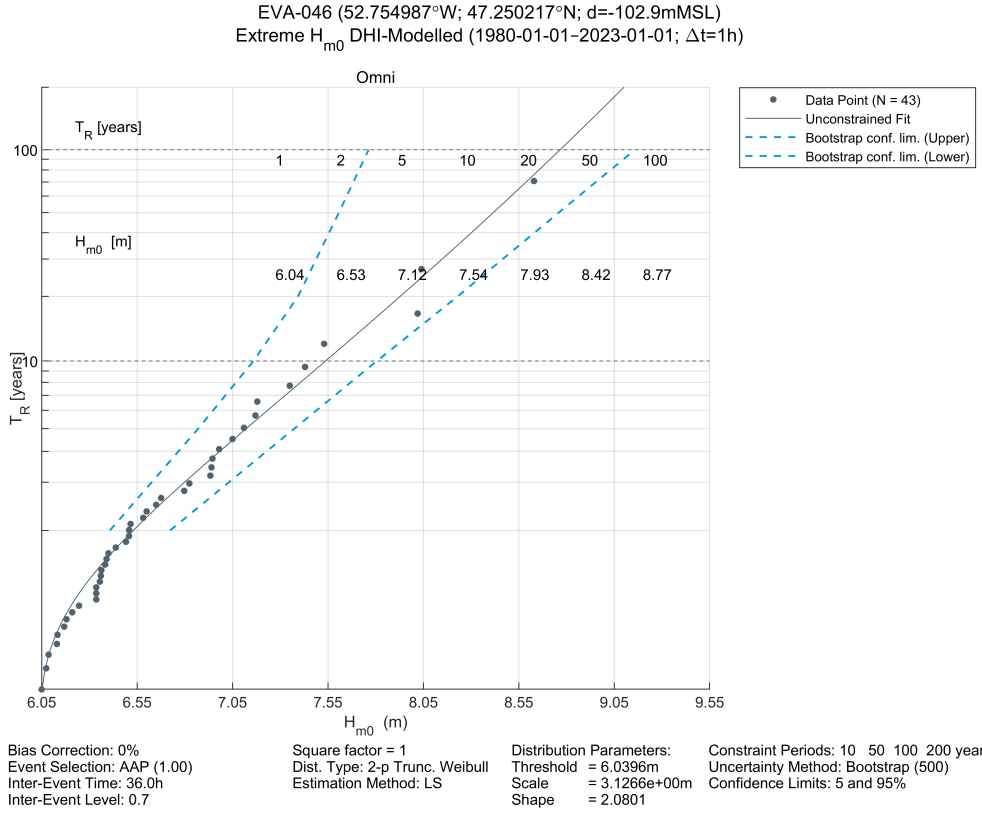


Figure C-293: Extreme value distribution fit at EVA-046.

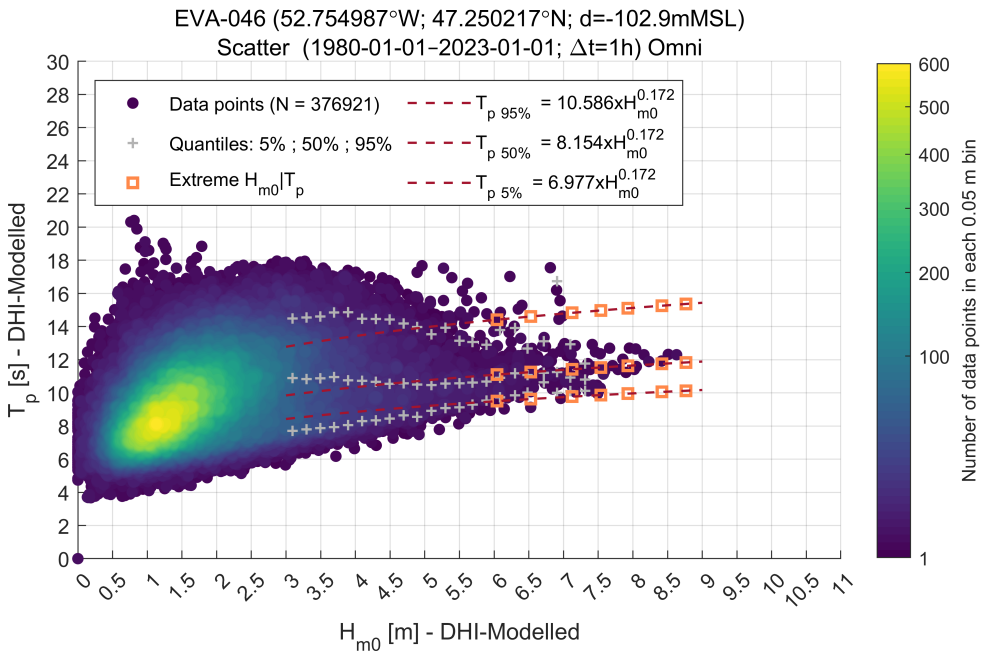


Figure C-294: Scatter plot of Hm0 x Tp at EVA-046 and quantile fit used to derived associated Tp to each extreme Hm0.

EVA-047

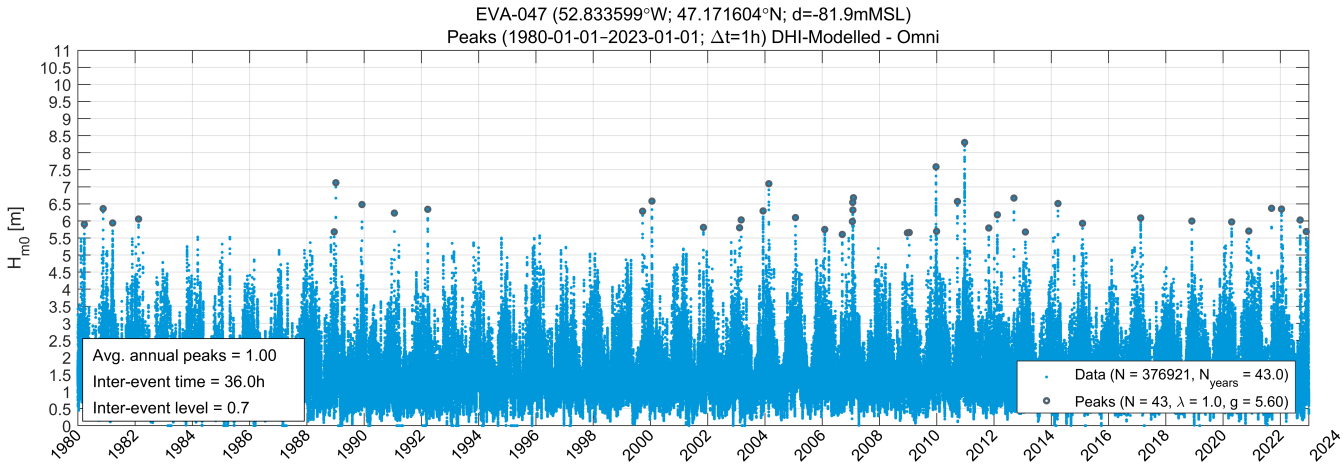


Figure C-295: Time series of significant wave height at EVA-047 and selected peaks.

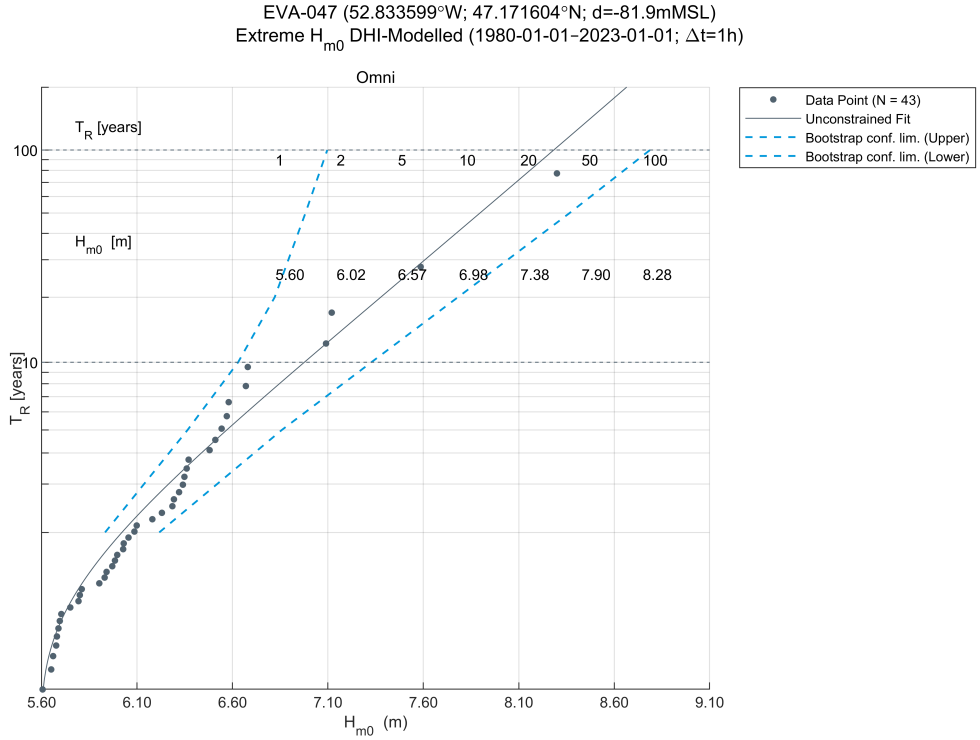


Figure C-296: Extreme value distribution fit at EVA-047.

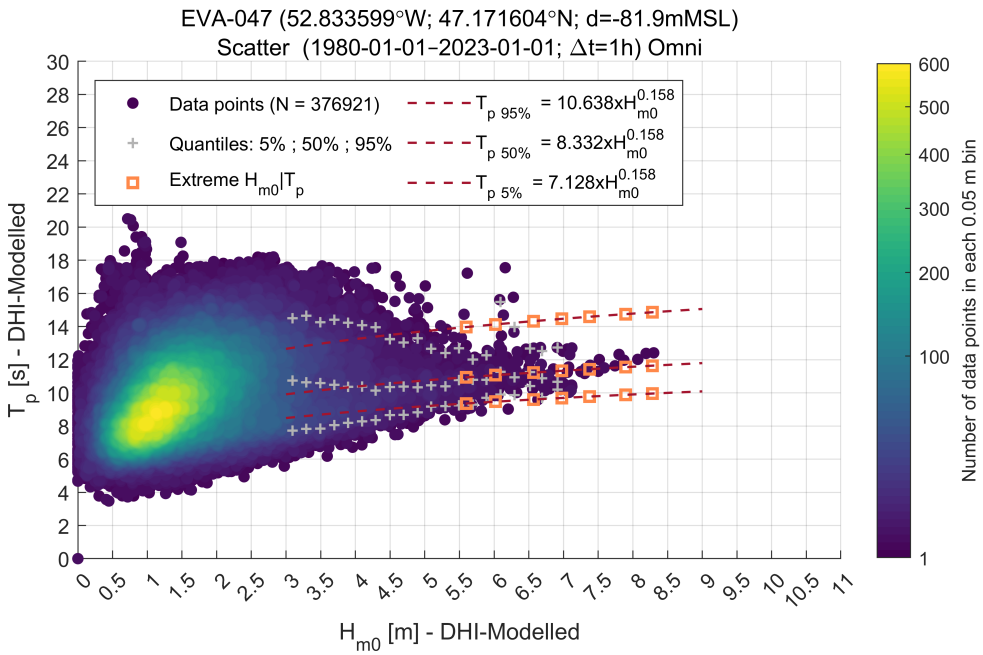


Figure C-297: Scatter plot of Hm0 x Tp at EVA-047 and quantile fit used to derived associated Tp to each extreme Hm0.

EVA-048

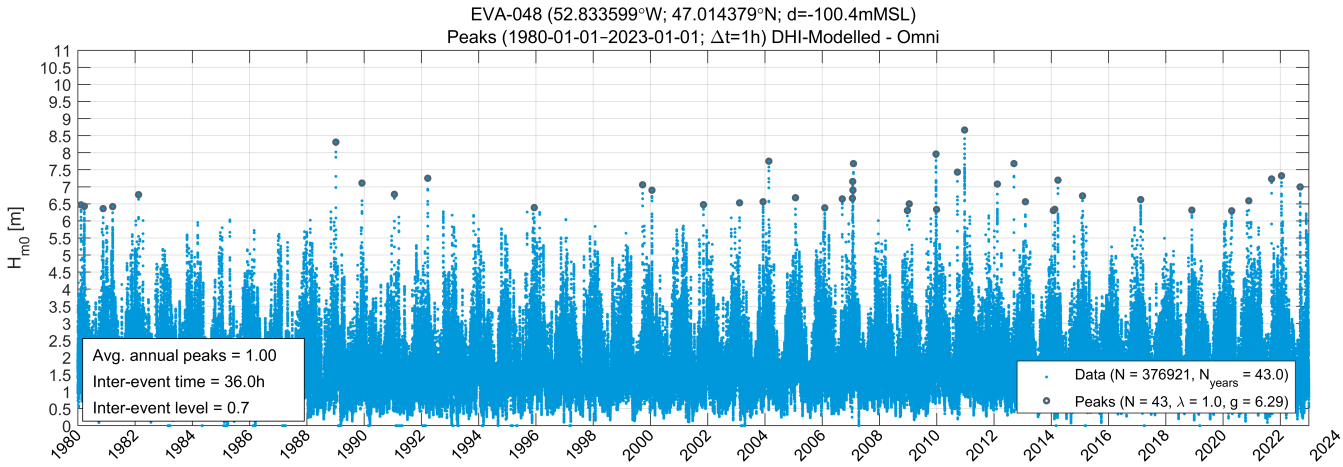


Figure C-298: Time series of significant wave height at EVA-048 and selected peaks.

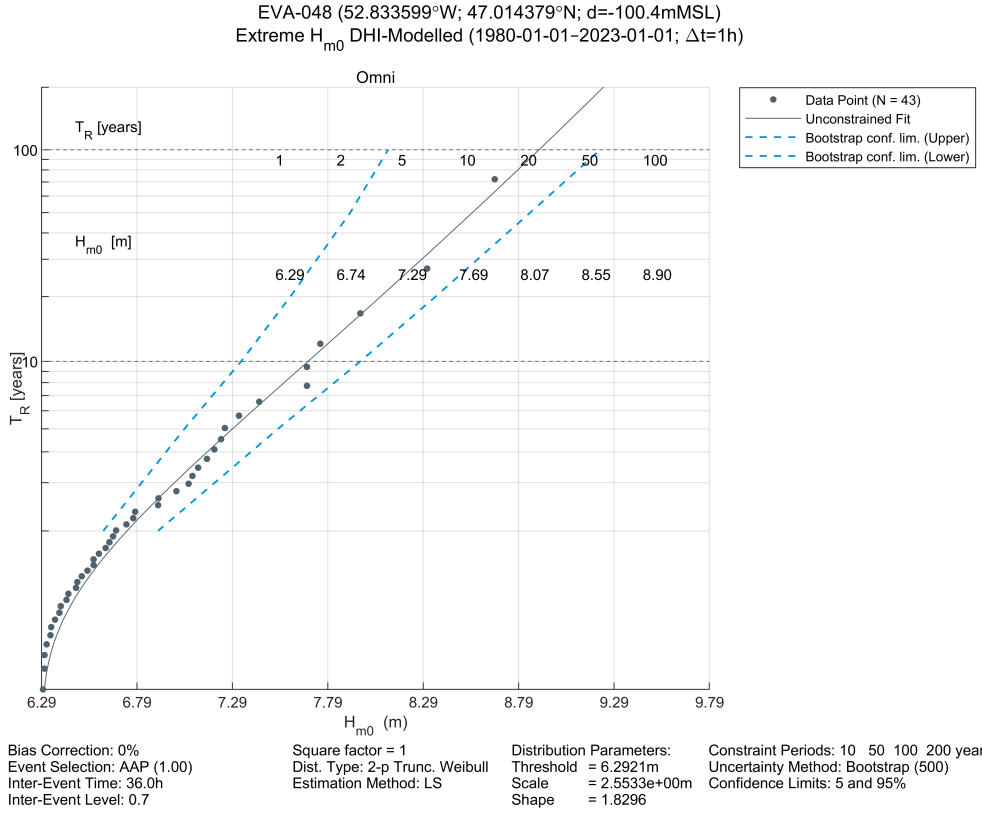


Figure C-299: Extreme value distribution fit at EVA-048.

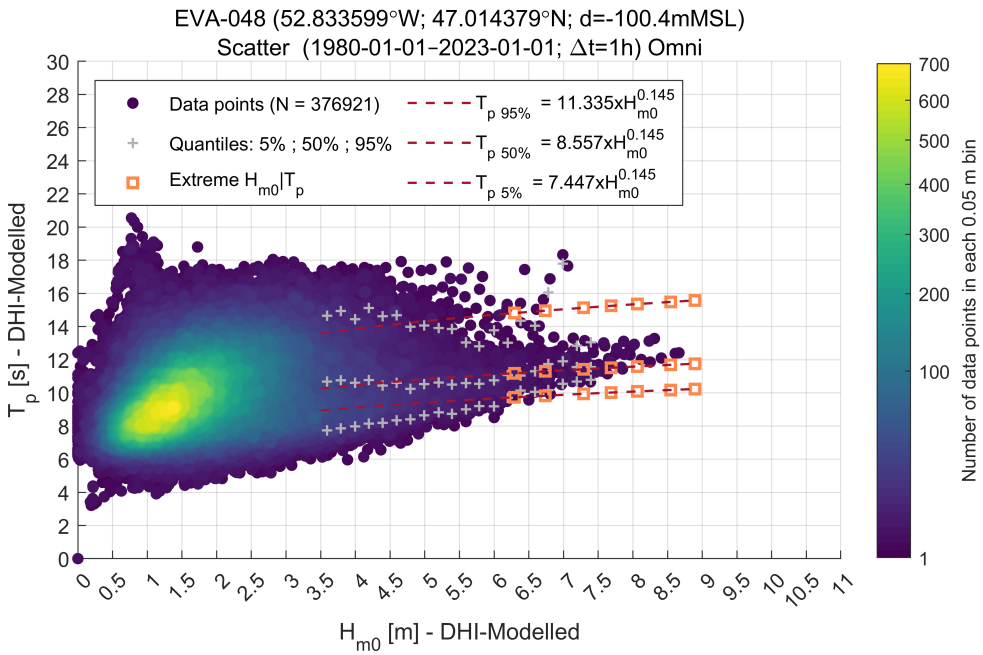


Figure C-300: Scatter plot of Hm0 x Tp at EVA-048 and quantile fit used to derived associated Tp to each extreme Hm0.

EVA-049

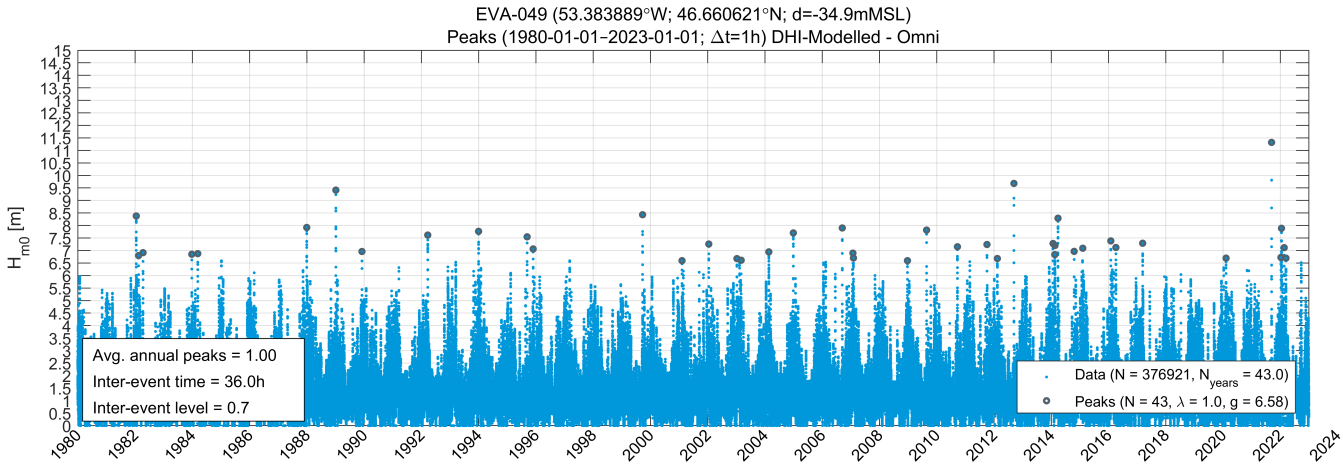


Figure C-301: Time series of significant wave height at EVA-049 and selected peaks.

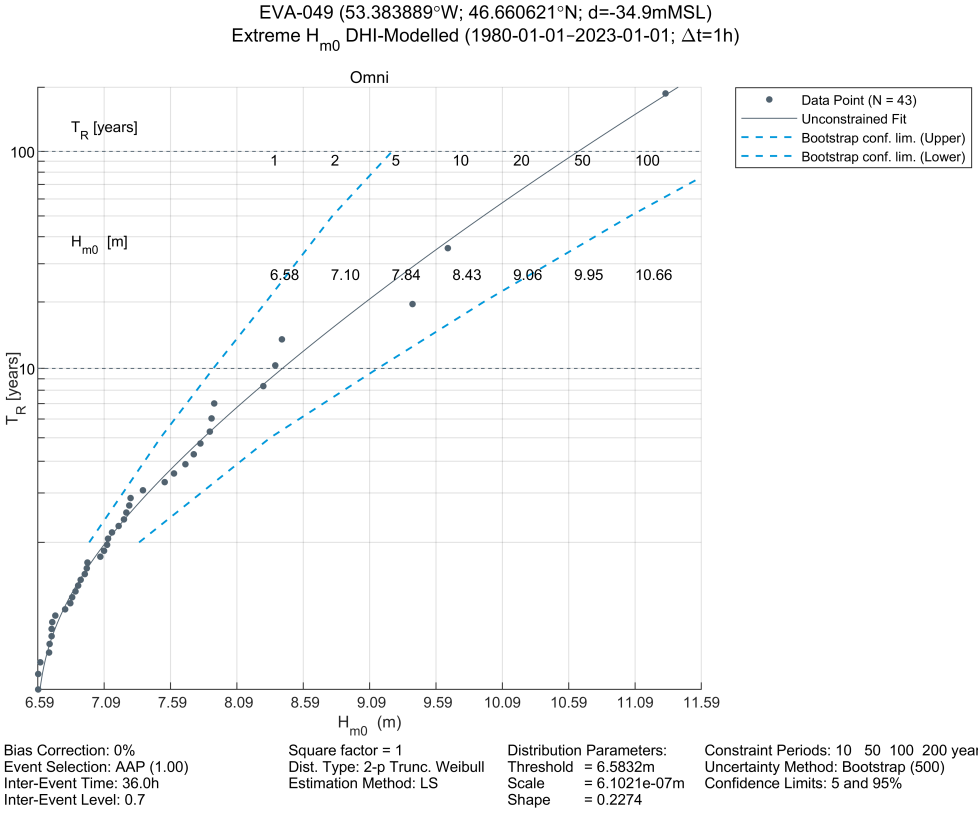


Figure C-302: Extreme value distribution fit at EVA-049.

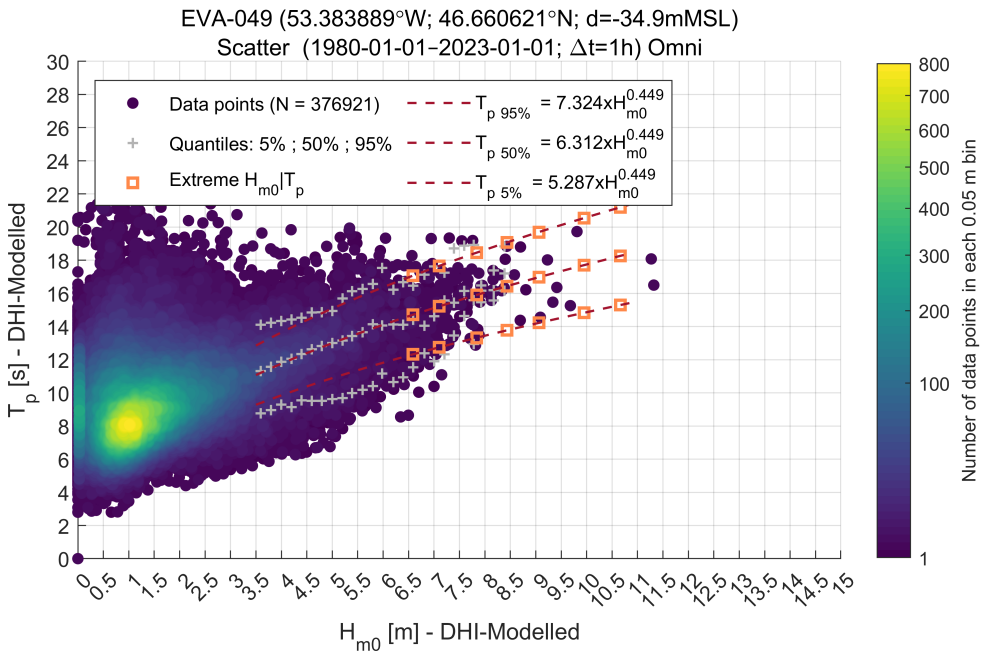


Figure C-303: Scatter plot of Hm0 x Tp at EVA-049 and quantile fit used to derived associated Tp to each extreme Hm0.

EVA-050

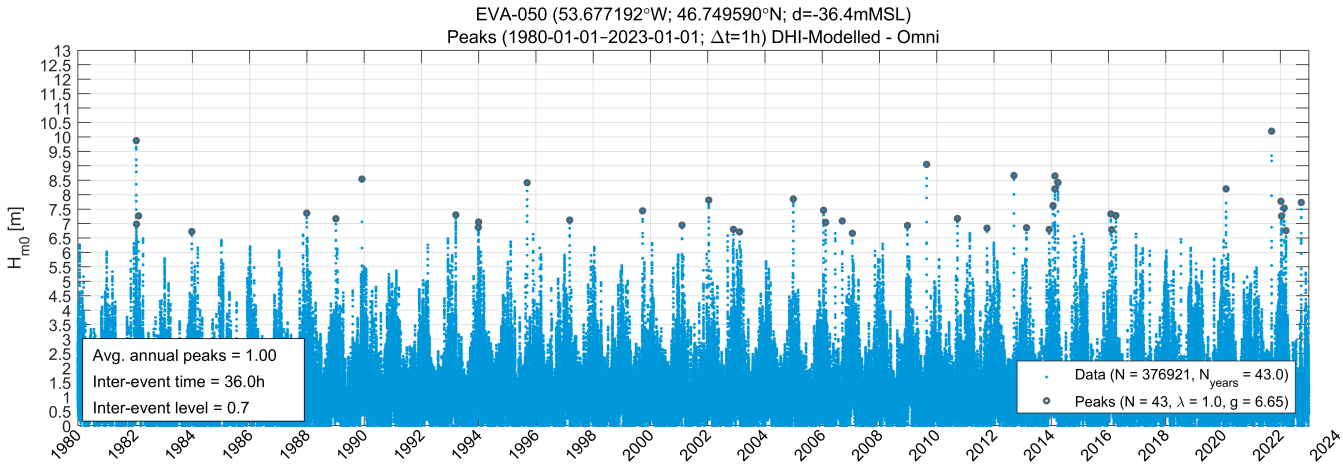


Figure C-304: Time series of significant wave height at EVA-050 and selected peaks.

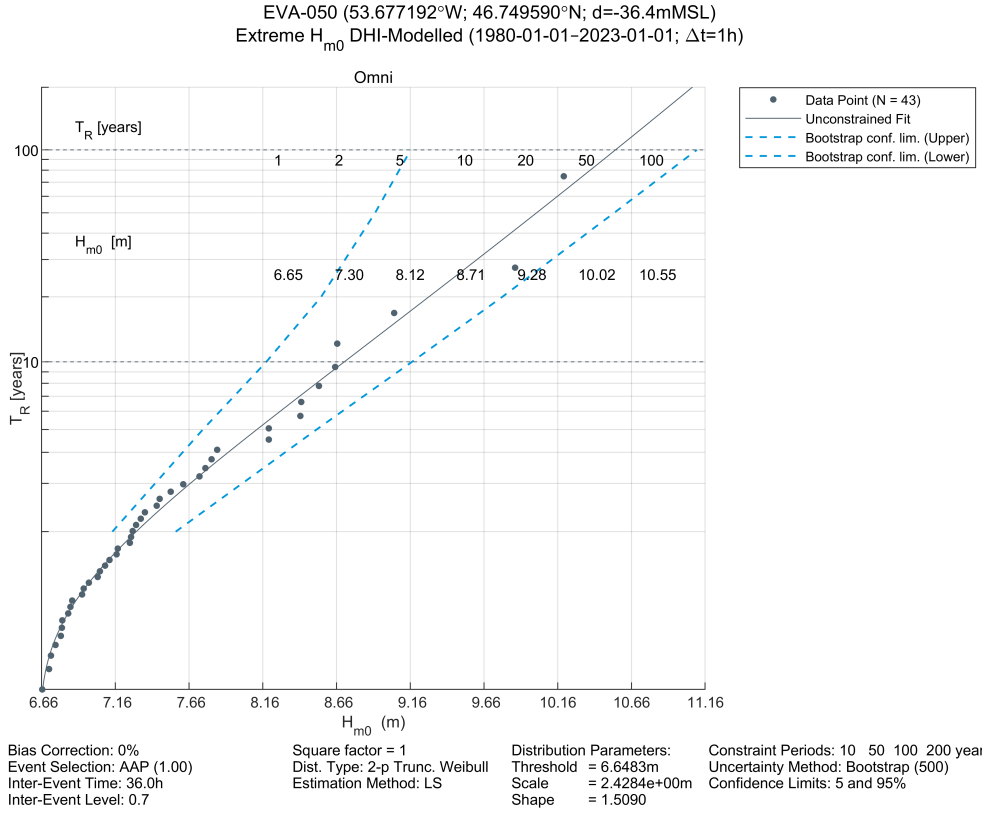


Figure C-305: Extreme value distribution fit at EVA-050.

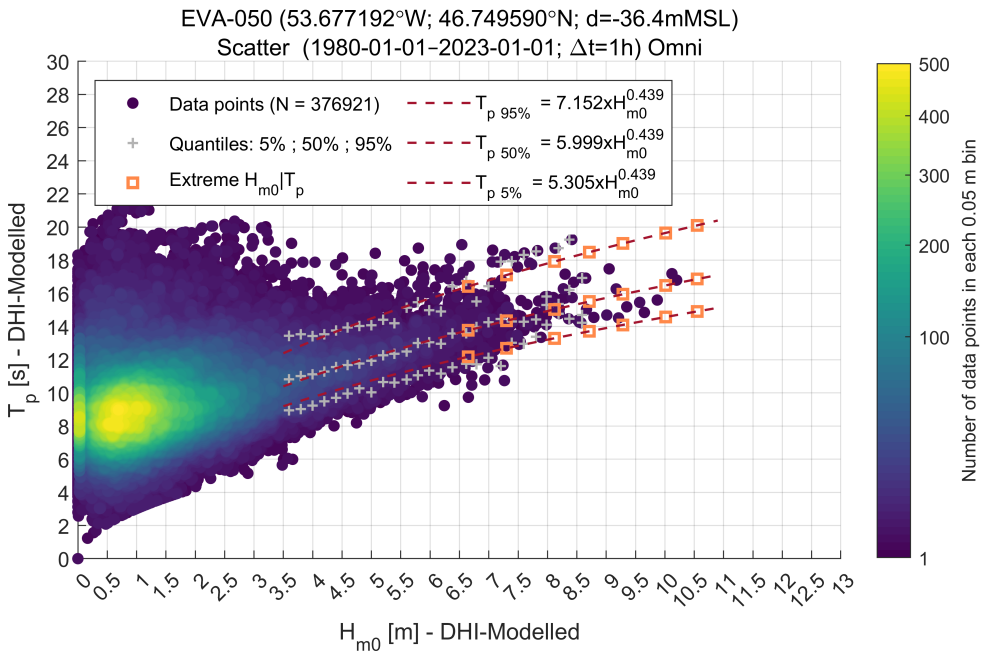


Figure C-306: Scatter plot of Hm0 x Tp at EVA-050 and quantile fit used to derived associated Tp to each extreme Hm0.

EVA-051

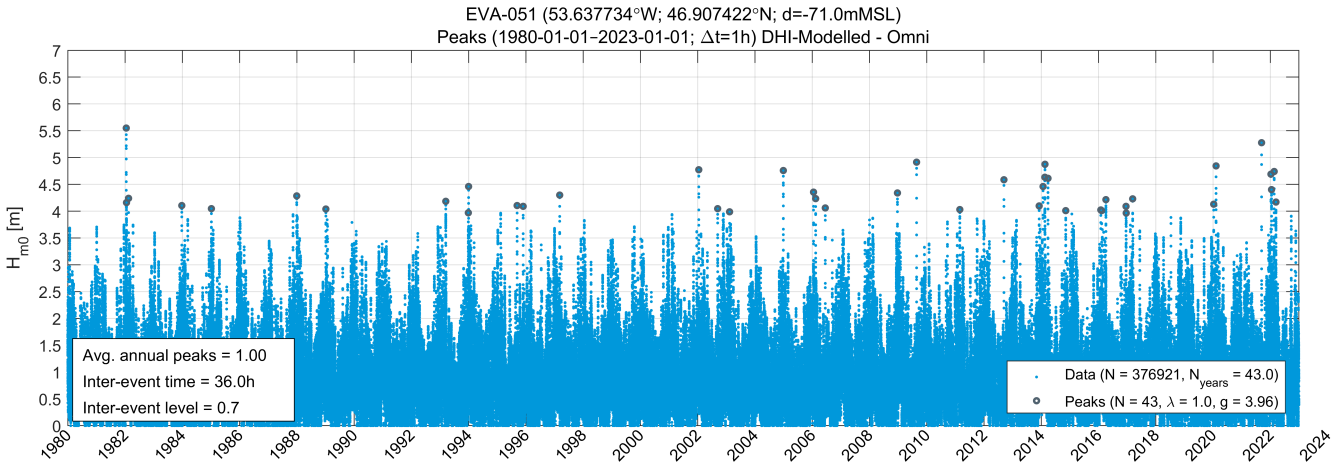


Figure C-307: Time series of significant wave height at EVA-051 and selected peaks.

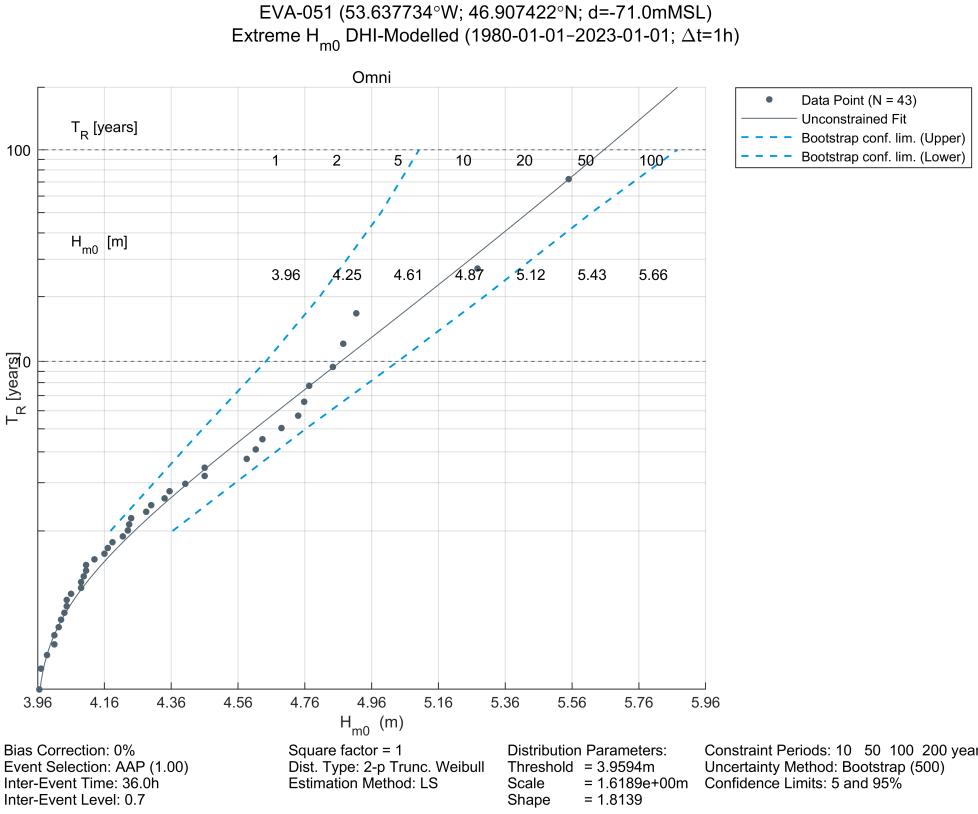


Figure C-308: Extreme value distribution fit at EVA-051.

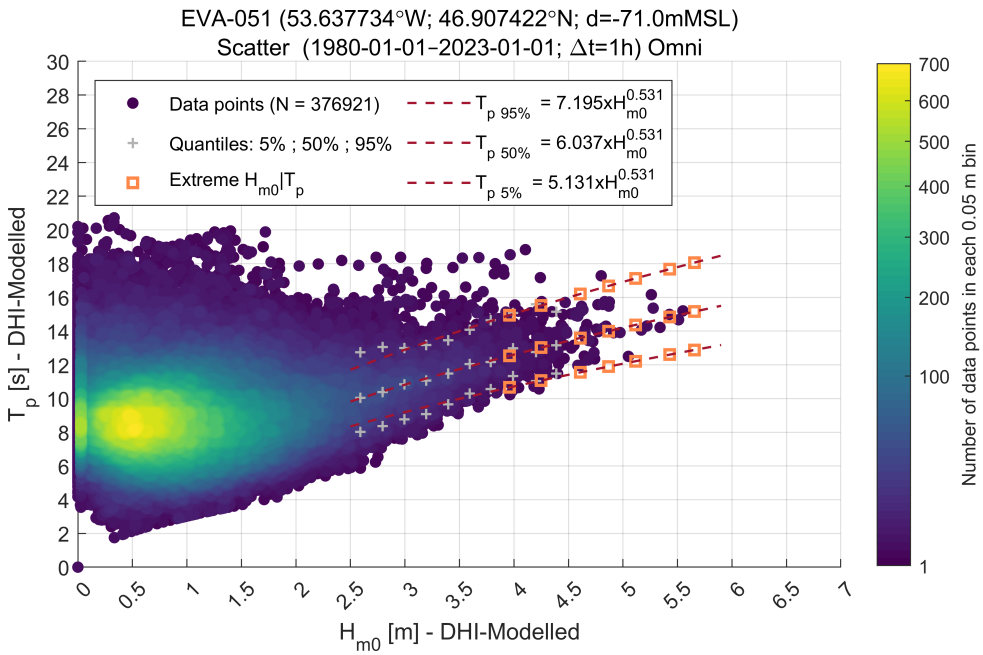


Figure C-309: Scatter plot of Hm0 x Tp at EVA-051 and quantile fit used to derived associated Tp to each extreme Hm0.

EVA-052

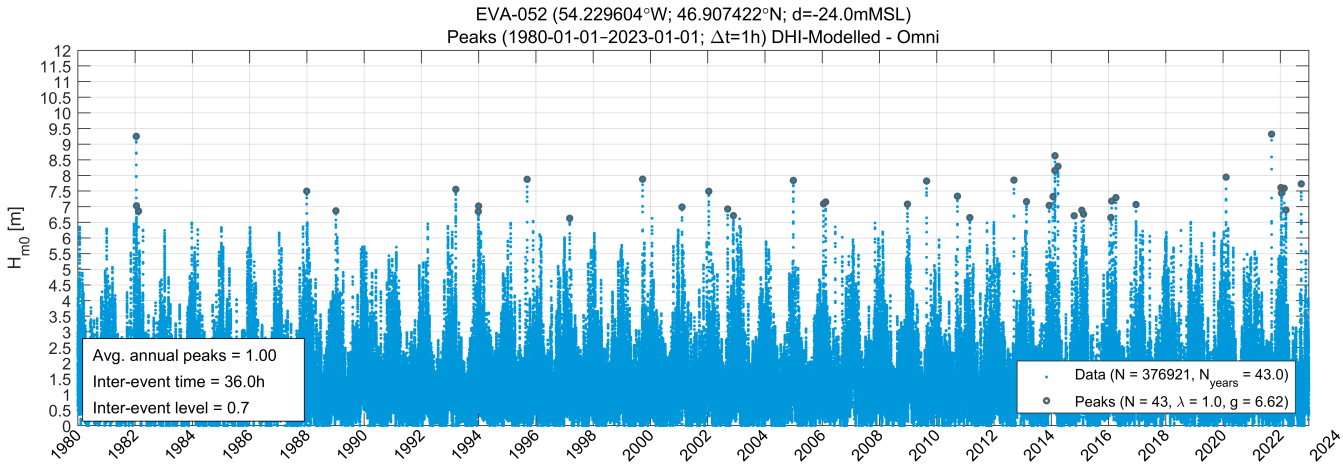


Figure C-310: Time series of significant wave height at EVA-052 and selected peaks.

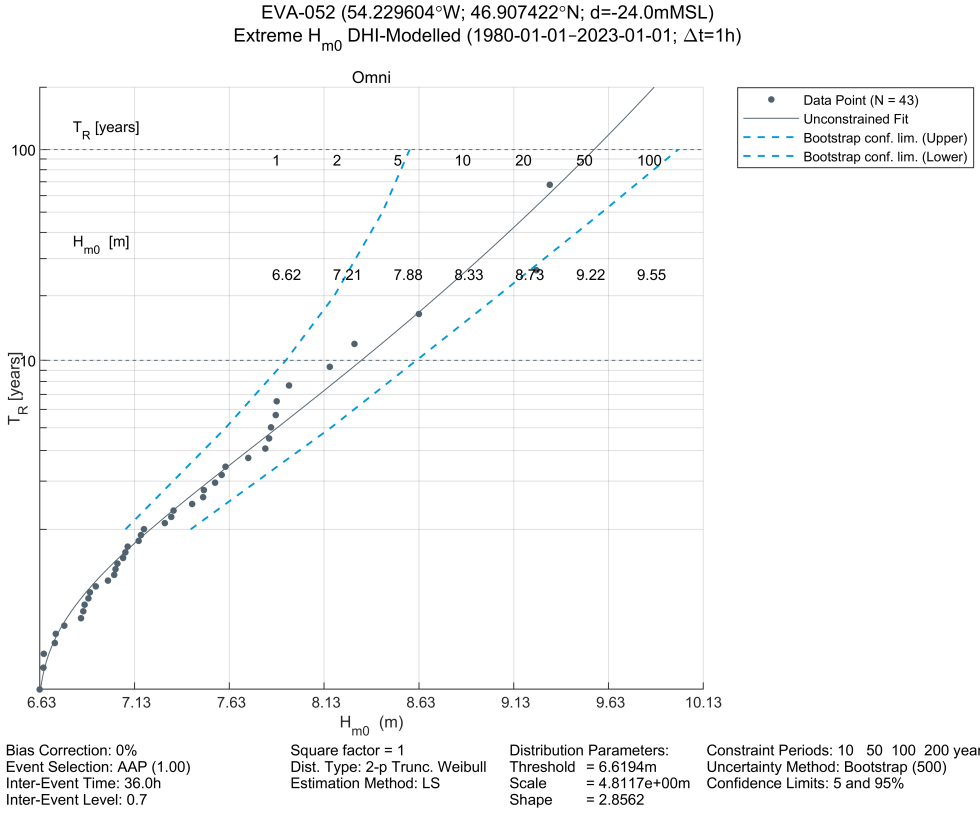


Figure C-311: Extreme value distribution fit at EVA-052.

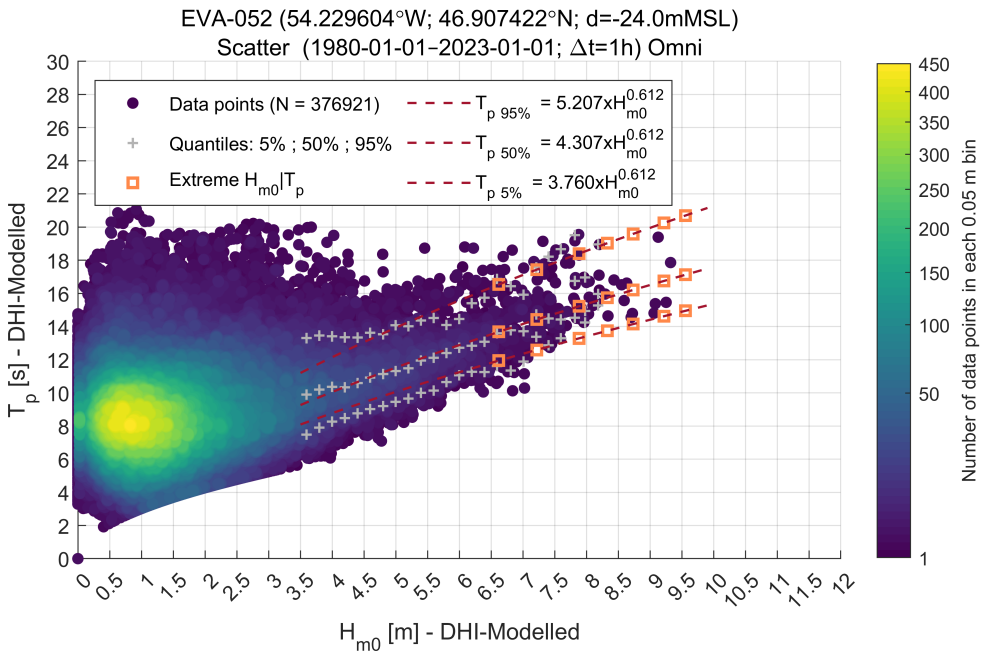


Figure C-312: Scatter plot of Hm0 x Tp at EVA-052 and quantile fit used to derived associated Tp to each extreme Hm0.

EVA-053

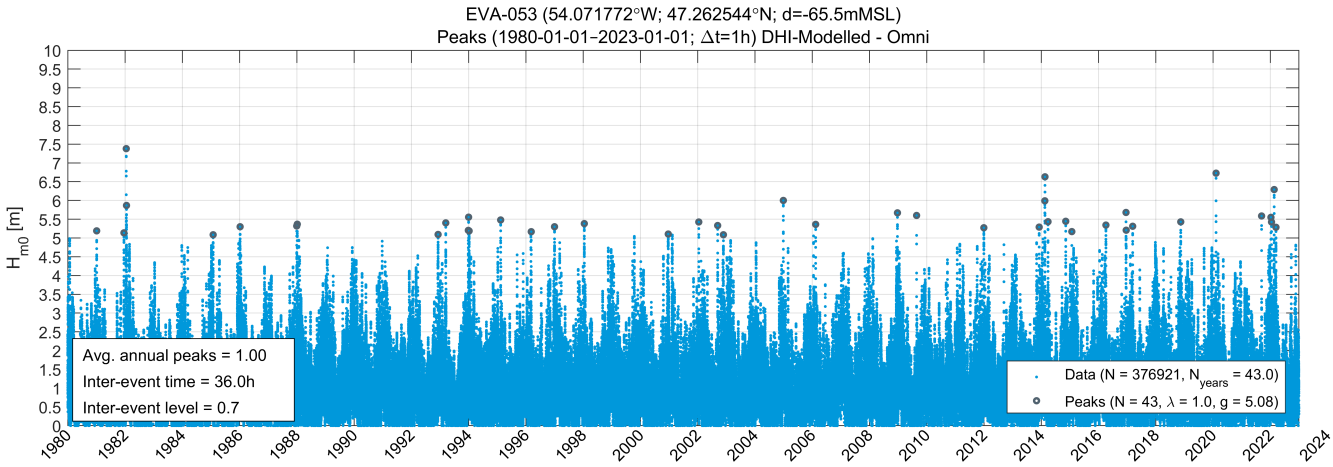


Figure C-313: Time series of significant wave height at EVA-053 and selected peaks.

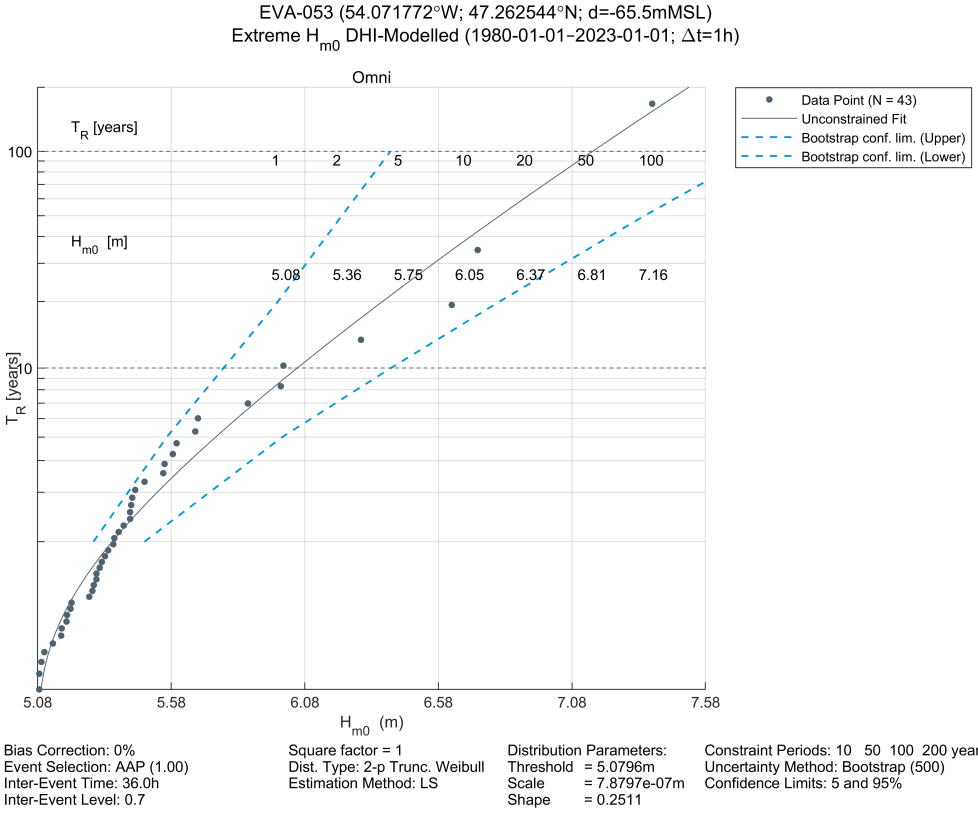


Figure C-314: Extreme value distribution fit at EVA-053.

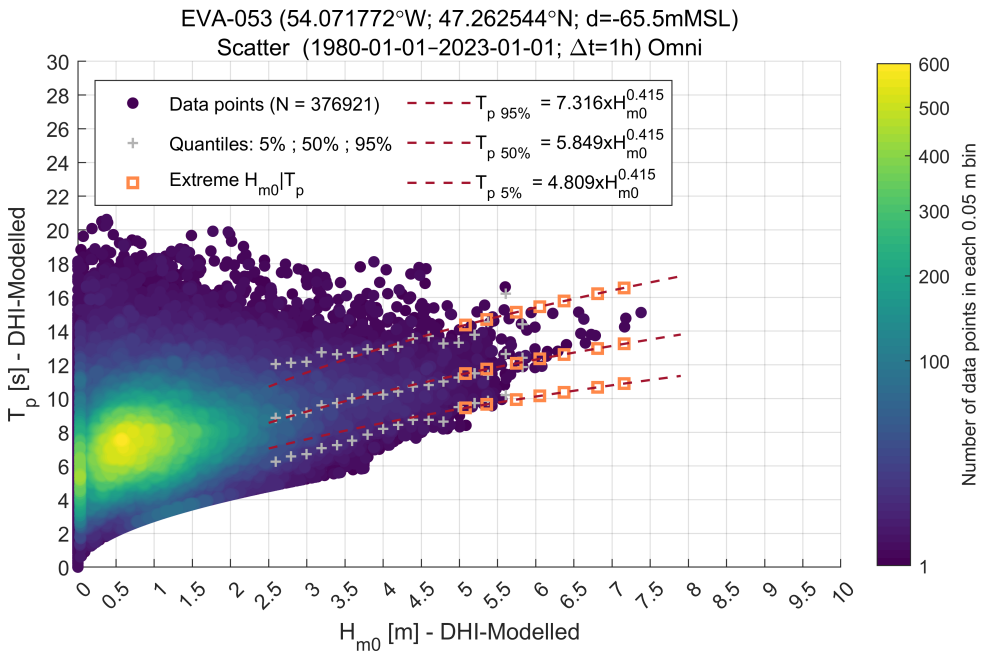


Figure C-315: Scatter plot of Hm0 x Tp at EVA-053 and quantile fit used to derived associated Tp to each extreme Hm0.

EVA-054

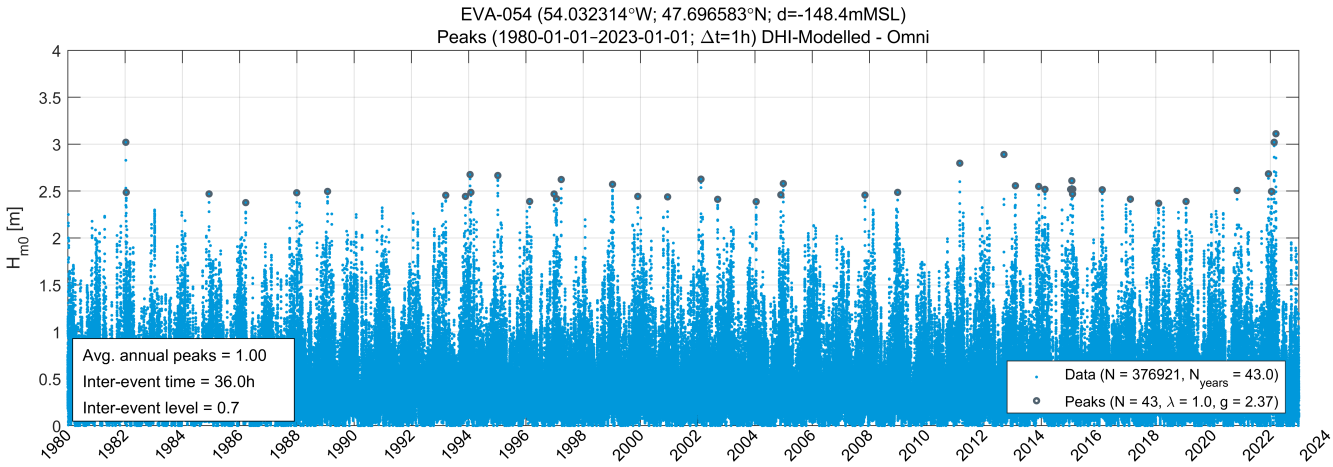


Figure C-316: Time series of significant wave height at EVA-054 and selected peaks.

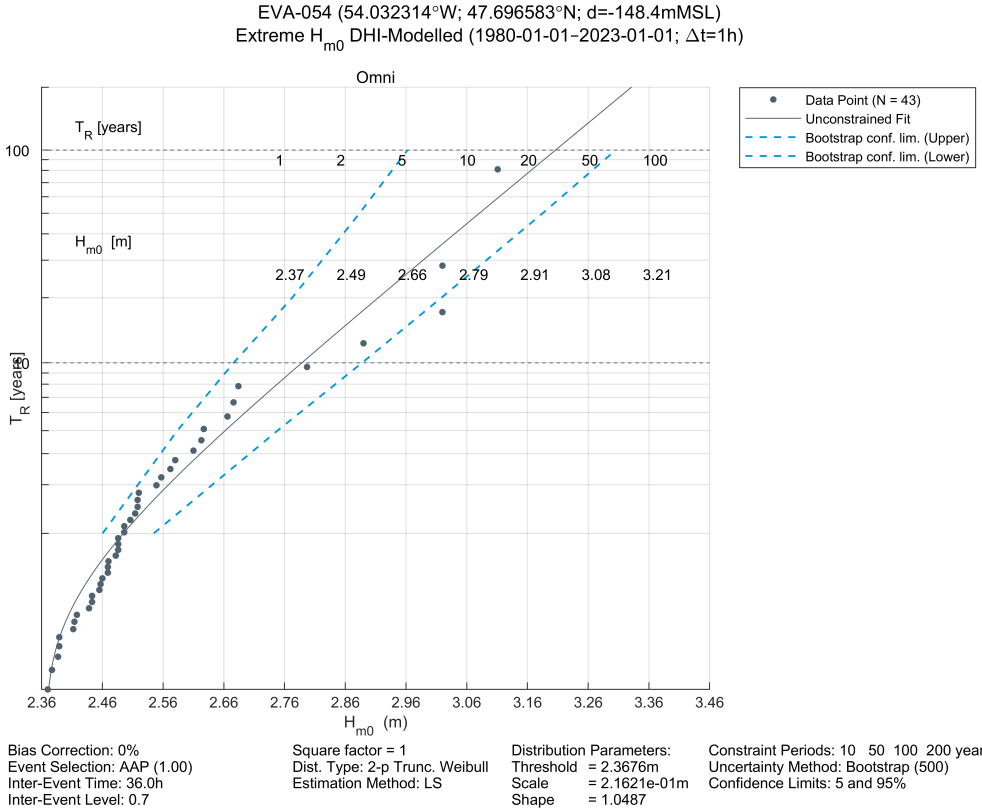


Figure C-317: Extreme value distribution fit at EVA-054.

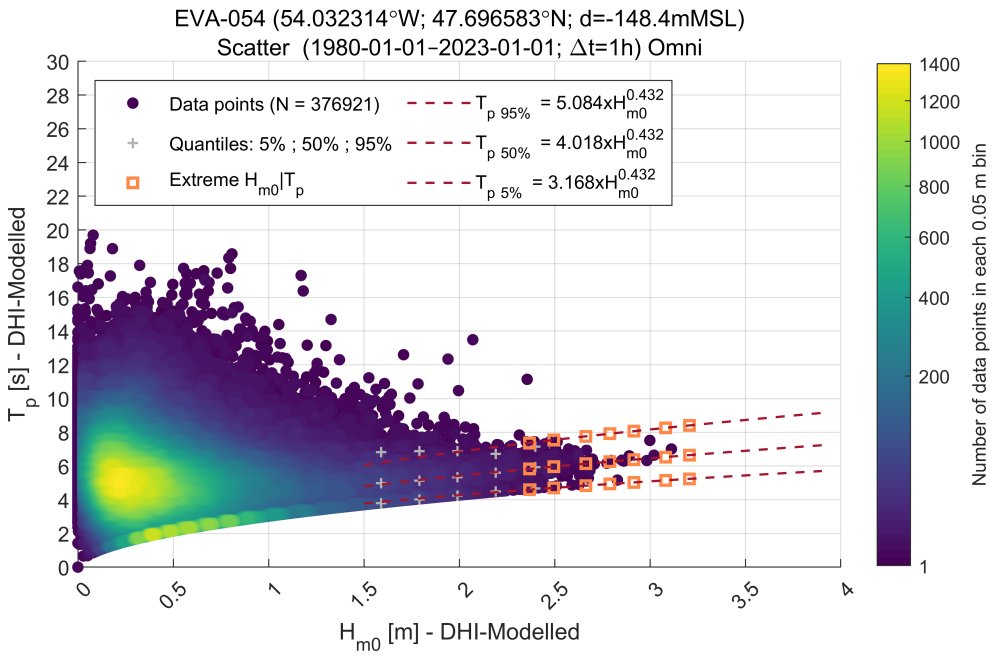


Figure C-318: Scatter plot of Hm0 x Tp at EVA-054 and quantile fit used to derived associated Tp to each extreme Hm0.

EVA-055

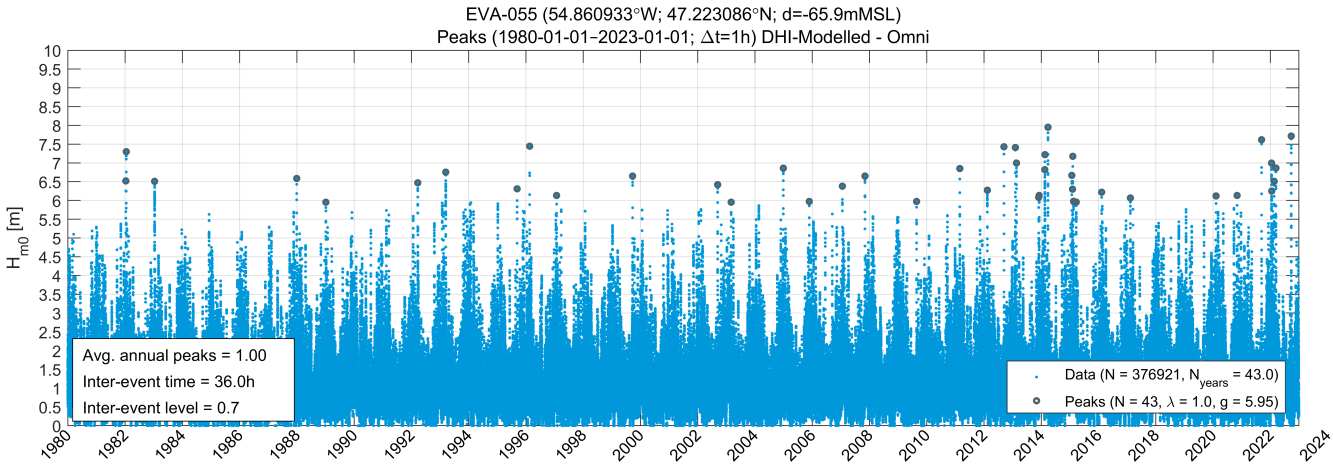


Figure C-319: Time series of significant wave height at EVA-055 and selected peaks.

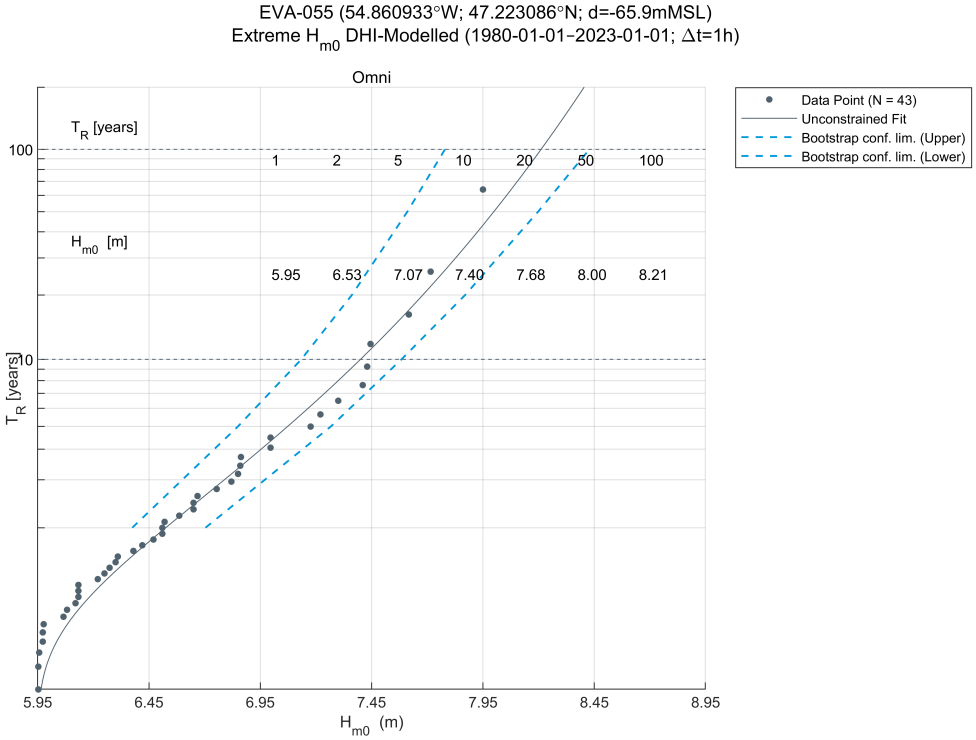


Figure C-320: Extreme value distribution fit at EVA-055.

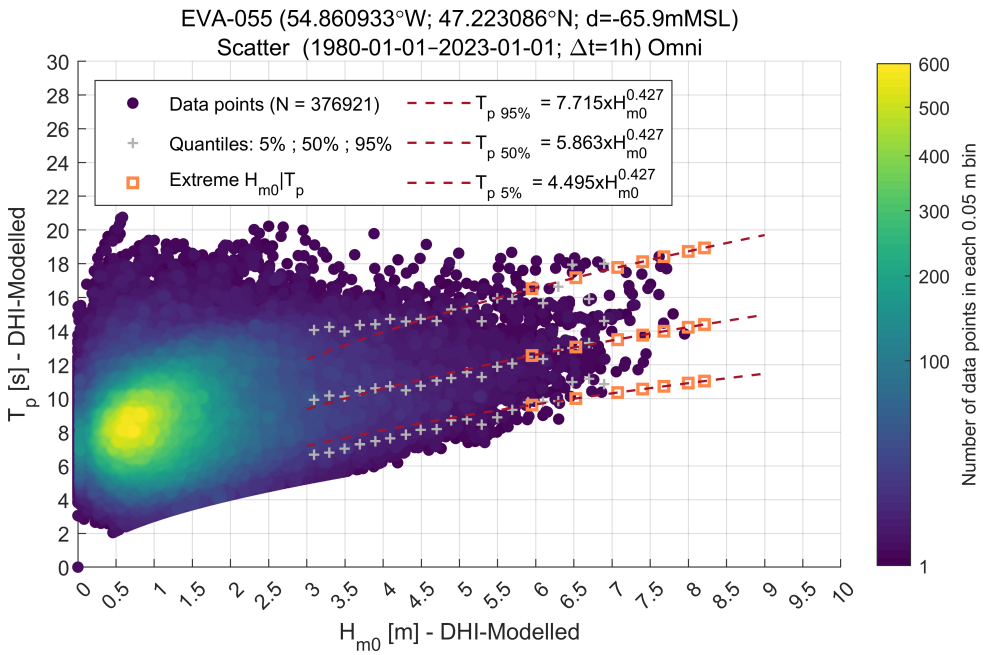


Figure C-321: Scatter plot of Hm0 x Tp at EVA-055 and quantile fit used to derived associated Tp to each extreme Hm0.

EVA-056

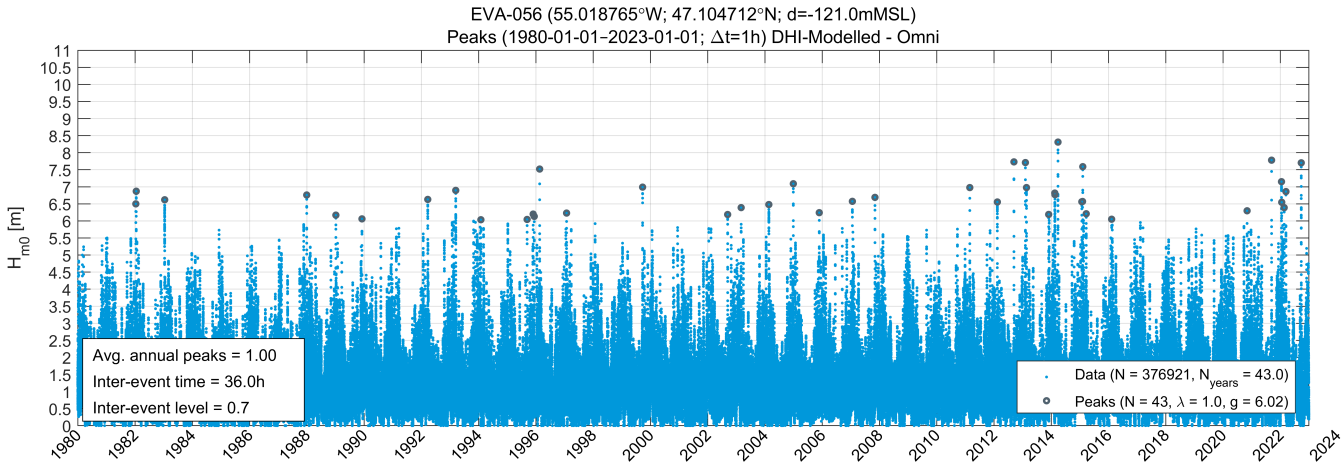


Figure C-322: Time series of significant wave height at EVA-056 and selected peaks.

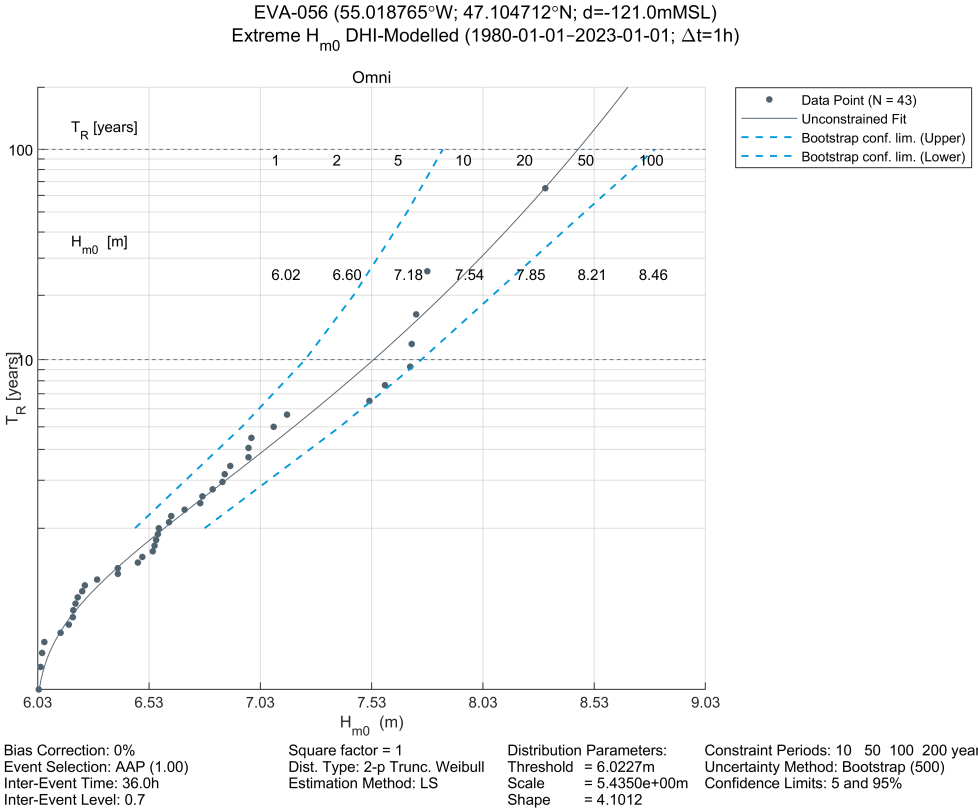


Figure C-323: Extreme value distribution fit at EVA-056.

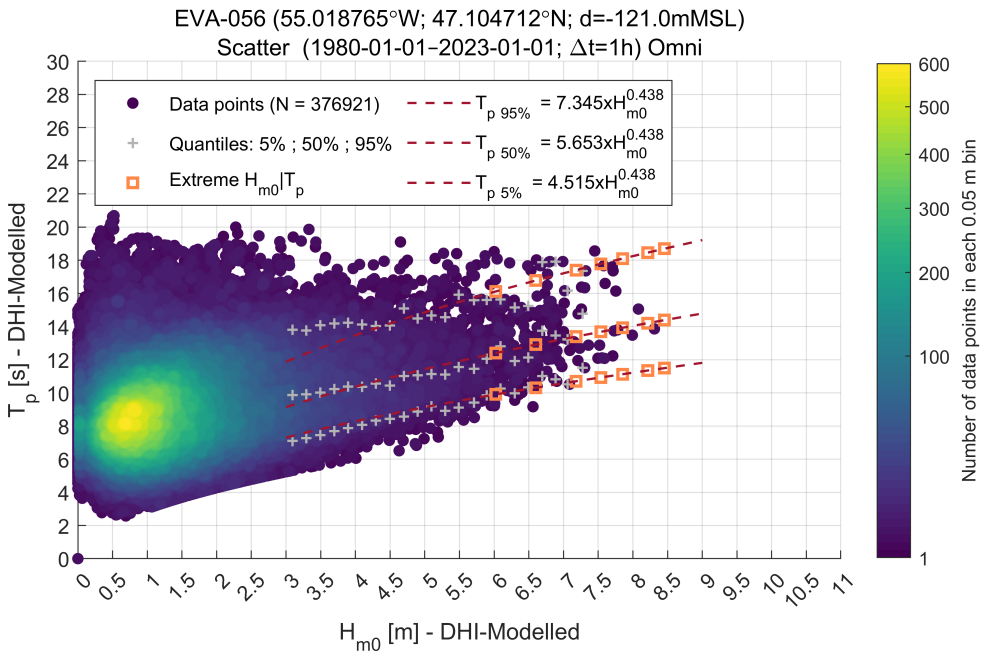


Figure C-324: Scatter plot of Hm0 x Tp at EVA-056 and quantile fit used to derived associated Tp to each extreme Hm0.

EVA-057

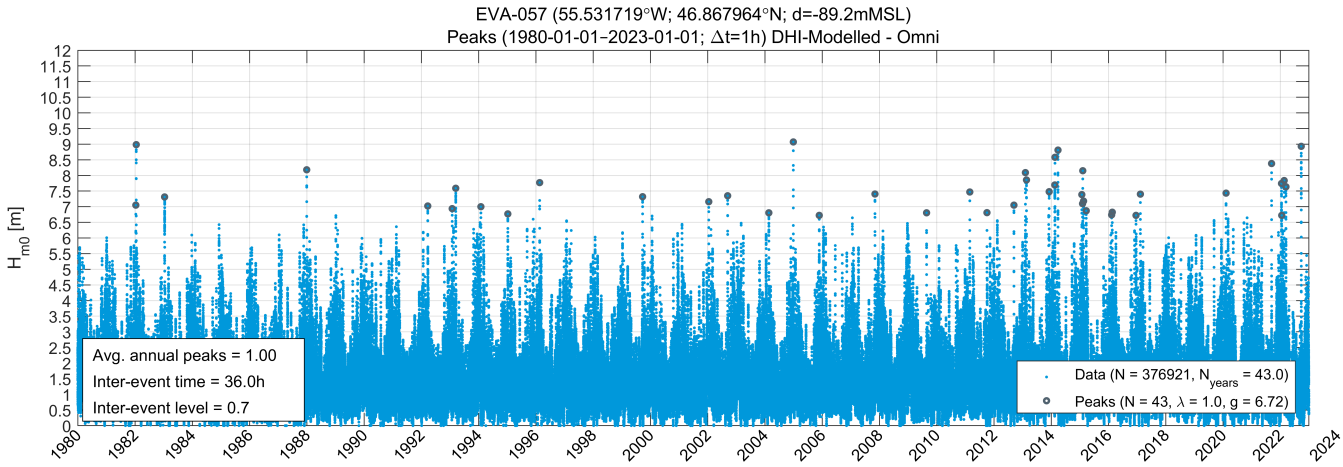


Figure C-325: Time series of significant wave height at EVA-057 and selected peaks.

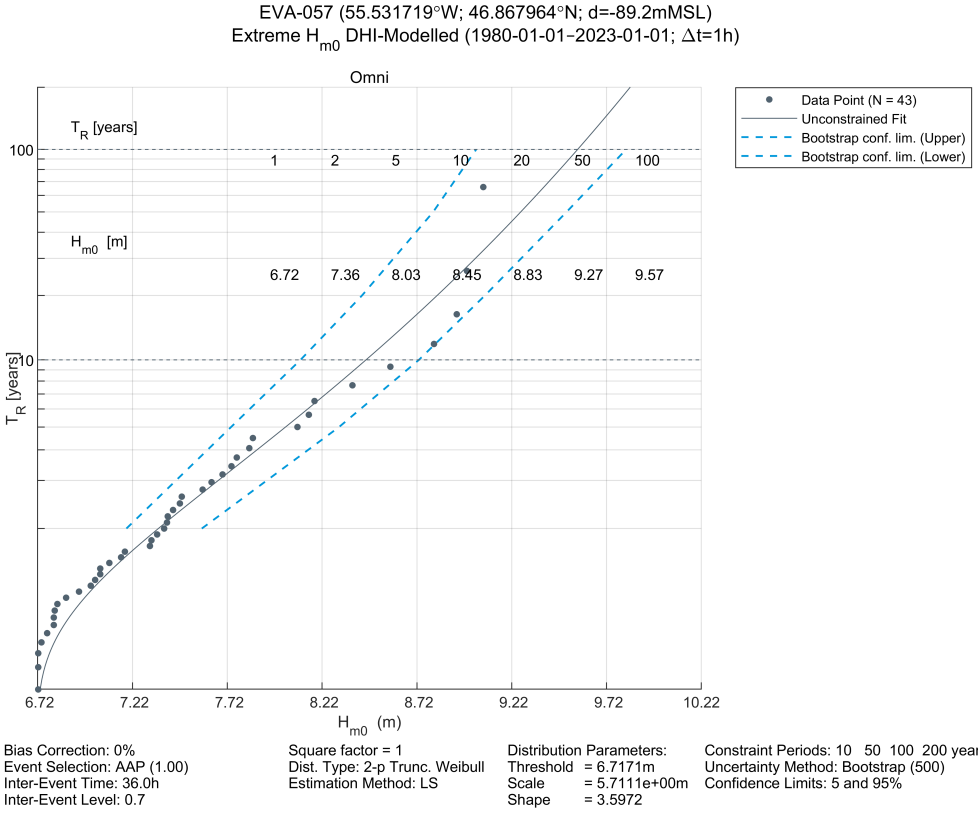


Figure C-326: Extreme value distribution fit at EVA-057.

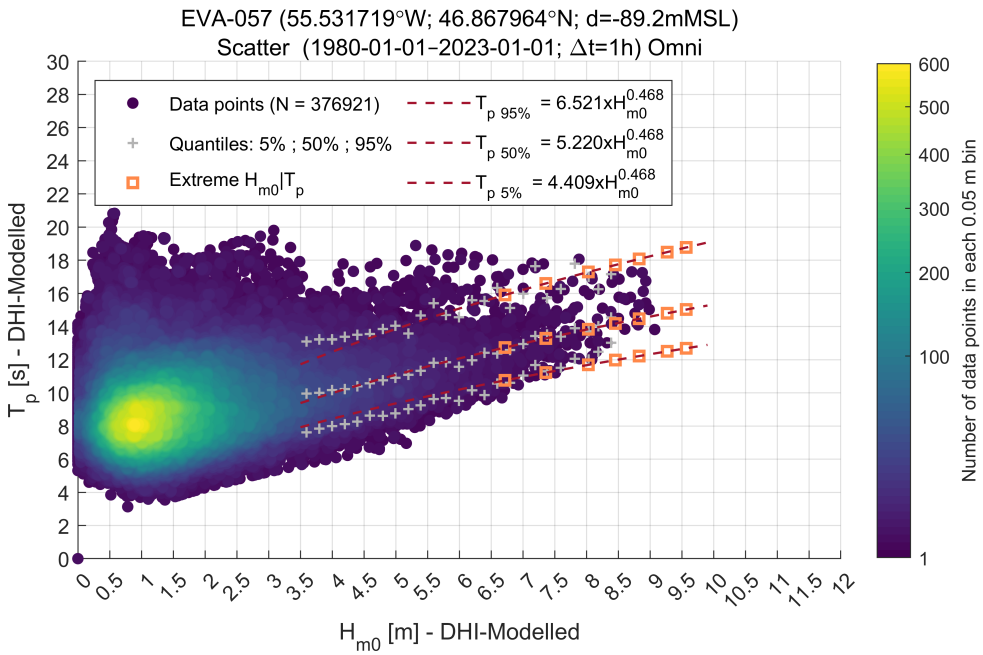


Figure C-327: Scatter plot of Hm0 x Tp at EVA-057 and quantile fit used to derived associated Tp to each extreme Hm0.

EVA-058

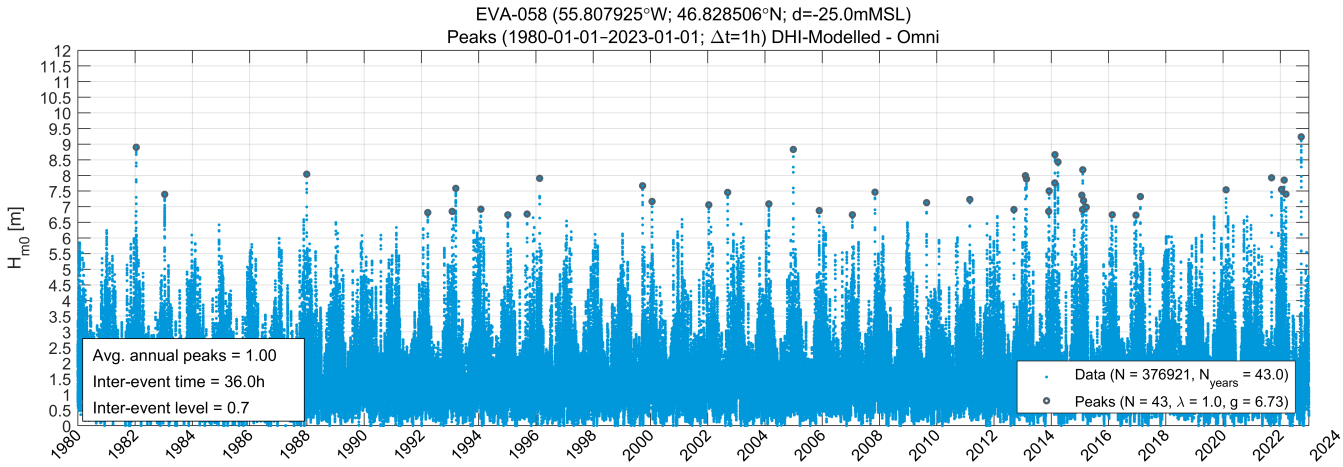


Figure C-328: Time series of significant wave height at EVA-058 and selected peaks.

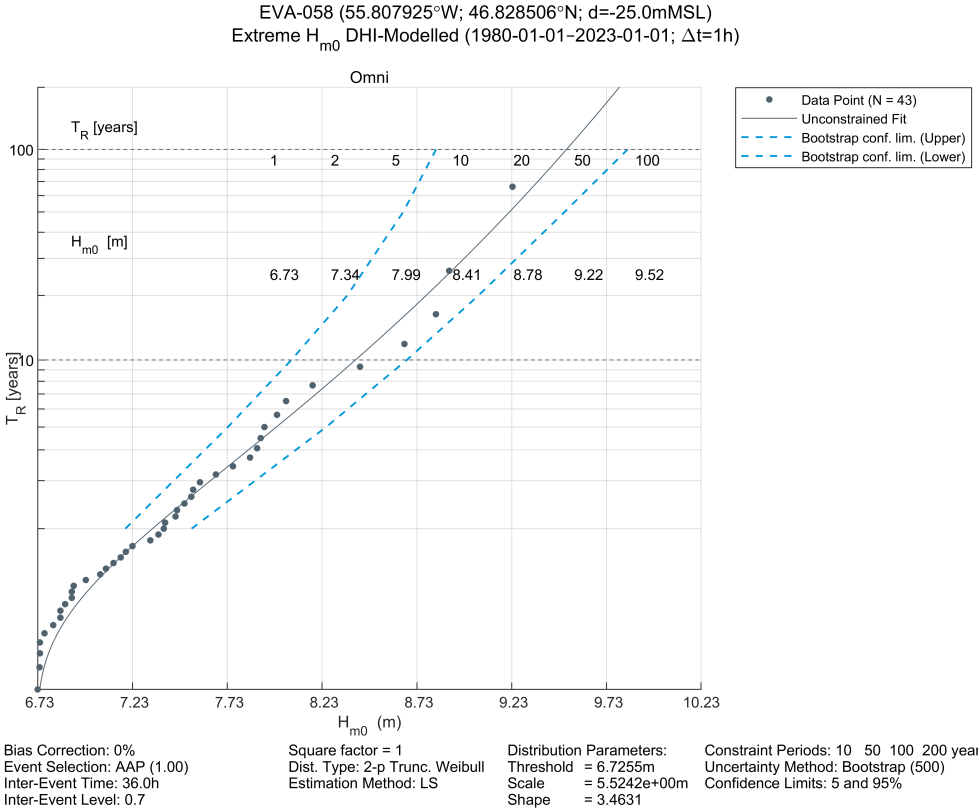


Figure C-329: Extreme value distribution fit at EVA-058.

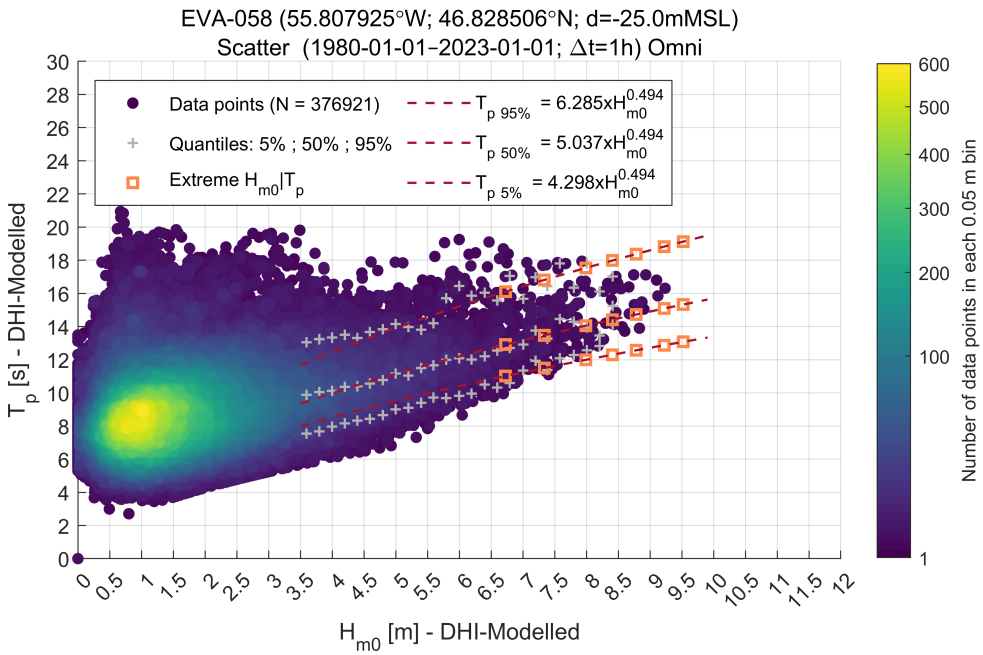


Figure C-330: Scatter plot of Hm0 x Tp at EVA-058 and quantile fit used to derived associated Tp to each extreme Hm0.

EVA-059

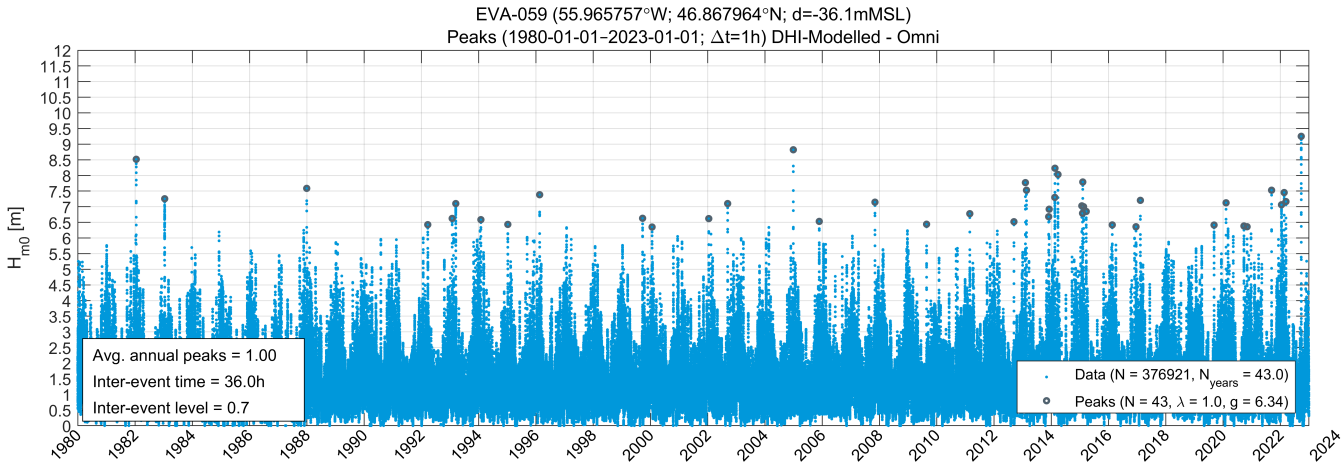


Figure C-331: Time series of significant wave height at EVA-059 and selected peaks.

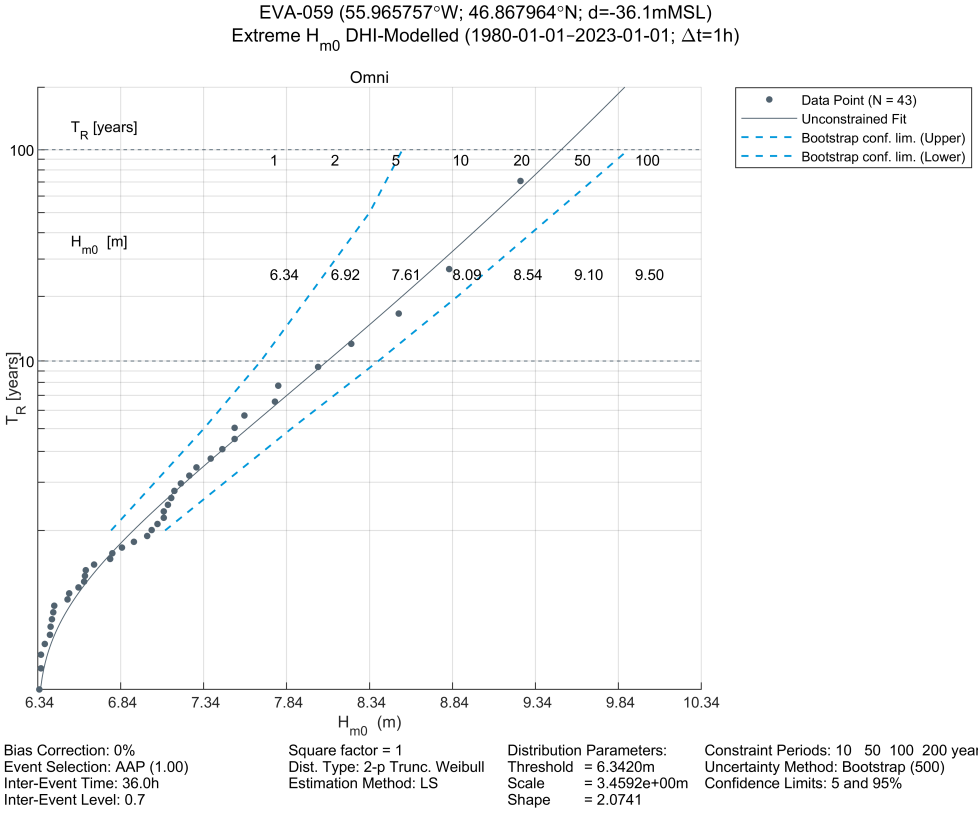


Figure C-332: Extreme value distribution fit at EVA-059.

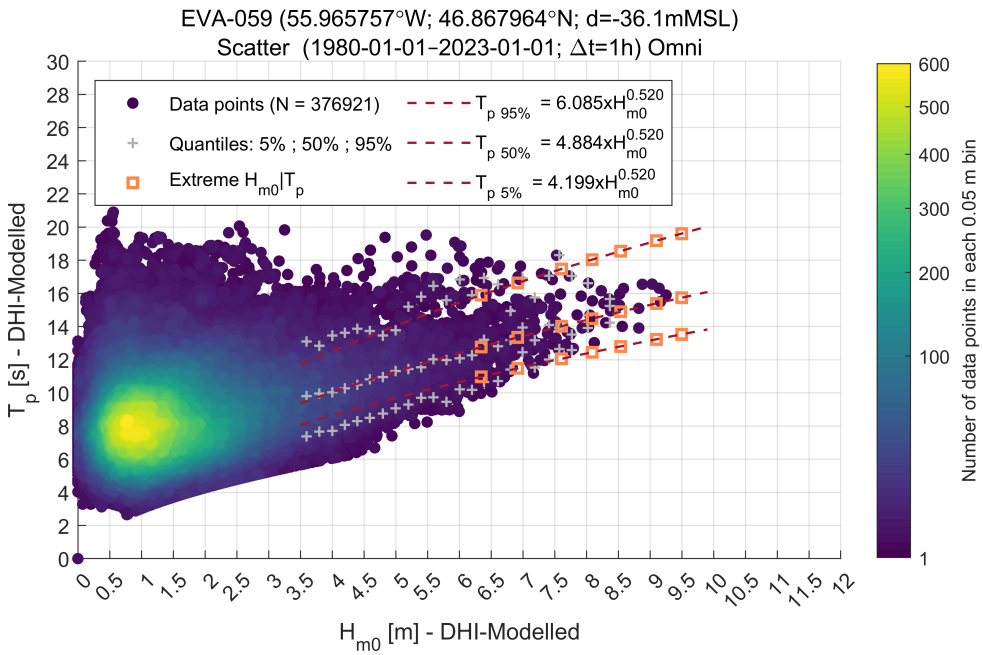


Figure C-333: Scatter plot of Hm0 x Tp at EVA-059 and quantile fit used to derived associated Tp to each extreme Hm0.

EVA-060

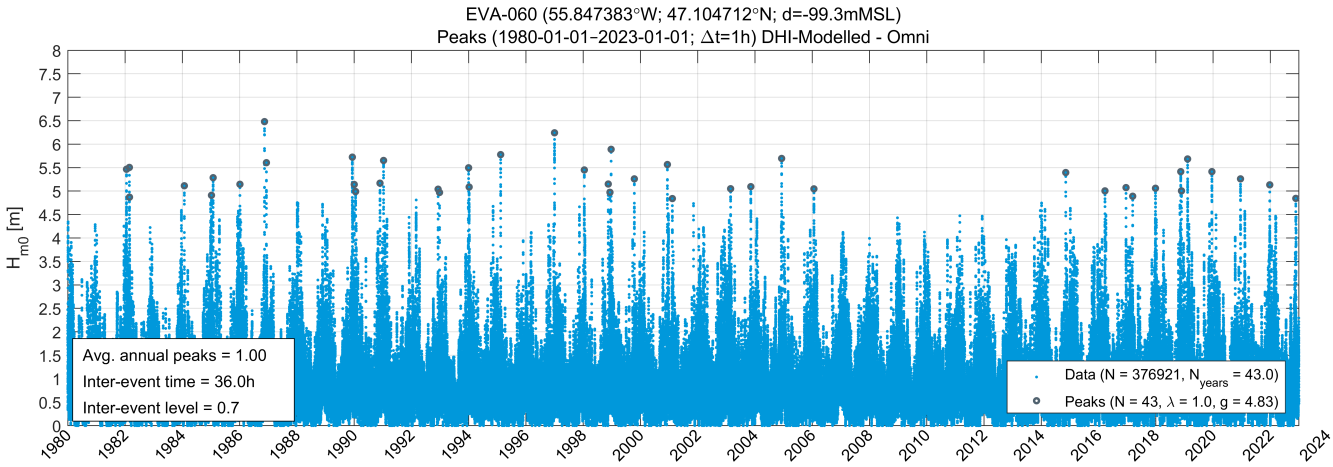


Figure C-334: Time series of significant wave height at EVA-060 and selected peaks.

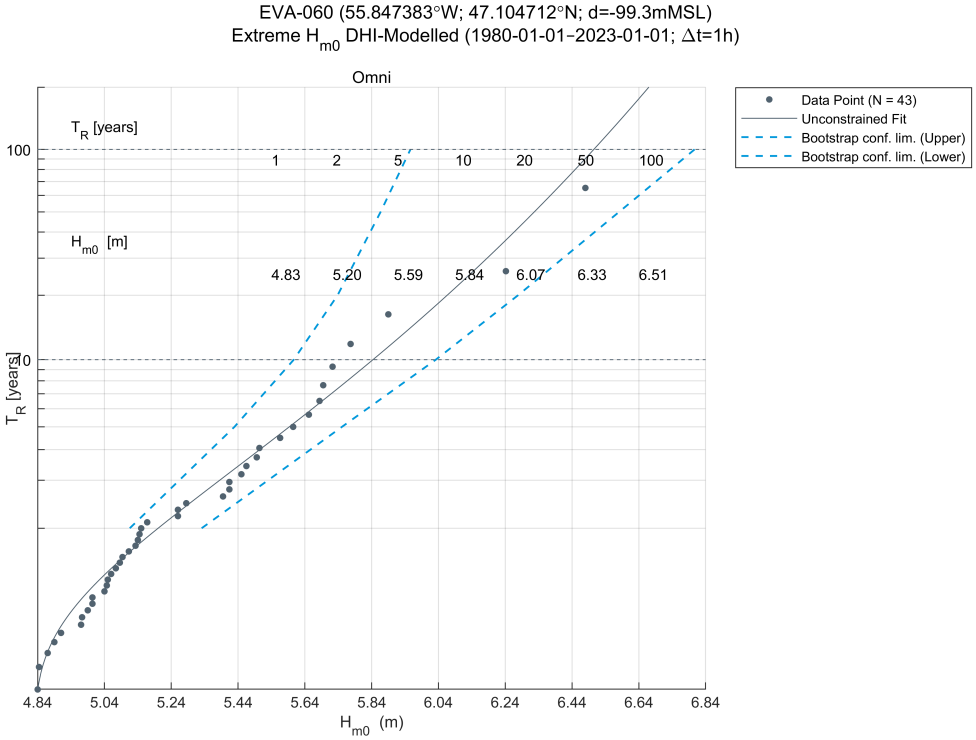


Figure C-335: Extreme value distribution fit at EVA-060.

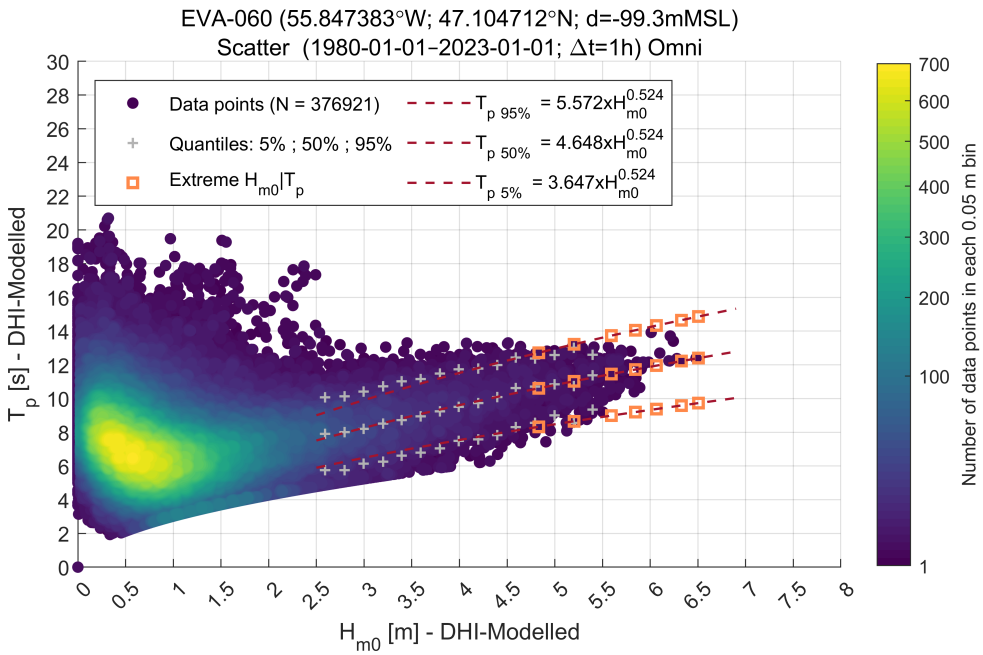


Figure C-336: Scatter plot of Hm0 x Tp at EVA-060 and quantile fit used to derived associated Tp to each extreme Hm0.

EVA-061

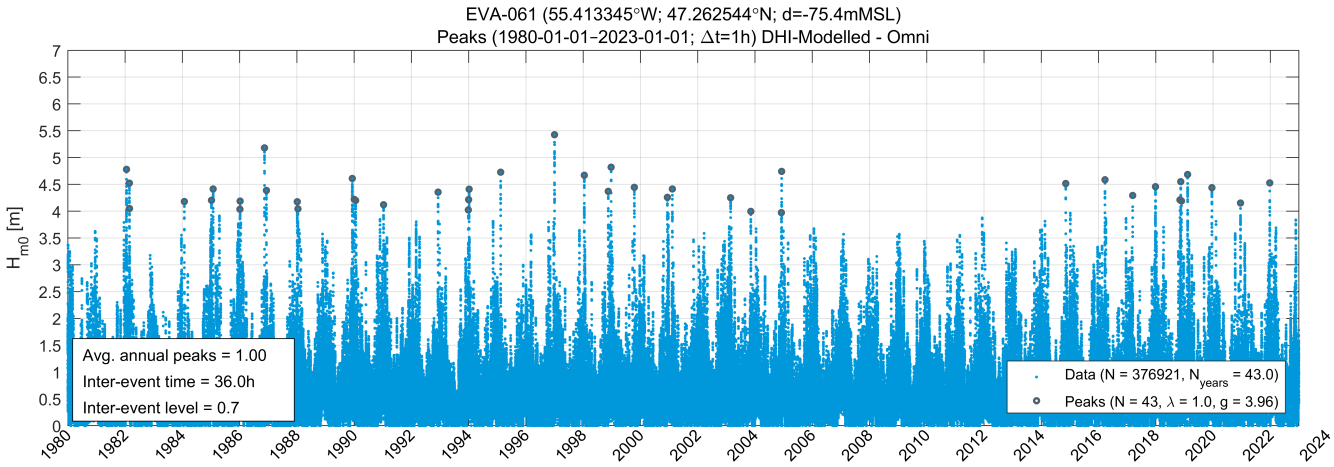


Figure C-337: Time series of significant wave height at EVA-061 and selected peaks.

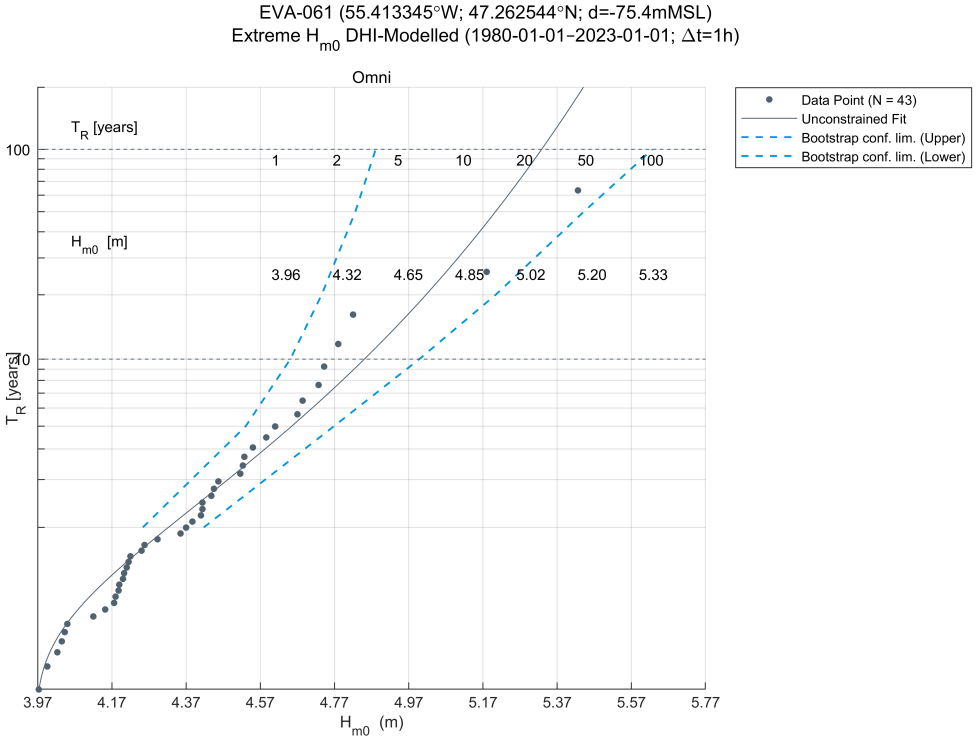


Figure C-338: Extreme value distribution fit at EVA-061.

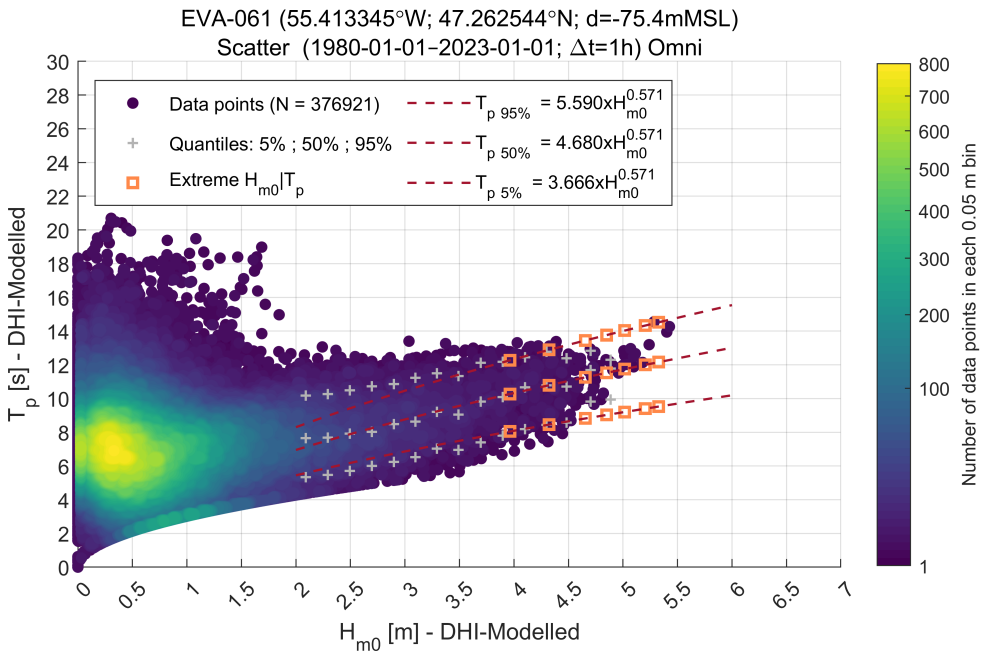


Figure C-339: Scatter plot of Hm0 x Tp at EVA-061 and quantile fit used to derived associated Tp to each extreme Hm0.

EVA-062

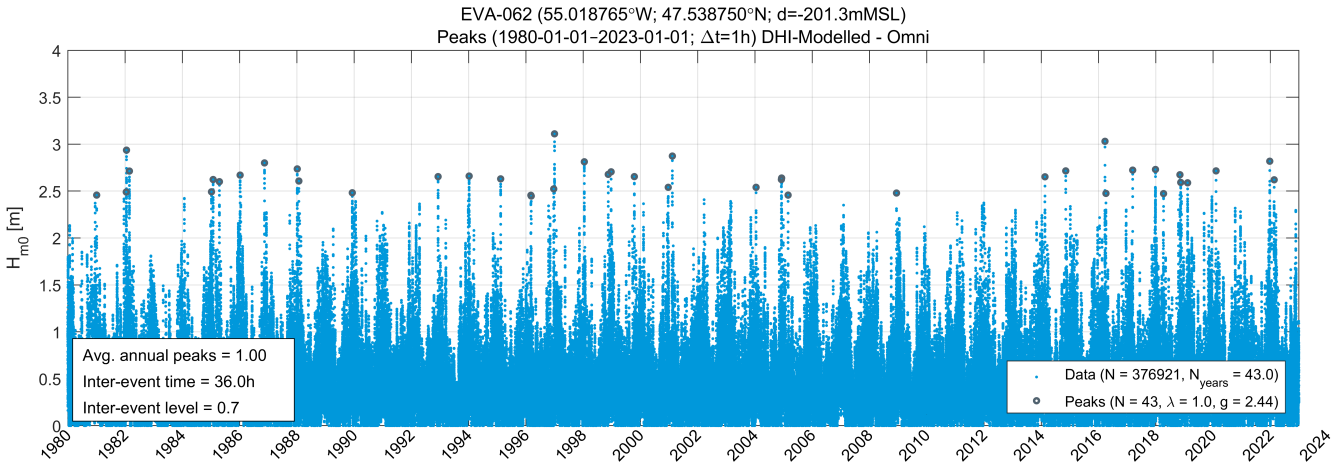


Figure C-340: Time series of significant wave height at EVA-062 and selected peaks.

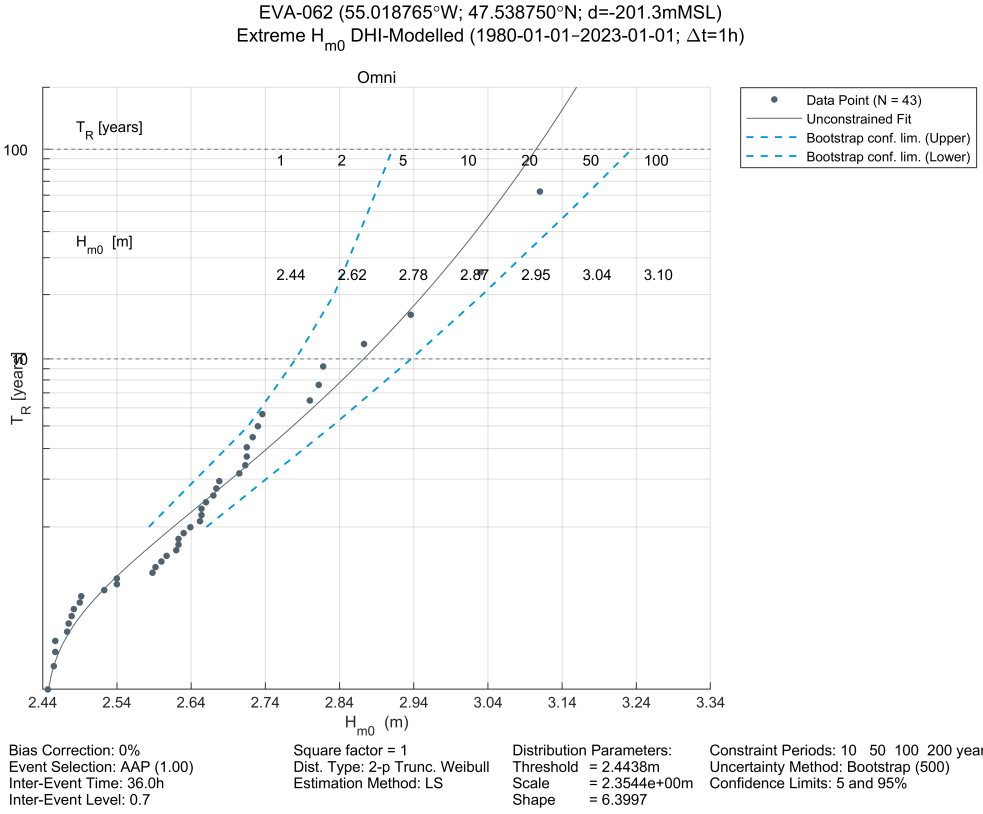


Figure C-341: Extreme value distribution fit at EVA-062.

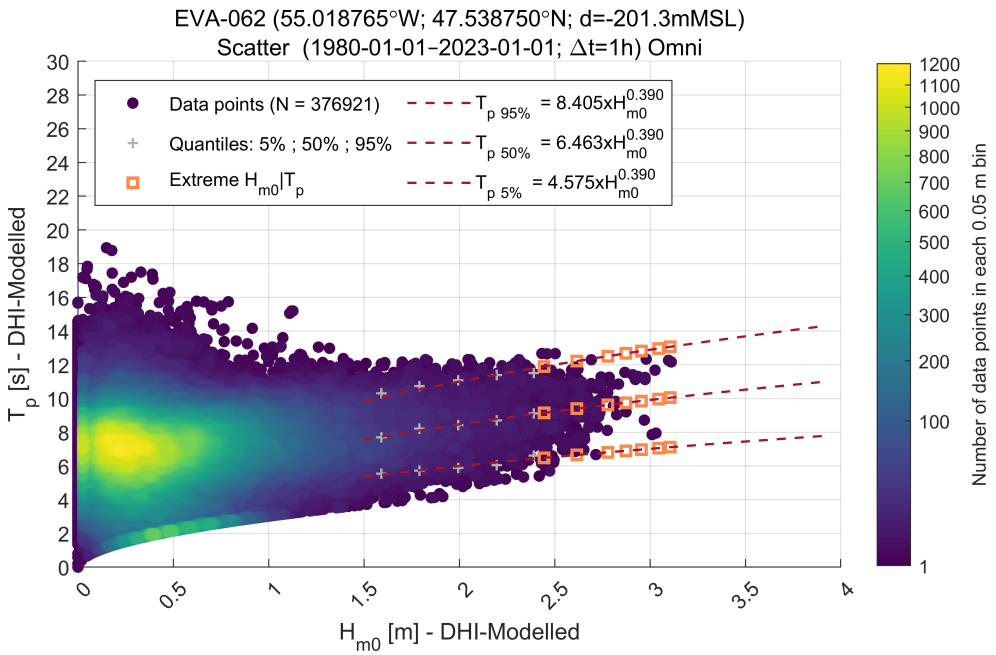


Figure C-342: Scatter plot of Hm0 x Tp at EVA-062 and quantile fit used to derived associated Tp to each extreme Hm0.

EVA-063

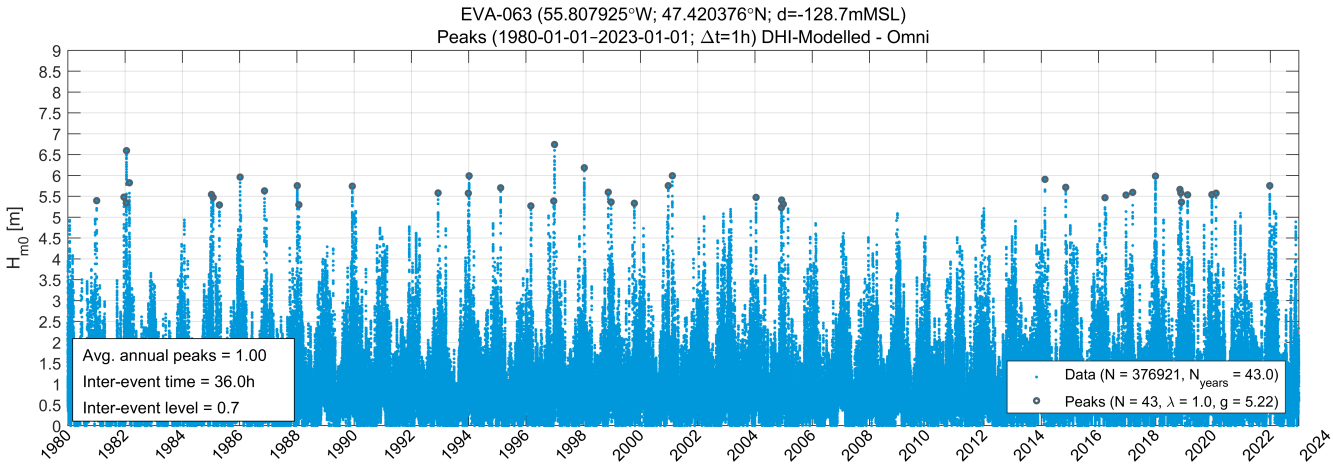


Figure C-343: Time series of significant wave height at EVA-063 and selected peaks.

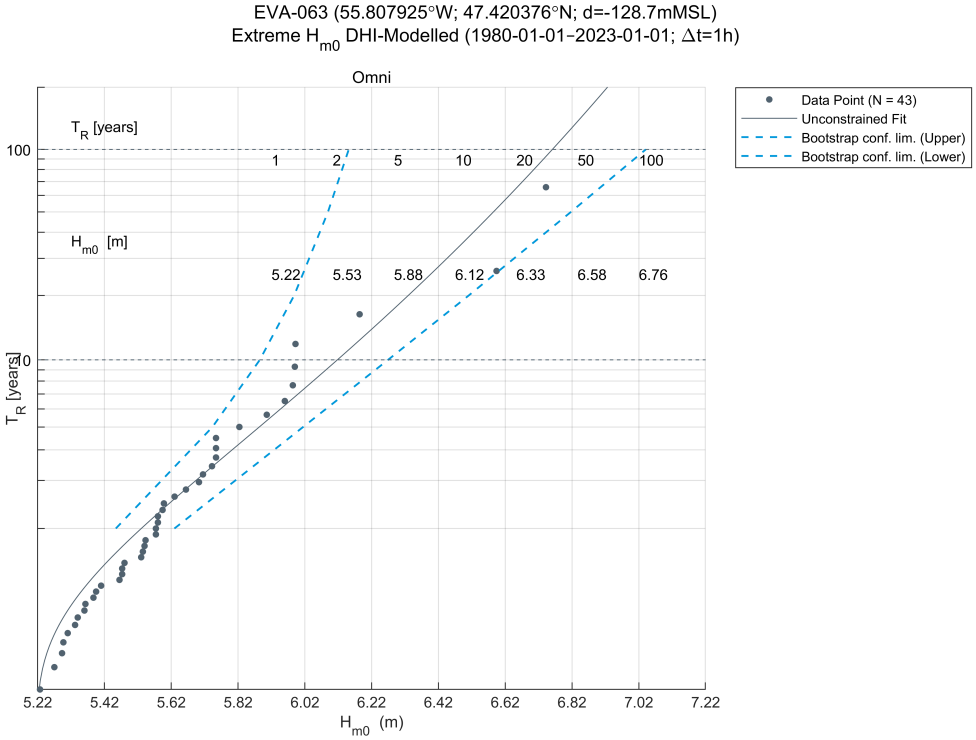


Figure C-344: Extreme value distribution fit at EVA-063.

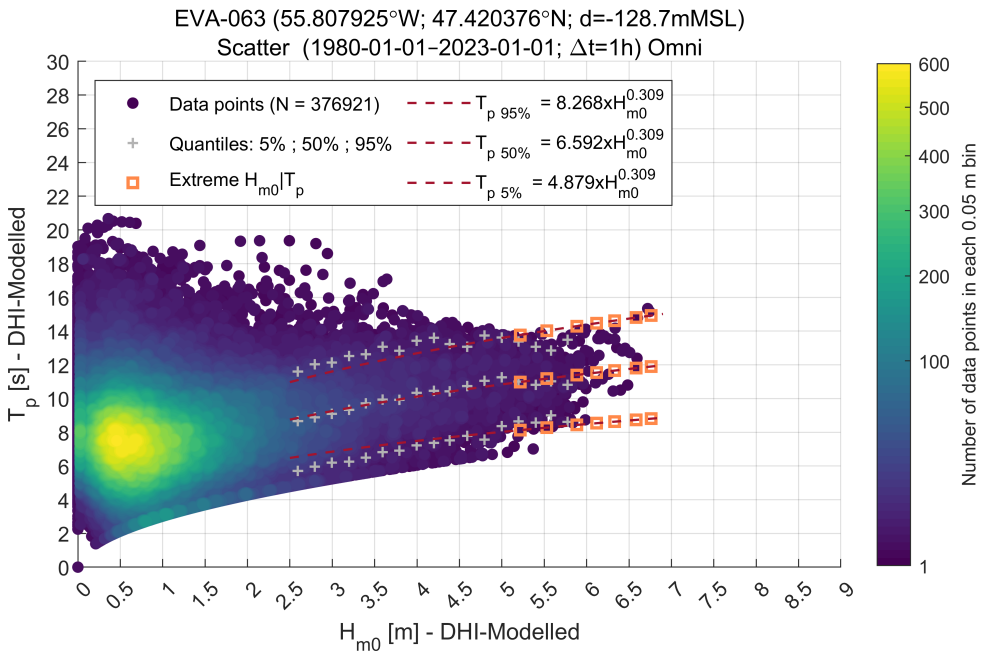


Figure C-345: Scatter plot of Hm0 x Tp at EVA-063 and quantile fit used to derived associated Tp to each extreme Hm0.

EVA-064

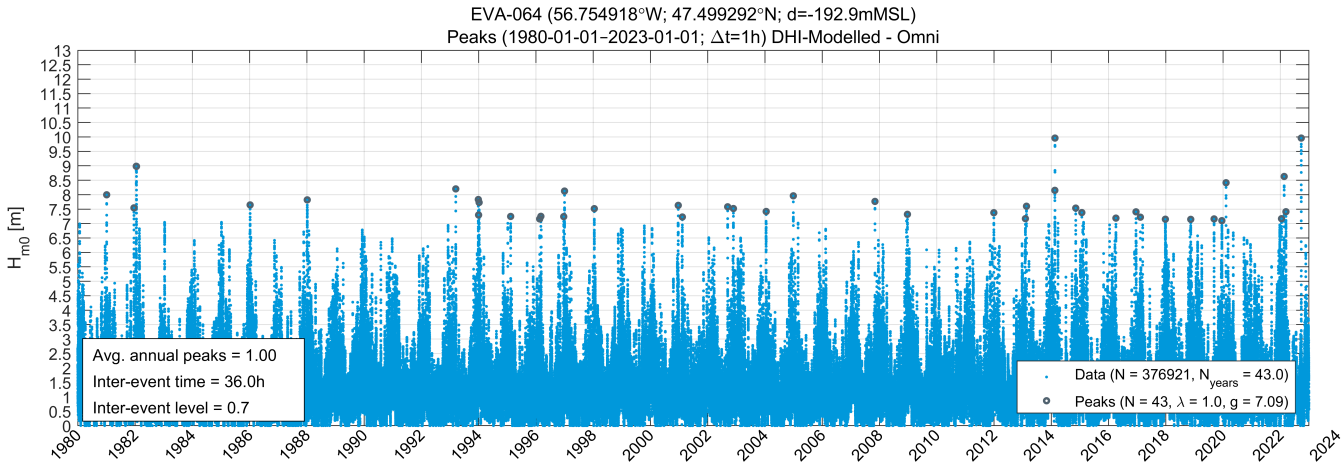


Figure C-346: Time series of significant wave height at EVA-064 and selected peaks.

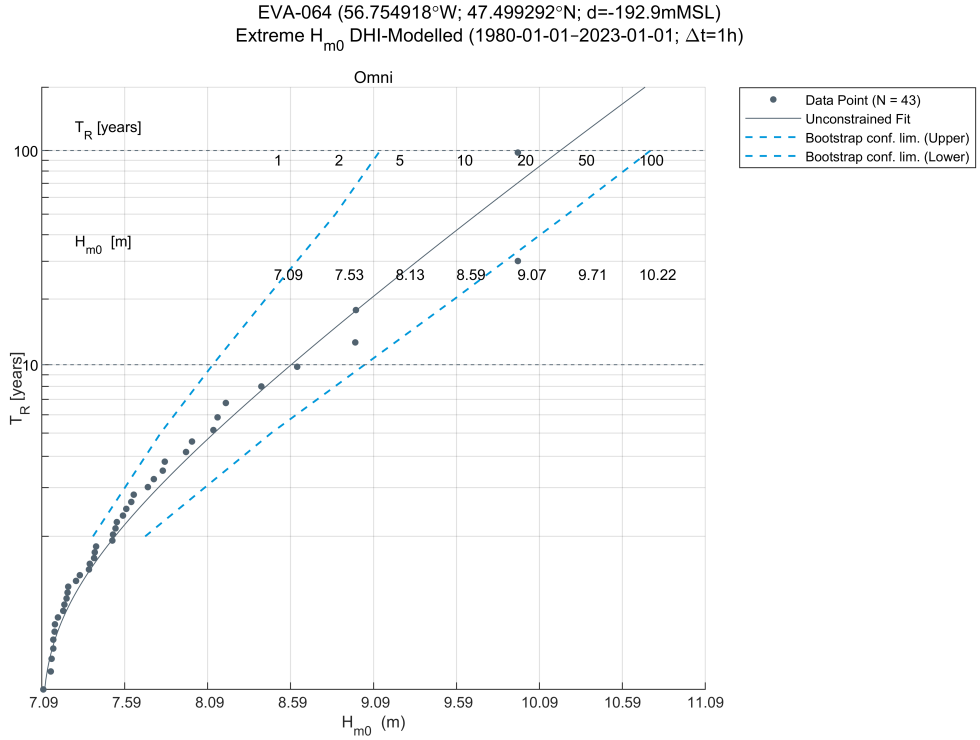


Figure C-347: Extreme value distribution fit at EVA-064.

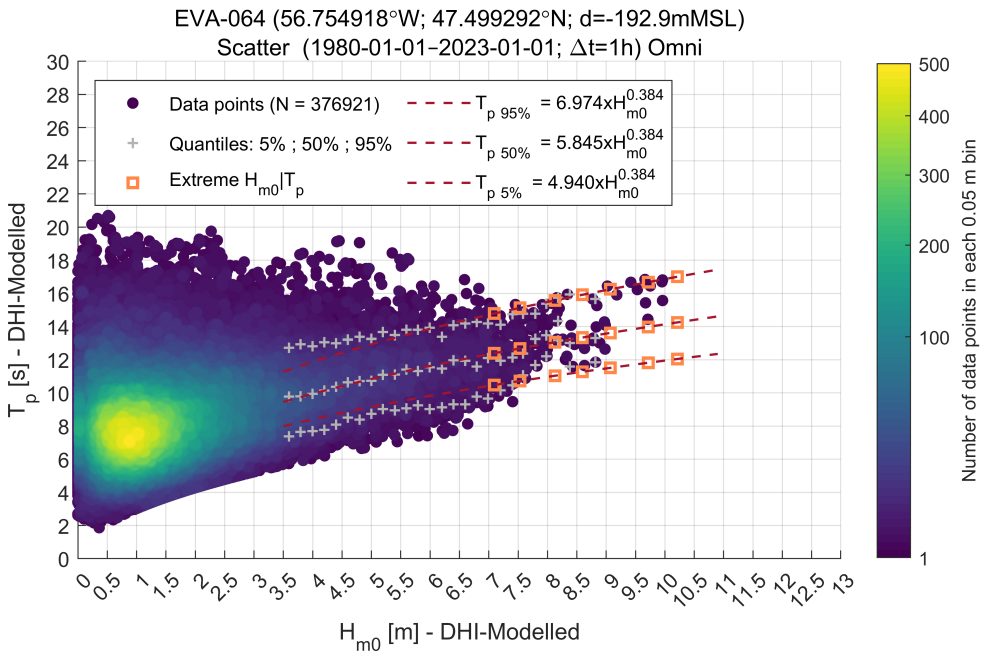


Figure C-348: Scatter plot of Hm0 x Tp at EVA-064 and quantile fit used to derived associated Tp to each extreme Hm0.

EVA-065

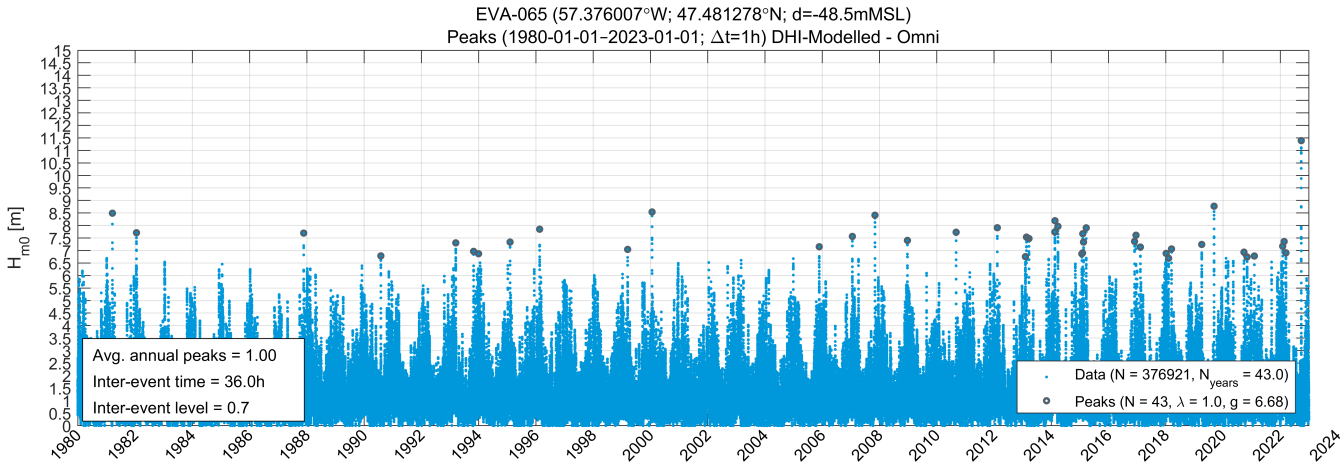


Figure C-349: Time series of significant wave height at EVA-065 and selected peaks.

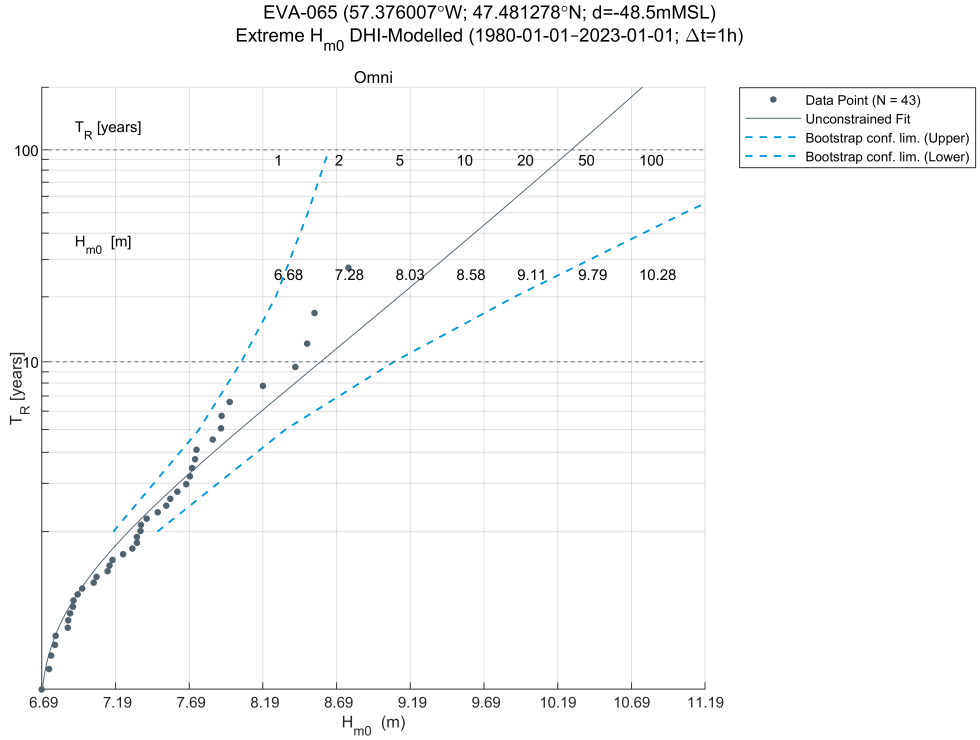


Figure C-350: Extreme value distribution fit at EVA-065.

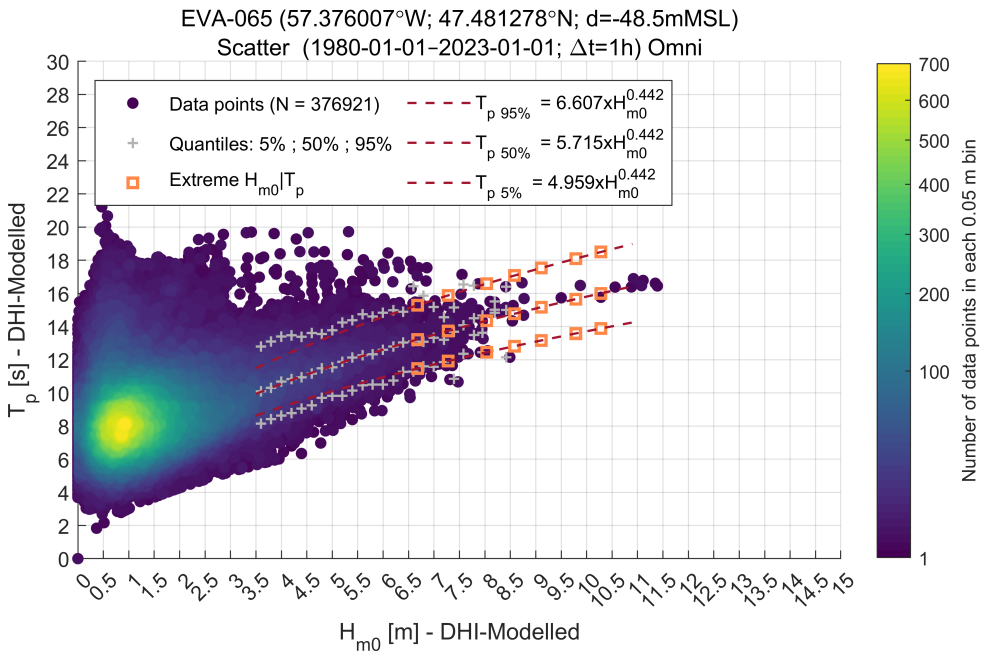


Figure C-351: Scatter plot of Hm0 x Tp at EVA-065 and quantile fit used to derived associated Tp to each extreme Hm0.

EVA-066

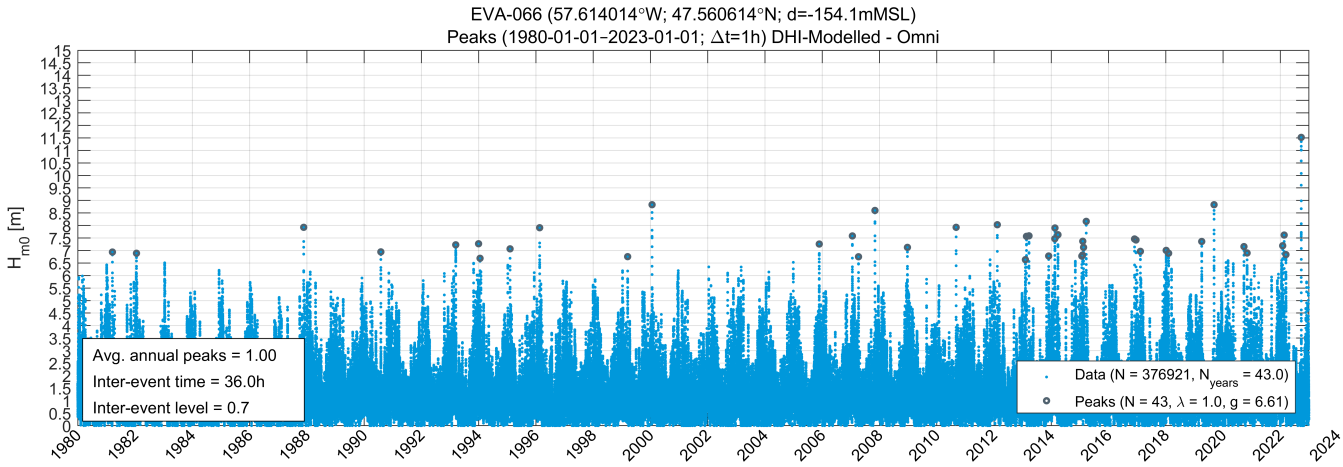


Figure C-352: Time series of significant wave height at EVA-066 and selected peaks.

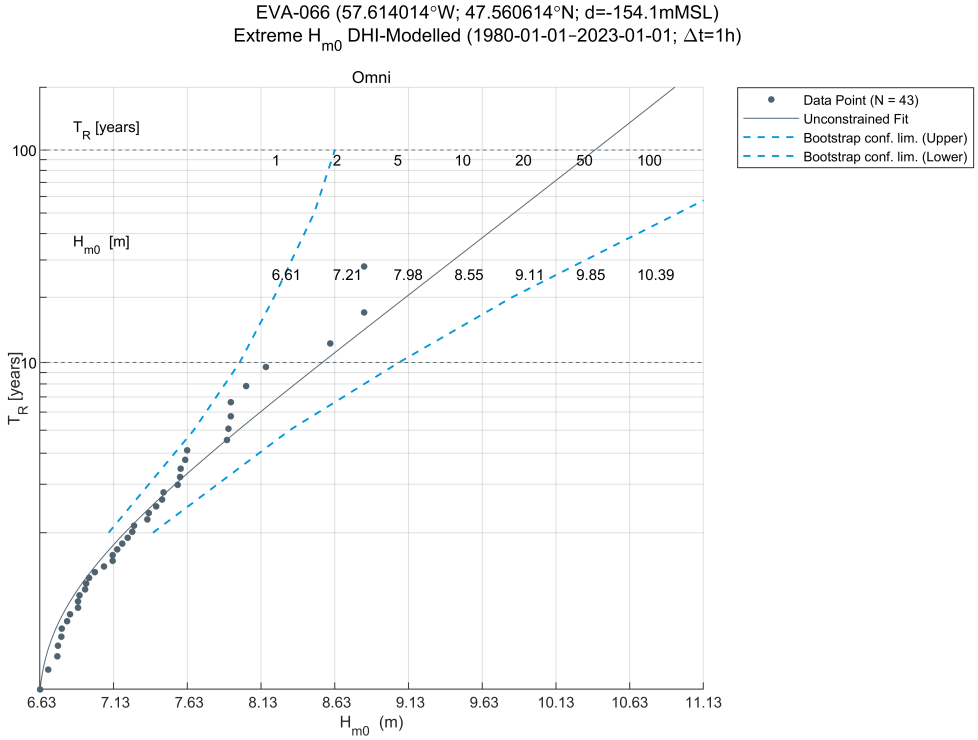


Figure C-353: Extreme value distribution fit at EVA-066.

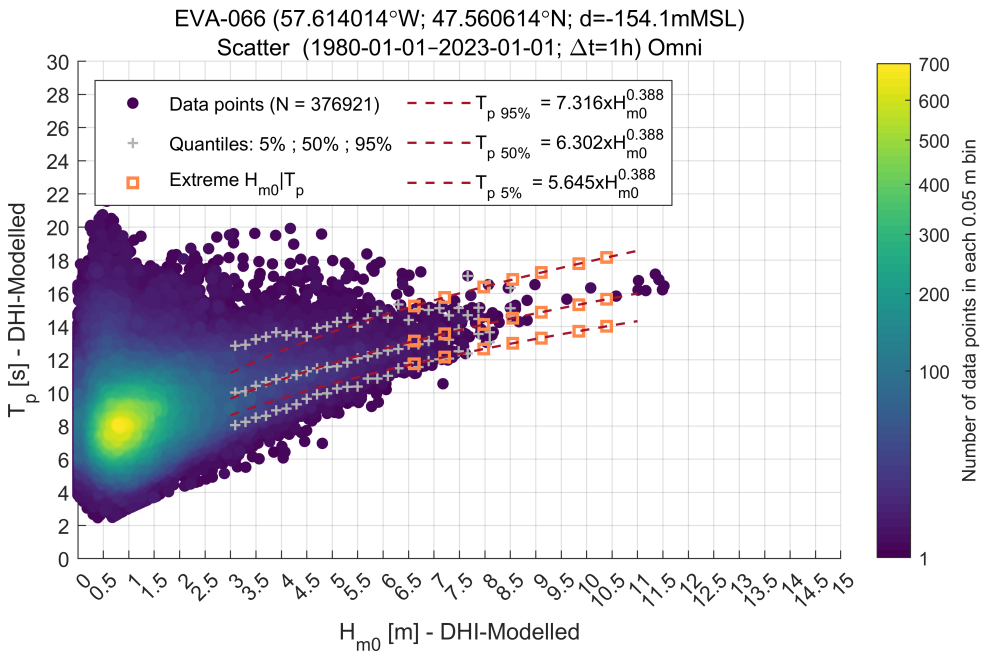


Figure C-354: Scatter plot of Hm0 x Tp at EVA-066 and quantile fit used to derived associated Tp to each extreme Hm0.

EVA-067

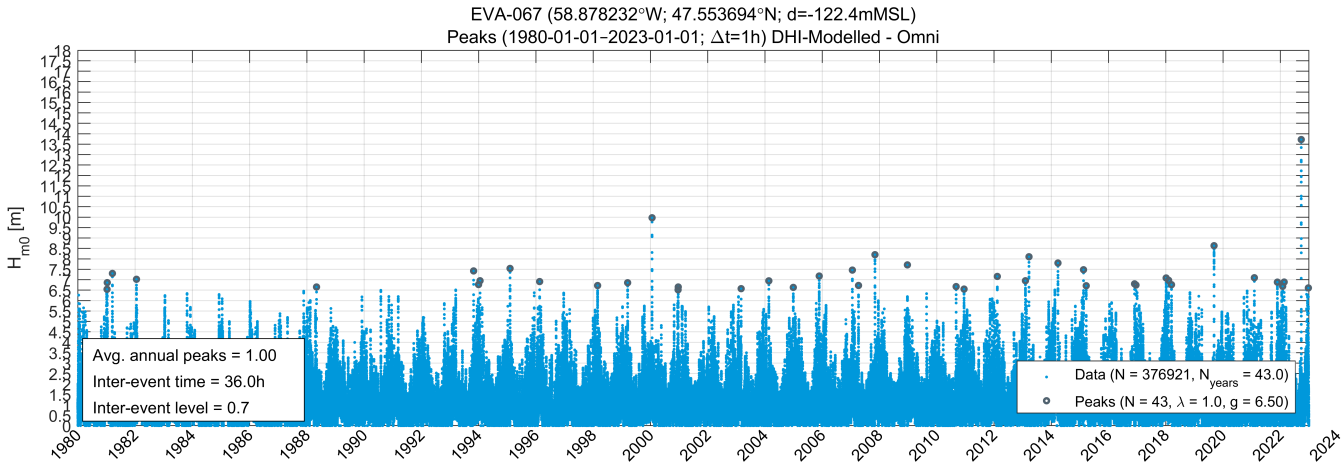


Figure C-355: Time series of significant wave height at EVA-067 and selected peaks.

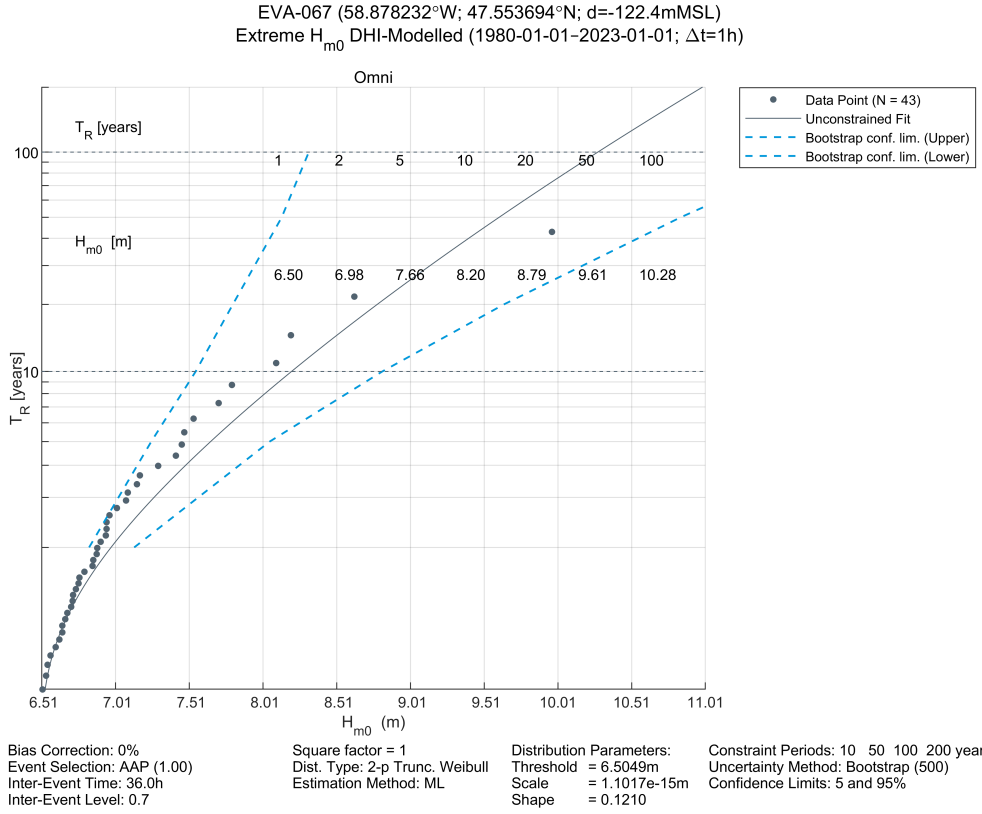


Figure C-356: Extreme value distribution fit at EVA-067.

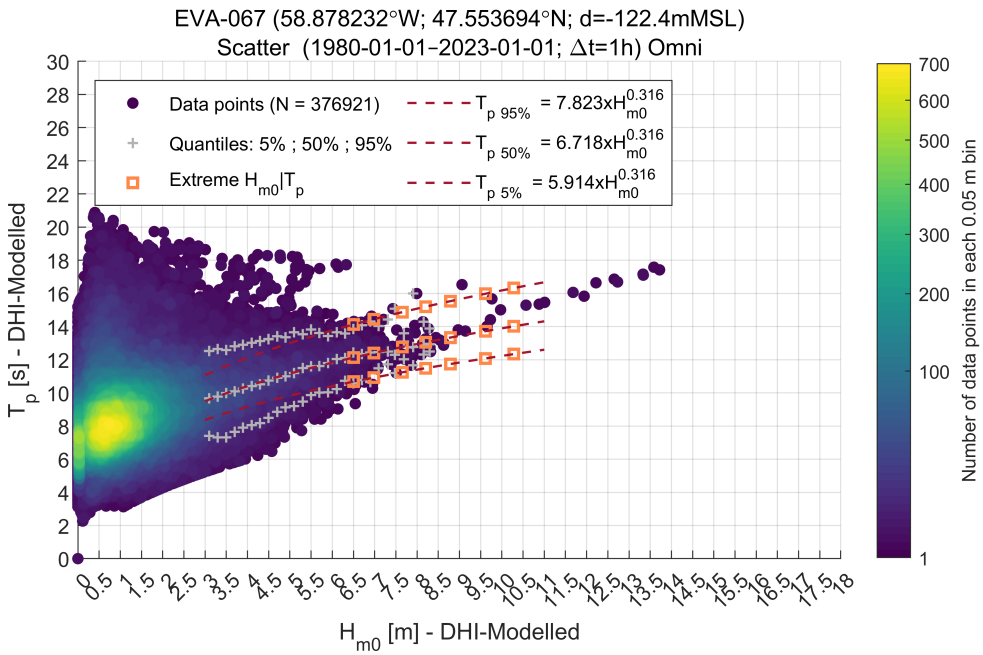


Figure C-357: Scatter plot of Hm0 x Tp at EVA-067 and quantile fit used to derived associated Tp to each extreme Hm0.

EVA-068

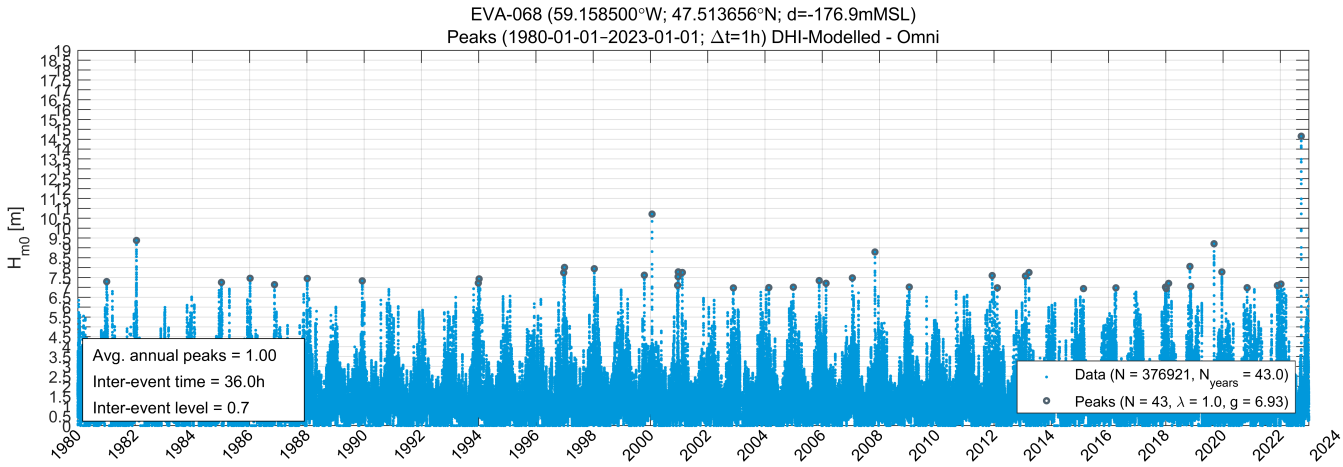


Figure C-358: Time series of significant wave height at EVA-068 and selected peaks.

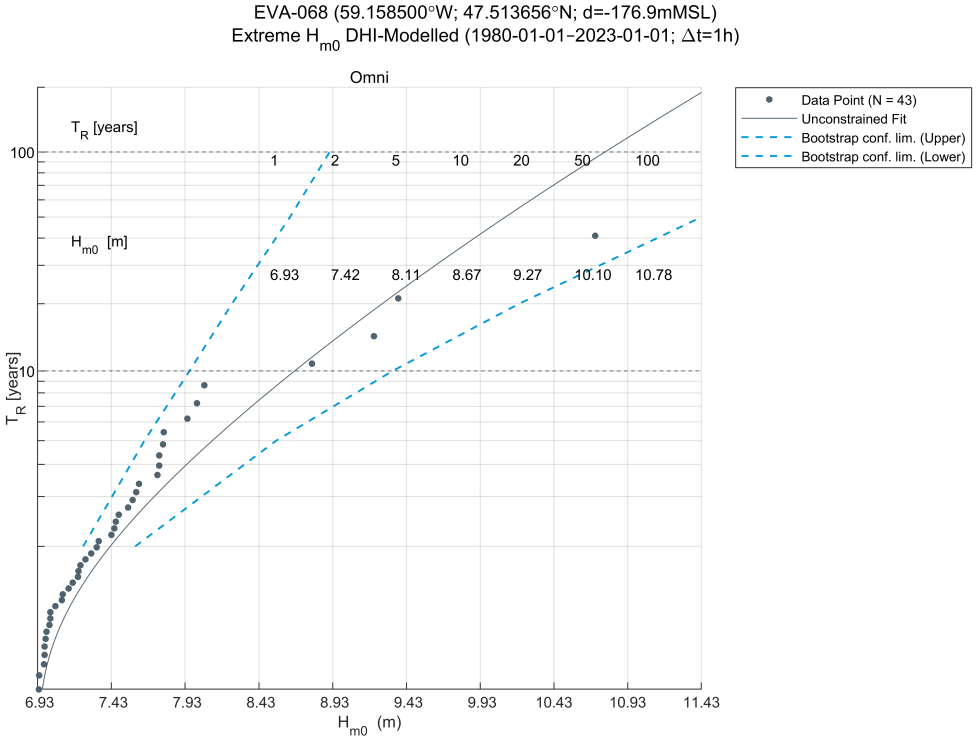


Figure C-359: Extreme value distribution fit at EVA-068.

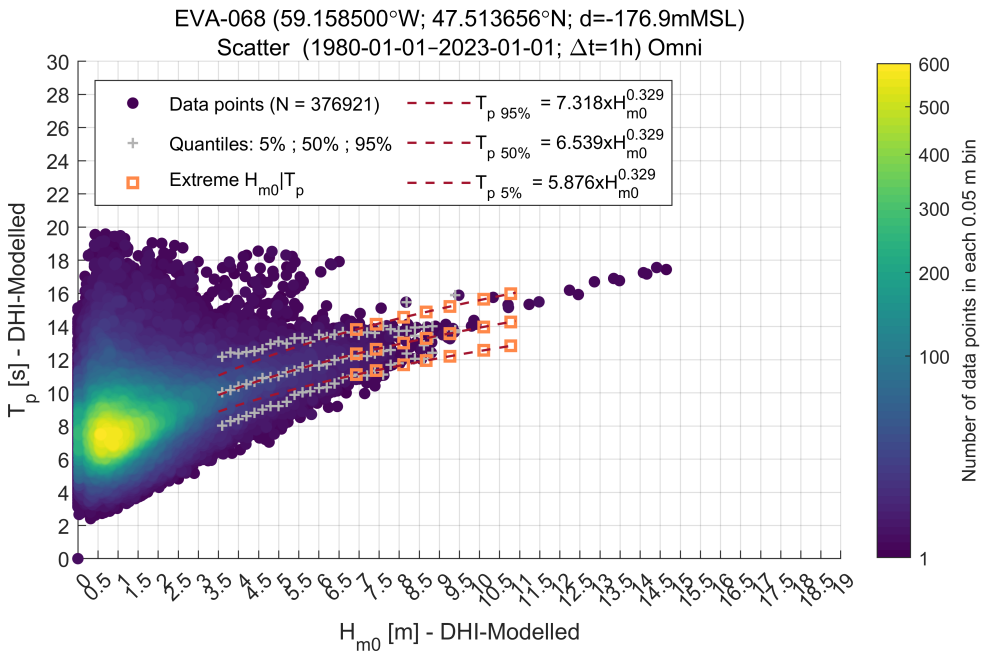


Figure C-360: Scatter plot of Hm0 x Tp at EVA-068 and quantile fit used to derived associated Tp to each extreme Hm0.

EVA-069

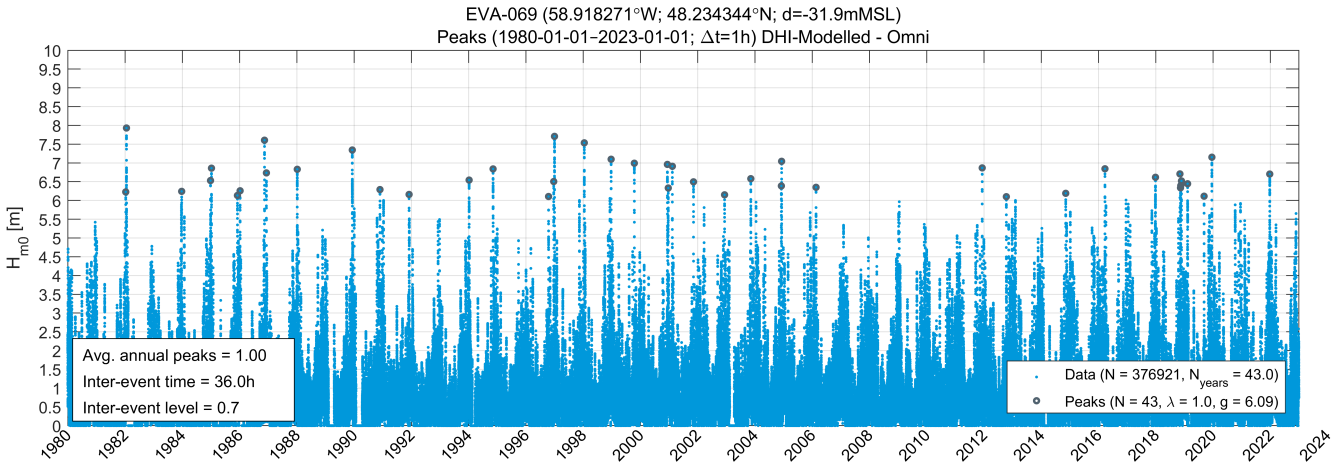


Figure C-361: Time series of significant wave height at EVA-069 and selected peaks.

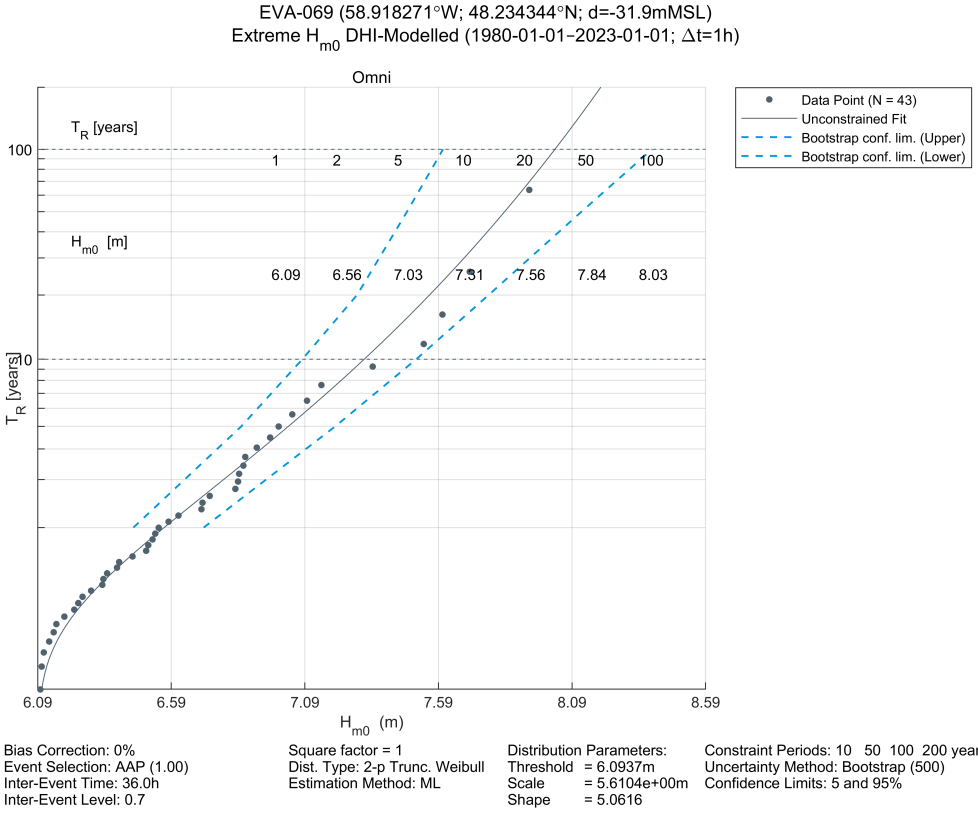


Figure C-362: Extreme value distribution fit at EVA-069.

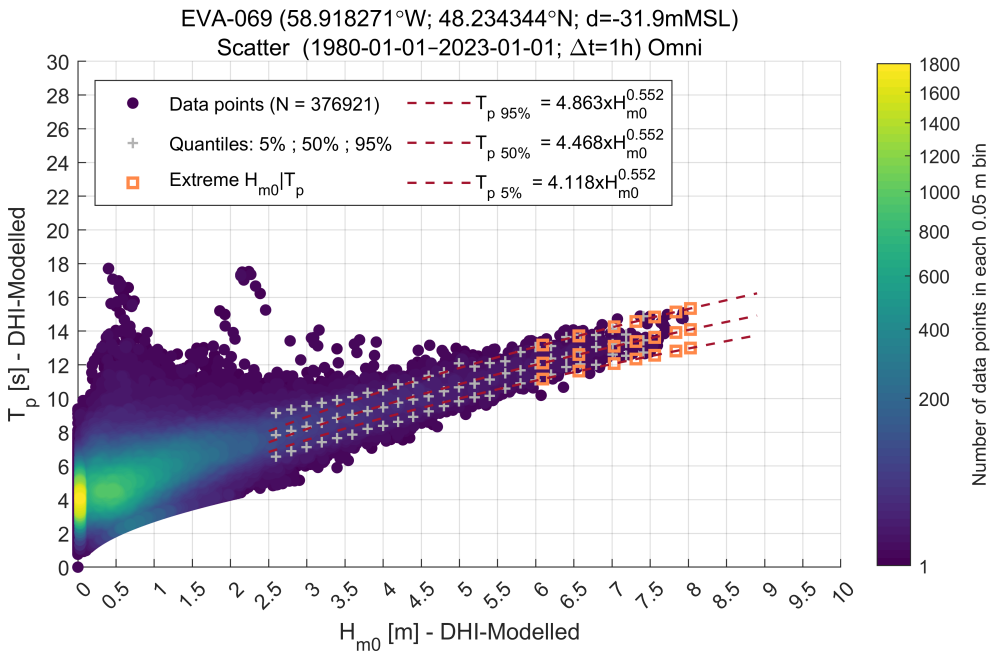


Figure C-363: Scatter plot of Hm0 x Tp at EVA-069 and quantile fit used to derived associated Tp to each extreme Hm0.

EVA-070

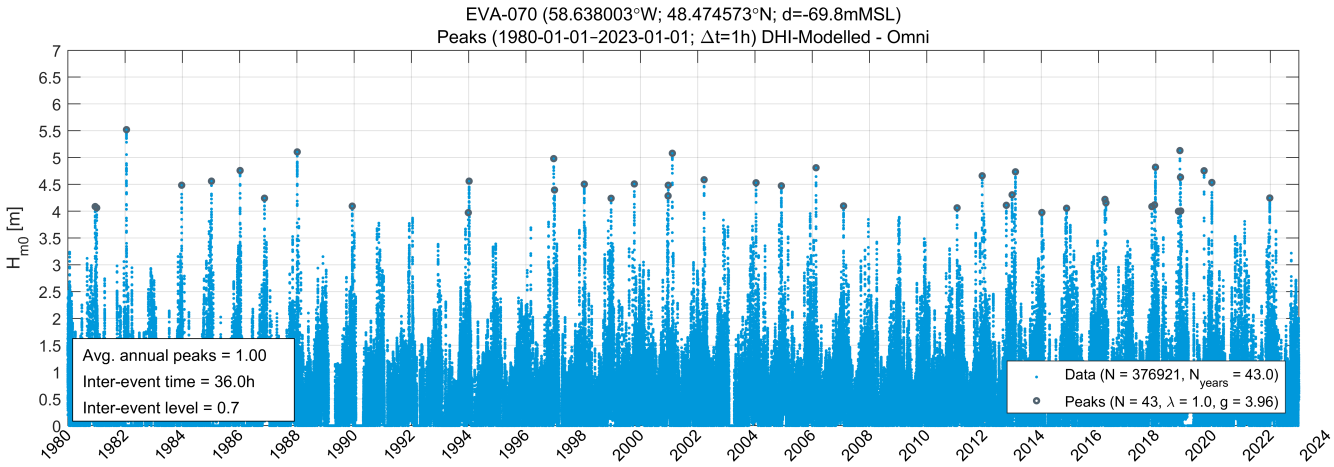


Figure C-364: Time series of significant wave height at EVA-070 and selected peaks.

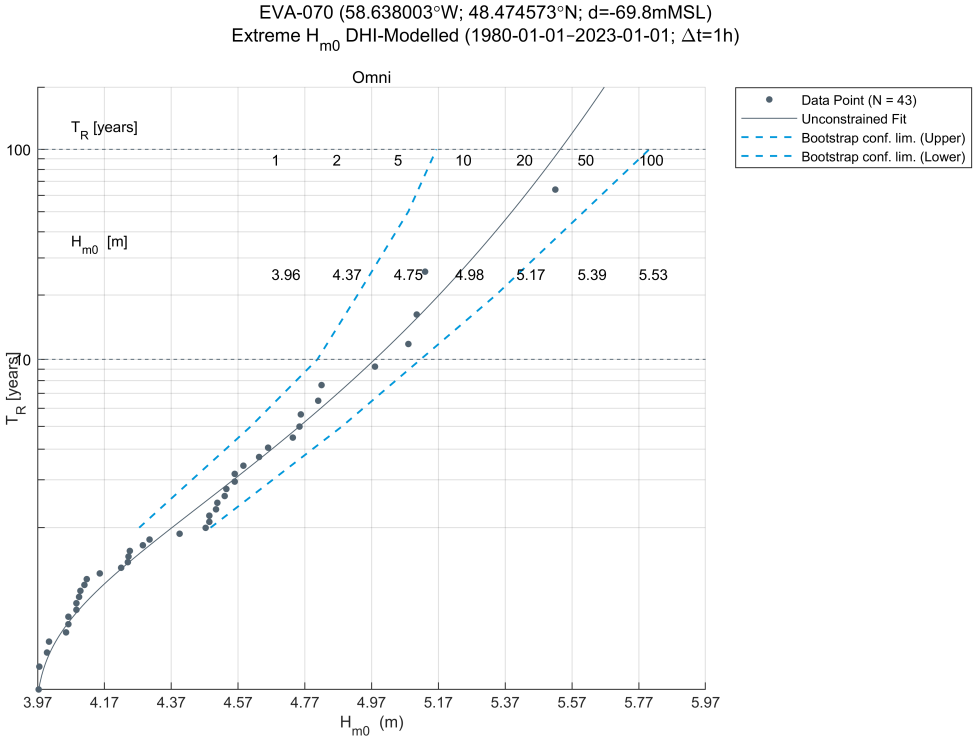


Figure C-365: Extreme value distribution fit at EVA-070.

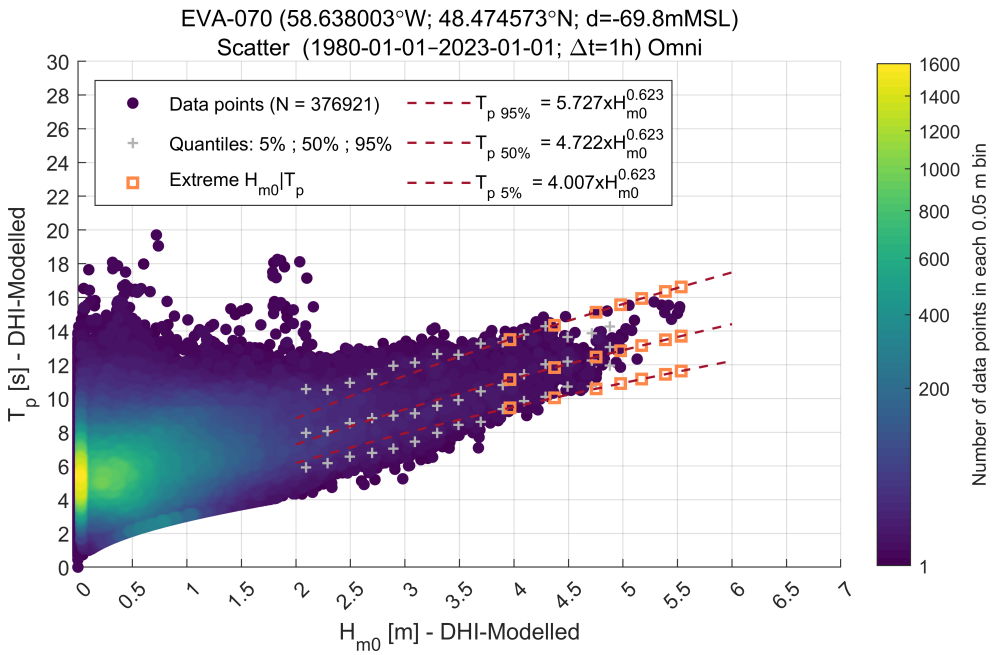


Figure C-366: Scatter plot of Hm0 x Tp at EVA-070 and quantile fit used to derived associated Tp to each extreme Hm0.

EVA-071

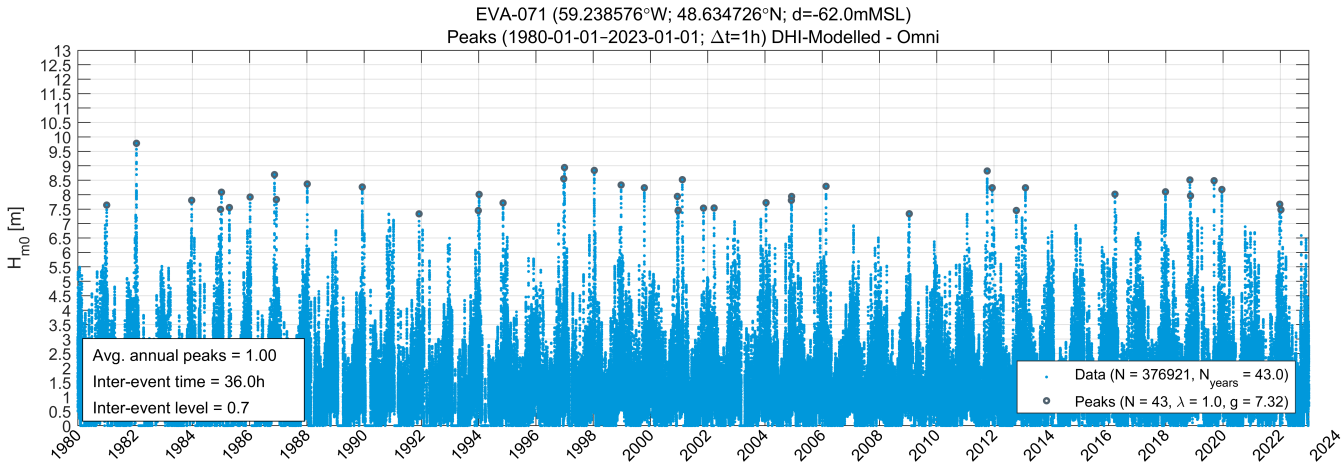


Figure C-367: Time series of significant wave height at EVA-071 and selected peaks.

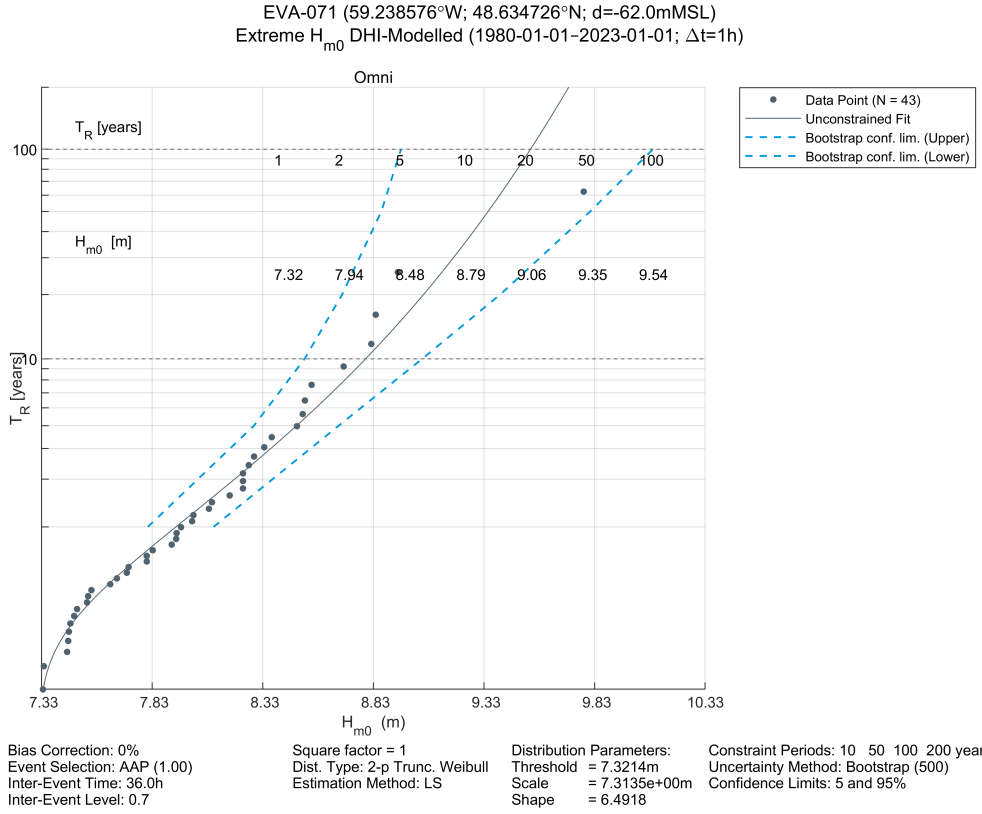


Figure C-368: Extreme value distribution fit at EVA-071.

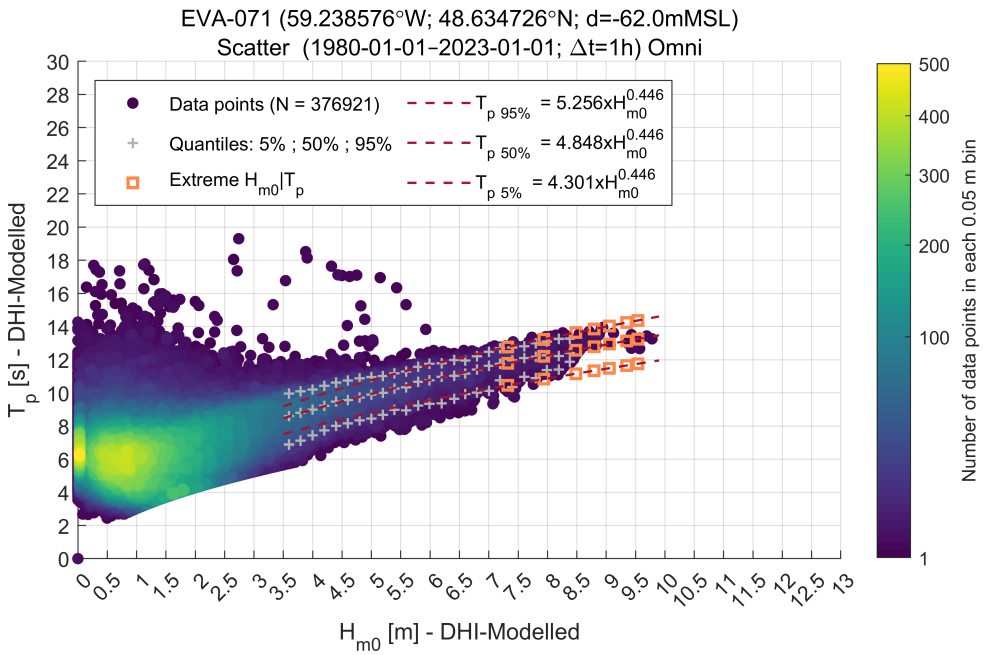


Figure C-369: Scatter plot of Hm0 x Tp at EVA-071 and quantile fit used to derived associated Tp to each extreme Hm0.

EVA-072

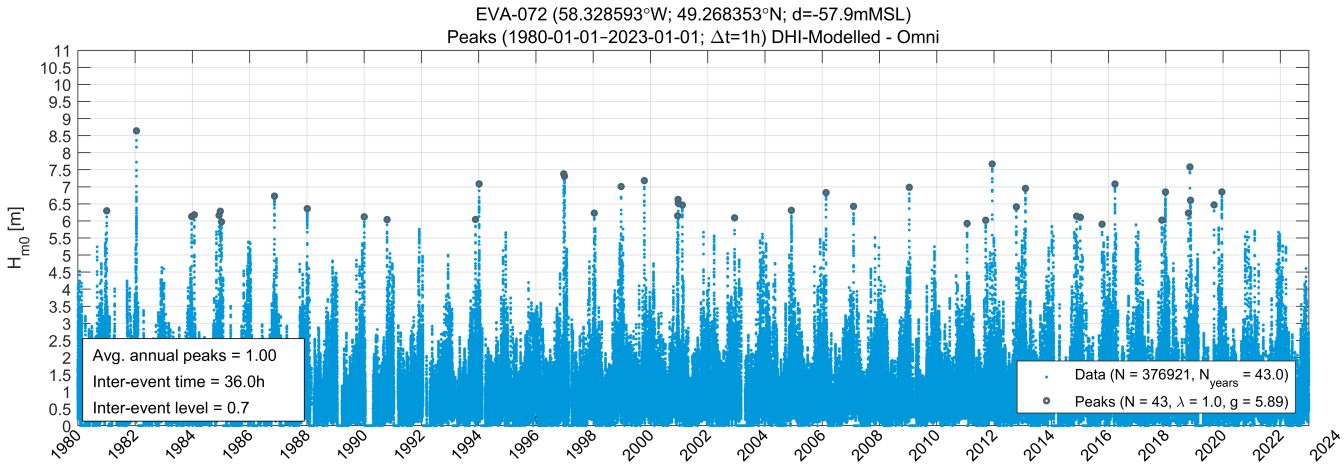


Figure C-370: Time series of significant wave height at EVA-072 and selected peaks.

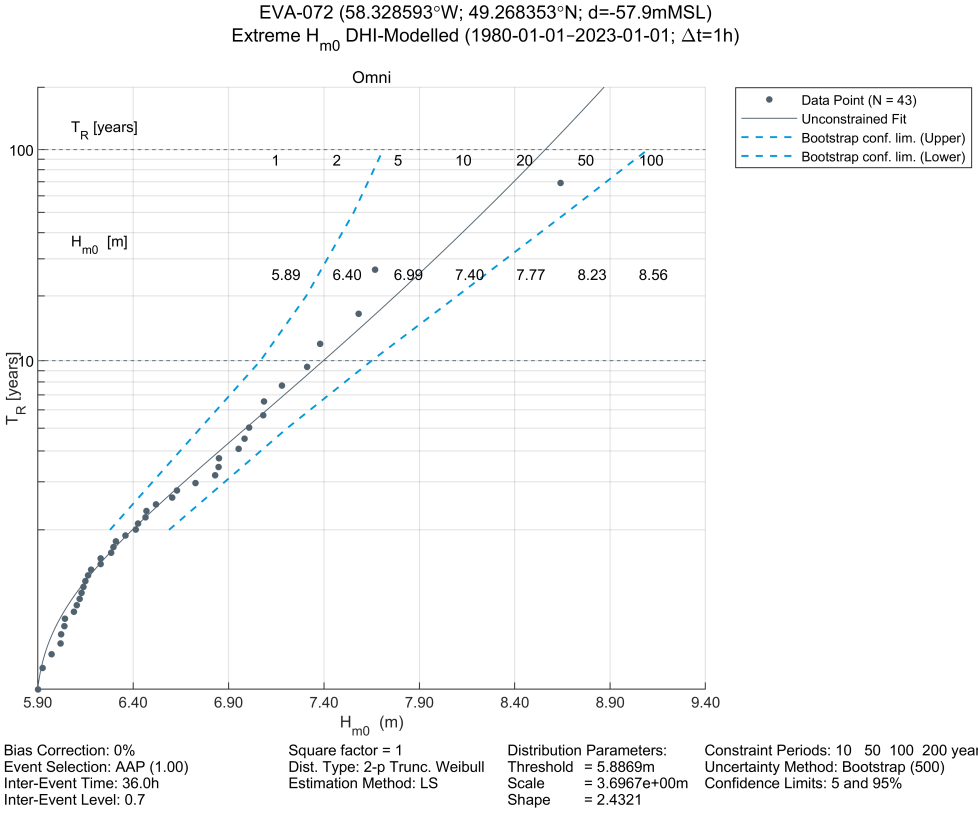


Figure C-371: Extreme value distribution fit at EVA-072.

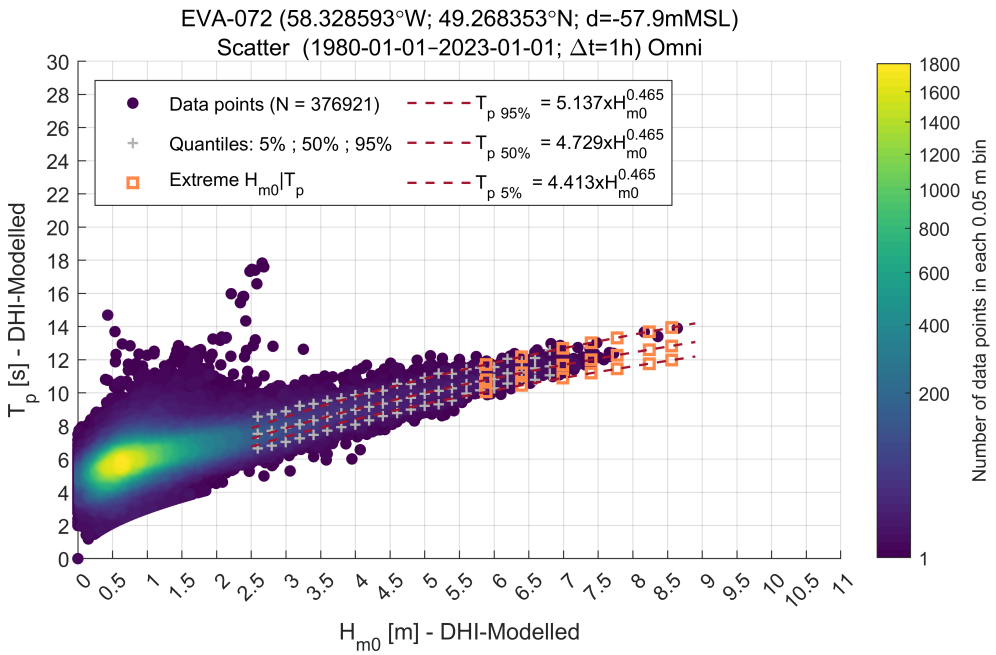


Figure C-372: Scatter plot of Hm0 x Tp at EVA-072 and quantile fit used to derived associated Tp to each extreme Hm0.

EVA-073

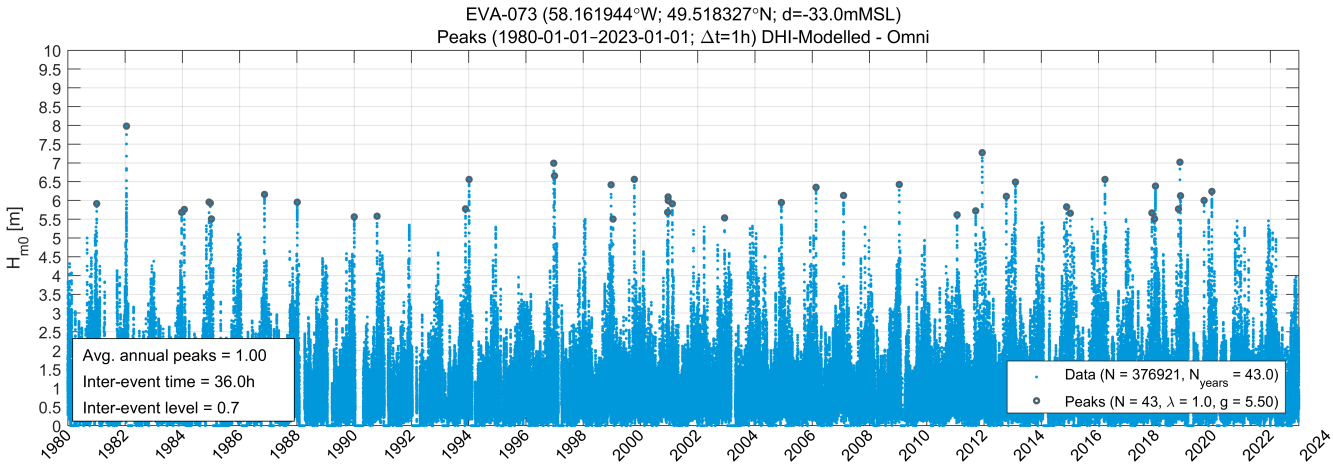


Figure C-373: Time series of significant wave height at EVA-073 and selected peaks.

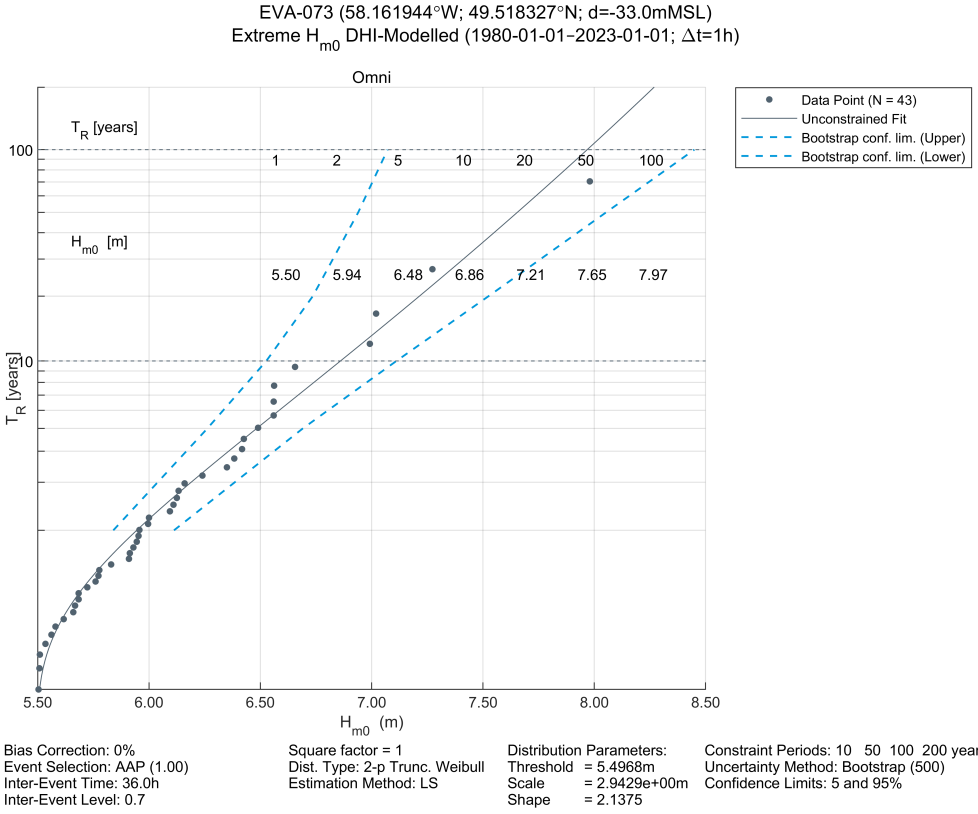


Figure C-374: Extreme value distribution fit at EVA-073.

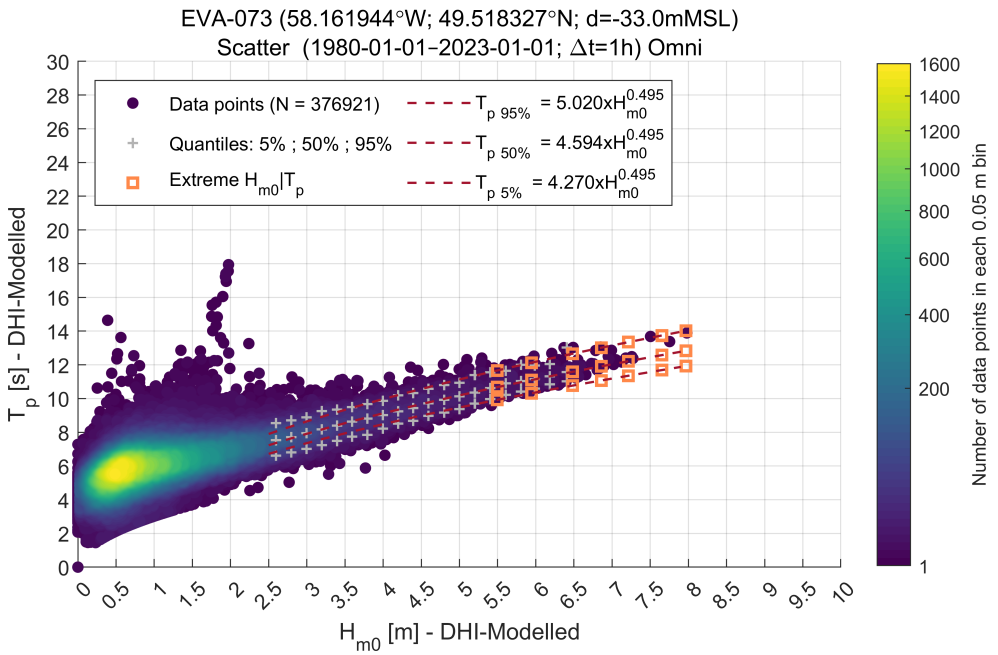


Figure C-375: Scatter plot of Hm0 x Tp at EVA-073 and quantile fit used to derived associated Tp to each extreme Hm0.

EVA-074

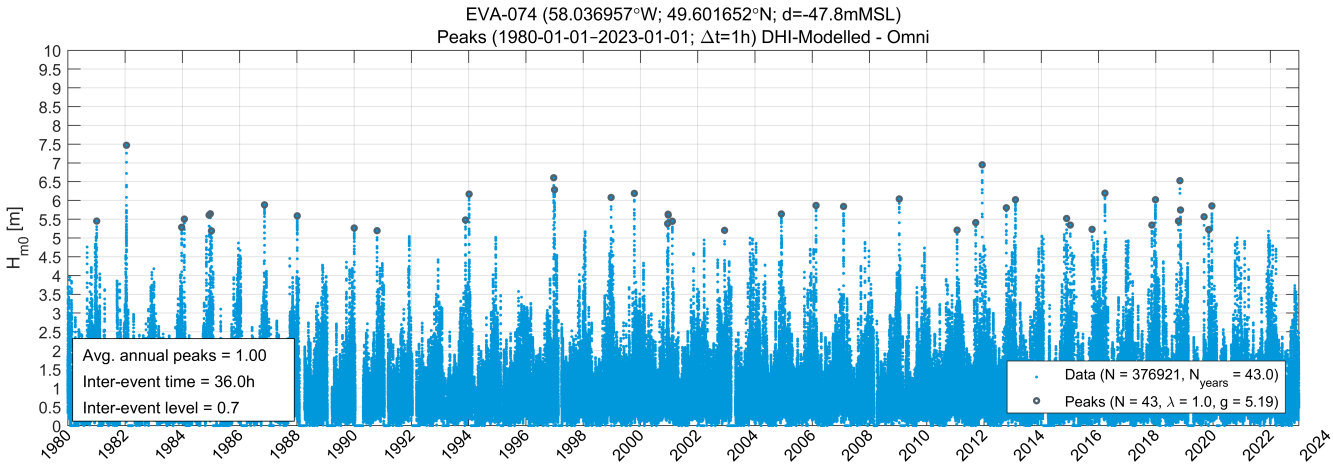


Figure C-376: Time series of significant wave height at EVA-074 and selected peaks.

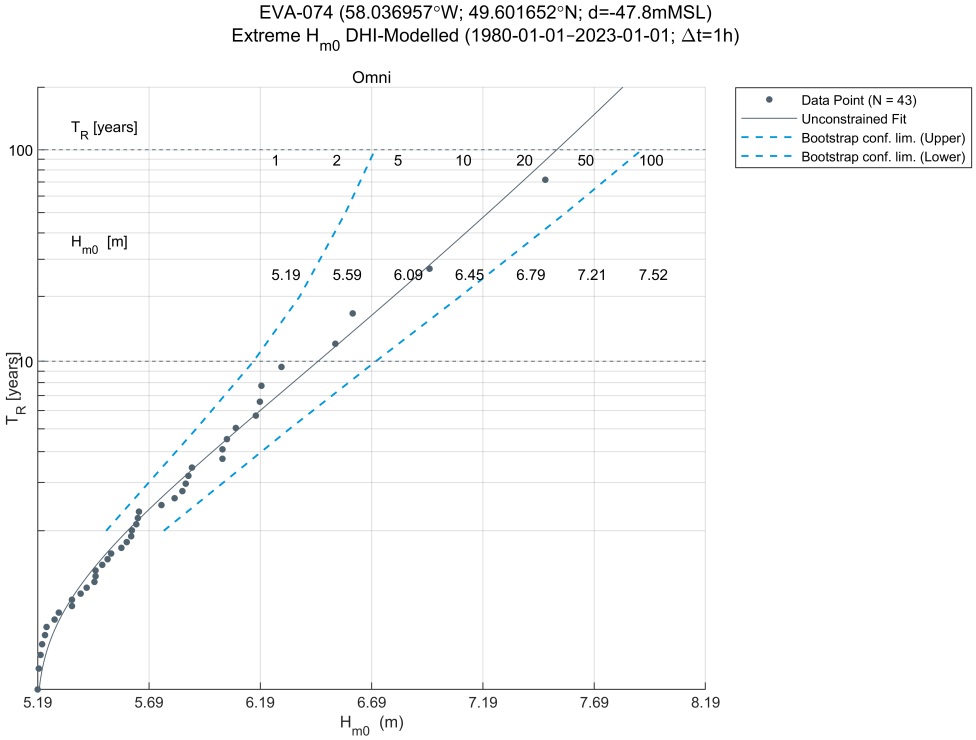


Figure C-377: Extreme value distribution fit at EVA-074.

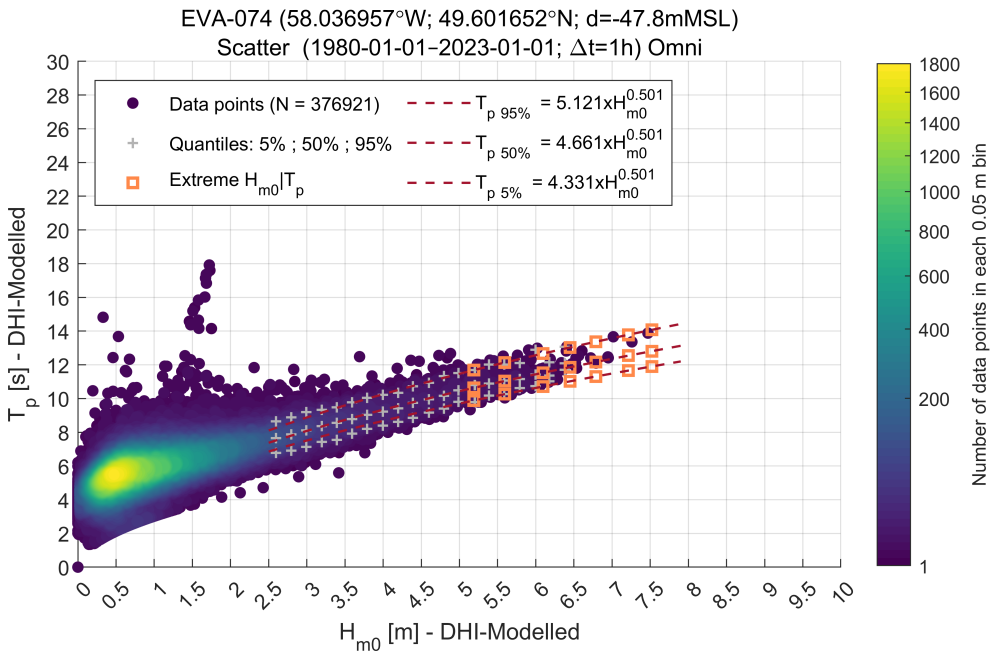


Figure C-378: Scatter plot of Hm0 x Tp at EVA-074 and quantile fit used to derived associated Tp to each extreme Hm0.

EVA-075

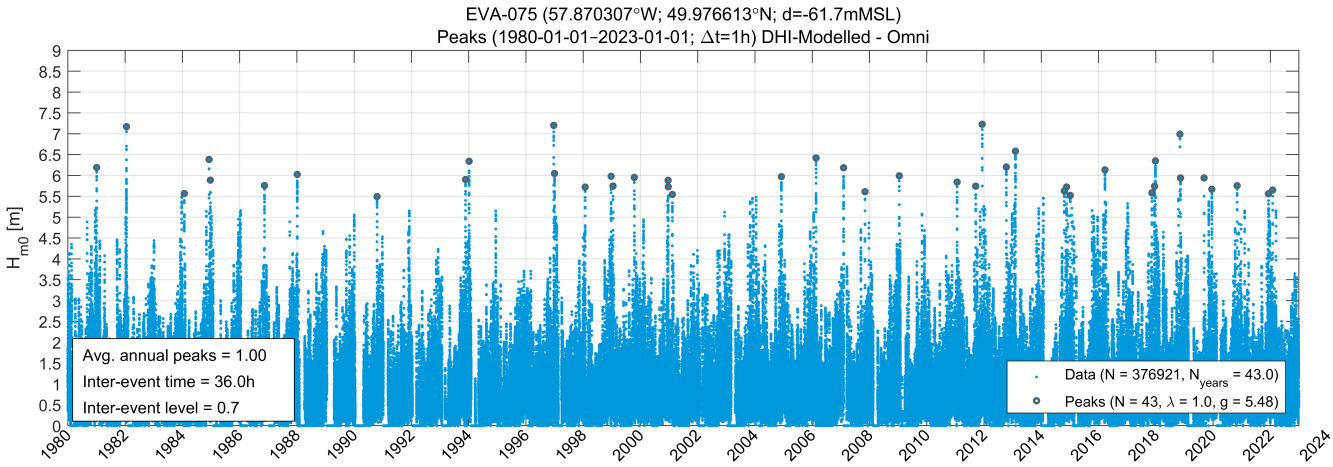


Figure C-379: Time series of significant wave height at EVA-075 and selected peaks.

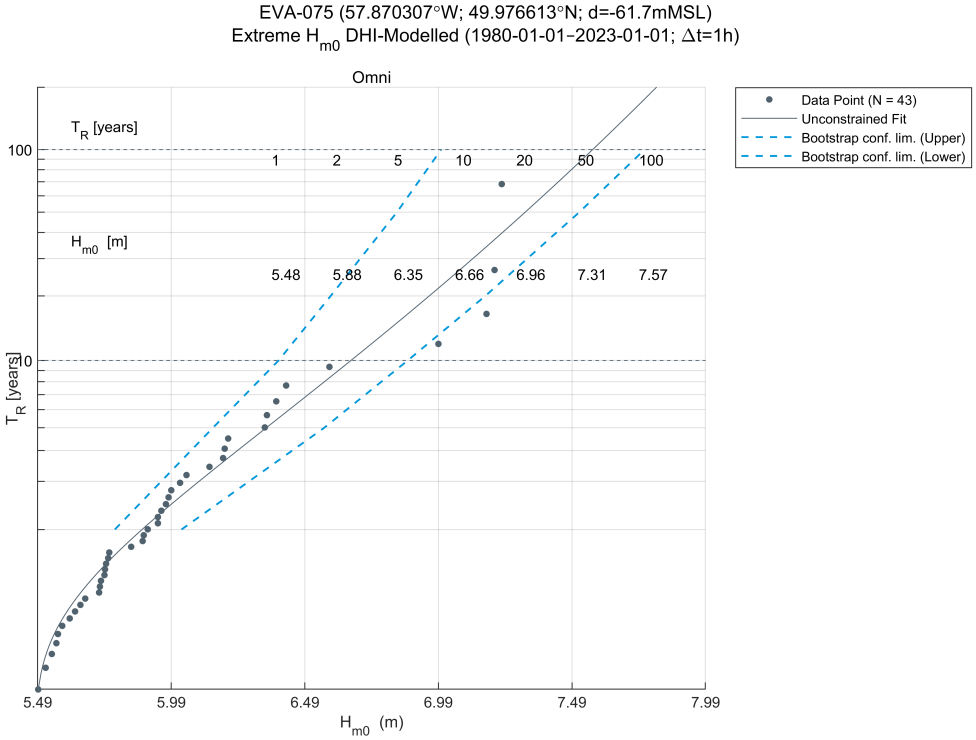


Figure C-380: Extreme value distribution fit at EVA-075.

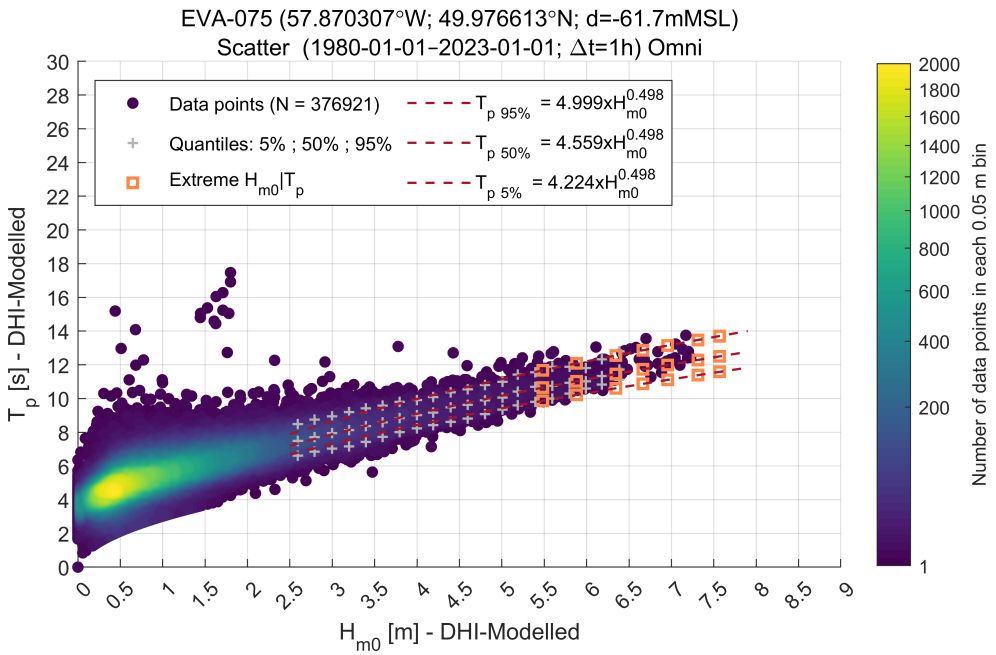


Figure C-381: Scatter plot of Hm0 x Tp at EVA-075 and quantile fit used to derived associated Tp to each extreme Hm0.

EVA-076

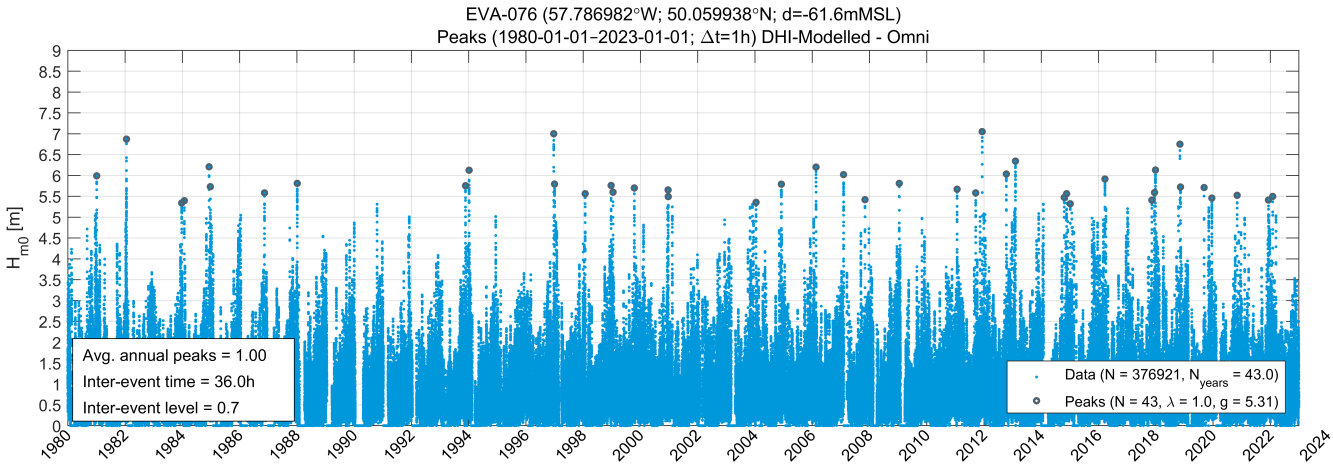


Figure C-382: Time series of significant wave height at EVA-076 and selected peaks.

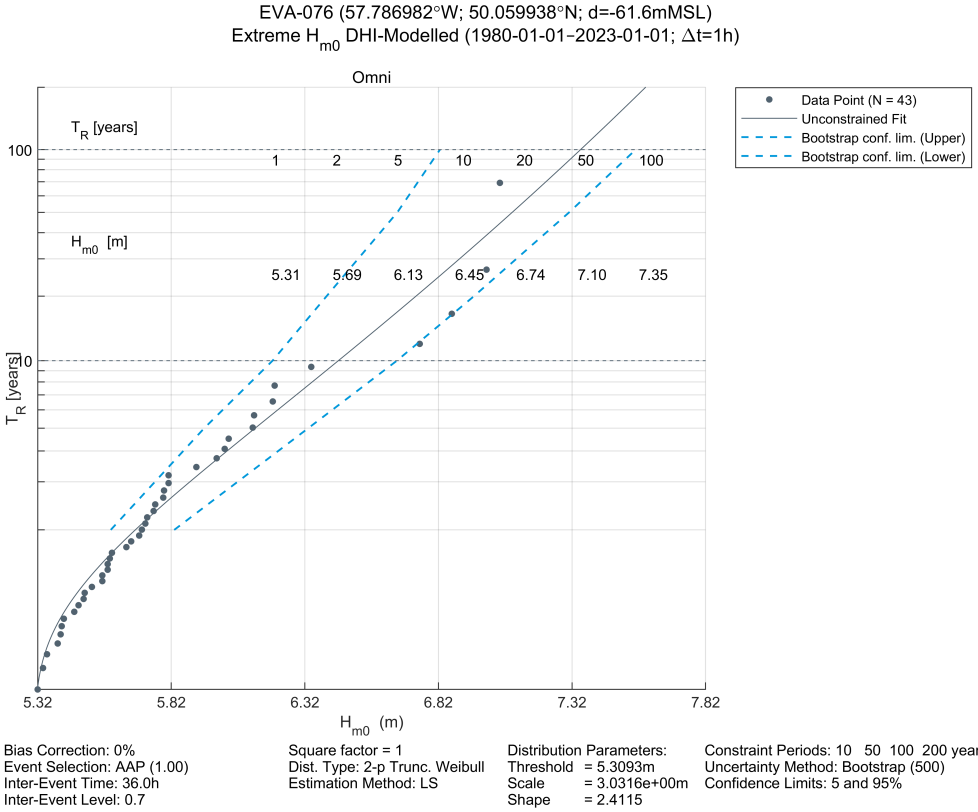


Figure C-383: Extreme value distribution fit at EVA-076.

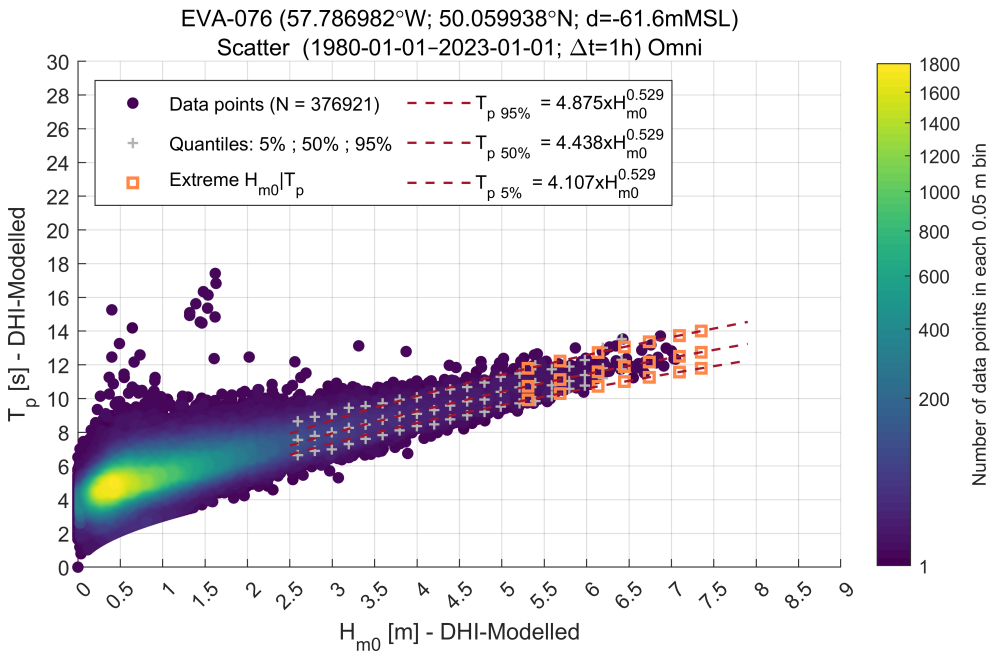


Figure C-384: Scatter plot of Hm0 x Tp at EVA-076 and quantile fit used to derived associated Tp to each extreme Hm0.

EVA-077

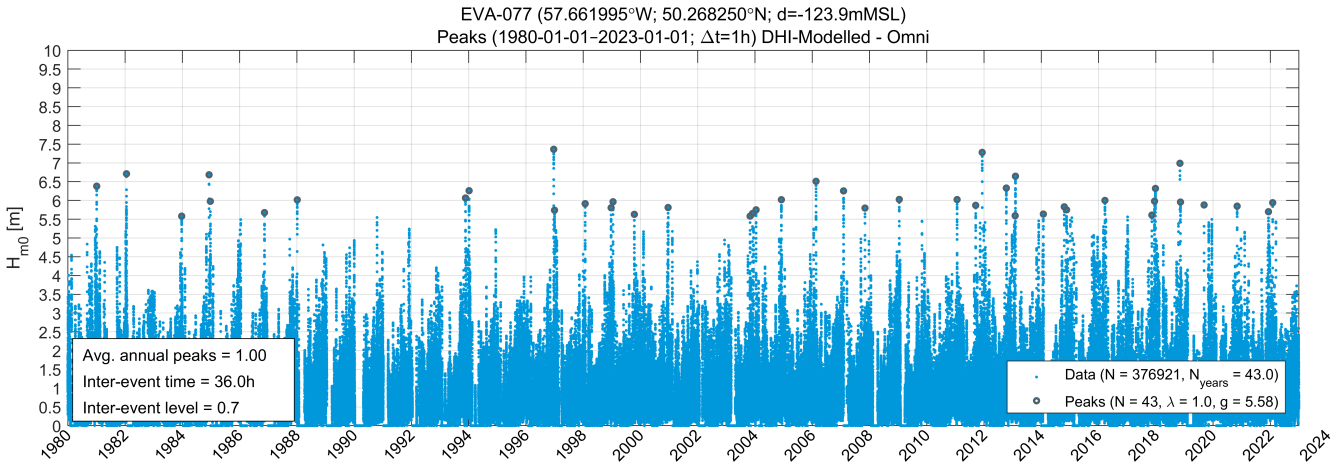


Figure C-385: Time series of significant wave height at EVA-077 and selected peaks.

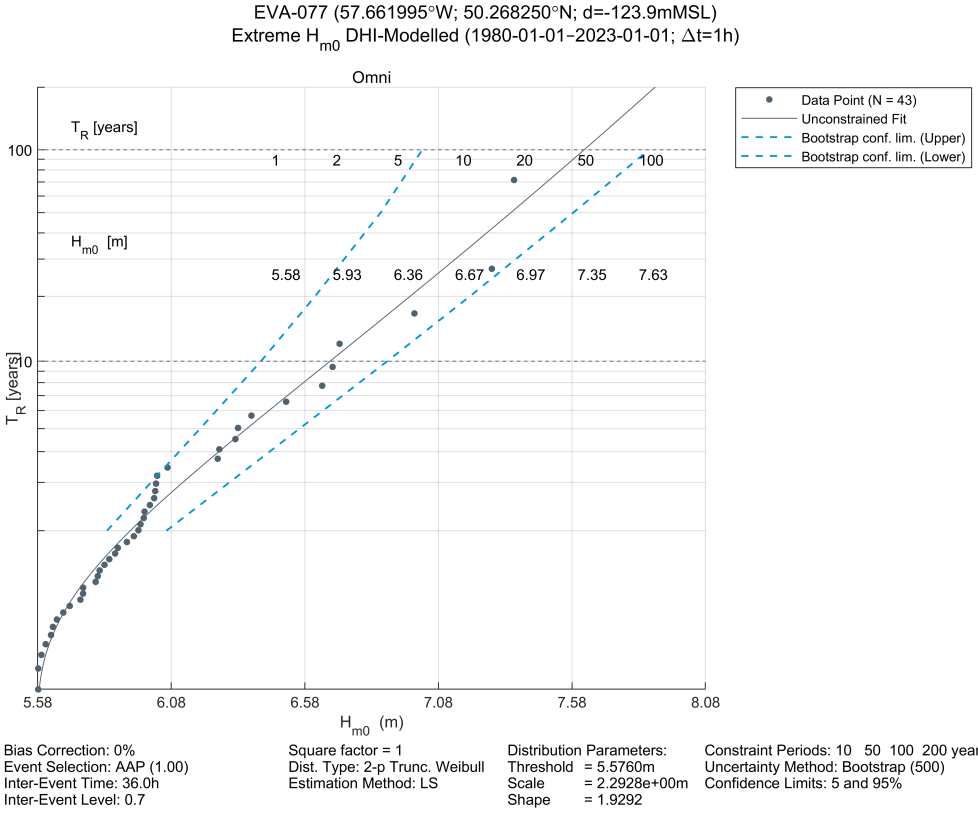


Figure C-386: Extreme value distribution fit at EVA-077.

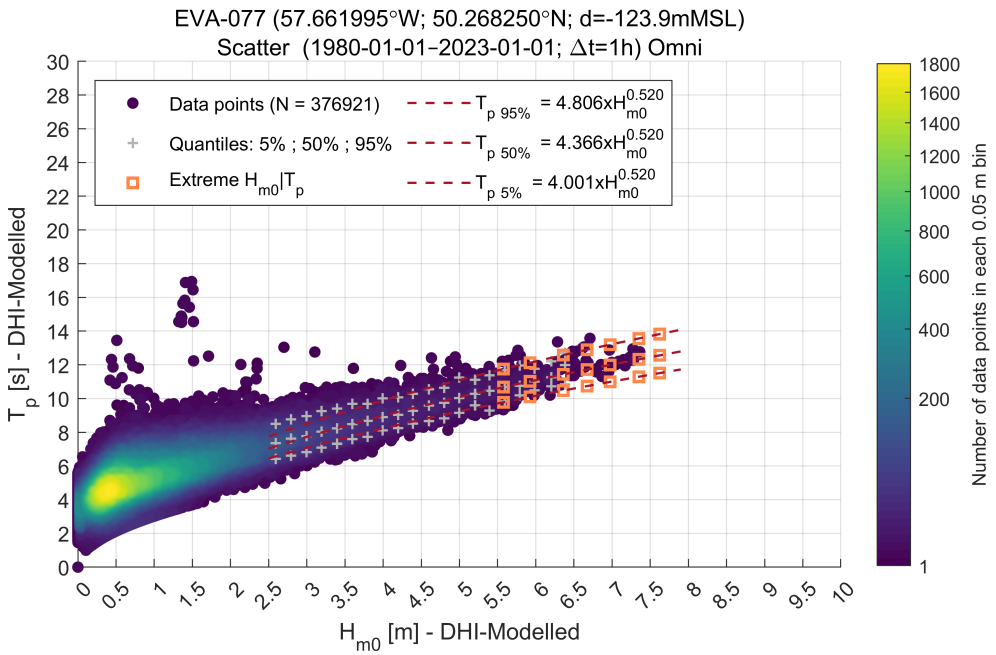


Figure C-387: Scatter plot of Hm0 x Tp at EVA-077 and quantile fit used to derived associated Tp to each extreme Hm0.

EVA-078

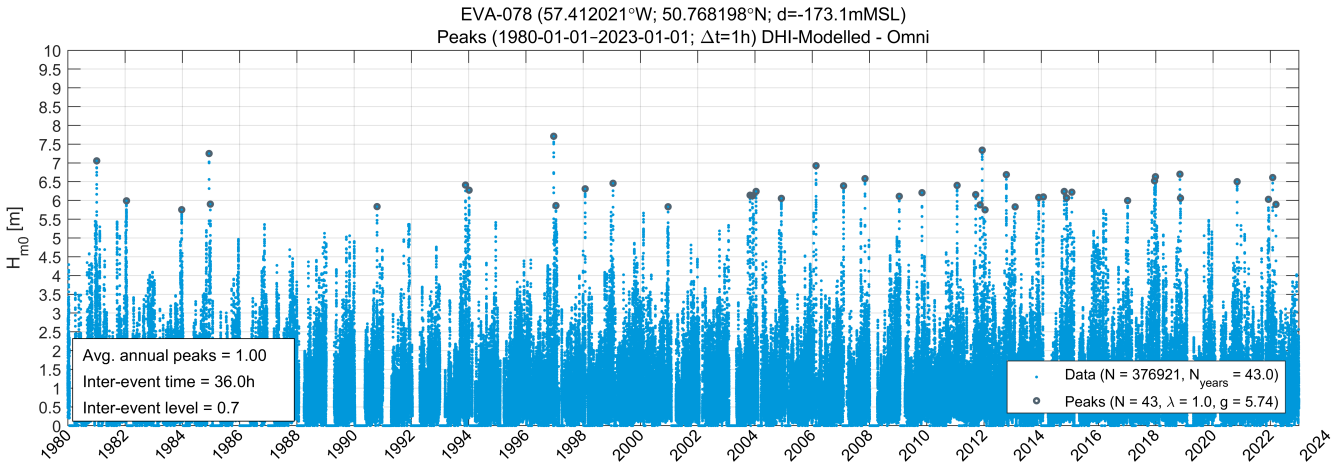


Figure C-388: Time series of significant wave height at EVA-078 and selected peaks.

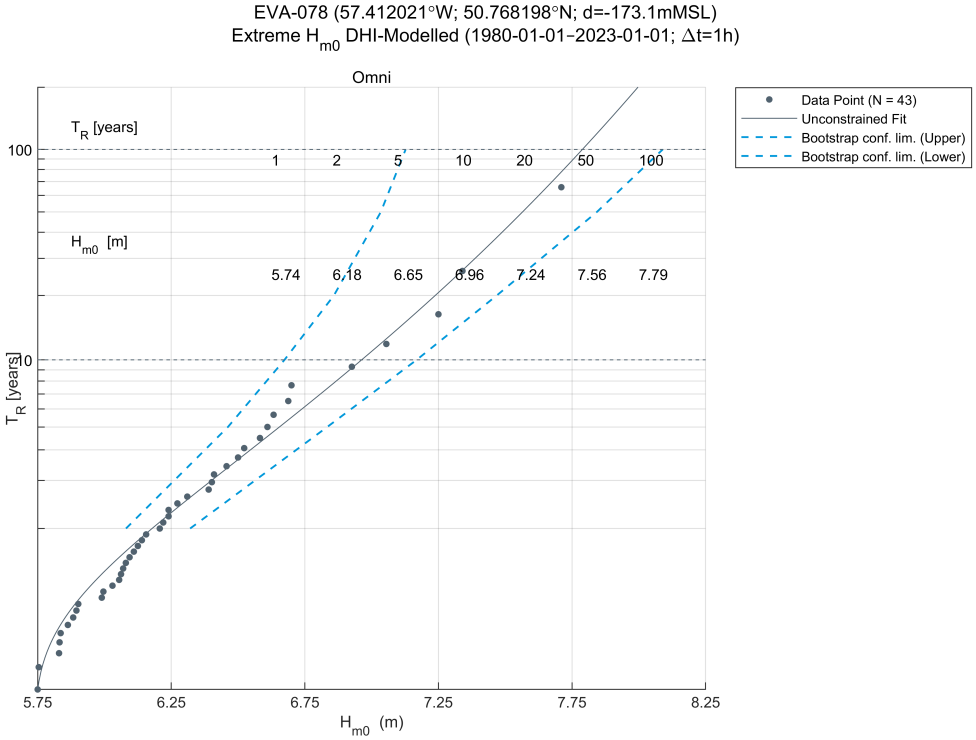


Figure C-389: Extreme value distribution fit at EVA-078.

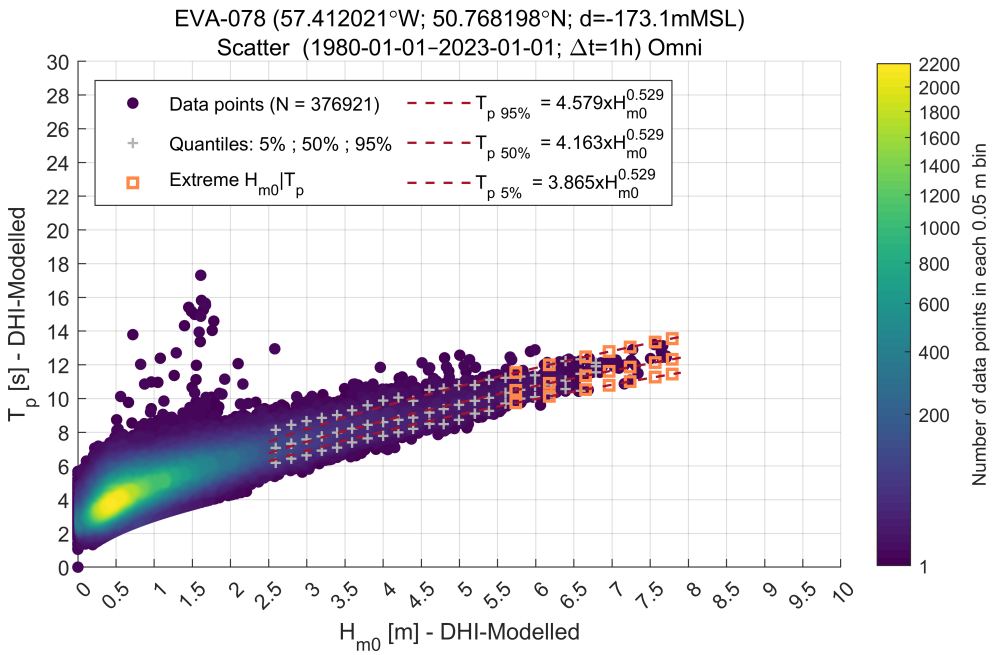


Figure C-390: Scatter plot of Hm0 x Tp at EVA-078 and quantile fit used to derived associated Tp to each extreme Hm0.